DISSERTATION

ISLAND DYNAMICS AND THEIR ROLE IN REGULATING SEDIMENT FLUX IN THE MIDDLE SNAKE RIVER, IDAHO

Submitted by

Dai B. Thomas

Department of Geosciences

In partial fulfillment of the requirements

For the Degree of Doctor of Philosophy

Colorado State University

Fort Collins, Colorado

Spring 2014

Doctoral Committee:

Advisor: Ellen E. Wohl

Deborah J. Anthony
Sara L. Rathburn
Brian P. Bledsoe

ABSTRACT

ISLAND DYNAMICS AND THEIR ROLE IN REGULATING SEDIMENT FLUX IN THE MIDDLE SNAKE RIVER, IDAHO

This study was conducted to provide an improved understanding of the dynamics of river islands and to investigate the role of islands in regulating sediment flux within the fluvial system.

The study showed that the islands in entrenched geomorphic subreaches of the MSR form, erode, and reform in locations controlled by lateral constrictions. The geometry of the islands adjust on a decadal or even longer time scale in response to a disturbance or changes in water and sediment supply, and thus, the islands form part of a temporal and spatial continuum of bedforms. The formation of the islands regulates sediment flux through the reach.

The study reach of the Middle Snake River (MSR) in Idaho contains over 300 islands within approximately 200 km between Swan Falls Dam and Brownlie Reservoir. The hydrology of the study reach has been significantly altered by upstream dams on the mainstem and dams on tributaries within the study reach.

Data used in the study include: (1) historical aerial photos (1938/1939) and topographic maps (c1894-1906), (2) topographic and bathymetric survey data collected in 1997 through 1999, (3) flow measurements from 1911 to present, (4) bed material samples, (5) morphostratigraphic mapping of 194 islands and (6) stratigraphic soil profile data collected on 95 islands. The soil profile data included soil stratigraphy, soil samples (used for sediment gradations and pollen analyses), pedological descriptions, historical artifacts and charcoal fragments (used for carbon dating). A previously developed 1-dimensional hydraulic model of the study reach was used to evaluate the hydraulic conditions along MSR and to calculate the overtopping discharges of the islands.

Comparison of historical aerial and topographic data with 2012 aerial photography showed evidence of the growth and erosion of islands and reworking of island chains to form new configurations, illustrating the dynamic nature of the islands over the last approximately 100 years. The historical document review also showed that the location of almost all larger islands and island groups are controlled by lateral constrictions such as tributary fans.

Soil profile data, pollen analyses, historical artifacts and radiocarbon dating of soil charcoal were used to determine the approximate age of islands and to evaluate the erosional and depositional activity of the islands. The soil profile data showed an extreme range in age at some islands where the gravel platform of the islands is old (circa 7,000 years), but the overlying sediments are young (on the order of hundreds of years).

Two-dimensional sediment-transport models were developed to evaluate the baseline conditions and simulate island development. Baseline conditions modeling showed the gravel- to cobble-sized material forming the core of the islands is not mobilized under the current hydrology. The islands formed in response to more recent floods from silt-sand sized sediment supply, which explains the relatively young soils overlying older gravel cores.

Modeling results showed that: (1) the island geometry adjusts to a disturbance or a change in sediment supply, (2) the formation of islands regulates sediment flux, and (3) the islands form, erode, and reform in the same general locations, which supports the study hypotheses that islands form part of a temporal and spatial continuum of bedforms.

ACKNOWLEDGEMENTS

This study would not have been possible without the help, guidance and support of many people, and I would like to sincerely thank all those who contributed.

The impetuous behind this study began back in the late 1990s when I was working for Mussetter Engineering, Inc. (MEI) , Fort Collins, CO as part of a study of the Middle Snake River conducted for the Idaho Attorney General's Office. Every soil pit was dug with a shovel, which was mostly enjoyable, even in +100^{O}F (+38^{O}C) weather and in freezing conditions, due to the good companionship on the river. We spent months on Snake River and had a lot time to discuss the dynamics of the islands - and this where the study began.

Firstly, thank you to my graduate committee members for their support, assistance and patience. I would like to especially thank Drs. Mike Harvey and Bob Mussetter for the invaluable assistance they have provided during this study and during my career. I would also like to thank everyone that I worked with while digging holes, including Mitch Peters, Chad Morris (MEI) and Dr. Maynord Fosberg (Univ. of Idaho) who provided soil science classes every day on the river and

Thank you to Ms. Bonnie Vail for her expert assistance in preparing the document and to Dr. Lyle Zevenbergen for his constructive editing. Also, thank you to Matt Iman and Brad Trabant for their GIS support and to Dr. Yong Lai (USBR) for providing the SRH-2D model.

Thank you to my parents for their support in everything and to my extended family in Colorado.

Finally, I would like to thank my wife Kirsten and our children Ben and Annie. This study began before our children were born, but it would not have been finished without everyone's support and encouragement.

TABLE OF CONTENTS

LIST OF TABLES

LIST OF FIGURES

1. Introduction

1.1. Background

The origin of this study was in the late 1990s when the State of Idaho filed an action to quiet title to 213 islands within the Snake River Islands Sector of the Deer Flat National Wildlife Refuge (DFNWR) within the State of Idaho (State of Idaho v. United States of America, Case CIV97-0426-S-BLW).

The DFNWR is located within the Middle Snake River (MSR), which extends from Swan Falls Dam downstream to Brownlee Reservoir, a distance of approximately 200 km, and contains over 300 islands (Figure 1.1). The islands along the MSR are owned by the Federal Government, the State of Idaho, the State of Oregon and private parties.

Mussetter Engineering Inc. (MEI) was retained by the Idaho Attorney General's Office to perform studies to determine ownership of the islands (Mussetter and Harvey, 2001a, b). To determine ownership of the islands, MEI performed analyses to determine the age of the islands. Islands that existed before the State of Idaho was formed belong to the federal government, while the islands that formed after the date of statehood belong to the State of Idaho. The studies were conducted by Drs. Mike Harvey, Bob Mussetter and Deb Anthony and supported by staff from MEI, including the author of this study. The data collected for the MEI studies are used in this study, including for the development of the 2-dimensional (2-D) hydraulic sediment-transport models. In addition, analyses and text reported in MEI Studies (Mussetter and Harvey, 2001a, b) are reproduced in this study with some limited modifications to fit the context of this study. A summary of the new work performed for this study and a description of the original work used in this study is listed in Table 1.1.

The MSR study reach is separated into three geomorphic subreaches (Figure 1.1). The upstream subreach (Subreach I) extends from Swan Falls Dam to the Boise River confluence, the middle subreach (Subreach II) extends from the Boise River to the Weiser River, and the downstream subreach (Subreach III) extends from the Weiser River to the upstream end of Brownlee Reservoir. The subreaches are primarily distinguished by the degree and character of anastomosing. The up- and downstream subreaches are entrenched and contain a mostly single-thread channel with multiple flow paths around the islands, which occur as single islands, island groups, and island chains (Figure 1.2). The middle subreach has an anastomosing planform with occasional multiple channels (Figure 1.3). Dams on the Snake River upstream of the study reach and dams on tributaries located within the study reach regulate the upstream flow and have significantly altered the sediment supply to the MSR compared to pre-dam conditions (Osterkamp et al., 2001).

1.2. General

River islands are found in many parts of a river's drainage network and span a wide range of energy conditions, but are most commonly located in montane, piedmont-valley, and coastal floodplain environments (Osterkamp, 1998). River Islands have long been recognized as part of the river continuum (Leopold et al., 1964; Gregory and Walling, 1973; Schumm, 1977), but there are very few studies that detail the evolution and/or dynamics of islands, or function(s) of islands within the river continuum. Osterkamp (1998) suggests the scarcity of research is due to the intimidating complexity of fluvial systems.

An improved understanding of the role of islands within fluvial systems is needed to better appreciate their role in regulating sediment transport within a reach, as well as to assess the extent of human impacts on river systems including management, restoration and conservation strategies. The factors that may influence island development and maintenance include hydrologic characteristics, geologic controls, local and reach-wide hydraulics, sediment supply/transport and the role of vegetation.

A fluvial island, as defined by Osterkamp (1998), is a

> "*geomorphic feature, surrounded by channel, that is higher than mean water level (or the principal network of adjacent ephemeral or intermittent stream channels) and that persists sufficiently long to permit the establishment of a permanent vegetation cover if adequate moisture is available" (*p531*)*.

River islands are a recognized bedform (Bridge, 2003) that can persist for up to thousands of years, with individual channels showing very low lateral migration rates due to the combination of relatively stable banks and well-established vegetation (Nanson and Knighton, 1996; Knighton and Nanson, 1993).

An anabranch is a metastable channel that diverges from a principal channelway and rejoins it downstream (Osterkamp, 1998), thereby forming an island between the anabranch and the principal channelway. "*An anabranching river is a system of multiple channels characterized by vegetated or otherwise stable alluvial islands that divide flows up to nearly bankfull discharge*" *(*Nanson and Knighton, 1996, p218)*.* There is some confusing nomenclature in the literature regarding the definitions of anabranching and anastomosing and commonly these terms have been used interchangeably. Nanson and Knighton (1996) examined rivers over a wide range of energy conditions. They apply the term anabranching as the generic term for all those multichannel rivers and limit the term anastomosing, by common usage, to those at the low-energy, fine sediment end of the range*.* In general, the term anastomosing is used in this study; however, in the literature review, the terms reported in the individual studies identified are used.

Islands form part of a temporal-spatial continuum of depositional features in rivers that vary from dune/ripple bedforms that are small-scale (in relation to the width of the river) and can rapidly adjust their geometry to daily discharge fluctuations, to gravel bars that have dimensions approximating the channel width and adjust their geometry to seasonal high-flow events, to vegetated islands that have dimensions on the order of the channel width and adjust their geometry on a decadal or even longer time scale (Figure 1.4). I hypothesized here that: (1) river islands adjust their geometry over decadal time periods in response to changes in water and sediment supply, and thereby regulate sediment transport, and (2) that where the hydraulic controls are fixed, the islands form, erode and reform in the same general locations following a disturbance or a change in sediment supply.

Stratigraphic soil analyses of 95 islands within the MSR show extreme variability at some islands where the island platform is old (based on soil characteristics and/or radiocarbon dates) but the overlying sediments are young based on the absence of pedogenic development or the presence of introduced pollen species. For example, at some islands, the basal gravels and/or the soils of the island platform are thousands of years old, whereas the overlying soils are on the order of decades to centuries in age (Mussetter and Harvey, 2001b).

1.3. Study Objectives

This study was conducted to develop an improved understanding of the dynamics of river islands and to investigate the role of islands in regulating sediment flux within the fluvial system. The MSR was selected to evaluate the following specific objectives:

1. Evaluate the dynamics of the islands within the MSR,
2. Test the hypothesis that islands in general, and specifically in the MSR, form part of a temporal-spatial time continuum by adjusting their geometry to regulate sediment flux
3. Test the hypothesis that, where the hydraulic controls are fixed, islands form, erode and reform in the same general locations following a disturbance or a change in sediment supply
4. Evaluate the extreme variability between the old island platform sediments and the young overlying sediments.

Data used in the study include:

1. Hydrologic data, including mean-daily flow and annual peak flow data measured at three gages along the MSR from Water Year (WY) 1910 to 2012.

2. Historical mapping, which includes early U.S. Geological Survey (USGS) topographic maps (c. 1894-1906) and mapping from the USGS 1914 Water Supply Paper.
3. Aerial photography collected in 1934/1936 and 1938, which covers the majority of the MSR study reach.
4. Topographic and bathymetric survey data along the majority of the MSR reach collected between 1997 and 1999.
5. Morphostratigraphic mapping of the 194 islands in the MSR conducted in 1997 by Othberg and Fosberg (2001).
6. Stratigraphic soil profile data collected on 95 islands, which include soil stratigraphy, soil samples (used to determine sediment gradations and used in the pollen analyses), soil descriptions, historical artifacts and charcoal fragments (that were used in carbon dating analyses).

1.4. Study Approach

This investigation of island dynamics included the following tasks:

1. A literature review of studies of islands in river environments.
2. A hydrologic analysis of the MSR flows was conducted for five selected hydrologic subreaches using gage records and hydrologic record extension techniques to quantify the flow-duration and flood-frequency characteristics along the study reach for the pre- and post-dam periods. In addition, historic flood hydrographs were evaluated in order to develop representative flood hydrographs that were used as input to the 2-D sediment-transport models developed to evaluate the sediment-transport characteristics at two selected subreaches.
3. Analyses of the morphologic changes of the islands along the MSR reported by Mussetter and Harvey (2001b) are detailed to show the dynamic nature of the islands over the last approximately 100 years. The analyses included: an historical map and

aerial photography analysis, identification and characterization of the local hydraulic controls on the islands, analysis of the island topography and morphology, and an evaluation of the change in island morphology through time.

4. A 1-D hydraulic model that extends along the majority of the MSR (from Brownlee Reservoir to upstream of Sign Island) was developed by Mussetter and Harvey (2001a). The model output was used to evaluate the hydraulic conditions and correlate them to patterns of erosion and deposition observed in the sequential aerial photographs. The results were used to develop the conceptual model of island development (Mussetter and Harvey, 2001b).

5. Soil profile data, pollen analyses, historical artifacts and radiocarbon dating of charcoal found in the soils were used to determine the approximate age of islands and to evaluate the erosional and depositional activity of the islands (Mussetter and Harvey, 2001b).

6. A review of 1-, 2-, and 3-D sediment-transport models was conducted. Based on the review, a 2-D sediment-transport model was selected.

7. Two 2-D sediment-transport models were developed to perform a detailed analysis of two study subreaches located in the entrenched geomorphic subreaches (Subreaches I and IIIA) to simulate island development and to evaluate the sediment-transport characteristics. The model output was used to evaluate the proposed hypotheses:
    a. islands adjust their geometry in response to changes in water and sediment supply, and
    b. islands form, erode, and reform in the same general locations in response to changes in sediment supply.

8. The 2-D model results were used to further develop the conceptual model of island formation and to resolve the apparent disconnection between the old island platform sediments and the young overlying sediments.

1.5. Figures and Tables

Table 1.1 Summary of the new work performed for this study and the original analyses and text (MEI, 2001a,b) used in this study.

Chapter	Section	Comment
1		New work
2		New work
3		The original text (2001b) was modified to fit the context of this study.
4	4.1	The original text (MEI, 2001b) was modified slightly to fit the context of this study. The hydrologic analyses (Section 4.1.2) were updated for this study using more recent flow data (up to Water Year 2012).
	4.2	New work
5		Original text modified slightly to fit the context of this study. Section 5.1.5 is new work. The analyses in Section 5.5.1 were updated using the more recent hydrologic data.
6		New work
7		New work

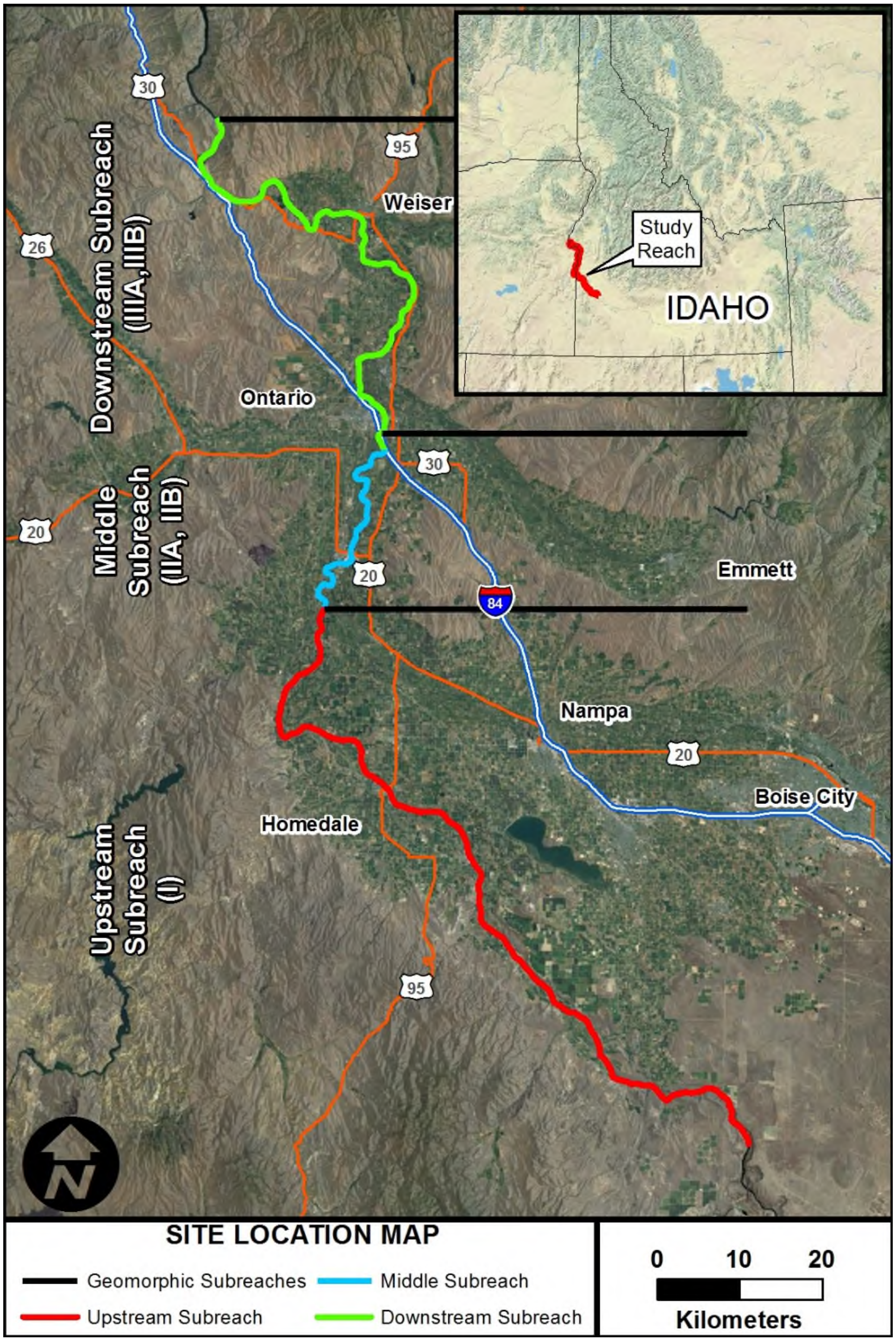

Figure 1.1 Site location map and geomorphic subreaches of the study reach (using Roman numerals, I, IIA, IIB, IIIA and IIIB).

Figure 1.2 Island chain located within the entrenched Geomorphic Subreach I.

Figure 1.3 Island located within the anastomosing subreach (Geomorphic Subreach IIA). Note: Figure 1.2 and Figure 1.3 are at the same scale.

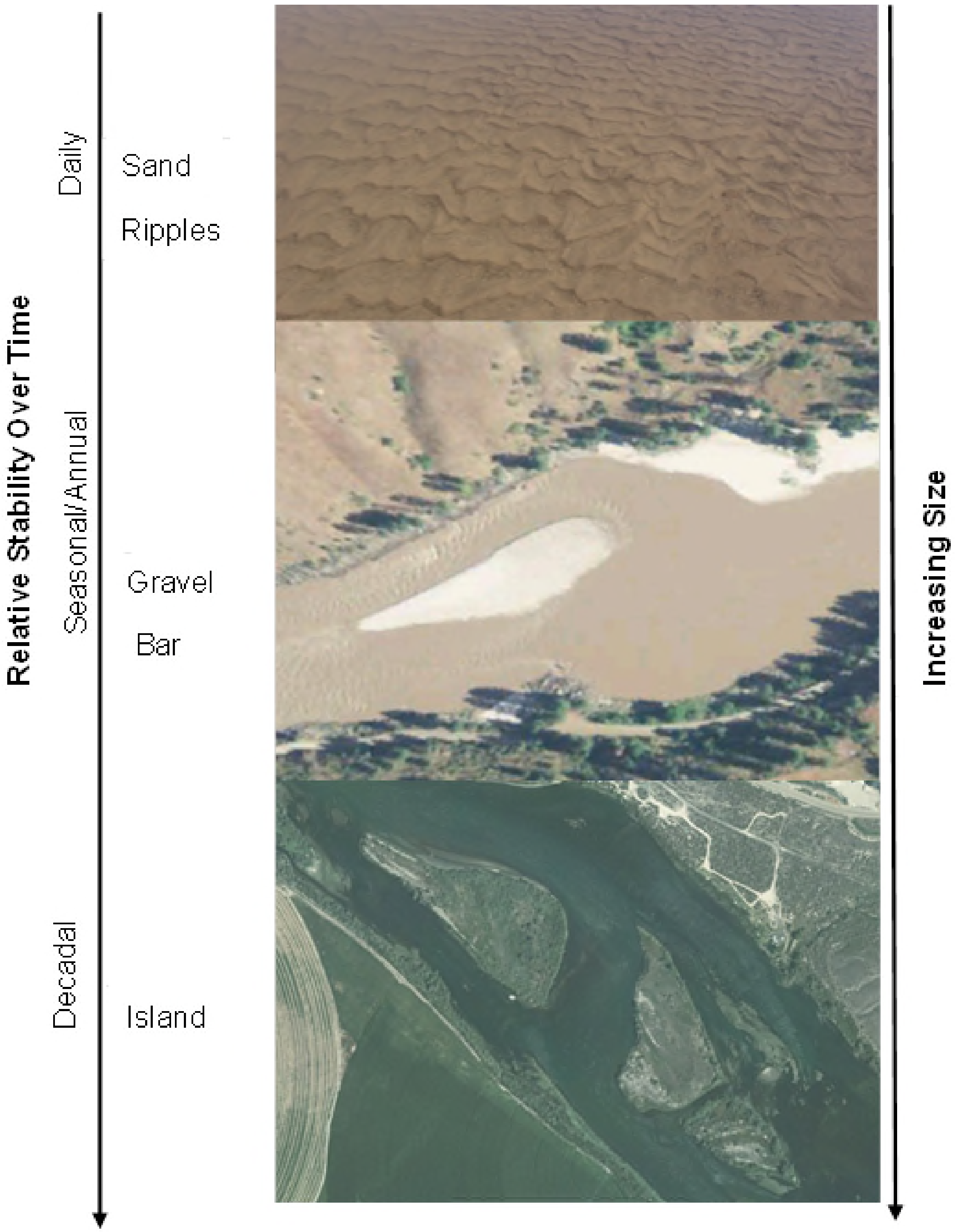

Figure 1.4 Relative stability of sand ripples, gravel bars and islands within the temporal and spatial continuum.

2. Literature Review

Numerous river classifications have been developed as a way to arrange rivers into groups based on descriptive or process criteria (Buffington and Montgomery, 2013). Davis (1899) first classified rivers into youthful, mature and old age based on their relative stage of adjustment. Lane (1957) classified rivers into braided, intermediate, and meandering streams based on planform and quantitative slope-discharge relationships, and Leopold and Wolman (1957) classified rivers into straight, meandering and braided, with anabranching channels placed in the braided category.

It is now generally recognized that anabranching rivers are classified separately from braided rivers. An anabranching river consists of multiple channels separated by vegetated and stable islands. The channel gradients are generally very low, whereas braided rivers consist of wetted areas separated by dynamic bars within the channel with have relatively steep gradients (Knighton and Nanson, 1993).

Several classifications have been developed that include islands and anabranching rivers, including Kellerhals et al. (1976); Brice and Blodgett (1978); Schumm (1985); and Nanson and Knighton (1996). The Brice and Blodgett (1978) classification is applied to this study. It characterizes three basic channel types based on the degree and character of channel sinuosity, braiding and anabranching (sinuosity is the ratio of channel length to valley length) (Figure 2.1). The Degree of Anabranching is the percentage of the reach length that is occupied by large islands and the Character of Anabranching describes the planform pattern of the anabranch. The middle anastomosing subreach of the MSR fits into the Class 1 (5 to 34 percent) of the degree of anabranching and in the composite category of the character of anabranching, while the upstream and downstream subreaches (Geomorphic Subreaches I and III) fit into Class 0 (<5 percent) of the degree of anabranching and in the split channel, sub parallel category of the character of anabranching.Islands occur in many parts of the stream network but most frequently occur in montane, piedmont-valley and coastal-floodplain environments (Osterkamp, 1998). Osterkamp's (1998) paper discusses the processes of fluvial island evolution in detail and proposes eight major causes of fluvial islands. These may occur preferentially in particular zones of a catchment and may develop over different timescales. The eight categories are:

1. Avulsion;
2. Gradual degradation of channel branches bounding a higher within-channel surface;
3. Lateral shifts in channel position during normal flows that isolate a central surface topographically higher than the channel braches bounding it;
4. Stabilization of a riffle, sand or gravel bar by accretion and vegetation establishment during a period of non-erosive peak discharges;
5. Steady degradation of channel branches along preferred paths of bedrock fractures or around structural features such as reef anticline, or through permeable zones of glacial deposits, leaving a medial feature of relative resistance to erosion between the channel branches;
6. Rapid incision of channel branches during recession of a flood or ponding event to isolate a higher surface during flood recession or a ponding event leaving a higher surface than the anabranches bounding it;
7. Lee deposition at a channel obstruction, generally in a braided or anabranched reach, and,
8. Deposition of various positive features by mass movement, such as hummocks of debris avalanche and possibly rare drumlin-like bars preserved as protuberances from basal-flow deposits of debris flow.

Osterkamp (1998) discusses Plum Creek, Colorado and the Middle Snake River, Idaho as examples. He suggests that many of the islands within the MSR were created by rapid incision following the Bonneville Flood and, therefore, he places the islands in the MSR into

Type 6. Osterkamp (personal communication, 2010 and unpublished document 2011) performed an analysis of the age of mussel shell fragments that were clearly related to aboriginal activity. The mussel shells were found on the low relief gravel core at Sign Island and were determined to be approximately 7,000 years. He determined the low gravel core formed from coarse Bonneville Flood debris (the Bonneville Flood occurred approximately 14,500 years ago). Mussetter and Harvey (2001b) indicated that only a minority of the islands are Bonneville age. The majority of the islands was formed due to sediment deposition during post-Bonneville flooding, and therefore belong in the Type 4 and 6 categories.

Anabranching channels form over a wide range of climatic and hydrologic environments and over a range of channel slopes and energy conditions (typically evaluated in terms of stream power) ranging from alpine rivers of Italy (Ward et al., 1999) to the very low gradient channels of northern Australia (Nanson and Knighton, 1996). They occur in channels with bed material sizes ranging from clay to boulders and occur with specific stream powers spanning two orders of magnitude (Nanson and Knighton, 1996).

Knighton and Nanson (1993) describe a general analysis of conditions that may lead to the development of multichannel systems based on their studies of very low-gradient rivers in Australia. They determined that anastomosing reaches are usually characterized by: flood-dominated flow regimes, often by a slight surplus in their local sediment budget that can result in aggradation; banks that are resistant to erosion relative to stream energy; and mechanisms that lead to channel damming and avulsion. They suggest that anastomosis is a transitional channel pattern, and that the advantage anabranching channels have over their single-channel counterparts is that, in situations where it is not possible to increase channel slope, the division of a single channel into two or more anabranches concentrates shear stress and stream power and enables the system to maintain or enhance the transport of water and sediment (Knighton and Nanson, 1993). The reported flow and sediment-transport advantages of anabranching are discussed more in the next section.

Nanson and Knighton (1996) proposed that anabranching channels are formed by both avulsion (involving erosion) and accretion and detailed the existence of six anabranching types that formed due to a number of mechanisms including highly variable flow regimens, resistant banks, factors leading to flow displacement (e.g., channel sedimentation or the formation of vegetation or ice jams) and tectonics.

The Canadian literature on anastomosing rivers has largely focused on mountain valleys (Smith and Smith, 1980; Smith, 1983; Smith, 1986; Abaddo et al., 2005; Tabata and Hickin, 2003) in which active tributary alluvial fans have reduced the channel gradient and induced channel aggradation, and as a result, anabranching channels have formed in the upstream aggradational reaches. Smith and Smith (1980) concluded that channels and islands aggrade over time and there is very little channel migration.

Smith et al. (1989) proposed a cyclical process of channel development where an initially single thread channel avulses to form an anastomosing channel. Over time, the anabranching channel reverts back to a single channel, and the cycle is repeated. A similar process was also reported by Sipos and Kiss (2004), who studied 12 islands long a 20-km-long section of the River Maros in Hungary. They studied island formation as a result of flow regulation and channel straightening using historical aerial photos, topographic surveys and tree dating. Flow regulation on the River Maros began in the middle of the 19th century and the channel straightening for flood protection purposes began in the 1920s, which increased the slope from 0.014 to 0.028. As a result, the river planform become slightly sinuous, there was a rapid establishment of vegetation (*Salix, Populus* spp.) and islands formed in locations where point bars previously existed. During the period 1950 to 2001, Sipos and Kiss (2004) observed that, within the study reach, the main islands coalesced and attached to the river banks, creating a single channel. Over time, two small island cores formed in the middle of the channel, which grew large enough to divide flow and the anabranching pattern was re-formed. Sipos and

Kiss (2004) concluded this represented a cyclical pattern of establishment, migration and elimination of islands, which represents a quasi-equilibrium state.

Schumm et al. (1996) studied the Oven and Kings Rivers in northeastern Victoria, Australia and determined that the anastomosing channels vary widely with age and the multiple channels develop by avulsion.

> "*The young channels have large bankfull flows, low sinuosity, large meander wavelength, steep gradients, and are unstable). They are incised channels that are rapidly eroding their bed and banks. Old channels, however, have small bankfull flows, high sinuosity, small meander wavelength, gentler gradients, and are relatively stable*" (p1212, Schumm et al., 1996).

Furthermore, Schumm et al. (1996) stated

> "*as individual channels become older and more sinuous, they also become more hydraulically inefficient. Thus, increasing proportions of flood discharge are displaced overbank. This overbank flow concentrates in relatively straight floodplain depressions, and it erodes a new channel, which develops by both up- and down-valley incision…with time, both channel segments join to form a new anabranch of the anastomosing-channel system*" (p1212).

Schumm et al. (1996) compared the differences between the Australian and Canadian anabranching river systems. In general, the Australian rivers "…*are sinuous, and they are not stable because they increase in sinuosity and avulse as a result of reduced channel efficiency*" (p1223). Furthermore, the Australian rivers are characterized by slow vertical deposition on floodplains. In comparison, the Canadian-type rivers described by Smith (1983, 1986) "*are relatively straight and stable, and they are characterizied by rapid vertical deposition in channels and on floodplains*" (p1223). Unlike the Canadian and Australian examples, under post-dam conditions, the MSR experiences very little overbank flow and the islands form by vertical accretion but not by avulsion.

Gurnell et al. (2001) studied the interaction of riparian vegetation and island development in the Fiume Tagliomento, Italy, and developed a conceptual model of island development. The Fiume Tagliomento is considered the last natural alpine river in Europe (Müller, 1995) and extends from the headwaters in the Italian Alps to the Adriatic Sea, a distance of approximately 170 km. The upper part of the reach has a slope of approximately 10percent, the middle braided section has a slope of approximately 1 percent, and the downstream meandering reach has a slope of 0.1 percent. The channel bed material is approximately 256 mm (D_{50}) in the upstream reach, 32 to 64 mm in the middle reach, and 0.2 mm in the downstream reach. Islands are located along the majority of the length of the river, but are most common in the middle and lower reaches of the river. Gurnell et al. (2001) observed that islands may develop on bare gravel bars, or be dissected from the floodplain by channel avulsion. An analysis of aerial photographs indicated that the largest and most established islands rarely survived longer than 20 years. Their conceptual model of island development illustrates how interactions between vegetation, large woody debris, local topography, sediments and hydrologic regime can produce different types of islands and also describes the mode of development, which includes the stabilization of medial bars and floodplain dissection. The islands in this study reach predominantly occur in the wide braided and meandering sections of the river; these conditions differ significantly from the MSR, but the Gurnell et al. (2001) study emphasizes the importance of many factors, including the influence of vegetation on island development.

Mussetter and Harvey (2001b) reported that island formation, erosion and re-formation over time in the Walters Ferry Reach of the Snake River appears to be a dynamic process that is a function of changes in discharge and sediment supply over time. Two-dimensional (2-D) hydrodynamic modeling (Mussetter and Harvey, 2001b) of the reach, which contains a 5-km-long chain of islands, suggested that the dynamics of the island reaches were dramatically different if the islands were removed down to the cobble/gravel platform. The analyses evaluated the incipient motion conditions using gravel-sized material at approximately half the bankfull discharge along the reach for with- and without-island conditions. The results of the analysis indicated that sediment continuity through the reach is not maintained if the accreted islands are not present, and thus sediment deposition occurs to form the islands, which

Mussetter and Harvey hypothesized would eventually lead to the re-establishment of sediment continuity.

The islands in the up- and downstream entrenched geomorphic subreaches of the MSR have developed in different conditions to those in representative Australian anabranching rivers, which generally have significant overbank flooding and develop either by avulsion or slow vertical accretion. The up- and downstream reaches also differ from the Canadian examples that mostly develop through rapid vertical accretion as a result of active tributary alluvial fans reducing the channel gradient and inducing channel aggradation.

Vegetation has been identified as playing an important role in both the creation of islands and the stabilizing effect on the islands and channel banks. The majority of the reviewed studies emphasized the important role of vegetation on island development and maintenance (Ward et al., 1999; Makakse, 2001; Maser and Sedell, 1994; Gautier and Grivel, 2006; Gurnell et al., 2000; Sipos and Kiss, 2004; Wende and Nanson, 1998; Tooth and Nanson, 1999, 2000; Jansen and Nanson, 2010). However, Rust (1981), who described an anastomosing river in an arid environment on a sparely vegetated floodplain, determined that the role of vegetation is less important on arid floodplains.

Maser and Sedell (1994) identified processes by which drift wood in streams helps create channel islands. Large woody debris can form the core of scroll bars (Nanson, 1981) and can become stranded or snagged to form bar apex jams (Abbe and Montgomery, 1996) and lateral jams (Fetherston et al., 1995) behind which sediment and organic matter accumulate to provide locations for the establishment of riparian trees. The establishment of forested floodplains and islands reflects different interactions between fluvial processes and vegetation colonization and establishment in gravel-bed streams in Missouri and Arkansas (McKenney et al., 1995), with the stable river reaches being associated with forested floodplains, whereas in the disturbed river reaches, the low energy reaches exhibit vegetation-banded bars and higher-energy reaches contain vegetated islands. Fetherston et al. (1995) suggest that wood accumulation at the head of the islands plays an important role in reducing boundary shear stress and protecting vegetated islands and vegetated bands on bars.

Gautier and Grivel (2006) studied a section of the middle Loire River in France that experienced a rapid growth in the number of islands over a 150-year period as a result of change in hydrology and land use. In 1850, there were 11 islands along the 16 km study reach and the river was described as a wide and active channel largely free of vegetation, with approximately 0.4 percent of the floodplain was comprised of naturally forested land. By 2002, there were approximately 30 islands along the reach and there was a significant increase in vegetation on the islands and lateral margins, with approximately 35 percent of the overbank comprised of forested land. The increase in islands was attributed to the significant decrease in number of large floods after 1866 and to the cessation of clearing in-channel vegetation for the purpose of navigation around the beginning of the 20th century.

In addition, Guatier and Grivel (2006) used repeat topographic surveys and sediment traps located on the islands coupled with grain-size analysis to measure deposition and erosion over two floods with 5- and 30-year return periods. Vegetation was shown to exert a major influence in sediment trapping on the islands and they noted the aggradation rates were varied across the islands during the two large floods. On average, the younger islands had aggradation rates of 80 to 200 mm/year and total deposition of up to 5 m over a 25-year period. The older islands experienced deposition of approximately 50 to 140 mm/year on the lateral margins and slight degradation or no change on the central part of the islands, indicating the rate of sedimentation is partly a function of the island's height.

Nadler and Schumm (1981) studied the South Platte and Arkansas Rivers in eastern Colorado and discuss how the change in flow regime changed the channel morphology. In the early 1800s, the river was relatively straight, wide, shallow, braided planform with transient bars, and the flow was intermittent. By the early 1900s, irrigation increased the groundwater table, flows became perennial and dam construction reduced the peak flows, which resulted in increased vegetation on floodplain and channel bars and subsequent stabilization of the bars. In addition, the rivers narrowed and became more sinuous due to perennial streamflow, abstraction of sediment occurred with irrigation water, and discharge decreased during drought. Over time, the vegetated bars coalesced with the channel banks, and the channel became a single thread channel. Similar to Sipos and Kiss (2001), this study shows how change in hydrologic regime alters the vegetation and channel planform, and thereby provides important information in regards to river management.

Jansen and Nanson (2010) conducted a study of Magela Creek in northern Australia to examine the water and sediment flux interaction in an anabranching river. They noted the importance of vegetation for "*increasing bank strength, raising flow drag, and restricting high velocity flow to a zone above the channel bed*" (p14), and argued "*that these interactions result in stabilizing mechanisms than ensure long-term stability of the channel floodplain system*" (p14).

In addition to recognizing the stabilizing effect of vegetation required for island development, Sipos and Kiss (2004) noted that the hydrologic regime plays an important role, in that a period of low-flow runoff years is required to provide the vegetation an opportunity to colonize and persist.

Smith (1976) performed a series of experiments on bank materials of anastomosed channels in floodplain silt deposits in the Alexandra Valley in Banff National Park, Alberta, to determine the effect of vegetation roots on bank erodibility and lateral migration of channels. The experiments were performed using a specially designed erosion box as a means to simulate natural erosion conditions and measure the influence of vegetation roots in reducing bank erosion. Smith's results indicate that bank sediment with 16 to 18 percent by volume of roots with a 5-cm root mat for bank protection had 20,000 times more resistance to erosion than comparable bank sediment without vegetation.

In summary, the majority of the reviewed studies (the exception being Rust, 1981) emphasized the important role of vegetation for the development and maintenance of islands and/or anabranching channels. In addition, the studies by Guatier and Grivel (2006) and Nadler and Schumm (1981) illustrate how changes in hydrologic conditions and river management affect the channel morphology.

Komar (1984) developed a set of measurement parameters to define the geometry of islands. Komar (1983, 1984) observed that streamlined islands in rivers have lemniscate loop shapes that are similar to symmetrical airfoils. (In mathematics, a lemniscate refers to figure 8 shaped curves. Komar was comparing the island shape to one side of the lemniscate loop). He measured islands along the Mississippi, Missouri and Columbia Rivers and found a strong linear relationship between the island length and width, with the length:width ratio averaging from 3 to 4, and the maximum width positioned at about a factor of 0.65-0.70 along the length from the point lee. Both of these relationship are consistent with the analytical lemniscate loop shape (Komar, 1984) and correspond to the minimum drag observed in airfoils, which Komar concluded supports the hypothesis proposed by Baker (1979) that islands acquire shapes that minimize the drag or resistance to the flowing fluid when they formed. In addition, Komar (1983) performed flume experiments to determine how the islands obtain their streamlined shape. He found that when the islands were partially submerged, "*most of the streamlining was brought about by deposition filling in the wake region*" (p651). In addition, "*when the islands were fully submerged, the flow over the top can become supercritical, producing a hydraulic jump in the island lee and focusing the erosion in that region, rapidly eroding the island to a streamlined shape*" (p651).

Many studies have shown that fluvially controlled rivers tend towards a stable channel configuration and an approximate equilibrium between the supply of water and sediment from upstream sources and the capacity of the channel to convey water and sediment. This is achieved by adjusting hydraulic geometry, planform and slope (Leopold and Maddock 1953;

Horton 1945; Lane, 1955; Simons, 1957; Leopold and Wolman, 1957; Leopold et al., 1964; Schumm, 1973). The results of studies on anabranching rivers provide some insight into the role that islands play in regulating sediment flux.

There has been debate in the literature regarding the water and sediment-transport efficiency of anabranching rivers and whether anabranching channels represent a dynamic equilibrium. Studies based on the Australian rivers indicate that anabranching rivers adjust their geometry (width, depth, number of channels) to enhance sediment transport and attain a dynamic equilibrium. Nanson and Knighton (1996) asserted that the major advantage of anabranching rivers over their single thread counterparts, is that in a situation where it is not possible to increase channel slope, the division of a single channel into two or more anabranches concentrates shear stress and stream power and enables the system to maintain or enhance the transport of water and sediment flux; however, this can only occur where stream banks are relatively cohesive and can resist increased stress.

Studies based on the Canadian rivers show that anabranching channels are not necessarily more efficient at transporting sediment and water compared to single channels (Abbado et al., 2005; Tabata and Hickin, 2003), but anabranching channels represent a dynamic equilibrium between the rates of channel creation and channel abandonment. In the following discussion, both the Australian and Canadian studies are compared in the context of a Jansen and Nanson (2004) study that demonstrated that both conditions can occur.

Nanson and Knighton (1996) explained the increase in flow efficiency of an anabranching channel in terms of Yang's (1971) minimum energy expenditure theory. Theoretically, a semi-circular cross section has the smallest ratio of skin resistance to discharge, and therefore is the most efficient at conveying flow. However, it is difficult for a channel and banks composed of unconsolidated material to maintain a semi-circular shape. As a result, the banks collapse and sediment is transported across the cross section, resulting in a wider, shallower cross section with a parabolic shape (Wolman and Brush, 1961).

In contrast, Pickup (1976) noted that a channel with broad, rectangular cross-sectional geometry is the most efficient at transporting sediment. However, due to the large boundary area and an associated increase in roughness, a wide-shallow system is hydraulically less efficient than a narrow, deep channel at conveying flow. Therefore, the form of an alluvial channel becomes a compromise between an efficient conduit for water and one able to transport bed material supplied to it (Knighton and Nanson, 1996). Furthermore, Knighton and Nanson (1996) state that the energy compromise from narrow and deep to wide and shallow channels involves an increase in gradient in order to maintain or increase the conveyance of water and sediment. In many river systems, an increase in gradient can be achieved by reducing the channel sinuosity. However, in a system that is unable to change the gradient, an alternative method to increase both flow and sediment-transport efficiency (by an increase in work per unit area) is to form an anabranching system with a number of channels that are typically narrower and deeper than a single thread channel.

The increase in efficiency of anabranching channels was demonstrated by Nanson and Huang (1999) using the basic hydraulic relationships, including flow continuity and channel roughness. The channel geometry was defined in terms of the width-to-depth ratio and sediment transport was evaluated in terms of velocity, since velocity has a highly non-linear relationship to sediment transport. Nanson and Huang (1999) showed that when channel roughness or sediment size and channel slope remain unchanged, flow discharge is determined only by cross-sectional area and a shape factor, and the channel having the least wetted perimeter for a given area has the maximum flow discharge; in open-channel flow, this is known as the most economic section (Chow, 1959). Furthermore, the best hydraulic section also provides the maximum velocity, and therefore provides the maximum sediment-transport capacity.

By comparing the sediment-transport capacities of single- and multiple-channel systems, Nanson and Huang (1999) showed that under conditions where gradients could not be readily increased, anabranches appear to provide the potential to increase, or at least maintain, sediment flux without an increase in slope. The maintenance of sediment flux can be achieved through the adjustment of the number of channels and channel shape (width/depth ratio); this shows how anastomosing rivers represent a balance between channel geometry and sediment and water transport, and illustrates why anastomosing rivers may develop (Nanson and Huang, 1999).

The results from two field studies (Abaddo et al., 2005; Tabata and Hickin, 2003) performed on anabranching reaches of the upper Columbia River in Canada reported no flow efficiency advantage in anabranching channels. Abaddo et al. (2005) performed sediment-transport analyses using the Bagnold (1977), Rouse (1937), and Van Rijn (1984a, b) sediment-transport equations with representative channel geometries, bed slope and grain sizes. Their analyses indicated a decrease in sediment-transport rates with an increasing number of channels, which led them to conclude that anastomosis of the Columbia River is "*maintained by a dynamic equilibrium between the rates of channel creation and channel abandonment*" (p16).

Tabata and Hickin (2003) performed analyses using a modified version of hydraulic geometry called interchannel hydraulic geometry, which they developed to study anabranching channels on the upper Columbia River. Similar to the conventional hydraulic geometry developed by Leopold and Maddock (1953), interchannel hydraulic geometry relates the channel geometry (width, depth, and slope) and hydraulic conditions (velocity, friction factor) to the bankfull discharge using a series of power equations. Tabata and Hickin's (2003) analysis showed an increase in flow resistance with an increasing number of channels, which they concluded led to a decrease in hydraulic efficiency. Furthermore, Tabata and Hickin (2003) summarize their study by stating,

> "*On the Columbia River, the cause of anastomosis more likely relates to local oversupply of sediment, channel aggradation, and consequent enhancement of channel avulsion behavior. Any change in hydraulic efficiency of anastomosing channels on Columbia River appears to be independent of the channel splitting process; change in channel conductivity is a result of anastomosis, not the cause of it*" (p850).

The results of Abaddo et al. (2005) and Tabata and Hickin (2003) appear to contradict Nanson and Huang's (1999) hypothesis that anabranching channels are more efficient than their single channel counterparts. An explanation for this apparent contradiction was provided by Jansen and Nanson (2004) based on field measurements and flume experiments. Jansen and Nanson (2004) collected hydraulic data along an 8.5-km anabranching reach of Magela Creek, Australia. The measurements were taken at discharges up to 14 times bankfull discharge and sediment-transport measurements were collected at discharges ranging up to 4 times the bankfull discharge. The field data indicated that, at the bankfull discharge, the flow in the anabranching channels was deeper and faster, and the flow efficiency was approximately 60 percent greater compared to the wide, single-channel sections.

Jansen and Nanson's (2004) flume experiments were conducted in a 10-m-long, 0.45-m-wide and 0.3-m-deep flume for the following three channel geometries: (1) a single 45-cm-wide channel, (2) three 10-cm-wide channels, and (3) a single 30-cm-wide channel. Channel Geometries 1 and 2 were developed to represent the Magela Creek conditions and Geometry 3 was developed to represent the Columbia River conditions identified in studies by Tabata and Hickin (2003); Abaddo et al. (2005). For the Magela Creek conditions, the flume experiment indicated an increase in flow in the anabranching channel (Geometry 2) compared to the single channel (Geometry 1). For the Columbia River conditions, however, the results indicated no flow efficiency advantage in anabranching (Geometry 3). Jansen and Nanson (2004) concluded that two types of anabranching are possible and that no flow efficiency advantage derives from anabranching if aggregated bed width of the anabranches equals that where flows converge into a single channel.

Nanson and Huang's (1999) analysis showed that development of anabranches appears to provide the potential to increase, or at least maintain, sediment flux without an increase in slope. They also indicate that not all anabranching channels are able to adjust their geometry and increase sediment-transport rates to achieve a stable equilibrium; this assertion appears to be supported by the studies of Tabata and Hickin (2003) and Abbado et al. (2005), which suggest that the anabranching on the Columbia River is a relatively inefficient disequilibrium system. Both Tabata and Hickin (2003) and Abbado et al. (2005) indicate that anastomosing rivers are formed by avulsions and the slow abandonment of older channels, and therefore are not a “graded” state.

Huang and Nanson (2007) extended their original theoretical analysis (Nanson and Huang, 1999), which used basic hydraulic relationships for bed-load transport, to include the number of anabranches as a variable to evaluate flow efficiency and the causes for the occurrence of anabranching systems. They reported a complex relationship between the number of anabranches, channel geometry (including width and width-depth rations), vegetation influence and the flow transport capacity. Furthermore, depending on the circumstances, an increase in the number of anabranches can lead to either an increase or a decrease in the sediment-transport capacity. Their analytical analysis showed that with an increase in the number of channels, some anabranching channels (both overloaded and under-loaded with sediment) can achieve stable equilibrium conditions. If the channel width can be significantly reduced either by vegetation or by cohesive sediments, then anabranching rivers can significantly increase sediment-transport capacity. Conversely, if the channel cannot significantly reduce width, then an increase in the number of channels can cause sediment transport to reduce significantly, which leads to rapid vertical accretion as observed in the Upper Columbia River, Canada (Smith and Smith, 1980).

In summary, studies based on mathematical analyses, field studies, and flume studies of anastomosing rivers in Australia indicate that under conditions where gradients could not be readily increased, the development of anabranches appear to provide the potential to increase, or at least maintain sediment flux (Nanson and Huang, 1999). In terms of this study of the MSR, the limits on slope adjustment come from geologic features such as bedrock control located at the downstream end of the reach and local constrictions caused by tributary fans.

In addition, a previous study of a subreach of the MSR (Mussetter and Harvey, 2001b) evaluated the incipient motion conditions along the reach at bankfull conditions for with- and without-island conditions. The results of the analysis indicated that sediment continuity through the reach is not maintained if the islands are not present, and thus sediment deposition occurs to form the islands, which Mussetter and Harvey hypothesized would eventually lead to the re-establishment of sediment continuity.

Although the Australian rivers vary significantly from conditions found in the MSR, and in particular from the entrenched conditions in the up- and downstream subreaches of the MSR, the idea of anabranching channels adjusting their geometry to more efficient transport sediment is applicable to evaluating the role of islands in regulating sediment flux in the non-anastomosing reaches of the MSR.

2.1. Figures and Tables

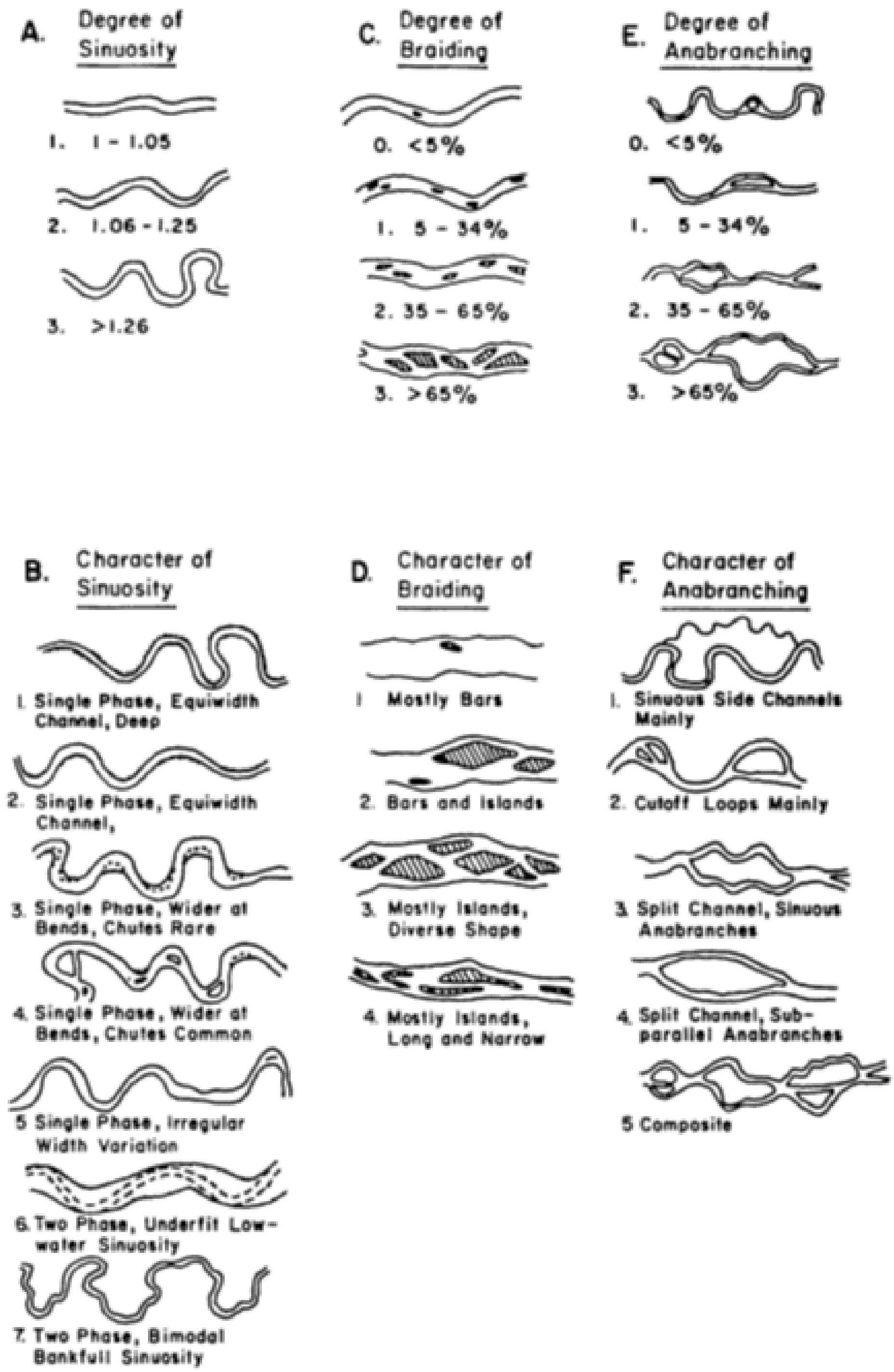

Figure 2.1 Types of channel patterns (Brice and Blodgett, 1978, reproduced from Schumm, 1985 p8).

3. Study Area

To describe the study area, a review of the geology and geomorphology of the Middle Snake River (MSR) was conducted, which includes a description of the extents and geomorphology of the three geomorphic subreaches.

To reference key locations within the study reach and facilitate identifying the location of the islands, development of the hydraulic models and interpretation of the model results, a main channel station line was developed that represents the distance along the approximate centroid of the flow. The origin of the station line (i.e., downstream end is located at Sta 0) is located near the head of Brownlee Reservoir and the upstream end of the station line (Sta 2009+20) is located at Swan Falls Dam (Figure 1.1). Table 3.1 identifies significant features along the study reach, including the stationing of features used in the hydrologic analyses and the hydraulic models; it also shows the correlation of the stationing with river miles (RM) shown on USGS 7.5-minute quadrangle maps at significant features along the study reach.

The naming convention for the islands was based on previous studies of the MSR (Mussetter and Harvey, 2001a, b). The islands are typically identified by a reference number, which may be followed by a letter/number combination. In general, single islands are identified with a single number, whereas islands within a larger group may be identified with a common number followed by a letter and/or another number. In addition to the unique reference number, many of the islands are also named. The unnamed islands are referenced to the river mile stationing shown on the USGS quadrangle maps. The reference number, name, coordinates of the island and the elevation of the top of the island are presented in Appendix A1 and the location of the islands are shown in reduced-scale USGS 7.5-minute quadrangle maps in Appendix A2.

3.1 Geology and Geomorphology of the Middle Snake River

3.1.1. Geology and Geomorphology

The Snake River basin upstream of Farewell Bend covers approximately 178,700 km^2 and extends into five states (Idaho, Oregon, Nevada, Utah, and Wyoming) (Figure 3.1). Elevations range from over 4,000 m along the highest peaks of the Teton Range in the southeast to about 600 m along the river valley near the downstream end of the study reach. The granite massif of the Idaho batholith forms the upland border of the drainage basin to the north, while the faulted mountain blocks of the Basin and Range (which include batholith outliers) form the southern border. The Snake River flows between these two physiographic areas in the broad Snake River Plain, prominent, curved lowland extending from Yellowstone National Park to the eastern edge of Oregon (Figure 3.1).

The Snake River Plain appears to be one simple topographic feature, but is actually formed by two different geologic mechanisms. The eastern Snake River Plain represents the path of the hot spot that currently fuels Yellowstone's geysers and fumaroles. The western Snake River Plain, which includes the MSR reach, is a downfaulted graben, very similar to the many basins found in the Basin and Range province to the south (Othberg, 1994). This graben formed in a rift zone initiated about 17 million years ago, and subsequently filled during the Miocene and Pliocene with a complex mixture of volcanic basalts, and lacustrine and fluvial sediments (Othberg, 1994). The basin filling was interrupted several times when the Ancestral Snake River eroded through the basin boundaries, causing erosion and incision. In the Late Pliocene or early Pleistocene, the final incision into this basin fill was initiated when the Snake River formed its current outlet near Farewell Bend. Prior to, and during, this incision, extensive Pleistocene basalt volcanism occurred, covering the Tertiary basin fill, preserving terraces left in the Boise River and Snake River valleys, and even damming the Snake River (Othberg, 1994).

The climate in the area of the project reach is temperate arid to semi-arid. Along the river and in the lowlands bordering the river, annual precipitation ranges from 150 to 300 mm, but in the surrounding highlands can range up to 600 mm (Othberg, 1994). Most of this precipitation falls in the colder months of the year, and usually falls as snow. Floods can occur due to snowmelt, rain-on-snow events or summer thunderstorms.

3.1.2. Bonneville Flood and Effects

About 14,500 years ago, near the end of the Pleistocene, Lake Bonneville (a large pluvial lake centered on the modern Great Salt Lake) overflowed its basin to the north, and drained into the Snake River Plain at Red Rock Pass near Preston, Idaho (Malde, 1968; O'Connor, 1993). Peak discharge from this overflow has been estimated at 1.0 million m^3/s (35 million cfs), with flows from Swan Falls to Marsing (including the upper portions of the MSR reach) estimated at 0.82 million m^3/s (29 million cfs, O'Connor, 1993). While this peak flow may have only lasted for a short time [O'Connor (1993) estimated 6 days of peak flow, with the entire flood lasting up to several months], the overflow from Lake Bonneville could have augmented Snake River flows for as long as 1,100 years, both prior to and after the primary flood (O'Connor, 1993).

This dramatic flood created extensive areas of scabland erosion, and in other locations deposited thick layers of sediment, including deposits of large basaltic boulders, with diameters up to 10 m, known as the Melon Gravels. These boulder deposits are especially evident in the most upstream section of the MSR, from upstream of Sign Island (88) (Sta 1852+67) to the Papike Island Chain (73-77) (~Sta 1710+20), where large boulder berms with boulders as large as 4.6 m in diameter border the Snake River (Figure 3.2). Downstream from these coarse-grained boulder deposits, much finer Bonneville Flood slackwater deposits mantle much of the Snake River valley, including lower terraces and portions of the tributary valleys of the Boise, Payette, and Owyhee Rivers (O'Connor, 1993; Othberg et al., 1997). These slackwater sediments were deposited due to ponding of the Bonneville flood at the constriction near Farewell Bend at the downstream end of the MSR reach.

Many of the islands formed on the low-elevation gravel cores, which are relic bar features formed from the coarse Bonneville Flood debris, and were likely formed under a hydrologic regime that experienced significantly higher flows, such as during the 1,100 year period following the Lake Bonneville flood. As discussed later in the study, the relic gravel bars are located up- and downstream of the fixed hydraulic controls. For example, in the 2-D modeling study reaches, Ketchup Island (in the Ketchup study reach) formed on a relic gravel bar downstream from a channel expansion, whereas Argy, Becky and Brooks Islands formed on relic gravel bars located upstream of contractions. No analyses were conducted to determine the percentage of islands located on relic bars.

3.1.3. Valley Geomorphology

The basin filling of the late Tertiary, and later incision and basaltic volcanism, created a varied valley geomorphology along the study reach. The extreme upstream end of the study reach is entrenched into the Tertiary basin fill (mostly the Glenn's Ferry Formation). High, basalt-capped bluffs bound the valley as far downstream as Marsing. The coarse-grained Melon Gravels form prominent riverside deposits as far downstream as the Papike Island chain (77a-e), (Sta 1710+20). The Whitney and Boise Pleistocene-age terraces begin upstream of Center Island (58) (Sta 1505+00), and are located on either side of the Snake River (Othberg, 1994) downstream to the Boise River confluence. The higher Whitney terrace (of Bull Lake age) occupies most of the valley between the bluffs capped with either basalt, later Tertiary/Early Pleistocene gravels (i.e., Tenmile Gravels), or early Pleistocene high terraces and gravels (the Deer Flat Surface). The Whitney terrace is generally covered with fine-grained Bonneville slackwater deposits, which bury a much older soil developed on the Bull Lake-age surface. The lower Boise terrace (of late Pinedale age) is inset in small, sometimes discontinuous, sections from Center Island (58), to the Boise and Owyhee River confluences (Sta 955+40 and Sta 958+90, respectively), and generally increases in width and connectivity in the downstream direction (Othberg and Stanford, 1992). From Sign Island (88) (Sta 1852+70) downstream as far as the Goose Egg Island (33) (Sta 1013+50), Holocene-age alluvium in the overbanks is rare, usually occurring in small pockets as floodplain fragments, attached islands or tributary fans, and the entire channel is entrenched slightly below the level of the Boise Terrace. This upstream section of the MSR is identified as Geomorphic Subreach I in Figure 1.1.

At Goose Egg Island (33), just upstream from the Boise River confluence, significant amounts of Holocene-age alluvium are present, and the river changes both its planform and slope (Figure 3.3). The Boise River delivers coarse bed load to the Snake River, and the Snake River has formed a broad active floodplain. While the slope steepens downstream from the confluence, the planform also changes from a single channel with interspersed island groups to an anastomosing channel planform. Multiple islands occur as both in-channel islands and dissected floodplain remnants.

The entire MSR has limited ability to adjust its slope as the valley is cut into a broad, flat Tertiary basin fill, and the downstream end is fixed by an extensive bedrock-controlled canyon. However, it is only in the middle, anastomosing section, between the Owyhee and Boise Rivers and the Weiser River, that significant coarse sediment has been introduced, and the channel planform has adjusted to transport this material. The Payette and Malheur Rivers (Sta 518+20 and Sta 569+40, respectively) also contribute flow and sediment approximately to the middle reach. The Owyhee, Boise, Weiser, Payette and Malheur Rivers are all dammed. The coarse sediment supplied from these rivers is derived from erosion of the channel banks downstream from the dams. The anastomosing planform is most pronounced just downstream of the Boise and Owyhee River confluences, but anastomosing sections occur as far downstream as the Goat/Patch/Long Island Group (~Sta 312+80) just upstream of the Weiser River confluence. Between the anastomosing reaches are short channel segments that commonly contain islands with forms similar to the upstream reach. Throughout the middle section of the MSR, Tertiary-age basin fill underlies the modern floodplain deposits, which are flanked by Pleistocene-age terraces ranging in age from early Pleistocene (Deer Flat Terrace) to late Pleistocene (Boise Terrace). This middle anastomosing planform section is shown as Geomorphic Subreach II in Figure 1.1. The subreach is subdivided into the highly anastomosing section, Subreach IIA (from the Boise and Owyhee Rivers confluence to just downstream of the large Morton/McPhearson's Island) and the moderately anastomosing Subreach IIB, extending farther downstream to the Weiser River (Sta 276+30).

Downstream of the Weiser River confluence, individual islands and island groups occur, but the Snake River channel no longer has an anastomosing planform. As the river approaches the mountainous region around Farewell Bend, the channel once again becomes entrenched and confined, similar to the extreme upstream reaches of the MSR near Sign Island (88). This is shown on Figure 1.1 as Geomorphic Subreach III. Subreach IIIA extends from the Weiser River to about Jackass Island (5) (~Sta 138+70), and the entrenched section downstream from Jackass Island (5) to Farewell Bend is Subreach IIIB.

3.2. Figures and Tables

Table 3.1 Correlation between stationing used in the hydraulic analysis with river miles (RM) at locations that are identified on USGS 7.5-minute quadrangle maps at significant features along the study reach.

Station (m)	River Mile (RM)*	Feature
0	333.6	Farewell Bend
276+30	351.3	U.S. 30N Bridge, Weiser
287+00	351.9	Weiser River confluence
506+40	365.0	SR 52 Bridge, Payette
518+20	365.7	Payette River confluence
569+40	368.5	Malheur River confluence
596+20	370.0	UPRR Bridge, Ontario OR
622+80	372.0	US 30 Bridge, Ontario OR
644+50	373.7	I-84 Bridge
838+80	385.0	US 20/26 Bridge, Nyssa OR
859+40	390.0	UPRR Bridge, Nyssa OR
953+70	395.4	Boise River confluence
959+20	395.7	Owyhee River confluence
1069+90	399.2	Adrian Bridge
1313+70	416.0	US 95 / SR 19 Bridge, Homedale
1449+80	424.0	Hwy 55 Bridge, Marsing
1751+90	441.9	SR 45 Bridge, Walters Ferry
1838+70	447.3	Guffy RR Bridge (abandoned)
2009+20	457.7	Swan Falls Dam

*Based on USGS 7.5' topographic maps.

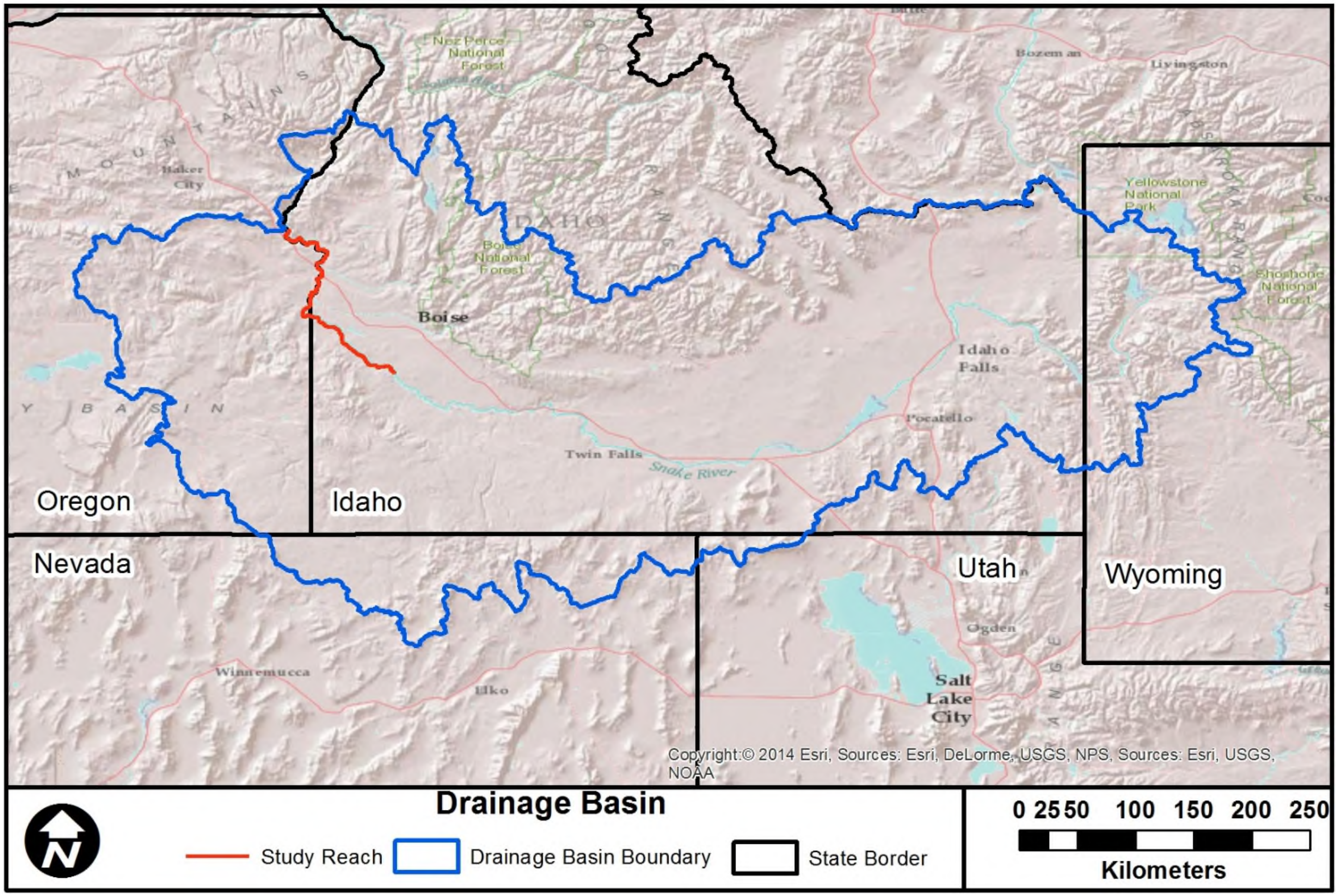

Figure 3.1 Snake River drainage basin from the upstream end of Brownlee Reservoir.

Figure 3.2 Looking downstream at the Melon gravels located above Sign Island (#88, Sta 1852+90), near the upstream end of the MSR.

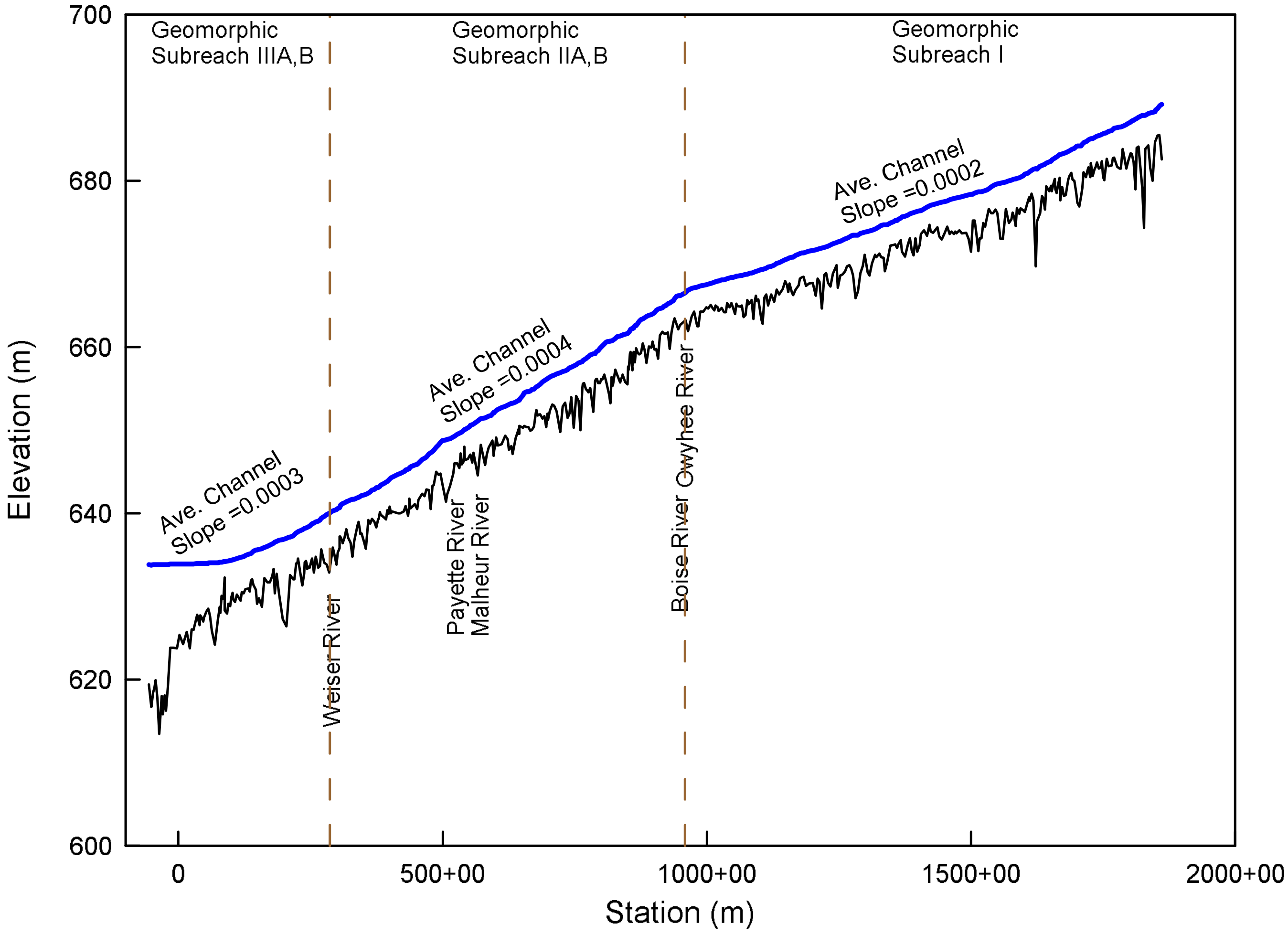

Figure 3.3 Longitudinal profile of the study reach from Brownlee Reservoir (Sta 0) to Sign Island (88, Sta 1852+90).

4. Methods

The study is separated into the following two components:

- Analysis of the island dynamics in the MSR, and
- Detailed 2-D sediment-transport modeling of two selected subreaches.

Each of these components is explained further in the following subsections.

4.1. Island Dynamics

To understand the island dynamics, it is important to understand whether islands are transient (temporal) features that occur in changing locations or whether islands form, erode, and reform at the same (spatial) locations. It is also important to determine how islands can be formed and subsequently altered by erosion and deposition. In addition, understanding the island dynamics requires an understanding of the ages of the islands.

Firstly, a review of historical documents was conducted to show how dynamic the islands have been over the last approximately 100 years. A historical document review was originally conducted by Mussetter and Harvey (2001b), but only included the islands within the DFNWR. The review was redone to include all of the islands within the MSR. The historical documents were compared with recent maps and the differences between the old and new mapping illustrate the erosional and depositional activity of the islands within the last approximately 100 years and provide a preliminary estimate of the age of some of the islands along the study reach. The results of the historical document review were used to answer the question of whether islands are transient (temporal) features that occur in changing locations or whether islands form, erode, and reform at the same (spatial) locations.

Following the historical document review, the results of an evaluation of the controls on the islands (Mussetter and Harvey, 2001b) are reported that show how the locations of the islands are spatially fixed by geomorphic controls.

The island geomorphology was then investigated using a time sequential analysis of early (1938/1939) and 1997 aerial photographs. Measurements of the islands were used to quantify the change in island geometry.

To augment information on island age obtained from analysis of the early aerial photographs and historical mapping, the soil stratigraphy of selected islands in the MSR was examined. The stratigraphic investigation was designed to examine the deposits making up the islands on a variety of morphological surfaces mapped by Othberg and Fosberg (2001). The soil stratigraphy was used to determine the relative soil development of the morphological surfaces, to reconstruct their history where possible, and to determine island age.

To understand how the morphologic changes on various island geomorphic surfaces might have occurred, a hydrologic analysis was performed to characterize the pre- and post-dam hydrology and a 1-D hydraulic model (HEC-2) was run over a range of flows. The 1-D model was developed using topographic and bathymetric data collected for the DFNWR project (Mussetter and Harvey, 2001a, b) and using USGS topographic mapping. The 1-D hydraulic model output used to determine the recurrence interval for post-dam floods capable of overtopping and altering the different geomorphic surfaces. In addition, the output from the 1-D model was used to evaluate the general hydraulic characteristics of the entire reach. In particular, the velocity, water-surface elevation and shear stress data from the HEC-2 model were reviewed to evaluate processes that explain the patterns of erosion and deposition observed in the time sequential aerial photographs.

4.1.1. Available Data

The data used in the analyses of island dynamics include historical and recent aerial photography and mapping, morphostratigraphic mapping, soil profile mapping, topographic survey data and hydrology data.

4.1.1.1. Aerial Photography and Mapping

The aerial photography and mapping includes:

1. Early USGS topographic maps (c. 1894-1906),
2. USGS Water Supply Paper 347 (1914),
3. 1938/1939 aerial photographs,
4. 1997 aerial photography,
5. 2010 USGS topographic maps, and
6. 2012 aerial photography obtained from the ArcGIS [a geographical information systems (GIS) software package].

For each data set, the following procedure was used:

1. The maps and aerial photographs were geo-referenced in ArcGIS on to the Idaho West State-Plane coordinate system.
2. For each map and aerial photograph, the groups of islands were identified and listed:
    - those that could be identified and correlated on both the older sets of maps and on 1997 aerial photography,
    - those that were clearly not shown on the older maps, but existed on the 1997 aerial photography,
    - islands found on the older maps that are not shown on the 1997 aerial photography, and
    - islands whose identification was difficult because of significant differences in shape and location between the two sets of maps.

3. For the 1938/1939 aerial photographs, the Komar (1983, 1984) indices were measured and compared with the 1997 aerial photography to show the changes in islands geometry over the approximately 60-year period.

4.1.1.2. USGS Topographic Maps

The earliest United States Geological Survey (USGS) maps range in age from 1894 to 1906 and all were reprinted in the 1940s. All the maps extend 30 minutes of latitude and longitude, at a scale of 1:125,000. They cover most of the MSR reach from upstream of Sign Island (88) to downstream of the confluence with the Weiser River. The portions of the maps showing the Snake River are provided in Appendix B, and include:

- Weiser, Idaho – Oregon (1897, reprinted 1948)
- Mitchell Butte, Oregon – Idaho (1906, reprinted 1948)
- Nampa, Idaho – Oregon (1898, reprinted 1948)
- Silver City, Idaho (1898, reprinted 1943)

The geo-referencing of the USGS maps showed significant variation compared to recent mapping. Within one 30-minute map, various island locations could be tentatively identified, but when one was matched with the modern island group, other island groups, and even the river itself shifted considerably. This is to be expected considering the available mapping technology when these early maps were produced. The final product was reasonably accurate at the scale to which these were originally produced. A comparison of the between the 1894 to 1906 topographic maps and the 2010 USGS topographic mapping is shown in Appendix B.

4.1.1.3. 1914 Water Supply Paper

A set of maps from U. S. Geological Survey Water Supply Paper (WSP) 347, published in 1914, cover a short length of river near the upstream end of the MSR; the maps extend from

Sign Island (88) at the upstream end to Raccoon Island (66) at the downstream end. Although the mapping is nearly 100 years old, there were sufficient identifiable landmarks to geo-reference the maps and identify the islands, but there appeared to be some distortion and it was not possible to accurately measure the size of the islands. A comparison between 1914 WSP mapping and the 2010 topographic mapping is shown in Appendix C.

4.1.1.4. Aerial Photography from 1938, 1939 and 1943

Aerial photographs taken of the study reach in 1938 and 1939 (with two photographs of the extreme downstream reach taken in 1943) were analyzed to evaluate the presence or absence of islands and to evaluate the changes in geometric characteristics compared to recent aerial photography. For convenience, this data set is referred to as the 1938/1939 aerial photography. The 1938/1939 aerial photos were the earliest available and have continuous coverage over the majority of the study reach. In general, there was a significant amount of overlap of the photos and the islands were georeferenced with reasonable accuracy. The discharge in the river at the time of each photo was estimated using flow records from the nearby gages. A comparison between 1938/1939 aerial photography and the 2010 topographic mapping is shown in Appendix D.

4.1.1.5. Morphostratigraphic Mapping

Morphostratigraphic mapping is a technique used to characterize landform surfaces. A morphostratigraphic unit is an informal stratigraphic term used to designate a body of rock that is identified primarily from the surface form it displays (“rock” usage here is broad and does not imply any degree of induration) (Frye and Willman, 1962). The term “morphostratigraphic unit” has been used synonymously with “geomorphic surface.”

Geomorphically, a morphostratigraphic unit is a surface, either depositional or erosional, that is recognized by its topographic character (Bates and Jackson, 1997). Morphostratigraphic units may employ the descriptive term “surface” instead of a genetic landform term such as “terrace.” Gile et al. (1981), in describing the specialized stratigraphic needs in mapping geomorphology and soils, stated Earth materials genetically related to a constructional phase of a geomorphic surface are often conveniently mapped as a morphostratigraphic unit.

Morphostratigraphic units are not strictly superposed with respect to one another, but we still apply stratigraphic principles in interpreting their relative positions (North American Commission on Stratigraphic Nomenclature, 1983). For example, a sequence of morphostratigraphic units is different from a layered sequence of strata in that the morphostratigraphic unit is defined on the basis of its bounding discontinuities instead of distinctive lithologies. For example, map units with identical lithologies but in different terrace positions can be given separate stratigraphic names. Likewise, island landforms with distinctive geomorphological positions can form a morphostratigraphy.

There are three major reasons for using morphostratigraphic units. First, morphostratigraphic units are records of geomorphic processes and are indispensable for reconstructing events. Second, this stratigraphic approach to the study of landforms allows the geomorphic events to be interpreted historically. Third, the correspondence between soil characteristics and morphostratigraphic units allows interpretation of the ages of the landforms.

Morphostratigraphic units must be placed in a chronology to properly analyze the geomorphic history. The relative ages of landforms typically are determined by topographic position, unit boundaries, surface morphology and physical characteristics, and cross-cutting relations among the morphostratigraphic units. The degree of soil development that takes place on the stable surface of a morphostratigraphic unit is a key indicator of age.

Morphostratigraphic mapping of 194 islands in the MSR was conducted by Othberg and Fosberg (2001), who identified morphostratigraphic units for the different surfaces making up the islands. The morphostratigraphic mapping was georeferenced in ArcGIS for comparison with other data, including aerial photography, topographic mapping and soil pit locations (Figure 4.1). The morphostratigraphic units are based on elevation of the surface, level of soil formation, and vegetation types. Table 4.1 details the morphostratigraphic units delineated by Othberg and Fosberg (2001). The morphostratigraphic units have been numbered from 1 (the highest elevation and oldest, with upland vegetation dominant) to 5 (the lowest elevation, most recently formed, with aquatic vegetation dominant). The level 2 unit was subdivided into 2+ and 2-, representing successively less developed soils.

The morphostratigraphic units range from high elevation surfaces found on island cores to lower elevation surfaces more often associated with berms. Island cores were assigned a morphostratigraphic unit number of 1, 2+, and 2-, indicating successively lower elevations, changing vegetation, and lower levels of soil development.

4.1.1.6. Island Stratigraphy

Ninety five soil pits were excavated on 93 islands in 1999 and 2000 (Mussetter and Harvey, 2001b) (Table 4.2). The islands were selected along the length of the MSR to provide a representative range of soil development and island ages. This included islands thought to be old [Jackass (5), Big Cottonwood (28) and Guffey (86) Islands], islands known to be relatively young (those not present or forming in the 1938/1939 aerial photographs), and many islands whose preliminary age determination was 100 years or less. Islands of various heights, soil types, sizes, and potential ages were chosen at approximately even spacing along the entire MSR reach.

The soil sampling program was overseen by Dr. Maynard Fosberg from the University of Idaho and the following procedures were used. At each island, a pit site was chosen to represent the location on the island thought to contain the oldest deposits based on island elevation and form. The pits were located in the highest core area, if a high core was present, and this was commonly roughly in the center of the island. The pits were located away from areas with large trees to avoid root bioturbation and to facilitate excavation.

Pit depths ranged from about 0.5 to 3.5 m. Each pit was excavated to a depth at which either the gravel/cobble basal platform of the island was encountered, or the water table prevented further digging. After excavation was complete, the pit face oriented to the maximum sun exposure was cleaned and photographed. Stratigraphic and pedogenic layers were identified and the individual layers were then measured (for total thickness and cumulative depth), logged, and described. The soil descriptions included descriptions of the soil horizons, identifying depth, horizon type, texture, color, carbonate content, structure, and boundary characteristics. Primary sedimentary structures, such as trough cross-bedding or horizontal laminations, and any modern artifacts were also identified and logged. Modern artifacts so identified included bottles, cans, shotgun shells, pistons and even a stove.

One large sample was then taken from each stratigraphic layer, starting at the bottom of the pit. A smaller soil sub-sample from each layer was retained for textural analysis and the remaining larger portion of the sample was provided to Paleo Research Laboratories for pollen analysis (Section 4.1.1.7). The bottom-up sampling method helped to avoid modern pollen contamination of lower, potentially older layers. If any layers in the pit contained charcoal fragments or wood, samples were collected for later ^{14}C dating.

After sampling was completed, the pits were refilled and compacted. After completion of the sampling program, the pit locations and elevations were measured using a survey-grade RTK-GPS.

Eleven samples containing datable carbon, carbon-rich sediment, and wood fragments were provided to Beta Analytic, Inc. for standard ^{14}C analysis. After separation, most samples underwent standard radiometric dating, with small samples requiring Accelerated Mass Spectrometry (AMS) dating.

The soil samples provided to Paleo Research Laboratories (PRL) were treated to separate pollen and phytoliths, which were then identified and counted for each separate sample. In total, 1,378 samples were provided to Paleo Research Laboratories, and 11 samples were provided to Beta Analytic, Inc. (Table 4.2).

4.1.1.7. Pollen Data

Pollen and phytolith analyses were conducted to determine the age of the sediments collected from the soil pits. Around the time of European settlement (Idaho became a state in 1890), non-native European crops (such as wheat, corn, and clover) were beginning to be cultivated along the MSR, and well non-native invasive plants such as Russian olive, tamarisk, and purple loosestrife began to occur. Other non-native plants, such as *Plantago lanceolata* (Ribwort Plantain), and *Plantago major* (broadleaf plantain) are associated with early European settlement and were dispersed in small-seeded legume crops (Mack, 1986). The timing of introduction for a selected subset of the non-native plants was investigated by Ms. Juanita Lichtardt of the Idaho Conservation Data Center. She concluded the following:

- Tamarisk was first collected near Weiser in 1938 (Robinson, 1969). By 1965, it occurred from Caldwell to Payette on the Snake River.
- Russian olive was first reported to have escaped from cultivation in Utah in 1924 (Knopf and Olson, 1984).
- White clover was found in South Dakota in 1896, in Kansas in 1893, in Pullman, Washington, in 1907, and in the Blue Mountains of Oregon in 1911.
- Teasel was collected in Walla Walla County, WA in 1896, and in Whitman County, WA in 1902.

- *Plantago lanceolata* was collected in Moscow, ID in 1907, Walla Walla, WA in 1911, and Ada County (Idaho) in 1939. *P. major* was collected in Canyon County (Idaho) in 1910 and in eastern Oregon in 1898.

The processing of the 1,378 soil pit samples conducted by PRL involved the separation of pollen by centrifuge and floatation. This involved a multi-step process of washings with hydrochloric acid and sodium hexametaphosphate, multiple rinses, floatation and centrifuge with sodium polytungstate, and final processing with hydrofluoric acid. This separated the sediment from the pollen and other organic remains, which were mounted on slides for identification at magnifications of 400X to 600X.

After preparation of each sample, the separated pollen and spores were identified to the most specific level possible based on pollen morphology. For many of the pollen grains, this included identification to genus or genus and species level. However, other groups, such as grasses (Family Poaceae) and Mustards (Family Brassicaceae) have pollen that can usually only be identified at the family level. For each sample, the identified pollen spores were placed in the following groupings, determined by an earlier survey of vegetation along the Snake River (Johnson et al., 1992).

- Obligate Wetland (OBL). Plants that occur almost always (>99 percent of the time) under natural conditions in wetlands.
- Facultative Wetland (FACW). Plants that usually occur in wetlands (estimated probability of occurring in wetlands is 67 to 99 percent), but occasionally are found in non-wetlands.
- Facultative (FAC). Plants that are equally likely to occur in wetland or non-wetland environments (estimated probability of occurring in wetlands is 34 to 67 percent).
- Facultative Upland (FACU). Plants that usually occur in non-wetlands (estimated probability of occurring in wetlands only 1 to 33 percent).

- Obligate Upland (UPL). Plants that may occur in wetlands in another region, but occur almost always in non-wetlands (<1 percent probability of being found in wetlands) in the MSR.
- Arboreal Pollen. Pollen known to travel by air, including trees that were not part of the local vegetation described in the Johnson et al. (1992) report.
- Non-Arboreal Pollen. Pollen from herbs and shrubs that are either not listed in the first five categories above, or were not described as local vegetation in the Johnson et al. (1992) report.

In addition to the above pollen types, charcoal abundance, spores, any contaminant pollen, and redeposited pollen were identified. A total pollen count for each stratigraphic horizon continued until 200 to 300 grains were identified (excluding any observed contaminants). When pollen concentration was very low, fewer pollen grains were observed, and the final count was consequently lower.

Contaminant pollen, which may have been accidentally introduced from the modern surface, was identified by relative preservation, with modern pollen having significantly less alteration than older, preserved pollen. In the process of sampling horizons in the soil pits, care was taken in sampling to prevent contamination, including the practice of sampling from the bottom to the top so that very recent surface pollen would not be introduced into lower layers. However, coarse grained (medium to coarse sand, occasionally pea gravel) stratigraphic deposits commonly contained very low pollen concentrations, so modern pollen from the surface could make its way into a coarse-grained layer during the process of excavating the soil pit and cleaning off the surface. If only very small amounts of pollen were originally contained in the layer, and contamination occurred, then these contaminant grains would likely be found during pollen identification. In addition, natural processes (such as the burrowing of earthworms and gophers) can allow more recent pollen to move lower in stratigraphic deposits, creating natural contamination. Identified contaminant pollen was noted if it was found in the pollen count for individual stratigraphic layers, but was obviously not included in any other category (such as introduced pollen) for that layer.

Redeposited pollen (pre-Quaternary) was also identified, especially in the lower sections of some of the upstream islands. This redeposited pollen was identified both by its poor preservation, flattening, differential stain uptake, and also because it could occasionally be identified as originating from plants that are now extinct (plants that grew at least as far back as the Tertiary). Most of this pollen comes from the basin-filling formations discussed in Section 3.1.1, such as the Glenn’s Ferry formation. While moderate amounts of redeposited pollen can be found in the lower layers of the upstream islands, redeposited pollen can also be found at any level in almost any island, since the formations occur throughout the western Snake River plain. Even though Pleistocene-age terraces and Holocene-age floodplain border the Snake River along most of the reach, and Tertiary-age formations only outcrop along the banks on a small percentage of the reach, small tributaries along the reach are eroding into the underlying Tertiary-age deposits. Any discharge that creates further erosion of these deposits introduces ancient pollen into the Snake River, which can later be redeposited on islands.

The pollen record for each island was organized by stratigraphic layers, showing the change in vegetation patterns through time. In addition, any pollen from introduced species was listed separately.

Determination of non-native or introduced species was originally developed from the Johnson et al. (1992) study, which was conducted for the U.S. Fish and Wildlife Service to determine the general effects of potential flow reductions on riparian vegetation in the Snake River reach from Swan Falls to the Idaho-Oregon border. The Johnson et al. (1992) report contains a listing of all plants found along this reach of the Snake River, including relative abundance, habitat (with the categories listed above, OBL, etc.), and whether each plant is native or non-native. The plant list was subsequently modified by Dr. Richard F. Harner of Harner Environmental, Dr. Maynard Fosberg of the University of Idaho, and Ms. Juanita

Lichthardt of Idaho Conservation Data Center, who added more 12 non-native plants. The final listing of non-native plants from the Johnson et al. (1992) is shown in Table 4.3.

An additional 62 species of non-native plants producing pollen were identified in the soil samples by PRL (Table 4.4). This final list is conservative because pollen from many introduced plants has not been counted. For example, of the 37 species of grasses (Family Poaceae) found and listed in the Johnson et al. (1992) report, 18 are non-native. Because identification of grass to species level is problematic, none of this pollen was counted as non-native. This also applies to other high level groups, such as the low-spine and high-spine Asteraceae, and the Cheno-Am groups discussed in the PRL report (Cummings and Moutoux, 2001). All of these groups contributed significant amounts of pollen to the stratigraphic record of the islands analyzed so far, and none of their non-native pollen has been counted as modern. The only family level group that was counted as modern was the Mustards (Brassicaceae). In the original Johnson et al. (1992) report, nine mustard species were identified, and of these seven were non-native. The remaining two were rare, and usually found around bank “seeps”—a location not identified on the islands surveyed. Therefore, the Brassicaceae were placed in the non-native category.

While the presence of non-native pollen in the stratigraphic layers of an island was considered evidence of its recent deposition, other criteria were also applied by PRL to identify those deposits that had been laid down in recent years. The presence of dung fungal spores (Sporormiella) indicated the presence of grazing animals. While herds of elk and deer may also deposit these spores, they are far more common and far more likely to be preserved in the stratigraphic record, when modern livestock are present (Davis, 1987). On several islands, the level of dung fungal spores was so high that PRL identified the island as a potential livestock grazing location.

An additional potential indicator of recent deposition was the charcoal abundance. After processing, the organic remains mounted on the slides for identification included not only pollen and spores, but also charcoal fragments. In general, charcoal abundance is lower (less than about 40-percent abundance) since the onset of fire suppression efforts during modern times. This of course did not apply if fires occurred on or near the islands in spite of suppression efforts, but it is an indirect indicator of post-settlement and recent sedimentary deposits.

4.1.2. Hydrologic Data and Analyses

A hydrologic analysis was performed to evaluate the mean-daily flow (MDF) and flood-frequency characteristics for the pre- and post-dam conditions in each hydrologic subreach and to develop input to the 1- and 2-D models. The results of the MDF and flood-frequency analyses were used with the 1-D hydraulic model output to provide information on the events that create the island morphology. The results of the flood-frequency analysis for the pre- and post-dam hydrology were used to show the effects that the reservoirs have had on peak flows along the study reach.

4.1.2.1. General

To facilitate evaluation of the frequency and duration of discharges, the project reach was subdivided into five hydrologic subreaches (Figure 4.2 and Figure 4.3, Table 4.5), and the available stream gage records (Table 4.6) were used to determine a record of flows for each hydrologic subreach. The subreach boundaries correspond to the major tributaries along the reach at which significant changes in the discharge characteristics in the mainstem occur (i.e., the confluences of the Boise and Owyhee Rivers, which are very close together, the Malheur River, the Payette River, and the Weiser River).

Numerous dams on both the mainstem and major tributaries regulate flow upstream of the study reach. Dam construction began in the early 1900s, and the dams that represent most of the storage were completed by the late 1950s (Figure 4.4). Palisade Dam, completed in

1957, is located upstream of the study reach and was the last major dam constructed. Today, total basin reservoir storage is approximately 13 km^3. This dam and reservoir complex, along with numerous diversion structures, is currently used for irrigation, power, flood control, recreation, and fish and wildlife conservation. There are no dams along the study reach, but most of the major tributaries are regulated, including the Owyhee, Boise, Payette, Owyhee and Malheur Rivers.

The potential effects of these reservoirs on peak flows within the study reach can be illustrated by comparing the frequency estimates for flood peaks recorded before and after the completion of Palisade Reservoir in 1957, the last major reservoir to be constructed in the Snake River Basin upstream of the study reach (Figure 4.5 and Figure 4.6). The development of the flood-frequency curves is described in Section 4.1.2.3. Figure 4.5 shows that floods at the Murphy gage greater than about a 5-year return period are consistently lower for the post-Palisade Reservoir period (1957 through 2012), most probably due to the effects of the reservoirs. At the Weiser gage, the reservoir effects are more pronounced, with all floods with the exception of three or four floods near the 10-year return period being lower for the post-Palisade period (Figure 4.6).

Figure 4.7 and Figure 4.8 show the recorded peak flows at the Snake River near Murphy and Snake River at Weiser stream gages, the two stream gages with long-term flow records for the MSR (Table 4.6). The Murphy gage is located near the upstream end of the study reach and the Weiser gage is located near the downstream end (Figure 4.3). Included on Figure 4.7 is the approximate 1894 peak flow at the location of the Murphy gage based on a previous estimate for the reach between Milner Dam and King Hill (Idaho Water Resource Board, 1993). This location is about 145 kilometers upstream of the Murphy gage, and there are no large tributaries in the intervening reach. The figures show that moderately large floods have occurred throughout the period of record, with particularly large floods near the turn of the 20^{th} century (the estimated 1894 flood at the Murphy gage and the recorded 1910 flood at the Weiser gage).

The flow record for the Murphy gage (1914 through 2012) includes four annual peaks that exceed 1,100 m^3/s (1914, 1918, 1921, and 1997). The flow record at the Weiser gage (1910 through 2012) includes four flows that equaled or exceeded 2,000 m^3/s in the pre-dam period (1910, 1912, 1921 and 1952) and five flows that equaled or exceeded 2,000 m^3/s in the post-dam period (1965, 1984, 1986, 1997 and 1998).

4.1.2.2. Mean Daily Flow Analysis

The development and erosion of the islands is a product of the flows that have occurred in the river over the past several years to decades, among other factors. A mean-daily flow analysis was conducted to develop mean daily flow estimates which were used to illustrate the changes in duration between the pre- and post-dam conditions and, in part, to develop the annual peak flow estimates.

To facilitate the analysis, mean daily flow-duration curves were developed for each hydrologic subreach (Figure 4.9). Because of the potential impact of upstream storage projects on the flow characteristics of the river, only the period after construction of Palisade Reservoir (1957-2012), which was the last major storage project to be completed, was included in the analysis. The flow-duration curves were developed from a combination of published flow records (Table 4.6) where available, and estimates of flows where data were not available. A detailed description of the methods and assumptions that were used to develop each flow-duration curve follows:

Subreach H1 (Swan Falls Dam to Owyhee/Boise River confluence): The flow-duration curve for Subreach H1 was developed from the recorded flows at the Snake River near Murphy gage (USGS Gage Number 13172500, Figure 4.3). This curve was applied to the entire subreach because the tributaries that enter this subreach are relatively small, drain generally dry, low-elevation terrain west of the river, and therefore do not contribute significantly to the total flow in the river. The largest tributary is Succor Creek, which drains about 1,280 km^2, or about one-third of the total contributing area between the Murphy gage and the Boise River and Owyhee River confluences. Flow records are available in Succor Creek for the period 1989 through 1992. During this period, the average flow in Succor Creek was about 1.2 m^3/s, which is only about 0.6 percent of the recorded flow at the Murphy gage during the same period.

Subreach H2 (Owyhee/Boise River confluence to Malheur River confluence): The flow-duration curve for Subreach H2 was developed from a combination of recorded flows at the Snake River at Nyssa gage (USGS Gage No. 13213100) for the periods for which data were available (1975 through 1986, 1989 through 2012), and estimated flows for the periods 1957 through 1974, 1987, and 1988, for which data were not available at the Nyssa gage.

The missing data at the Nyssa gage were estimated using the Maintenance of Variance Extension (MOVE.1) technique (Maidment, 1992). This technique involves development of a relationship between the observed flows in the reach that has missing data (i.e., the "short-record station") and a hydrologically similar reach for a concurrent time-period (i.e., the "base station"), and then use of that relationship to estimate the missing flows at the short-record station. The principle of the MOVE.1 technique is to derive a set of coefficients for the relationship that transforms the base station data to estimates of the missing data at the short-record station in such a way that the mean and variance of the population are preserved. (This differs from the more commonly applied linear regression technique, which preserves the mean but does not necessarily preserve the variance.) In applying the technique, it is common to use the log-transform of the basic data to provide a more linear relationship that has more constant variance over the range of the data than occurs with the untransformed data.

In applying the technique, Subreach H3 (described in the following section) was used as the base station, and the MOVE.1 relationship was developed based on the logarithms of the data (Figure 4.10). The estimated flows in Subreach H3 were used as the base station because they showed the least scatter of any of the other possible choices, which included recorded flows at the Murphy gage, recorded flows at the Weiser gage, or estimated flows in Subreach H4.

Subreach H3: Flows in this subreach were estimated by subtracting recorded mean-daily flows in the Weiser River (USGS Gage No. 13266000) and the Payette River (USGS Gage No. 13251000) from the corresponding mean-daily flows in the Snake River at Weiser (USGS Gage No. 13269000). Based on examination of recorded hydrographs at the Weiser and Nyssa gages, the travel time in the reach is less than one day, which indicated that lagging the hydrographs was not necessary.

Subreach H4: Flows in this subreach were estimated by subtracting recorded mean-daily flows for the Weiser River (USGS Gage No. 13266000) from the corresponding mean-daily flows from the Snake River at Weiser (USGS Gage No. 13269000).

Subreach H5: The Snake River at Weiser gage (USGS Gage No. 13269000) was used to represent the flows in this subreach.

The resulting flow-duration curves (Figure 4.11) show that flows increase in the downstream direction, as would be expected based on the tributary inflows, for exceedence probabilities greater than about the 90 percent exceedence flows. This relationship does not hold at lower flows, particularly in Subreaches H3 and H4. The reason for the change is not known, but could either be an indication of flow loss in the downstream direction due to diversions, seepage, and evapotranspiration under these conditions, or could be due to uncertainty in the data in this range of flows. In either case, the change does not affect the conclusions that are drawn from this study because the formation of the islands is primarily controlled by the higher flows. A summary of the mean annual discharge, as well as the median (50 percent), 10-, 5-, 2- and 1-percent exceedence discharges, is shown in Figure 4.11.

A comparison of the pre- and post-dam mean-daily flow curves developed from the Murphy and Weiser flow records shows contrasting changes for the low-flow conditions. At the Murphy gage (Hydrology Subreach H1), the 90-percent exceedence is higher under pre-dam condition (202 m^3/s) compared to post-dam conditions (178 m^3/s) (Figure 4.11); whereas, at the Weiser gage, the 90-percent exceedence is lower under pre-dam conditions (238 m^3/s) compared to post-dam conditions (268 m^3/s) (Figure 4.11). The decrease in baseflows at the Murphy gage is due to the dam and the increase in base flow at the Weiser gage is likely due to irrigation return flows.

4.1.2.3. Flood Frequency Analysis

Estimates of the magnitude and frequency of floods in each of the hydrologic subreaches were developed from a combination of published flow records (Table 4.6), where available, and estimates of the annual peak flows where data were not available.

The annual peak flow estimates for the locations and times where data were not available were derived from the mean daily flow estimates, which were discussed in the previous section. The mean daily flow estimates were utilized in making the annual peak flow estimates because it is not possible to make the estimates directly from the recorded peak flows at different locations. This is due to the following:

- Peak flows from tributaries for the same event will not in general coincide in time with peak flows on the mainstem,
- The combination of inflow from tributaries may result in annual peak flows occurring for different events at different points through the system, and
- Peak flows translate and attenuate along the river.

The following basic procedure describes how the mean daily flow estimates were used to develop the annual peak flow estimates:

1. The annual maximum mean daily flow and the corresponding date were determined using the mean daily flow estimates.

2. If the date of the annual maximum mean daily flow was within two days of the date of the recorded annual peak flow at the Weiser gage, the annual maximum mean daily flow was multiplied by the ratio of the recorded annual peak to the corresponding recorded mean daily flow at the Weiser gage. The ratios varied from 1.01 to 1.18, with an average of 1.04.
3. If the date of the annual maximum mean daily flow was not within two days of the date of the recorded annual peak flow at the Weiser gage, the annual maximum mean daily flow was multiplied by 1.04, the average ratio of recorded annual peak to corresponding mean daily flow at the Weiser gage.

Table 4.7 summarizes the data used to develop the peak flow estimates for each of the hydrologic subreaches. The estimates were developed for the post-Palisade Reservoir period, 1957 through 2012.

Flood-frequency curves were developed for each hydrologic subreach by plotting the individual annual peaks on a log-probability scale using the Weibull plotting position and connecting the points with a straight line. The points were not fit to theoretical probability distributions such as a Log-Pierson type III distribution, as is common in flood-frequency analyses, because regulation by upstream reservoirs cause a poor fit to the distributions. The resulting curves, shown in Figure 4.12, indicate show that the 2-year event varies from about 644 m^3/s in Subreach H1 to about 1,158 m^3/s in Subreach H5, the 10-year event varies from about 962 to 1,993 m^3/s, and the maximum flow during the 57-year, 1957 through 2012, varies from 1,141 to 2,381 m^3/s.

4.1.3. Hydrographic and Topographic Surveys

Topographic data for the study were derived from several sources, with the primary source being a set of contour maps and digital terrain models (DTMs) of the riverbed and near-overbank areas that were developed by Ayres Associates (Ayres). The overbank topography covers an area that extends approximately 100 m from the top of the riverbank on each side of the river for the entire project reach from near the upstream end of Brownlee Reservoir (Sta 7+00) to just upstream from Sign Island (Sta 1883+70). This topography was developed using photogrammetric methods, with aerial photographs of most of the reach taken during May 1997, and additional photographs of the middle portions of the reach taken in November 1998 and April 1999. The topography for the below-water portions of the river between Sta 1+50 and Sta 1066+80 was developed from bathymetric surveys that were conducted by Ayres Associates in June 1997 and April 1999 using a sonic depth sounder linked to a survey-grade, real-time kinematic GPS. Additional bathymetry in the vicinity of Adrian, Oregon and between the mouth of Reynolds Creek and the Highway 45 Bridge at Walters Ferry, Idaho was developed from surveys conducted by Ralston and Associates in October 1998. Other data sources included river cross sections that were surveyed by the U.S. Geological Survey in the portions of the project reach upstream from the Boise River confluence (Kjelstrom, 1992). A schematic showing the portions of the project reach that are covered by each of the data sources is presented in Figure 4.13.

Additional topographic survey data were collected along the project reach to accurately locate the horizontal position and elevation of the soil pits, top of the islands and sediment samples, to measure water-surface elevations for the purpose of hydraulic model calibration, to obtain additional channel bathymetry to supplement the existing bathymetry, and to better define the topography of certain islands. These surveys were conducted using a differentially corrected, real-time kinematic Global Position System (RTK-GPS).

All the surveys were tied to survey bench marks that were established by Ayres Associates in 1997. The ground-control surveys were conducted using methods that conform to or exceed horizontal Class 2, vertical Class 3 survey standards, and criteria specified in the "Geodetic Accuracy Standards and Accuracy Specifications for using GPS Relative Positioning Techniques" (Federal Geodetic Control Subcommittee, 1998).

4.1.4. One-Dimensional Hydraulic Model Development

An existing 1-D hydraulic model (Mussetter and Harvey, 2001a) of the MSR from Brownlee Reservoir to just upstream of Sign Island was used to determine water-surface elevations over a range of flows (Table 4.8).

Output from the hydraulic models was used to determine the magnitude of flows required to overtop the islands and other identified geomorphic features. This analysis was conducted as part of the Mussetter and Harvey (2001b) study, but was updated for this study using the more recent hydrologic data. The flood-frequency curves and flow-duration curves developed from the post-Palisades Reservoir data (Section 4.1.2) were used in conjunction with the overtopping discharges to determine the frequency and duration of the overtopping discharge for islands. The output of the hydraulic models was used to develop a preliminary model regarding the formation of the islands (Mussetter and Harvey, 2001b).

4.1.4.1. General Modeling Approach

The hydraulic analysis was conducted using the U.S. Army Corps of Engineers (USACE) HEC-2 step-backwater computer program (USACE, 1990). HEC-2 is a 1-D gradually varied flow model that uses standard-step backwater procedures along with user-defined input values describing the channel topography, roughness and energy-loss characteristics to compute water-surface profiles and associated hydraulic conditions for specific, steady-state discharges. HEC-RAS is now the most commonly used 1-D hydraulic model and has replaced the older HEC-2 model, which was widely used in the engineering community to develop water-surface profiles and analyze hydraulic conditions in rivers. At the time of the model development, HEC-RAS did not contain the split flow routines required to properly model the multiple split flow conditions. The computational procedures in both HEC-RAS and HEC-2 are essentially the same; therefore, the HEC-2 model of the study reach has not been updated to HEC-RAS.

To model the multiple flows paths in HEC-2, separate hydraulic models were set up for each well-defined flow path. Figure 4.14 shows as an example the cross-section spacing and alignments applied to the HEC-2 model to represent three split flow paths in the vicinity of Nadeau and Buttermilk Islands. For each steady-state discharge profile that was analyzed, the amount of the total discharge in the river in each flow path was determined by balancing the computed elevation of the energy-grade line at the upstream end of each branch. Because of the many branches considered in the analysis, an automatic procedure for performing the energy balance was developed.

Three hydraulic models were developed to represent the lower, middle and upper subreaches (Figure 4.2):

1. The **Lower Reach** extends from just below Farewell Bend near the upstream end of Brownlee Reservoir (Sta -61+00) (Note: the station line was extended downstream from the origin, Sta0+00, to incorporate the upstream end of Brownlee Reservoir) to Ontario, Oregon (Sta 644+50), a river distance of about 70.5 kilometers. In portions of the lower reach, the model indicated that limited areas in the overbanks that extend beyond the limits of the detailed contour mapping were subject to inundation at high flows. To ensure that these areas were properly considered in the model, the affected cross sections were extended beyond the limits of the DTMs using the USGS 7.5-minute quadrangle maps.
2. The **Middle Reach** extends from Ontario, Oregon (Sta 644+50) to the confluence with the Boise River (Sta 956+60), a river distance of about 31 kilometers. Cross-sectional data for this reach were taken from the DTM, and supplemented with overbank topography from the USGS 7.5-minute quadrangle maps, where necessary. As discussed above, the DTM for this reach was developed using aerial photography and bathymetry that were taken in May 1997, November 1998, and April 1999.

3. The **Upper Reach** extends from the Boise River confluence (Sta 644+50) to just upstream of Sign Island (Sta 2006+00), a distance of about 105 kilometers. Topographic data sources for this reach include the 1999 topographic mapping (above and below water) that covers the portion of this reach downstream from Sta 1105+10 (see discussion above for the Middle Reach), the 1997 overbank topography that extends from Sta 1186+80 (the Idaho/Oregon border) to Sta 1883+30, and the USGS cross sections from Kjelstrom (1992) of the portion of the reach from the Owyhee River confluence to the upstream end of the study reach.

In general, the cross-section spacing within the models was approximately one channel width apart. Additional cross sections were incorporated into the model in topographically complex areas such as around islands and bridges. In the Lower model, there are 221 cross sections along the main channel (does not include the cross sections along the split-flow channels) at an average spacing of 320 m, The Middle model has 101 cross sections along the main channel at an average spacing of 298 m. The Upper model has 263 cross sections along the main channel at an average spacing of 346 m.

Geometric data for bridges within the project reach were obtained from a variety of sources including the Idaho Transportation Department (ITD), the Union Pacific Railroad (UPRR), the Oregon State Highway Department, the Malheur County (Oregon) Road Department, Ascott Farms (private owner of one of the bridges), photographs, and topographic mapping. A total of 20 bridges were incorporated into the model. Because the low chord of the bridges are generally above the highest modeled flows, all the bridges were modeled using the HEC-2 Normal Bridge Routine. The Normal Bridge routine is based on standard-step backwater calculations, which are generally the most appropriate way of determining energy losses for low-flow situations when friction and expansion/contraction losses dominate. In addition to the complexities caused by well-defined multiple flow paths, flow conditions in the overbank areas are very complex due to the presence of low areas that are not connected to the main channel. Some of these low areas are depressions such as old meander scars, and others are low areas separated from the main channel by berms or levees. Encroachments were employed to ensure that the low areas not connected to the main channel would not flow until the intervening high ground (in some cases berms or levees) was overtopped.

4.1.4.2. Channel Roughness and Energy Loss Coefficients

The roughness and energy loss characteristics of the river channel and overbanks are accounted for in HEC-2 through the use of Manning's *n* roughness coefficients and expansion and contraction losses. Main-channel Manning’s *n* coefficients were initially selected using standard references (Chow, 1959; Barnes, 1967), but were refined during model calibration (see Section 4.1.4.4). Manning’s *n* coefficients for the overbanks were selected to reflect roughness conditions in the overbanks and ranged from 0.065 for areas with sparse upland vegetation to 0.12 for areas with dense riparian vegetation.

4.1.4.3. Downstream Boundary Condition

The model requires a water-surface elevation to be specified at the downstream boundary for each discharge being modeled. The starting water-surface elevation for the downstream model reach depends on pool elevations in Brownlee Reservoir, which, in turn, depend on the operation of the reservoir, as well as the discharge in the river. When the pool elevations are relatively high, a backwater condition is created that causes water-surface elevations in the downstream portion of the project reach to be higher than they would be in the absence of the reservoir. This affects the duration at which the water-surface is at any given elevation for those islands located within the backwater area of Brownlee Reservoir.

An analysis of the range and duration of the reservoir stages was conducted to assist in selecting reasonable starting water-surface elevations for the hydraulic model. The analysis was conducted using the recorded daily reservoir stages (i.e., water-surface elevations) at Brownlee Dam, which is located approximately 76 kilometers downstream from Farewell Bend, for the period October 1958 to September 1998. The reservoir stage data were obtained from Idaho Power Company (IPC).

A stage duration curve of the data that indicates the reservoir water-surface elevations varied over a range of about 31 m, from approximately 603.2 m to approximately 634.7 m (Figure 4.15). The median reservoir stage during the period was 631.6 m, and exceeded 633.6 m about 10 percent of the time and exceeded 631.6 m approximately 50 percent of the time. A scatter plot of the daily reservoir stages versus the corresponding discharge in the Snake River at Weiser indicates that reservoir stages varied over a wide range for any given range of discharges in the upstream river; thus, a single-valued relationship between the two is not present (Figure 4.16).

The reservoir stages plotted in Figure 4.15 and Figure 4.16 represent the water-surface elevation at Brownlee Dam. The water-surface elevation at the downstream boundary of the project reach at Farewell Bend is higher than the reservoir stage at the dam due to energy losses in the intervening approximately 76-kilometer reach of the reservoir. To evaluate the magnitude of the increase, a separate HEC-2 model was developed for the reservoir. Cross sections used in the reservoir model were derived from 1996-1998 bathymetric data provided by IPC.

A sensitivity analysis was performed to evaluate the effect of the Brownlee Reservoir water-surface elevations on the water-surface profiles in the downstream portion of the project reach. A river discharge of 1,322.4 m^3/s and water-surface elevations at Brownlee Dam ranging from 602.3 to 633.7 m were used in the evaluation. The analysis indicates that when the water-surface elevation at the dam is less than 631.6 m (corresponds to 50-percent exceedence), the large riffle that is located just upstream from Rapids Island (Sta 88+40) is not drowned out by backwater from the reservoir, and the upstream water-surface profile is not affected by the reservoir. At the highest recorded reservoir elevation (634.7 m), the backwater causes an increase in water-surface elevation of about 1.4 m compared to the elevations with no backwater effect at the riffle, and minor effects of greater than 3 centimeters extend upstream to approximately Sta 225+60 in the vicinity of the Aulbach Island group. Approximately 17 islands fall within backwater-affected reach between Whitehill and Aulbach No. 3 (7).

The starting water-surface elevations for the 1-D models were set at the 10-percent exceedence water-surface elevation, which corresponds to an elevation of 633.6 m.

4.1.4.4. Model Calibration

The HEC-2 models were calibrated by adjusting main-channel Manning's *n* roughness coefficients within a physically reasonable range to match, to the extent possible, available water-surface elevation data. These data include water-surface elevations that were measured during the various surveys (Table 4.9) and USGS rating curves at the Snake River at Weiser and Snake River at Nyssa stream gages.

Water-surface elevation data were available for discharges ranging from 317.1 to 1,682 m^3/s in the reach downstream from I-84 near Ontario, Oregon; from 291.7 to 934.5 m^3/s in the middle reach between the Boise River and I-84; and from 205.3 to 478.6 m^3/s in the reach upstream from the Boise River (Table 4.10). In general, the data are well distributed throughout the lower and middle reaches. In the upstream reach, the data were more limited, particularly for high flows.

The Snake River at Weiser gage is located in the Lower reach and the rating curve (Figure 4.17) shows that the computed water-surface elevations fall 0.07 to 0.3 m below the rating curve when the curve is plotted using the published gage datum of 637.0 m (NAVD88). Comparison of water-surface elevations in the vicinity of the gage that were measured during the field surveys suggests that the published datum for the gage is approximately 0.24 m too high. When the rating curve is adjusted for this difference, the computed water-surface elevations match the curve very well (see dashed line in Figure 4.17). The calibration of the downstream reach was achieved using main-channel Manning's *n*-values, which ranged from 0.025 to 0.035, and were held constant for the range of modeled discharge. SRH-2D does not have the ability to adjust Manning's n-values over the duration of a hydrograph.

An example of the calibration profile for the downstream section of the Lower model is shown in Figure 4.18 and a summary of the deviation of the computed water-surface elevations from the measured water-surface elevations at each of the data points is shown in Table 4.10.

In the reach downstream from I-84, the mean difference between the computed and observed water-surface elevations for the Ayres (1997) data set, which was collected at discharges in the river ranging from 934.5 to 1,682.0 m^3/s, is essentially zero, with a standard deviation of 0.08 m (i.e., about 2/3 of the points fell within 0.08 m of the observed value), and a maximum deviation of 0.25 m.

In the middle reach, the average deviation between the computed and observed water-surface elevations for the two most extensive data sets varies from –0.04 m at discharges between 291.7 and 331.3 m^3/s to 0.04 m at discharges between 574.8 and 784.4 m^3/s.

The rating curve for the Snake River at Nyssa gage was also used in the calibration of the middle reach (Figure 4.19). The published vertical datum for the gage appeared to be approximately 3.7 m different from the measured water-surface elevations in the area. As a result, a datum was computed for the curve by comparing stage readings from the USGS gage data with the surveyed water-surface elevations. The resulting curve shows excellent agreement for discharges above 283 m^3/s (10,000 cfs). To achieve the indicated calibration for this reach, it was necessary to reduce the main-channel Manning's *n* with increasing discharge for discharges between 283 and 566 m^3/s (10,000 and 20,000 cfs). The best calibration was achieved with a 10-percent reduction over this range of discharges. A constant *n*-value was used for discharges above 566 m^3/s. Main-channel *n*-values for the lower flows ranged from 0.025 to 0.04, and from 0.022 to 0.036 for the highest flows.

As previously discussed, the available calibration data for the reach upstream from the Boise River are more limited; the water-surface elevations were collected at discharges ranging from 205.3 to 291.7 m^3/s. The agreement between the observed and computed water-surface elevations is very good, with mean deviations of less than 0.02 m, and standard deviations of 0.15 m or less. Main channel Manning's *n*-values used in the upstream reach varied from 0.025 to 0.035, and were not varied with discharge.

4.2. Two-dimensional Hydraulic Model Development

Two-dimensional sediment-transport models of two subreaches were developed to simulate the processes of island formation and evaluate the role of the islands in regulating sediment flux through the reach.

4.2.1. Site Selection

The two study reaches were selected based on the results of the historical photo and map analysis (Section 5.1).

4.2.1.1. Walters Ferry

The Walters Ferry subreach was selected because it contains the longest island chain in the MSR, with 10 islands along the 5.2-km subreach (Figure 4.20). It is located in Geomorphic Subreach I and extends from approximately 750 m downstream of Reynolds Creek Fan to the Walters Ferry Bridge (Sta 1699+00 to Sta 1751+00).

The Walters Ferry subreach is confined along the right side from the downstream end of the reach (Sta 1699+00) to approximately Argy Island (Sta 1717+50) by a steep slope formed at the base of basalt rim-rock which is elevated approximately 150 m above the river (Figure 4.20). From Argy Island to the upstream end of the reach, the right bank is confined by an approximately 25-meter-high terrace composed of Glenns Ferry Formation sediments deposited during the Bonneville Flood. The left side of the channel is mostly confined by a terrace with a representative elevation of about 7.5 m above the channel. The left bank determines the channel capacity of the subreach, which is approximately 2,265 m^3/s (80,000 cfs). The high elevation surfaces on both sides effectively create an entrenched channel, which has likely retained the same channel alignment since the Bonneville Flood. The highest recorded peak flow at the Murphy Gage was 1,340 m^3/s in 1918, but a flood in 1894 was estimated to have a peak discharge of 2,265 m^3/s (Idaho Water Resource Board, 1993).

The channel width along the subreach ranges from a minimum of approximately 120 m near the downstream end below Reynolds Creek (Sta 1707+00) to a maximum of approximately 380 m in the vicinity of Bayha Island; the representative reach width is 300 m.

The Reynolds Creek fan creates a significant contraction and there are five islands (Wright, Bayha, Becky Argy and Papike) located upstream of the contraction (Figure 4.20). Another channel contraction located approximately midway along the subreach (Sta 1730+00) was formed by two opposing unnamed tributaries. The Brooks Group of Islands has formed just upstream of the contraction. The Blind Group of islands formed in the channel expansion just downstream of the Walters Ferry Bridge.

Seven bed-material samples and 14 soil samples were collected along the subreach (Figure 4.21). The seven bed material samples were collected in 1997 and the median bed material sizes (D_{50}) ranges from 16 to 33 mm (Figure 4.22). A representative bed-material gradation was developed based on the 7 samples and it has a D_{50} of 23mm and a D_{84} of 33 mm (Figure 4.22).

Soil sampling of Blind and Papike Islands indicates that the islands are composed of silt to sand-sized material, with the median (D_{50}) sizes ranging from 0.07 to 0.28 mm (Figure 4.23) and the D_{84} ranging from 0.2 to 0.3 mm.

The morphostratigraphic mapping of the Walters Ferry reach (Figure 4.24 and Figure 4.25) shows that the upper surfaces of the higher and generally older islands, which include Bayha (74), Argy (75), Becky (76), Papike (77), 78.3 and Blind (79.1), have morphostratigraphic values of 2- and 2+, whereas the lower and younger islands, which include Wright (73), Brooks Group (78.1 and 78.2) and 79.2 in the Blind Group, have a morphostratigraphic value of 3 (Table 4.11).

4.2.1.2. Ketchup Island Study Reach

The Ketchup Island subreach is located in Geomorphic Subreach III and extends from Sta 405+00 to Sta 465+00, a distance of approximately 6 km (Figure 4.26). The subreach was selected because historical photo analysis and morphostratigraphic mapping indicated that Annear Island appeared relatively young in 1938/1939 aerial photographs and that Oglesbee Island was not present; therefore, the presence of relatively young islands indicated this reach would be appropriate for simulating the processes of island development.

The Ketchup Island study reach has a floodplain along the right bank, which has a representative height of approximately 5.5 m above the channel bed. The right bank determines the channel capacity of the subreach, which is approximately 2,832 m^3/s (100,000 cfs).

The eastern (right) side of the study reach is bounded by a railway track that was constructed c1900 and the crest of the railway embankment is elevated approximately 2 m above the floodplain. The western boundary of the subreach from the downstream end to approximately Sta 450+00 is confined by a terrace, which is approximately 13 m higher than channel bed. Along the west bank from between Sta 45,000 and the upstream end of the model, the terrace recedes to the west and there is a short floodplain segment between the terrace and the river.

There are four islands located in the study reach: Ketchup, Annear, Oglesbee Islands and an unnamed island (Figure 4.26). Ketchup Island formed downstream from a channel expansion (Sta 442+00) and Annear Island formed on the downstream side of Ketchup Island. The morphostratigraphic mapping of Ketchup and Annear Islands shows that the upper surfaces of the islands are 2+ and 2-, respectively (Figure 4.1).

The Ketchup Island subreach ranges in channel width from a minimum of approximately 170 m near the upstream end (Sta 450+00) to a maximum of approximately 390 m at Ketchup Island, with a representative reach width of 230 m.

A single surface bed-material sample was collected at the head of Ketchup Island in 1997. The median size (D_{50}) of the gradation is 54 mm and the D_{84} is 78 mm (Figure 4.27). Soil samples were collected at six locations on Ketchup Island and the D_{50} ranges from 0.04 to 0.15 mm and the D_{84} ranges from 0.14 to 0.28 mm (Figure 4.28).

4.2.2. Model Selection

Several hydraulic models were evaluated to determine an appropriate model for simulating the processes of island formation and maintenance and to evaluate the hydraulic and sediment-transport characteristics of the two subreaches.

One-, two- and three-dimensional models were evaluated and the benefits and limitations of these models are summarized in Table 4.12. A 1-D model (e.g., HEC-2 and HEC-RAS) is developed using cross sections, the flow is assumed to be perpendicular to the cross section, and the main-channel and overbank velocities are averaged across each portion of the cross sections. A 1-D model cannot simulate secondary currents, transverse movement, transverse variation or lateral diffusion, and therefore, a 1-D model cannot simulate such phenomena as island development, river meandering, point bar formation, pool-riffle formation, and many plan form changes. A 1-D model has the advantage that both the modeled reach and simulation times can be very long (Table 4.12).

A 2-D model computes both the magnitude and the direction of the flow at each point within the model grid, and therefore, flow separation, eddy patterns, lateral velocity variation and circulation and bed shear stresses can be evaluated. The hydrodynamic output from the 2-D model can be coupled with sediment-transport equations to predict the bed-load and suspended sediment load at each node in the model. The 2-D model is simulated with both time-varying discharge and sediment hydrographs, and the models can predict both localized areas of sediment aggradation and degradation.

A 3-D hydraulic model can simulate flow velocity variations in three directions (x, y, z). Such models are typically used to simulate complex hydrodynamic conditions such as detailed flow characteristics around hydraulic structures and reservoir and lake stratification. Typically, 3-D models are significantly more detailed and the reach lengths are smaller compared with 2-D models, they require a greater amount of input data, they produce a greater amount of output and they require a lot of computer power.

Based on the review of the 1-, 2- and 3-D models, it was determined that a 2-D model would provide the best compromise between the ability to simulate the processes of island development and computational run time.

Three 2-D sediment-transport models were evaluated: SRH-2D, CCHE2D and MD_SWMS. Each of these models is publically available and contains bed-load and suspended sediment-transport equations with the ability to simulate deposition and erosion processes. Some key features of these models are listed in Table 4.13.

In general, each of these models computes scour and deposition in rivers and reservoirs by simulating the interaction between sediment transport and the hydraulics of the flow. The models simulate vertical changes in bed elevations and changes in the surface bed material gradation. In general, the models simulate bed elevation changes by estimating the bed-material transport capacity at each element based on the flow hydraulics and bed-material characteristics, comparing the estimated capacity with the upstream sediment supply, and adjusting the bed elevations to account for the differences between the sediment supply and the transport capacity (i.e., the net addition or loss of sediment to the element). Each of these models routes the sediment through the reach by size-fraction; thus, model output reflects changes in the bed-material gradation that result from differences between the supply and transport capacity of the individual size fractions.

The CCHE2D model was developed by the National Center for Computation Hydroscience and Engineering (NCCHE) at the University of Mississippi in Oxford, Mississippi (NCCHE, 2006). CCHE2D is a 2-D finite volume, unsteady, flow and sediment-transport model (Table 4.13).

The MD_SWMS program was developed by the U.S. Geological Society (McDonald et al., 2006). The MD_SWMS program is a finite element model. Both the CCHE2D and MD_SWMS programs use a curvilinear grid. An example of the CCHE2D mesh for the Walters Ferry Reach is shown in Figure 4.29.

The SRH-2D Version 3 beta program was developed by the Bureau of Reclamation and the mesh for SRH-2D was developed with Version 10.1 of the Aquaveo Surface Water Modeling System (SMS) graphical user interface (Aquaveo, 2010). SRH-2D is a finite-volume, hydrodynamic model that computes water-surface elevations and horizontal velocity components for sub-, super-, and trans-critical, free-surface flow in 2-D flow fields. SRH-2D uses a flexible mesh composed of triangular and trapezoidal elements, which allows the resolution of the computational elements to vary throughout the model domain. This provides a significant advantage over models with a structured mesh (i.e., the orthogonal mesh used by CCHE2D and MD_SWMS) because the density of the computational points can be increased in areas with large topographic variability and areas of special interest, while a lower resolution can be used in other areas to maintain reasonable model size and computational efficiency.

SRH-2D computes scour and deposition by simulating the interaction between sediment transport and the hydraulics of the flow. The model simulates both vertical changes in bed elevations and the associated changes in surface bed-material gradation. In general, the bed elevation changes are simulated by estimating the bed-material transport capacity in each element based on the flow hydraulics and bed-material characteristics, comparing the estimated capacity with the sediment supply from adjacent elements, and adjusting the bed elevations to account for the differences between the supply and the transport capacity (i.e., the net addition or loss of sediment to the area within the element). SRH-2D routes the sediment through the reach by size-fraction; thus, model results reflect changes in the bed-material gradation that result from differences between the supply and transport capacity of the individual size fractions. This capability allows the model to simulate fining and coarsening of the bed surface in response to changes in hydraulic conditions and upstream sediment loads. SRH-2D contains an unsteady total load algorithm that automatically partitions "suspended load, bed load or mixed load depending on the transport model parameter of local flow hydraulic" (p1142) (Greinmann et al., 2008), A full description of the sediment-transport calculations is presented in Greinmann et al. (2008).

The CCHE2D, MD_SWMS and SRH-2D programs were evaluated by developing models of the Walters Ferry subreach for the baseline and without-islands conditions and comparing the ability of the model to simulate island development. A more detailed description of the model development for the final selected model is provided in Section 4.2.3, but for the purposes of model selection, the following is a brief description of the model development.

A baseline model was developed to represent the 1997 topography and was calibrated to measured water-surface elevations. A "without-island" conditions model was developed by removing the islands from the baseline model down to the elevation of the gravel core. The "without-island" models were used to simulate the 1997 flood hydrograph, which had a peak discharge of 1,140 m^3/s (50-year return interval). The representative bed-material gradation

(Figure 4.22) was applied to the model and a representative input sediment-transport load was developed and applied. CCHE2D was run using the Wu et al. (2000) sediment-transport equation, MD_SWMS was run using the Wilcock and Kenworthy (2002) sediment-transport equation and SRH-2D was run using the Parker (1990) and Engelund-Hansen (1972) equations.

The CCHE2D “without-island” model predicted deposition in the low shear stress locations along the reach where islands had previously been located. Although the CCHE2D model was able to successfully predict island development, it often became unstable and was not able to complete a full simulation. The MD_SWMS program did not adequately predict sediment deposition in either the baseline or “without-island” conditions and the program would often stop for unidentified reasons; the model input and output were checked to investigate possible reasons including excessive erosion/deposition, excessive change on bed material and large time step changes. The initial results from the SRH-2D model indicated it was able to predict sediment deposition and was stable over the duration of the hydrograph.

The SRH-2D model was selected for the study due to the stability of the model, the ability to simulate island growth and the observation that the unstructured grid was better at representing the complex topography of the study reaches. The instability of the CCHE2D and MD_SWMS models can likely be attributed to user inexperience (although a significant effort was made to make the models run), and, although not a deciding factor in the final model selection, the CCHE2D and MD_SWMS models took significantly more time to develop and apply compared to SRH-2D.

4.2.3. SRH-2D Model Development

4.2.3.1. Topographic Data

The SRH-2D model uses a mesh composed of triangular and quadrilateral elements that represent the plan form geometry and topography of the study reach. The topography is represented by elevations assigned to each node in the mesh. The elevations for the Ketchup mesh were derived from the 2-foot contour mapping and in-channel bathymetric survey data collected by Ayres and Associates in 1997. In the Walters Ferry reach, the elevations for the overbank portion of the mesh were derived from the Ayres (1997) and the Ralston and Associates (1998) survey (Section 4.1.3).

The SRH-2D mesh is limited to no more than approximately 16,000 elements for sediment-transport simulations due to computational limitations. The mesh resolution for both the Ketchup and Walters Ferry models was varied to maintain greater mesh density within the channel and at the islands where most of the topographic changes are expected to occur, with lower mesh density in the overbank areas.

In the Ketchup Island model, the typical size of the channel elements is approximately 15 m wide (lateral to the flow direction) by 23 m long (Figure 4.30). The overbank portion of the model is generally comprised of triangular elements with side lengths ranging from 20 to 45 m. The resulting Ketchup mesh is 5,990 m long and contains 13,798 elements and 11,675 nodes.

The Walters Ferry mesh is 5,235 m long and contains 9,814 elements and 9,665 nodes. Similar to the Ketchup mesh, the typical size of the channel elements is approximately 15 m wide (lateral to the flow direction) by 23 m long (Figure 4.31). Due to the entrenched channel of the Walters Ferry reach, the mesh was constructed up to the top of the left bank and to an equivalent elevation along the right overbank. As a result, there is very little overbank area, which was represented mostly with trapezoidal elements with similar sizes to the in-channel elements.

4.2.3.2. Downstream Boundary Conditions

To execute the model, it is necessary to specify the boundary conditions at the outflow boundaries for each discharge being modeled. The downstream boundaries of the Ketchup and Walters Ferry meshes were located at HEC-2 model cross sections and the hydraulic output from the HEC-2 models was used to develop stage-discharge rating curves for the Ketchup and Walters Ferry 2-D models (Figure 4.32 and Figure 4.33, respectively).

4.2.3.3. Model Validation and Material Properties

The SRH-2D model uses Manning's *n*-values to define boundary friction losses and a parametric turbulence model was used to calculate the energy loss due to internal turbulence.

Different roughness material types were used to represent the main channel, islands and various overbank roughness zones (Figure 4.34 and Figure 4.35). The overbank roughness ranged from 0.04 for the gravel bars to 0.1 for overbank areas with thick vegetation (Table 4.14). Main-channel Manning's *n*-values of 0.023 and 0.025 were used in the Ketchup and Walters Ferry models, respectively, for the entire channel area and for the entire range of discharges. (SRH-2D does not have the ability to vary the Manning's *n*-values during a simulation.) These values produce water-surface elevations that are consistent with measured elevations, and they are generally consistent with recommended values in standard references (Chow, 1959; Barnes, 1967; Hicks and Mason, 1991; Julien, 1995).

The hydrodynamic portion of the models was validated to measured water-surface elevations that were surveyed at discharges ranging from 328.5 to 1,608.4 m^3/s in the Ketchup reach (Figure 4.36) and at approximately 257.7 m^3/s in the Walters Ferry reach (Figure 4.37). [The discharge at the Walters Ferry reach varied during the survey from 219.5 to 259.7 m^3/s, with the most of the water-surface elevation measured at approximately 257.7 m^3/s. For model validation purposes, the model was run at each specific discharge corresponding to the water-surface elevation measurement.]

The agreement between the computed and measured water-surface elevations using the selected Manning's n roughness values is very good for both models. The Ketchup model calibrates reasonably well at the lowest discharge of 328.5 m^3/s, with an average difference between the predicted and measured water-surface elevation of -0.1 m (Figure 4.36). At higher discharges, the Ketchup model calibrates very well, with differences of 0.04 m at 1,506.5 m^3/s and 0.04 m at 1,608.4 m^3/s (Figure 4.36).

For the Walters Ferry model, the average difference between the predicted and measured water-surface elevation is -0.03 m; the maximum difference of -0.20 occurs at Sta 1733+20 (Figure 4.37).

4.2.3.4. Representative Flood Hydrographs

Representative flood hydrographs were developed as input to the 2-D sediment-transport models. As discussed later, the islands located within the Ketchup and Walters Ferry subreaches were formed before flow measurements were collected and therefore it was not possible to recreate the flood series that created the islands. In addition, the sediment-transport conditions that formed the islands are not known. It was originally anticipated that the 2-D models would be simulated using recorded flow hydrographs. After initial testing of the models, it was concluded that the simulations were taking a considerable time to run due to the variation in annual peak flow hydrographs, which included multiple peaks and significant variation in volumes. Therefore, to simplify the modeling and decrease the simulation times, representative flow hydrographs for the Ketchup and Walters Ferry Reaches were developed based on the characteristics of the measured hydrographs.

To develop the hydrographs, the mean daily flow values for representative annual peak flow hydrographs were plotted. The representative hydrographs typically showed reasonably steady increase in flow up to the peak discharge, then remained reasonably constant, followed by a steady decrease in flow back to the base flow. Flow hydrographs with multiple peaks or unusual flow characteristics were not considered in the analysis.

Because the individual hydrographs peak at different times each year, the timing of each of the annual hydrographs was adjusted by shifting the hydrographs so that the rising limbs of the hydrographs match as closely as possible and a representative slope was calculated that represents the increase in flow. Similarly, the timing of the hydrographs was adjusted so that the falling limbs of the hydrographs matched and a representative slope was calculated to the decrease in flow. Comparison of flood hydrographs indicated the slope of the rising and falling limbs were similar at both sites. A representative change in flow (increase and decrease) of 4.25 and 5.0 m^3/s/hour was selected for the Walters Ferry and Ketchup subreaches, respectively. An example of the representative hydrographs is shown in Figure 4.38. A comparison of the representative hydrograph developed for the Walters Ferry reach with measured peak flow hydrographs is shown in Figure 4.39.

4.2.3.5. Sediment-transport Measurements

An evaluation of the sediment-transport measurements along the study reach was conducted to develop sediment input rating curves for the 2-D model. No bed load transport measurements were found for the study reach. Suspended sediment-transport measurements collected at the Murphy (USGS Gage No. 13172500) and Weiser gages by the USGS were obtained. Unfortunately, most of the measurements do not report the wash load portion of the sample (percentage of suspended sediment less than 0.0625 mm). At the Murphy gage, only 8 of the 26 samples report the wash load fraction, and the majority of these measurements indicate that entire sample was mostly comprised of wash load. A suspended sediment sample collected at the Murphy gage during the 1997 flood when the discharge was approximately 1,096 m^3/s indicated a sediment concentration of 81 mg/l, but the wash load component was not reported. Due to the lack of suspended sediment-transport measurements, it was not possible to develop a suspended-sediment-transport discharge relationship.

At the Weiser gage, there were 53 suspended-sediment-transport measurements reported with the associated wash-load component. The measurements were collected between 1977 and 1986 and over a range of flows from 244 to 1,950 m^3/s. The highest sediment concentration of 158 mg/l occurred at a discharge of 578 m^3/s. No apparent explanation was found for this comparatively high value, but it may have been due to sediment inflow from a tributary.

4.3. Tables and Figures

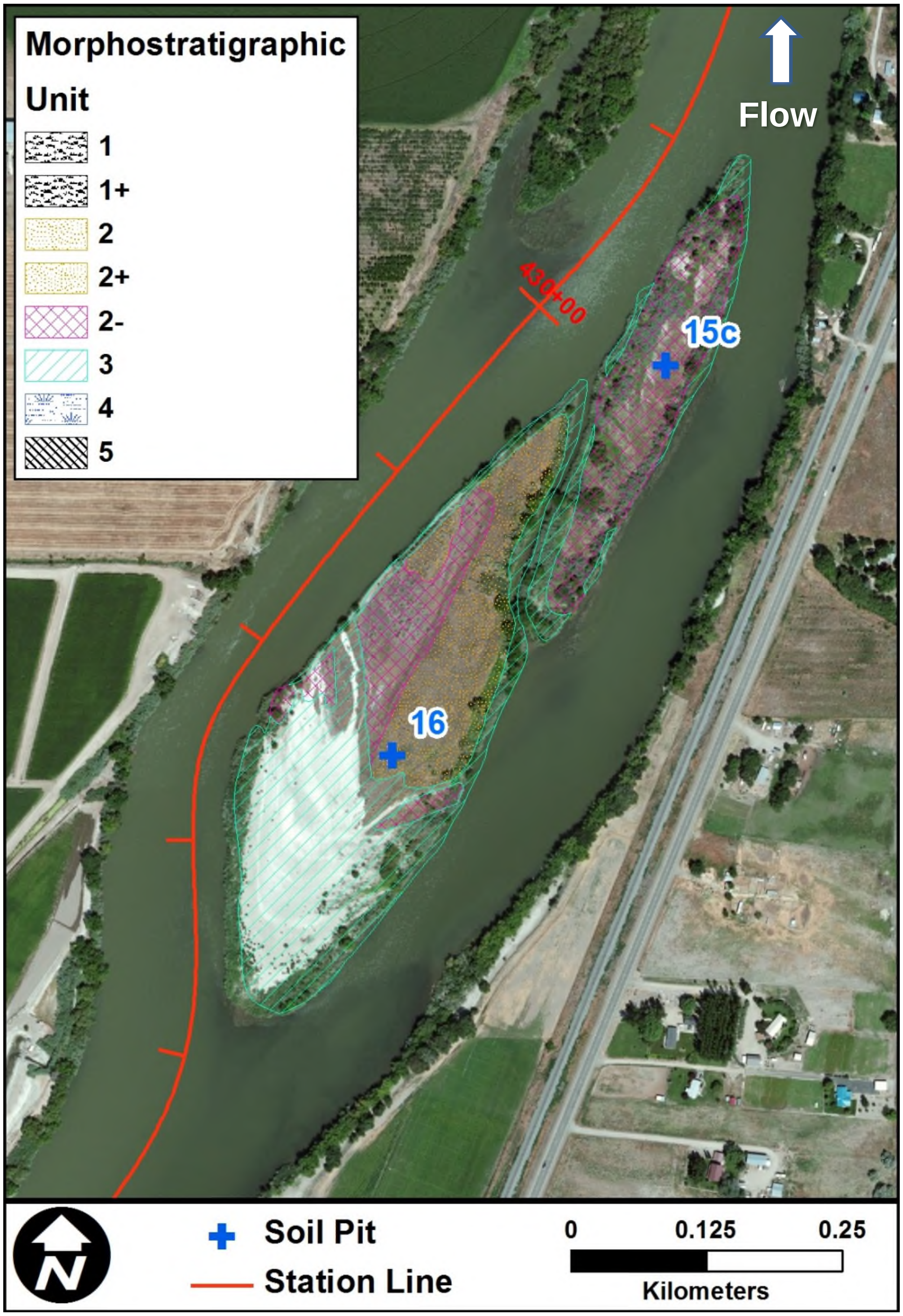

Figure 4.1 Example of morphostratigraphic mapping conducted by Othberg and Fosberg (2001) at Ketchup (16) and Annear Islands (15c).

Table 4.1 Description of morphostratigraphic units delineated by Othberg and Fosberg (2001).

Morpho-stratigraphic Unit	Description
1	Landform with greatest average surface height and oldest relative soil development. Composed of thin layers of sand and silty sand alluvium. Unit 1 surfaces are the most stable among the islands, i.e., not overtopped by high stream flows for the longest period of time. Vegetation typically reflects height above mean water-surface elevation and degree of soil development. Label of 1+ for Big Rocky and Rail islands indicates inclusion of a remnant of Bonneville Flood gravel.
2+	Landform with second-greatest average surface height above mean water-surface elevation. Composed of thin layers of sandy alluvium interbedded with minor silty layers. Lacks the relatively well-developed soil B horizons of unit 1; typically has greater occurrence of B horizons and buried A and B horizons. Unit 2+ surfaces show evidence of stability, i.e., infrequently overtopped by high stream flows. Vegetation typically reflects height above mean water-surface elevation and degree of soil development.
2-	Landform with average surface heights a few feet above mean water-surface elevation. Composed of thin layers of sand interbedded with minor silty layers. Unit 2- was both eroded and received deposits during the spring high stream flows of 1997. Unit 2- represents a surface that is relatively unstable, i.e., frequently overtopped by high stream flows. Soil development ranges from none (all C horizons) to some incipient A and B horizons. Vegetation reflects closeness to mean water-surface elevation and common disturbance.
3	Landform with surface heights typically at or slightly above mean water-surface elevation. Composed of thin sand layers, but gravel is common. Locally deposited coarse sand accumulated in association with willow thickets and larger trees is also important sediment. Unit 3 represents an unstable surface that is frequently overtopped. Soil development is largely absent with the exception of mottling from fluctuating water level. Vegetation reflects nearness of water, unstable conditions, and common annual disturbance. Unit 3 predominantly comprises small islands, most of the fringes that are formed typically at the upstream ends of larger, higher islands.
4	Landform with surface height just exposed during low summer discharges. Composed of gravel and thin sand. Vegetation beginning to take hold.
5	In a few locations, field observations and aerial photography obtained during low river flows indicate locations of gravelly shallows that may be incipient island growth.

Table 4.2 Summary of samples collected.

Date	Islands Sampled	Soil Pits Dug	Total Samples
9/8/1999 to 9/9/1999	5	5	60
5/9/2000 to 5/22/2000	30	31	442
8/14/2000 to 8/23/2000	24	24	346
8/29/2000 to 9/21/2000	35 (one repeat)	35	530
TOTALS	93	95	1,378

Table 4.3 Non-native plant species developed based on the Johnson et al. (1992) report - separated by Habitat (no grasses).

OBL	FACW	FAC	FACU	No indicator
Ammannia robusta*	Chenopodium rubrum*	Chenopodium album	Acer negundo	Cardaria draba
Asclepias incarnata	Conium maculatum	Chenopodium glacum*	Anthemis cotula*	Carduus nutans
Iris pseudacorus	Mentha piperita	Elaeagnus angustifolia	Asparagus officinalis	Catalpa speciosa
Juncus articulatus*	Polygonum lapathifolium*	Fraxinus pennsylvanica	Cerastium vulgatum	Convolvulus arvensis*
Lythrum salicaria	Polygonum persicaria	Gleditsia triacanthos	Cirsium arvense	Descurainia sophia
Nasturtium officinale	Rumex crispus	Kochia scoparia	Cirsium vulgare	Dipsacus fullonum
Polygonum hydropiper	Salix alba	Lactuca serriola*	Lepidium perfoliatum	Erodium cicutarium
Potamogeton crispus	Tamarix chinensis	Lepidium latifolium	Melilotus alba	Juglans nigra
Veronica anagallis-aquatica	Tamarix ramosissima	Nepeta cataria	Plantago lancolata	Malva neglecta
		Plantago major	Salsola iberica	Morus alba
		Populus deltoides	Sisymbrium altissimum	Sisymbrium loeselii
		Portulaca oleracea	Trifolium repens	Solanum rostratum*
		Solanum dulcamara	Verbena brachteata*	Tribulus terrestris*
		Xanthium strumarium*		Ulmus pumila
				Verbascum thapsus

*Added as non-native by Juanita Lichthardt and Dr. Rick Harner.

Table 4.4 Non-native pollen found in sediment samples.

Genus	Common Name
Acer	boxelder, maple
Acer negundo	boxelder
Acer saccarinum-type	sugar maple
BRASSICACEAE	mustand family
Carya	hickory
Cerealia	cereal crops
Cirsium - type	thistle
Convolvulus arvensis	field bindweek
Dipsacus	teasel
Elaeagnus	russian olive
Erodium cicutarium	filaree, heron's bill
Fraxinus	ash
Juglans	walnut
Liquidambar (cf)	black gum
Lythrum	purple loosestrife
Malva	common mallow, cheeseweed
Morus	mulberry
Ostrya / Carpinus - type	hornbeam, hop hornbeam
Plantago	plantain
Platanus	sycamore
Polygonum persicaria	Lady's Thumb
Portulaca	purslane
Rumex	curly dock
Scabiosa - type (knautia)	scabiosa
Scabiosa- type	scabiosa
Tamarix	tamarisk
Trifolium pratense	red clover
Trifolium repens	white clover
Trifolium-type	clover
Ulmus	elm
Zea mays	corn

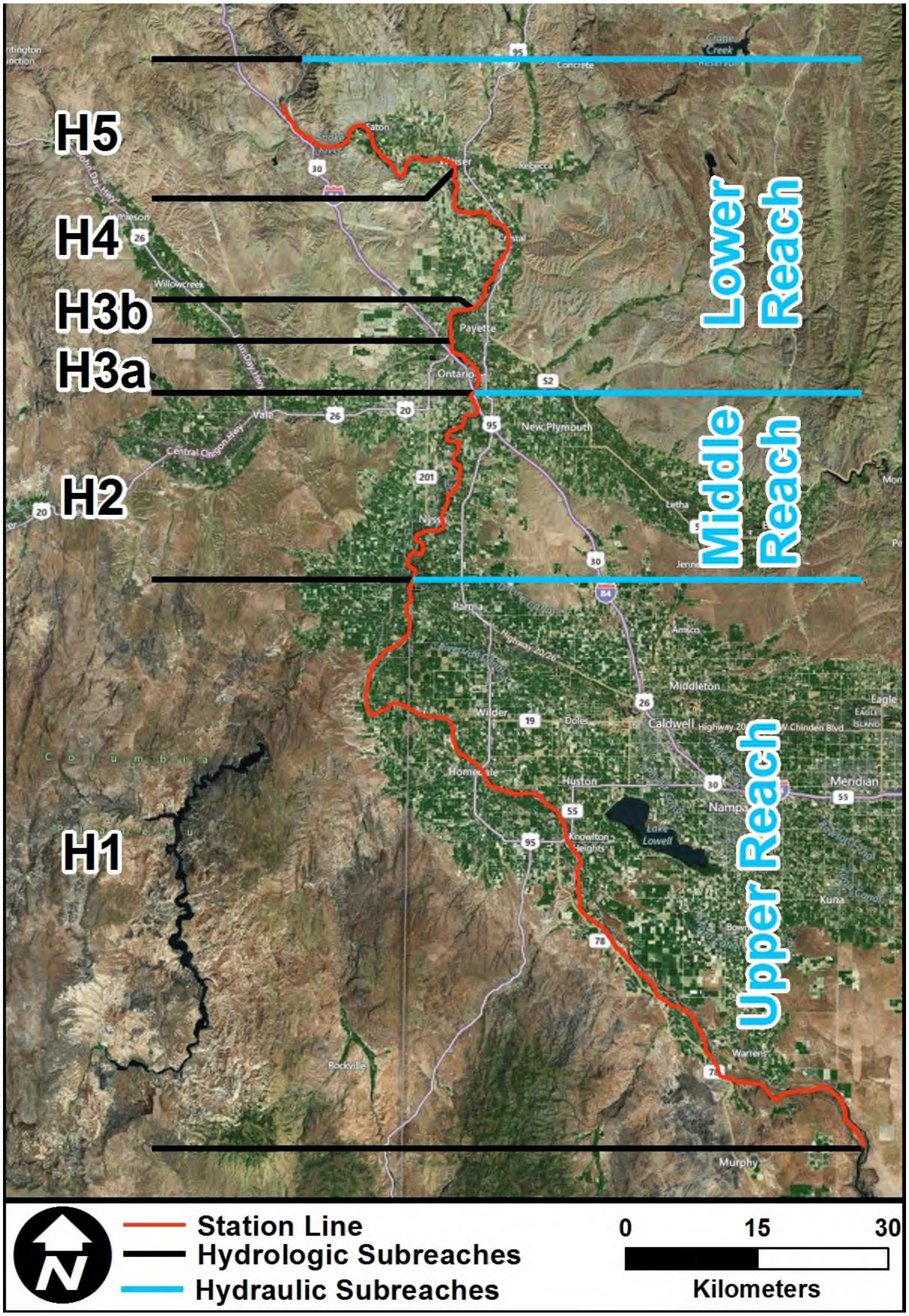

Figure 4.2 Map of the Snake River study area showing the limit of the hydrologic and hydraulic model subreaches.

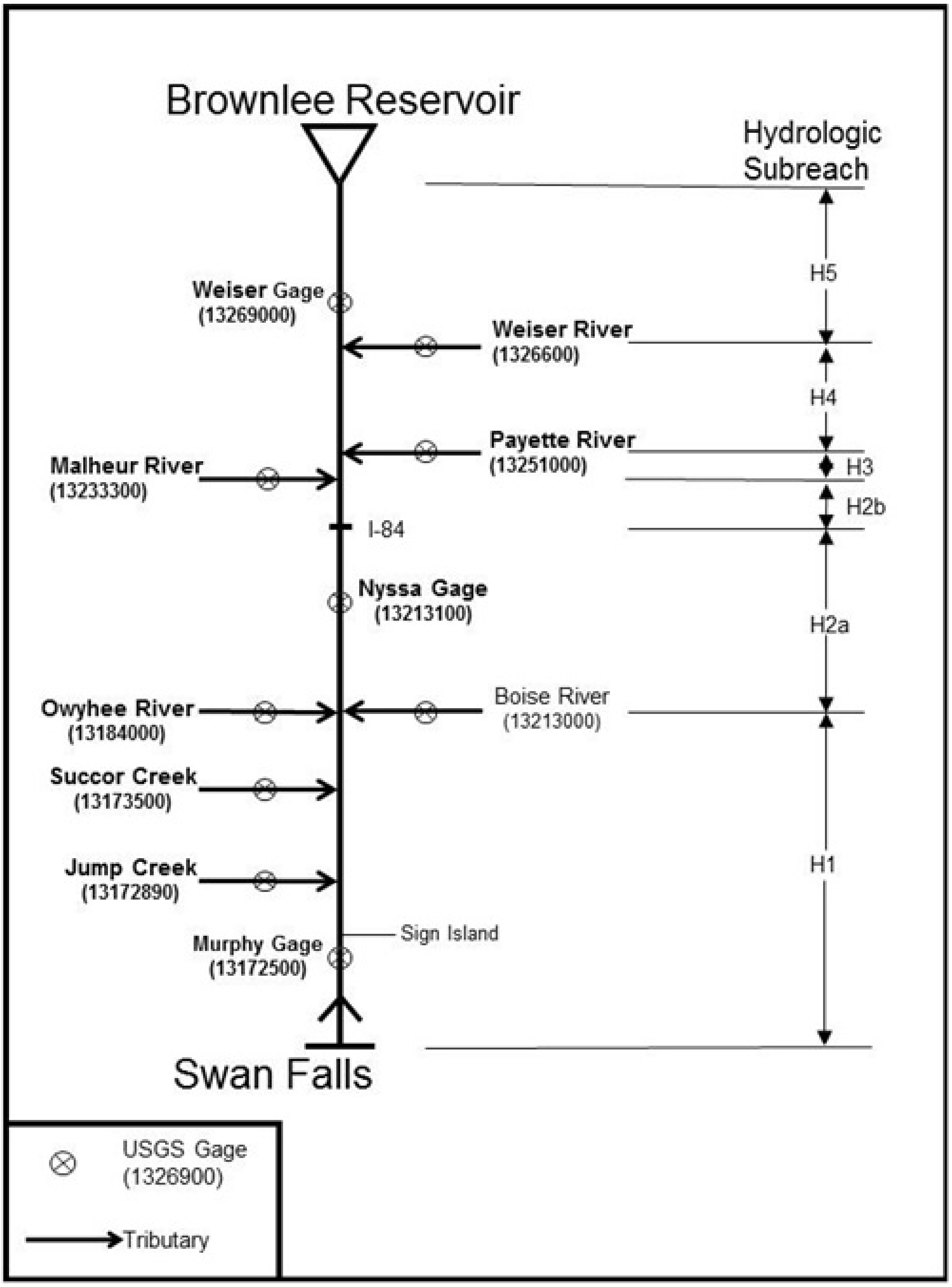

Figure 4.3 Schematic diagram of the study reach of the Snake River showing major the major tributaries and USGS stream gages considered in the hydrologic analysis.

Table 4.5 Hydrologic subreach boundaries.

Subreach	Upstream Limit	Downstream Limit
H1	Swan Falls	Owyhee/Boise River confluence
H2	Owyhee/Boise River confluence	Malheur River
H3	Malheur River	Payette River
H4	Payette River	Weiser River
H5	Weiser River	Upstream end of Brownlee Pool

Table 4.6 Summary of the stream gages in the hydrologic analysis of the study reach of the Middle Snake River extending from Swan Falls to Brownlee Reservoir.

USGS Gage Number (see Figure 4.9)	Gage Name	Drainage Area (km^2)	Period of Record*
13172500	Snake River near Murphy, ID	108,520	1912-2012
13172890	Jump Creek near Homedale, ID	n/a	1989 – 1995
13173500	Succor Creek at mouth nr Homedale, ID	1,280	1903 - 1910, 1988 – 1993
13184000	Owyhee River at Owyhee, OR	29,270	1890-1897, 1903-1916, 1920-1929, 1979-1986
13213000	Boise River near Parma, ID	10,280	1971-2012
13213100	Snake River at Nyssa, OR	152,030	1975-1986, 1989-2012
13233300	Malheur River below Nevada Dam near Vale, OR	10,050	1926-1934, 1951-1954, 1980-1981, 1994-2012
13251000	Payette River near Payette, ID	8,390	1935-2012
13266000	Weiser River near Weiser, ID	3,780	1895-1905, 1911-1915, 1922-2012
13269000	Snake River at Weiser, ID	179,230	1911-2012

*Water years contained in the record. May contain missing values.

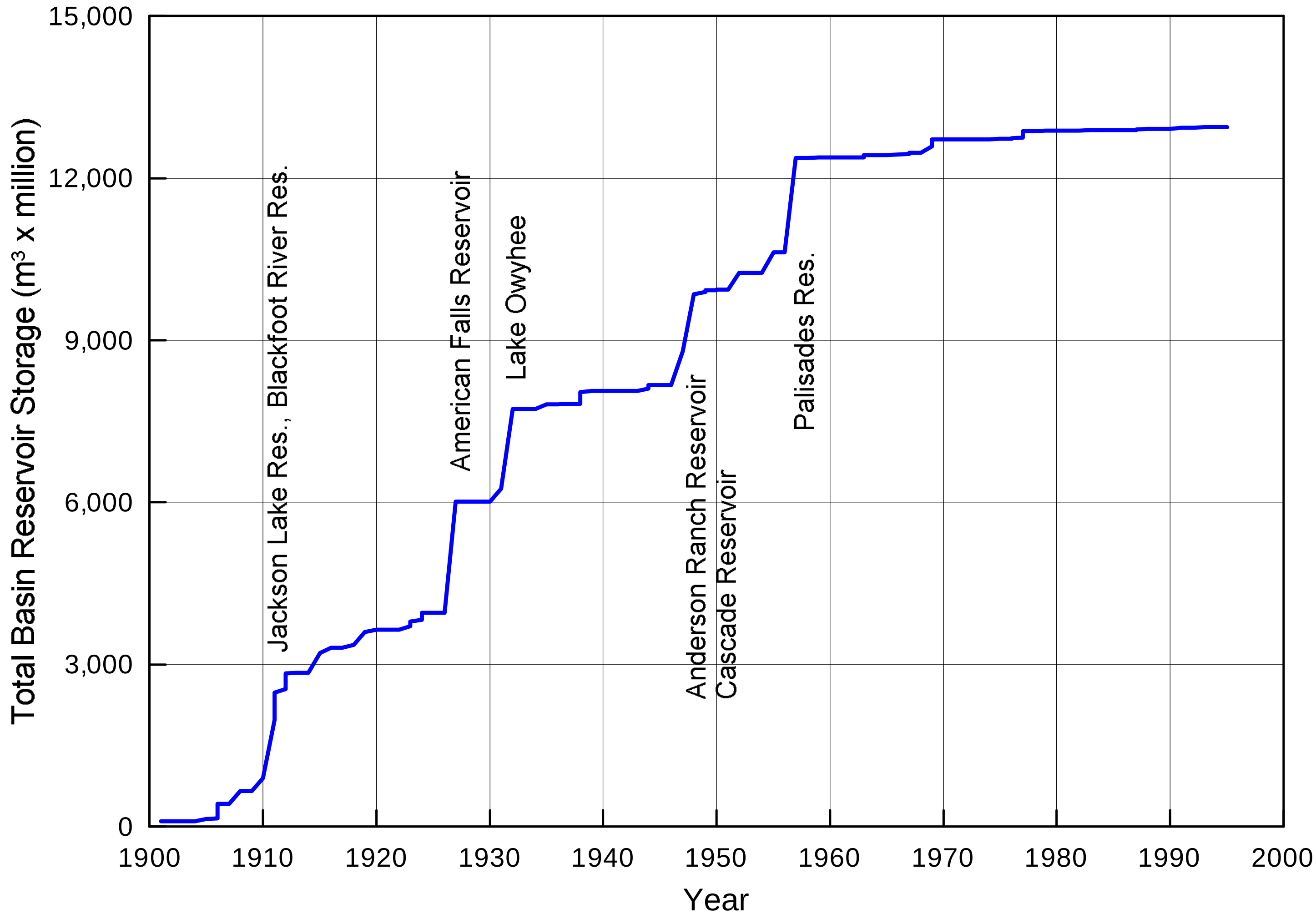

Figure 4.4 Change in total reservoir volume upstream from Brownlee Reservoir over time.

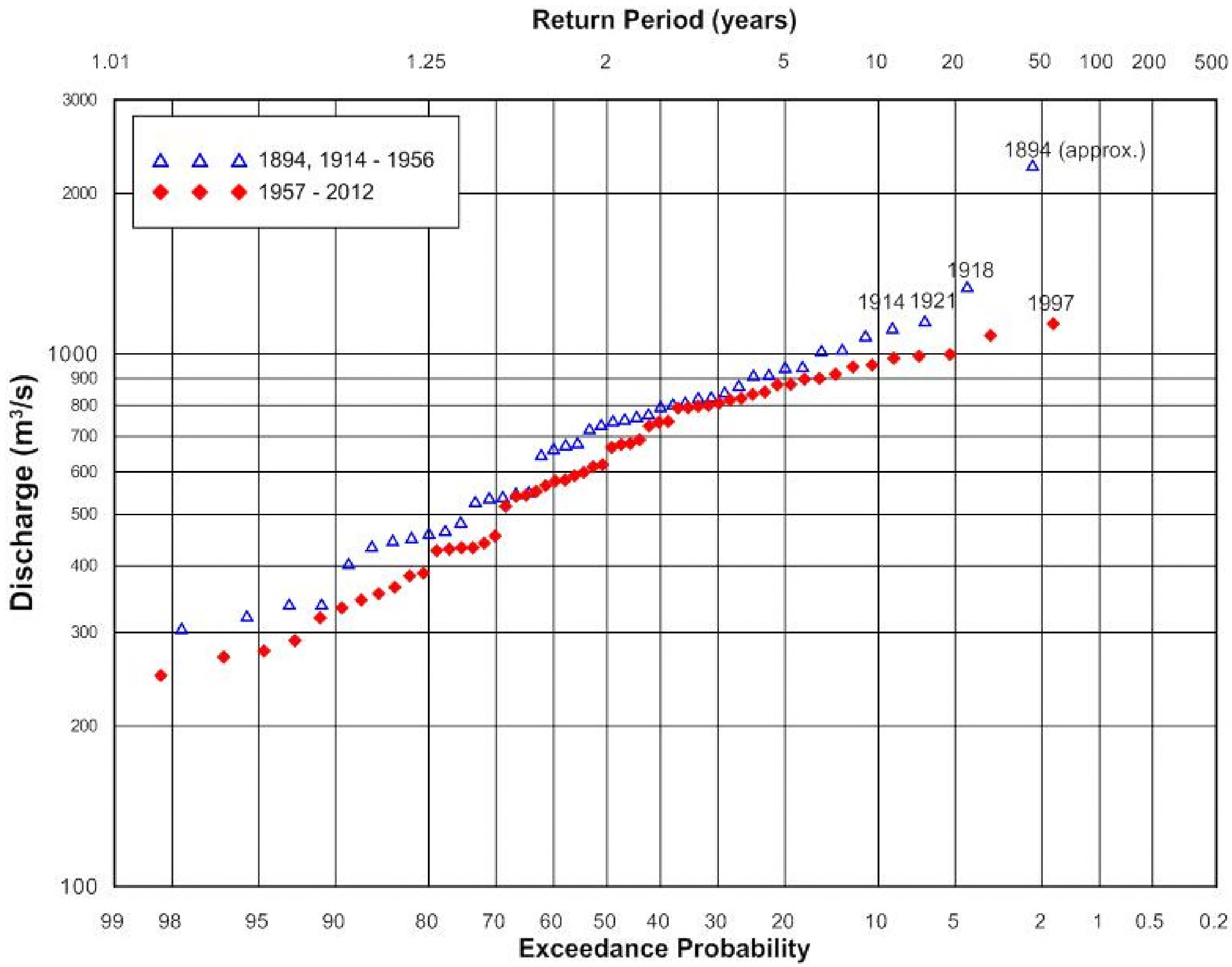

Figure 4.5 Comparison of flood frequency estimates for the pre- and post-Palisade Reservoir periods at the Snake River near Murphy gage (USGS Gage No. 13172500).

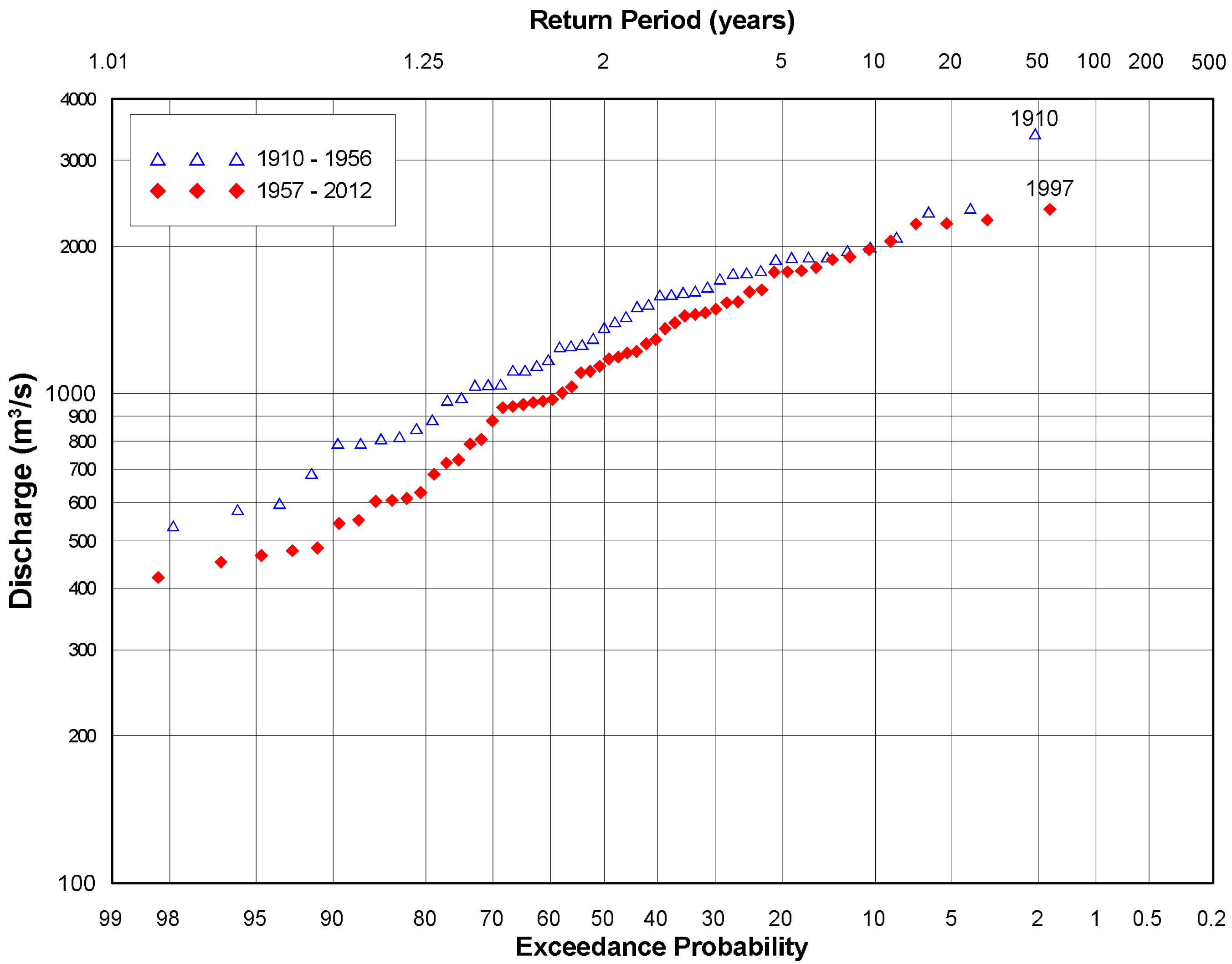

Figure 4.6 Comparison of flood frequency estimates for the pre- and post-Palisade Reservoir periods at the Snake River at Weiser gage (USGS Gage No. 13269000).

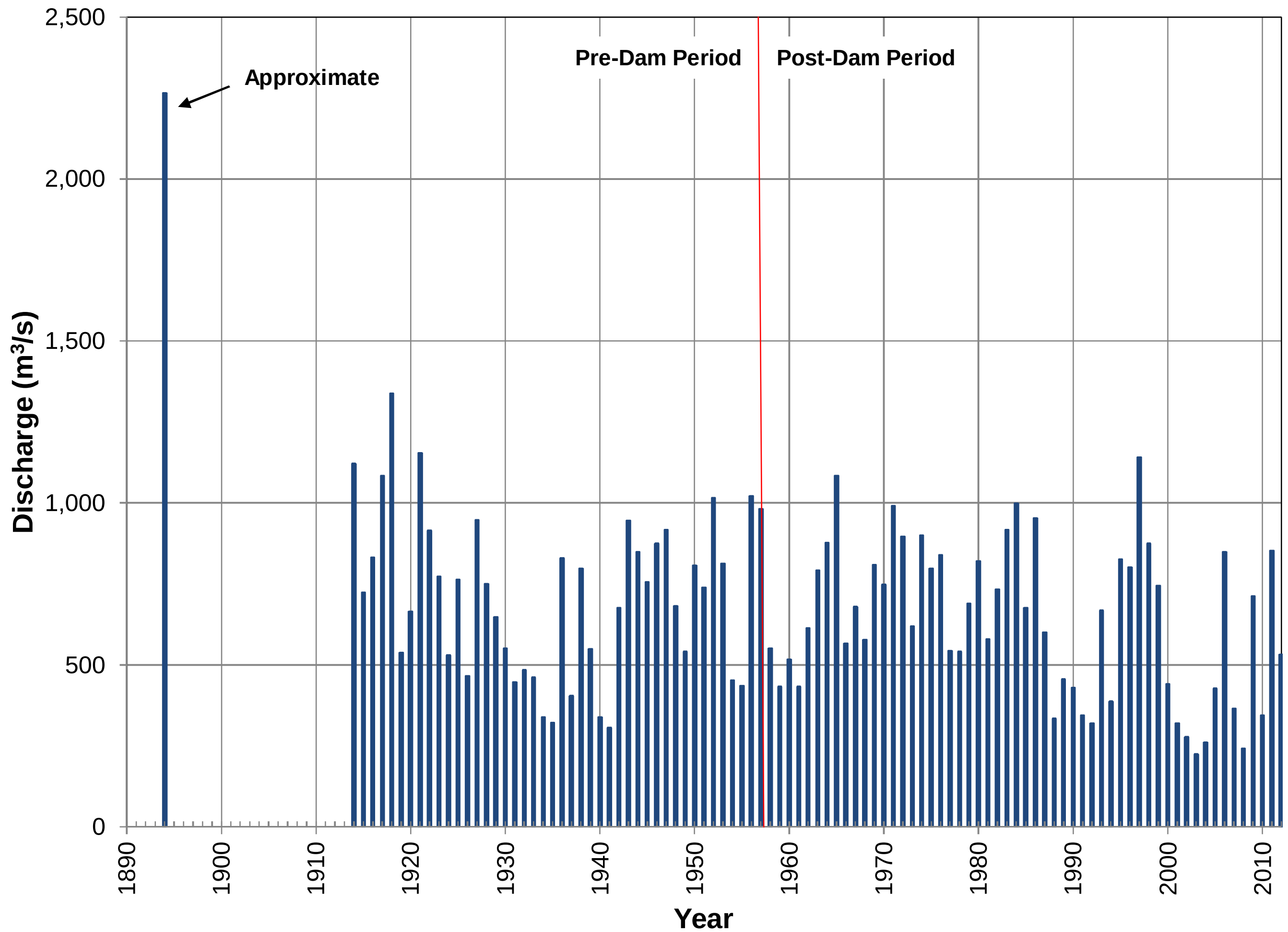

Figure 4.7 Annual peak flows recorded at the Snake River near Murphy gage (USGS Gage No. 13172500).

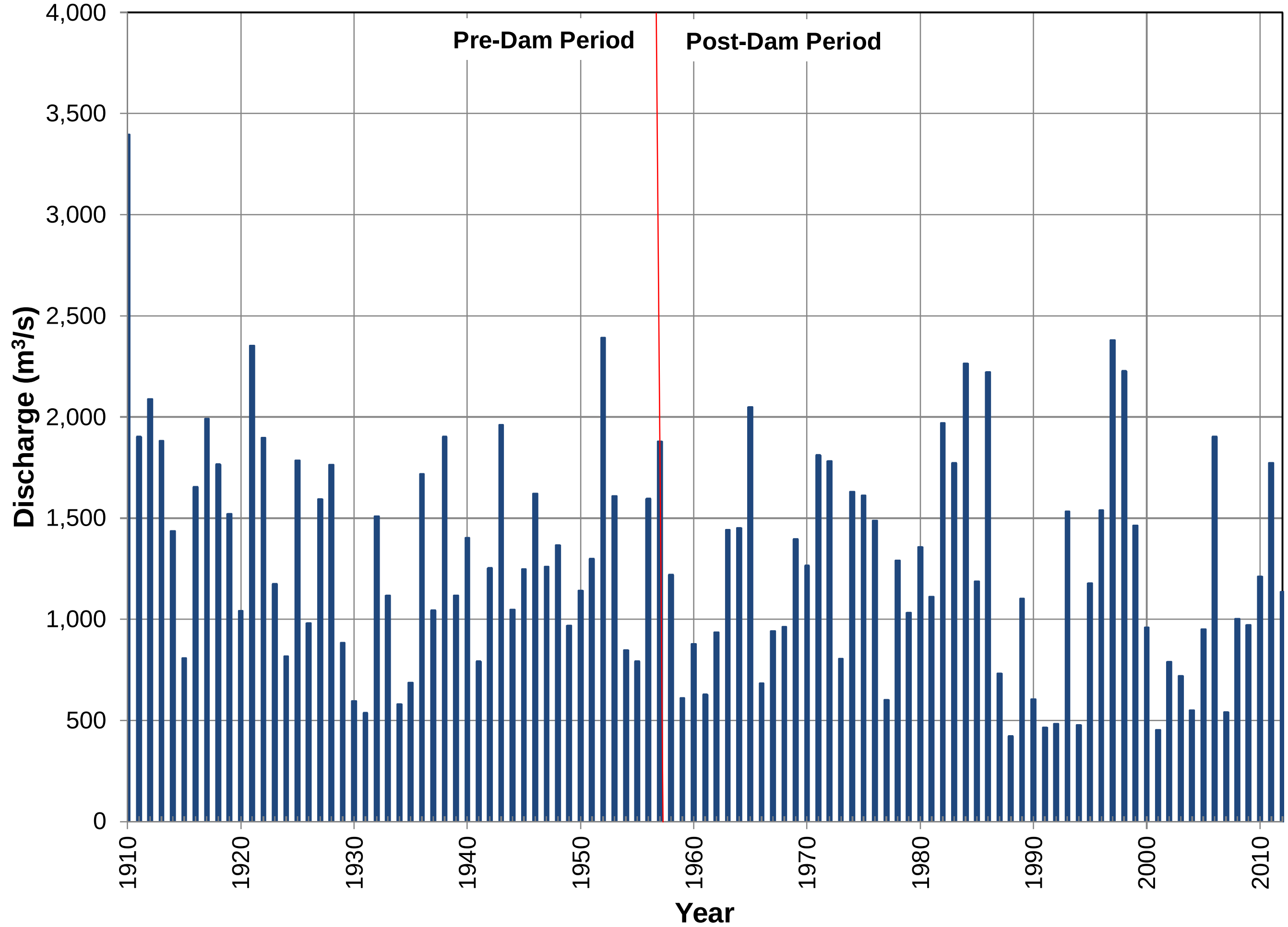

Figure 4.8 Annual peak flows recorded at the Snake River at Weiser gage (USGS Gage No. 13269000).

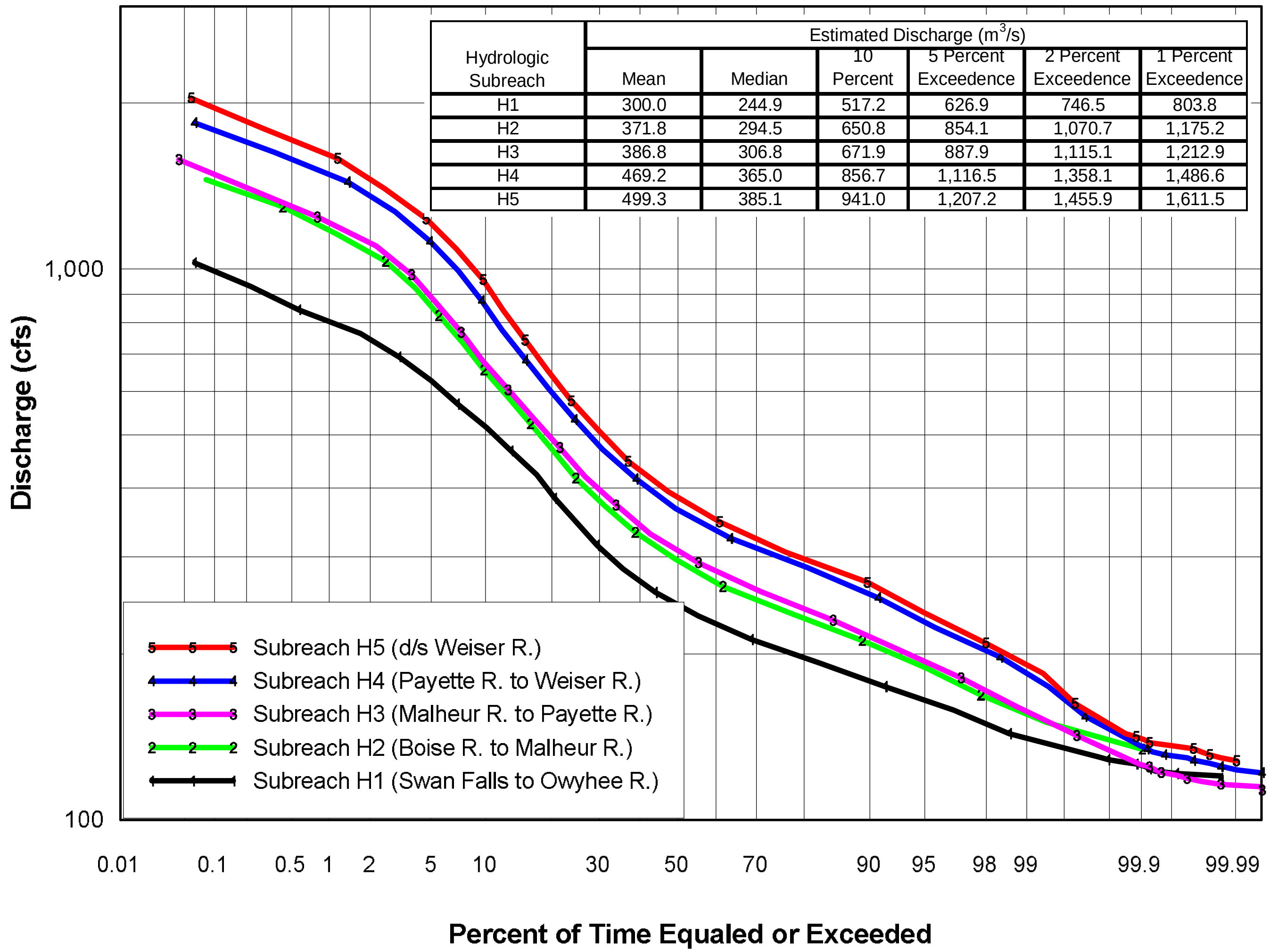

Hydrologic Subreach	Estimated Discharge (m^3/s)					
	Mean	Median	10 Percent	5 Percent Exceedence	2 Percent Exceedence	1 Percent Exceedence
H1	300.0	244.9	517.2	626.9	746.5	803.8
H2	371.8	294.5	650.8	854.1	1,070.7	1,175.2
H3	386.8	306.8	671.9	887.9	1,115.1	1,212.9
H4	469.2	365.0	856.7	1,116.5	1,358.1	1,486.6
H5	499.3	385.1	941.0	1,207.2	1,455.9	1,611.5

Figure 4.9 Mean-daily flow duration curves for the post-dam period for the five hydrologic subreaches along the Snake River study reach.

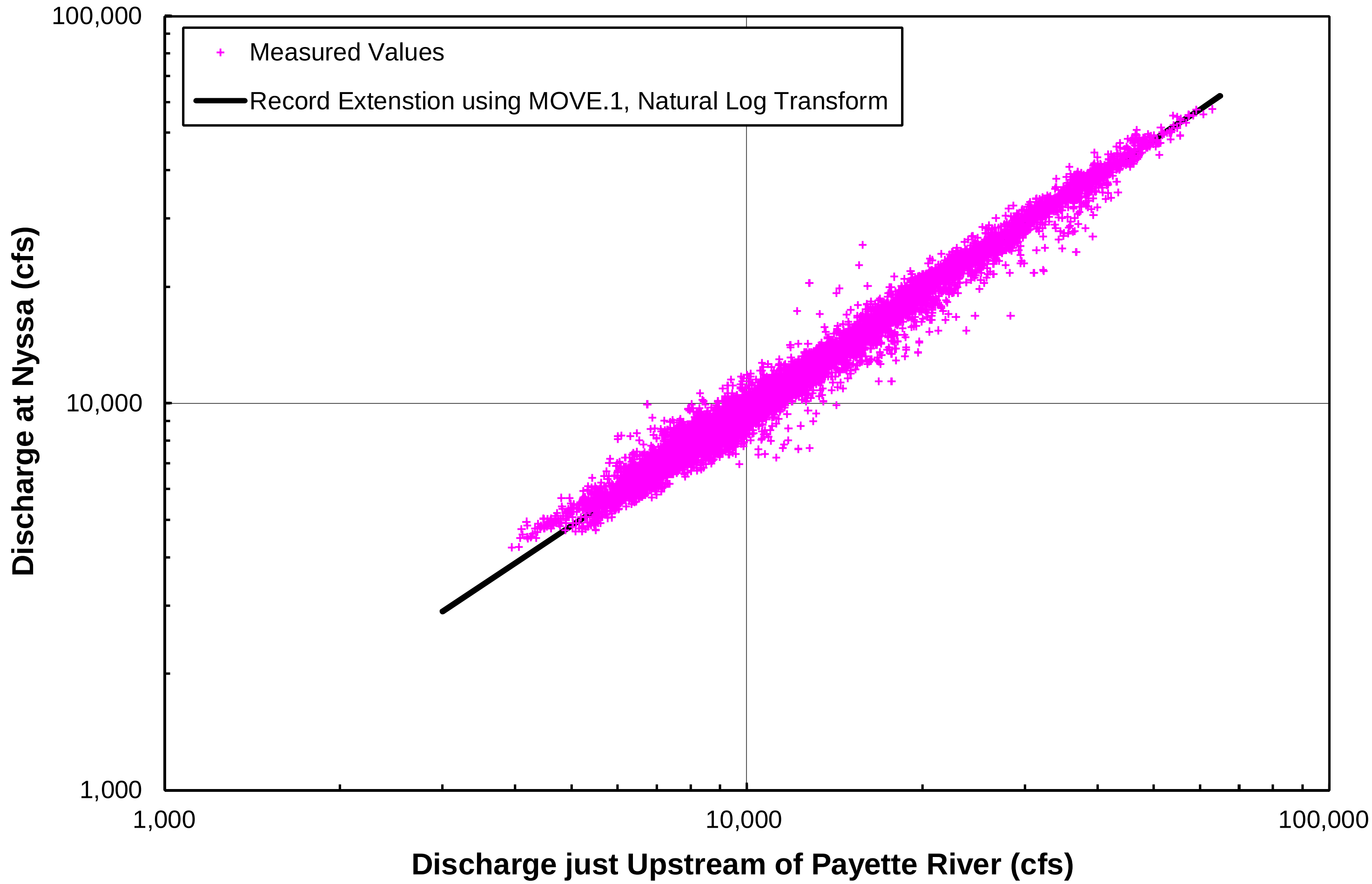

Figure 4.10 Plot of the measured discharge at the Snake River at Nyssa gage versus the estimate discharge upstream from the Payette River.

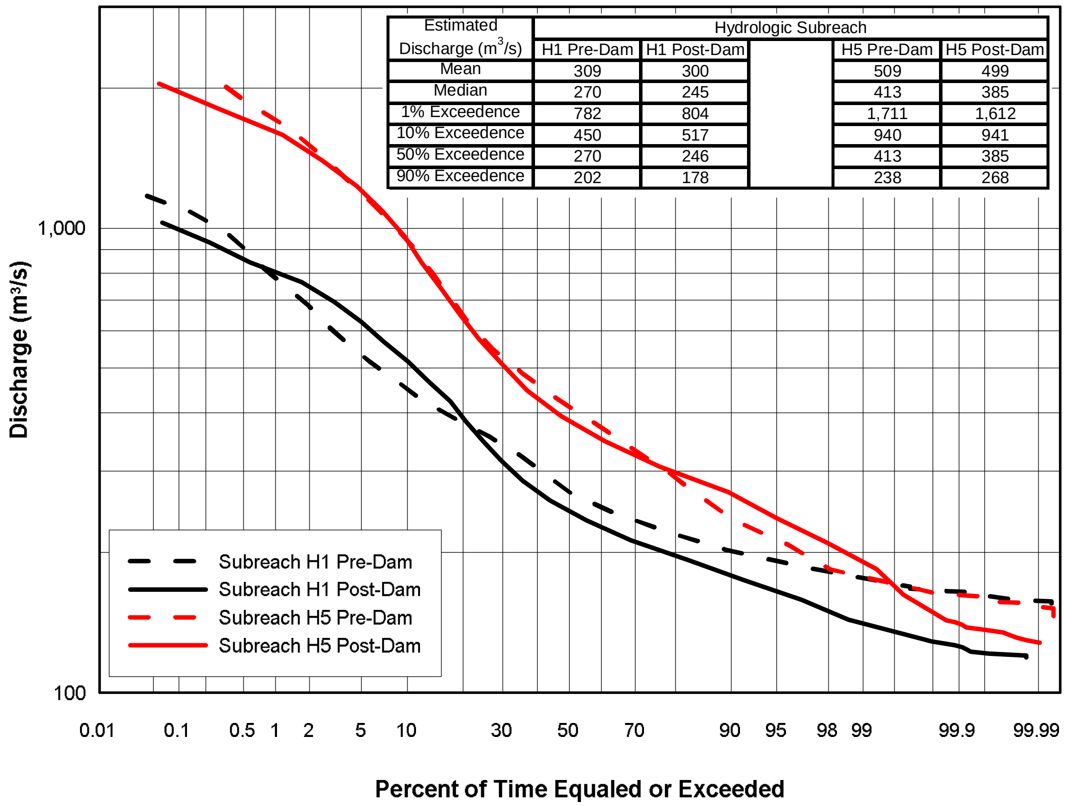

Figure 4.11 Comparison of the pre- and post-dam mean-daily flow-duration curves for the Murphy and Weiser gages.

Table 4.7 Summary of data used to estimate the annual peak flows in the various hydrologic subreaches.

Subreach	Data Used
H1	Recorded peak flows at the Murphy gage.
H2	Recorded peak flows at the Nyssa gage where available (1975 - 1986; 1989 - 2012). Otherwise, estimated mean daily flows in Subreach H2.
H3	Estimated mean daily flows in Subreach H3.
H4	Estimated mean daily flows in Subreach H4.
H5	Recorded peak flows at the Weiser gage.

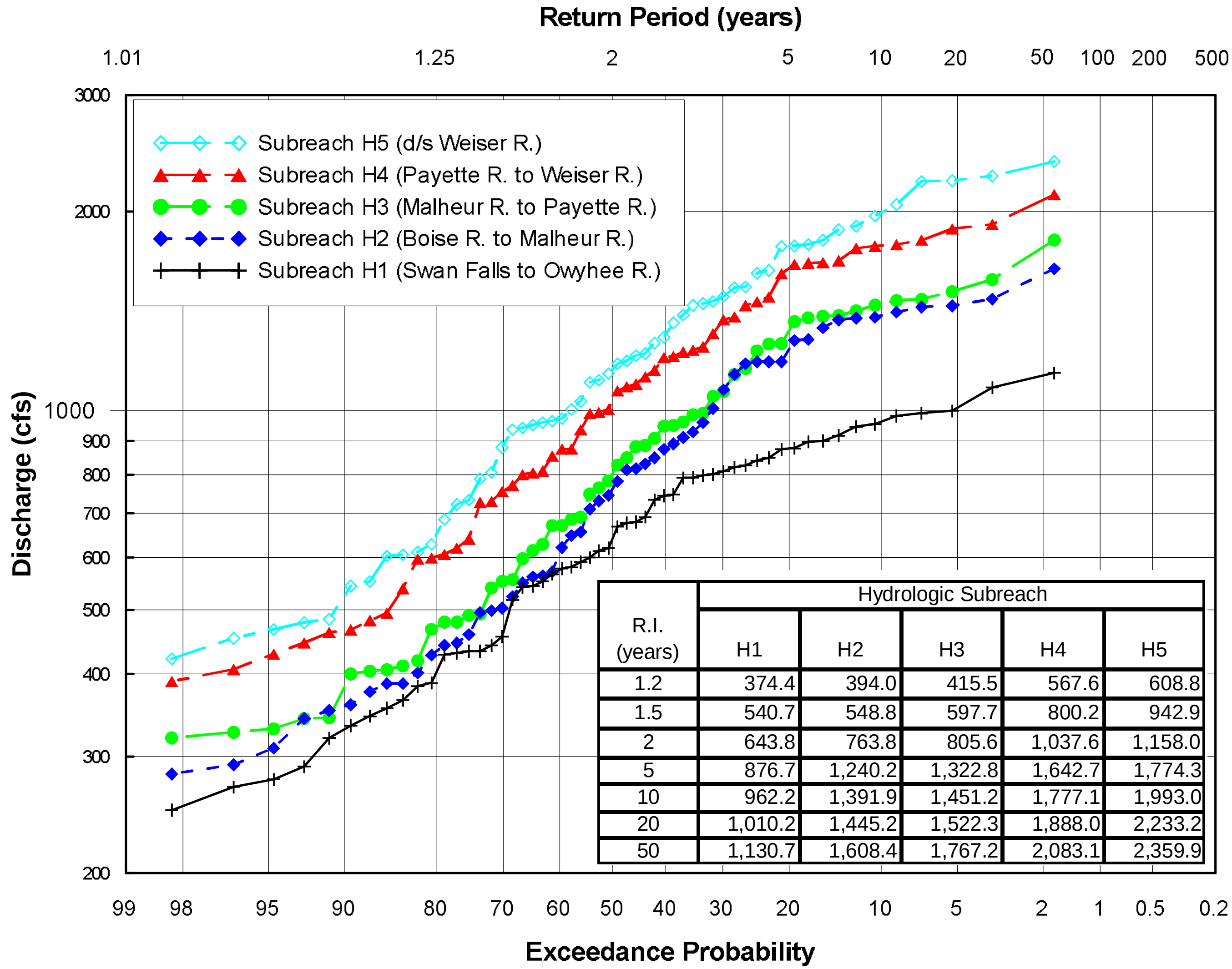

R.I. (years)	Hydrologic Subreach				
	H1	H2	H3	H4	H5
1.2	374.4	394.0	415.5	567.6	608.8
1.5	540.7	548.8	597.7	800.2	942.9
2	643.8	763.8	805.6	1,037.6	1,158.0
5	876.7	1,240.2	1,322.8	1,642.7	1,774.3
10	962.2	1,391.9	1,451.2	1,777.1	1,993.0
20	1,010.2	1,445.2	1,522.3	1,888.0	2,233.2
50	1,130.7	1,608.4	1,767.2	2,083.1	2,359.9

Figure 4.12 Estimated flood-frequency curves for the post-dam period for the five hydrologic subreaches along the study reach.

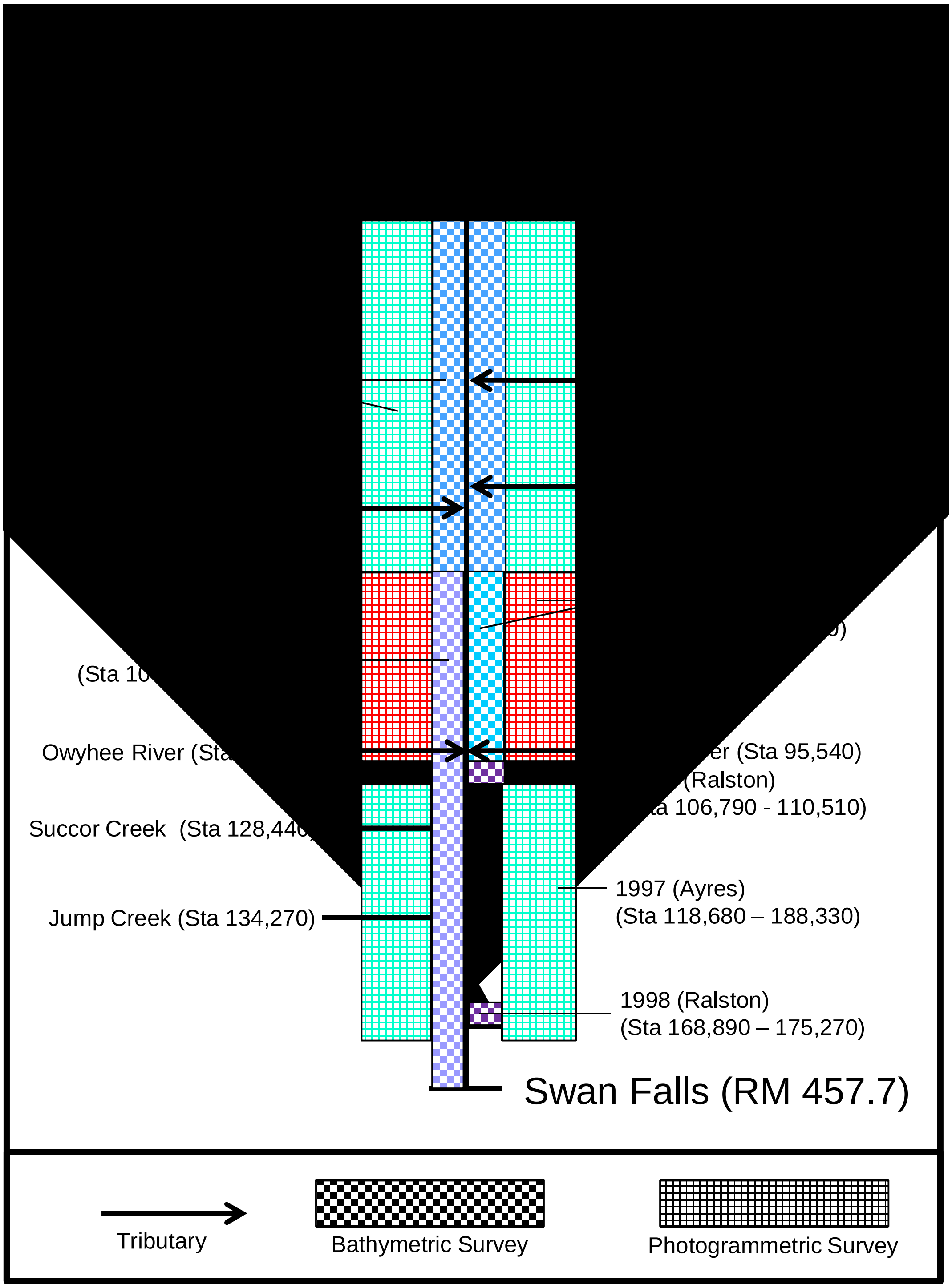

Figure 4.13 Schematic of the study reach showing the areas covered by each source of bathymetric and topographic data that was used in the hydraulic model.

Table 4.8 Range of discharge profiles created by the HEC-2 model, by hydrologic subreach.

Hydrologic Subreach	Range of Discharges (m^3/s)
H1	127 - 1,982
H2a	142 - 2,124 (middle reach)
H2b	139 - 2,761 (downstream reach)
H3	139 - 2,945
H4	140 – 3,276
H5	142 – 3,681

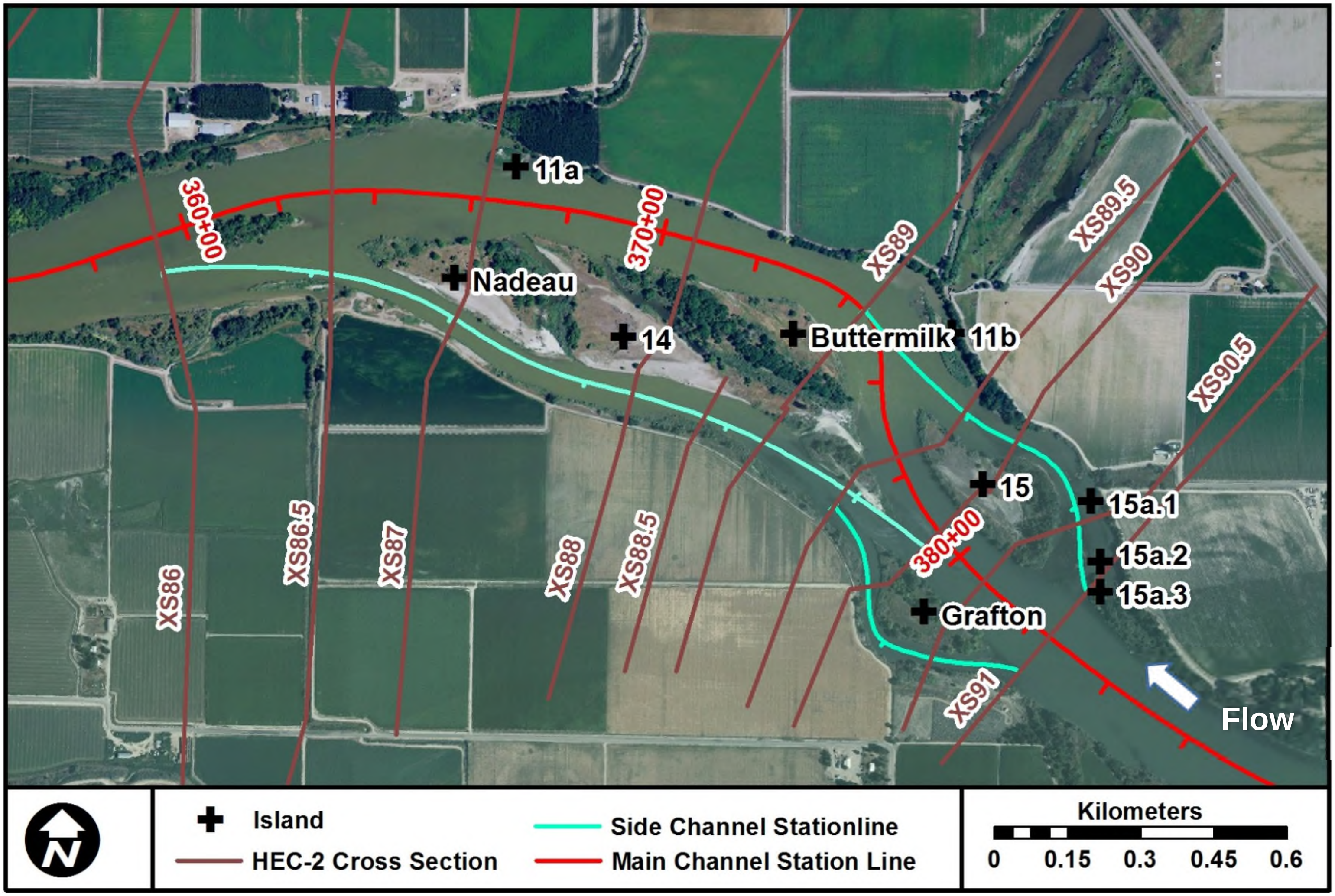

Figure 4.14 Example of the HEC-2 cross section layout for a HEC-2 model.

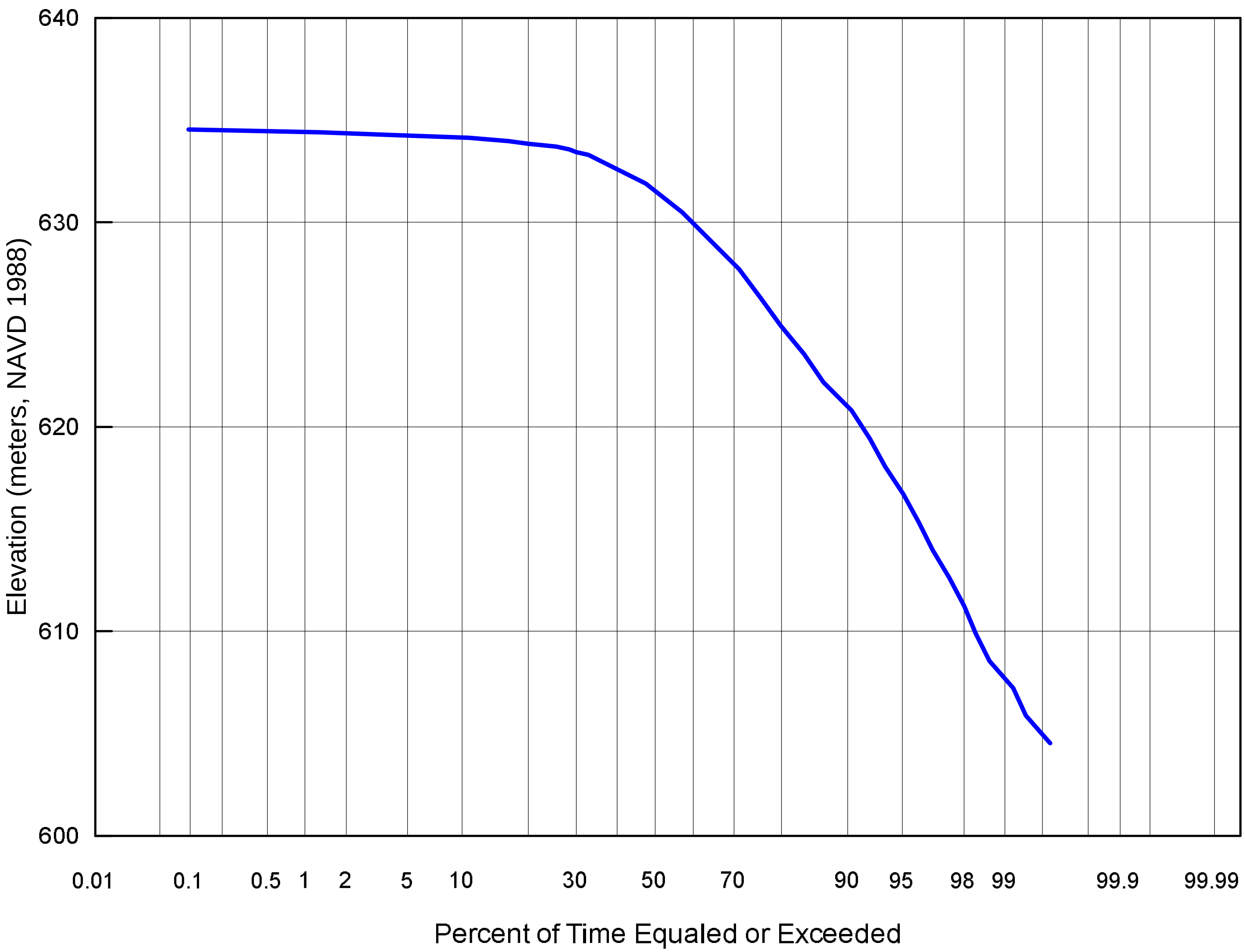

Figure 4.15 Duration curve of mean-daily reservoir elevations at Brownlee Dam for WY1958 through WY1998.

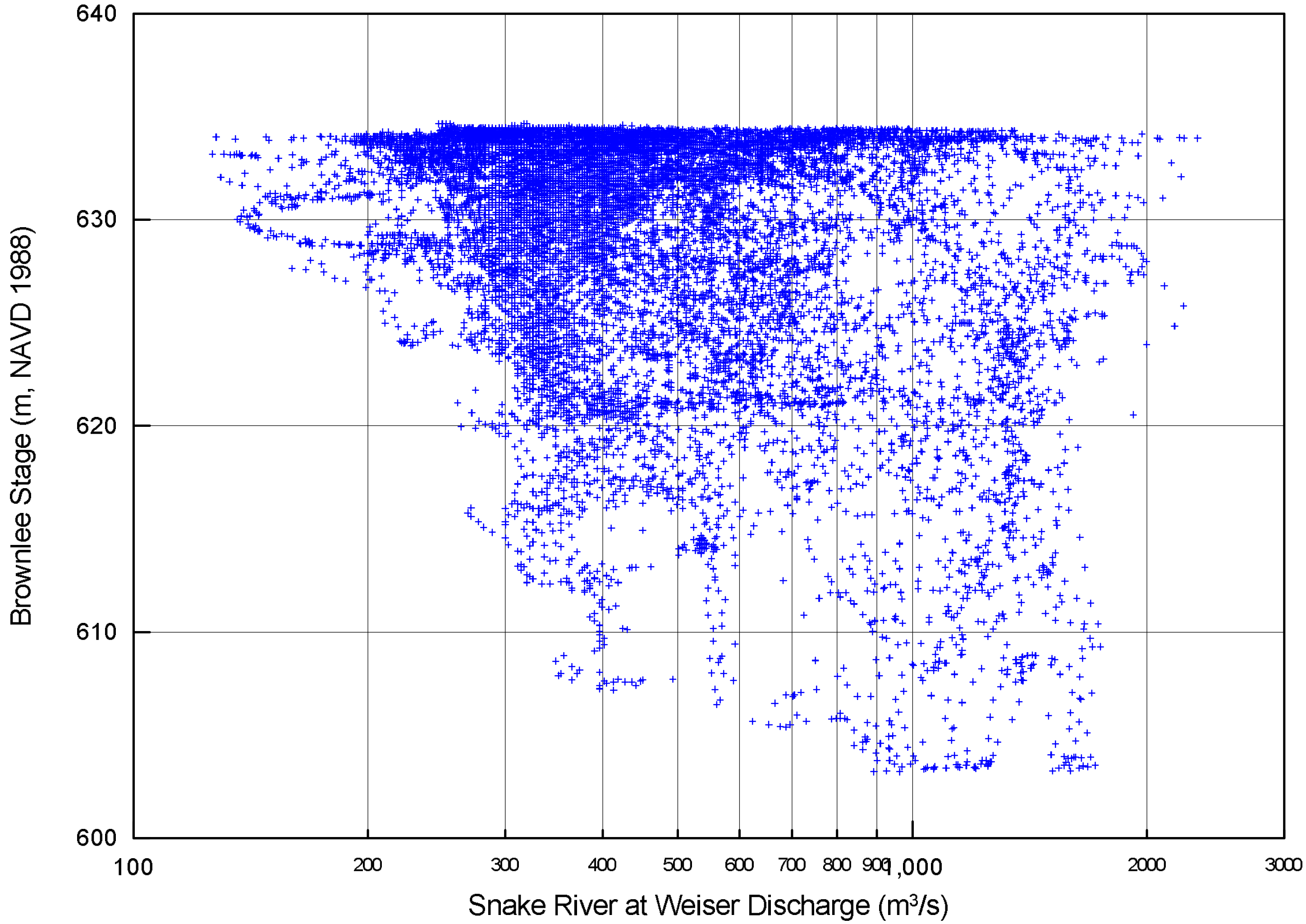

Figure 4.16 Reservoir stages at Brownlee Dam versus the measured discharge in the Snake River at Weiser gage for the period October 1958 to September 1998.

Table 4.9 Summary of survey data used to calibrate the hydraulic models.

Description	Date	Coverage (Station, m)	Reaches included			Number of Points
			Lower	Middle	Upper	
Ayres 1997 hydrographic survey	June 12 - 22, 1997	-6,010 to 66,600	X	X		238
MEI 1998 field survey*	Oct. 13 - 15, 1998	43,030 to 43,750; 107,710 to 108,040	X		X	42
Ayres 1999 hydrographic survey	Apr. 20 - Apr. 26, 1999	65,170 to 99,090		X	X	206
MEI 1999 field survey	Aug. 29 - Sep. 12, 1999	9,730 to 185,490	X	X	X	207
MEI 2000 field survey	Oct. 11 - Oct.15, 1999	72,620 to 606,160	X	X	X	62

*Survey data for Ketchup and Suzy Islands, only

Table 4.10 Summary of deviations between the computed and surveyed water-surface elevations.

Survey	Discharge Range (m^3/s)	Number of Points	Deviations (m)			
			Mean	Standard Deviation	Minimum	Maximum
Lower Reach						
Ayres, 1997	934.5 - 1682.0	230	0.00	0.08	-0.25	0.25
MEI, 1998	413.4	38(1)	0.07	0.06	-0.16	0.22
MEI, 1999	317.1 - 362.5	55	0.00	0.13	-0.30	0.28
MEI, 2000	359.6 - 399.3	16	-0.02	0.11	-0.20	0.15
Middle Reach						
Ayres, 1997	934.5	8(2)	-0.04	0.07	-0.12	0.11
Ayres, 1999	574.8 - 784.4	195	0.04	0.10	-0.29	0.52
MEI, 1999	291.7 - 331.3	52	-0.04	0.12	-0.30	0.27
MEI, 2000	365.3	5	-0.07	0.11	-0.19	0.09
Upper Reach						
MEI, 1998	278.9	4(3)	0.02	0.07	-0.05	0.09
Ayres, 1999	478.6	11(4)	0.29	0.07	0.15	0.40
MEI, 1999	205.3 - 256.6	100	-0.01	0.12	-0.61	0.23
MEI, 2000	258.0 - 291.7	41	-0.01	0.15	-0.65	0.33

(1)All points on Ketchup Island

(2)Data cover lower 1,430 m of reach, only

(3)All points on Suzy Island

(4)Data cover lower 3,690 m of reach, only

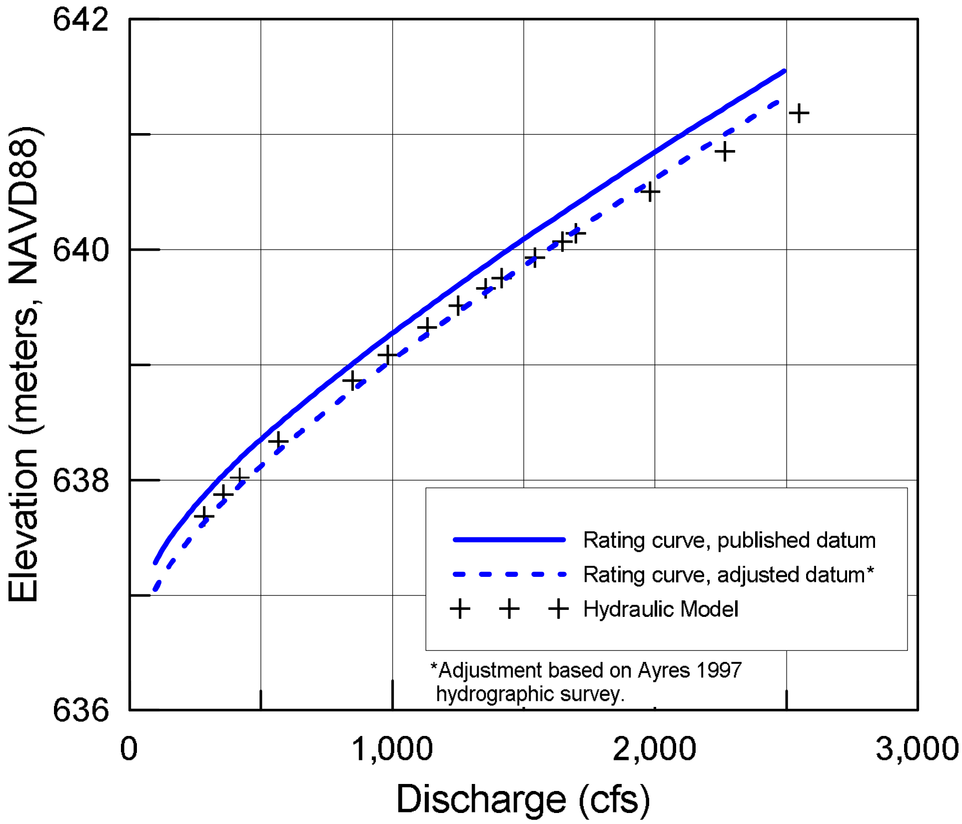

Figure 4.17 Comparison of the USGS rating curve for the Snake River at Weiser gage and the predicted water-surface elevations from the HEC-2 hydraulic model.

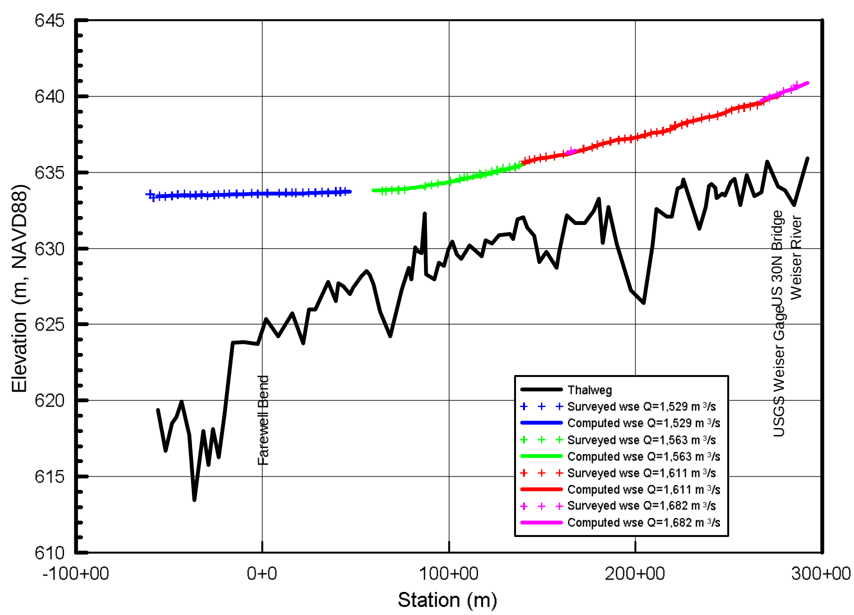

Figure 4.18 Comparison between the measured and predicted water-surface elevations in the downstream section of the Lower model for a range of flows from 1,529 m^3/s to 1,682 m^3/s.

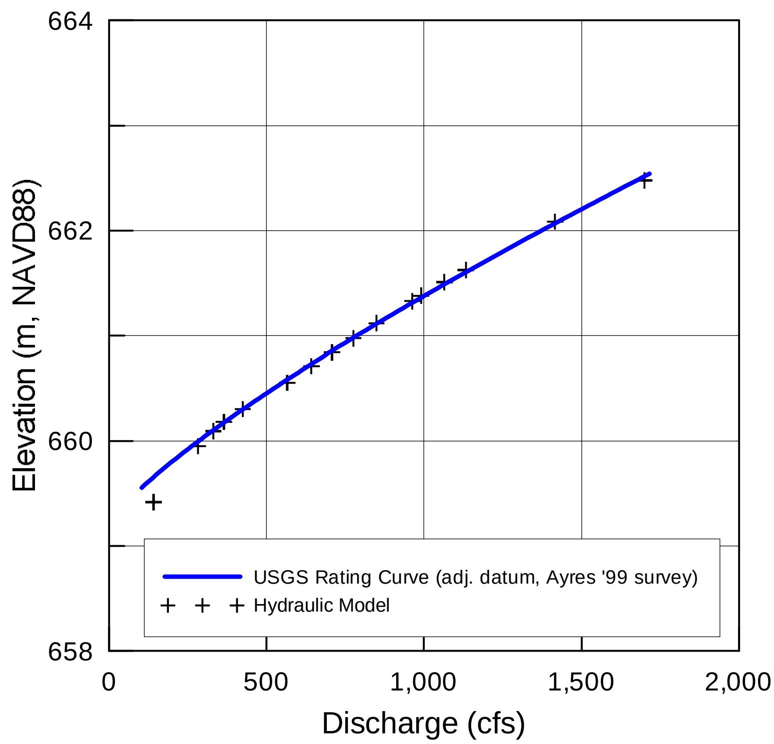

Figure 4.19 Comparison of the USGS rating curve for the Snake River at Nyssa gage and the predicted water-surface elevations from the HEC-2 hydraulic model.

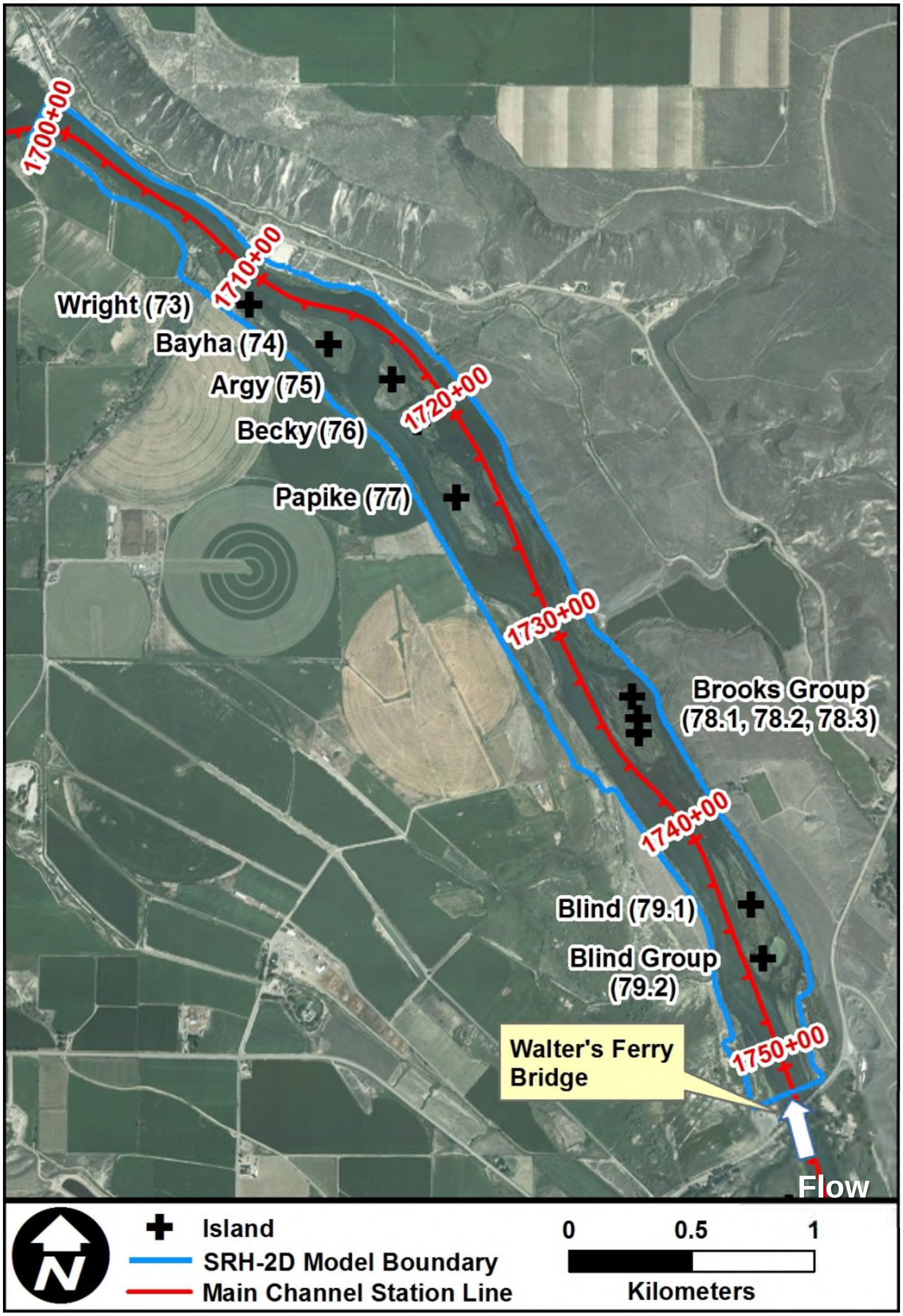

Figure 4.20 Extents of the Walters Ferry subreach and SRH-2D model.

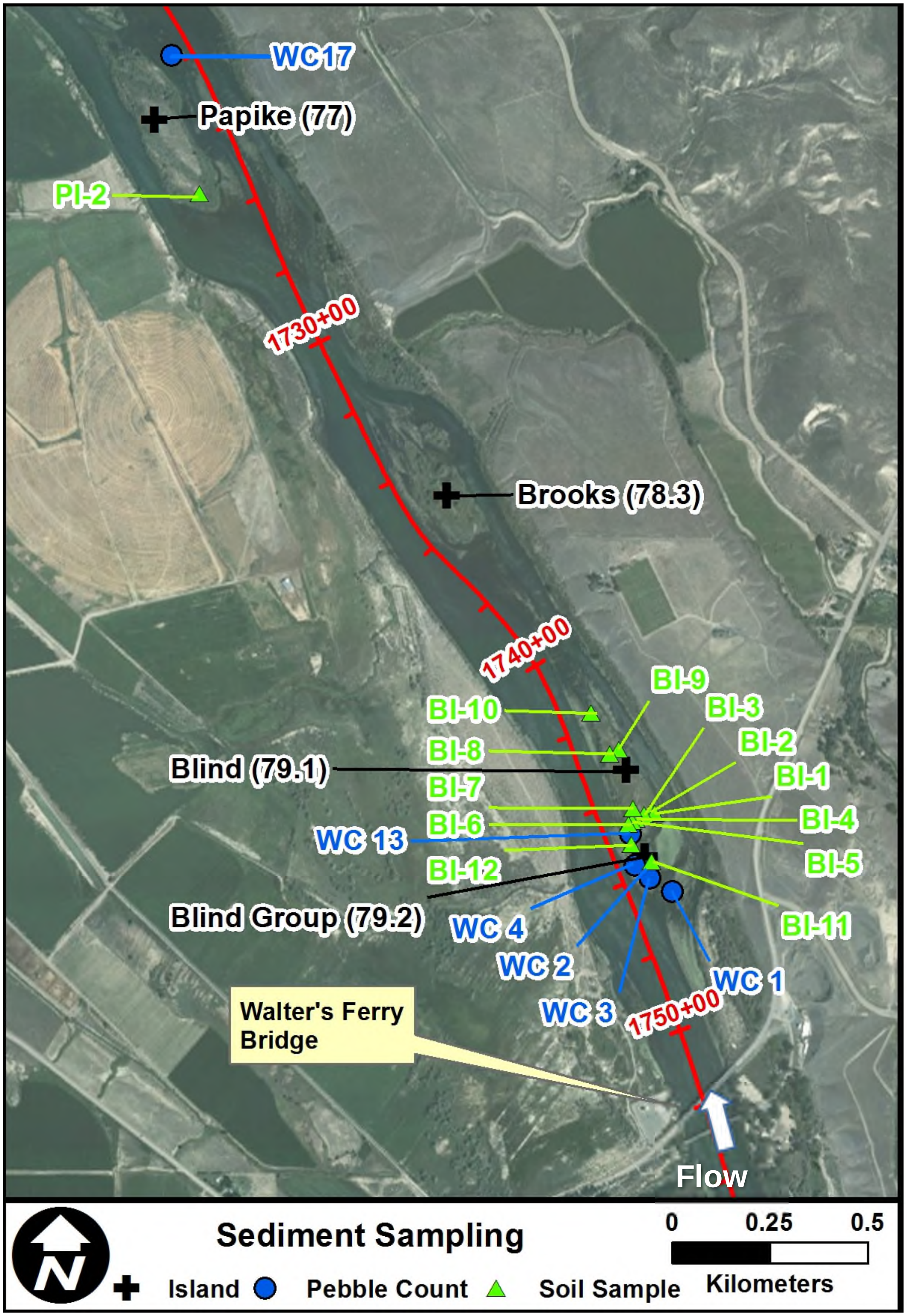

Figure 4.21 Walters Ferry sediment sampling location.

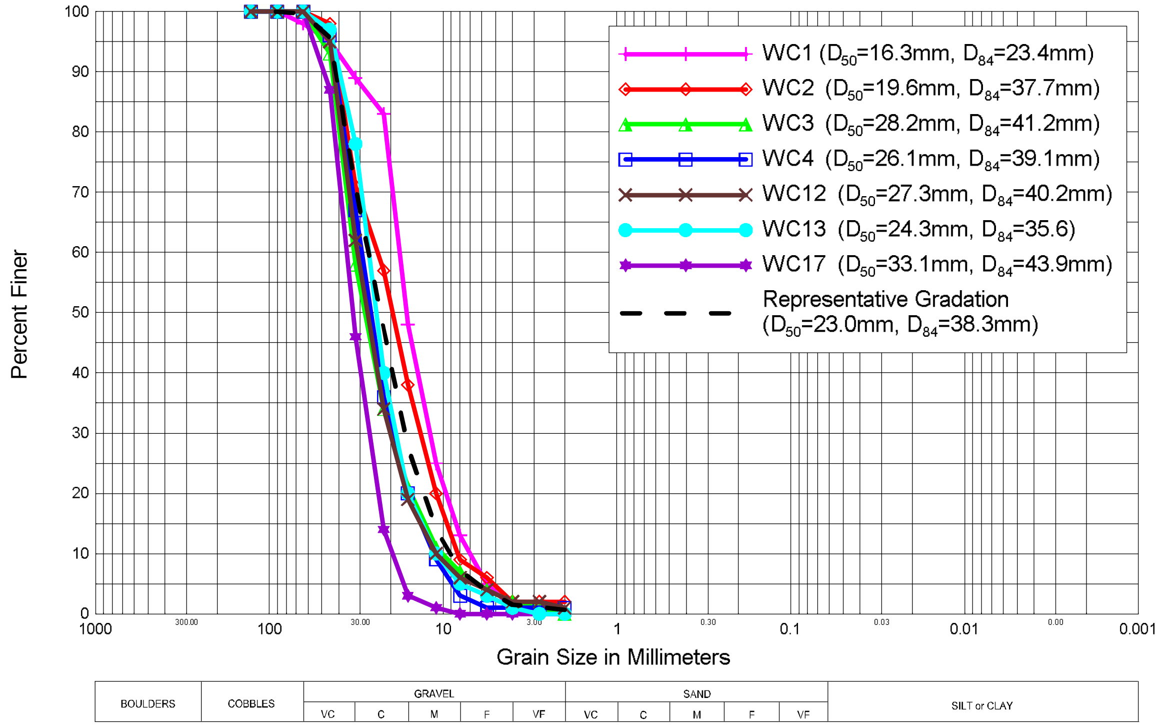

Figure 4.22 Wolman count measurements collected in the Walters Ferry reach in 1997.

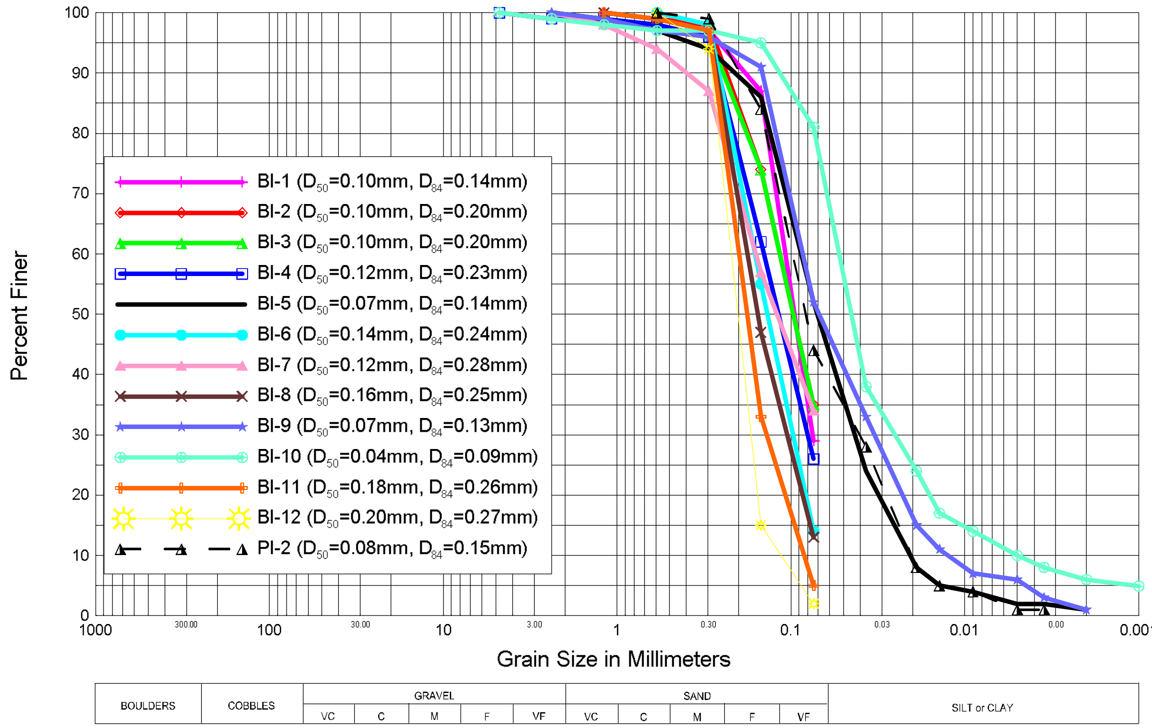

Figure 4.23 Soil samples from Papike and Blind Island.

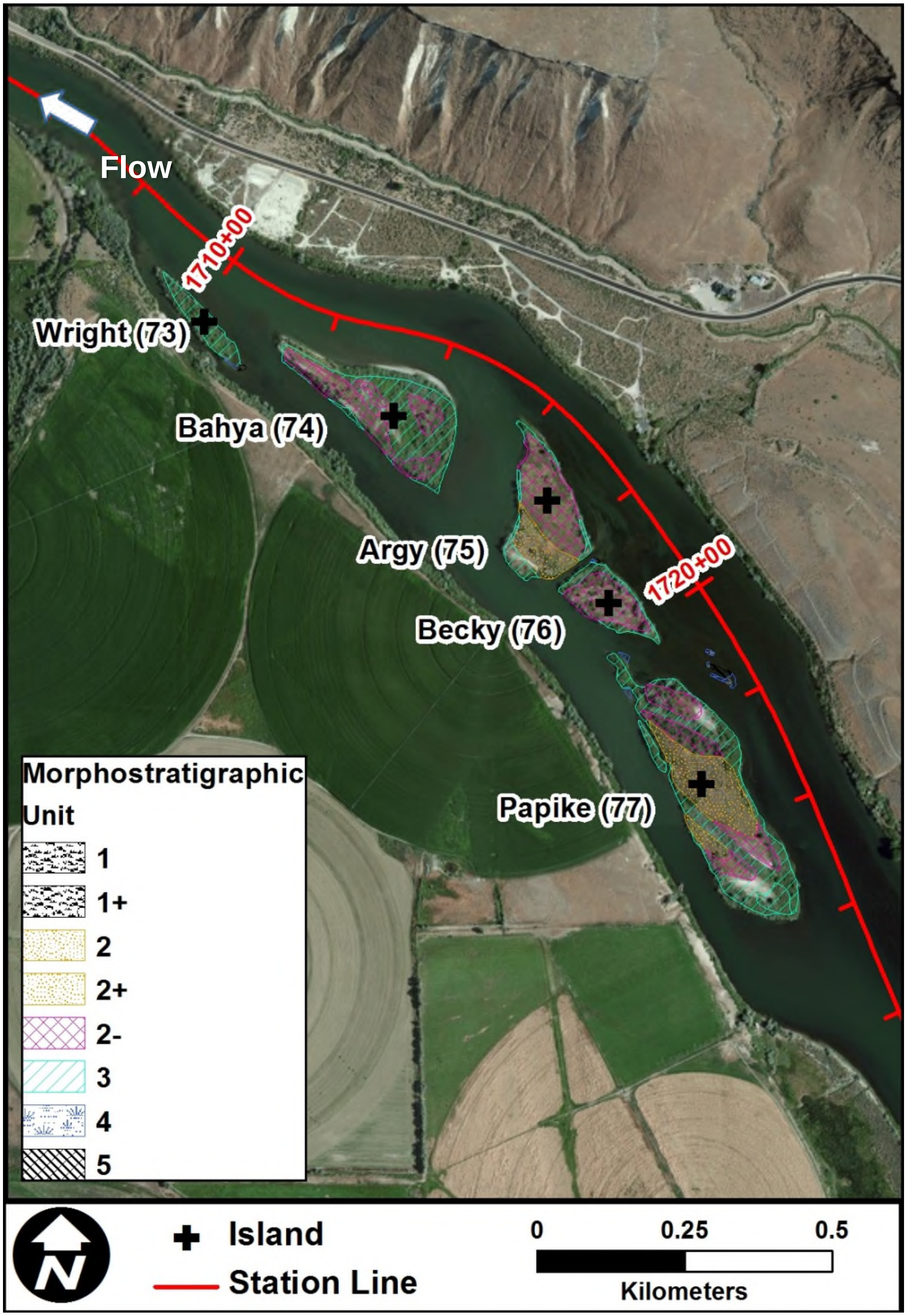

Figure 4.24 Morphostratigraphic mapping of the downstream portion of the Walters Ferry reach. Mapping conducted by Othberg and Fosberg (2001).

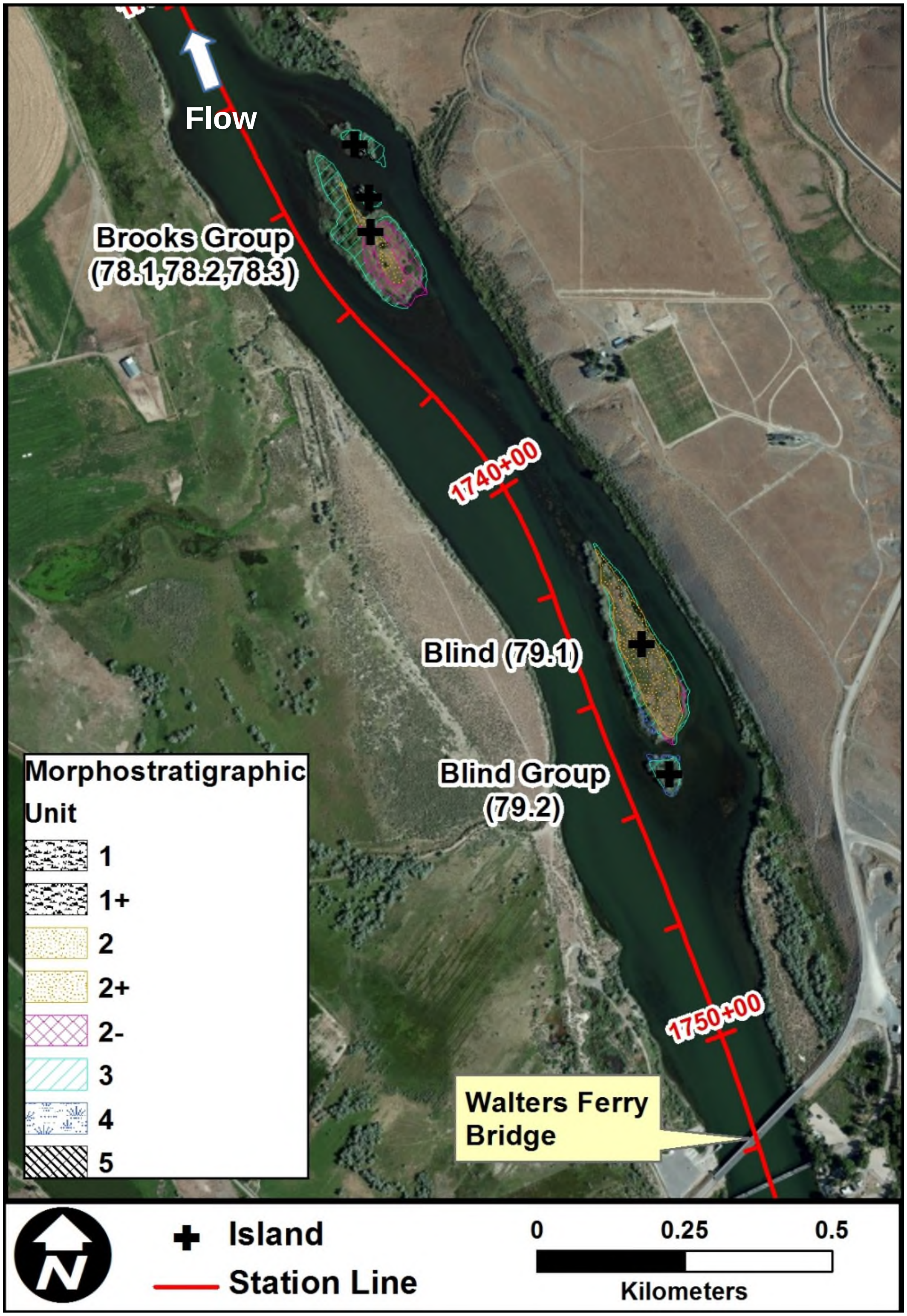

Figure 4.25 Morphostratigraphic mapping of the upstream portion of the Walters Ferry reach. Mapping conducted by Othberg and Fosberg (2001).

Table 4.11 Soil Morphostratigaphic Units for Islands in the Walters Ferry subreach.

Island No.	Island Name	Core Morphostratigraphic Unit
73	Wright	3
74	Bayha	2-
75	Argy	2+
76	Becky	2-
77	Papike	2+
78.1	Brooks Group	3
78.2	Brooks Group	3
78.3	Brooks Group	2+
79.1	Blind	2+
79.2	Blind Group	3

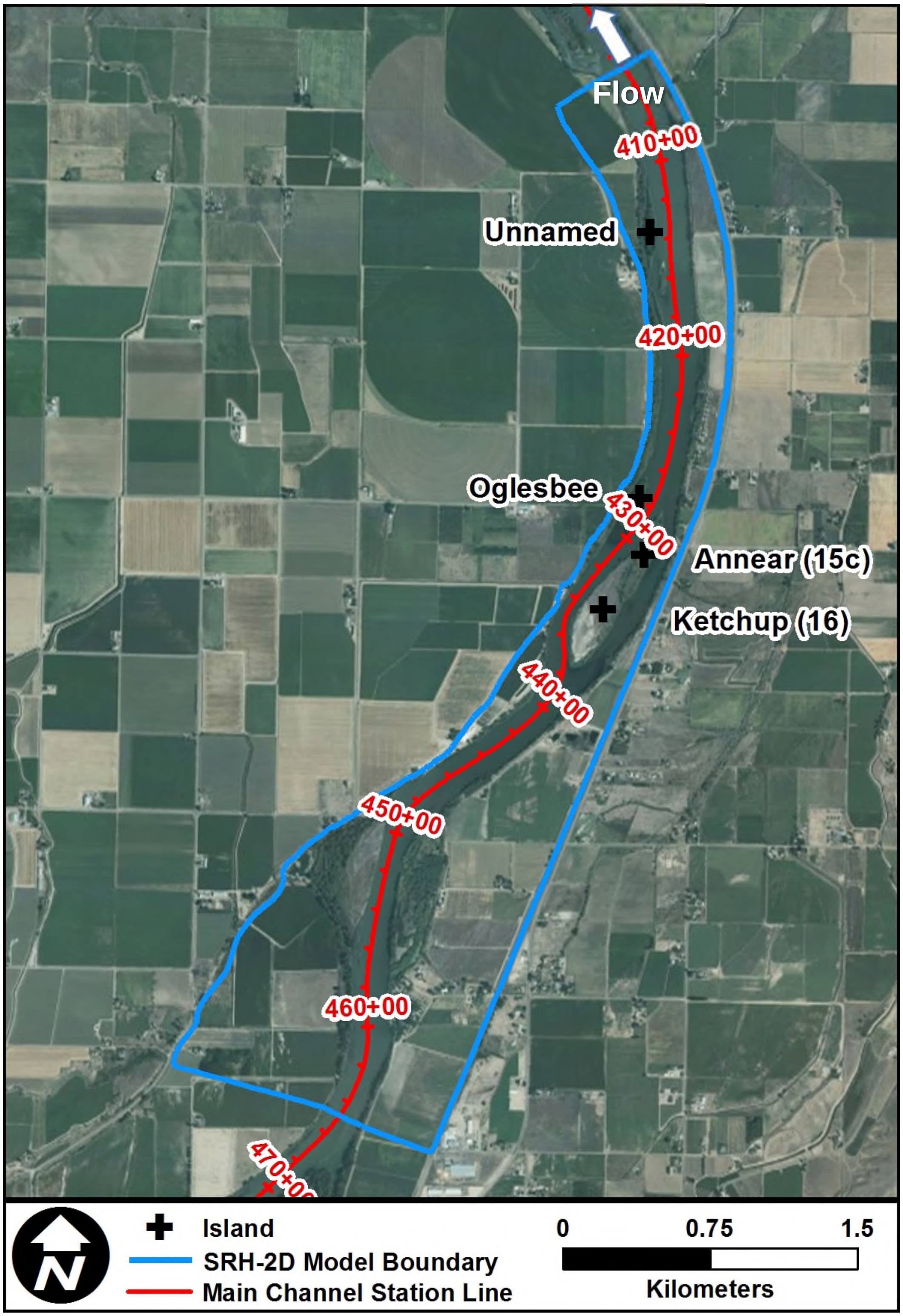

Figure 4.26 Extents of the Ketchup Island SRH-2D model.

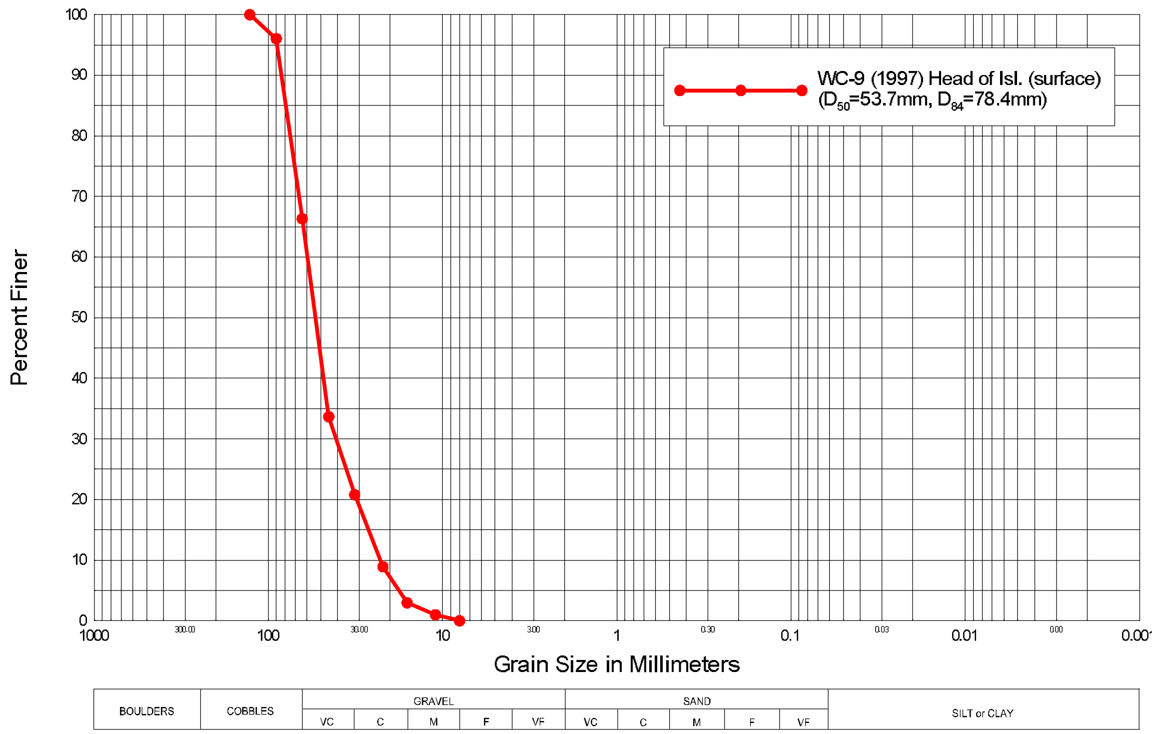

Figure 4.27 Sediment sample collected at the head of Ketchup Island.

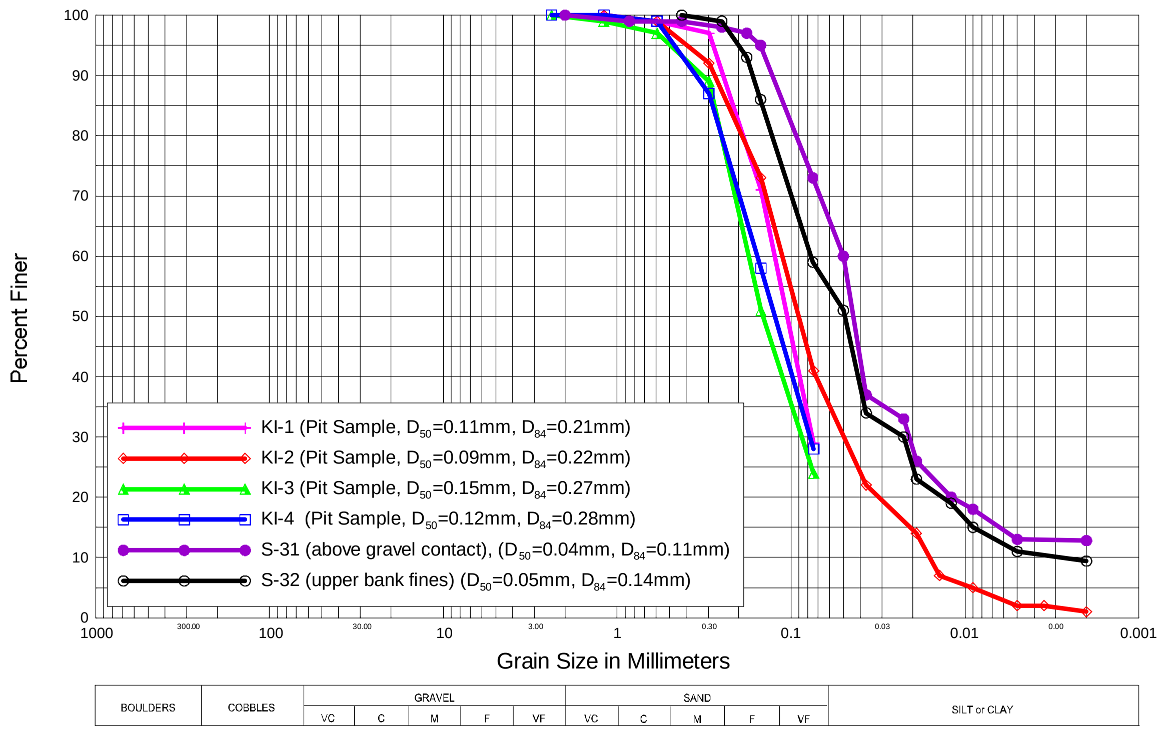

Figure 4.28 Sediment gradations measured at Ketchup Island.

Table 4.12 Summary of advantages and disadvantages of 1-, 2-, and 3-D models.

Model	Advantage(s)	Disadvantage
1-D	Reaches can be 100s of kilometers long and simulations times up to 100 years.	Cross-sectionally averaged results. Cannot simulate secondary currents, transverse movement, transverse variation or lateral diffusion.
2-D	Predict transverse flows, lateral diffusion	High data and computer requirements. Reaches typically less than 10 kilometers long and simulations times less than 1 year.
3-D	Predict secondary flows (e.g. helical flow), lateral and vertical diffusion	Extreme data and computer requirements. Reaches are typically less than 2 kilometers and simulation times less than 1 year.

Table 4.13 2-D models evaluated for the study.

Feature	2-D Sediment-transport Model		
	CCHE2D	MD_SWMS	SRH-2D
Model Type	Finite Volume	Finite Element	Finite Volume
Mesh Type	Curvilinear Grid	Curvilinear Grid	Unstructured Grid
Sediment-transport Equations	• Wu, Wang, and Jia (2000) • modified Ackers and White (Proffitt and Sutherland, 1983) • modified Engelund and Hansen (Wu and Vieira, 2000) • SEDTRA module (Garbrecht et al., 1995)	• Engelund-Hansen (1972) • Wilcock and Kenworthy (2002) • Yalin (1963)	• Engelund-Hansen (1972) • Meyer-Peter Müller • Parker (1990)

.

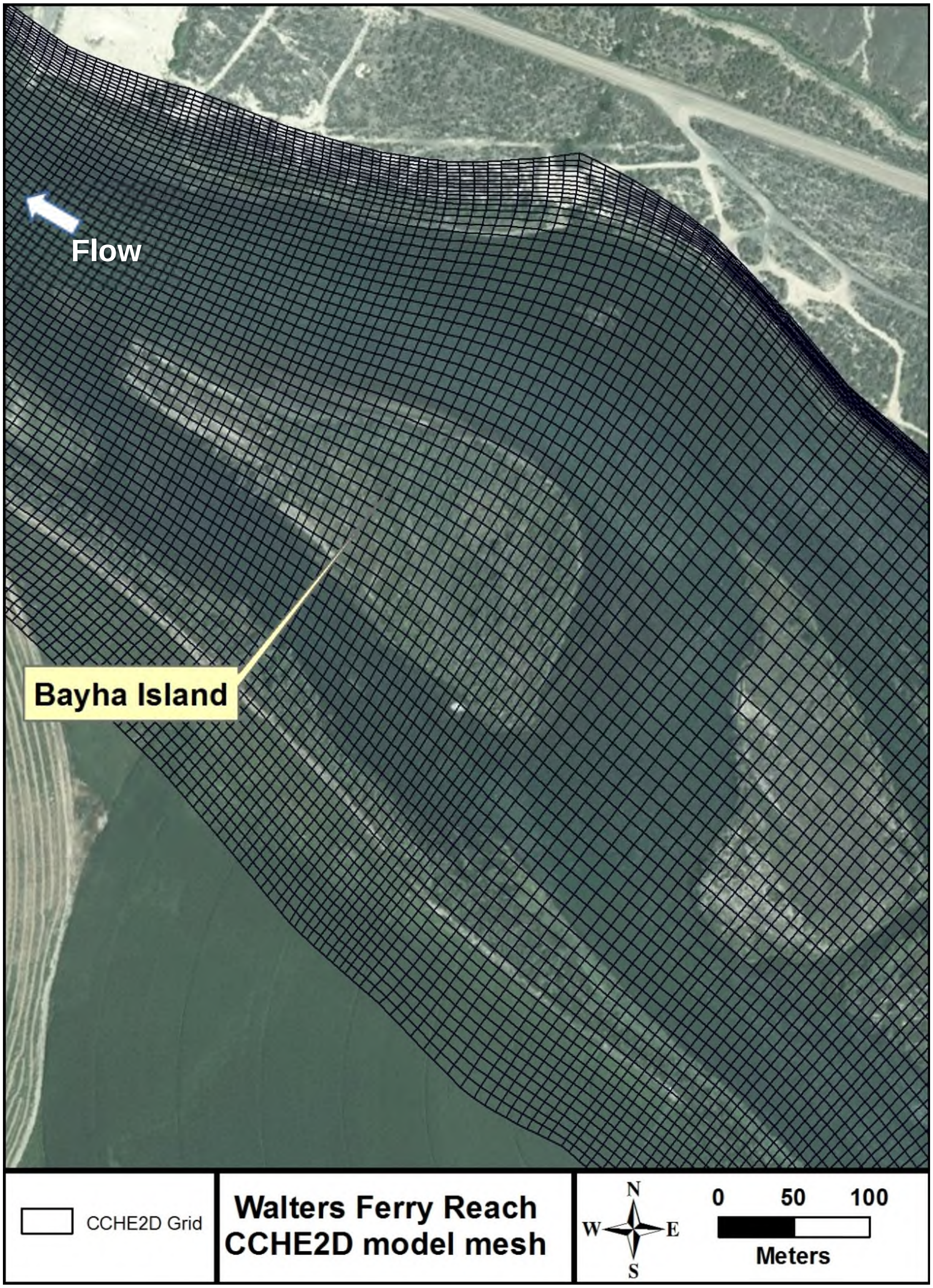

Figure 4.29 Close-up view of the CCHE2D curvilinear mesh of the Walters Ferry reach.

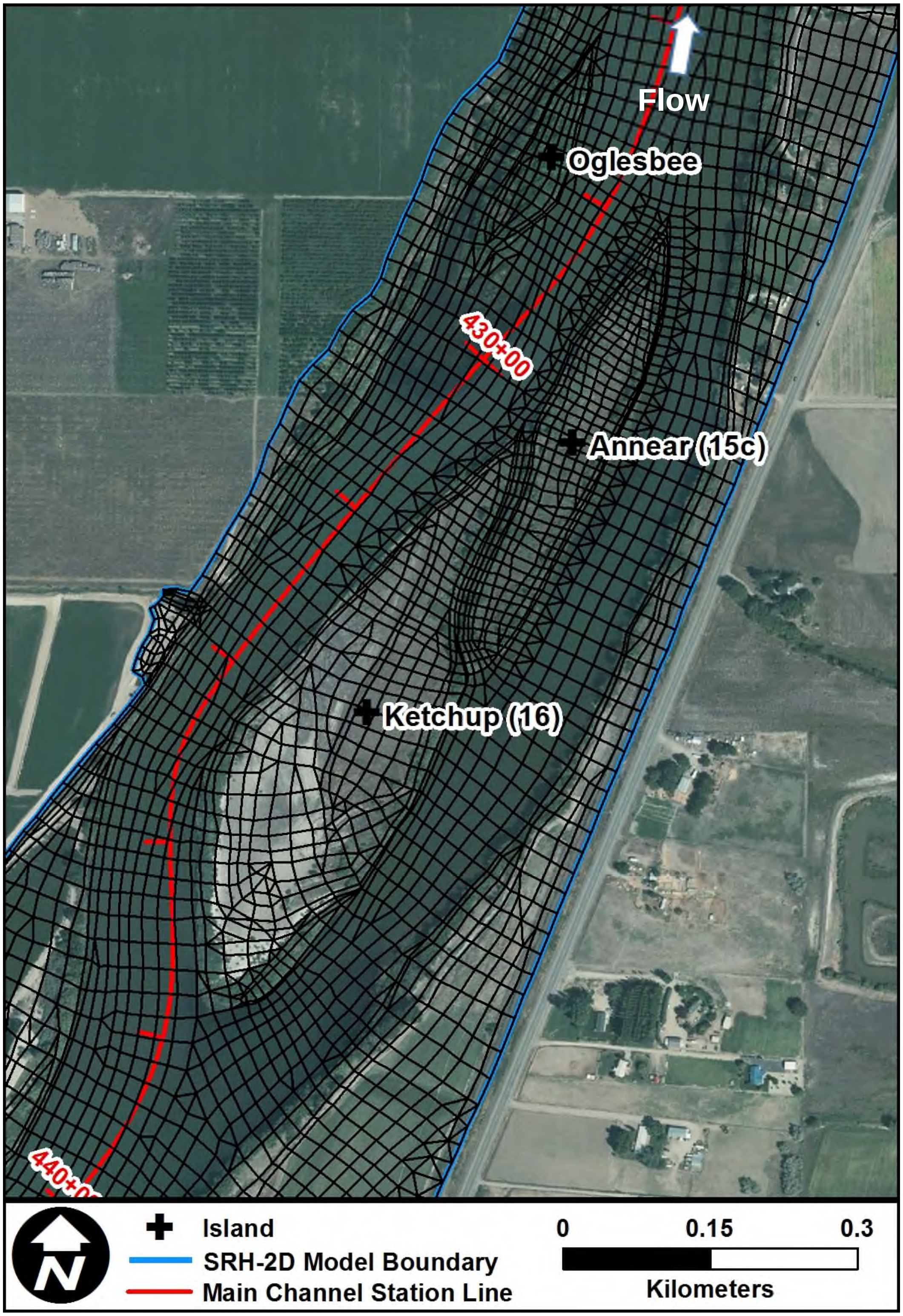

Figure 4.30 Close-up view of a portion of the Ketchup SRH-2D model around Ketchup and Annear Islands.

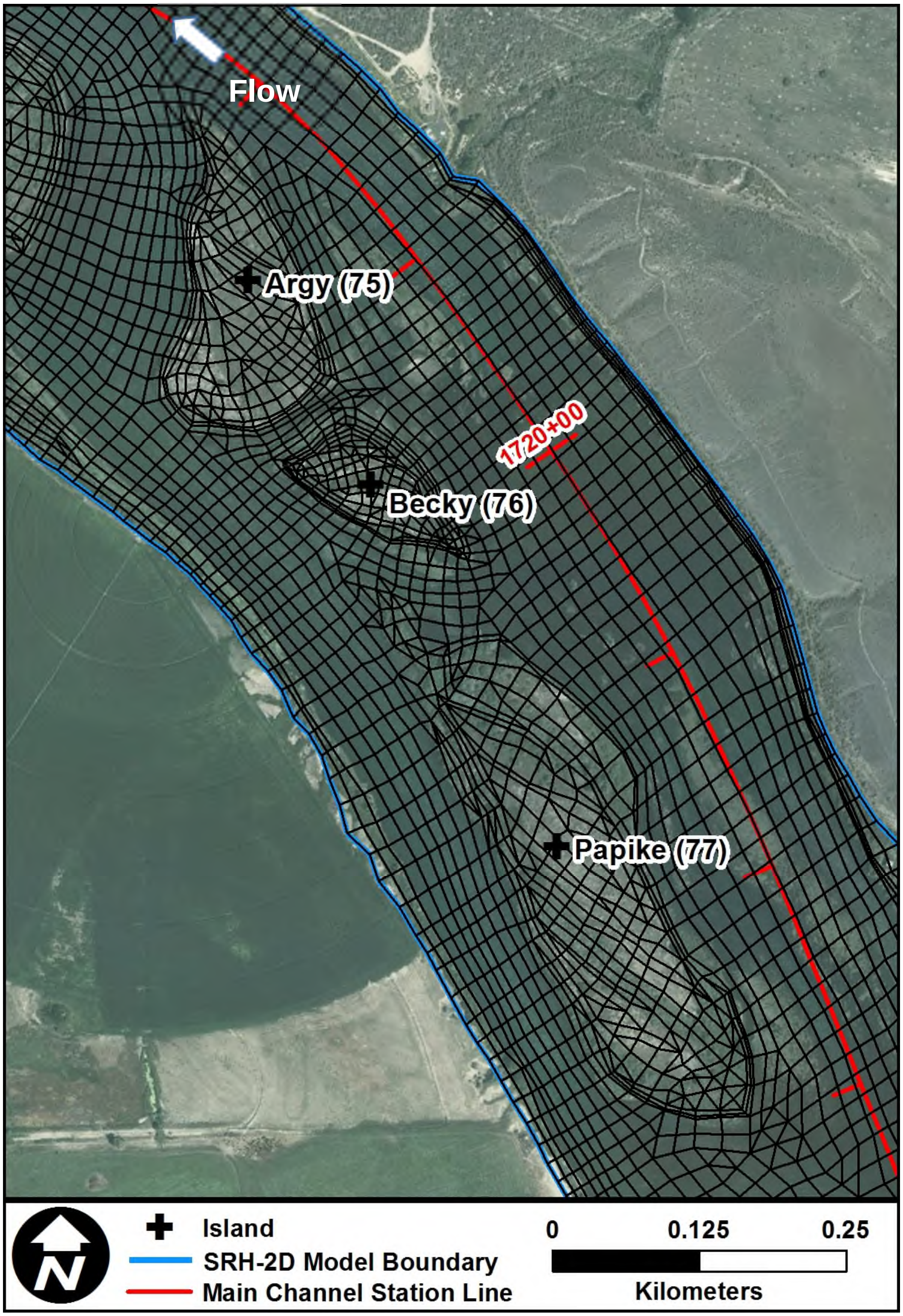

Figure 4.31 Close-up view of a portion of the Walter's SRH-2D model around Argy, Becky and Papike Islands.

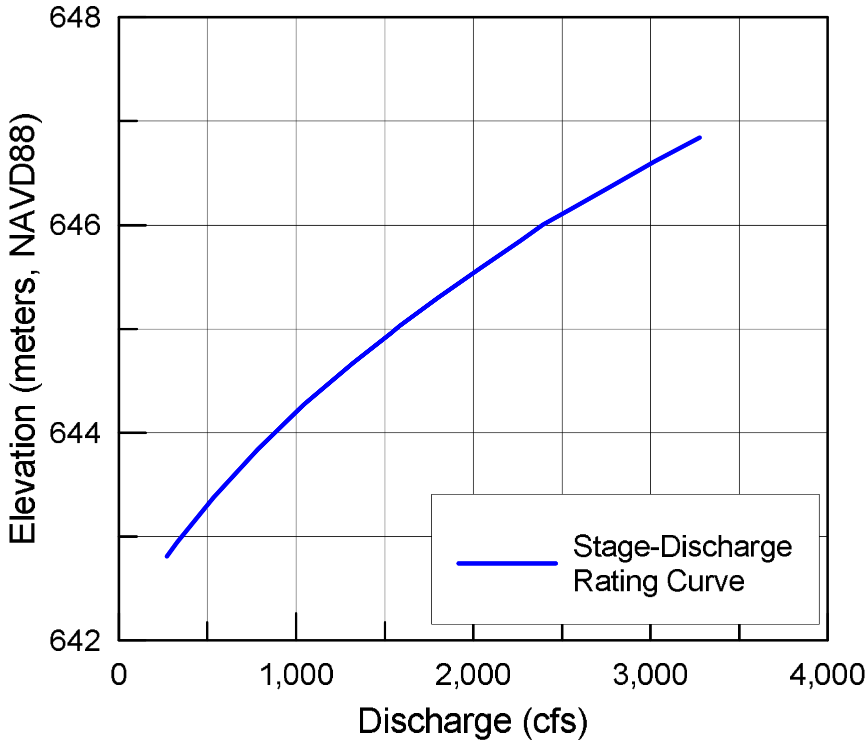

Figure 4.32 Stage-discharge rating curve applied to the 2-D model for the Ketchup model.

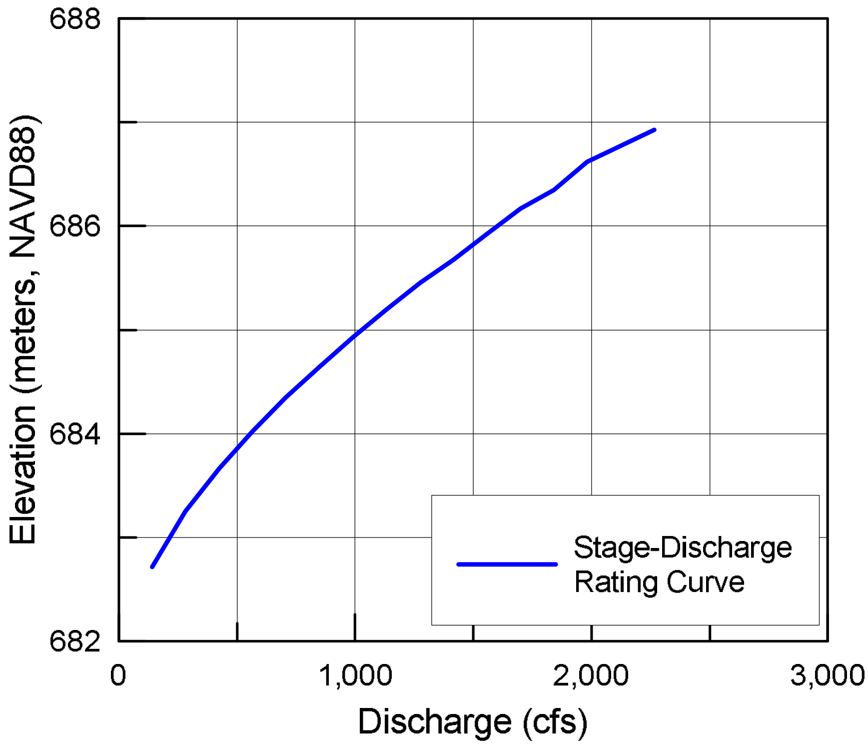

Figure 4.33 Stage-discharge rating curve applied to the 2-D model for the Walters Ferry model.

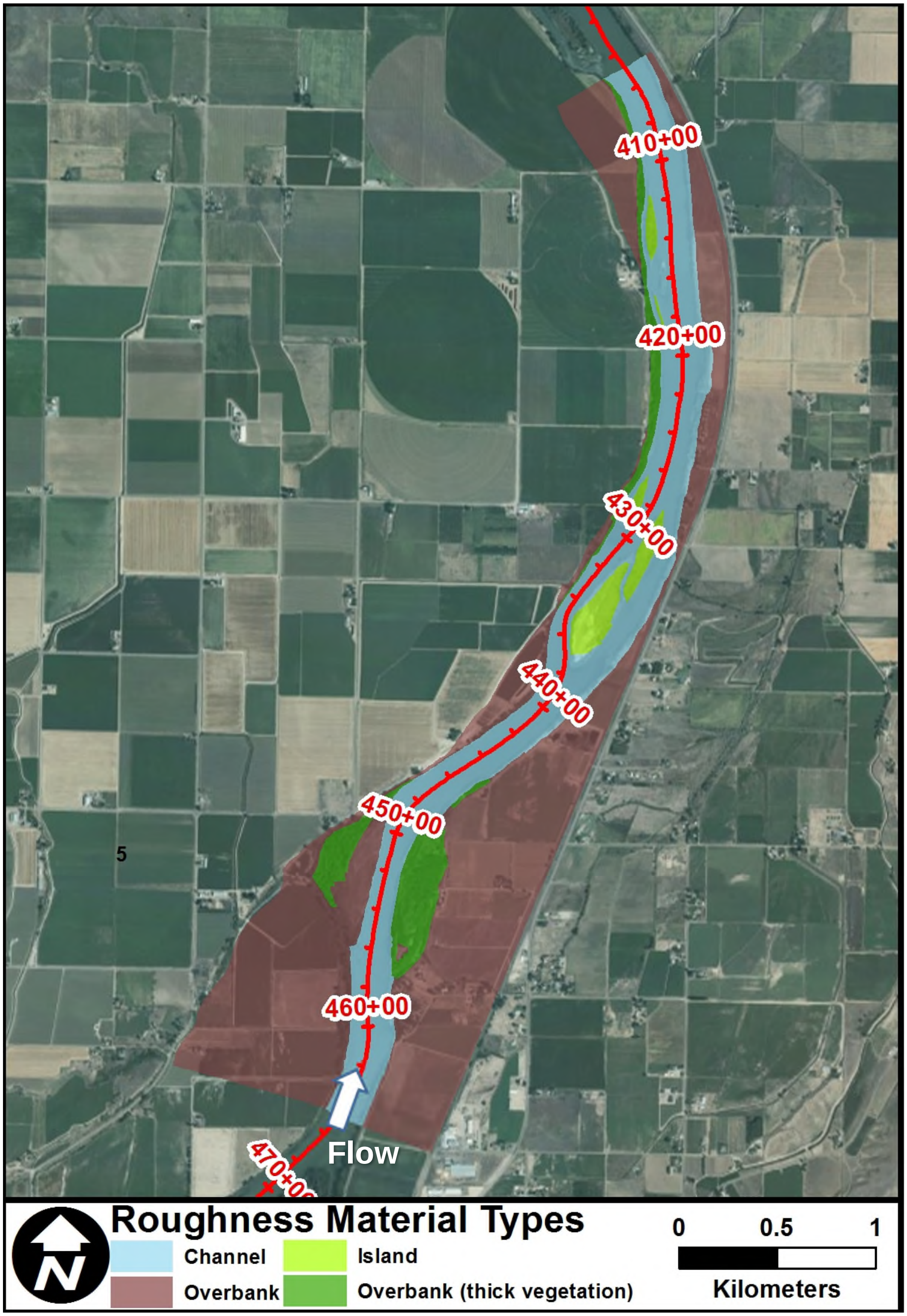

Figure 4.34 Distribution of the material types used to define the Manning's *n*-values in the Ketchup model.

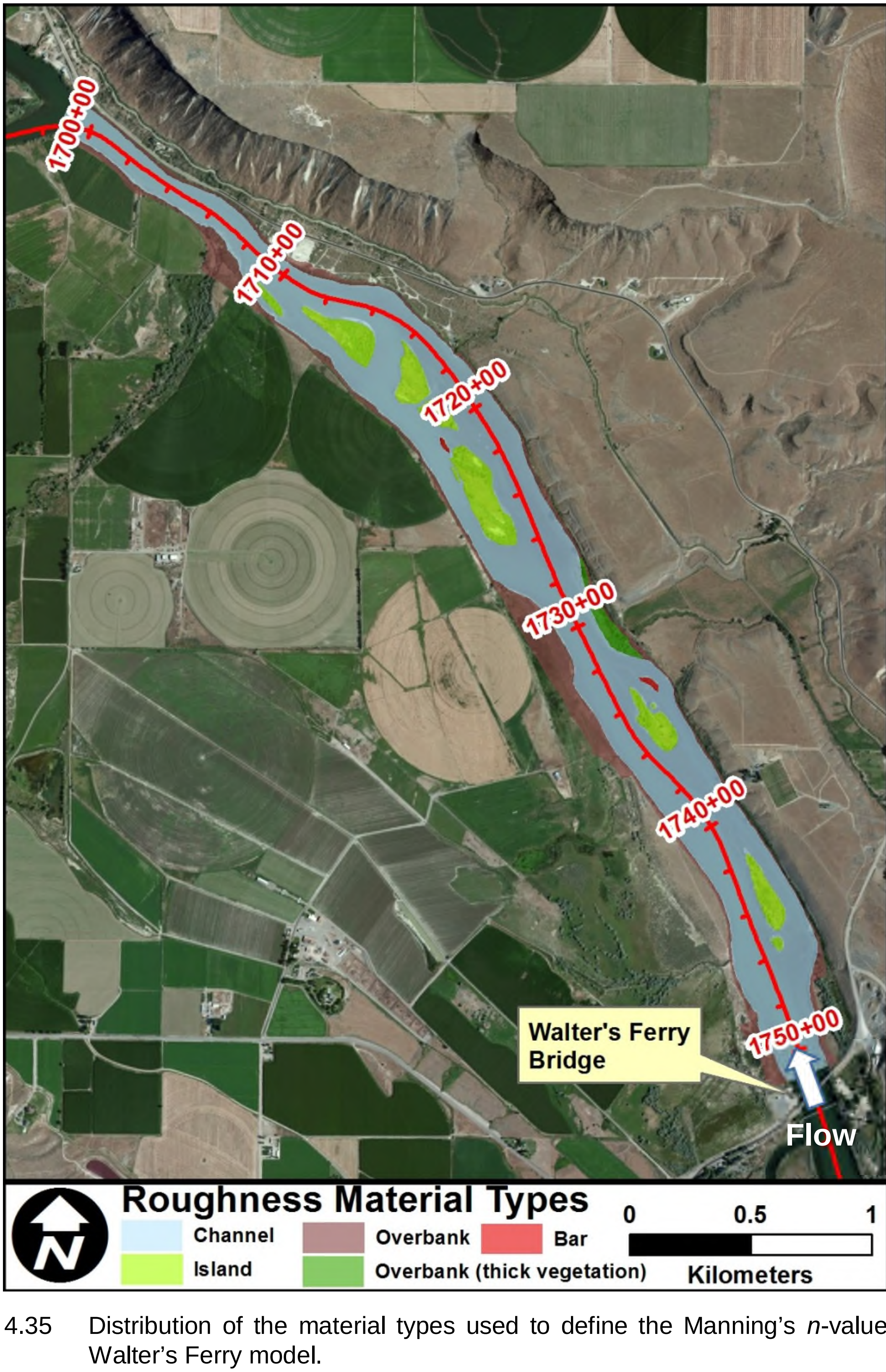

Figure 4.35 Distribution of the material types used to define the Manning's *n*-values in the Walter's Ferry model.

Table 4.14 Manning's *n*-roughness values.

Material Roughness Type	Model	
	Ketchup	Walters
Channel	0.023	0.025
In-channel Bar	0.04	0.04
Island	0.065	0.065
Overbank (light vegetation)	0.065	0.065
Overbank (thick vegetation)	0.1	0.1

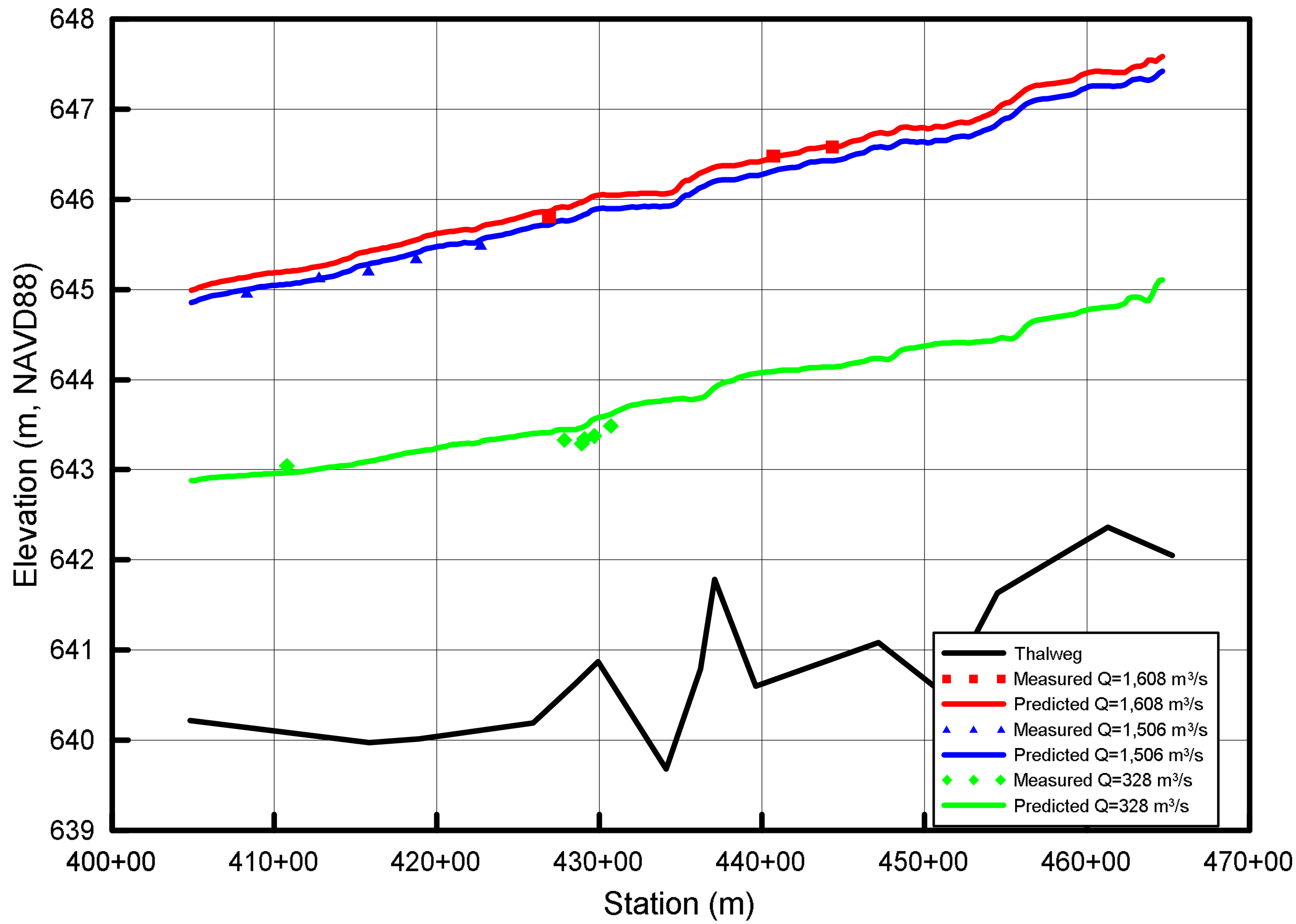

Figure 4.36 Comparison of the predicted water-surface profiles and measured water-surface elevations in the Ketchup model at 328, 1,506 and 1,608 m^3/s.

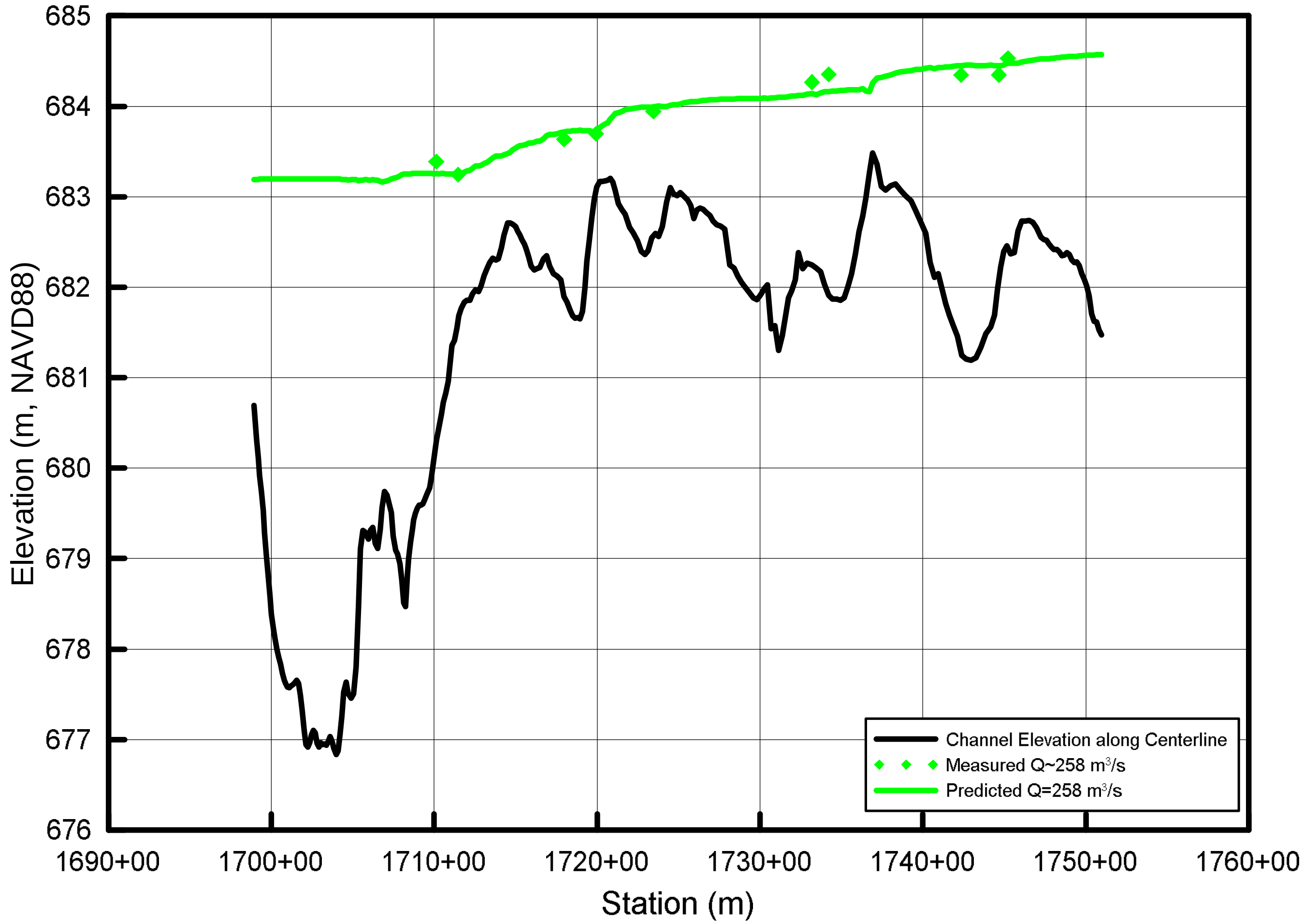

Figure 4.37 Comparison of the predicted water-surface profiles and measured water-surface elevations in the Walters Ferry model at 257.7 m^3/s.

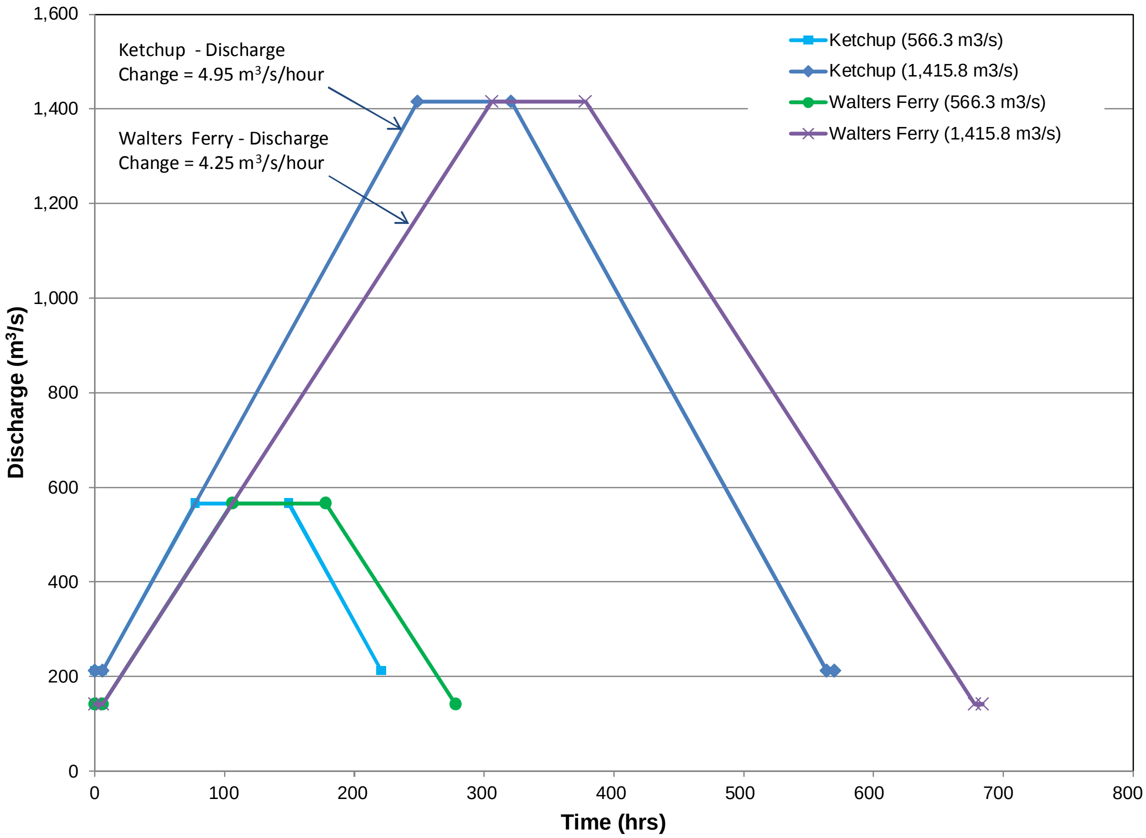

Figure 4.38 Examples of representative flood hydrographs developed for the Ketchup and Walters Ferry 2-D models.

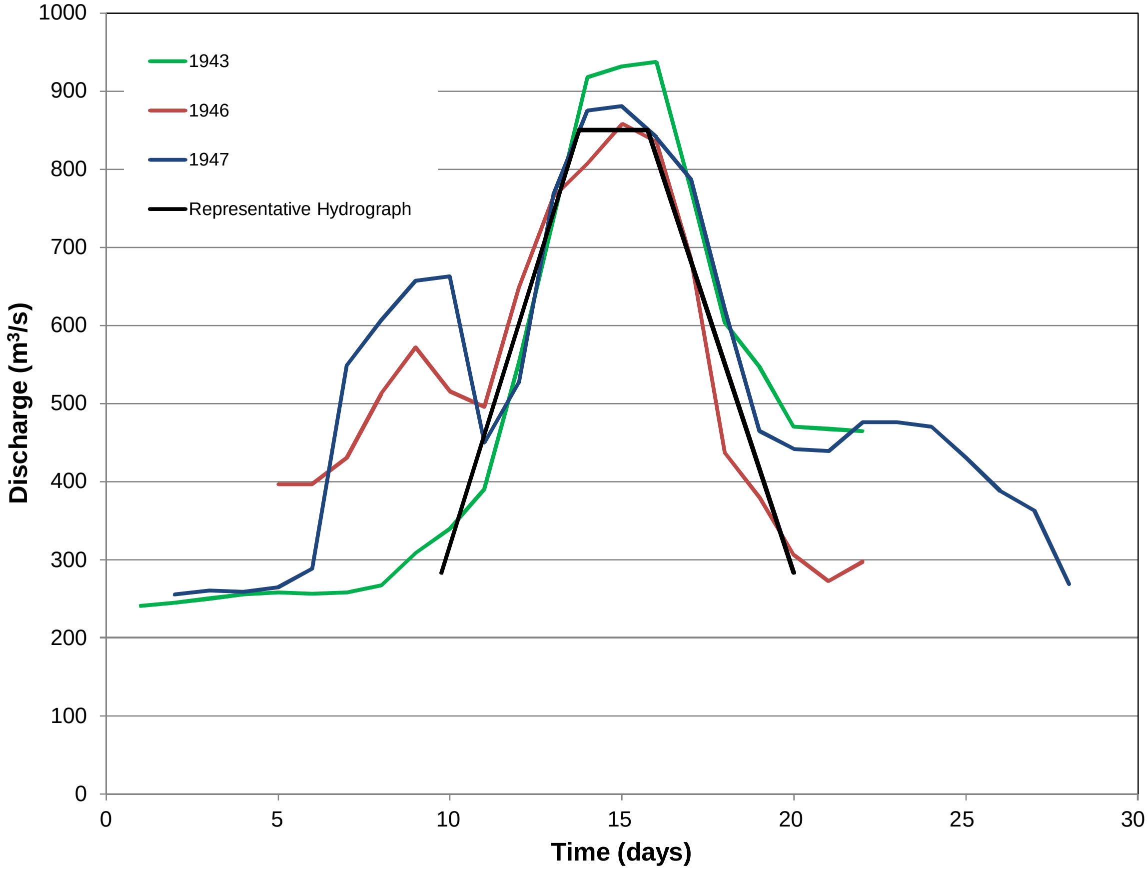

Figure 4.39 Comparison of the 850 m^3/s representative hydrograph for the Walters Ferry reach with the 1943, 1946 and 1947 peak flow hydrographs measured at the Murphy gage (USGS Gage No. 13172500).

5. Middle Snake River Island Dynamics

5.1. Historical Photo and Map Analysis

A review of early maps and early aerial photography with the 1997 aerial photography shows the dynamic nature of the islands within the MSR. In the early USGS topographic maps (c. 1894-1906), many of the larger islands could be identified, but most smaller islands could not be clearly identified. The 1938/1939 aerial photos are the earliest available and have continuous coverage from the modern Brownlee Reservoir to upstream of Sign Island. They provide clear evidence for the presence or absence of islands, and they provide an excellent benchmark for island formation over the approximately 60-year period from 1938/1939 to 1997.

Table F.1 summarizes the islands identified in the early USGS maps, the 1914 USGS Water Supply Paper and the 1938/1939 aerial photography. The following naming convention was applied in developing Table F.1. If no historic map of the island was available, the island was identified as No Map. Islands that could not be identified on the older maps were listed as NP for Not Present. Islands that are in areas where the locations and shapes of the islands are different from the present configuration are listed with a question mark (?), since their identity is unclear. Those that are clearly present are listed with a P. Islands determined to be still forming are listed with an “F”. Appendix A1 lists the 300 identified islands and their locations and Appendix A2 shows their location on topographic maps.

In addition, the historical photo analysis showed a new island forming in the downstream portion of the Ketchup study reach. A comparison of a sequence of aerial photographs from 1994 to 2010 shows the changes in geometry and influence of vegetation over the period.

5.1.1. Early USGS Topographic Maps

Of the 300 listed islands in the MSR, 180 are not present and 53 are probably present in the early USGS mapping. The rest are either outside the early map coverage area (21 islands) or their identity is uncertain.

To show the erosional and depositional activity along the reach, the early USGS topographic maps are compared to current 7.5-minute topographic maps. Although it is possible that smaller islands would not have been mapped at the scale of the older maps, the changes in island size and location, the presence of new islands, the absence of previously mapped islands, and changes in the river channel itself, attest to the dynamic state of the islands along the MSR. This is especially evident downstream from the Boise River and Owyhee River confluences.

For the Weiser, South, ID-OR map area, the older maps show Patch and Long Island, but Goat Island (10) or the smaller adjacent islands are not shown (Figure B.5). The Smith Island (11.1-11.3) reach showed one very large island located due south of Island 11 that is now part of the floodplain (Figure B.6). Several islands are shown on the older map that are not now present: one in the vicinity of Nadeau, one upstream of Larson Island (14), one small island near what may be either Sundstrom Island (15) or Grafton Island (Figure B.7); Buttermilk Island is not shown. Resch, Pruitt, Ketchup (16), and Annear (15c) are also not shown on the map (Figure B.8).

In the Payette, ID-OR map area, the older map showed Pool, Scarecrow (18), and Duncan Islands, but island shapes and channel locations on the early maps were different from modern maps (Figure B.9). The confluence areas of both the Payette River and the Malheur River were entirely different from today, and it is not clear if Banks and Little Banks (18f.1) Islands were mapped, since the geometry is so modified (Figure B.10). Depending on which features are used to line up the channel, the Ontario, Welsh, and Johnson Island Group could have been part of the early floodplain, with the possible exception of one large island, which could be either Ontario or Welsh Island (Figure B.11). Ramey Island, now part of the floodplain, was shown as a fully detached island (Figure B.12).

The old map of the current Nyssa, ID-OR map region displayed the large Morton/ McPhersons's island, and also displayed a downstream island (near Sta 670+00) that is now part of the floodplain (Figure B.13). Half of Perrin Island was present, but not Crow Island (18n.1). Gamble Island was shown as four islands, but Beaver Island (19) was not present. There were also two islands at the approximate current location of P-1, and it is unclear whether they are both part of the modern island (Figure B.14).

The current Parma, ID-OR map shows only the corner of Bridge Island. The older map showed Bridge Island, and a possible portion of the main island in the Cable Island group (23.4) (Figure B.15). This could also have been the center of a modern bend. Two small islands were present in the general location of the Quail Islands (20 and 21) an area that currently has three islands (Figure B.15).

The area around the confluences of the Boise River and the Owyhee River with the Snake River, shown on the current Owyhee, OR-ID map, has changed dramatically. Although the two large islands downstream of the confluence (Bridge and Gold Islands) were shown on the older maps, other channel and island geometry is very different (Figure B.15). Bridge Island was mapped as two islands on the older map, and Prati Island may have been part of Bridge Island. No islands existed in the western branch channel around Bridge Island. Heron Island (29) was present southeast of Gold Island, but to the southwest, the modern Big and Little Cottonwood (27 and 28) and Squatters (26) Islands were shown as one island. Upstream from the confluence, the Boise (31.1-31.3) and Barney (9.1-9.3b) groups of islands were not present on the older maps. Farther upstream, Goose Egg Island (33) was shown, but upstream of Goose Egg Island (33), the Big Willow (12-12b) and Billy Goat (34.1-34.4) island groups were not mapped (Figure B.16).

Upstream from this confluence area, the changes are more subtle. On the modern Adrian, OR-ID map area, all of the major islands are shown on both sets of maps, including Main & East Shack (35), Rhubarb (36), Adrian (37), Suzy (38), Airport (39), Peachtree, Grassland and Border (Figure B.17). However, the Tule Group (39a-39a.2) was not present (Figure B.17). The Wilder, Idaho, map area shows few major changes: two small islands were present in the general location of the Channel Island Group (39b, 39d); small islands such as Avocet (40a.1) were not mapped; and a channel shift to the northeast at Succor Creek was shown on the older map (Figure B.18). The older Homedale, Idaho, map area showed no Homedale/Rabbit Island Group (41-43.6b), and upstream of this group an island was shown that does not exist today (Figure B.19).

On the Marsing, Idaho map area, most change has occurred in the chain from Tiny (50) to Poison Ivy (55) Islands (Figure B.20). On the older maps, it is unclear if Tiny Island (50) was shown, Gosling Island (51) was composed of two small islands, Jensen Island (52) was not shown, Cigar Island (53) was mapped as a curved island and upstream of the present location, Marsing (54) was not shown, and Poison Ivy (55) Island was mapped as two islands. This may be important in reconstructing island evolution for long, narrow islands, because this reach is today broad and shallow with minor constrictions and very long, narrow islands. Also, while Center Island (58) was present on the older maps, there appears to have been a subtle meander shift on the Snake River between Poison Ivy (55) and Center (58) Islands.

The older maps in the Opaleen Gulch, Idaho area are difficult to match with modern maps. One large island was mapped that may or may not be Fruit Island (the position is wrong), and the Dilly Group (59 and 60) and smaller islands (58a-58e) were not mapped, unless they were all included in that large island (Figure B.21). Cottontail Island (61) could be represented on the older Opaleen Gulch, Idaho, and Givens Hot Springs, Idaho, map areas, but it is offset from its modern position. Upstream, the older map of Fogler’s Island (62) showed a mid-channel island (not the current bank-attached island), and in the area of Blackburn (63), Dredge (64), and Goldeneye (65) Islands, it is somewhat difficult to reconcile the older and current maps (both due to changes in location and island shape), especially for Blackburn Island (63). The older maps showed an island in the general area of Raccoon Island (66), which could be Raccoon or Stanley (64a) Island. On the older maps, only the larger islands in the Hermit / Rippee Group (67-68.5) were present, and their shape and location were shifted. The Ware Group (69-72) was also present, but distorted (Figure B.22).

The modern chain of islands from Wright to Papike (73-77) looks much different on the old maps (Figures B.22 and B.23). In the general location of the modern Papike to Wright chain (73-77), there were three large islands on the older maps, but the shapes do not match the current islands. The upstream-most island overlapped Papike Island (77); Becky (76), Argy (75) and Bayha (74) Islands were located in the modern river channel; the entire channel was shifted; and Wright (73) did not exist. The final portion of the maps upstream from this chain shows only minor changes. Present in both maps were Big Rocky (83), Noble, Guffey (86), Rail (87), and Sign (88) Islands. Other islands, such as Little Rocky (84) and Menning (85) Islands, were not present in the older maps, while islands were shown near Menning Island (85) on the older maps that are not present in the recent topographic mapping.

5.1.2. 1914 Water Supply Paper

The maps from USGS Water Supply Paper 347, published in 1914, cover the MSR from Sign Island (88) at the upstream end to Raccoon Island (66) at the downstream end, and they were compared to 2010 topographic mapping of the same area. This comparison was a simple visual comparison, and the results are compatible with the findings for the earlier maps, with a few exceptions. The major islands or island groups were present: Raccoon (66), the Hermit/Rippee Group (67-68) (Figure C.1), the Ware Group (69-72) (Figure C.1), the Papike Chain (74-77), Brooks (78), Blind (79) (Figure C.2), Walters Ferry (80), Big and Little Rocky (83-84) (Figure C.2), Noble, Menning (85), Guffey (86), Sign (88), and Rail (87) Islands (Figure C.4).

The two islands in this group that were not present on the earlier maps were Menning (85) and Little Rocky (84) Islands. Several of the 1914 mapped islands showed different configurations from modern maps:

- Raccoon Island (66) was mapped as two islands (Figure C.1).
- Hermit Island (67) was present but had a different shape (Figure C.1).
- Two lower islands in the Rippee Group, 68.5 and 68.2, were smaller than at present, which shows that they were still forming (Figure C.1).
- Current Island (69) was present, but its shape has changed (Figure C.1).
- Fisher Island (70) was either not present or mapped as part of Ware Island (71) (Figure C.1).
- In the Papike Island chain, Bayha (74) and Becky (76) Islands display different shapes, and Papike Island (77) was mapped as two islands (Figure C.2).
- Brooks (78.3) Island had a different shape (Figure C.2).
- One small island was present on the downstream end of Big Rocky Island (83). This could have been Kim’s Island (82), Jim’s Island (81), or a downstream, low elevation extension of Big Rocky Island (83) (Figure C.3).
- Noble, Guffy (86), Rail (87) and Sign (88) are shown, but the smaller adjacent islands are not shown in the older maps (Figure C.4).

The smaller, lower elevation islands between Sign (88) and Raccoon (66) Islands are generally not found on the 1914 maps (see Table F.1). Although this map set did not cover the entire study reach, or even the area covered by the earlier maps discussed above, the 1914 data also give the impression of a moderately dynamic river reach where new islands were forming and older islands were eroding and changing form.

5.1.3. Aerial Photography from 1938, 1939 and 1943

Of the islands listed on Table F.1, 107 of the 300 islands were not present on the 1938/1939 aerial photographs, 62 were in the process of formation, five were questionable (they are located at the mouth of the Boise River) and 3 were located downstream of the aerial photograph coverage. In total, the 1938/1939 aerial photographs show 174 of the 300, indicating that 60 percent of the islands were forming or had not yet formed.

The 1938-1939 period is nearly midway between the date of the early USGS maps and the comprehensive 1997 aerial photographs and mapping that was used to develop the 1- and 2-D models. In 1938/1939, 174 of the 300 or 60 percent of the islands were forming or had not yet formed.

5.1.4. Summary of Topographic and Aerial Photograph Review

The early UUSGS topographic maps (c. 1894-1906) showed that many of the larger islands and island groups in existence today could be identified on these maps, but smaller islands could not be clearly identified. Many of the island groups and chains showed significant variation between the early and current maps. Although some of this “change” could be due to early mapping techniques (due to the date on which the maps were made, and the technology available then), the comparisons indicate there has been significant erosional and depositional activity within the MSR during the last century.

The 1938/1939 aerial photography clearly shows both the larger and smaller islands along the reach. A comparison between the 1938/1939 and 1997 aerial photography shows clear evidence of the growth and erosion of islands along the study reach. The comparison of early maps with the review of early aerial photography, both show the islands are dynamic along the MSR.

In the early USGS mapping, 53 of the 300 islands were probably present, 180 were not present, and the rest are either outside the early map coverage area (21 islands) or their identity is uncertain.

Half a century later, in the aerial photographs, 123 islands were present, 107 were not present and the remaining 70 are either outside the early map coverage area (3 islands) or their identity is uncertain.

In summary, the entire length of the MSR shows activity (i.e., erosion of older islands no longer present, formation of new islands where none were mapped before, reworking of island chains to form new configurations, and shifting and reworking of the MSR channel itself). The persistent pattern of change along the entire study reach strongly suggests an active channel with forming and reforming islands.

5.1.5. Time-sequential Aerial Photographs of New Island Forming

The review of the historical photographs showed an unnamed island (Sta 416+00) forming in the Ketchup Island study reach. A time-sequential series of Google Earth aerial photographs illustrate the changes in island geometry and vegetation between 1994 and 2011 (Figure 5.1 through Figure 5.8). The unnamed island is barely visible in the April 1994 aerial photograph (Figure 5.1) at a relatively low discharge of 339 m^3/s (11,960 cfs). By 2001, the island is clearly visible and vegetation has established towards the downstream end of the island (Figure 5.2). From 2001 to 2004, the vegetation appears to become more established and covers the entire island (Figures 5.3 and 5.4). Figure 5.5 shows the island following a flood with a peak discharge of approximately 1,781 m^3/s (62,900 cfs, an approximately 5-year recurrence interval) and shows the amount of vegetation is significantly less than shown in photo taken two years prior. It is unclear if the vegetation was removed during the flood or significant deposition occurred on the island covering the vegetation. Three years after the flood, the vegetation is re-establishing (Figure 5.6) and by 2010, the vegetation appears to have re-established to pre-flood conditions (Figure 5.7). Figure 5.8 shows the islands approximately 4 months after a flood with a peak discharge of approximately 1,602 m^3/s (56,570 cfs, an approximately 4-year recurrence interval) and shows that the vegetation on the islands was relatively unaffected by the flood.

The series of aerial photographs show that the frequent periods of overtopping followed by low-flow periods created conditions for the establishment of vegetation provided and island growth.

5.1 Island Controls

The historical document review showed that almost all larger islands and island groups are located either upstream and/or downstream of lateral constrictions along the main channel (Table F.2). These constrictions are either due to fans created by small side tributaries, or small floodplain fragments that create narrowing in the main channel. The small floodplain fragments are usually about the same height as the top surface of nearby islands, and some may be attached islands. Some, however, are higher, and may be remnants of earlier terraces bordering the channel.

An analysis of the lateral constrictions and islands patterns around the various controls was conducted by Mussetter and Harvey (2001b) using the following procedures. The constrictions were identified on aerial photographs, and no attempt was made at the measurement stage to determine the cause of the constriction (other than the obvious cause of tributary fans), or its relationship to island formation. Instead, the narrowest portion of the channel within one island-length of each island group was measured up- and downstream of each island or island group. Constrictions were classified as either abrupt or gradual. Abrupt constrictions showed dramatic narrowing within the length of about a channel width. Gradual constrictions occurred over multiple channel widths. The gradual constrictions may not be true constrictions, but simply the channel gradually narrowing to the river width typical of a reach without islands.

Abrupt constrictions, however, influence island location. If islands are located downstream of a constriction, in the zone where the channel widens dramatically, then these islands are likely to have formed due to deposition caused by flow expansion. This is especially likely if the upstream constriction is due to a tributary fan, with the tributary supplying additional sediment to form the islands. Abrupt downstream constrictions also facilitate island formation. These constrictions create backwater zones upstream, forcing sediment deposition.

In the following discussion, islands are listed by geomorphic subreach and in order from downstream to upstream. The discussion reviews the island patterns found with various constriction morphologies. For each geomorphic subreach, constrictions and their associated islands, or island groups, were reviewed to determine the differences in island morphology between:

- Type of Constriction: constrictions formed by tributaries fans vs. those formed by floodplain or terrace fragments;
- Form of Constriction: abrupt vs. gradual constrictions; and
- For both type and form, differences between upstream vs. downstream constrictions.

In the upstream reach (Geomorphic Subreach I), constrictions were equally divided between tributary fans and floodplain/terrace fragments, with most island groups being associated with both types of constriction. Tributary fans form constrictions for 23 of the 37 islands or island groups (62 percent) between Sign Island (88) and Goose Egg Island (33), with 10 islands or island groups bounded by upstream fans, six bounded by downstream fans, and seven bounded on both the upstream and downstream ends by fans (including the islands in the Walters Ferry study reach). The largest island groups or chains [Rabbit (43.1-43.6b), Cigar (53), Fruit/Dilley (59-60), Rippee (68.1-68.5), Ware (69-72), Big Rocky (81-84), Noble, and Rail/Sign

(88-87) Groups] are bounded by upstream fans, while downstream fans generally constrict individual islands (Helton's, Cottontail (61), and Raccoon (66) Islands).

Of the same 37 islands or island groups, 33 are bounded by floodplain/terrace fragments, with 10 bounded on the upstream side, 10 on the downstream side, and 13 bounded on both ends. The pattern for floodplain/terrace fragments is reversed from that of the tributary fans, with upstream floodplain fragments bounding individual islands [Poison Ivy (55), Feedlot (56), Center (58), Cottontail (61), and Raccoon (66) Islands), and the larger island groups or chains having floodplain fragments either downstream, or at both ends (Rabbit (43.1-43.6b), Clark/Olive (45.2), Cigar (53), Fruit/Dilley (59-60) Rippee (68.1-68.5), Papike (73-77), Noble, Big Rocky (81-84), and Ware (69-72) Groups].

In the anastomosing middle reaches (Geomorphic Subreaches IIA and IIB), no constrictions are created by tributary fans. Changes in channel width are rarely due to obvious features such as attached islands, and are most frequently simple expansions or contractions of channel width. This is logical, since the entrenched upper reach experiences channel narrowing as small, steep tributaries build fans into the main channel. Because Geomorphic Subreach I is entrenched into either Tertiary formations or confined between later terraces, when the tributary fans build into the channel, the Snake River is forced against the opposite, erosion-resistant bank, where lateral erosion is limited. In the anastomosing section, few small tributaries enter the main channel, and when they do, the Snake River erodes laterally, preventing formation of a constriction. At the major tributary junctions (e.g., Malheur and Payette Rivers), the combined rivers create broad, active floodplains with rapidly changing topography. This implies that the upstream islands and island groups, while they may be eroded and reformed, are generally fixed in place by the presence of tributary fan constrictions (and some terrace fragments), while the islands formed in the areas of broad, active floodplain may be more dynamic in terms of both their shapes and locations.

In the extreme downstream reach (Geomorphic Subreach IIIB), where the channel once again becomes entrenched, tributary fans again create constrictions that control island location. All islands from Whitehill (1) to Rapids Islands have fans upstream, and all but Huffman Island have fans downstream.

5.3. Island Topography and Morphology

Larger islands in the non-anastomosing reaches are composed of a high elevation core (some with multiple higher surfaces), and a lower elevation berm that typically surrounds the island. The central cores of the larger islands are approximately 2 m higher than the average upstream berm elevation (with a greater elevation difference for other berms). The two surfaces have different vegetation types, different soils, and have different overtopping frequencies. Some smaller islands do not display these two elevation zones, but instead have surfaces that are close to the elevation of the lower berms, with vegetation and soil profiles to match.

In the anastomosing sections (Geomorphic Subreach II), the largest islands can have a very complex form, because they are surrounded by separate reaches of gently curved to meandering channels. Although almost all of the islands have a high core with relatively minor berms, they may also contain dissected portions of the floodplain. Within individual channels of the anastomosing reaches, islands are found that are similar to those in the non-anastomosing reaches. While some may also contain high cores and lower berms, the berms can be smaller, the high cores are often more irregular, and the elevation difference between core and berms are less pronounced. Many of the islands in the anastomosing reaches are also low islands that have no higher elevation discernable core, and sometimes have very irregular shapes.

Large islands with high elevation cores have berms that surround all or part of the island. The berms can be subdivided into upstream, lateral, and downstream berms, each with distinctive forms (Figure 5.9). Most berms show some evidence of deposition on recent and earlier photographs, but the sediments that form the berm can be deposited on top of erosional surfaces. The upstream berms that have accreted to islands with high cores typically have a distinctive, rounded, upstream-pointing arrow shape. This wraps around the upstream portion of the island core, which can also be pointed at the upstream end. The upstream berms are frequently associated with island-dissecting chutes. Some of the chutes cut across the berm at high angles, but most chute channels are located between the berm and the high core. The lateral berms vary, but most are narrow and surround the island perimeter downstream from the much more distinctive upstream berms. Distinctive downstream berms (as opposed to simply a downstream continuation of the lateral berm) do not exist on many islands. However, most islands in the upstream portion of the upstream reach [Center Island (58) to Sign Island (88)] do contain these distinctive downstream berms, which are usually asymmetric (i.e., occurring mostly or only on one side of the island) and are often detached (i.e., separated from the main island by a shallow chute). It appears that these distinctive asymmetric forms are found where two flow paths around an island create flow separation and/or an elevated backwater where they converge, which allows deposition at the downstream end of an island.

5.4. Island Changes through Time (Aerial Photography Comparison)

A comparison of the island changes was conducted using aerial photographs taken in 1938/1939 and 2012. Example of the types of change discussed below are provided in Appendix D. This appendix contains 19 sets of 1938-1939 photographs matched with 2012 aerial photography. Each set of photographs is annotated by island number or name, and the appendix is arranged in order, from downstream islands to upstream islands (Figures D.1 through D.19).

In the earliest photographs (from 1938-1939), the central cores of the larger islands have a range of different shapes, varying from streamlined forms to highly irregular (possibly dissected) forms. The surfaces usually display low vegetation (shrubs and grasses) with occasional patches of exposed sediment (natric soils or recent deposits). The larger islands with wide, high cores commonly have a 3-D surface that appears braided; with channels that would be active only at flows that are close to overtopping the island (examples are Rippee (68.1), Ware (71), and Big Rocky (83) Islands). Some islands contained deeper chutes dissecting the high core, which would be active at much lower flows (such as Papike Island, 77). Many island cores displayed steep, bare banks (possibly eroding) along their perimeter in the 1938/1939 photos. Examples are Squatter's (26), Goose Egg (33), Rabbit (43.1) and Center (58) Islands. Some islands showed visible erosion between the earliest and later photos (examples are Airport (39), Peachtree, Jensen (52), and Cottontail (61) Islands). In later photos, however, berm growth and expansion of the riparian vegetation zones into the steep banks (frequently including non-native trees such as Russian olive and tamarisk near the base of the banks and on the lower berm) had stabilized the steep and possibly eroding island edges; these changes are most likely due to dam effects.

Formation of some of the extremely elongate island cores (such as Cigar Island, 53) appears to be a process of narrow, streamlined, en-echelon island formation and eventual merger. An excellent example is Schledewitz Island (8.4, a.k.a. W-7, Figure D.4). The first step in this process is the formation of a normal streamlined island, then later the formation of another island just downstream and slightly offset. Berm growth on both islands causes merger of the islands, and subsequent erosion of the core and berm distorts the prior form, leaving an elongate, irregular island with an uneven core. Several other islands have been identified at different points in this evolutionary cycle: Ketchup/ Annear (15c-16, Figure D.6), Pheasant #1 and #3 (48-49), Cottontail (61), and Raccoon (66, Figure D.17) Islands. Others that may have formed this way are Goat (10), Quail #2 (20), Channel #3 (39c), Gosling (51), Jensen (52), Cigar (53), Dilly #1 (59), Blackburn (63) and Sign (88) Islands. Gosling and Cigar Islands were mapped as two islands on the earliest maps, providing support for the above hypothesis.

On the larger islands with high cores, many of the upstream berms have shown significant growth during the period covered by aerial photographs (1938 to 1997). Good examples include Jackass (5, Figure D.1), Rhubarb (36), Grassland, Channel #2 (39d), Homedale (41), Rabbit (43.1, Figure D.14), Poison Ivy (55), Center (58), Dilly #1 (60), Blackburn (63), Blind (79), and Menning (85) Islands. Almost all islands have shown at least minor growth of the upstream berm. Some show vegetation zoning, which would indicate episodic growth during less frequent high flows (Wright Island, 73). Others display additions to the berm with topographic variation: inner and outer berms, also indicating formation during multiple, successive high discharge events [Little Cottonwood (27), Rick (30, Figure D.10), Blackburn (63), Dredge (64), and Cottontail (61), Figure D.16) Islands].

The amount of vegetation has progressively increased on the upstream berms during the period covered by the aerial photographs. In the earliest photographs, the upstream berms generally consist of mostly unvegetated sediment in the center, with a fringe of low vegetation at the water's edge. Now, the vegetation has generally covered the entire berm (including the new berm areas), and that vegetation usually includes trees with underbrush. Figures D.1, D.5, and D.12 provide excellent examples of increases in vegetation on the upstream berms.

Lateral berms have shown moderate growth and vegetation increase since 1938-1939. Examples of islands with significant growth of lateral berms include Rhubarb (36), Center (58), Fruit, Dilly #1 (60), Richards (72), Becky (76, Figure D.19), Papike (77), Blind (79), and Little Rocky (84) Islands. Islands that have shown distinctive downstream berm growth include Silo (40), Tiny (50), Center (58), Fruit, Cottontail (61, Figure D.16), Hermit (57), Ware (71), Richards (72), and Guffey (86) Islands. As with the other berm types, these areas have experienced vegetation growth since 1938, with dense tree stands that include non-native tree species (e.g., tamarisk and Russian olive).

Vegetation establishment has been a persistent trend since the time of the earliest photographs. The 1938/1939 aerial photographs usually show very narrow zones of low riparian vegetation, either along the riverbanks or along the island perimeters. The 1997 and 2012 aerial photography shows that riparian vegetation zones have usually surrounded the islands, and also line much of the banks of the Snake River and its tributaries (Figures D.1, D.3, D.12, and D.15).

The trend of increase in riparian vegetation on the islands also appears to be steadily moving upstream. In the 1938-1939 aerial photos, the berms and lower islands in the downstream, anastomosing reach from the Weiser River to the Boise River confluences (Geomorphic Subreach II) appear to be somewhat more heavily vegetated than the berms and low islands in Geomorphic Subreach I (and also, in Subreach IIIB). While Subreach II showed dramatic increases in riparian vegetation from 1938 to 1987, it appears that significant amounts of riparian vegetation already existed on some islands in 1938. By the time of the 1987 aerial photographs, the expanded riparian zones on at least the lower elevation islands and some of the berms had moved upstream to Sign Island (88). But in the upstream reach between the Cigar Island Chain (50-53) and Sign Island (88), significant increases in riparian vegetation occurred on some islands from 1987 to 1997. This upstream-moving expansion of riparian vegetation has also found expression in the pollen record (see Section 5.1.6). Non-native pollen from riparian zones is only found sporadically in the stratigraphic record of some upstream islands that were substantially formed by 1938/1939.

Comparison of aerial photographs also shows the formation and erosion of smaller islands. While numerous islands have formed since the 1938/1939 aerial photographs (these are discussed further in Section 5.1.3, see Figures D.1, D.3, D.6, D.7, D.8, D.9, D.13, and D.17 for good examples), other islands present in the earliest aerial photographs have later eroded (Figures D.11 and D.19). Examples of these include small islands present in 1938 and 1938 in the channel around the Cable (23.1-23.4), Little Cottonwood (27), Heron (29), Grass, Bayha (74), and Big Rocky (83) Islands. Larger islands, such as the original Boise and Barney Islands, have also been eliminated by erosion.

The final pattern observed in the analysis of the time-sequential aerial photographs has been a metamorphosis in shape and size in some island groups or chains. While the primary change seen in most island groups has been island growth (due to berm growth), and the formation of new islands, some island groups or chains have displayed more complex patterns of erosion and deposition. This is best displayed in the Papike Island chain that encompasses Papike (77) to Wright (73) Islands (Figure D.19). In the earliest photographs, only a narrow channel separates Papike (77) and Becky (76) Islands, and Becky Island has a roughly rectangular shape. In the 1987 and 1997 photographs, the upstream end of Becky Island has been eroded (the island is now triangular in planform) and the downstream end of Papike Island has been modified and extended. In addition, the downstream end of Bayha (74) Island has been eroded and the island shown in earlier photographs just downstream is now gone. This particular island group may also have experienced planform metamorphosis in the period between the earliest maps and the earliest aerial photographs. Such change would explain the differences between the 1938 island form and the oldest maps, which showed only three islands of vastly different form in the location of the modern 5-island chain.

Island group metamorphosis was also demonstrated by a variety of changes that have occurred downstream of the Boise River and Owyhee River confluences. In this reach, islands in the earliest aerial photographs became attached to the floodplain or other islands (a good example is the area around Heron Island (29) in Figure D.10), medium size islands coalesced into larger islands (such as the Nadeau / Larson (14) / Buttermilk Group), Figure D.5), and single islands became island groups (the Ketchup (16) / Annear (15c) / Ogelsbee Group, Figure D.6).

The changes between 1938/1939 and 2012 show that the river is forming new islands, eroding and eliminating islands already formed, and modifying entire island chains. While the location of individual island groups appears more fixed in the entrenched reaches, the Snake River is capable of modification of all islands along the MSR reach, which is consistent with the findings from the review of early maps (Sections 5.1). However, under post-dam conditions, the river is less dynamic compared to pre-dam conditions. The increase in riparian vegetation and the development of berms in the post-dam period are stabilizing the islands; this is a similar effect to that reported by Nadler and Schumm (1981), where the increase in base flows, reduction in peak flows and the establishment of vegetation altered the channel planform.

5.5. Hydraulics

The HEC-2 model was run for the range of discharges (Table 5.1) and the model output was used to determine the overtopping discharge of the islands. The flood-frequency curves developed for the post-Palisades dam period were used to determine the frequency of the overtopping discharge for islands and selected upstream berms (which are higher than lateral and downstream berms).

5.5.1. Island Overtopping Discharges

The highest elevation of the islands and some berms were determined from either direct survey of the island or from the 1997 topographic mapping. Overtopping discharges were determined by linear interpolation between discharge profiles developed from the HEC-2 model.

The results are presented in Table F.4, and show for each island listed the overtopping discharge, the exceedence percent, the return interval, and the highest elevation morphostratigraphic unit assigned by Othberg and Fosberg (2001). Because both the exceedence percent and the return interval are developed from post-dam data, they do not reflect the large floods experienced in the early parts of the 20th century. To put the post-dam overtopping recurrence intervals presented in Table F.4 in context with the pre-dam conditions, the pre-dam recurrence interval are listed for a range of flows (Table 5.2) for hydrologic subreaches H1 and H5 based on the flood-frequency curves (flood frequency curves were not developed for hydrologic subreaches H2, H3 and H4). For example, in the upstream reaches (hydrologic subreach 1), a discharge of 1,000 m^3/s has a recurrence interval of 6.2 years based on the pre-dam flood-frequency curve and 19.1 years based on the post-dam flood-frequency curve (Table 5.2). Similarly, in the downstream hydrologic subreach (H5), the recurrence intervals for 2,250 m^3/s are 14.3 years under pre-dam conditions and 24.0 years under post-dam conditions (Table 5.2). The dam impacts are less pronounced in the downstream reaches due to the tributary inflows.

To understand island evolution and the history of different morphostratigraphic units, it is necessary to evaluate their different overtopping history. The islands were separated by morphostratigraphic unit and also by geomorphic subreach and the overtopping discharges are summarized in Table 5.3 and Figure 5.10 through Figure 5.13. The discharge necessary to overtop most level 1 and 2+ islands has only rarely been exceeded during the period of record (Figure 5.10 through Figure 5.13).

The maximum known upstream flood is listed at 2,265 m^3/s for the Murphy Gage, and 3,398 m^3/s for the Weiser Gage, values slightly greater than those listed on Figure 5.10 for level 1 and 2+ islands. However, average values listed with a ">" sign are too low, because several islands included in these averages were not overtopped by the maximum flow run in the HEC-2 model for that reach. The overtopping discharge value used for those islands was simply the maximum discharge modeled. Discharges sufficient to overtop all islands were not run in the HEC-2 model, because they would have exceeded the lateral boundaries built into the model. However, it is also apparent that floods have occurred during the period of the gage records that have overtopped some level 1 and 2+ islands (Figure 5.10 and Figure 5.13).

Morphostratigraphic units 2-, 3, 4, and 5 overtop at lower discharges. For the lower units (level 3, 4, and 5), discharges are listed that have a relatively frequent recurrence interval, even within the post-Palisades Dam period. Recurrence intervals for average overtopping discharges for these morphostratigraphic levels range from 4 to less than 1.1 years, with most values less than 2 years for level 3, 4 and 5 surfaces (Table 5.3). This is to be expected, since many of these islands formed during and after the dam-building period (i.e., they were not present on the earliest aerial photographs). Floods overtopping the level 2- islands are less frequent, as would be expected on older and higher surfaces. The average overtopping discharge for level 2- islands in Geomorphic Subreach III (downstream of the Weiser gage) is 1,849 m^3/s. This discharge has a recurrence interval of 6.9 years. Discharges greater than 1,982 m^3/s (70,000 cfs) have been equaled or exceeded at the Weiser Gage in at least 9 years during the period of the gage record (1910-2012), and discharges greater than 2,265 m^3/s (80,000 cfs) have been recorded in 5 years. In the upstream reach (Geomorphic Subreach I), the average overtopping discharge for the level 2- islands is 1,244 m^3/s. This has a recurrence interval greater than the length of the post-Palisades Dam record (55 years). Floods exceeding 1,133 m^3/s (40,000 cfs) have occurred three times during the total gage period (excluding the estimated maximum flood of 2,265 m^3/s (80,000) cfs in 1894).

5.5.2. HEC-2 Model Output

The output from HEC-2 model runs for each hydrologic subreach (Table 5.1) was reviewed to determine whether patterns in water-surface elevation, average channel velocity, hydraulic depth, total shear stress, or other variables could provide insight into channel dynamics and help to explain the type of island change described in previous sections. The most informative data were the total shear stress and water-surface elevations with increasing discharge.

The water-surface profiles show significant variation along the reach (Figure 5.14, Figure 5.15 Figure 5.16). At the locations of individual islands or island groups, the water-surface profile is commonly steep, especially at lower discharges. At these island locations, the thalweg elevations are relatively high, creating a broad, shallow section of channel surrounding the islands or island groups. Deep pools were located between islands or island groups. These pools were typically found at channel constrictions, and were also typically associated with tributary fans in geomorphic subreach I (e.g., Jump Creek, Succor Creek, Hardtrigger Creek, Reynold's Creek and Rabbit Creek locations on Figure 5.16). Tributary fans create the constrictions that cause deep pools to form opposite the fans.

At low discharges, water-surface slope is relatively level over deep pools, and steep at island locations (especially on the downstream end of large island groups). This indicates that at low flows, the islands are areas of high bed shear stress, where erosion may be occurring, and the pools are areas of low bed shear stress that are accumulating sediment. As discharge increases, the differences in slope of the water surface between islands and pools decreases, and the overall profile becomes more even, changing the relative shear stress available to move sediment.

The above-described pattern was also visible in the anastomosing reach (Figure 5.14 and Figure 5.15). In addition to the relative steepness over individual island reaches, very steep water surfaces were observed at the downstream end of anastomosing reaches where two or more separate channels came together (i.e., see the downstream end of Bridge Island, the Perrin/Crow Island group, and the downstream end of the Patch/Goat/Long Island group).

A comparison of the total shear stress was conducted to evaluate the changes in relative shear stress between islands and pools at all discharges (Figure 5.17 through Figure 5.21). The patterns observed confirmed the hypothesis of shear stress reversal obtained from the analysis of water-surface and bed elevations (Mussetter and Harvey, 2001b). In all geomorphic subreaches, a consistent pattern of shear stress change could be identified between islands or island groups and intervening pools. Excellent examples include Westlake, Aulbach (6, 7) (Figure 5.17), and Smith (11.1-11.3) Islands (Figure 5.18), Beaver (19) and Baxter Islands (Figure 5.19) and Peachtree, Channel (39c, 39d) (Figure 5.20), and Fruit/Dilly (59, 60) (Figure 5.21). This pattern can be observed at most island locations along the channel. The pattern of narrower and broader ranges of shear stress values with discharge is apparent along the entire MSR, with the pools being the zones with a wide range of shear stress values and the islands being the locations where the range of shear stress is narrower.

At low discharges, the shear stresses are higher at island locations and lower at pool locations. Because bed shear stress is a relative measure of the river's ability to move sediment, this implies that at low discharges the island locations are potentially more erosional than the pools. Even though the stresses are relatively higher in the island locations than in pool locations, the shear stresses need to be of sufficient magnitude to cause sediment transport. Any sediment eroded from island cores or berms is deposited in the next pool downstream where shear stress is relatively lower, and the river's ability to move sediment is decreased. At higher discharges, this pattern reverses, and the island locations are zones of relatively low shear stress (and probably deposition) between upstream and downstream pools where sediment that was deposited at low flows is mobilized. This can be seen more clearly in Figure 5.22 through Figure 5.30, which show the shear stress patterns of broader and narrower ranges in selected reaches surrounding individual islands or island groups, and illustrate the change in total shear stress with discharge at specific channel locations. The figures present one example from each of the geomorphic subreaches to illustrate how this variation of relative shear stress with discharge can influence island growth and change.

In the downstream reach (Geomorphic Subreach III), the reach of the Snake River immediately adjacent to the Aulbach group illustrates this point (Figure 5.22 and Figure 5.24). As discharge increases from 283 m^3/s to 3,681 m^3/s, the total shear stress at both island cross sections (cross sections 58.7 and 59) remains relatively stable, decreasing slightly from 283 m^3/s to about 1,699 or 1,982 m^3/s, then rising slightly. At low discharges, the shear stress in both the upstream pool (cross section 60) and the downstream pool (Cross Section 58) is much lower than near the islands. With increasing discharge, the pool shear stress values increase rapidly. Between 1,416 and 2,214 m^3/s, the relative magnitudes change, and pool shear stresses are greater than island shear stresses. This means that at flows less than about 1,416 m^3/s, the islands are potentially in a net erosional zone, because the river may be able to transport more sediment than is being delivered from the upstream pool. At discharges higher than about 2,124 m^3/s, the islands become depositional zones, because shear stresses do not change significantly and the sediment supply from the upstream pools increases as a result of increasing shear stress in the pools.

This same pattern is seen with some variation in the middle anastomosing reach (Geomorphic Subreach II). Here, instead of relatively smooth curves, some island areas exhibit a secondary peak (in both island and pool cross sections) between about 850 and 1,982 m^3/s (30,000 and 70,000 cfs). The 1,416 m^3/s (50,000 cfs) discharge at the center of this secondary peak corresponds to the break between the morphostratigraphic levels 2 and 3 in Geomorphic Subreach II. The final result is the same, with pool shear stress values increasing above island shear stress values at higher discharges (at about 1,699 m^3/s (60,000 cfs) in Figure 5.25 and Figure 5.27).

The same pattern occurs with regularity in the upstream reach (Geomorphic Subreach I). For example, in the Fruit/Dilly Island reach (Figure 5.28, Figure 5.30), as discharge increases, shear stress decreases rapidly, then decreases more slowly while pool shear stresses increase steadily. The crossover point in this example is just above 850 m^3/s (30,000 cfs).

The shear stress patterns are typical of the pool-riffle velocity reversal found in moderate gradient, coarse bed channels (Keller, 1971; Richards, 1976; Keller and Melhorn, 1978). (Velocities were also investigated, and velocity reversals were shown to occur. However, shear stress is a better indicator of relative sediment-transport ability than velocity, so that parameter was more fully investigated.)

In summary, the MSR has a pool/island morphology that is analogous to the pool/riffle morphology found on smaller rivers. Thompson et al. (1999) found that a velocity reversal (and subsequent reversal of sediment-transport capacity) is reinforced by constrictions in the pool (that reduce the pool's cross-sectional area), which accords with findings in this study of pools associated with channel constrictions in the Snake River. Richards (1976) found that riffle cross sections were about 15 percent wider than pool cross sections because central bars of coarse bed material diverted flow against the channel banks. The island reaches in the MSR are shallow and steep, similar to the riffle reaches, and they are also wider than the pool reaches. The islands have a central platform or base of coarse material, which is analogous to the central bar of Richards (1976). It is upon this central platform that the finer grained material that makes up the island core and berms are deposited at higher discharges.

5.5.3. Conceptual Model of Island Formation

Island formation and reformation in the MSR appears to be a dynamic process that is a function of discharge and sediment supply. At frequent, low discharges, typical of those that overtop berms and low elevation islands (morphostratigraphic units 3, 4, and 5), shear stresses are relatively higher within the island reaches than in pool reaches up- and downstream. At higher discharges, typical of those overtopping 2-, 2+ and 1 level surfaces, the islands are depositional zones, which explains the formation of the higher elevation cores.

The 1938/1939 aerial photographs show the berms were much smaller and less vegetated than at present, and many of the edges of the higher cores in the islands appear to be erosional. These small berms are likely due to dam effects. Today, the islands are more stable, with wider, vegetated berms surrounding and protecting the cores.

5.6. Island Stratigraphy and Island Age

5.6.1. Soils Data

The morphostratigraphic mapping (Section 4.1.1.5) was developed based on the level of soil formation, elevation of the surface, and vegetation types. The morphostratigraphic units were numbered from 1 (the highest elevation and oldest, with upland vegetation dominant) to 5 (the lowest elevation, most recently formed, with aquatic vegetation dominant). The level 2 unit was subdivided into 2+ and 2-, representing successively less developed soils.

Soil horizons identified in the pits ranged from completely undeveloped soils to those with very complex stratigraphy, including evidence of previously truncated surfaces. Table F.5 lists islands on which pits were dug, and identifies for each the morphostratigraphic level identified by Othberg and Fosberg (2001), and the general soil stratigraphy, discussed in the paragraphs below.

The least developed soils identified were those that contained only multiple C horizons, which represent unaltered parent material, in this case Snake River alluvium [e.g., unnamed island 18h, and one of the Cable Islands (23.1)]. The alluvium usually contained mostly silt and sand size material, but occasional zones of fine clay loams or coarse gravel were present. These deposits commonly displayed primary sedimentary structures, such as cross-bedding, ripple drift, or horizontal laminations, all features created as the sediments were deposited by the river. The multiple C horizons identified on the islands can represent multiple depositional events (e.g., individual floods), or stacked horizons showing fining upward characteristics may represent deposition during one larger event. These soils are identified in Table F.5**.** as “all C’s”.

Slightly more developed soils than the C’s, were those soils that contained one A horizon. This could be either a surface A horizon over multiple C horizons [“A/C” on Table F.5**.**, such as Annear (15c) and Quail #2 (20) Islands), or one buried A horizon (identified as Ab on Table 17) over multiple C horizons and overlain by at least one C horizon (Ross (25) and Wegman (42) Islands]. For all soils, the lower case “b” following a capital letter horizon designation indicates burial by more recent deposits. In several cases the Ab horizon was covered with sediment that appeared to originate in the 1997 flood. An A horizon contains organic material in addition to primary sediment, and develops when a surface is stable for long enough that plants become established, die, and add their organic matter to the upper soil layers. This process can occur relatively rapidly in as little as a few decades. Constraints on the minimum time for development of A horizons are discussed in Section 5.6.4 after pollen data and ^{14}C dating have been presented.

Slightly more developed soils found in island pits included those with multiple A and Ab horizons (indicated in Table F.5 by the number of A and/or Ab horizons present). These buried A horizons, interspersed between multiple C horizons containing primary sedimentary structures, were additional evidence for various modes of island formation. These islands experienced episodes of deposition (displayed by the C horizons), followed by periods of stability (to develop the A horizons). Later episodes of island formation that buried the A horizons did not erode the entire pre-existing surface, leaving a complete or partial Ab horizon. Good examples of this soil burial are found on Jackass Island (5) and the Aulbach Islands (6 and 7). Islands with the least developed soils (those with only stacked C horizons) could also have experienced these periods of stability, but subsequent periods of higher energy island formation may have eroded the surface below any previously developed A horizon before depositing additional sediment.

After development of the surface A horizon, the next soil horizon to develop on a stable surface is generally a Bw horizon that forms beneath the surface A (Smith Island #2, 11.3). This horizon couplet is indicated on Table F.5 as “A/Bw”. The B horizon is one that shows pedogenic accumulation of material after deposition, and the lower case “w” indicates a weak horizon at the very earliest stages of development. The Bw horizon is a weakly developed layer that may show only slight alteration from the primary parent material. The alteration may be a slight accumulation of clay, salt, or carbonate, or it could be a subtle color change. The subtle characteristics that distinguish a Bw horizon could also be in part depositional. Information on the time required to form this weak Bw horizon was also determined from pollen analysis, and is discussed in later sections.

In addition to the relatively poorly developed soils discussed above, a few of the soil pits demonstrated much more advanced and complex soil formation. These included multiple stacked A, B, and altered C horizons showing significant accumulation of organics, clay, salt and carbonate. These complex soils are indicated on Table F.5 as “>Bw”. These soils displayed the level of pedogenic development typical of surfaces that have either been stable for a long period of time, or have experienced only very minor aggradation over time (thin flood layers are soon incorporated into the upper A horizon). Some of these complex soils were buried to significant depths by more recent deposits, including multiple buried A horizons. A few of these more complex soils also displayed evidence of truncation, leaving behind only buried B and altered C horizons (originally developed deep in the soil profile) that were subsequently overlain with deposits containing less well-developed, more recent soils. Some of these soils are discussed in more detail in the section on the time required for soil development (Section 5.6.4).

In general, the soil stratigraphy correlated well with the morphostratigraphic units that were originally developed by Othberg and Fosberg (2001). Soil pits were not excavated on the simplest level 4 and 5 soils. The level 4 and 5 islands consistently displayed either very shallow soils (too shallow to dig and sample) or they were exposed gravel bars, with no surface fine deposits. Level 3 islands displayed mostly stacked, multiple C horizons (61 percent), or sometimes contained one or two A horizons on the surface or buried (17 percent). Only two level 3 islands had more than two Ab horizons. Level 2- soils were more complex and had a greater range of soil horizon types. A few consisted of only C horizons (14 percent), but most contained either a single A or Ab horizon, or an A/Bw couplet (60 percent). Level 2- islands with multiple A or Ab horizons represented the remaining 26 percent of the sampled islands. The advanced soil formation displayed by multiple stacked A, B, and altered C horizons was found only on soils of morphostratigraphic levels 2+ and 1, but some level 2+ surfaces displayed multiple A horizons (33 percent).

5.6.2. Pollen Analysis

The 93 islands that were analyzed are listed in Table F.5. The islands represent a range of soil stratigraphy from the most simple (all C horizons) to the most complex (multiple A, B, and altered C horizons, with evidence of erosion and redeposition) and they are considered representative of the islands along the MSR.

Patterns can be seen in the pollen and soil records from this smaller sample of island stratigraphy. Islands whose central morphostratigraphic unit level is 3 are all very similar. Thirty-six of the 41 level 3 islands have relatively continuous levels of non-native pollen either throughout the stratigraphic column to the cobble/gravel basal platform or the bottom of the pit. Of the remaining level 3 islands, only one (77e) has a relatively shallow depth of non-native pollen in the stratigraphic column.

All but one of the islands (Wright Island) display at least sporadic dung fungal spores to the island basal platform (or bottom of the pit), and all have lower charcoal abundance throughout their stratigraphy, which indicates that all level 3 islands listed in Table F.5 have formed since the time of European settlement.

Islands assigned a morphostratigraphic level of 2- also showed consistent patterns, with a few exceptions. All but one of the 2-level islands (87a) showed relatively continuous non-native pollen throughout the stratigraphic column. However, this non-native pollen concentration generally was lower on the higher elevation islands upstream from Tiny Island (50). On several of these higher-elevation islands, non-native pollen is only present sporadically throughout the stratigraphic column, a consequence of the relatively late arrival of the non-native riparian species that provide most of the non-native pollen. All but two (Raccoon (66) and Bayha (74) Islands) showed at least sporadic dung fungal spores throughout their stratigraphic columns, and all but three (Sundstrom (15), Hoffman (24), and Bayha (74) Islands) showed low charcoal abundance. This convergence of evidence demonstrates that level 2- islands are young, having formed since the time of European settlement, introduction of non-native plants and livestock, and fire suppression.

The one possible outlier in this group is Bayha Island. This island is part of the Papike Chain (73 to 77), located in the Walters Ferry study reach. This island chain has experienced modification since both the time of the earliest maps and aerial photographs (Section 5.1). However, non-native pollen is only found sporadically through the stratigraphic column, no layers contain dung fungal spores, and the charcoal abundance is as high as 65 percent, becoming lower near the surface. This would seem to indicate a pre-European settlement period for accumulation of the island core. However, a ^{14}C date of 110 BP at 1.3 m below the surface indicates that a maximum age for the upper horizons is roughly equal to the time of European settlement and later. In addition, the soil horizons identified for Bayha Island are only a surface A over multiple C horizons, a soil that usually takes only a short time to develop.

Islands assigned a morphostratigraphic level of 2+ and 1 showed a much weaker signal for modern deposition. If this signal was moderately strong, it was only in the top few layers. The non-native pollen was sporadic throughout the stratigraphic column, being only continuous in the surface layers. The dung fungal spores were normally found in only a few layers, and these were usually at the surface. Finally, low carbon abundance was only found in surface layers, and lower layers displayed much higher values. Combined, this information indicates that the 2+ and 1 level islands were substantially formed prior to the period of European settlement, even though significant thicknesses of overtopping surface deposits may be modern.

This is consistent with the information on overtopping discharges presented in Section 5.5.1. Islands of morphostratigraphic level 3, 4, and 5 have overtopping discharges with recurrence intervals of from 4.0 to less than 1.1 years, and therefore these islands should show evidence of frequent reworking in the form of either multiple C horizons or Ab horizons. Table F.5 shows that islands with core soil morphostratigraphic levels of 3 all contain either only C horizons, A/C horizons, or multiple A horizons. Higher elevation, level 2- islands are overtopped less frequently, and thus have time for slightly more advanced soil development, to the level of the A/Bw couplet. Several 2- islands have developed this soil horizon character. Islands with core levels of 2+ and 1 have even less frequent overtopping intervals, and it is on these higher, older surfaces that soils with more developed horizons (Bt, Bk, Ck) have formed. Even on these islands, however, truncated and buried older surfaces are found, still showing evidence of reworking, but not as frequently as the lower elevation islands.

5.6.3. Carbon 14 Dating

Datable carbon was recovered on nine islands, with two samples being collected on Bayha Island (74), and one sample recovered from the Snake River bank near the Boise River and Owyhee River confluence (on the left bank opposite Boise Island, 31.2). The 11 samples are listed in Table 5.4, with age and location of the sample in the stratigraphic section for each island. The carbon samples included wood fragments, charcoal fragments, and organic-rich sediments. All material was dated using normal radiometric methods. .Several of the larger samples of organic sediment required pre-dating concentration, due to large sample size and low carbon concentration. Samples from three islands (Jackass (5), Pheasant #2 (47), and Fisher (70) Islands) were small and required accelerator mass spectrometer (AMS) dating.

The dates determined from the radiometric dating are listed as years BP (before present, with BP = 0 in 1950) and the standard deviation for each date is listed as well (Table 5.4). This is the conventional ^{14}C age recommended by Beta Analytic, Inc., as opposed to the measured radiocarbon age. The conventional ^{14}C age is the result of applying a C^{13}/C^{12} correction (based on the PDB-1 international standard) to the measured age, and is the most appropriate radiocarbon age for use in this analysis. In most cases, conventional and measured radiocarbon ages were identical. With all radiocarbon dates, the measured date is for the material contained in the stratigraphic layer. The actual date of deposition for each stratigraphic layer may be later than the age of the dated material, because older, existing material is eroded, transported, and re-deposited in the depositional events that make up individual islands. As such, each radiocarbon date should be considered a maximum age for that stratigraphic layer.

The radiocarbon dates ranged from relatively young (110 to 120 years BP) to almost 3,000 years old [Olive Island (45.2)]. Although the number of islands with radiocarbon dates was insufficient to use this technique exclusively for determining the age of the islands, it nonetheless provided significant information on the time required for soil development. This information augmented the data obtained from aerial photograph analysis and pollen analysis, and allowed constraints on the ages of different morphostratigraphic units to be identified and quantified.

5.6.4. Time Required for Soil Horizon Development

To develop an estimate of the age of the islands, analyses of the results from pollen analysis of the 93 pits and the nine carbon samples were used to develop an estimate of the time required to develop the various soil horizons, and the extension of this analysis to other islands identified within the various morphostratigraphic units (Mussetter and Harvey, 2001b). Detailed information used in this analysis can be found in the stratigraphic logs (Appendix E).

Stratigraphic columns composed of stacked C horizons with no pedogenic alteration are the most recently formed. Islands that were not present in 1938-1939 aerial photographs contain either all C horizons (islands 18h, 31.1 and 64a) or only slightly more complex A/C horizons (island 31.2). Several islands that were forming (low elevation gravel bars) in 1938/1939 were also found to contain only C horizons (39a, 86a).

Islands with a simple surface A horizon above stacked C horizons, or with one buried A horizon (Ab) between unaltered C horizons, were the next level of soil development investigated. Only Boise Island (31.2) was not present in 1938/1939, and contained an A/C horizon, but several islands forming during that period contained at least one A horizon (8.4, 15c, 25, and 48b).

Islands that were at the formation stage in 1938/1939 were also found to contain multiple surfaces and buried A horizons (4a, 8.2, 8.5, 8c, 9.2, and 11.1). Islands forming in the earliest aerial photographs with more than two A horizons (surface or buried) usually only occur near or downstream of the Weiser confluence. This could be due to backwater effects from Brownlee Reservoir or the canyon constriction during high flows. It may also be due to the differences in the timing of flows on the Weiser River and the Snake River. If so, this could create frequent sedimentation and burial of these low elevation islands, and subsequent preservation of quickly formed A horizons. At the very least, the evidence from islands not present or forming in 1938-1939 indicates that at least two (possibly more under the right circumstances) A horizons could have formed during the 60-year period from the time of the earliest aerial photographs to the time of the island pit excavation.

The most extensive pedogenic development found on islands that were forming in 1938-1939 was from Island 8.5 near the Weiser River confluence. This island has two different A/Bw couplets, and represents a level of development similar to the multiple A horizons found on islands of this age in the same area. This one example is tentative evidence that up to two A/Bw couplets could form in 60 years. However, it could be that the first couplet had already formed at the time of the earliest aerial photographs, because the island was forming at that time.

The pollen, spore, and charcoal evidence clearly indicate a level of soil development that is possible within the last 100 years. Numerous islands with the most basic level of development (all C's, A/C, soils with two A horizons) are found in Table F.5. Examples of islands present in the 1938/1939 aerial photographs, but with abundant pollen evidence for development since European settlement, include 11.2, 18a, 29a.1, 30, 44, 49, 57, 68.5.

Several islands with more than two A horizons (43.5, Aulbach #1) also show abundant evidence for recent development. The highest level of development seen in islands with abundant non-native pollen (and other positive indicators) are Smith #2 (11.3), Cliff (22), 18h.1 and Beaver (19) Islands. These islands both contain the A/Bw couplet, one slightly buried (22). This, in conjunction with the two A/Bw couplets found on Island 8.5, clearly shows that multiple A horizons or an A/Bw couplet can form within 110 years.

Information from artifacts found while excavating island pits also supports this level of soil development since European settlement. On islands 4a and 8.2, three A or Ab horizons were found above modern artifacts. On Aulbach #1 and Aulbach #3 (6), four A or Ab horizons were located above modern artifacts, and on Sign Island (88), a buried A/Bw couplet was found near the surface above buried artifacts.

The ^{14}C dates provide information on the age constraints of the more developed soils. This can best be illustrated by looking at each island separately:

- Jackass Island (5) had a carbon date of 146 years BP below eight buried A horizons. This follows the trend observed for multiple A horizon development and burial at, and downstream of, the Weiser River.
- Cottonwood Island (28) had a carbon date of 350 years BP for an Ab horizon, with two older Ab horizons separated below by C horizons. Above this dated horizon were four younger C horizons capped with a developed A horizon.
- Olive Island (45.2) had a carbon date of 2960 years BP topping a complex soil. This soil contained an A horizon, multiple Bk horizons (a Bk horizon is more well developed than a Bw, and contains significant amounts of carbonate), and Ck horizons (a Ck horizon is an altered C horizon that has accumulated carbonate). Above this surface were multiple C horizons, and the relatively young surface contained a buried A/Bw couplet.
- Pheasant Island #2 (47) had a carbon date of 2190 years BP for a horizon that was part of a stripped surface that could have been similar to the older soil described for Olive Island (45.2). However, only the lower Ck horizons remained, and above the dated horizon were six more recent A or Ab horizons, separated by five depositional C horizons.
- Jensen Island (52) had a carbon date of 690 years BP for a surface topping a buried soil containing A, Bw, and Bt horizons. Bt horizons are better developed than Bw horizons, and

contain increased amounts of pedogenic clay. Above the 690 year BP surface were one Ab and one surface A horizon, separated by multiple depositional C horizons.

- Fisher Island (70) had a carbon date of 290 years BP on a surface that had only developed one A horizon before it was buried and surface soil development ceased. Younger deposits above the 290-year BP surface included one buried A horizon, one buried A/Bw couplet and a modern A layer developing on the surface.
- Bayha Island (74) had a carbon date of 110 years BP in an unaltered C deposit. This C horizon, deposited 110 years BP or later, had above it eight depositional C horizons with an A layer developed on the surface. Slightly above the base of the island a carbon date of 890 years BP was obtained, indicating that the lower section of the island was formed or reformed in less than the last 1,000 years, and that the upper portion has formed since in the post-European settlement period.
- Brooks Island (78.3) had a carbon date of 280 years BP for an Ab horizon 45 cm below the surface. Above this, with an age of less than 280 years BP, is a thick depositional C layer and an A horizon that has developed on the surface.
- Sign Island (88) had a carbon date of 120 years BP just above a buried A/Bw couplet. Above the buried couplet are 3 C horizons that were deposited more recently.

The ^{14}C data support the time required for soil development determined from evidence obtained from the earliest aerial photographs, non-native pollen, dung fungal spores, charcoal abundance, and modern artifacts. In summary, a conservative estimate of the time required for soil development shows that at least two A horizons can form in 60 years, and multiple A horizons (on islands experiencing multiple episodes of deposition) or at least one A/Bw couplet can form in about 100 years. Evidence found on Fisher Island (70) indicates that in less than about 300 years, an A/Bw couplet and two other A horizons can form. However, a more complex soil containing an A/Bw/Bt sequence (such as that found on Jensen (52) Island) may require about 700 years to form, but could also require much less, because it is not known when that soil sequence was buried and development ceased. This evidence, in conjunction with the soil horizon information found on Table F.5, indicates clearly that all islands of morphostratigraphic level 3, 4, and 5 have very recently formed soils. It also indicates that, although the soils that have developed on morphostratigraphic level 2- surfaces are somewhat older, they also have clearly developed since the time of European settlement.

5.7. Figures and Tables

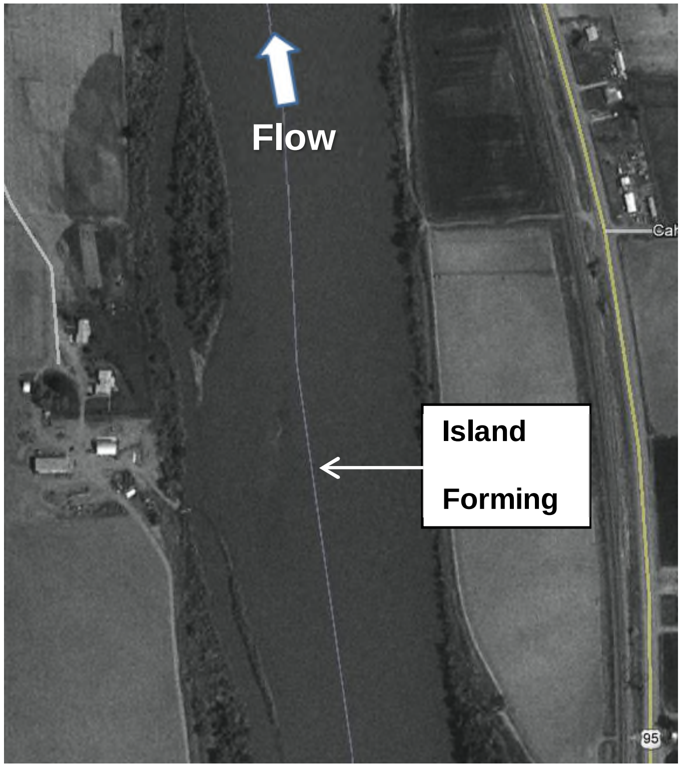

Figure 5.1 Aerial photograph of un-named island taken on 4/30/1994 when the discharge at the Weiser gage was approximately 399 m^3/s (11,960 cfs).

Figure 5.2 Aerial photograph of un-named island taken on 8/4/2001 when the discharge at the Weiser gage was approximately 194 m^3/s (6,840 cfs).

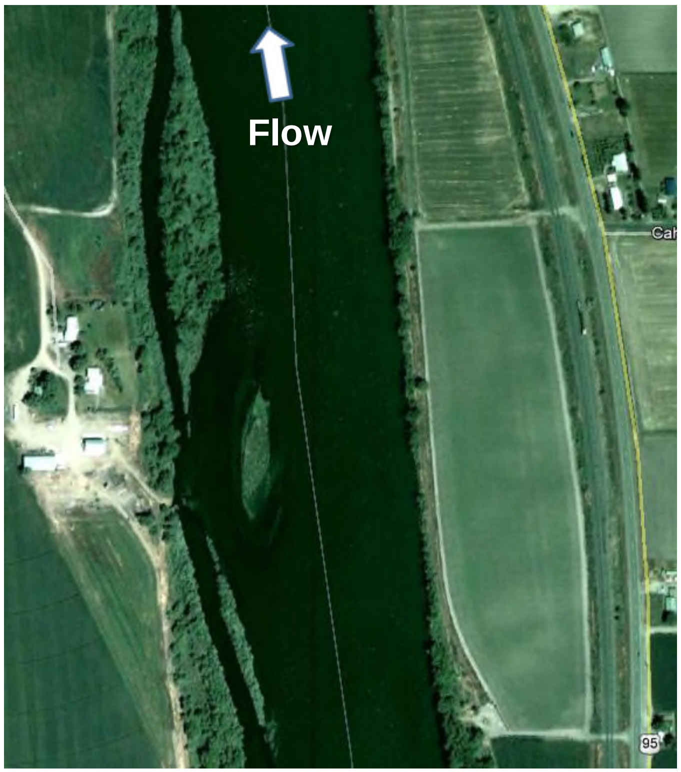

Figure 5.3 Aerial photograph of un-named island taken on 7/6/2003 when the discharge at the Weiser gage was approximately 236 m^3/s (8,230 cfs).

Figure 5.4 Aerial photograph of un-named island taken on 9/14/2004 when the discharge at the Weiser gage was approximately 266 m^3/s (9,380 cfs).

Figure 5.5 Aerial photograph of un-named island taken on 8/17/2006 when the discharge at the Weiser gage was approximately 295 m^3/s (10,420 cfs).

Figure 5.6 Aerial photograph of un-named island taken on 8/19/2009 when the discharge at the Weiser gage was approximately 273 m^3/s (9,650 cfs).

Figure 5.7 Aerial photograph of un-named island taken on 7/11/2010 when the discharge at the Weiser gage was at approximately 309 m^3/s (10,920 cfs].

Figure 5.8 Aerial photograph of un-named island taken on 5/20/2011 when the discharge at the Weiser gage was at approximately 255 m^3/s (9,020 cfs).

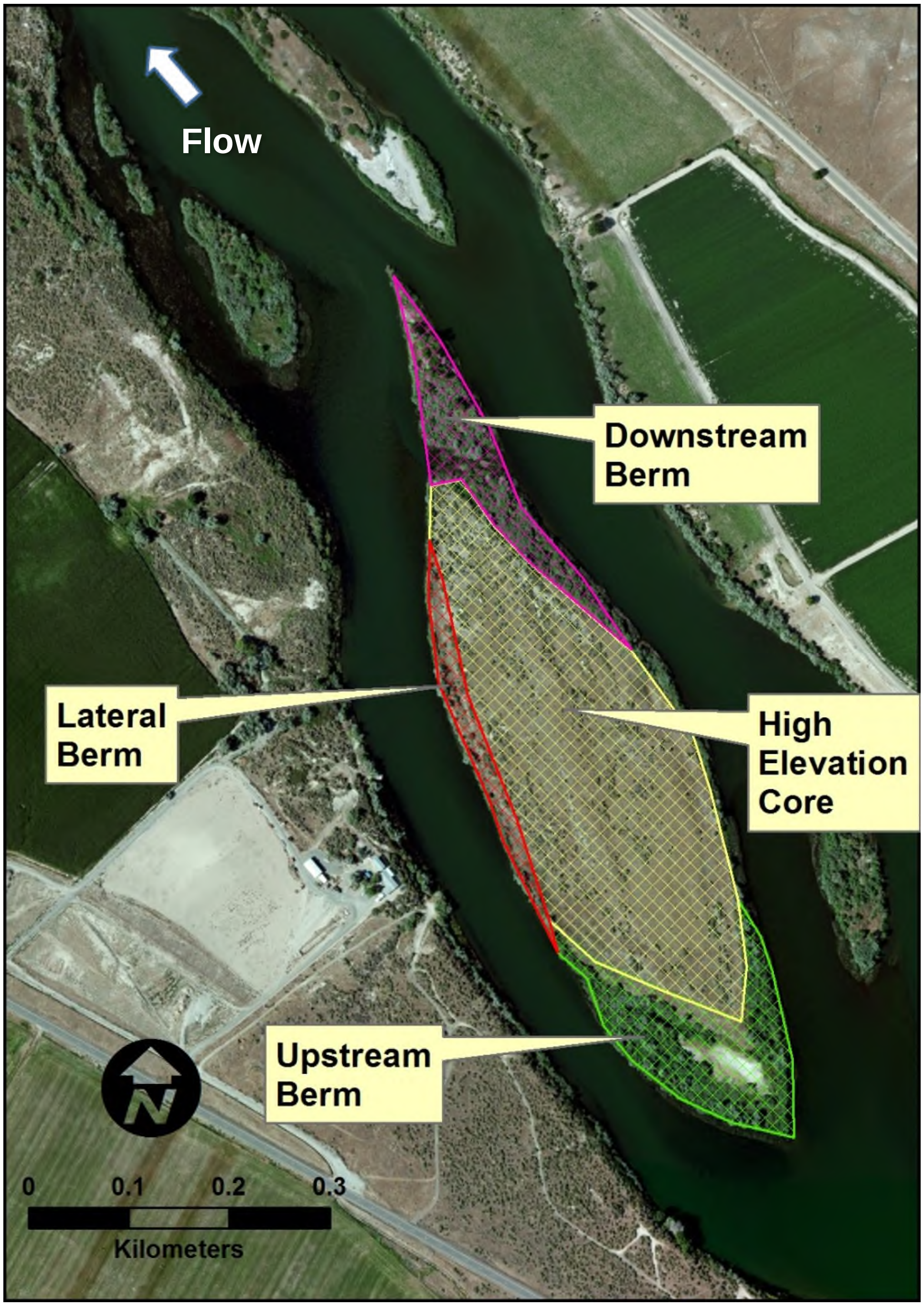

Figure 5.9 Schematic showing different types of island berms.

Table 5.1 Range of discharge profiles created by the HEC-2 model, by hydrologic subreach.

Hydrologic Subreach	Range of Discharges (m^3/s)
H1	127 - 1,982
H2a	142 - 2,124 (middle reach)
H2b	139 - 2,761 (downstream reach)
H3	139 - 2,945
H4	140 – 3,276
H5	142 – 3,681

Table 5.2 Comparison of the flood frequency return intervals for a range of flows at Hydrologic Subreaches 1 and 5.

Discharge (m^3/s)	Return Interval (years) Hydrologic Subreach 1			Return Interval (years) Hydrologic Subreach 5	
	Pre-Dam	Post-Dam		Pre-Dam	Post-Dam
500	1.3	1.5			
750	2.0	2.6		1.1	1.3
1,000	6.2	19.1		1.3	1.7
1,250	18.6	>55-YR		1.7	2.3
1,500	26.0	>55-YR		2.3	3.4
1,750	31.7	>55-YR		3.6	4.7
2,000	37.9	>55-YR		9.7	10.2
2,250	44.6	>55-YR		14.3	24.0
2,500	51.8	>55-YR		26.1	>55-YR
2,750	59.4	>55-YR		31.3	>55-YR
3,000	67.5	>55-YR		37.2	>55-YR
3,250	76.1	>55-YR		43.8	>55-YR

Table 5.3 Overtopping discharges and elevations for morphostratigraphic units by geomorphic subreach.

Morphostratigraphic Unit	Geomorphic Subreach	Average Overtopping Discharge (m^3/s)*	Recurrence Interval for Average Discharge (years)**	Discharge Standard Deviation (m^3/s)	Number of Islands	Number of Islands Outside Discharge Range
1	I	>>1,850	>55	233	16	8
1	II				0	
1	III				0	
2+	I	>1,723	>55	171	16	2
2+	IIA	>2,308	>55	325	6	5
2+	IIB	>2,830	>55	162	2	0
2+	III	>3,261	>55	365	3	0
2-	I	1,244	>55	292	15	0
2-	IIA	1,745	>55	472	5	1
2-	IIB	2,058	>55, 29.2	437	10	0
2-	III	1,849	6.9	441	5	0
3	I	749	2.3	312	43	0
3	IIA	<1,076	<2.9	682	30	2
3	IIB	899	1.9, 1.6	413	6	0
3	III	727	2.1	475	6	0
4	I	479	1.5	118	24	0
4	IIA	708	2.3	299	14	0
4	IIB	<417	<1.4	242	11	0
4	III	<610	<2.0	733	2	0
5	I	516	1.2	167	8	0
5	IIA	527	1.9	226	7	0
5	IIB	885	4.0	849	2	0
5	III				0	

* Discharges indicated as either greater than (>) or less than (<) indicate that the average contained maximum and minimum values, limited by the range of discharges run through the HEC-2 model.

** Return Intervals for discharges that have a ">" sign are minimum Recurrence Intervals, and for discharges that have a "<" sign are maximum Recurrence Intervals

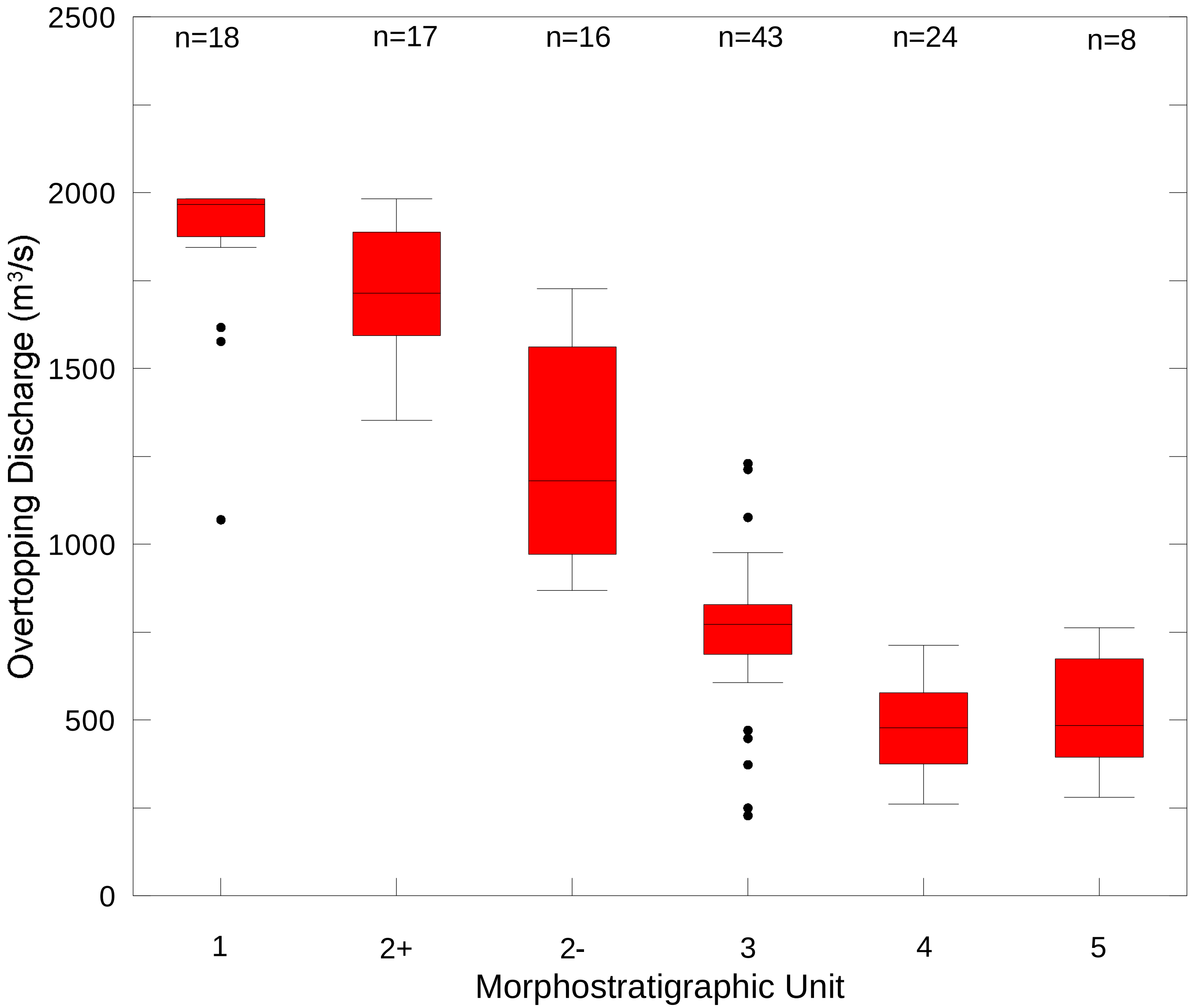

Figure 5.10 A box and whisker plot of the overtopping discharges for each morphostratigraphic unit in Subreach I.

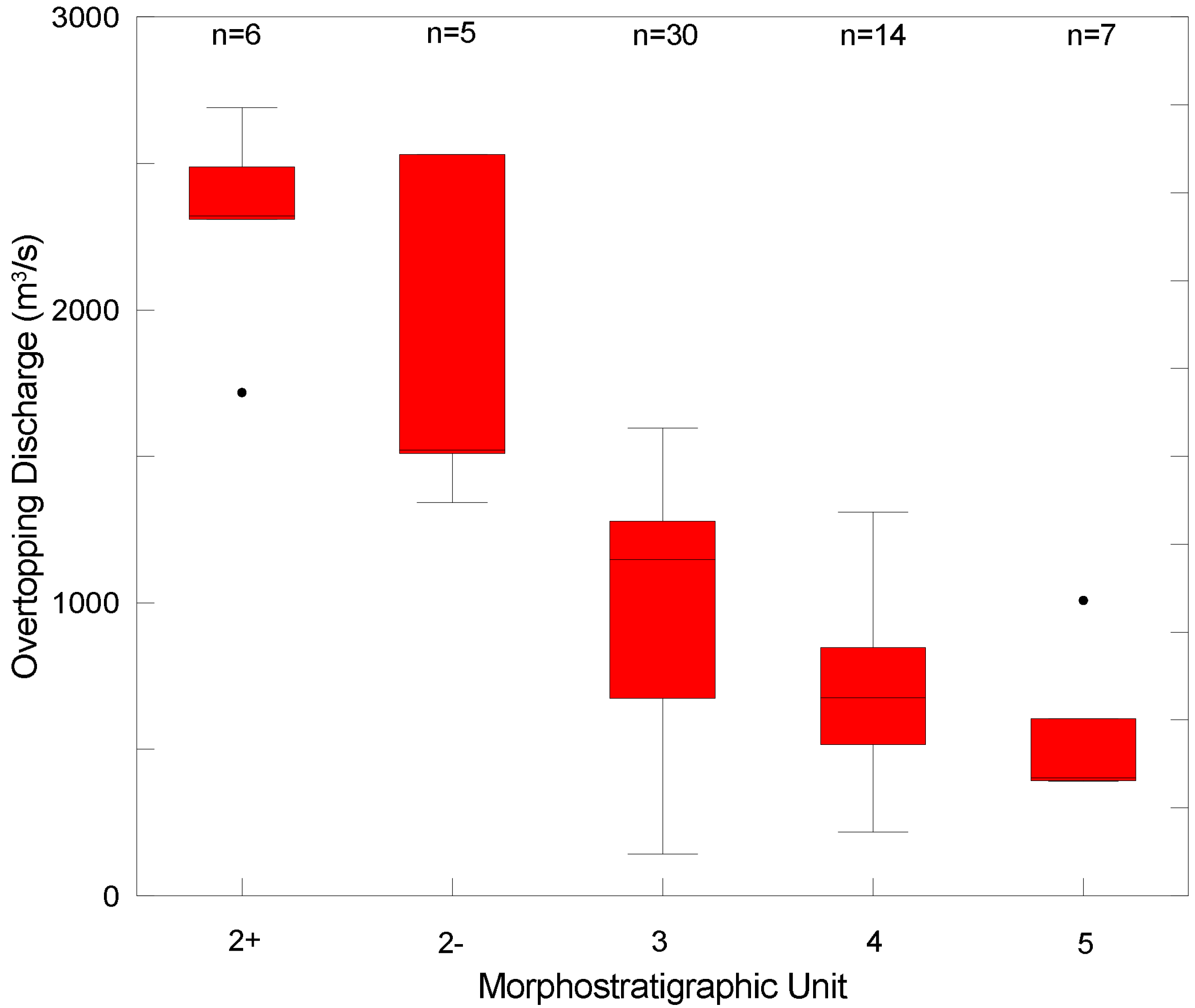

Figure 5.11 A box and whisker plot of the overtopping discharges for each morphostratigraphic unit in Subreach IIa.

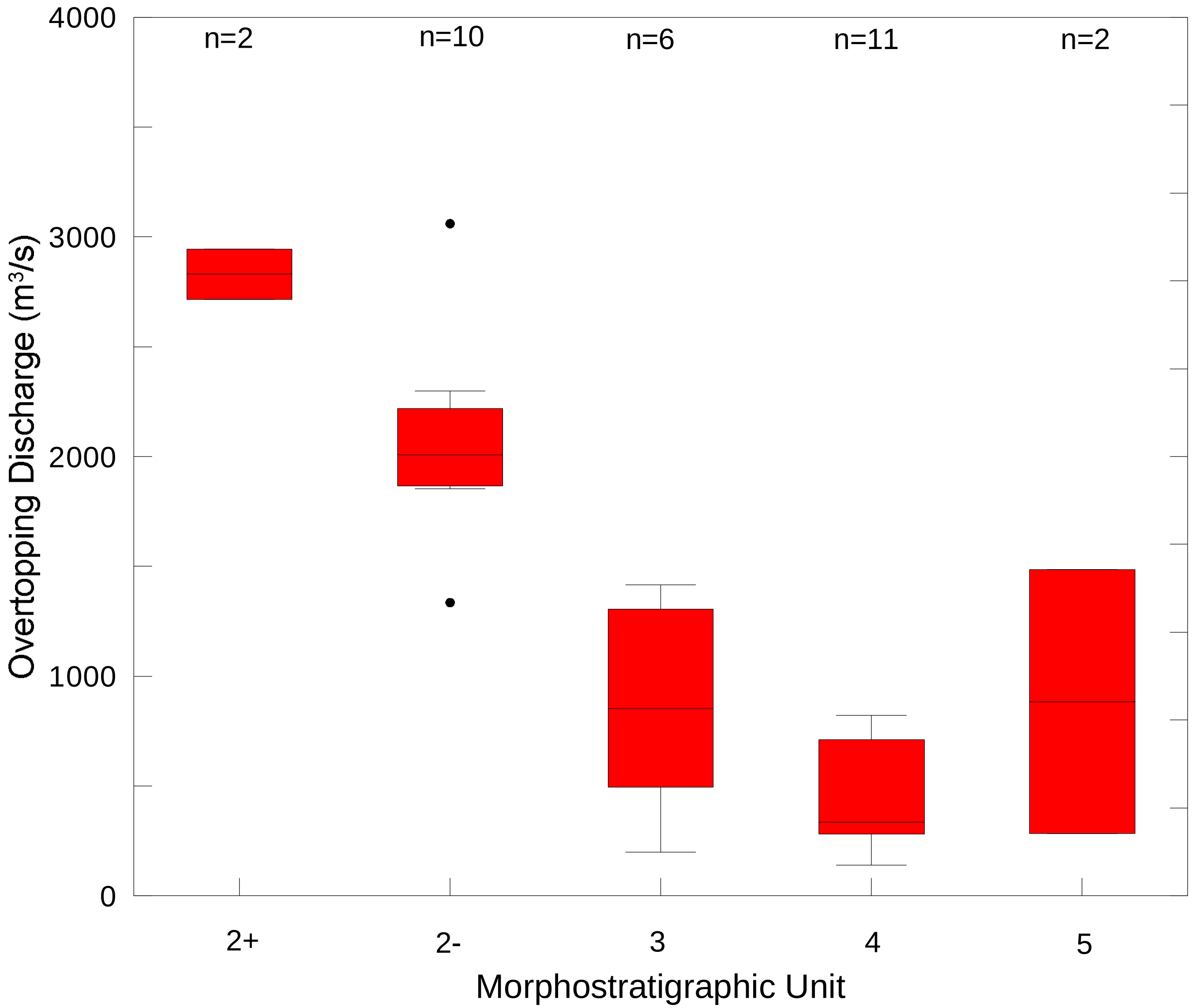

Figure 5.12 A box and whisker plot of the overtopping discharges for each morphostratigraphic unit in Subreach IIb.

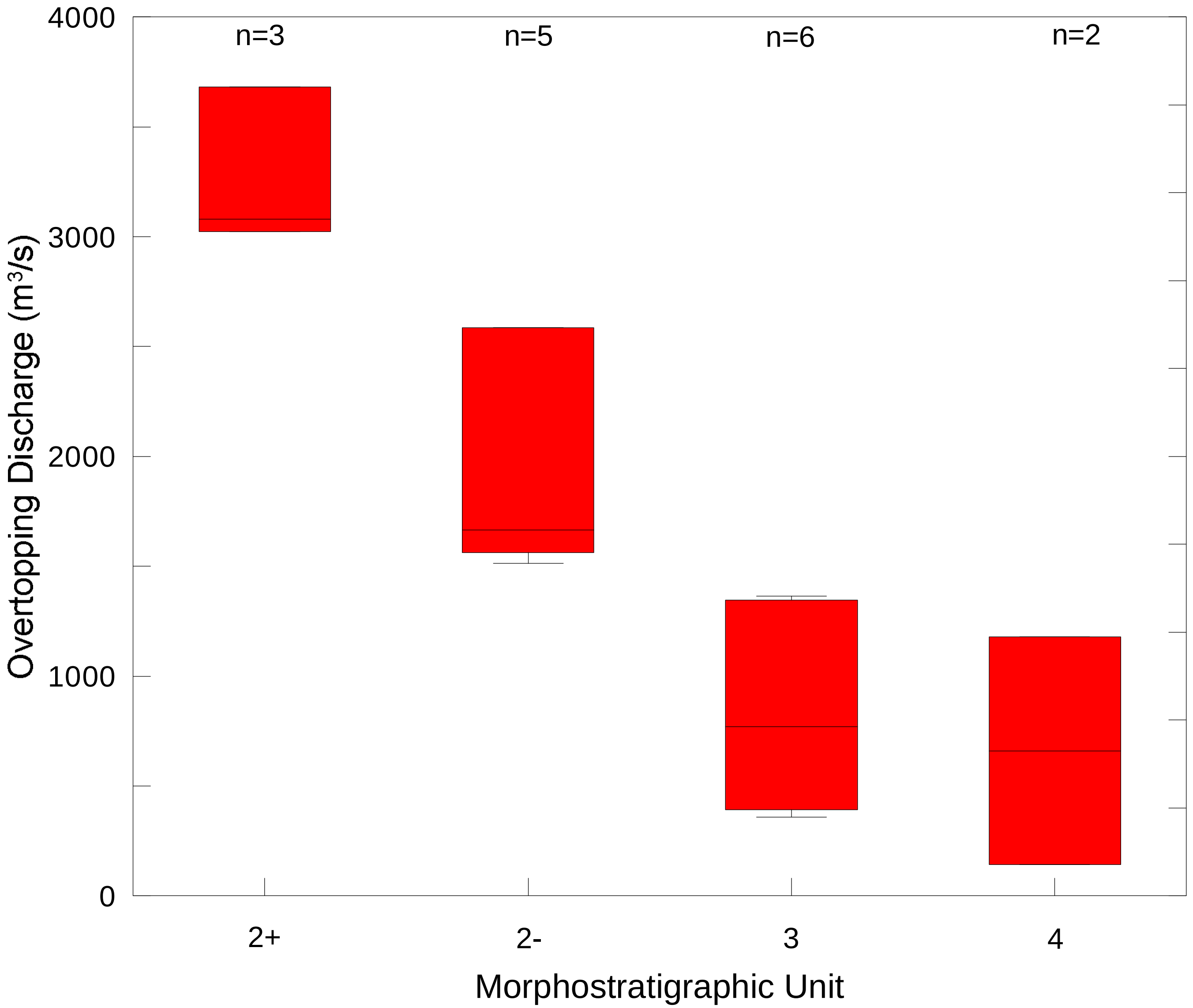

Figure 5.13 A box and whisker plot of the overtopping discharges for each morphostratigraphic unit in Subreach III.

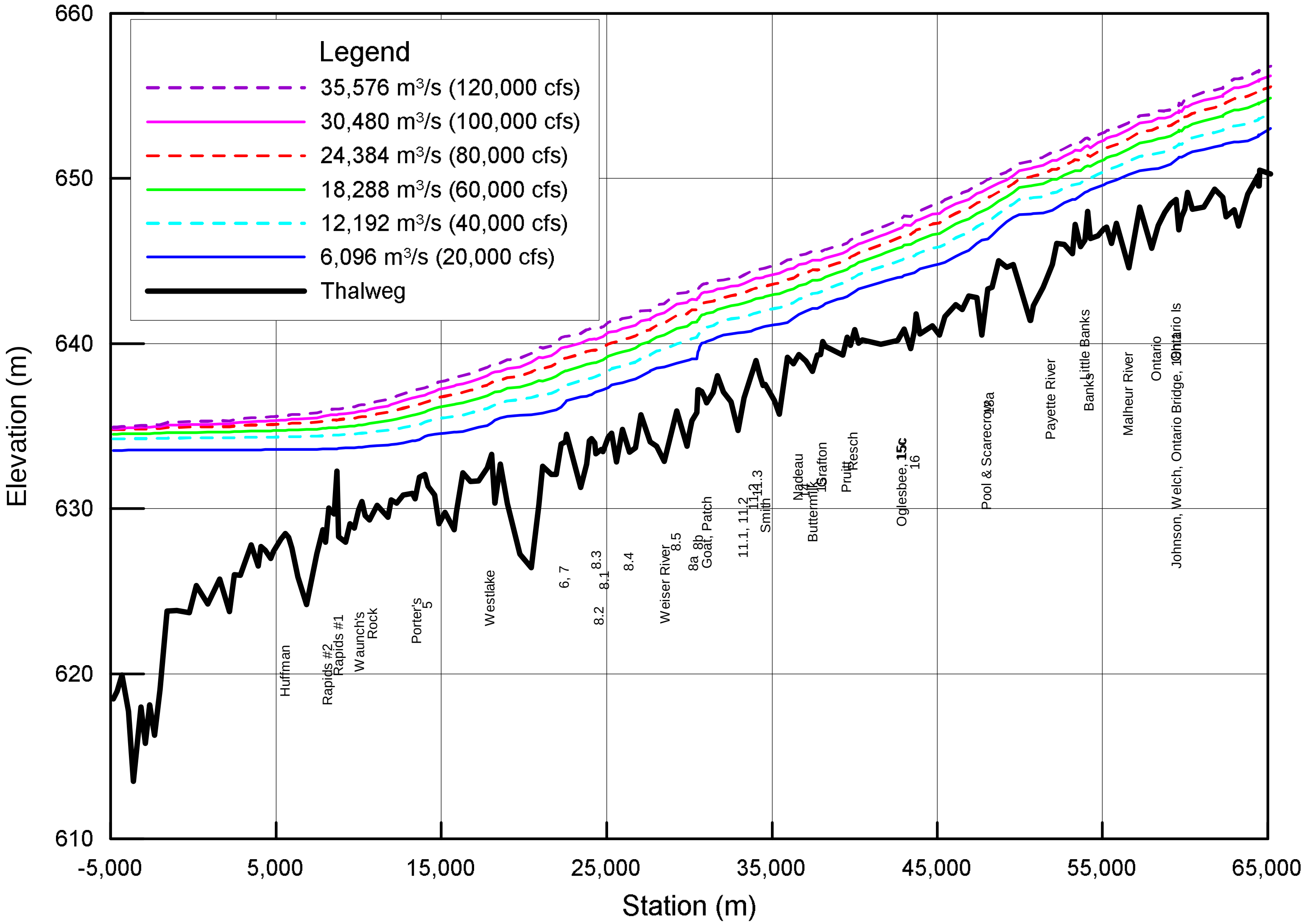

Figure 5.14 Water-surface profiles and the thalweg profile for the Lower section of the study reach, which includes Geomorphic Subreaches IIB and III.

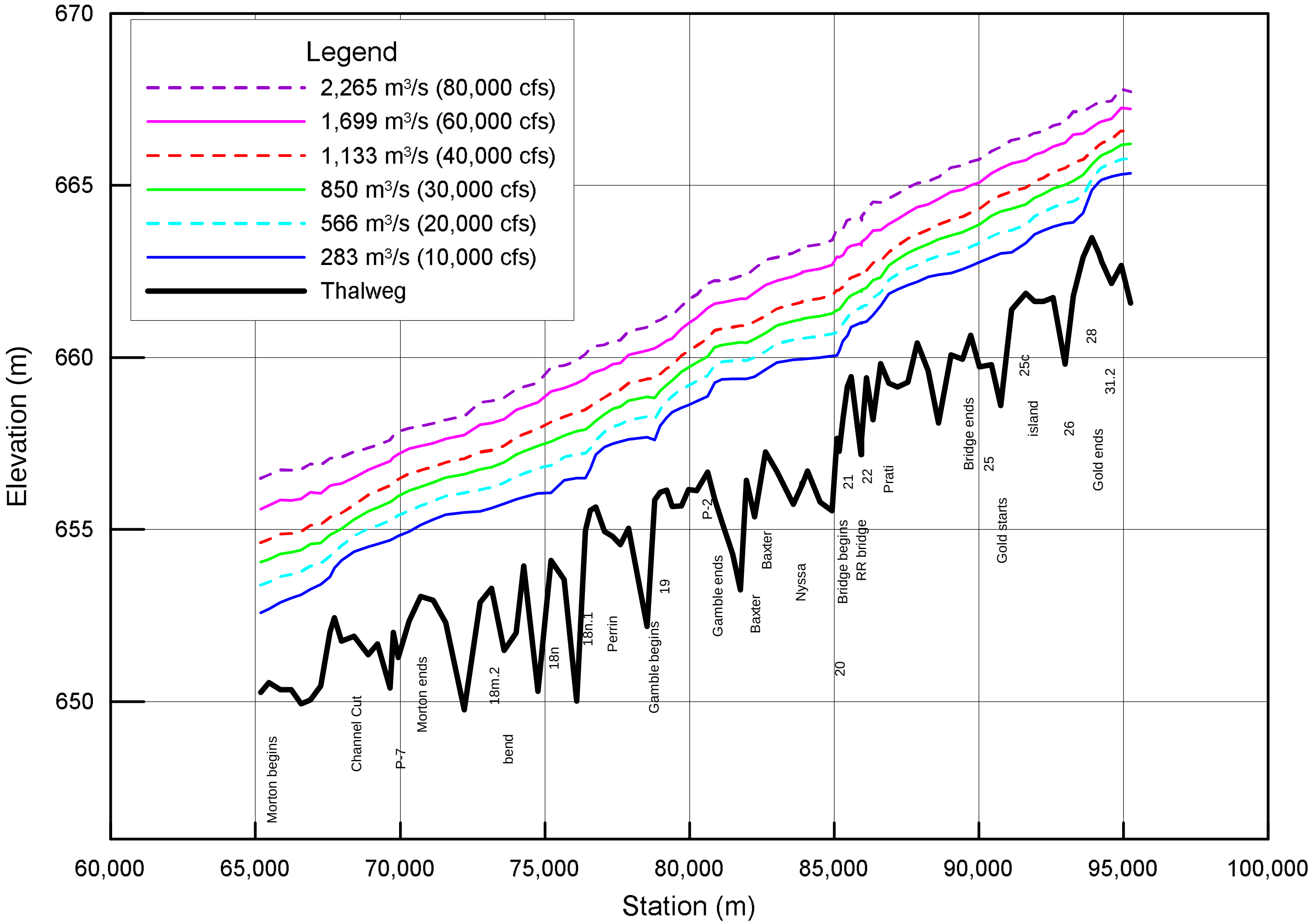

Figure 5.15 Water-surface profiles and the thalweg profile for the Middle section of the study reach, which includes Geomorphic Subreach IIA.

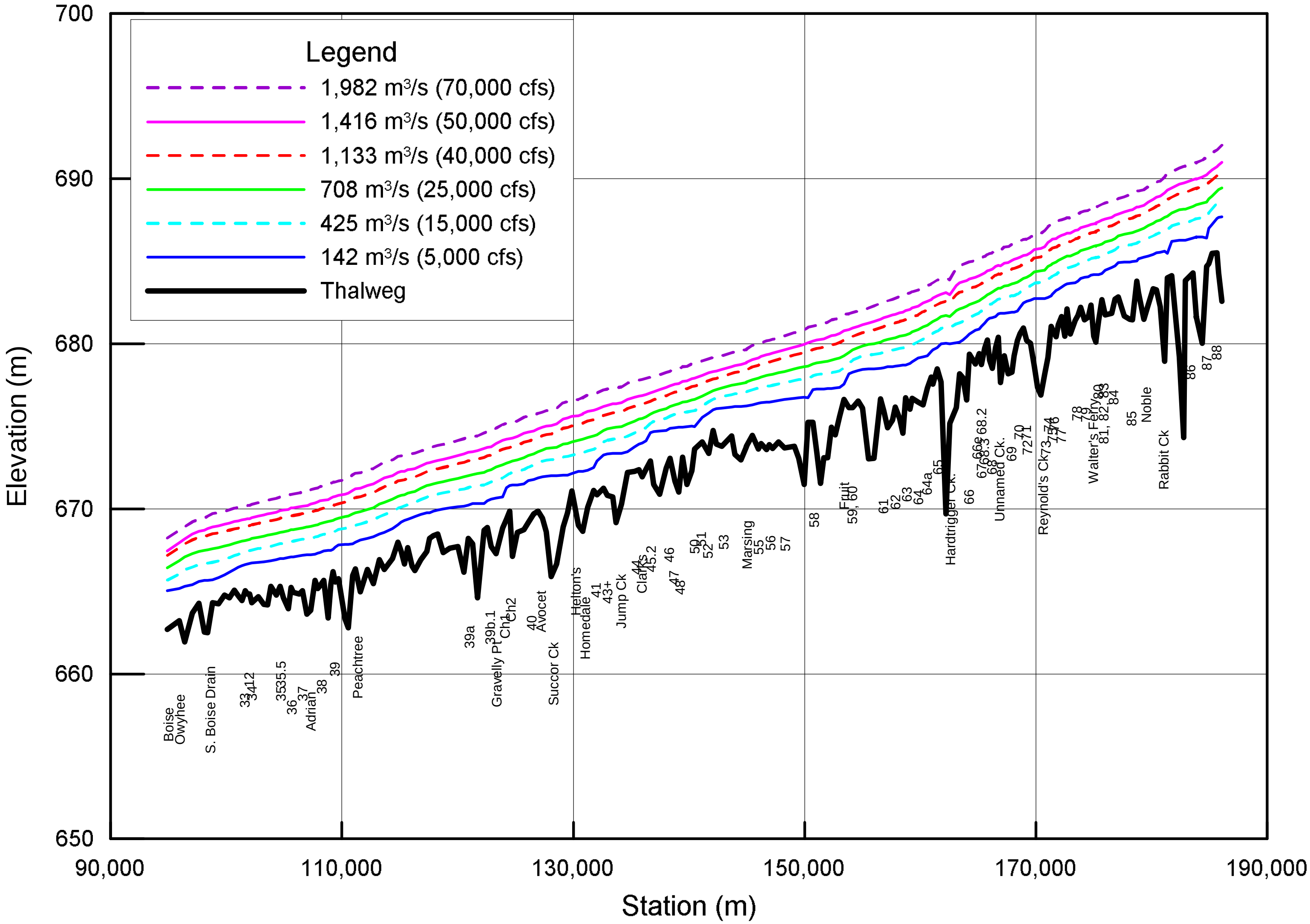

Figure 5.16 Water-surface profiles and the thalweg profile for the Upper section of the study reach, which includes Geomorphic Subreach I.

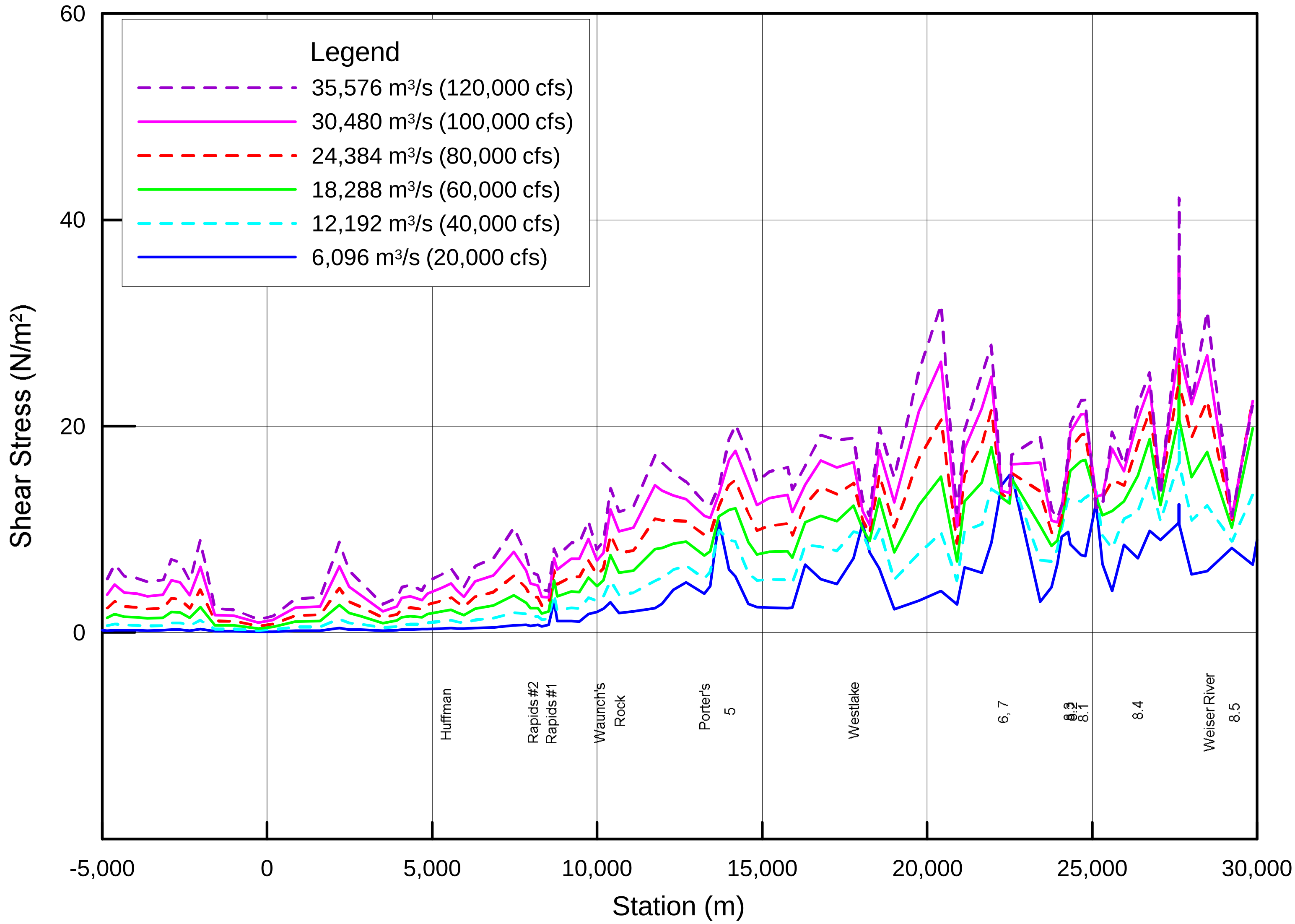

Figure 5.17 Shear-stress profile for the Lower section of the study reach (Sta -50+00 to Sta 300+00), which includes Geomorphic Subreaches IIB and III.

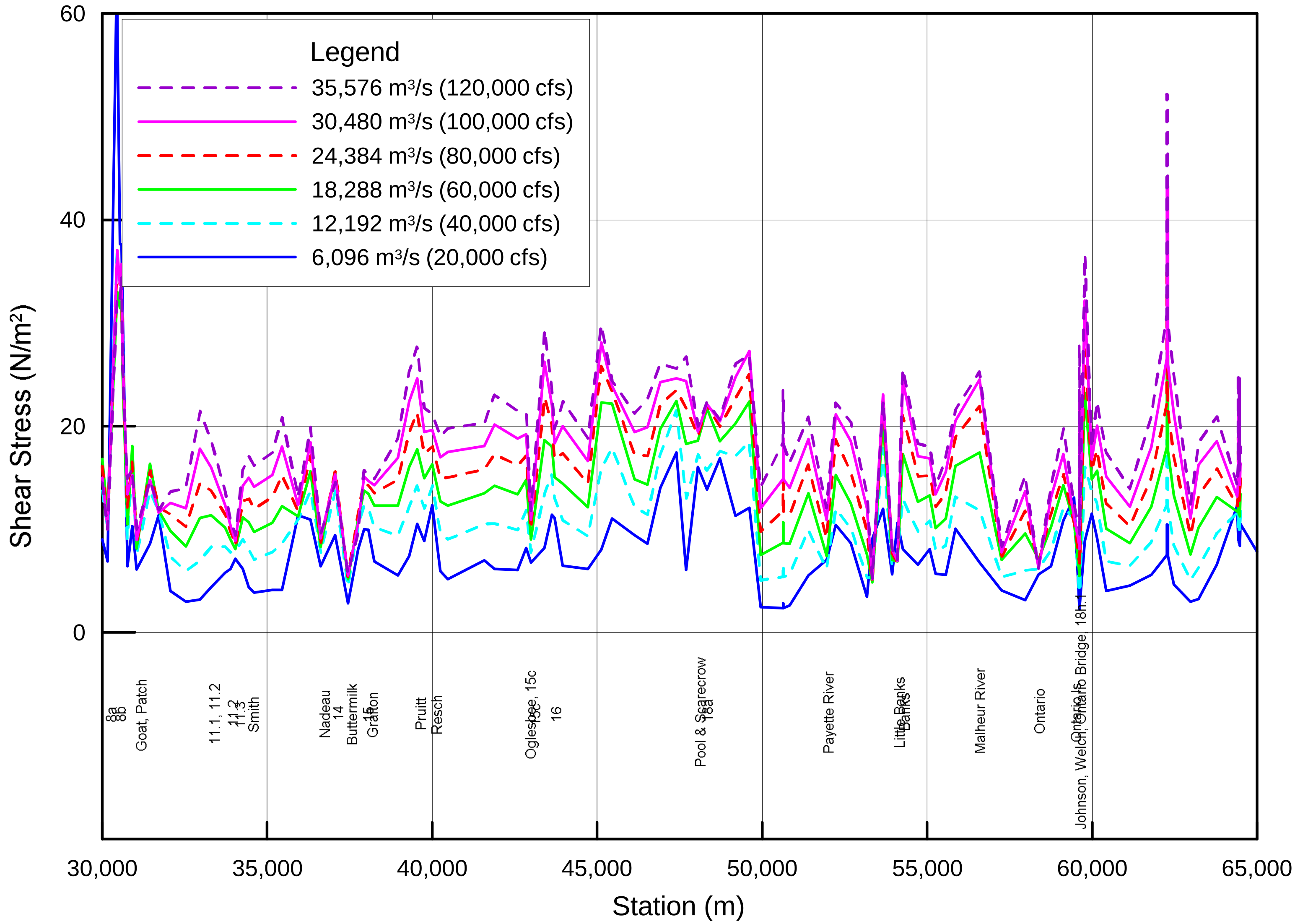

Figure 5.18 Shear-stress profile for the Lower section of the study reach (Sta 300+00 to Sta 650+00), which includes Geomorphic Subreaches IIB and III.

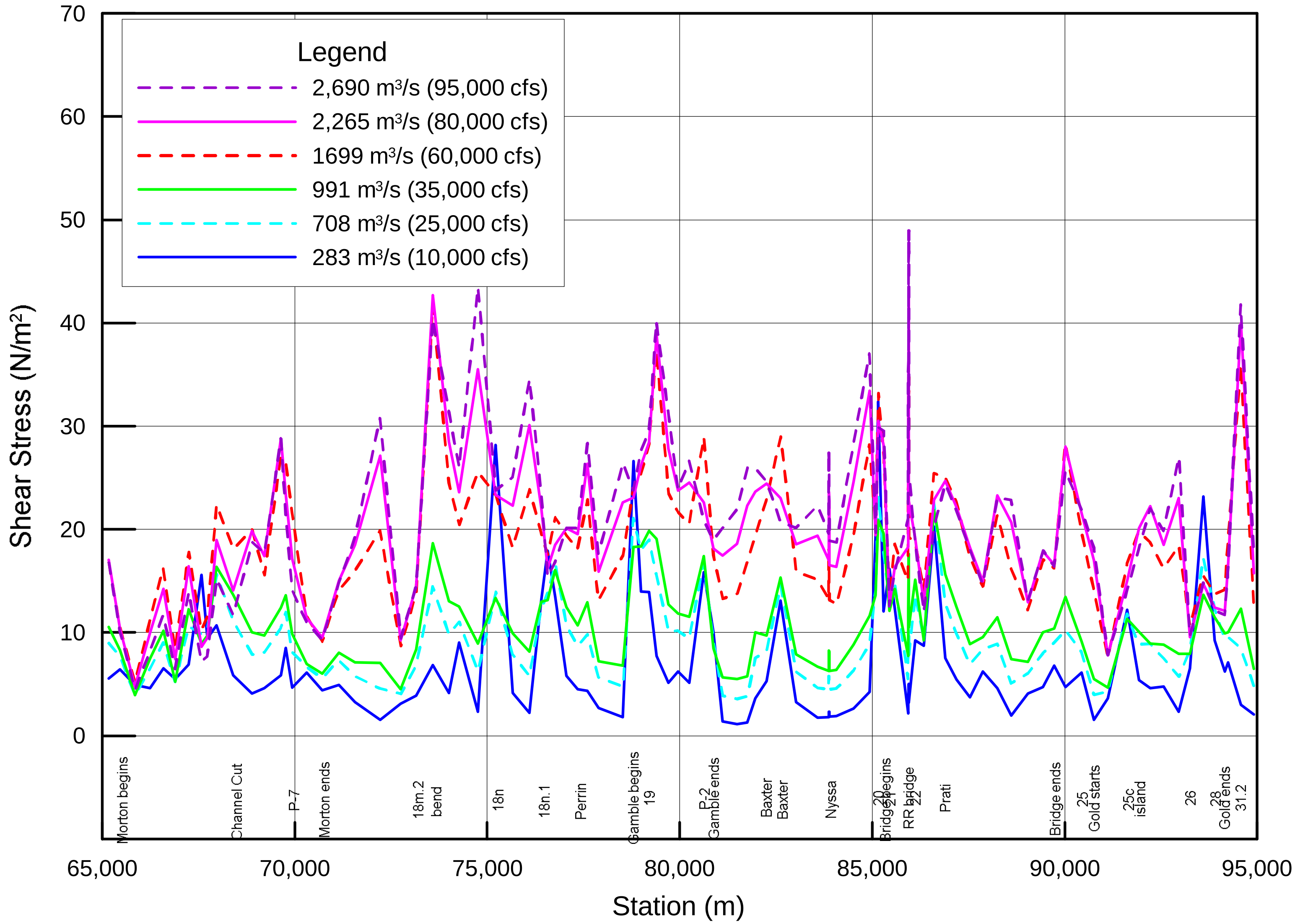

Figure 5.19 Shear-stress profile for the Middle section of the study reach (Station 65,000 to 95,000), which includes Geomorphic Subreach IIA.

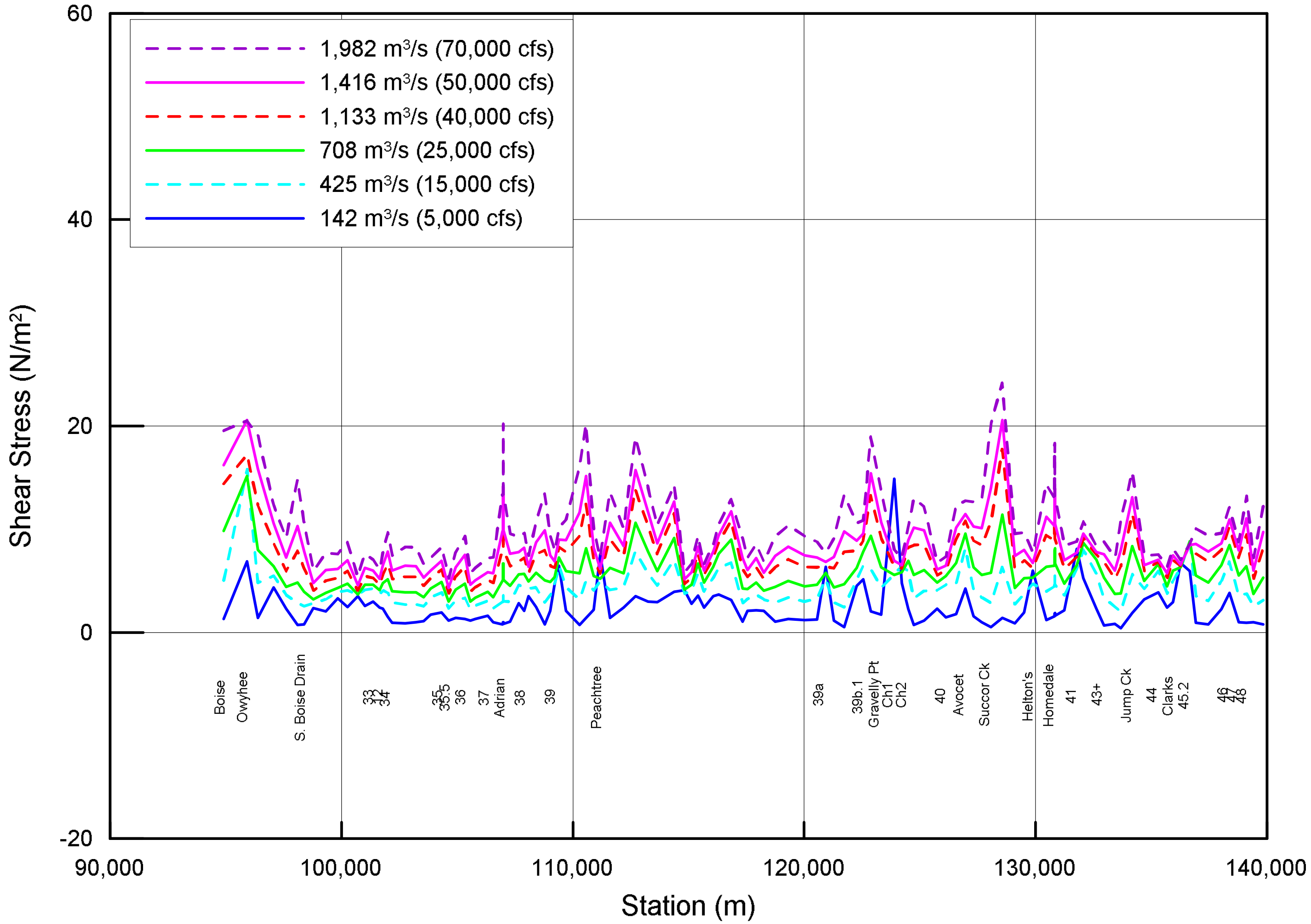

Figure 5.20 Shear Stress profile and the thalweg profile for the Upper section of the study reach, which includes Geomorphic Subreach I.

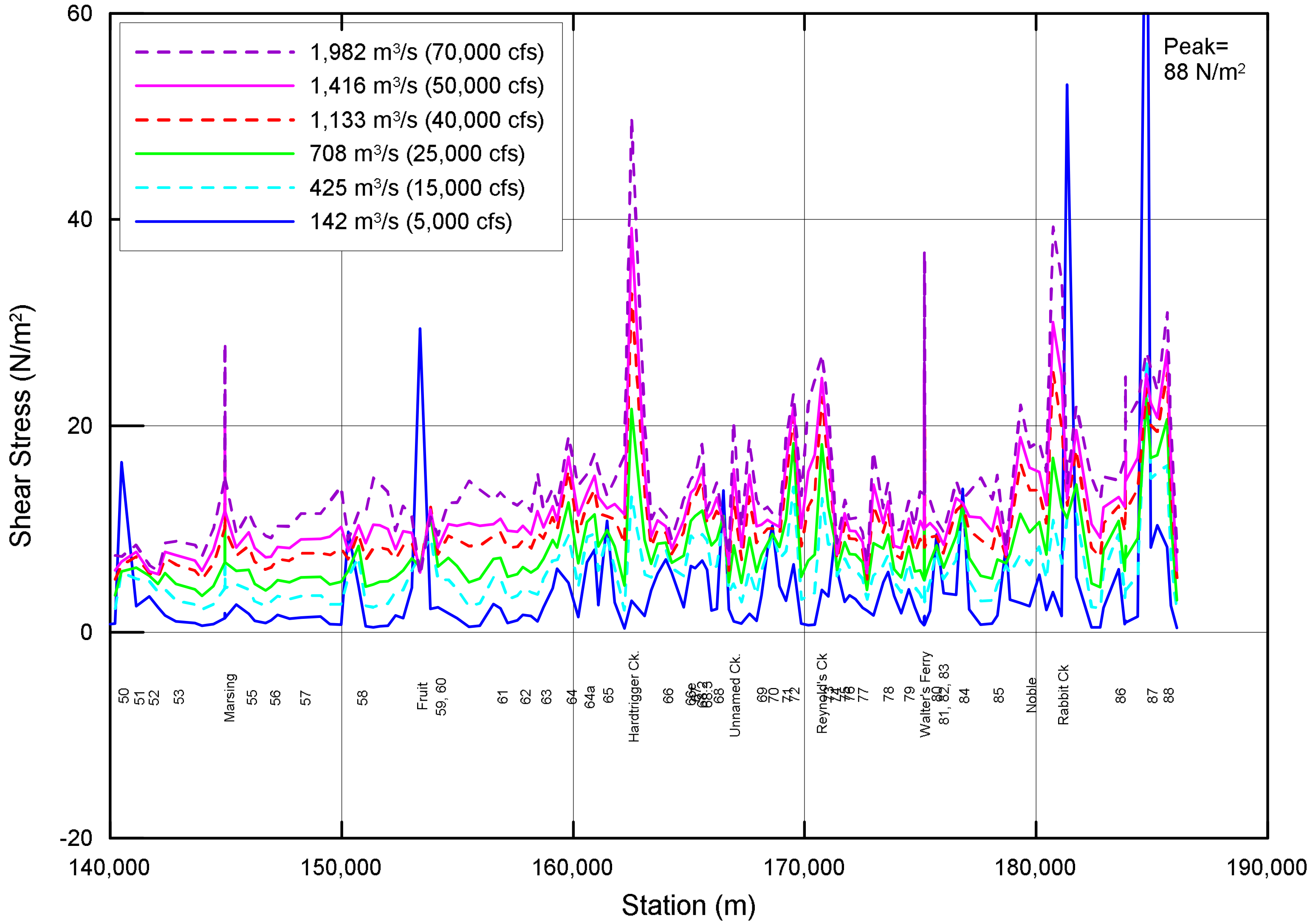

Figure 5.21 Shear Stress profile and the thalweg profile for the Upper section of the study reach, which includes Geomorphic Subreach I.

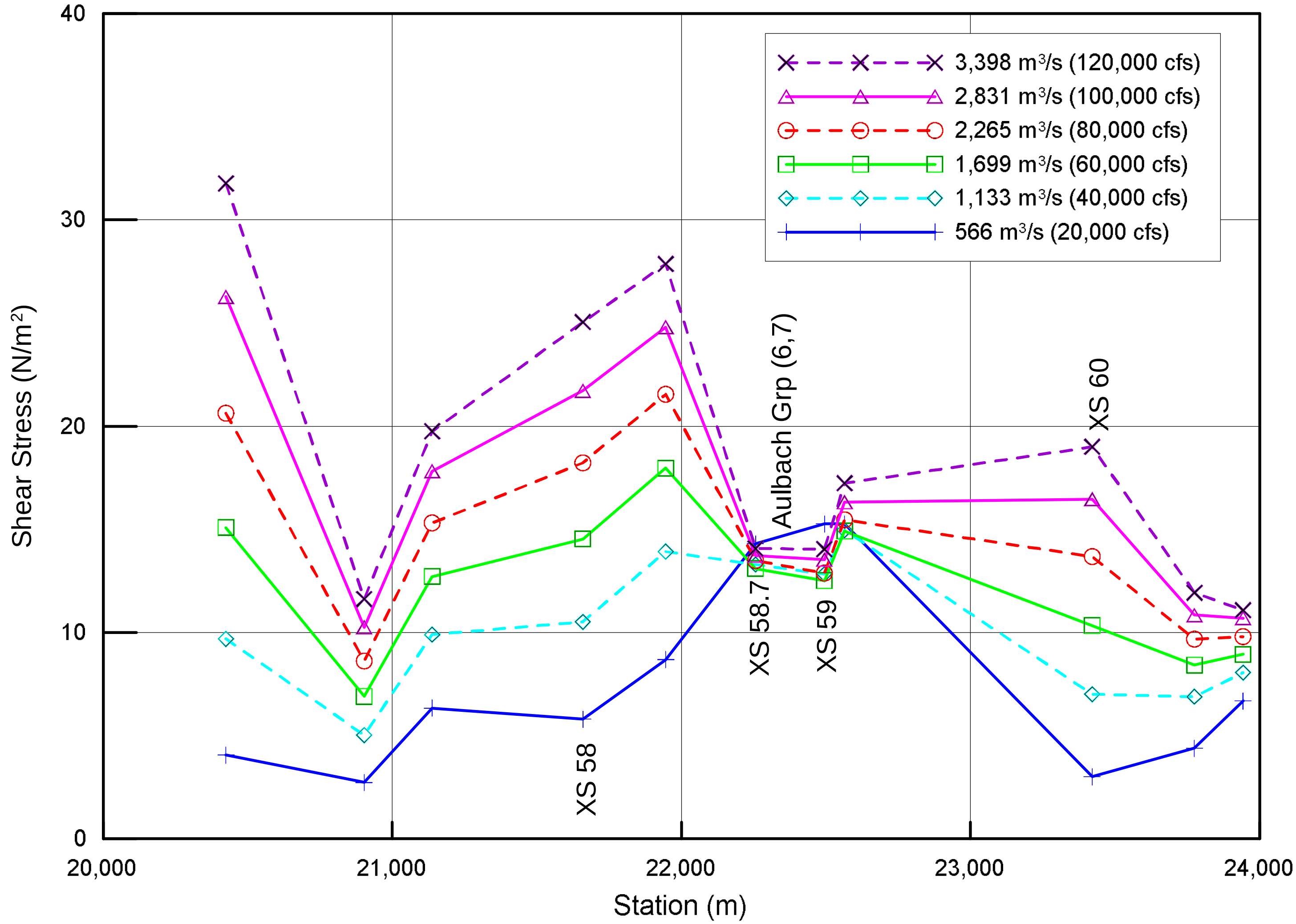

Figure 5.22 Shear stress profile in the vicinity of the Aulbach Island Group (6, 7). Note: the shear reversal in the vicinity of the Aulbach Group. The location of the cross sections is shown in Figure 5.23.

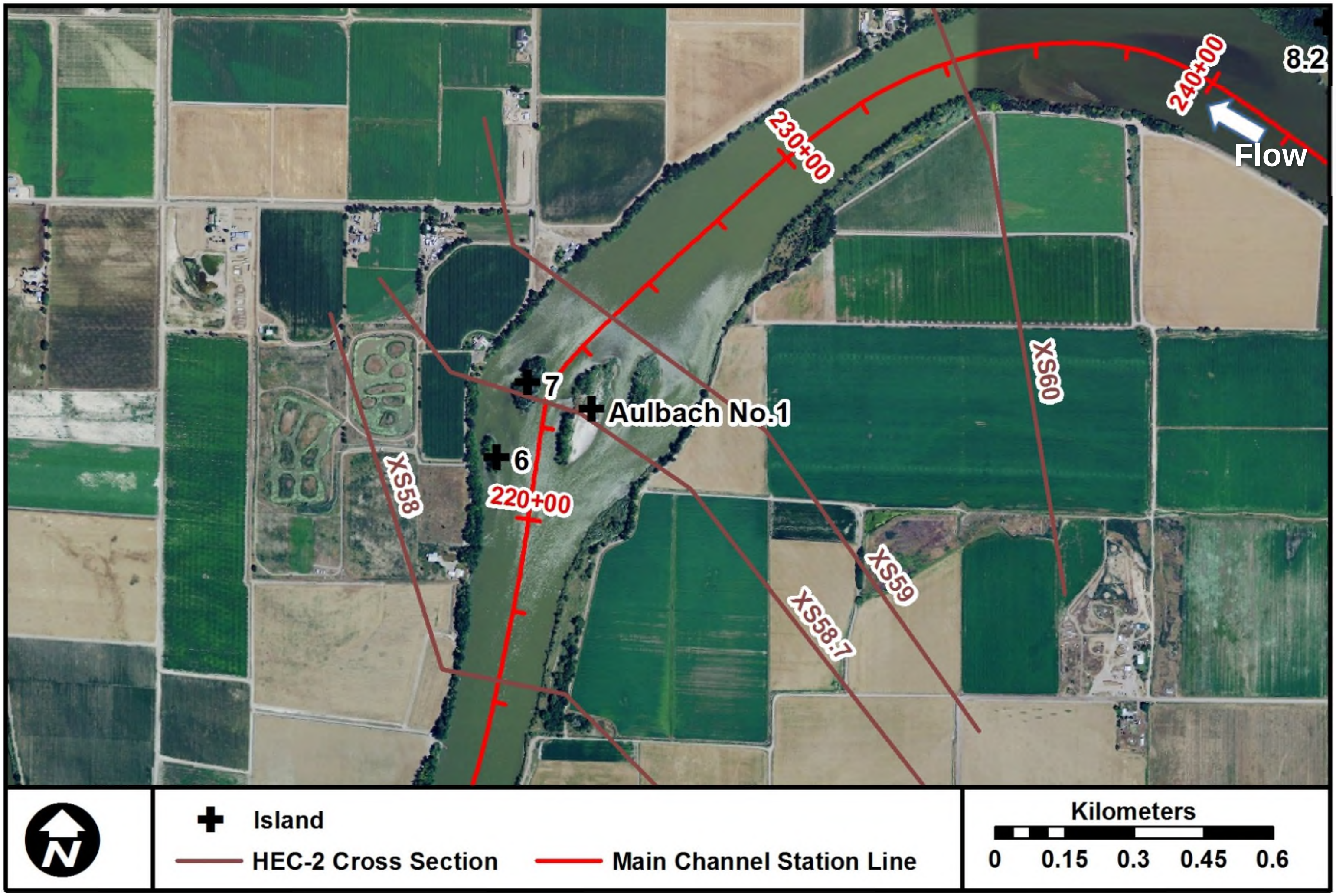

Figure 5.23 Location of Cross Sections 58, 58.7, 59 and 60 shown in Figure 5.22 and Figure 5.24.

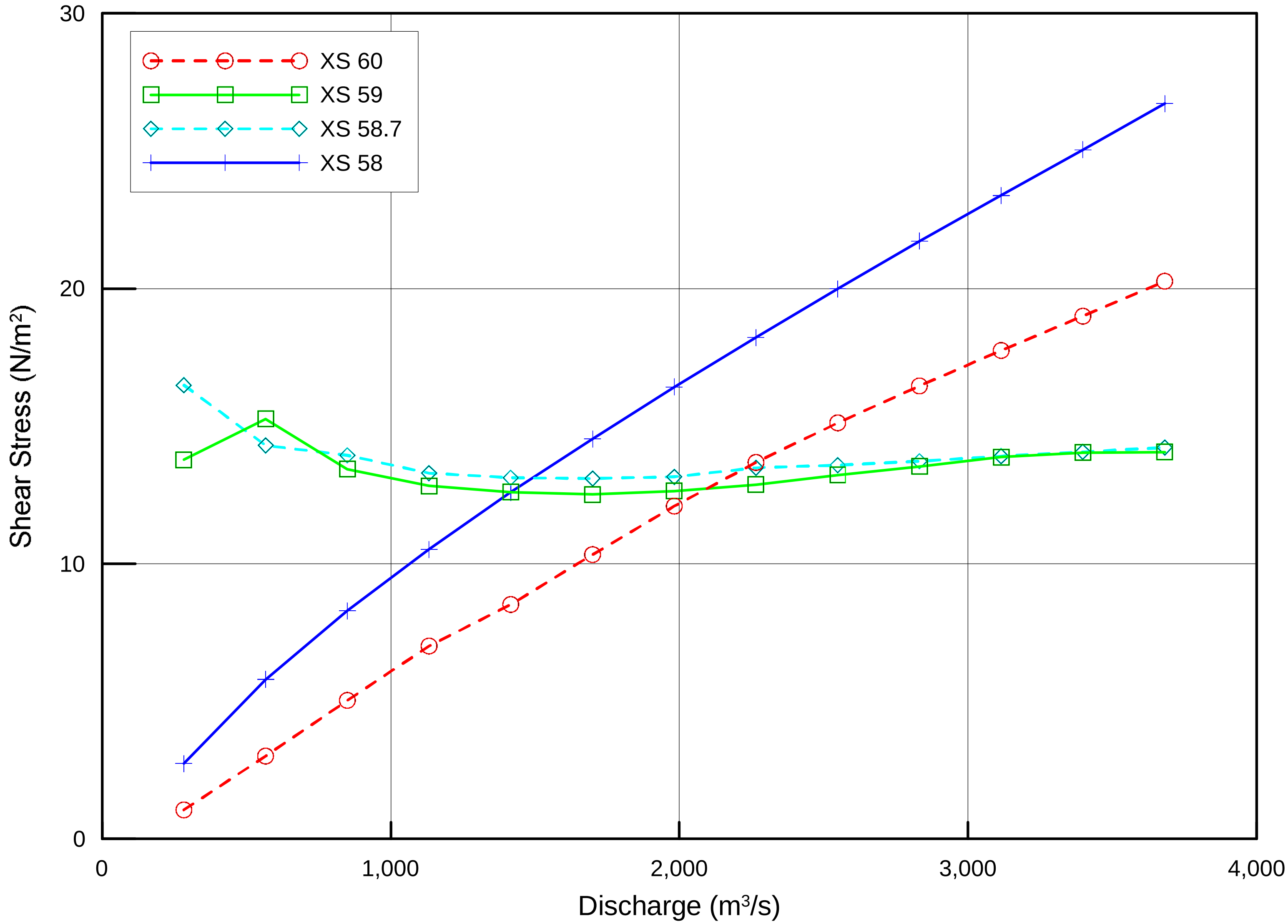

Figure 5.24 A plot of the upstream (Cross Section 60) and downstream (Cross Section 58) pool shear stress values versus the shear stress values at the island cross sections (58.7 and 59) for the Aulbach Island Group (6, 7). The location of the cross sections is shown in Figure 5.23.

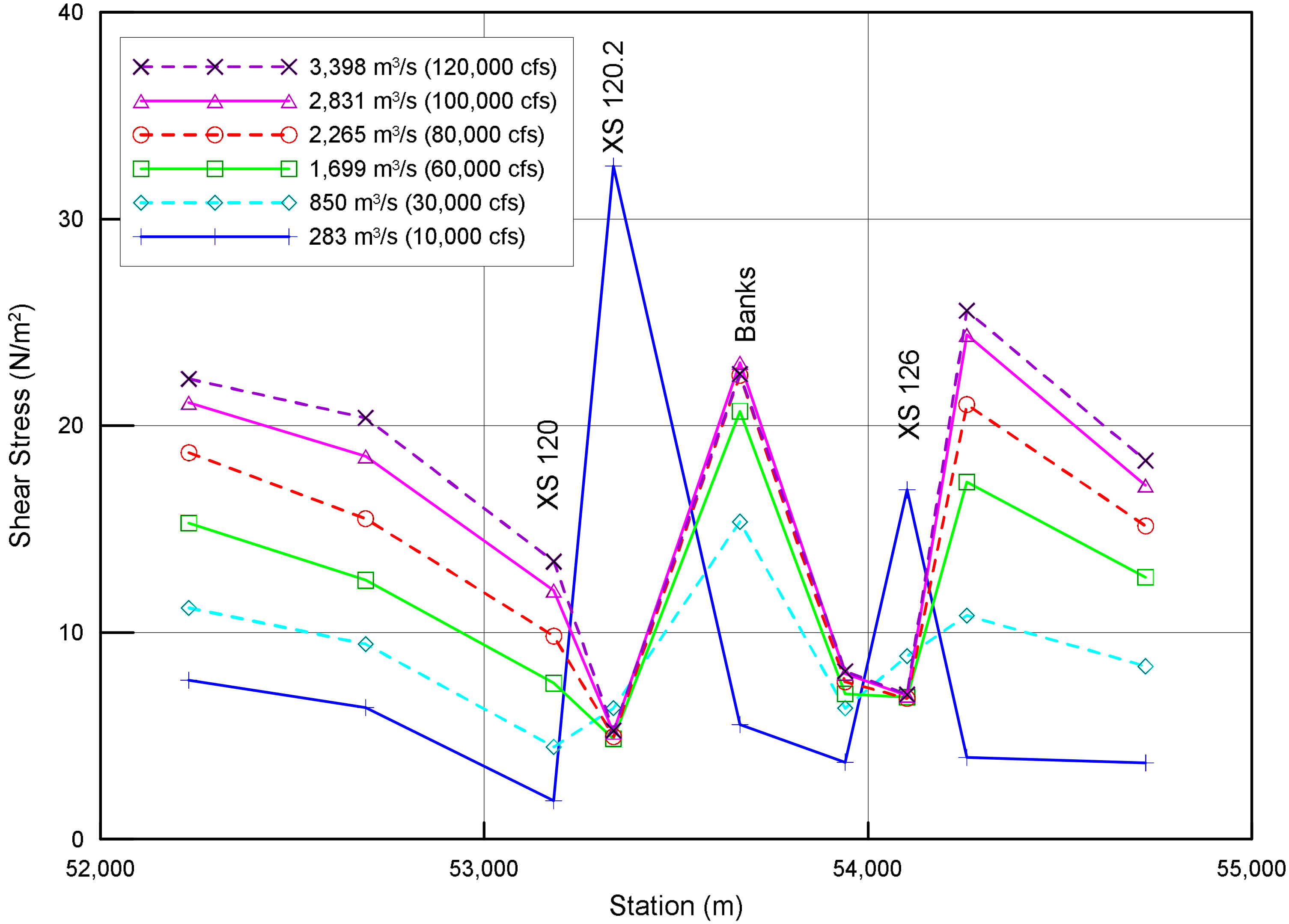

Figure 5.25 An expansion of Figure 5.18 for the reach in the vicinity of the Banks Islands and the unnamed Island 18h. The location of the cross sections is shown in Figure 5.26.

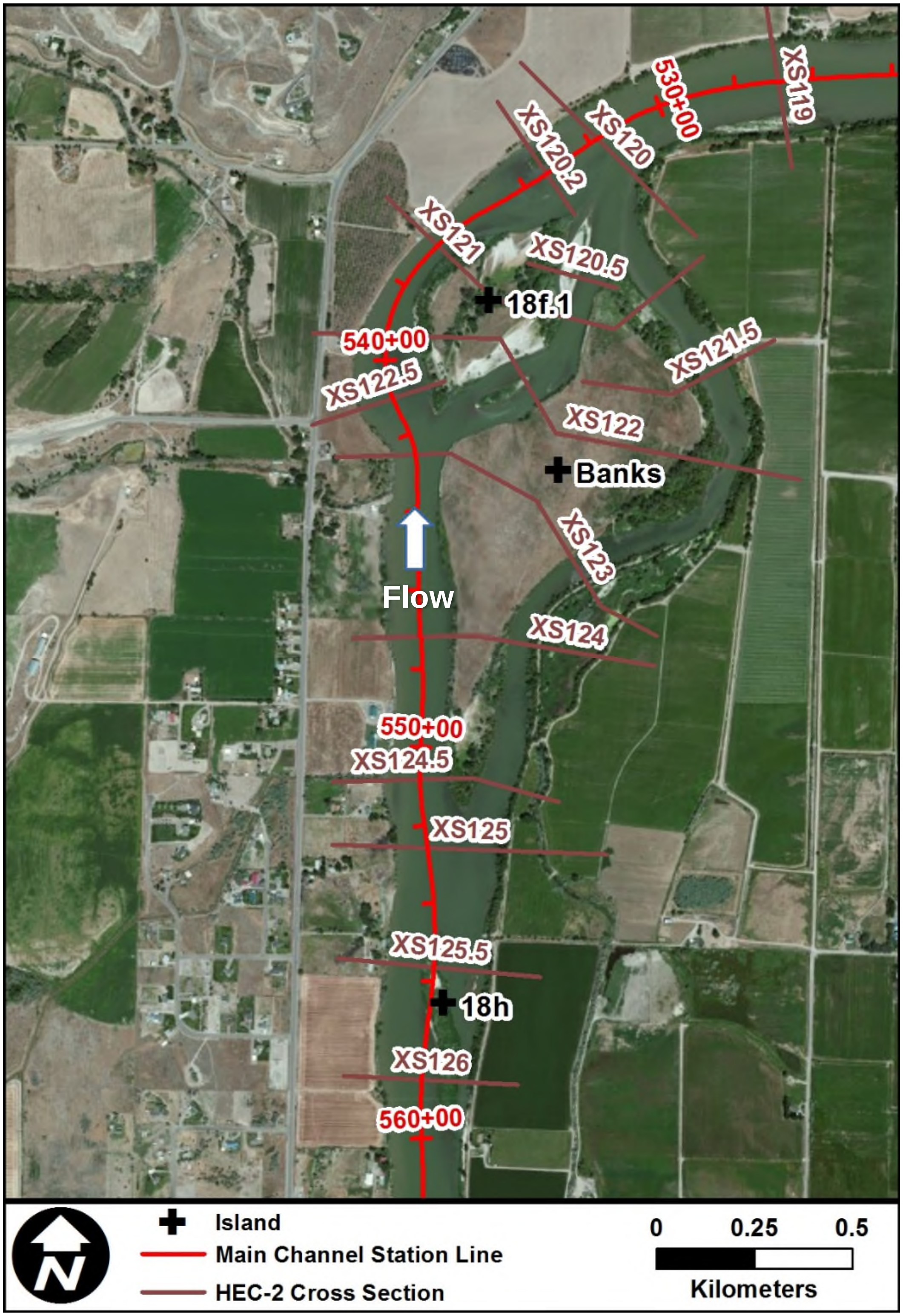

Figure 5.26 Location of Cross Section 120, 120.2 and 126 shown in Figure 5.25 and Figure 5.27.

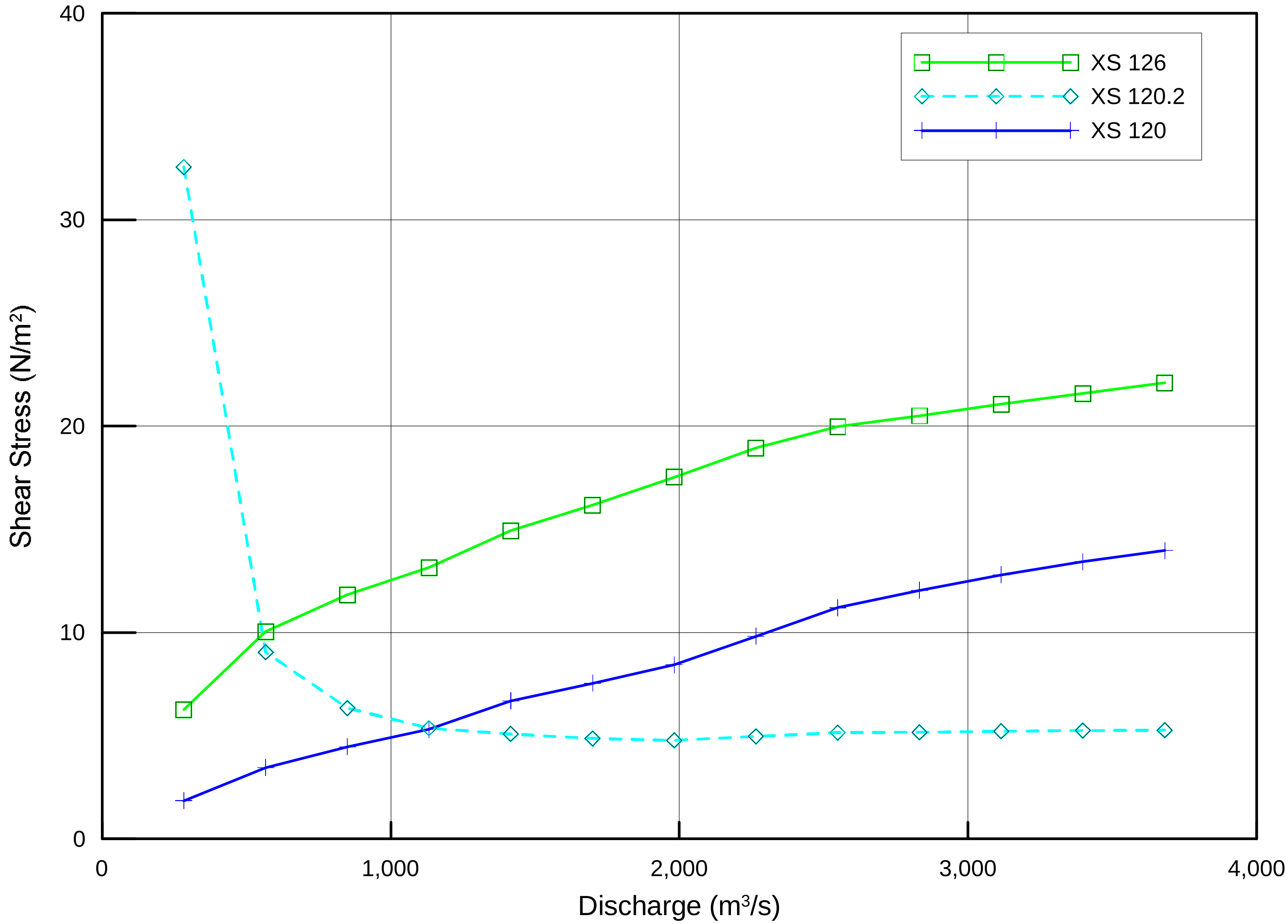

Figure 5.27 A plot of the upstream (Cross Section 126) and downstream (Cross Section 120) pool shear stress values versus the shear stress values at the island cross section (120.2) for Banks Island and 18h. The location of the cross sections is shown in Figure 5.26.

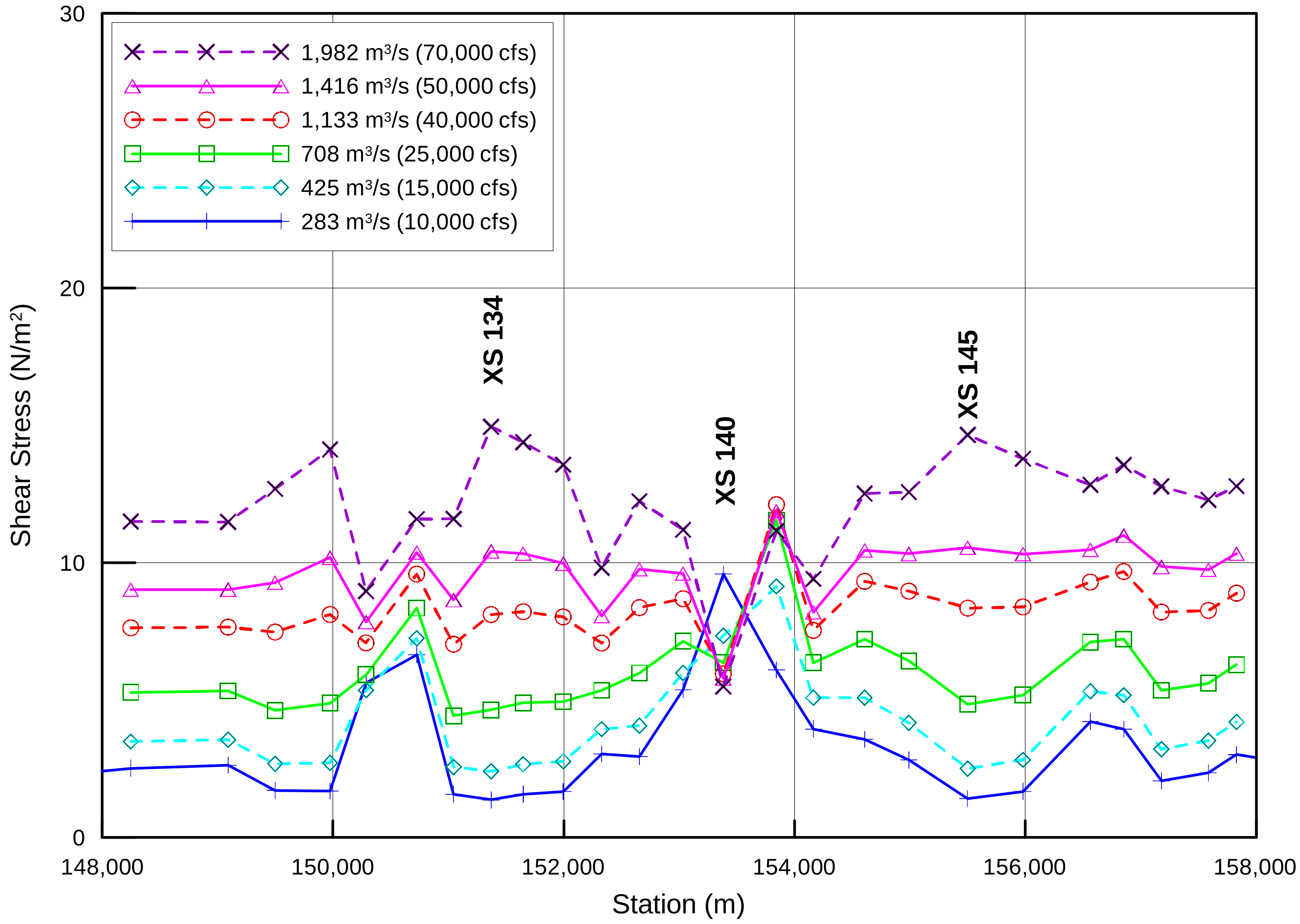

Figure 5.28 Shear stress profiles in the reach around the Fruit/Dilley Island Group (59, 60) The location of the cross sections is shown in Figure 5.29.

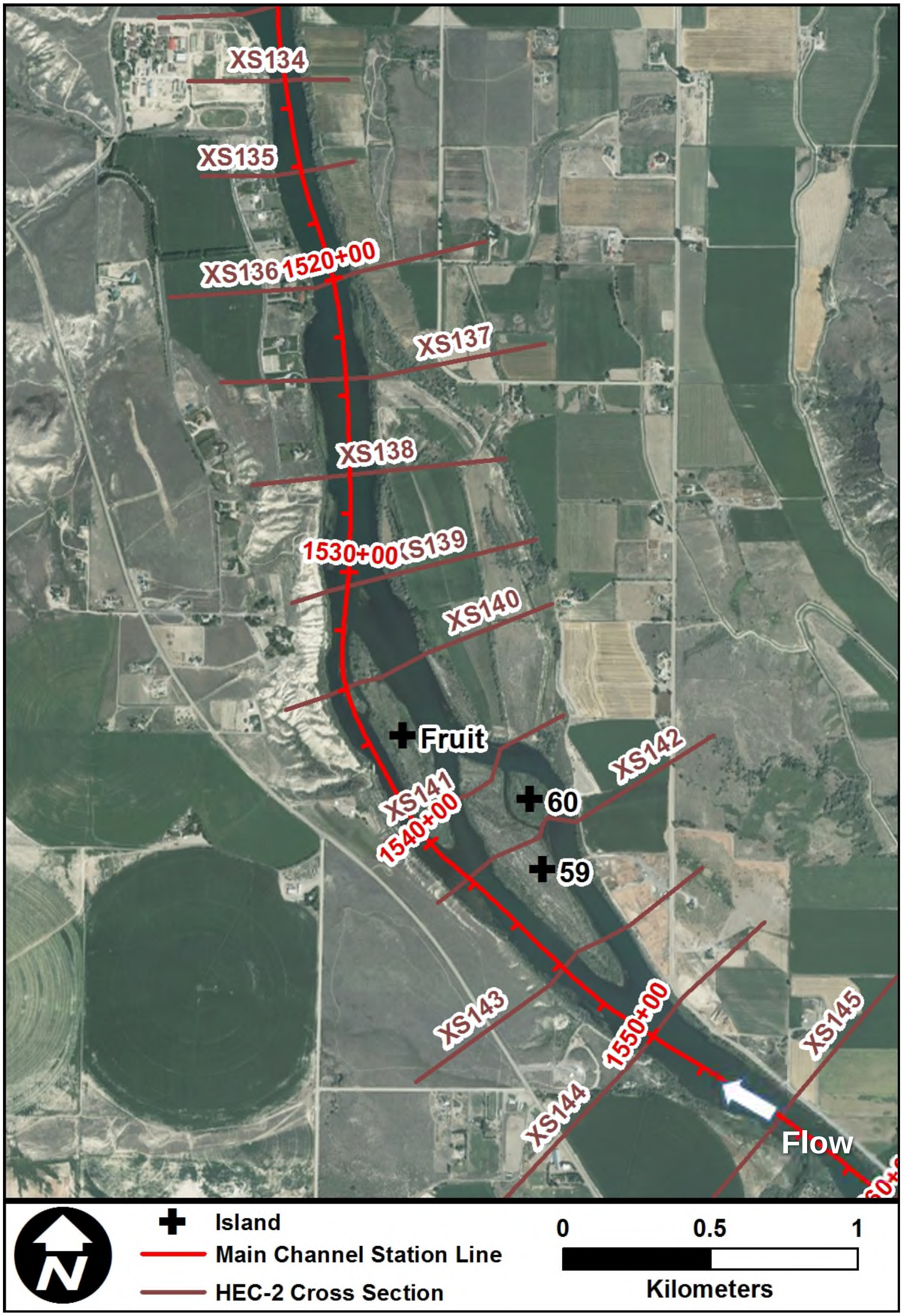

Figure 5.29 Location of Cross Section (134, 140 and 145) shown in Figure 5.28 and Figure 5.30.

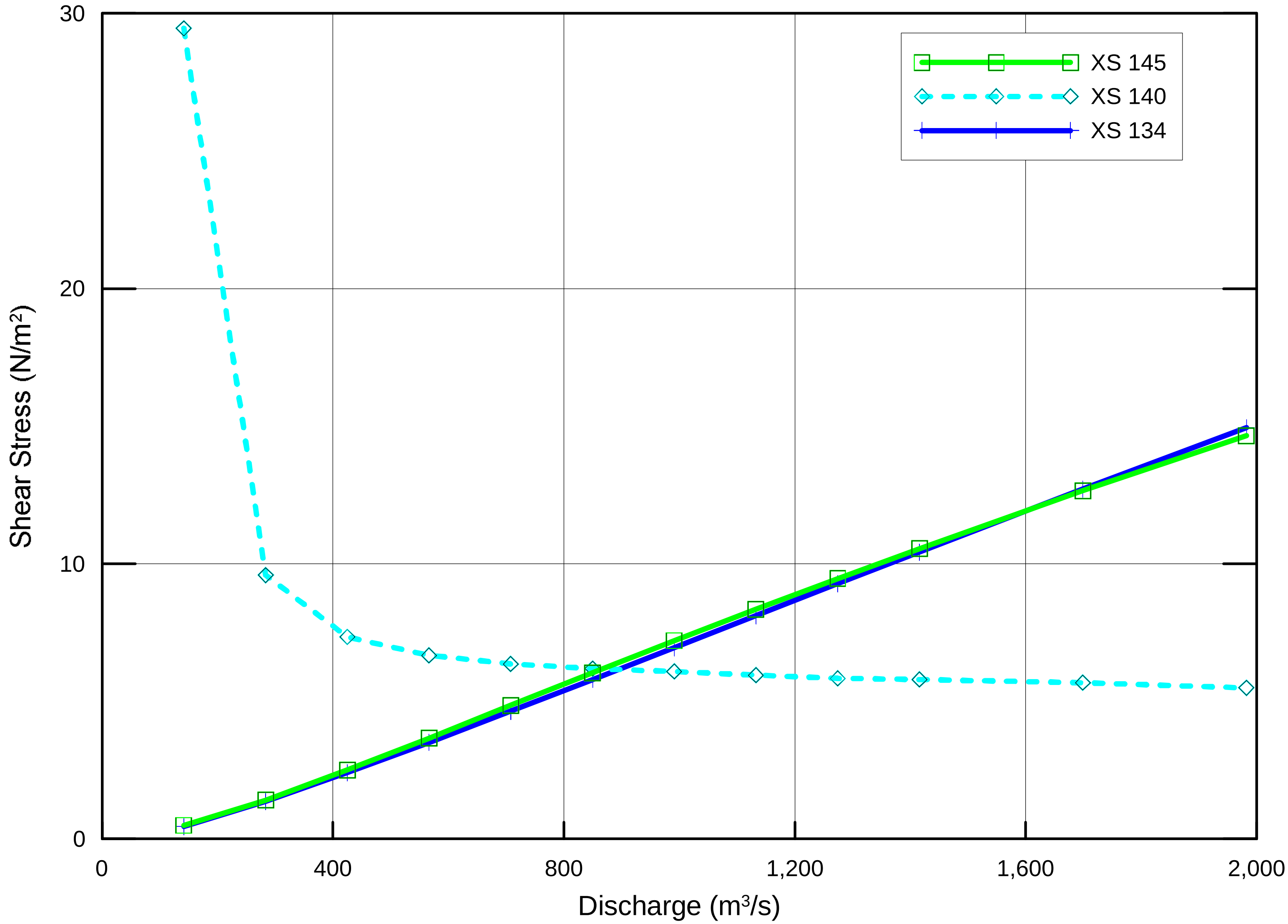

Figure 5.30 A plot of the upstream (Cross Section 145) and downstream (Cross Section 134) pool shear stress values versus the shear stress values at the island cross section (140) for Fruit/Dilley Group (59, 60). The location of the cross sections is shown in Figure 5.29.

Table 5.4 Carbon 14 results.

Island Number	Island Name	Material	Age BP	+ / - years	Depth of Layer (cm)
5	Jackass	wood	145.9	0.70%	175-180
28	Big Cottonwood	organic sediment	350	70	56-64
	River Bank	organic sediment	930	80	
45.2	Olive	organic sediment	2960	80	155-165
47	Pheasant #2	organic sediment	2190	40	137-150
52	Jensen	organic sediment	690	60	61-79
70	Fisher	charred material	290	40	71-76
74	Bayha	charred material	110	40	117-130
74	Bayha	organic sediment	850	60	218-226
78.3	Brooks	organic sediment	280	60	46-47
88	Sign	organic sediment	120	60	36-41

*This values presented in percent; all others in years.

6. Two-dimensional Sediment-transport Modeling

Two-dimensional sediment-transport models of the Ketchup and Walters Ferry reaches were developed and run to test the following study hypotheses: (1) where the hydraulic controls are fixed, islands will form, erode and reform in the same general locations, and (2) the islands regulate sediment transport by adjusting their geometry to maintain sediment continuity. In addition, the results of the 2-D modeling were used to evaluate the apparent discrepancy between the young soils and the older gravel cores in many islands and to further develop the conceptual model of island formation. Evidence supporting the hypotheses may help explain this discrepancy because older cores may persist, whereas the overlying soils may cycle through erosion and development.

The baseline 2-D hydraulic models of the Ketchup and Walters Ferry reaches, which were developed using the 1997/1999 topography and bathymetry, were used to perform an incipient motion analysis to evaluate the mobility of the bed material to provide a better understanding of the baseline conditions and to develop the sediment transport modeling methodology. In addition, the incipient motion analysis was used in part to explain the existence of relatively young soils overlying old gravel cores.

2-D sediment-transport models were developed by modifying the Ketchup and Walters Ferry baseline models to represent the geometry of the reach without the islands, and by incorporating the required sediment-transport parameters, which include the sediment-transport equation, representative bed-material sediment gradations and input discharge versus sediment-transport rating curve.

The historical hydraulic, hydrologic and sediment transport conditions that the islands formed under are not known, and therefore, it was not possible to recreate historical hydrologic and sediment inflow conditions. Due to the lack of sediment-transport measurements, representative inflow sediment-rating curves and flow hydrographs were developed. In short, the 2-D sediment-transport modeling was performed to simulate the dynamics and processes of island development and not to recreate historical conditions.

The without-island models were run over a series of representative hydrographs (Section 4.2.3.4). A methodology was developed to represent the stabilizing effect of vegetation. The models were validated, to the extent possible, by comparing the predicted island sizes to the 1997/1999 baseline conditions. The model output was used to develop soil profiles, which are compared to the measured soil profiles. To test whether the islands adjust to maintain sediment continuity, the variations in sediment transport rates were compared at several locations along the reach.

6.1. Sediment-transport Model Development

6.1.1. Incipient Motion Analysis

The channel bed in the Ketchup and Walters Ferry reaches is composed primarily of gravel- to cobble-sized material, while the islands are composed of silt to sand sized materials. An incipient motion analysis was conducted to determine the mobility of the bed material for flows up to the bank full discharge, and to determine whether the bed material was mobilized under pre-dam conditions.

The incipient-motion analysis was performed by evaluating the effective shear stress on the bed material in relation to the amount of shear stress that is required to move the material. The normalized grain shear (NGS) stress (τ^*) for a specific discharge, which is defined as the ratio of the grain shear stress (τ') to the critical shear stress (τ_c), provides a measure of the relative ability of that discharge to mobilize the bed material (Shields, 1936). Values of the normalized grain shear stress less than one (corresponding to a Shields value of 0.03) indicate that the bed material is not mobile and values greater than one indicate bed-material mobility.

Additionally, when the normalized grain shear stress is between 1 and about 1.5 (Shields value of 0.045), the bed-material transport rate is very low. Under these marginal transport conditions, when the upstream supply is also low, the bed will armor and significant channel bed adjustments will not typically occur (Parker et al., 1982; Andrews, 1984).

The normalized grain shear stress (τ^*) was computed using the sediment-transport routines in SRH-2D with a Shields value of 0.03 for all flows. Wilcock and Crowe (2003) developed a sediment transport equation for the transport of sand/gravel mixtures based on flume experiments and field data. Their study details the highly non-linear effect of the sand content of gravel transports rates. As the sand content increases, the channel bed transitions from a clast- to matrix-supported bed, resulting in an increase in the mobility of the gravel sized materials. When the surface content of the sand increases from approximately 15 to 25 percent, there is a corresponding decrease in the Shields parameter from 0.03 to 0.021, resulting in an increase in the mobility of the surface material. The bed material sampling along the MSR indicated very little sand-sized material and therefore the Shield's value of 0.03 is appropriate for baseline conditions. Two subsurface samples of the bed-material were collected at the heads of islands along the MSR indicated that approximately 15-percent of the subsurface material was sand-sized or finer, which is on the lower end of the transition range specified by Wilcock and Crowe (2003). Although the pre-dam conditions are unknown, the higher flows and presence of sand in the subsurface indicate the possibility that the bed material may have been more mobile under the pre-dam conditions.

Representative sediment gradations were applied to the models to define the distribution of bed and subsurface materials. For the Ketchup model, the bed-material gradation curve for the sample collected at the head of Ketchup Island was applied to the reach; this sample has median (D_{50}) and D_{84} sizes of 53 and 78 mm, respectively (Figure 4.27). No representative subsurface gradation was available for input to the model. However, as shown in Section 6.1.1.1, the surface, and therefore, the subsurface material is not mobilized.

For the Walters Ferry model, a representative surface bed-material gradation curve was developed for the study reach based on the average of seven measurements that were made during 1997 using the pebble count method (Wolman, 1954). The representative gradation curve of the surface material has median (D_{50}) and D_{84} sizes of 23 and 38 mm, respectively (Figure 4.22).

The Ketchup and Walters Ferry models were run at the peak flows recorded during the post-dam period of 2,124 and 1,141 m^3/s, respectively, and at the bankfull discharges in each reach of 2,832 and 2,265 m^3/s, respectively.

6.1.1.1. Results of the Incipient Motion Analysis (Baseline)

The results of the incipient motion analysis of the Ketchup reach indicate that the majority of the channel bed is not mobilized at the post-dam peak discharge (2,124 m^3/s) (Figure 6.1) or at the bankfull discharge (2,832 m^3/s) (Figure 6.2). At the post-dam peak discharge, the normalized grain shear (NGS) values along the reach range from 0.5 to 1.8, with a representative value of 0.7 for the main channel. (Note: in Figure 6.1, Figure 6.2, Figure 6.6 and Figure 6.7, the NGS values for the range from 0 to 0.5 are shown as clear to make the figures more readable). The highest NGS values in the main channel occur at the constriction in the vicinity of Sta 450+00; the NGS values are approximately 1.1, which indicates very low sediment transport rates. The highest NGS values along the reach occur at the head of the islands, with values of 1.2 at the head of Ketchup Island, and 1.8 at the head of Oglesbee Island (Sta 429+00) and un-named island (Sta 418+00). At the head of Ketchup Island, the pattern of the highest NGS values approximates the exposed gravel and vegetation-free area visible in Figure 6.1 and indicates this gravel forming the island core is not mobilized at discharges up to bankfull.

At the bankfull discharge of 2,831 m^3/s, the NGS values are generally less than 0.5 along the majority of the reach. The peak NGS values of 0.7 occur at the head of Ketchup Island (Sta 437+00) and Oglesbee Island (Sta 429+00).

The incipient motion analysis indicates that bed material is not mobilized under post-dam conditions. At higher than bankfull flows, there would likely have been extensive floodplain inundation. As a result, the stage and bed shear would not increase significantly with increasing discharge under pre-dam conditions

In the Walters Ferry reach, the incipient motion analysis indicates that the majority of the channel bed material is not mobilized at the post-dam peak discharge (1,141 m^3/s) (Figure 6.3). In general, the NGS values upstream of the constriction created by the Reynolds Creek fan range from 0.3 to 1.3, indicating low sediment transport rates. Upstream of the Reynolds Creek fan, the lowest NGS values (≤0.5 shown as clear) typically occur in the low velocity area between islands (e.g., between Bayha, Argy, Becky and Papike Islands), in the expansion zones (e.g., in the expansion below the contraction at Sta 1728+00) and along the right side of the channel adjacent to Argy and Becky Islands (Sta 1718+00 and Sta 1720+00), just downstream of Brooks Island (approximately Sta 1733+00) and along the right side of the channel from approximately Sta 1736+50 to Sta 1748+00. This pattern of low shear stress up- and downstream of the constrictions is consistent with the 1-D model results (Section 5.5.2).

In the vicinity of the Reynolds Creek fan, the NGS values range up 2.0, indicating significant sediment transport is occurring in this area at 1,141 m^3/s (Figure 6.4). No bed sample measurements were collected in the vicinity of the Reynolds Creek, but it is probable that the channel bed is significantly coarser than the representative size of 23 mm. The critical grain size (D_{50}) in this area is approximately 32 mm, compared to the representative size of 23 mm.

At the bankfull discharge, significant sediment transport occurs (NGS>1.5) from the downstream end of the reach (Sta 1700+00) to approximately 600 m upstream of the Reynolds Creek fan (Sta 1690+00), as well as in the vicinity of the contraction located midway along the reach at Sta 1730+00. In the area between these two contractions, the NGS values typically range from 0.3 to 1.3, with localized higher NGS values at the head of the islands.

In summary, the results of the incipient motion analysis of the Ketchup reach indicate that the bed material is not mobilized at the peak post-dam discharge or at the bankfull discharge, thus indicating that the bed is armored.

These results from the NGS analysis of the Walters Ferry and Ketchup Island reaches indicate that the bed of the channel is not mobilized at flows up to the bankfull discharge. The channel bed armored during a previous hydrologic flow regime such as the Bonneville flood and the gravel cores are relic bar features. This is supported by the evidence of mussel shells found within the low relief gravel core at Sign Island that were determined to be approximately 7,000 years (W.R. Osterkamp, USGS, personal communication, 2010 and unpublished document 2011). As shown later in the study, the islands formed in response to more recent flood hydrology and the silt-sand sized sediment supply, which explains how there can be relatively young soils overlying older gravel cores .

Historically, the gravel-cobble sediment supply to geomorphic subreach I was low due to the absences of upstream tributaries capable of supplying bed load to the river and a very flat gradient incapable of transporting coarse bed material Osterkamp et al. (2001).

The historic gravel-cobble sediment load in the middle and lower geomorphic subreaches was likely low (Osterkamp, 2001). The middle anastomosing reach, which receives tributary inputs, does not have sufficient-transport capacity to transport the gravel-cobble size material and, as a result, has aggraded and formed an anastomosing planform.

6.1.2. Shear Stress (Baseline Conditions)

Truncated soil profiles were observed at Pheasant Island #2 (47) and at Homedale Island (41). Pheasant Island #2 (47, Figure E.59) had a carbon date of 2190 years BP for a horizon that was part of a stripped surface. Homedale Island (Figure E50) showed a stripped B horizon at a depth of approximately 150 cm. Evidence of significant erosion can also be found at the head of Ketchup Island (Figure 6.5 and Figure 6.6), the downstream end of Aulbach #1

Island and at the head of Smith (11.1) Island (Figure 6.7). The truncated soil profiles are evidence of significant erosion resulting from floods with sufficient shear stress to erode the surface of the island.

The baseline Ketchup Island model was run at the bankfull discharge (2,832 m^3/s). The left side of Figure 6.4 shows the erosion at the head of the 2012 aerial photograph and the right side shows the predicted shear distribution. The high shear stress area at the head of the island approximates the eroded gravel area (Figure 6.6) and is consistent with the incipient motion analysis. In addition, relatively high shear stress areas are predicted over the surface of Ketchup and Oglesbee Islands and along the right side of Annear Island.

The predicted shear stresses over surface of the island range from approximately 35 Pa near the head of the island to approximately 6 Pa midway along the island. In comparison, the critical shear stress for surface erosion of sand sized particles is approximately 1 Pa and shear stress values for soils with cohesion range up to 3 Pa (USBR, 2006) based on laboratory experiments. Therefore, the predicted shear stress at the bankfull discharge is sufficiently large to erode the surface of the island.

The high shear stress over the islands explains how the surface of the islands can erode, resulting in a truncated soil profile. This could happen by the following means. An island that has remained relatively undisturbed for sufficient time to develop A and B horizons could be overtopped by a flood with sufficient shear to erode the upper A horizon, leaving the B horizon. Subsequent overtopping floods could deposit sediment (a C horizon) over the B horizon, which would appear as a truncated surface in the soil profile.

6.1.3. Without-Island Mesh Geometry

The without-island models were developed by lowering the elevations of the mesh nodes in the baseline models to represent removing the islands (down to the measured elevation of the top of the gravel platform). In the Ketchup model, five islands were lowered, including:

Ketchup, Annear, Oglesbee and two un-named islands (Figure 6.8). Eleven islands in the Walters Ferry model were removed (Figure 6.9).

6.1.4. Bed-material Transport Capacity Relationship and Upstream Sediment Supply

A discharge versus sediment transport rating curve was developed to input sediment into the models at the upstream boundary and a sediment-transport equation was selected to estimate the bed-material transport capacity.

It was originally anticipated that the Parker (1990) surface-based bed-load equation would be applied because it is appropriate for the range of bed-material sizes in the Ketchup and Walters Ferry reaches. A discharge-sediment transport rating curve based on the Parker Equation (1990) was developed and the models were run over a range of flows. The model output indicated negligible rates of sediment transport of the gravel- to cobble-sized material, which supports the incipient motion analysis that also showed very low rates of sediment transport and that the channel bed is armored at the Ketchup and Walters Ferry reaches.

Due to the negligible sediment transport loads in the gravel- to cobble-sized range and because the islands above the gravel platform are composed primarily of sand-sized material, the Engelund-Hansen (1967) bed-load equation was selected to estimate the sediment load. The Engelund-Hansen (1967) bed-load equation was developed for a similar range of sediment sizes and channel bed slopes found in the study reach. As mentioned previously, SRH-2D contains an unsteady total load algorithm that automatically partitions suspended load, bed load or mixed load depending on the transport model parameter of local flow hydraulic (Greinmann et al., 2008). Because the islands were likely formed from both suspended load and bed-load (as evidenced in the bedforms observed in the soil profiles), the Engelund-Hansen (1967) and SRH-2D sediment transport routines were determined to be appropriate for this study.

In SRH-2D, the sediment supply to the model is either calculated by the model using a user-defined input sediment-rating curve, a sediment-transport hydrograph, or the “capacity” option in the model that estimates the supply based on the transport capacity at the upstream boundary.

No sediment-transport measurements were available within the Ketchup or Walters Ferry reaches to directly develop a sediment-rating curve or a sediment inflow hydrograph. Because the bed of the channel is composed of cobble-sized material and the sediment supply to the reach is primarily sand-sized material, the capacity option predicted an unrealistically low-sediment supply. As a result, a sediment-transport versus discharge rating curve was developed using the following methodology. One method of developing a sediment-transport rating-curve is to develop an initial rating curve, run the model over a known hydrograph and compare the predicted magnitude and patterns of bed elevation changes with measured data. Obviously, this requires measured bed elevation data before and after the hydrograph. Because no such data are available, a representative sediment-transport rating-curve was developed.

The rating curve requires sediment transport rates for each size fraction for a range of modeled flows. A series of rating curves with varying sediment gradations and sediment concentrations were tested to select a rating curve that created reasonable sediment deposition patterns along the reaches. The rating curve was developed for six different sand-size fractions (0.0625 to 2 mm) for a range of flows from 142 to 2,832 m^3/s in 142 m^3/s increments.

The following method was used to develop the sediment rating curve:

1. An initial representative sediment gradation was selected based on the sediment samples collected at the islands.
2. An initial sediment concentration and sediment load (m^3/s) was assumed for each discharge in the rating curve.

3. The sediment-transport load (m^3/s) for each size fraction was calculated by multiplying the total sediment load by the percentage of sediment of each size class to obtain the sediment load per size class.
4. The model was run over a series of hydrographs using the developed sediment rating curve.
5. The model output at the end of the simulations was evaluated to determine the sedimentation patterns and the amount and rate of island building. Based on the results, and if deemed necessary, a new sediment rating curve was developed and tested.

The results of the testing indicated that sediment rating curves with lower sediment concentration (i.e., 5 ppm for flows up to 212 m^3/s and 200 ppm for the highest modeled flow of 2,832 m^3/s) caused islands to form, albeit at a very slow rate. Conversely, sediment rating curves tested with high sediment concentrations (i.e., 1,000 ppm for the highest modeled flow of 2,832 m^3/s) caused significant deposition at the upstream boundary of the model. During the testing, it was apparent there was significant deposition occurring on the receding limb of the hydrograph. To prevent this, the rating curve was modified to represent a hysteresis loop, which is consistent with the typical behavior observed in sand-bed rivers.

Based on the testing, the final rating curve was based on the KI-3 gradation (Figure 4.27) and has a sediment concentration of 30 ppm for flows up to 212 m^3/s and a maximum sediment concentration of 400 ppm at the peak discharge of 1,982 m^3/s on the rising limb and maximum sediment concentration of 218 ppm at 1,982 m^3/s on the falling limb (Figure 6.10). A log-log interpolation was used to calculate the sediment concentrations for the intermediate discharges. The resulting rating curve predicted reasonable sediment deposition patterns and rates in both reaches, and was therefore selected as the representative sediment-rating curve.

6.1.5. Modeling Methodology

The representative flood hydrographs discussed in Section 4.2.3.4 were applied to the models. For the Ketchup model, the flood hydrographs were developed to represent a range of peak flows from 850 to 1,982 m^3/s and were increased in increments of 283 m^3/s. The hydrographs started at a baseflow, increased to the peak discharge at a uniform rate, remained constant at the peak discharge for approximately three days, then decreased at a uniform rate to the base flow conditions and remained constant at the baseflow discharge for 10 days. The extended baseflow period at the end of the hydrograph provides time for sediment deposited in the channel to be transported out of the reach, as would normally occur during extended low- to intermediate flow periods. Each series of runs from 283 m^3/s up to the maximum modeled discharge was called a cycle (Figure 6.11).

The same procedure was used for the Walters Ferry model and the hydrographs were run for a range of peak flow hydrographs from 850 to 1,982 m^3/s, and increasing in increments of 283 m^3/s.

Both the Ketchup and Walters Ferry without-islands models were run over eight cycles. Over the duration of the hydrograph simulation, sediment deposited in the channel and the islands formed. To prevent the deposited material from completely eroding during the following hydrograph, it was necessary to artificially stabilize the island by re-setting the elevation corresponding to the upper surface of the deposition. In effect, this represents the stabilizing effects of the vegetation and/or sediment cohesion and is an indication of the interaction between fluvial processes and vegetation. As shown later in Section 6.2.2.3, if the islands are not stabilized, they erode down to the elevation of the gravel core. This methodology was necessary because SRH-2D did not have the ability to model vegetation or represent the cohesion from the clay- tosilt-sized materials. Other models such as the 3-D model SSIMM (Olsen, 2009) have represented the effects of vegetation as an additional energy loss or sink term. Under field conditions, it is likely the vegetation traps more sediment than predicted and the island growth may be faster than predicted by the model. In addition, the presence of clay- to silt-sized materials provides cohesion and typically results in steeper banks. At Ketchup Island, the left bank mostly consisted of non-cohesive sand-sized material, whereas the downstream right side bank of Annear Island contained cohesive materials and was steeper than the angle of repose. In general, the modeling methodology is thought to represent the observed processes of island formation reasonably well.

A Manning's n-value of 0.065 was applied to the islands. Based on the photo analysis and field observations of the Ketchup and Walters Ferry study sites, this value reasonably represents both the establishing vegetation on the islands and the older island surfaces.

The 2-D sediment transport modeling was conducted to represent the pre-dam conditions. Under present conditions, the islands in the Ketchup and Walters Ferry reaches are vegetated with grasses, shrubs and a few large trees; they appear more vegetated compared to pre-dam conditions, but they are significantly less vegetated compared to some of the low to intermediate height islands which are covered in thick vegetation. Therefore, the Manning's n-value of 0.065 is appropriate for simulating the pre-dam conditions, but under post-dam conditions, the roughness may be too low for the intermediate age islands.

6.2. Model Results

The models were validated by comparing the predicted island geometries (location, size and height) with the existing island geometry at various times over the simulation. The variation in sediment-transport capacity along the reaches was evaluated to determine the change in sediment transport continuity as the islands developed.

6.2.1. Ketchup Reach

6.2.1.1. Shear stress

The baseline and without islands conditions models were run at the 2-year post-dam peak flow event. Under the without-island conditions, there is a significant zone of low shear, and corresponding low sediment transport, in the channel expansion area (Figure 6.12). The area of low shear extends from just upstream of Ketchup Island (Sta 437+00) to downstream of Oglesbee Island (Sta 427+00). This low transport capacity zone creates a strong depositional tendency, and as a result, the island forms in this location. This depositional trend was observed over the full range of modeled flows for the without-islands conditions and is consistent with the 1-D model results.

6.2.1.2. Island Geometry

Figure 6.13 shows the predicted island development midway (end of cycle 4) and at the end of the simulations (end of cycle 8). At the end of cycle 4, sediment deposited along the left and right margins of the island to form levee-type features. The sediment deposition along the left and right sides ranged up to 2 m, but there was significantly more deposition along the right side of the island compared to the left. After four cycles, the elevation of the right levee was approximately 0.9 m higher than baseline conditions in the same location; this was the only location in which the predicted elevation exceeded baseline conditions at the end of four cycles. Natural levees form as a result of sediments dropping out of suspension adjacent to the channel margin. The sediment-transport capacity of the river is typically much higher than that of the overbank. As the suspended sediment is conveyed from the channel into the overbank, it quickly drops out of suspension, with the largest particles and largest amount of deposition occurring near the channel margins and smaller amounts of deposition occurring farther away from the channel margin (Pizzuto, 1987). The model predicted sediment deposition in the range of 0.25 to 1 m between the levees on Ketchup Island.

At the end of cycle 4, the model predicted no sediment deposition at the head of Ketchup Island due to the high shear stresses in this area. At Annear Island, the model predicted very little deposition across most of the island, but it did predict deposition in the range of 0.4 to 1.4 m along the left side of the island. In general, the model predicted significantly more deposition at Ketchup Island compared to Annear Island, supporting the historical aerial photographs and soil profiles showing that Annear Island formed after Ketchup Island.

The model predicted deposition at other areas along the reach, including: (1) up to 0.5 m along the left bank (Sta 440+00) upstream of Ketchup Island, (2) deposition of up to 0.5 m along the left bank in the vicinity of Sta 420+00, and (3) deposition of up to 0.7 m near the downstream end of Unnamed Island at Sta 410+00.

The island geometry at the end of the simulation (eight cycles) approximates the baseline conditions reasonably well, validating the model and the modeling procedures (Figure 6.13). The spatial location, length, width and lemniscate-loop. [In mathematics, a lemniscate refers to figure-8-shaped curves. Komar (1983, 1984) compared the island shape to one side of the lemniscate loop.] A significant difference was that the model predicted a single large island, whereas, under baseline conditions, there is an approximately 10-m-wide channel separating Ketchup and Annear Islands (Figure 6.13). After eight cycles, the model predicted approximately 0.2 to 0.4 m of additional aggradation along the margins of the island compared to the end of cycle 4. Most of the deposition occurred between the levees and from approximately midway along the length of the island towards the downstream end of the island. Furthermore, after eight cycles, the location, size and shape of the island are very similar to baseline conditions (Figure 6.13).

A comparison of the cross-section geometry shows the development of the Ketchup Island (Figure 6.14). The cross section is located perpendicular to the channel and crosses the blue triangle shown on Figure 6.13. At the end of cycle 4 (green line), levees have formed on both sides of the island and there was approximately 0.4 m of deposition near the center of the island. At the end of cycle 8, the levee along the right side of the island has continued to increase in elevation and the center portion of the island has increased in height. The width of the island is slightly wider compared to baseline conditions. The elevations along the left and right side of the island compare well to the baseline elevations, but the elevations near the center of the channel are lower than under baseline conditions.

The model predicted the island to form in the following sequence. Initially, levees formed along the upstream right side of the island followed by a levee along the lower left side of the islands. After the initial levee building period, deposition occurred towards the downstream half of the island, followed by general infilling of the center portion of the island. The predicted formation of the levees and the slightly convex shape of the cross-section are consistent with field observations at Ketchup Island, at other islands in the study reach, and with other studies (Makaske, 2001, Nanson and Knighton, 1996).

At the end of cycle 8, the maximum elevation of the island is overtopped at a discharge of 1,416 m^3/s, which corresponds to a recurrence interval of four years based on the post-dam flood frequency analysis. Based on the soil analyses, islands with this frequency of overtopping were mostly in Morphostratigraphic Soil Class 3.

A comparison of the change in elevation on the right levee and near the center of the island shows different rates of aggradation (Figure 6.15).The location of the levee is shown as a blue triangle and the center of the island is shown as a green triangle on Figure 6.13. In the vicinity of the right levee, the aggradation was initially very rapid, with approximately 1.4 m of aggradation at the end of cycle 1 (Figure 6.15). After cycle 1, the rate of aggradation on the right levee decreased significantly, with an additional 0.5 m of aggradation over the next seven cycles. After eight cycles, the levee was still aggrading, albeit at a much slower rate.

The shape of the aggradation curves (Figure 6.15), in particular for the right levee, is similar to the floodplain aggradation curve developed by Wolman and Leopold (1957) and described by the rate law (Wu et al., 2012).

A comparison of the predicted rates of aggradation over eight cycles is shown in Figure 6.16. During cycle 1, there is a small amount of aggradation over the first two simulations (850 and 1,133 m^3/s), followed by significant aggradation at 1416, 1699 and 1982 m^3/s. During the second cycle, the island is not overtopped at the lowest flow (850 m^3/s) because of the aggradation during the previous cycle. After every cycle, the island aggrades and frequency of overtopping decreases, resulting in less opportunity for additional aggradation. The aggradation rates shown in Figure 6.16 would be different under natural conditions because the order of the floods would be more random, with smaller floods occurring between the large floods. In addition, the methodology applied to model the floods has the same number of small and large floods. In nature, the large floods would occur much less frequently (Table 6.1). Using the same methodology as applied to Table 6.1 and using the post-dam Weiser gage flood frequency results, on average, the 850 m^3/s hydrograph occurs 20 times per 100 years and the 1,982 m^3/s hydrograph occurs six times per 100 years.

These results show that, over time, increasingly larger flows are required for continued aggradation. The maximum height of the island will be limited to approximately the elevation of the lowest channel bank. Based on the modeled aggradation rates, it is apparent that the islands adjust over decades (or longer).

In addition to the decrease in frequency of overtopping as the island increases in height, under natural conditions there would be a decrease in sediment concentration near the top of the water column. To illustrate what occurs under natural conditions, suspended-sediment concentration profiles in the channel near the right levee (shown as a blue triangle in Figure 6.13) were estimated using the Rouse equation (Vanoni, 1977). The analysis is based on the channel bed elevation and estimated hydraulic conditions in the channel immediately to the right of the levee. The analysis was conducted using the sediment concentrations developed from the input sediment-rating curve for the 2-year peak flow (1,070 m^3/s) and the highest peak flow during the post dam-period (2,150 m^3/s). The reference concentration (Ca, concentration at the channel bed) that is necessary to apply the Rouse equation was estimated by iteratively adjusting the value until the total transport including both the bed and suspended load matches the estimated total bed-material transport capacity at the location of interest, assuming that the bed layer thickness is 1/20th of the flow depth (Figure 6.17). The 2-D sediment-transport model calculates depth-averaged sediment concentrations, whereas the sediment concentration shown in Figure 6.17 approximates actual river conditions.

At the 2-year peak flow, the average sediment concentration over the entire water column is 195 ppm. The concentration near the bed of the channel is approximately 840 ppm, and approximately 12 ppm at water surface; the island is not overtopped during the 2-year peak flow. At the highest peak post-dam flow, the average sediment concentration is 436 ppm; the sediment concentrations are about 975 ppm near the bed of the channel, about 136 ppm at the elevation of the island and about 12 ppm at the water surface. It is important to note that the concentrations represent only the suspended sand portion of the total sediment load that is controlled by the hydraulic conditions and bed-material characteristics. The Snake River also carries a fine sediment (silt/clay) load that is controlled by upstream watershed conditions and not by local conditions in the vicinity of the study site.

A soil profile was developed at the levee location shown as a blue triangle on Figure 6.13. In Figure 6.18, deposition events larger than approximately 10 cm are shown as individual layers. To avoid showing numerous thin soil horizons that occurred over a cycle and are difficult to distinguish in the soil profile, the total deposition over a cycle is shown and the corresponding number of horizons is shown.

The island building and island eroding events that formed Ketchup Island are not known, but the soil profile predicted by the modeling (Figure 6.18) has similar characteristics to the sampled profile (Figure 6.19). The sampled profile shows a thick sand deposit at the bottom of the profile, and then a range of small to medium size deposits in the upper third of the profile. In comparison, the predicted soil profile has thick layers in the lower half of the profile and a range of small to medium size deposits that are comparable in thickness to the measured sediment layers. From approximately cycle 3 onwards, the majority of the sedimentation occurred as relatively thin horizons at discharges greater than 1,415 m^3/s (Figure 6.18). The model predicted 10 significant deposition events (deposition thickness of approximately 10 cm or larger) and approximately five thinner soil horizons to form Ketchup Island. Coincidently, the measured soil profile also shows 10 significant soil layers and four thinner horizons (Figure 6.19).

In addition to Ketchup Island, a low elevation island began to form along the left side of the channel in the vicinity of Sta 411+00. No islands existed at this location under baseline conditions. Farther upstream along the left bank, two islands are forming where islands exist under baseline conditions. One island was forming in the vicinity of an unnamed island (Sta 411+50) and had aggraded by 1.2 m over eight cycles; a second island was forming in the vicinity of Sta 418+00, where a low-elevation island exists under baseline conditions. No island was predicted to form at Ogleesbee Island. However, an island was forming immediately downstream of this location and aggraded by approximately 1 m over eight cycles. In addition, there was continued aggradation between the ends of cycles 4 and 8 along the left bank (Sta 440+00) upstream of Ketchup Island and localized areas of aggradation on the left overbank of up to 1 m between Sta 419+00 and Sta 416+00.

6.2.1.3. Sediment-transport Continuity

Results from the model were used to evaluate the variability in bed material transport along the reach and the associated tendency for aggradation (island growth) to occur. The variation in sediment transport was compared at 10 monitor lines through the modeled reach using the predicted sediment transport rates (Figure 6.20). A monitor line is a modeling option in

SRH-2D used to compute flow and sediment flux across a specified line that is defined by connecting a series of mesh nodes.

The sediment supply to any particular location is represented by the sediment-transport capacity of the river immediately upstream. Where the upstream supply exceeds the transport capacity at the location of interest, the river will adjust by depositing the excess material on the bed, which results in a general raising of the bed elevation and the formation of mid-channel bar, bank-attached bars, and islands. Where the upstream supply is less than the transport capacity at the location of interest, the river will adjust by eroding material from the bed, resulting in general bed-lowering or channel-armoring.

Figure 6.21 shows the variation in sediment transport along the reach at the 2-year peak flow under baseline conditions, under without-island conditions (conditions at the start of the simulations) and at the end of cycles 4 and 8.

Under baseline conditions, the rate of sediment supply into the reach is slightly higher than the amount leaving the reach, indicating that the reach is slightly depositional.

At the end of cycle 4, the variation in sediment transport decreased due to the formation of the islands, which reduce the channel width, confine the flow path, and increase the sediment transport capacity in the vicinity of the islands (Figure 6.19). At the end of cycle 8, the variation in sediment-transport capacity continued to decrease as a result of continued island formation, resulting in more uniform sediment transport through the reach. There was an approximately 5-percent increase in sediment transport efficiency at the downstream end of the reach from the start of the simulation to the end of cycle 8. At the end of cycle 8, Ketchup Island and Annear Island were still forming and the sediment transport rates along the reach were still approaching a uniform sediment flux through the reach.

6.2.2. Walters Ferry Reach

6.2.2.1. Island Geometry

Under the without-island conditions, there are significant zones of low shear, and corresponding low sediment transport, in the area located up- and downstream of the contractions (Figure 6.22). For example, low shear areas are located upstream of the Reynolds Creek contraction in the area of Argy Island (Sta 1717+00), and in the vicinity of Papike Island (Sta 1723+00), which is located approximately midway between two channel contractions. Low shear zones are also located in the vicinity of Brooks Island (Sta 1735+00), which is located upstream of a contraction, and in the vicinity of Blind Island (Sta 1743+00), which is located in a channel expansion area (Figure 6.22).

At the end of cycle 1, the model predicted the development of a single island that extends from near the downstream end of Argy Island (Sta 1715+00) to near the upstream end of Papike Island (Sta 1724+00) (Figure 6.23). The location, width and length of the predicted island approximate the location and combined size of Argy, Becky and Papike Islands. The model did not predict a channel between Argy and Becky Islands, or between Becky and Papike Islands. The average amount of aggradation at the end of cycle 1 was approximately 0.5 m and the highest amounts of aggradation—up to 2 m—occurred near the center of Becky Island and near the downstream end of Argy Island (Figure 6.23). Notably, the model did not predict any island growth in the area of Wright and Bayha Islands due to the high shear stresses in this area under without-island conditions (Figure 6.22). Under baseline conditions, Wright Island is located just upstream of the contraction formed by Reynolds Creek and Bayha Island is located slightly upstream of Wright Island. Wright Island and the downstream end of Bayha Island experience relatively high shear over a range of flows (Figure 6.22), which prevented island formation. The soil profile of Wright Island had a total depth of approximately 1 m and showed carbonate accumulation near the upper surface, indicating that recently the island has been stable.

The model predicted islands to form in the areas of Brooks and Blind Islands. In the area of Brooks Island, an island formed that extends from slightly downstream of the baseline location to approximately halfway up Brooks Island. At the end of cycle 1, there was up to 1 m of aggradation near the downstream end of Brooks Island (Figure 6.24). The location of the cross sections in Figure 6.24 and Figure 6.25 is shown on Figure 6.23.

In the area of Blind Island, an island formed in a similar location and with similar geometry characteristics as Blind Island. As with Brooks Island, the highest amounts of deposition (up to 1.5 m) at Blind Island occurred near the downstream end of the island. The average deposition over the island was 0.7 m (Figure 6.25).

In addition to the islands, relatively small amounts of aggradation were predicted to occur on the floodplains, including isolated areas along the left bank adjacent to Bayha Island and along the right overbank (up to 0.3 m) at the contraction near Sta 1730+00.

At the end of cycle 4, the single large island covering the area of Argy, Becky and Papike islands continued to aggrade, but the length and width of the island did not increase significantly (Figure 6.23). No significant aggradation occurred in the locations of Wright and Bayha Islands. The island in the vicinity of Brooks Island continued to aggrade, but did not increase in area significantly. The island in the area of Blind Island continued to aggrade significantly near the center of the island as well as increasing in length in a downstream direction. The model predicted approximately 0.2 m of aggradation from the downstream end of Blind Island to just upstream of Brooks Island.

At the end of cycle 4, continued aggradation was predicted to occur in the same floodplain locations observed at the end of cycle 1, as well as approximately 0.2 m of aggradation along the left bank in the vicinity of Sta 1730+00. In addition, there was approximately 0.2 m of aggradation along the right side of the channel on the upstream side of Blind Island (~Sta 1747+00).

At the end of cycle 8, the single large island covering the area of Argy, Becky and Papike islands continued to aggrade and infill the low elevation areas. At the end of the simulation, the island was approximately 30 m narrower compared to baseline condition. In general, the island did not increase in length, but there was approximately 0.3 m of aggradation along the left channel in the vicinity of Sta 1720+00.

Brooks Island continued to aggrade and the island extended in an upstream direction. The downstream end of the island remained in the same location as it was at the end of cycles 1 and 4. Blind Island continued to aggrade near the center of the island and there was continued aggradation on the downstream side of the island. The aggradation trend at Blind Island indicated that, with continued model simulations, Blind Island may attach to the right overbank. At the end of the simulations, Blind Island was approximately 30 m wider compared to baseline conditions (Figure 6.25).

In general, the predicted location and sizes of the island match the baseline conditions reasonably well, thereby validating the model. However, as noted previously, the model did not predict islands to form in the location of Wright and Bayha Islands due to the high shear stresses in the area.

A comparison of the aggradation rates at four locations over the duration of the eight cycles shows an initial steady increase in aggradation followed by slower aggradation towards the end of the simulations (Figure 6.26). The highest rates of aggradation occurred at Blind and Papike Islands with approximately 1.3 m of aggradation at the end of cycle 2. After cycle 2, the rate of aggradation at Papike slowed and by the end of cycle 8, there was a total of approximately 2 m of aggradation. The highest rates of aggradation occurred at Blind Island, with approximately 1.3 m of aggradation at the end of cycle 1 and 2.7 m of aggradation at the end of cycle 8. The aggradation trends at Argy and Brooks Island were similar and experienced slower aggradation rates than Blind and Papike Islands. At the end of cycle 2, there was approximately 0.5 m of aggradation at Argy and Brooks Islands, and at the end of cycle 8, there was approximately 2 and 1.8 m of aggradation at Brooks and Argy, respectively. The rate of aggradation slowed after cycle 2 at Papike Island, and slowed after cycle 6 at Brooks and Blind islands, while Argy Island continued to steadily increase in elevation.

At the end of cycle 8, the highest surfaces of Argy, Papike, Brooks and Blind Islands are overtopped at approximately 1,320 m^3/s, which corresponds to greater than the 50-year return interval on the post-dam flood-frequency curve. Based on the soil dating analyses, islands with this frequency of overtopping are generally classified as Morphostratigraphic Soil Class 2+. Othberg and Fosberg (2001) applied a 2+ classification to these four islands.

A comparison of the aggradation rates at Blind Island is shown in Figure 6.27**.** During cycles 1 and 2, aggradation occurs over the range of flows from 566 to 1,699 m^3/s. The aggradation trends are similar to those observed at Ketchup Island, with decreasing amounts of deposition over time as the height of the island increases.

Based on the model output, stratigraphic profiles were developed for Argy (75), Papike (77), Brooks (78.3) and Blind Islands (79.1) (Figure 6.28, Figure 6.29, Figure 6.30 and Figure 6.31, respectively). The locations of the soil profiles are shown as green triangles on Figure 6.23. The predicted soil horizons for Argy (Figure 6.28), Papike (Figure 6.29) and Blind (Figure 6.31) all show the islands are formed by approximately 10 to 12 events with deposition of approximately 10 cm or more. In comparison, the measured soil profiles for Becky Island (76) (Figure 6.32) and Brooks Islands (78.3) (Figure 6.33) show approximately 15 and 10 depositional events, respectively, of approximately 10 cm or more

.

6.2.2.2. Sediment-transport Continuity

The variation in sediment transport was compared at 10 monitor lines through the modeled reach using the predicted sediment transport rates (Figure 6.34). Figure 6.35 shows the variation in sediment transport along the reach at the 2-year peak flow under baseline conditions, under without-island conditions (conditions at the start of the simulations) and at the end of cycles 1, 4 and 8. Under the without-island (Figure 6.35) conditions, the sediment-transport load is significantly higher at the upstream end of the reach compared to the downstream end, indicating the reach is more depositional than under baseline conditions. Under the initial conditions, the largest changes in sediment transport rates, and therefore the most depositional conditions, occur between Papike and Bayha Islands, which coincides with the low shear stress area illustrated in Figure 6.22.

At the end of cycle 1, the variation in sediment transport decreased due to the formation of the islands. At the end of cycle 4, the predicted sediment transport rates in the upstream half of the reach are very similar to baseline conditions, but in the downstream half of the reach, the sediment transport rates increased significantly, to the point that they were higher than baseline conditions (Figure 6.35), indicating the reach was more efficient at transporting sediment at the end of cycle 4 compared to baseline conditions. The increase in efficiency is due to the formation of the single large island in the area of Argy, Becky and Bayha Islands. At the end of cycle 8, there was a relatively small increase in the sediment transport rate at the downstream end of the model compared to the end of cycle 4. There was an approximately 25-percent increase in sediment transport efficiency at the downstream end of the reach from the start of the simulation to the end of cycle 8. At the end of cycle 8, all of the islands were still aggrading, albeit slowly, and the sediment continuity along the reach was continuing to approach uniform sediment flux along the reach.

6.2.2.3. Stabilizing Effect of Vegetation and Sediment Cohesion

To simulate aggradation and island growth in the models, it was necessary to set the deposited sediment as a ‘non-erodible’ material to represent the stabilizing effect of vegetation. This condition forms one end of an erosion scale (i.e., no erosion); the other end of the erosion scale would occur when there is no vegetation and no particle cohesion. In reality, the surfaces of the islands fall somewhere between these two conditions, with the vegetation providing significant erosion resistance (Smith, 1976) and the silt/clay fraction of the sediments providing limited cohesion. Unfortunately, it was not possible to simulate the silt/clay fraction or erosion resistance in the SRH-2D model. However, it was possible to model the two extremes and draw some conclusions from them.

To show the stabilizing effect of the vegetation, the material type of the islands was changed from non-erodible to erodible. The Walters Ferry reach baseline geometry and a representative sediment size of 1 mm were applied from the surface of the islands to the gravel platform of the channel. The model was run over the representative hydrograph with a peak flow of 1,141 m^3/s. At the end of the simulation, all the islands in the Walters Ferry reach had eroded to near the gravel platform (Figure 6.36 and Figure 6.37).

This highlights the stabilizing effect of the vegetation and cohesion. In reality, the presence of vegetation and limited cohesion of the soils would likely prevent the islands from being eroded to the gravel core.

6.3. Low Sediment Supply Conditions

The 2-D modeling was conducted by applying a sand-sized sediment load that was developed to represent pre-dam conditions. An unresolved question from the modeling is, under pre-dam conditions, what happened to the islands during periods of low sediment load to the river? During low-sediment supply conditions, the sediment transport capacity of the channel will exceed the sediment supply and the islands should not adjust the geometry by eroding to regulate the lower sediment loads through the reach. In addition, there is no efficiency gained with the islands in place under low sediment load conditions. The channel will change from dynamic to a regime type channel, and, in the absence of large floods, the islands will remain stable.

Under pre-dam conditions, the islands experienced larger floods and were less vegetated, and therefore more prone to erosion. During large floods and under low sediment load conditions, the river may have eroded the margins and/or the surfaces of the islands, thereby partially restoring the sediment deficit. During subsequent higher sediment load periods, the islands will reform in locations fixed by hydraulic controls and re-establish sediment flux though the reach. This cycle supports the hypothesis that islands form part of a temporal-spatial time continuum.

6.4. Figures and Tables

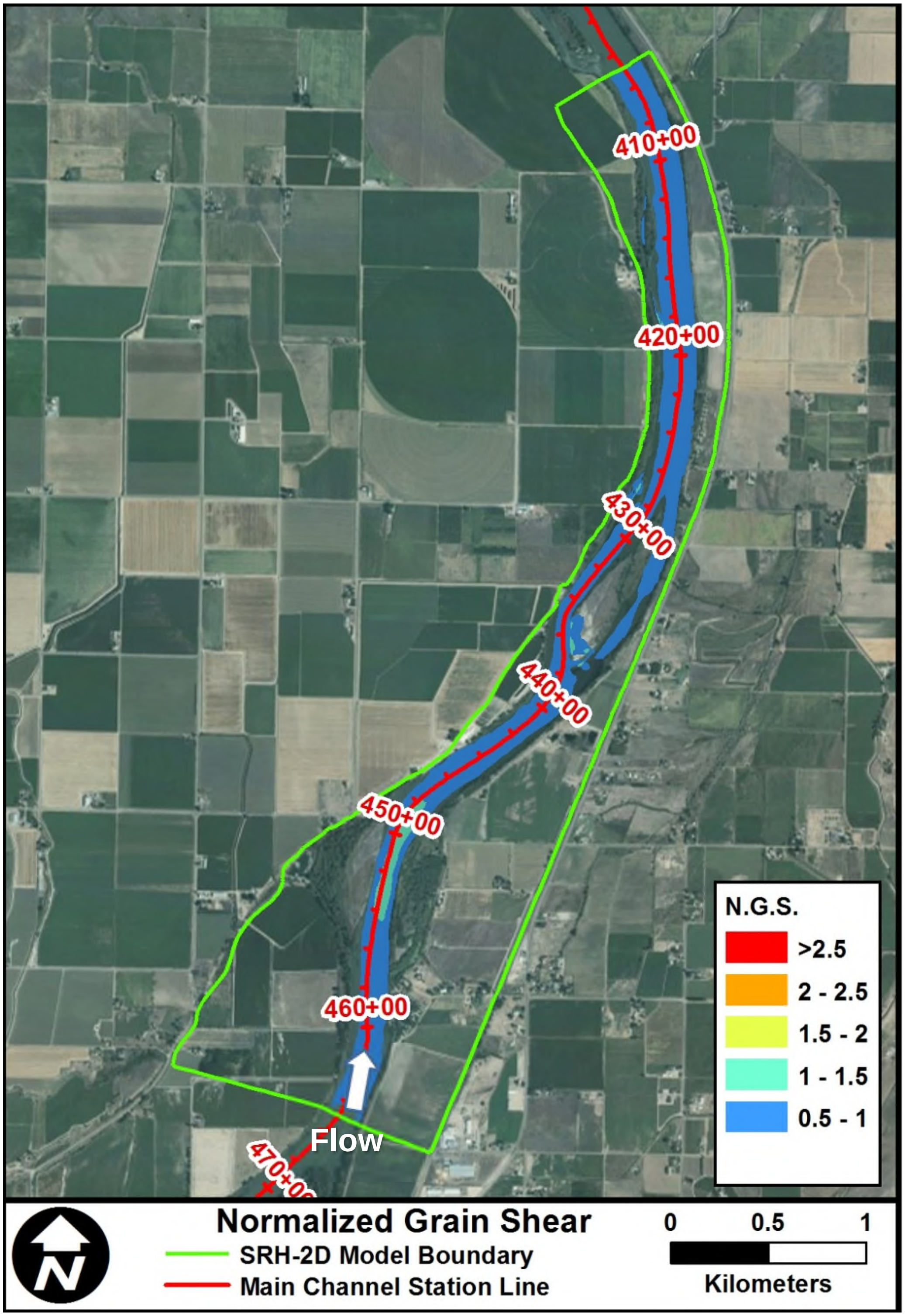

Figure 6.1 Normalized grain shear (NGS) in the Ketchup reach at the peak discharge during the post-dam period of 2,124 m^3/s.

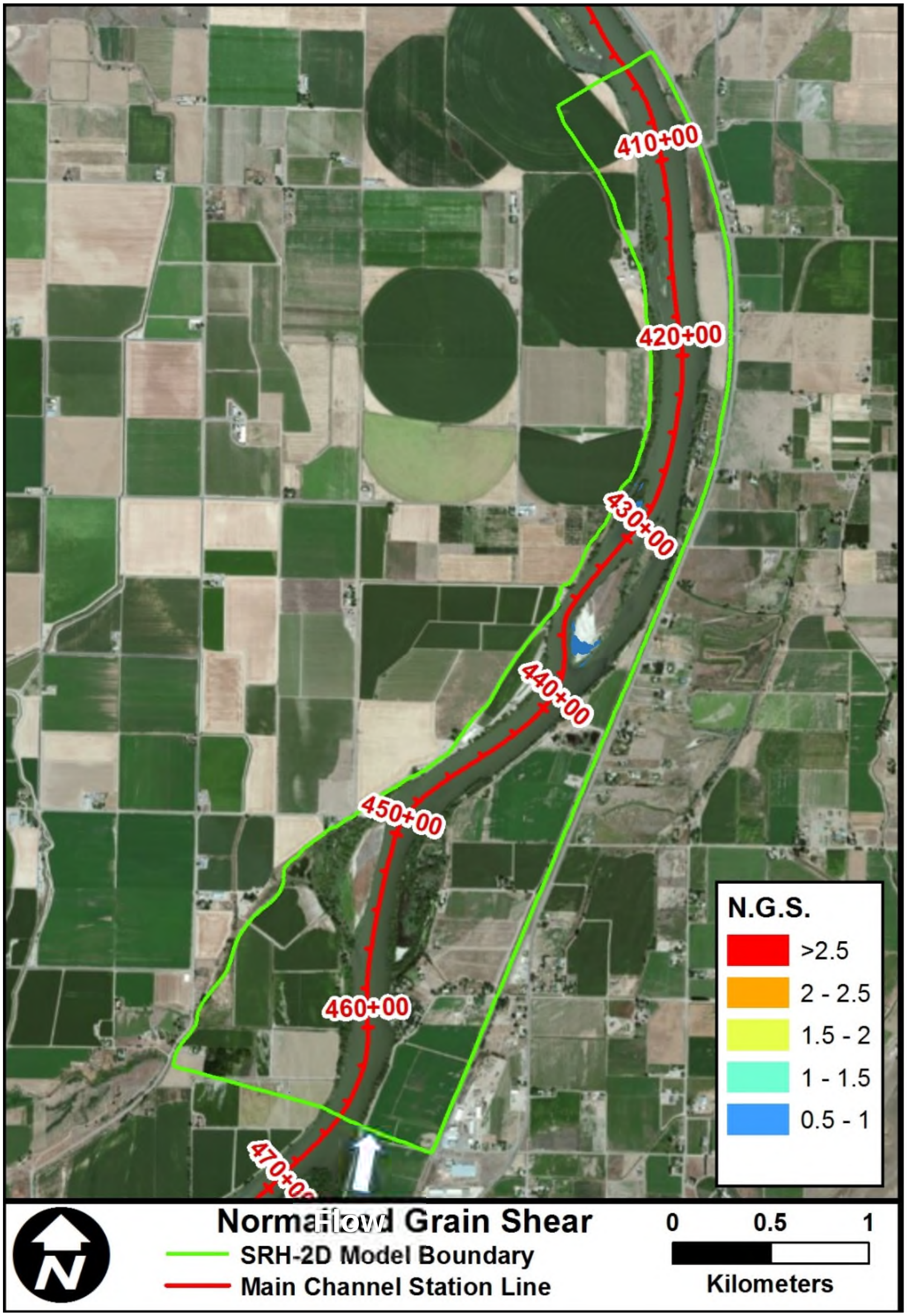

Figure 6.2 Normalized Grain Shear (NGS) in the Ketchup reach at bankfull discharge of 2,832 m^3/s.

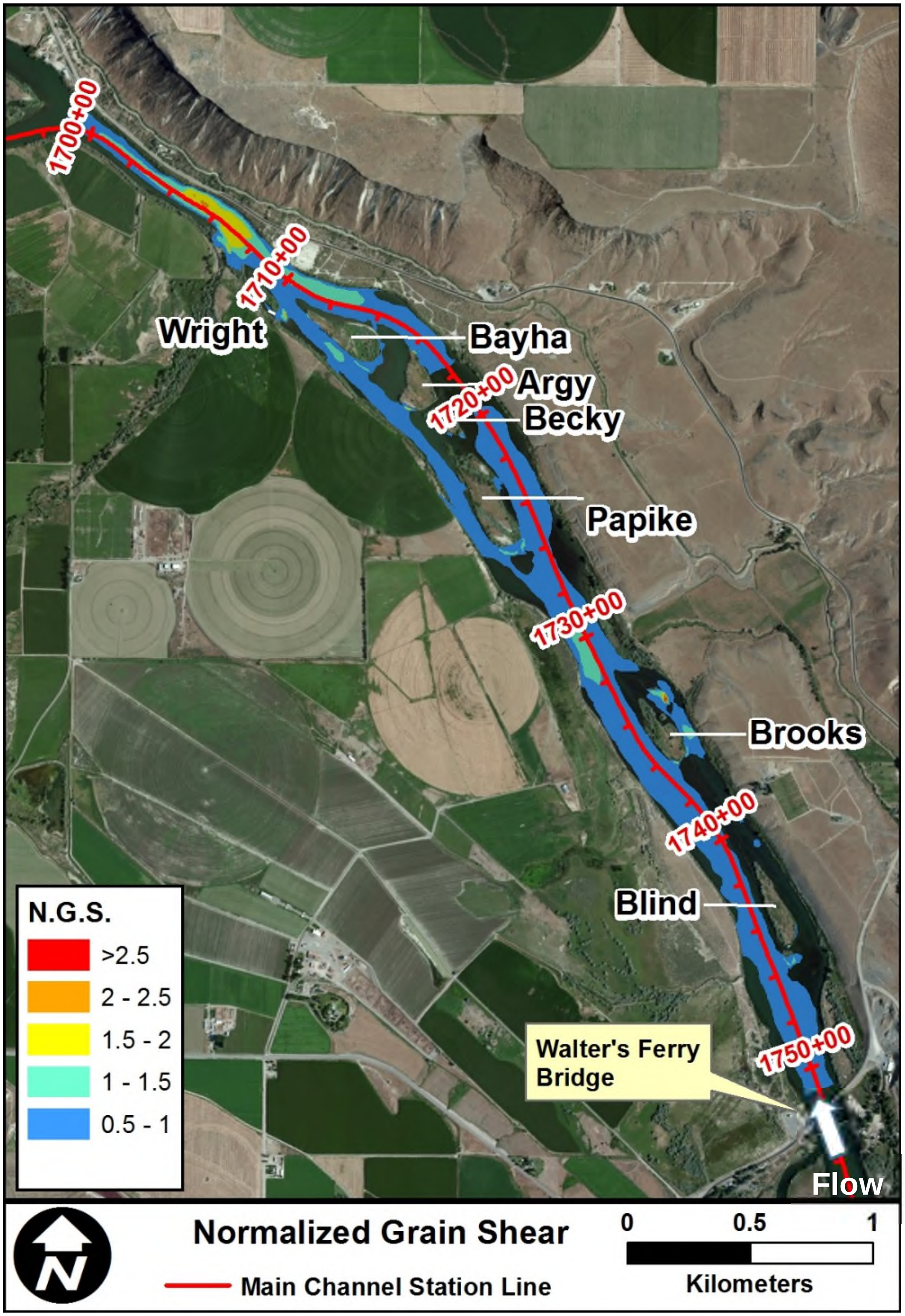

Figure 6.3 Normalized Grain Shear (NGS) in the Walters Ferry reach at the peak discharge during the post-dam period of 1,141 m^3/s.

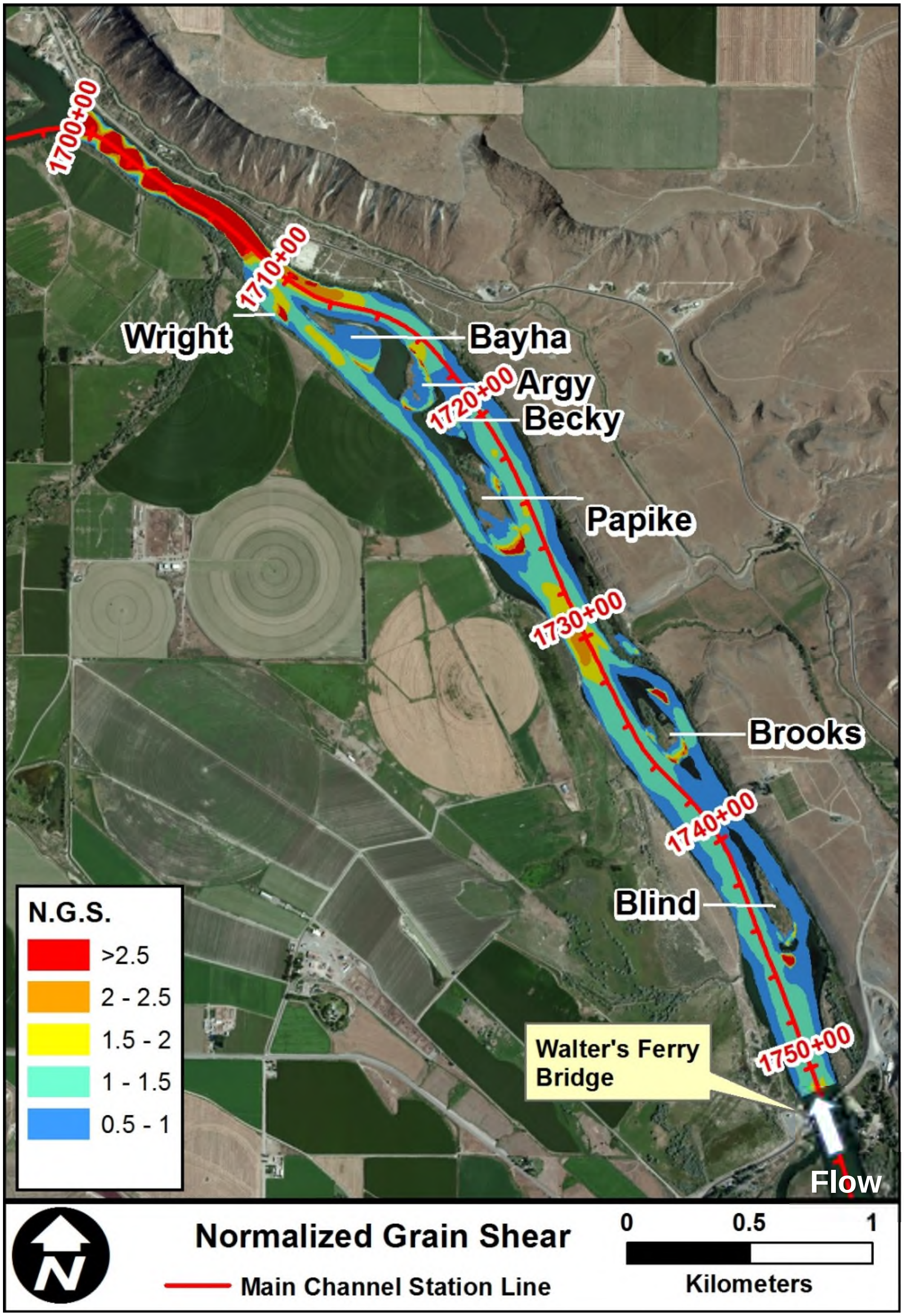

Figure 6.4 Normalized Grain Shear (NGS) in the Walters Ferry reach at bankfull discharge of 2,265 m^3/s.

Figure 6.5 View looking downstream from the head of Ketchup Island. Photo taken by Dr. R.A Mussetter.

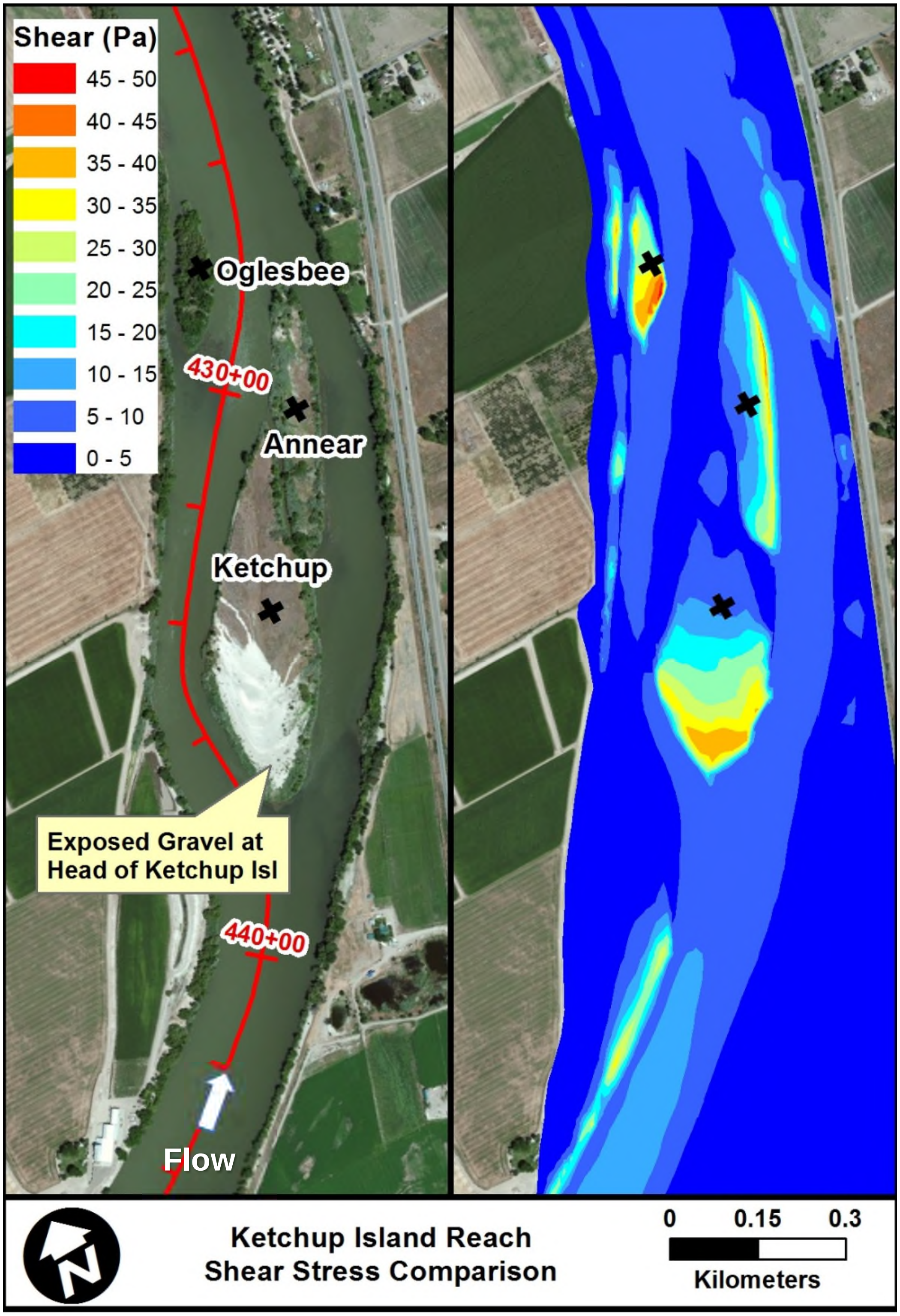

Figure 6.6 Predicted shear stress distribution at 2,832 m^3/s under baseline conditions along the Ketchup Island reach.

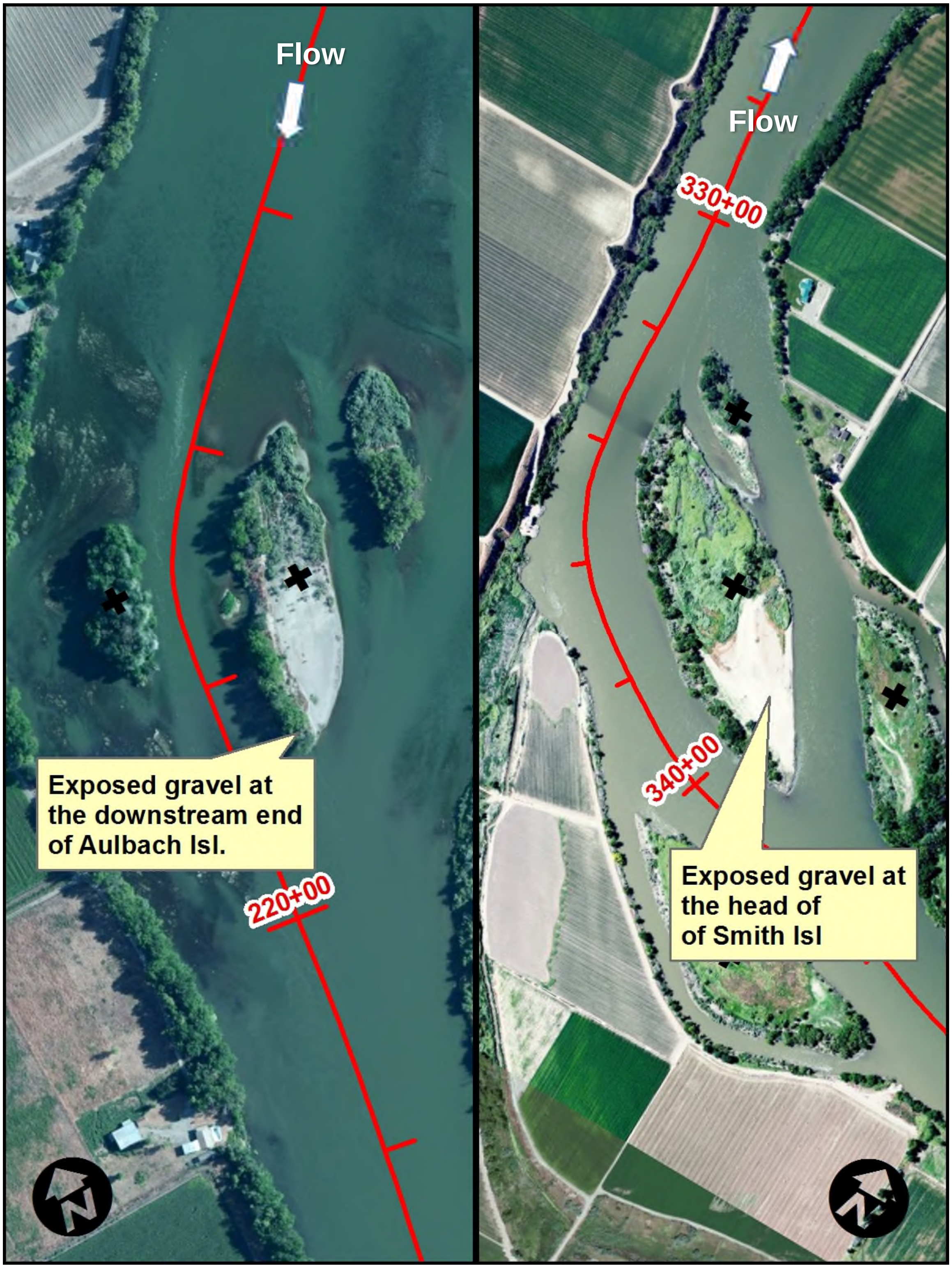

Figure 6.7 Eroded gravel surfaces at Aulbach #1 and Smith (11.2) Islands.

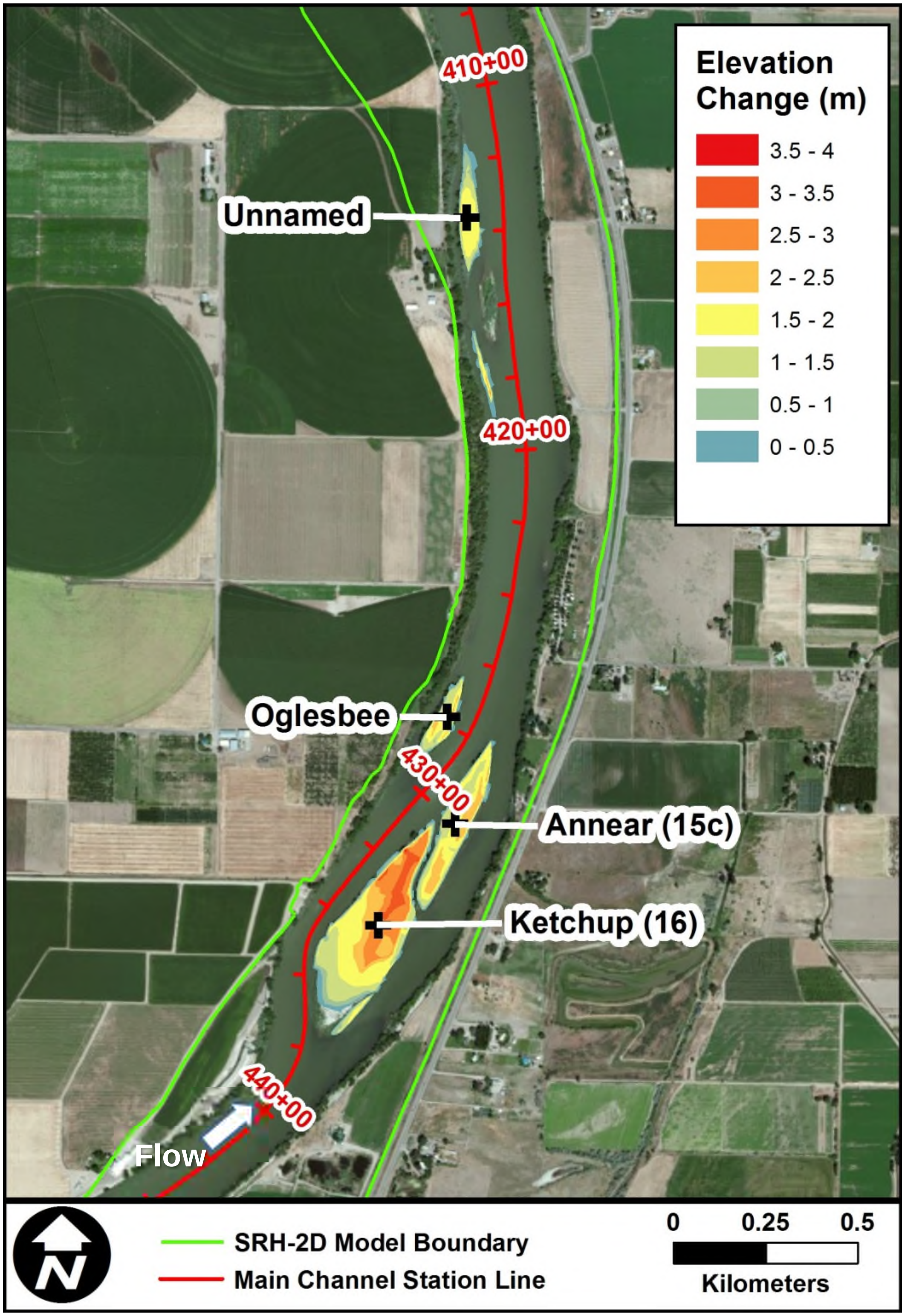

Figure 6.8 Difference in elevation between the baseline and without-islands conditions for the Ketchup model.

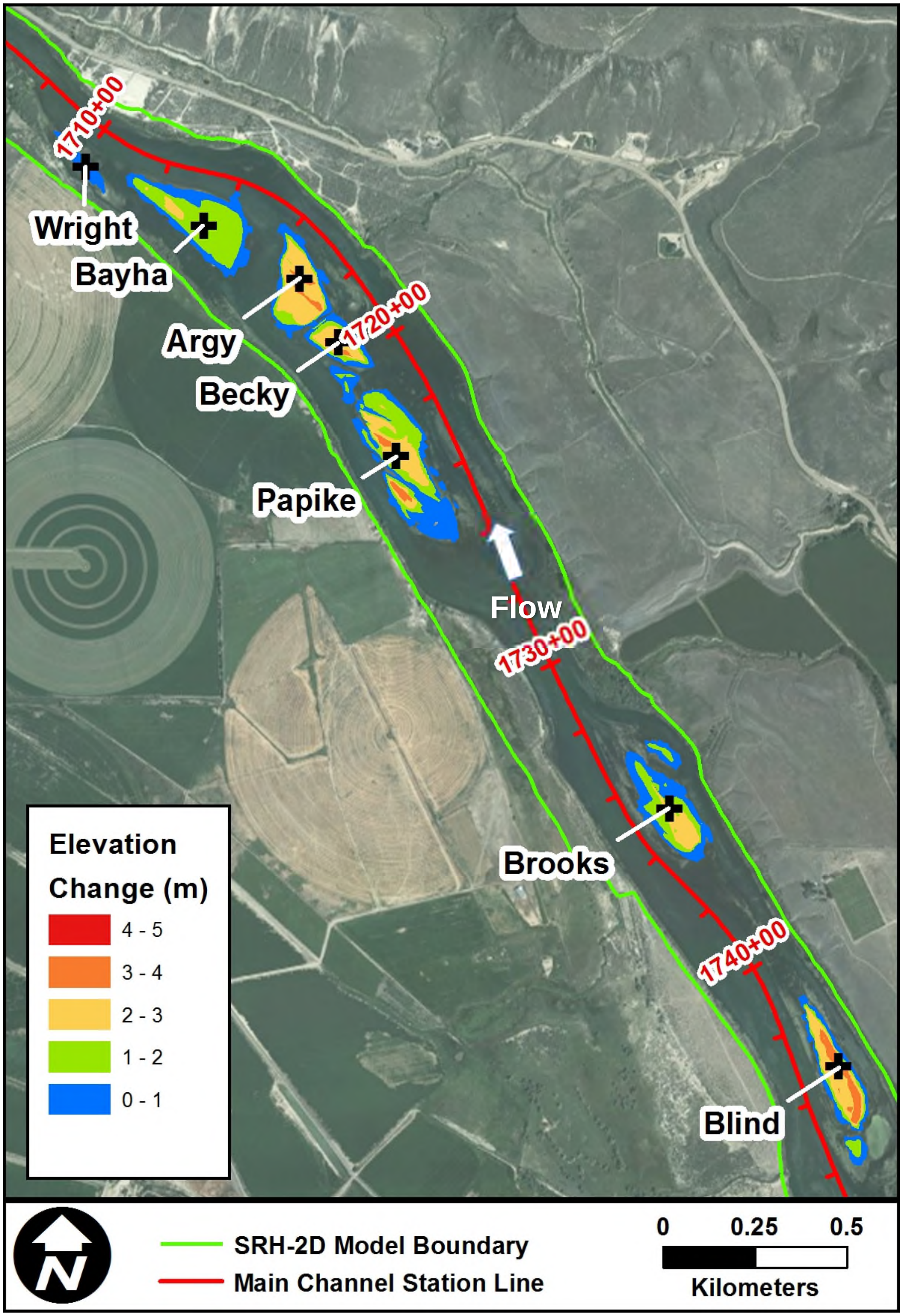

Figure 6.9 Difference in elevation between the baseline and without-islands conditions for the Walters Ferry model.

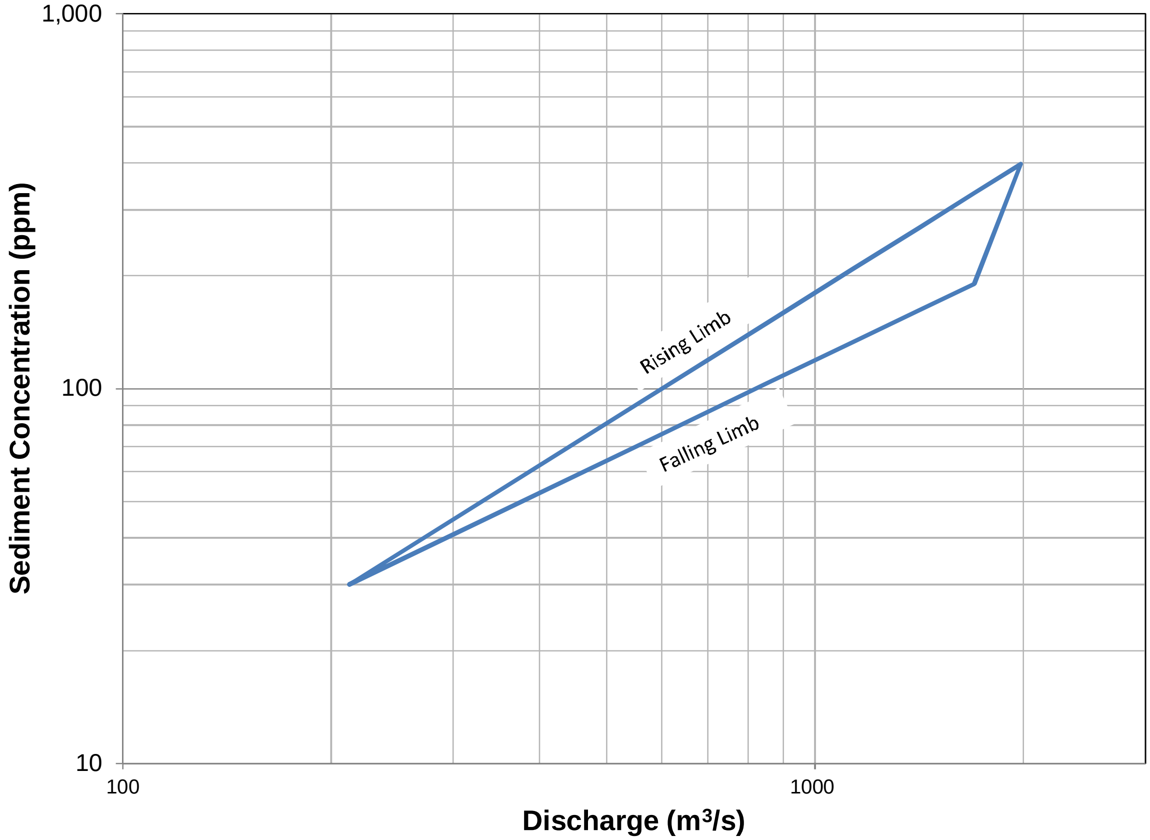

Figure 6.10 Discharge-sediment-transport rating curve developed to input sediment to the Ketchup and Walters Ferry 2-D sediment-transport models.

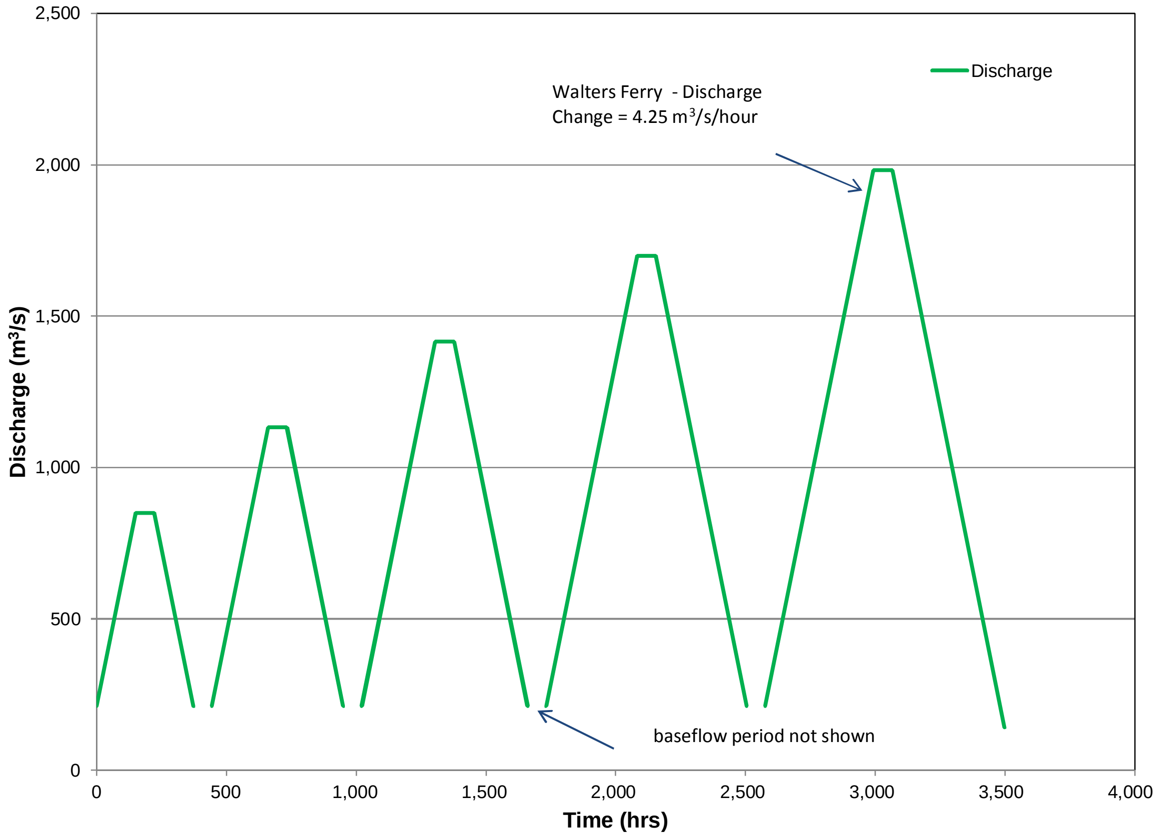

Figure 6.11 Example of the sequence of modeled hydrographs ranging from 850 m^3/s to 1,982 m^3/s. This set of hydrographs represents 1 cycle.

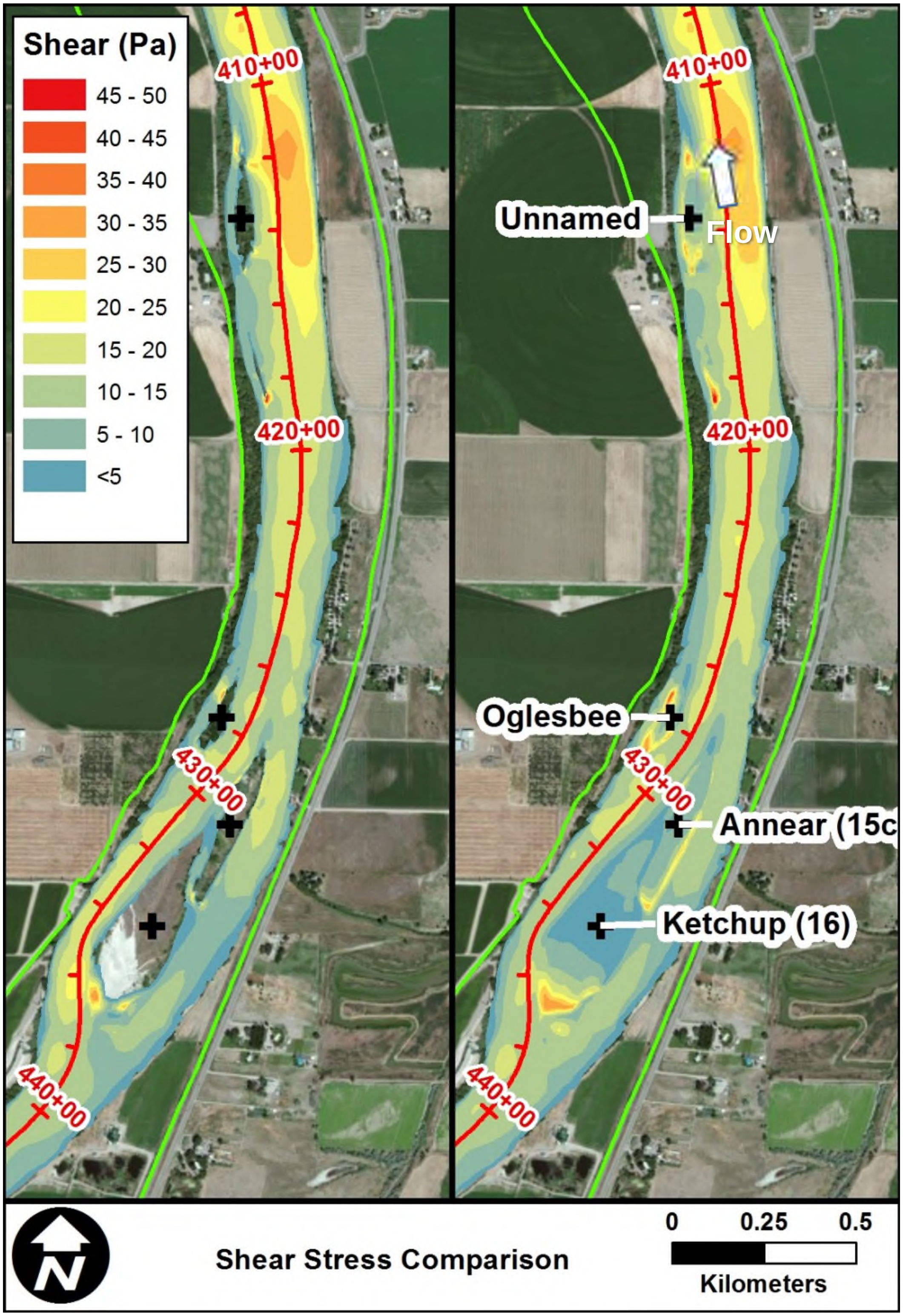

Figure 6.12 Shear stress comparison at the Ketchup Reach between the baseline conditions (left side) and the without-islands conditions (right side) at the 2-year peak flow.

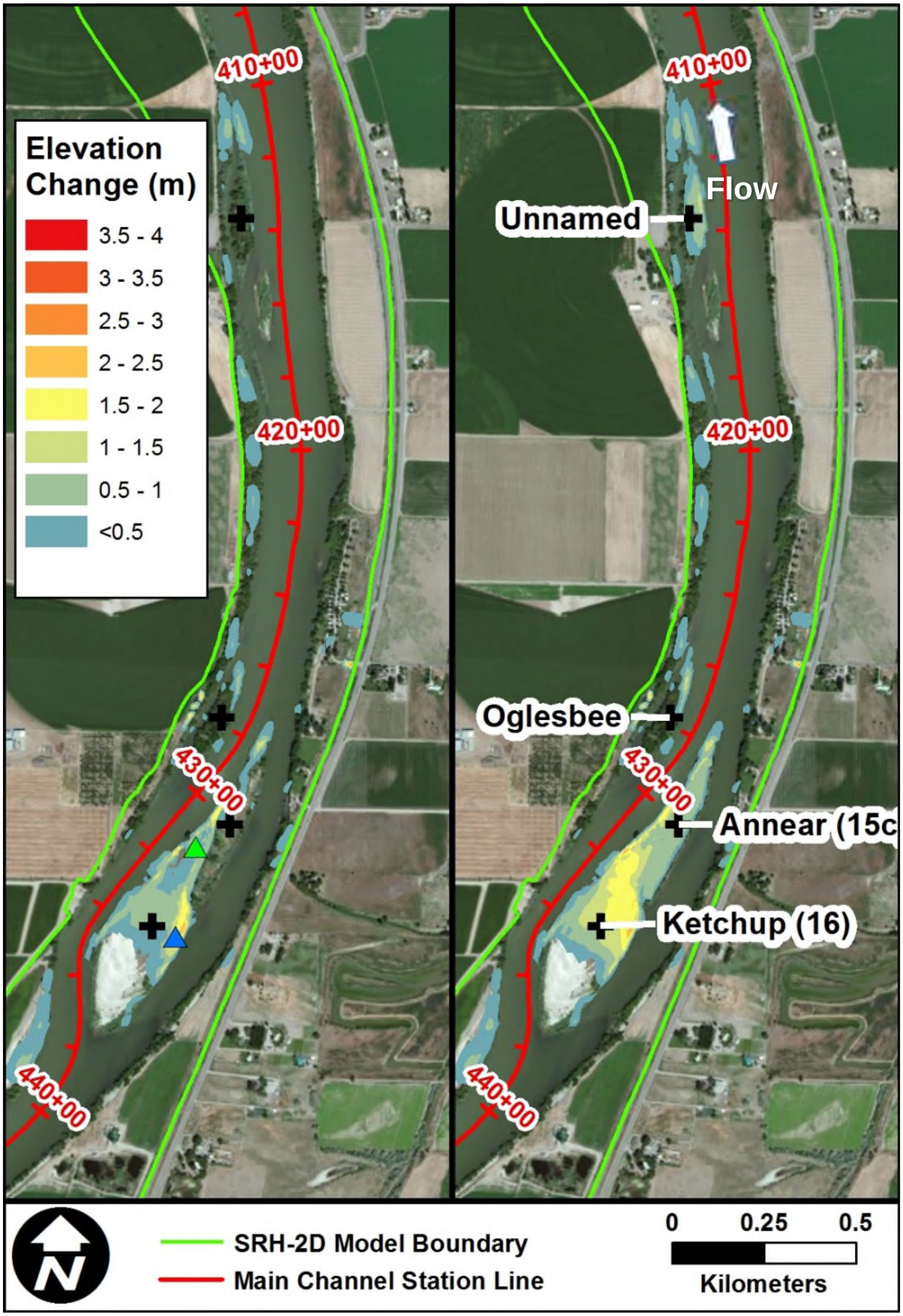

Figure 6.13 Change in bed elevation in the Ketchup reach at the end of cycle 4 (left side) and cycle 8 (on the right side).

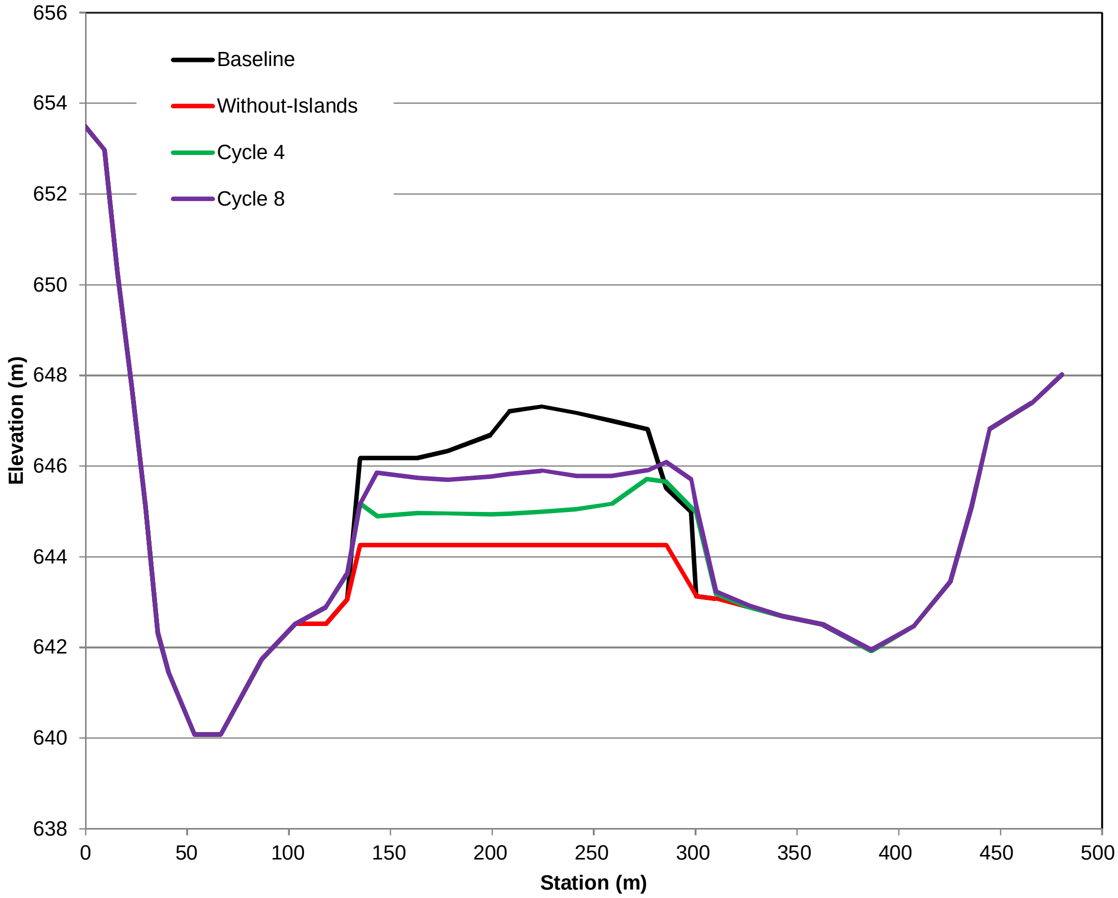

Figure 6.14 Comparison of the cross-section geometry across Ketchup Island for the baseline, without-islands, end of cycle 4 and end of cycle 8 conditions, as well as the predicted water-surface elevation at 2-year peak-flow recurrence interval (post-dam conditions).

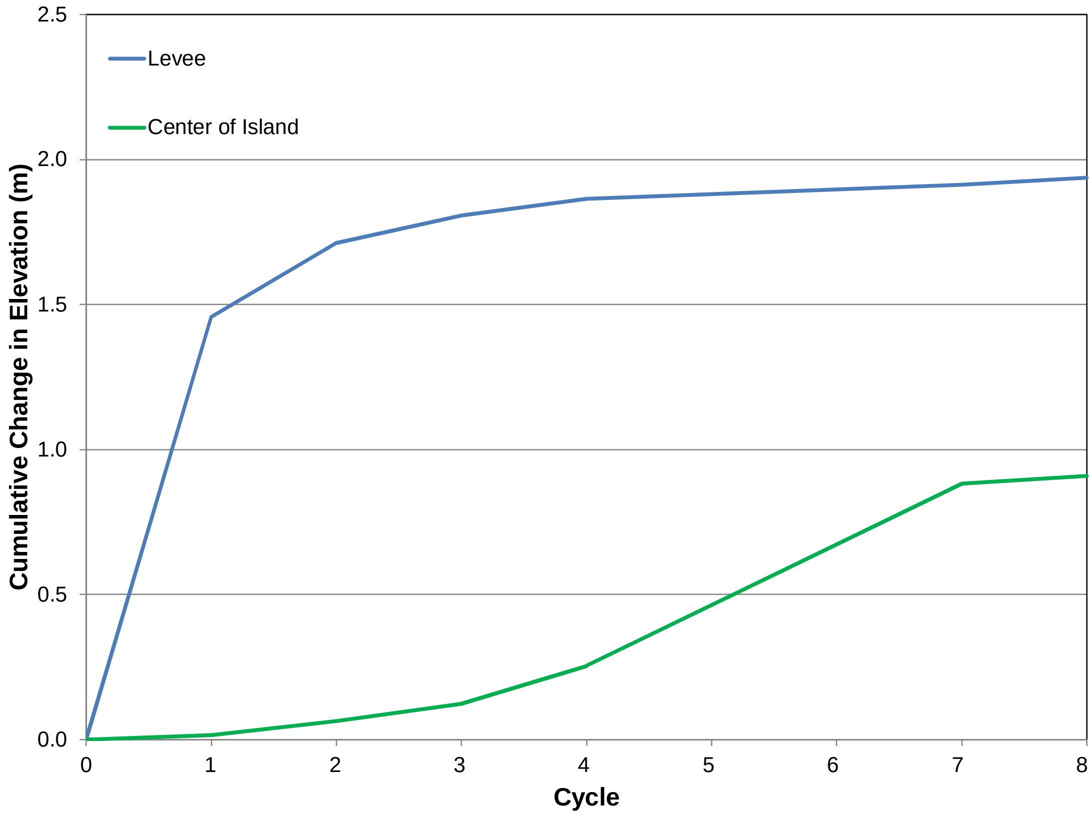

Figure 6.15 Comparison of aggradation rates at two locations on Ketchup Island.

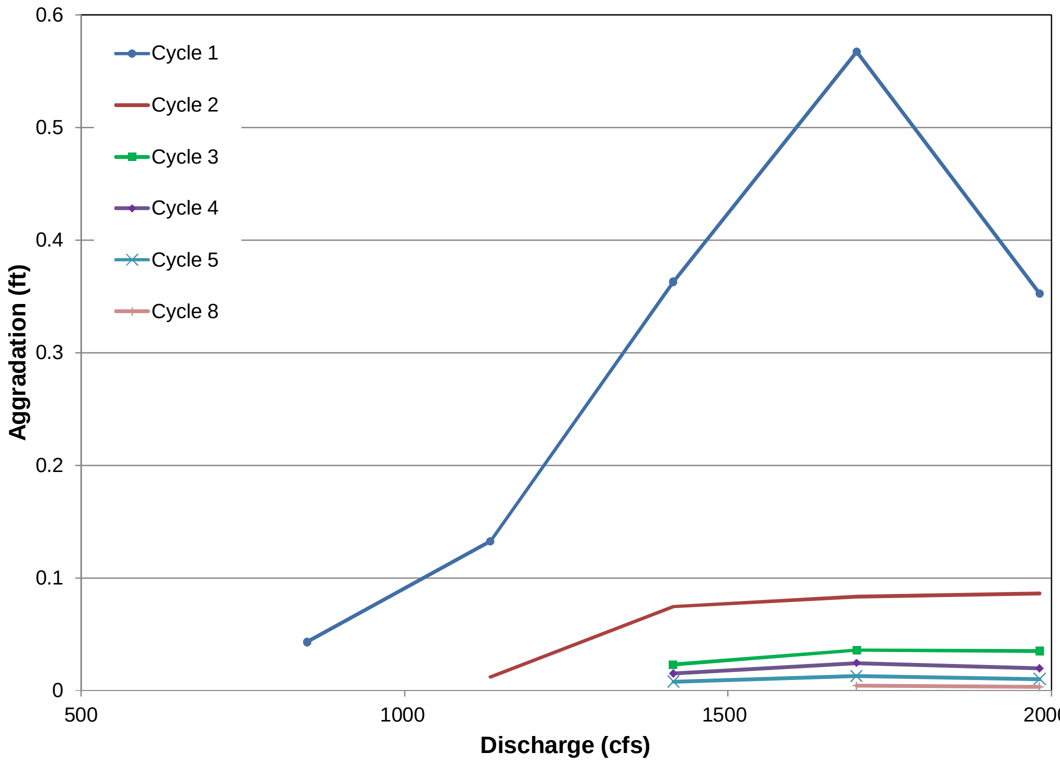

Figure 6.16 Comparison of the predicted amount of aggradation for each cycle at the levee location on Ketchup Island.

Table 6.1 Average number of occurrences per 100 years for selected return intervals.

Return Interval (years)	Discharge (m^3/s)	Average number of occurrences per 100 years
2	1,368	30
5	1,889	10
10	2,010	5
20	2,376	3
50		1
100		1

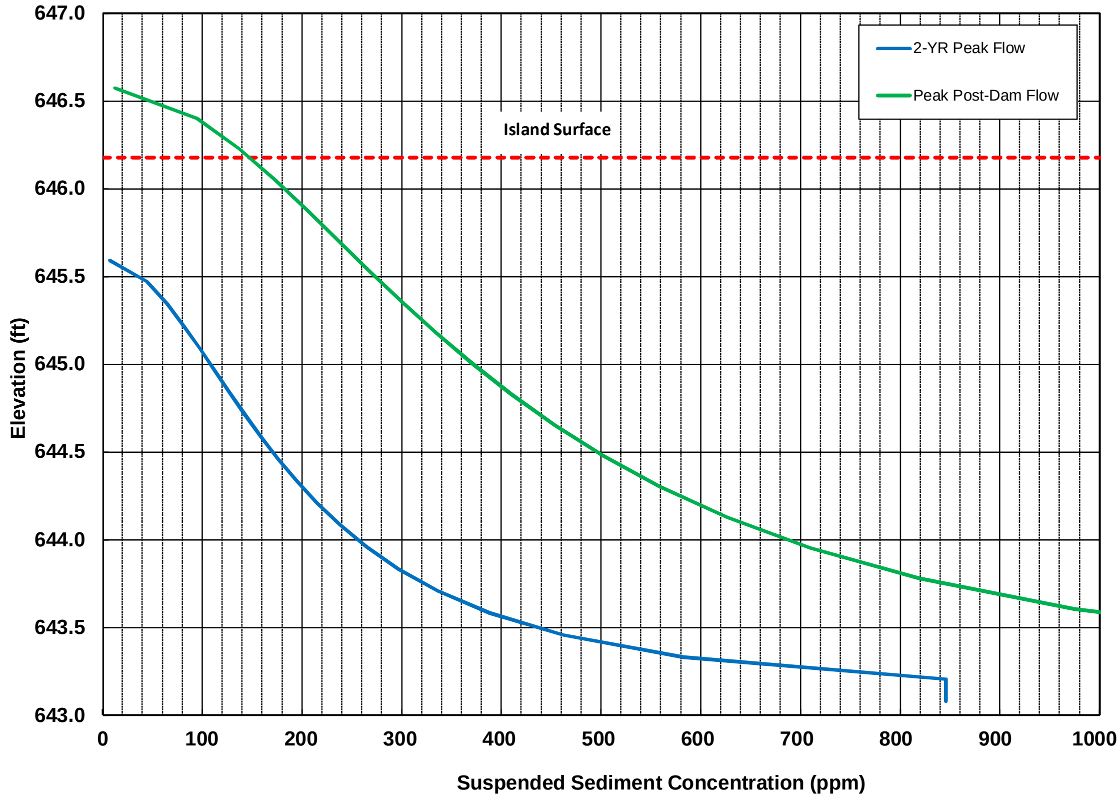

Figure 6.17 Estimated suspended concentration profiles along the right side of Ketchup Island at the 2-year peak flow and at the highest peak flow during the post-dam period.

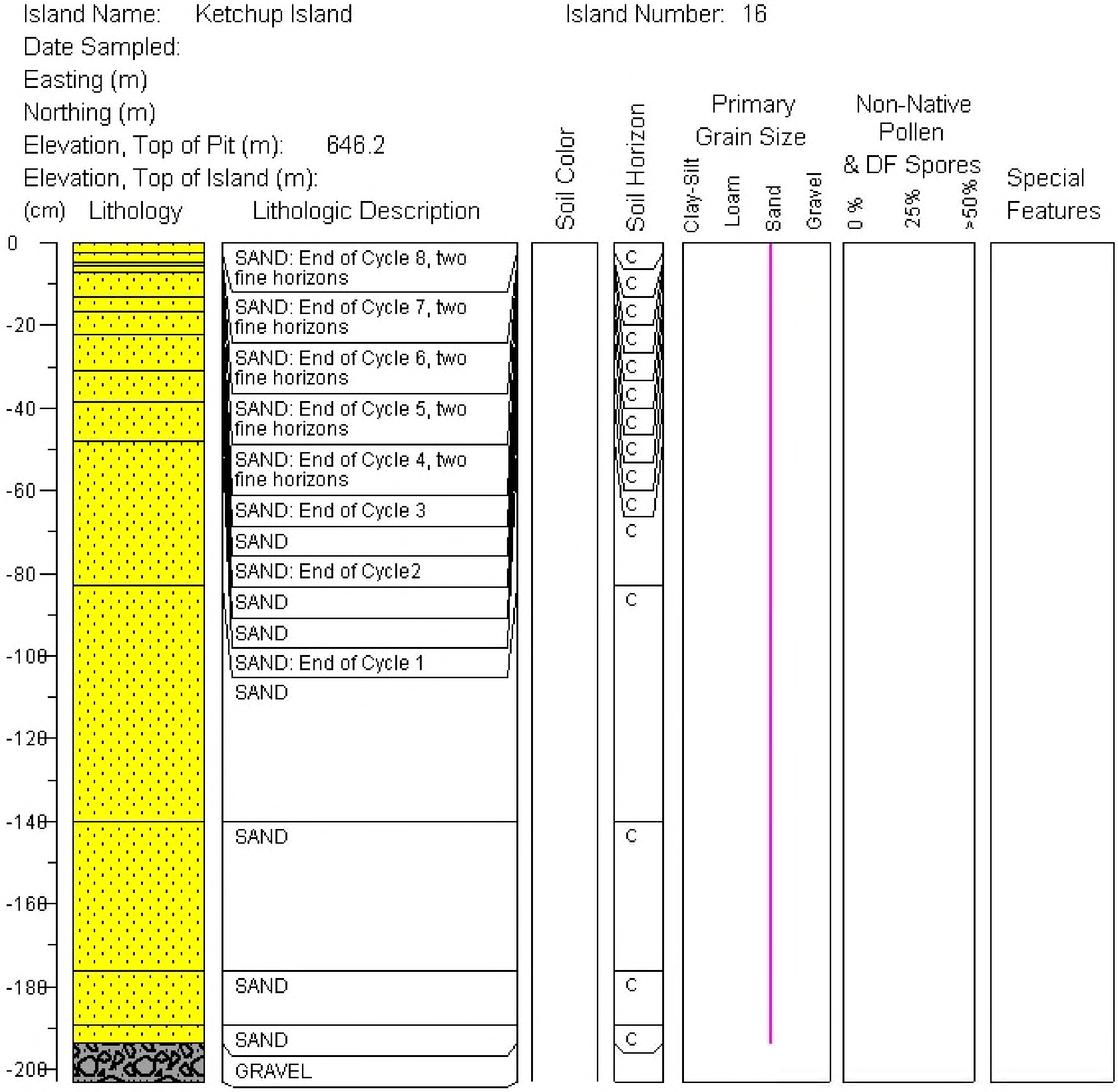

Figure 6.18 Soil profile for Ketchup Island developed from the 2-D model output.

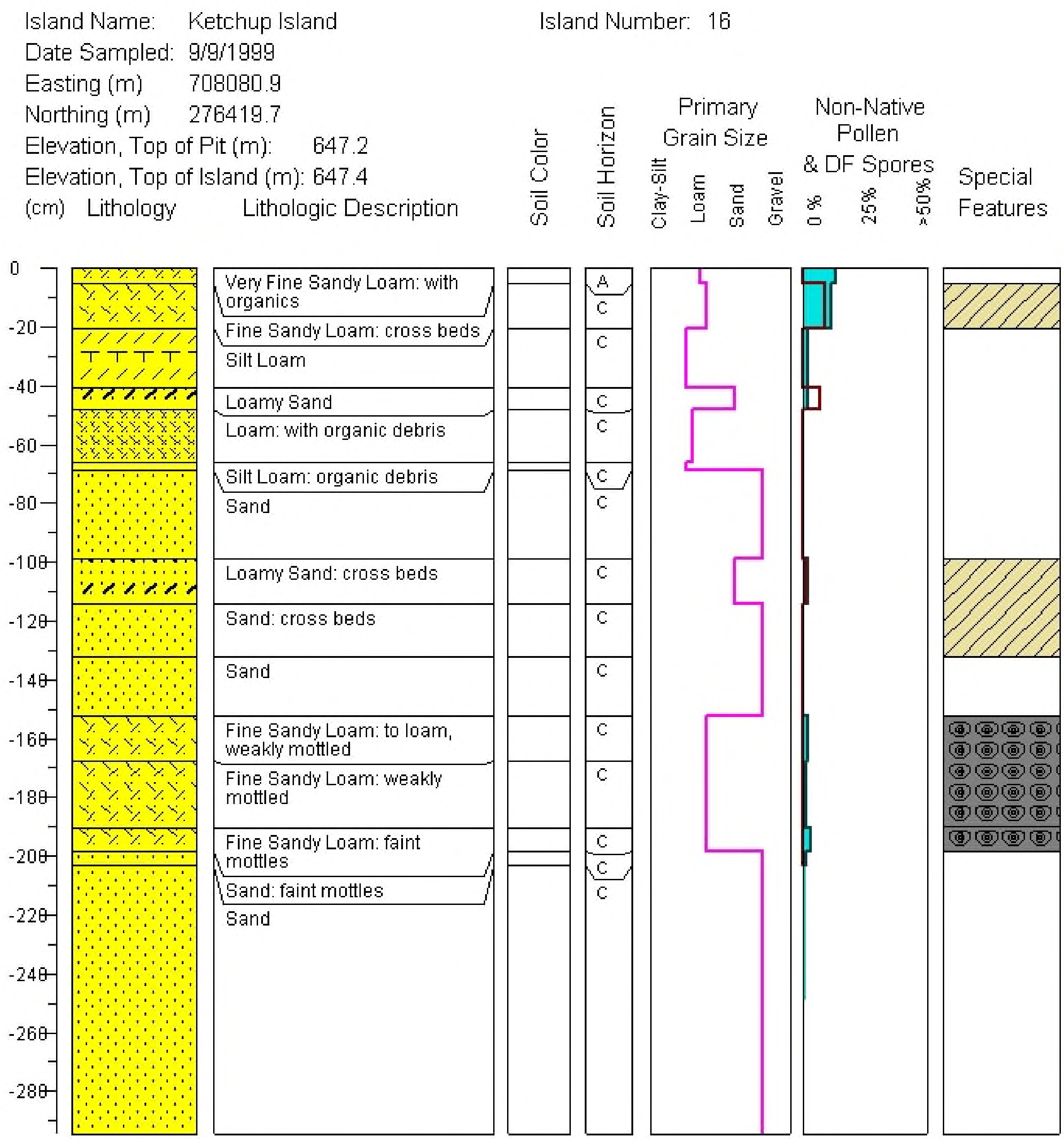

Figure 6.19 Measured soil profile for Ketchup Island.

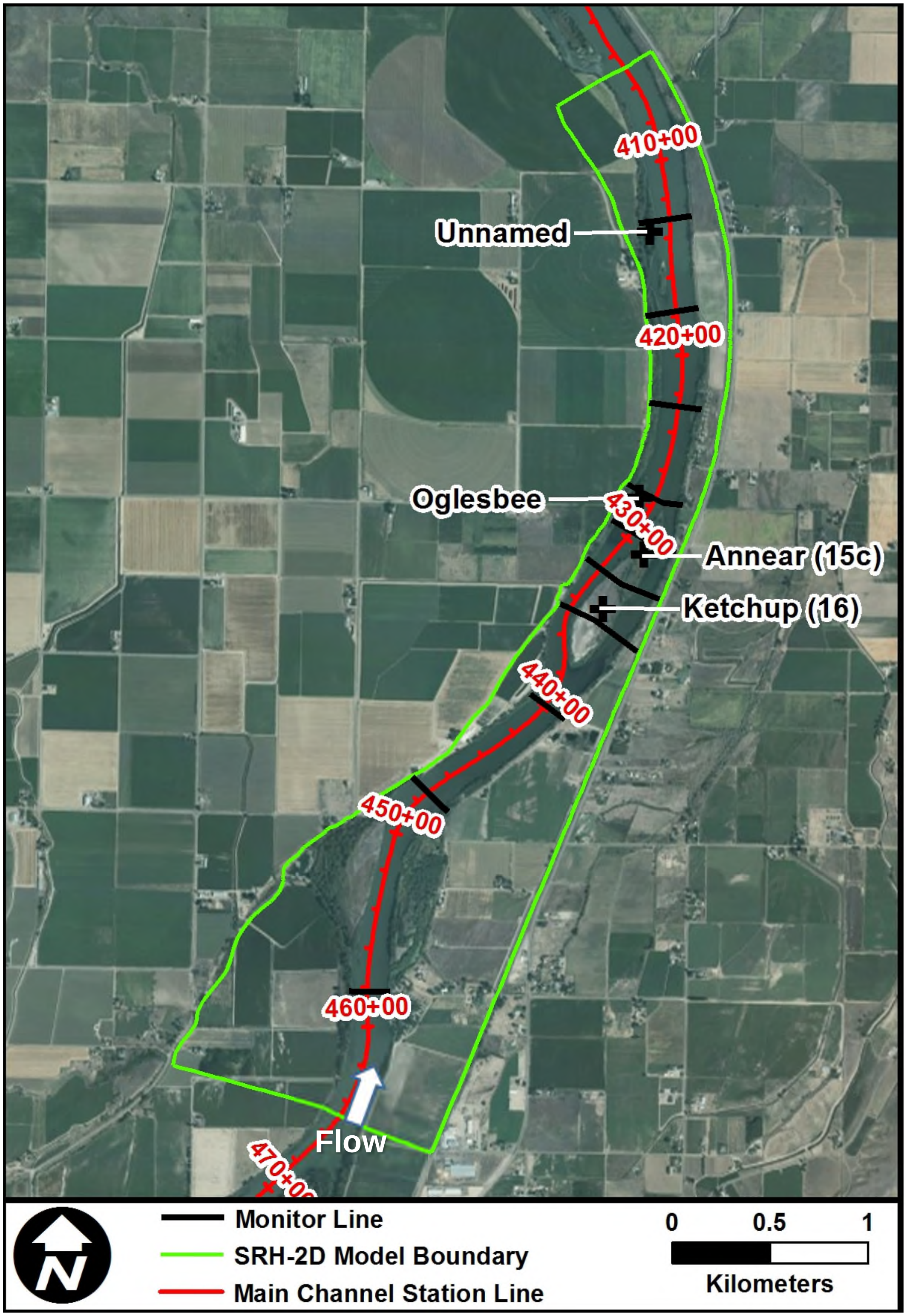

Figure 6.20 Monitor lines in the Ketchup Reach used to evaluate the sediment continuity along the reach.

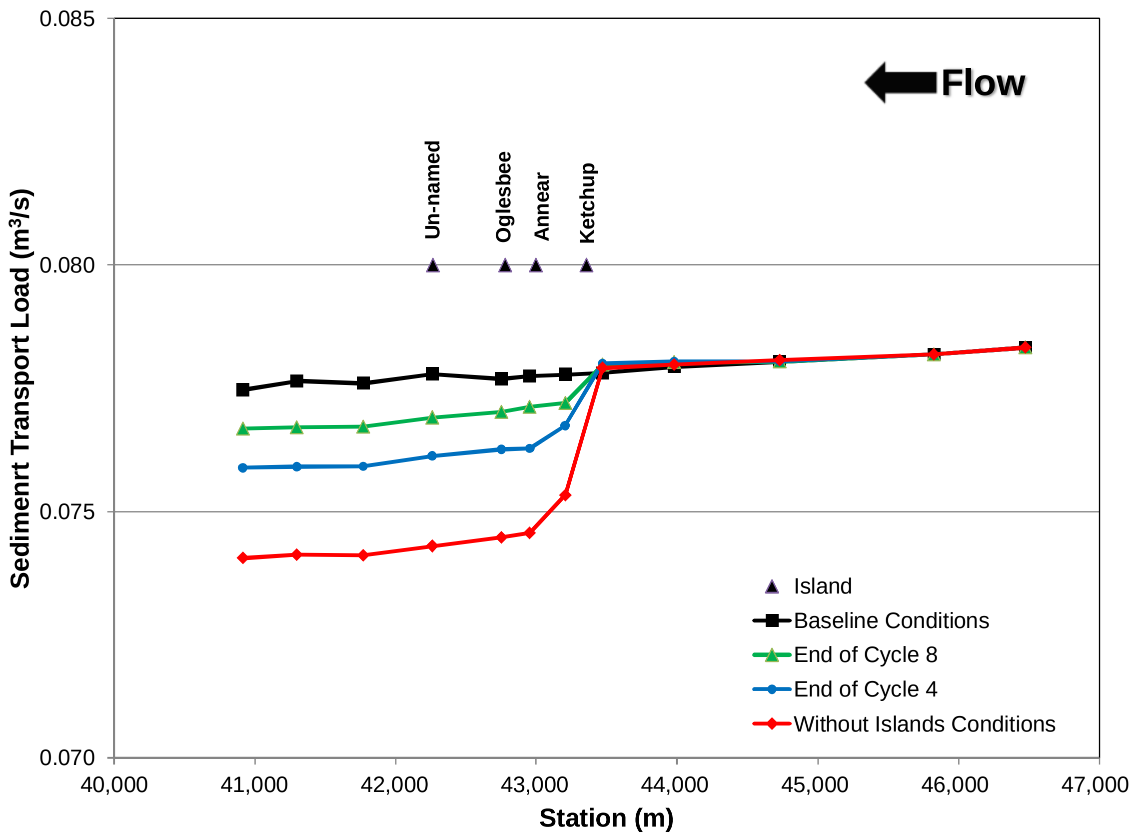

Figure 6.21 Variation in sediment transport along the Ketchup reach at the 2-year peak flow.

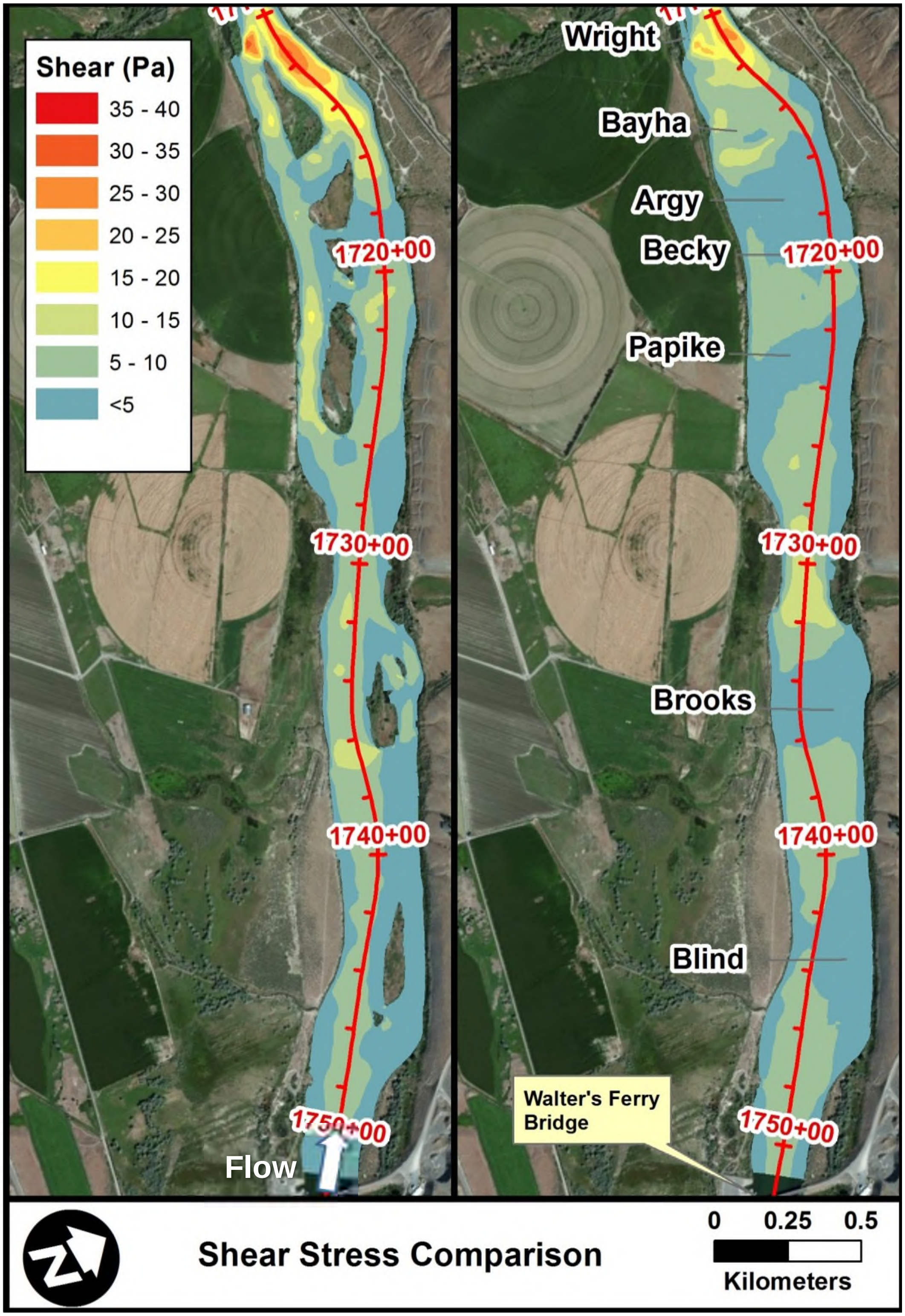

Figure 6.22 Comparison of predicted shear stress in the Walters Ferry subreach for the baseline (left side of figure) and without-islands (right side of figure) at the 2-year post-dam peak flow.

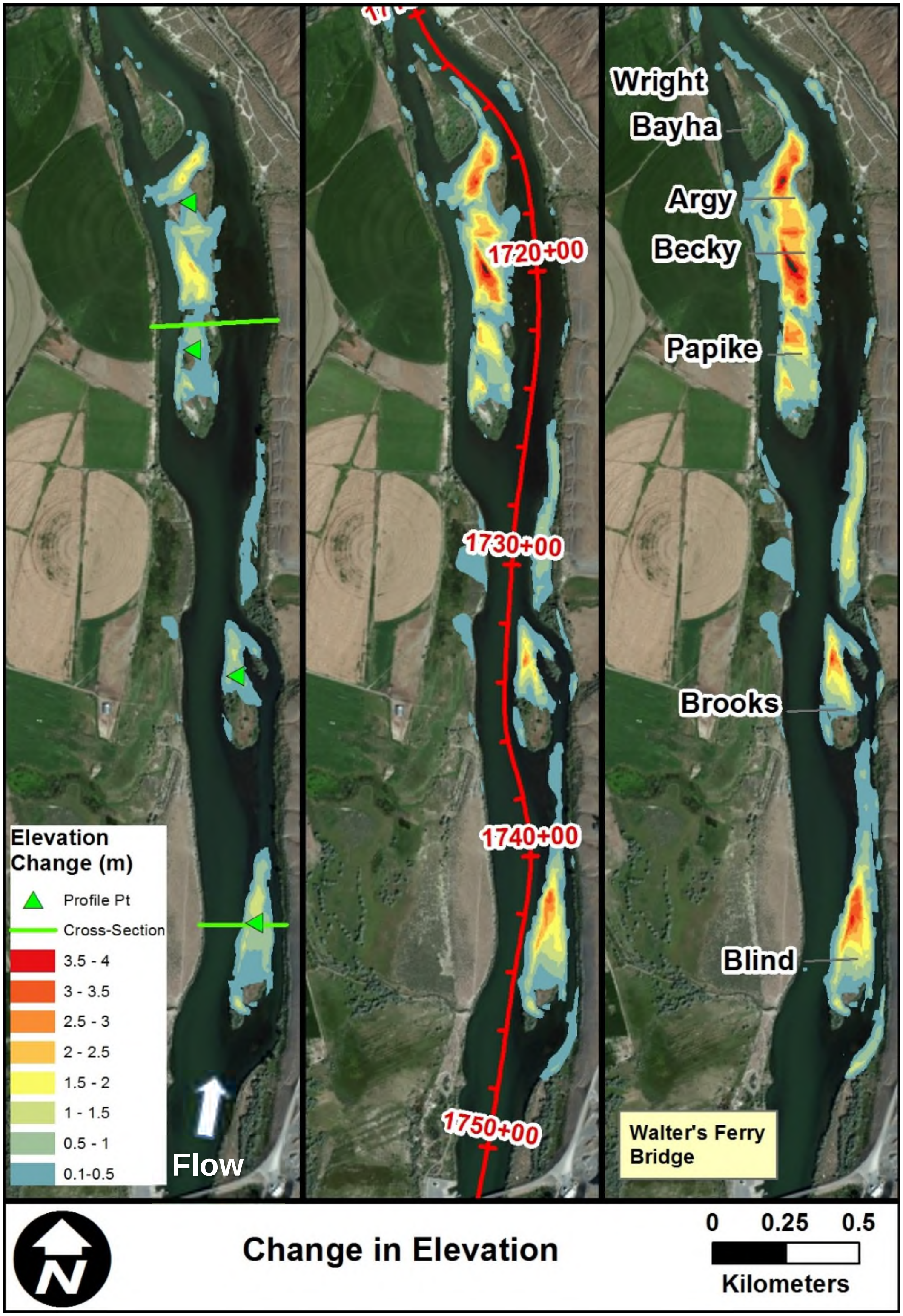

Figure 6.23 Change in bed elevation in the Walters Ferry Reach at the end of cycle 1 (left side), cycle 4 (center) and cycle 8 (right side).

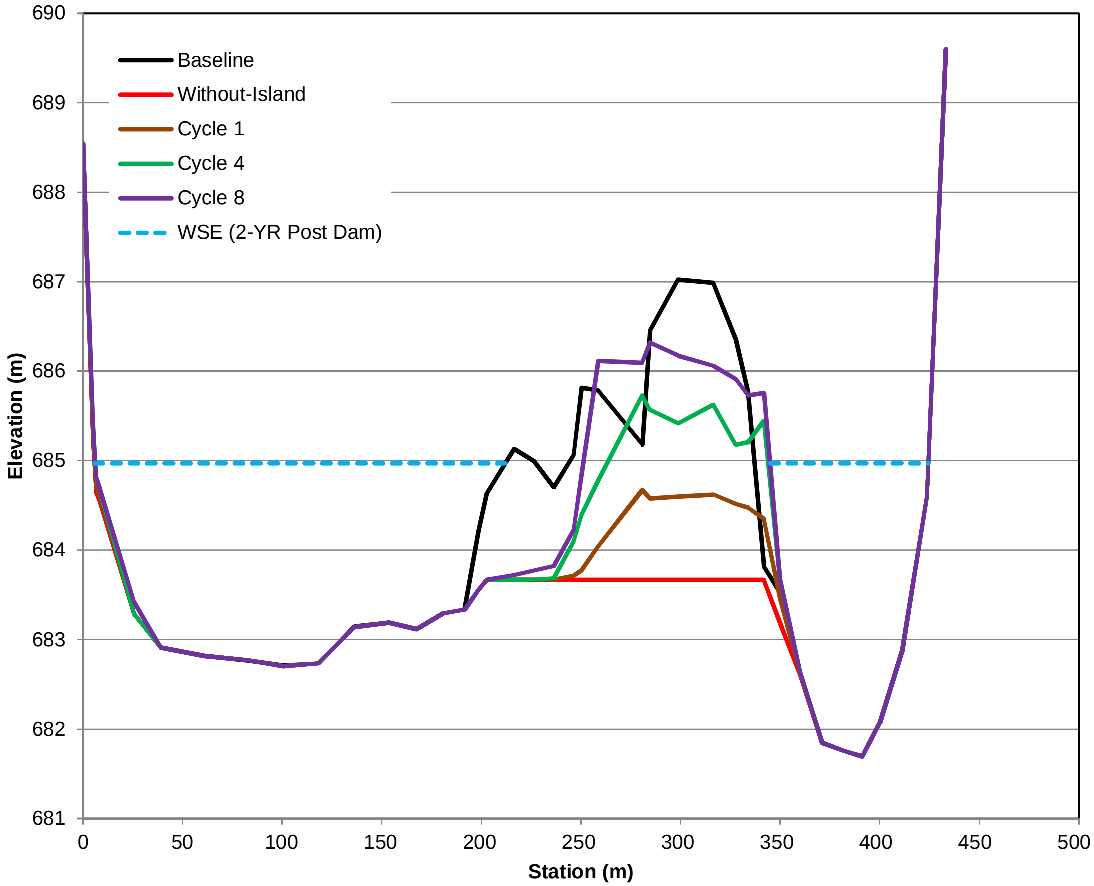

Figure 6.24 Comparison of the cross-section geometry across Papike Island for the baseline, without-islands, end of cycle 1, end of cycle 4 and end of cycle 8 conditions, as well as the predicted water-surface elevation at 2-year post-dam peak flow.

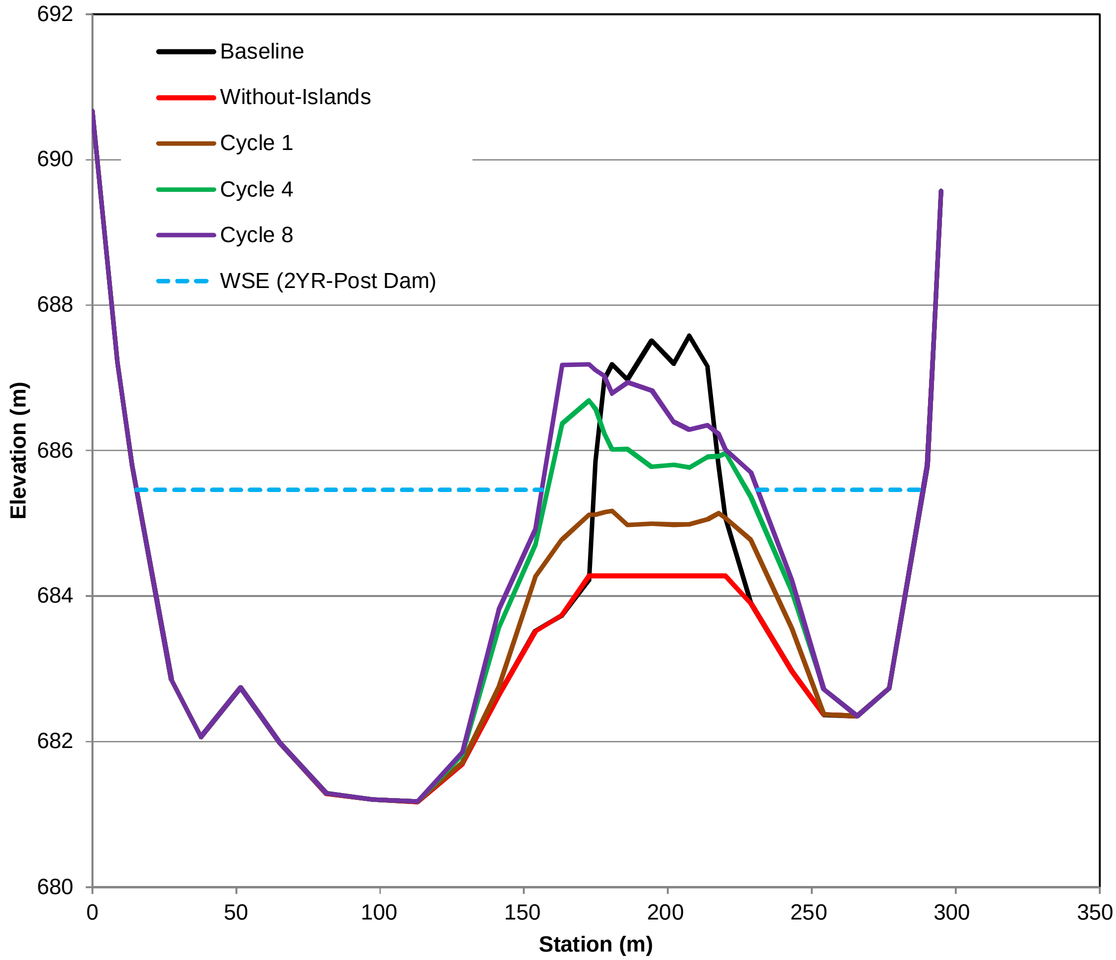

Figure 6.25 Comparison of the cross-section geometry across Blind Island for the baseline, without-islands, end of cycle 1, end of cycle 4 and end of cycle 8 conditions, as well as the predicted water-surface elevation at 2-year post-dam peak flow.

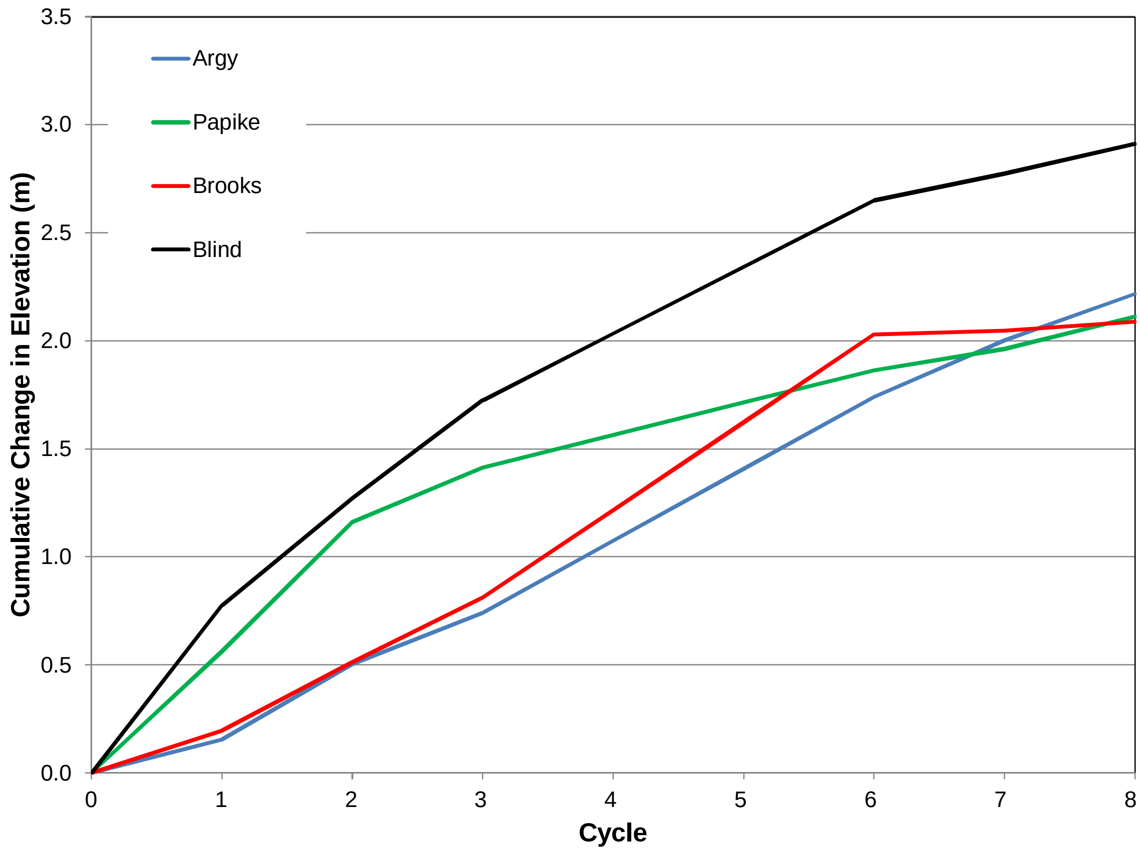

Figure 6.26 Comparison of the aggradation rates at four islands in the Walters Ferry reach.

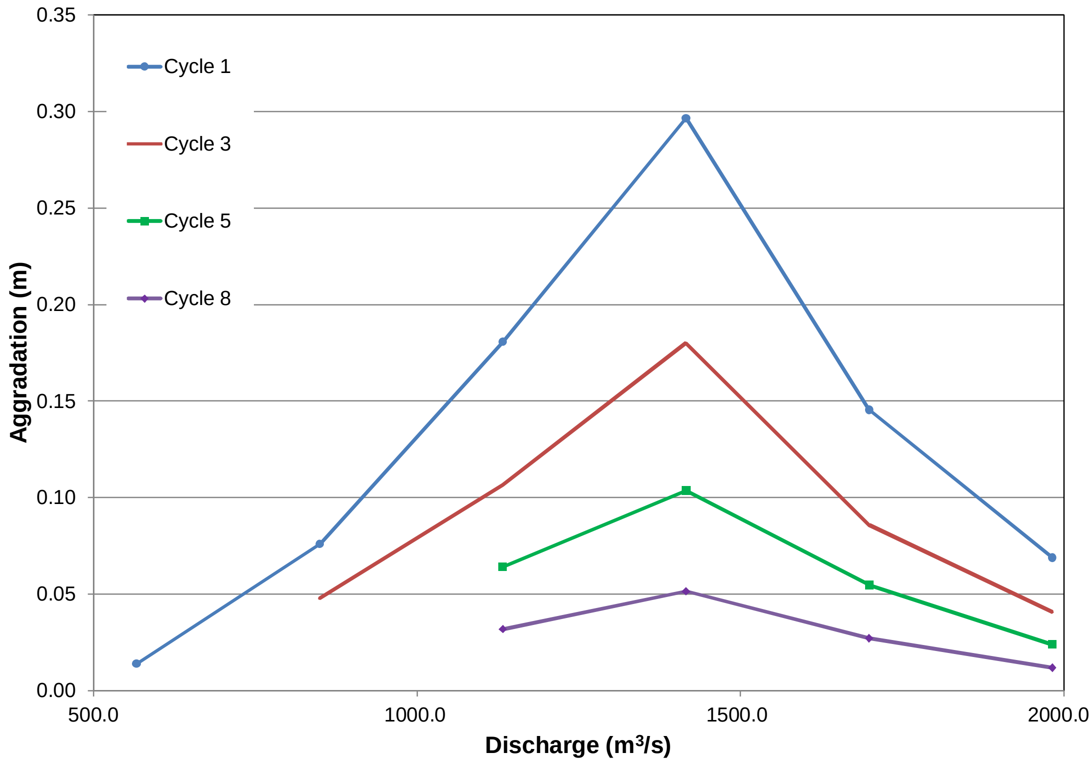

Figure 6.27 Comparison of the predicted amount of aggradation at the Blind Island.

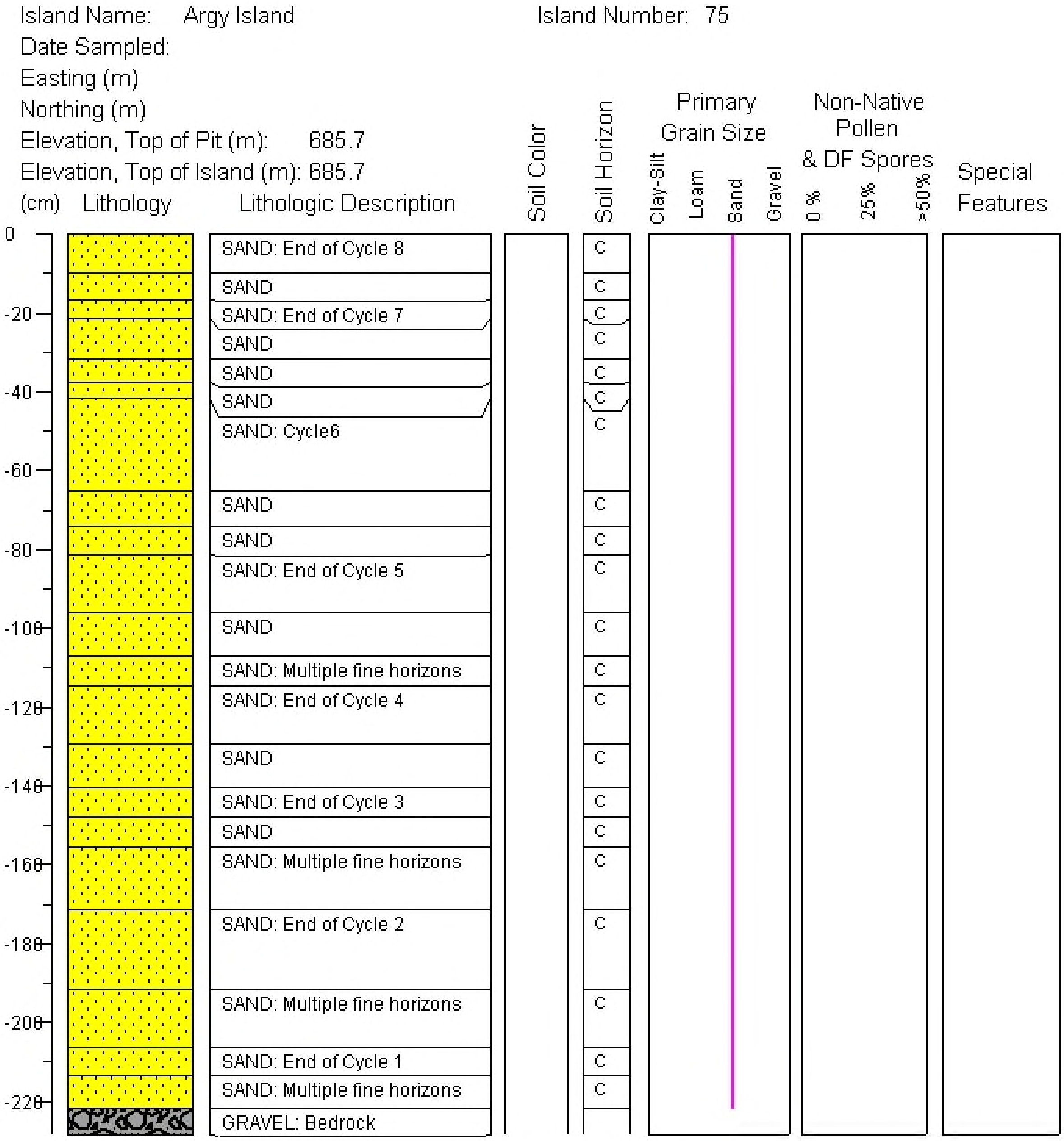

Figure 6.28 Soil profile for Argy (75) Island developed from the 2-D model output.

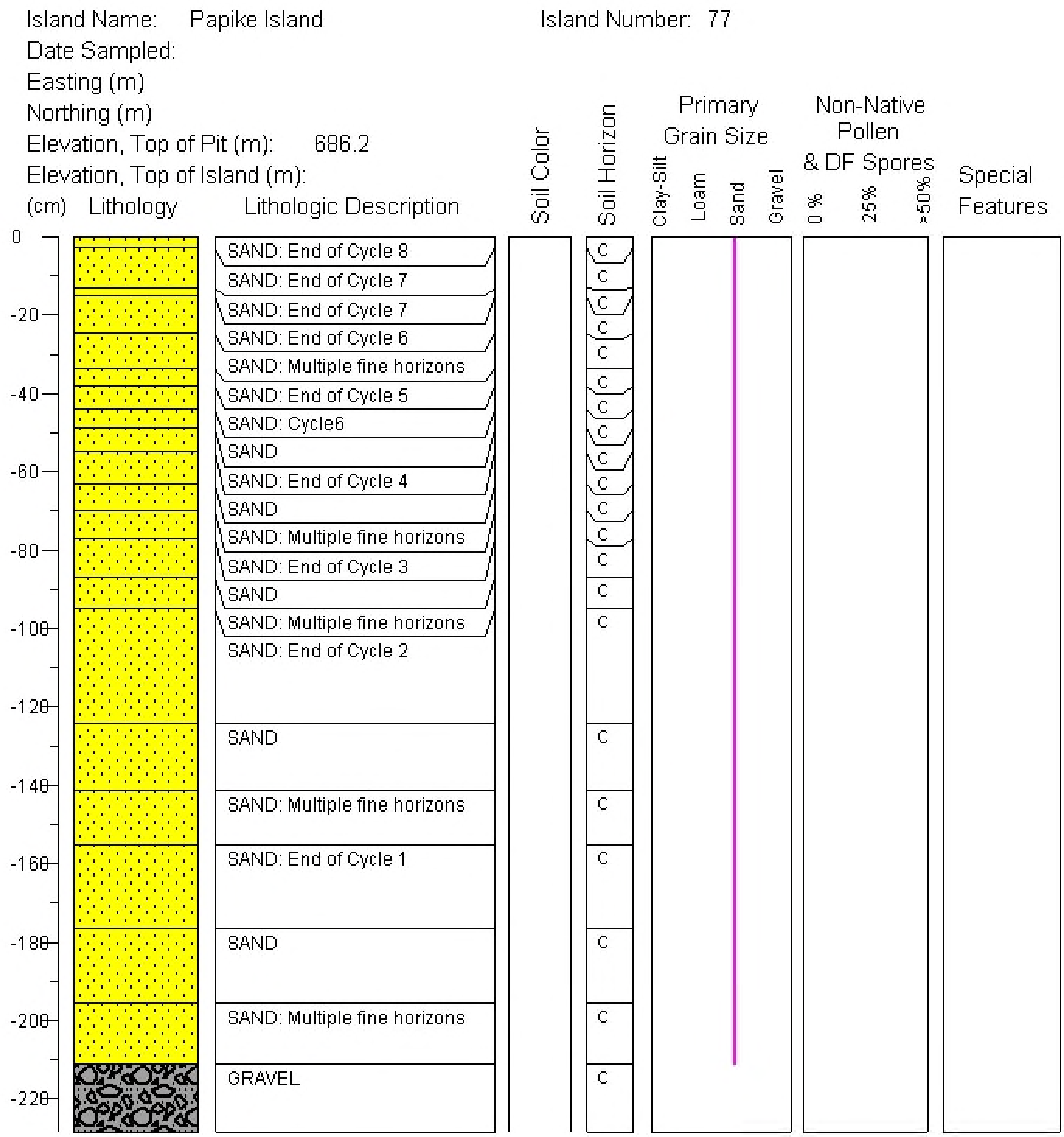

Figure 6.29 Soil profile for Papike (77) Island developed from the 2-D model output.

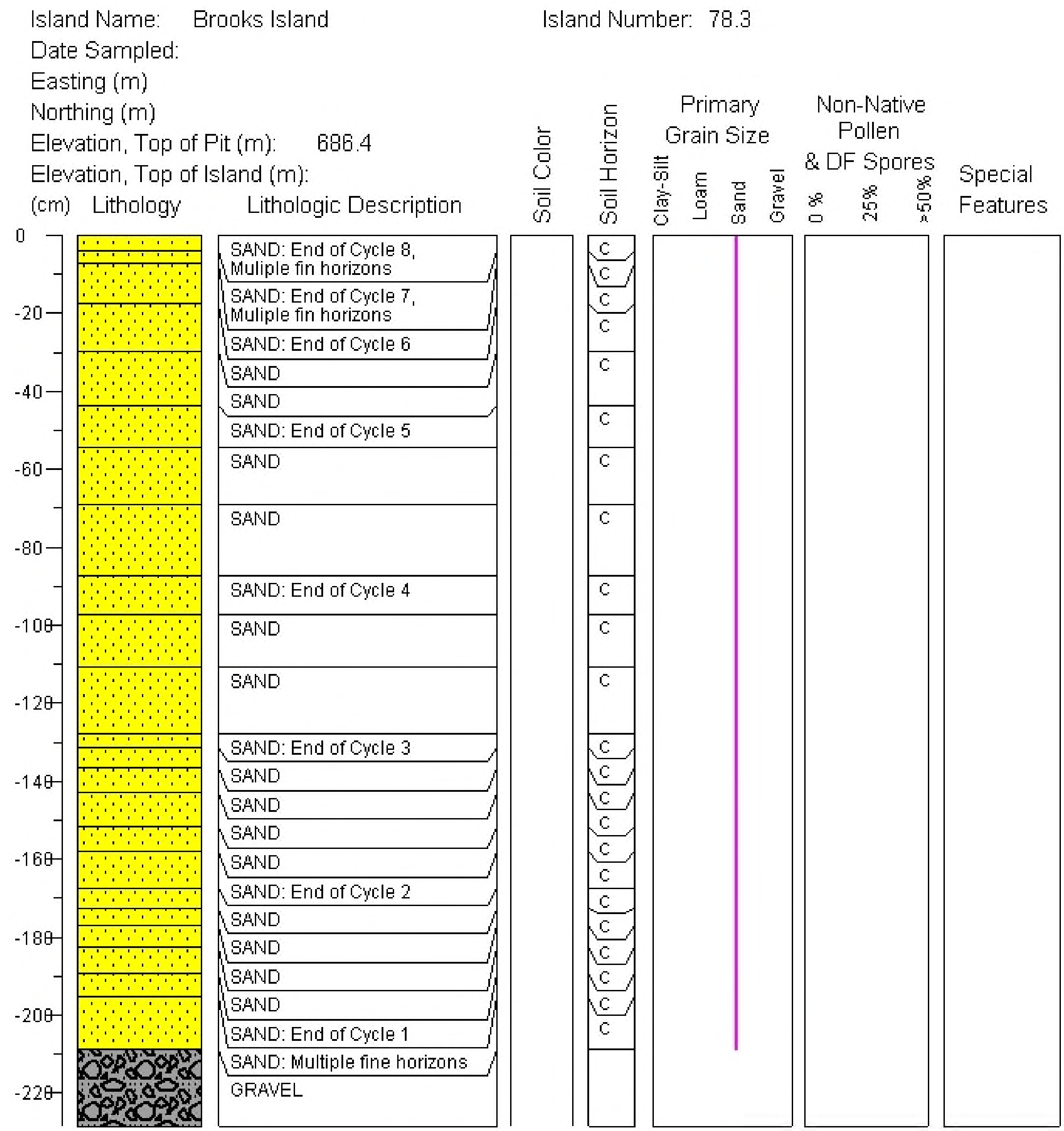

Figure 6.30 Soil profile for Brooks (78.3) Island developed from the 2-D model output.

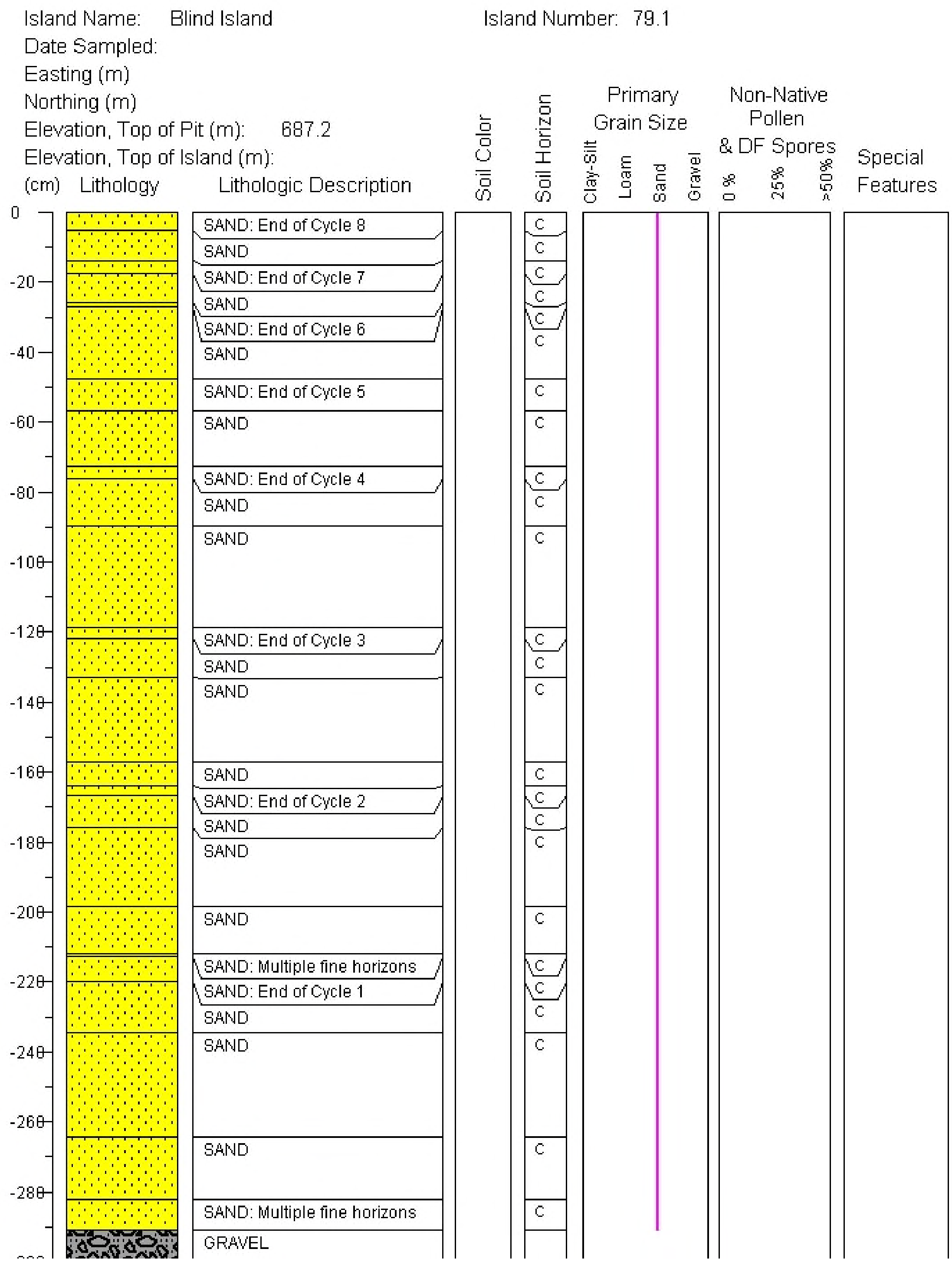

Figure 6.31 Soil profile for Blind (79.1) Island developed from the 2-D model output.

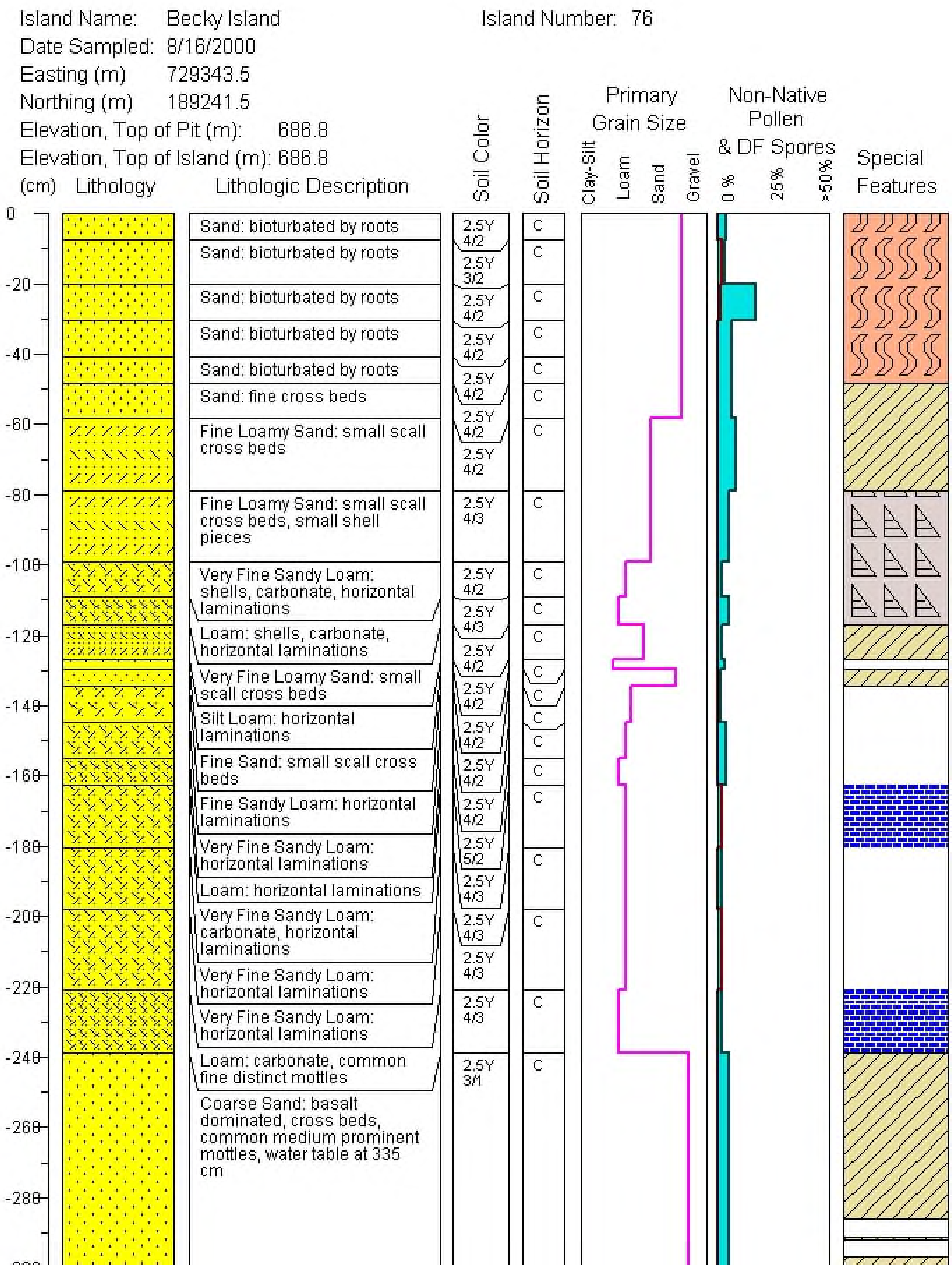

Figure 6.32 Measured soil profile at Becky Island (76).

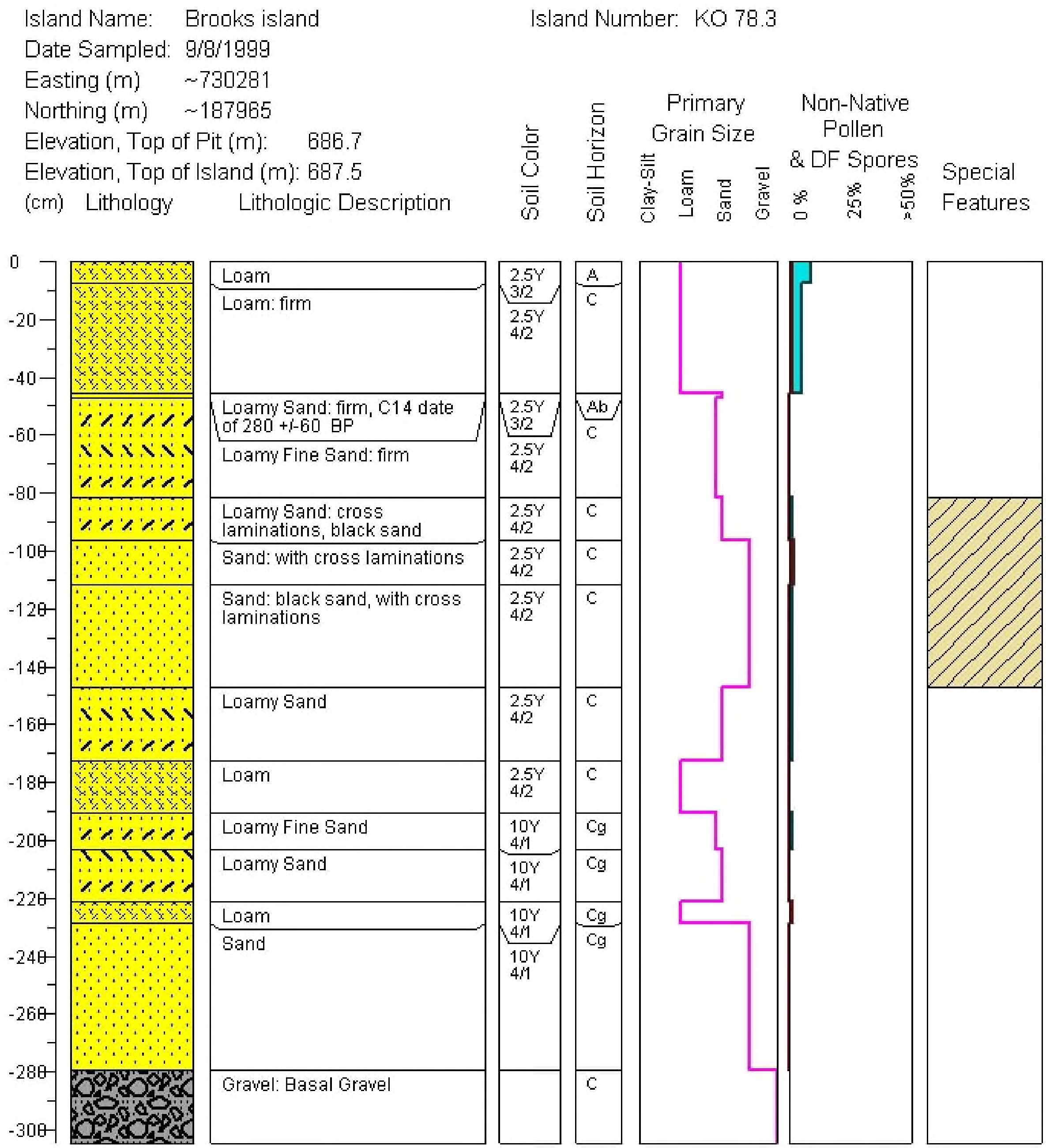

Figure 6.33 Measured soil profile at Brooks Island (78.3).

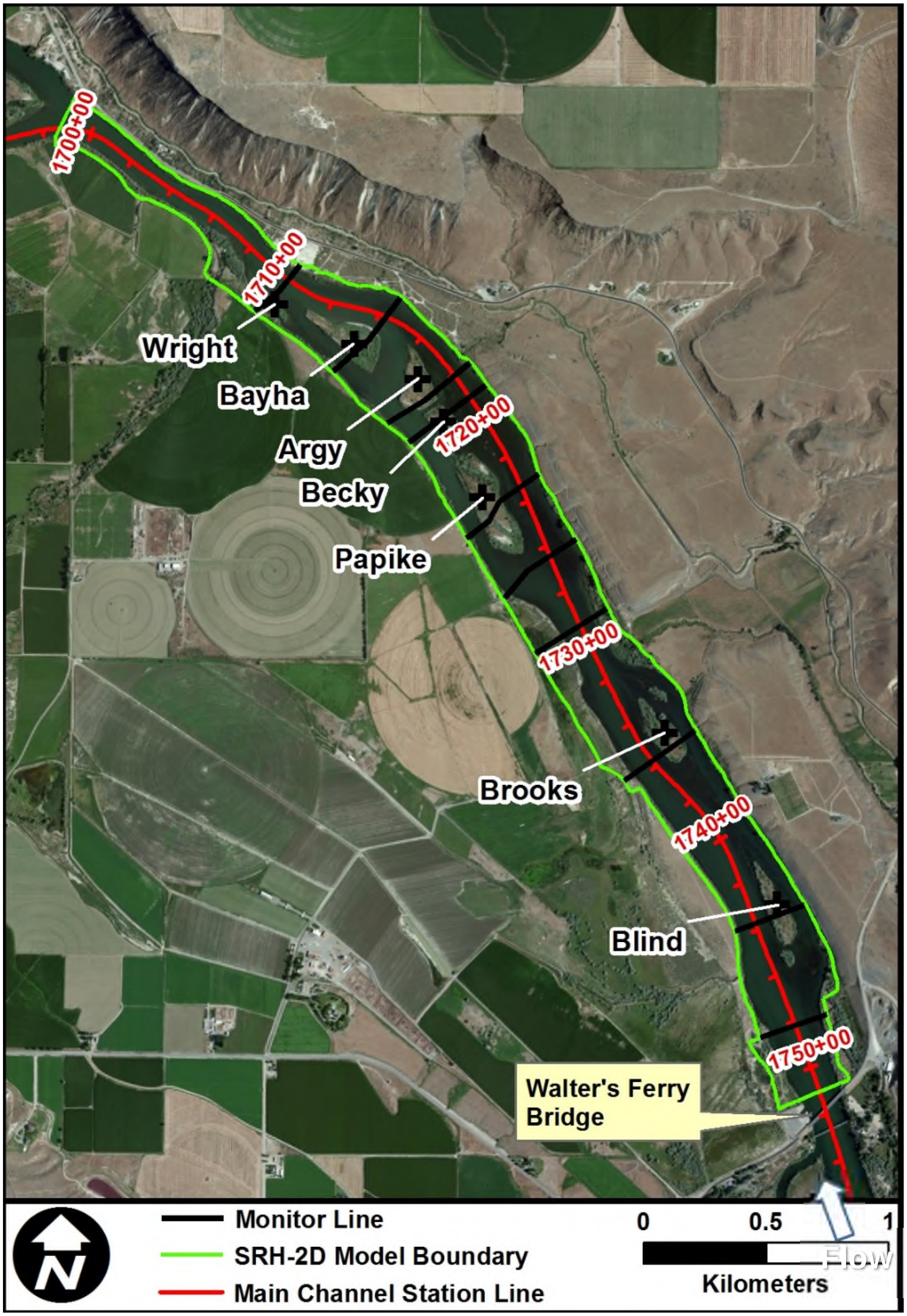

Figure 6.34 Monitor lines in the Walters Ferry Reach used to evaluate the sediment continuity along the reach.

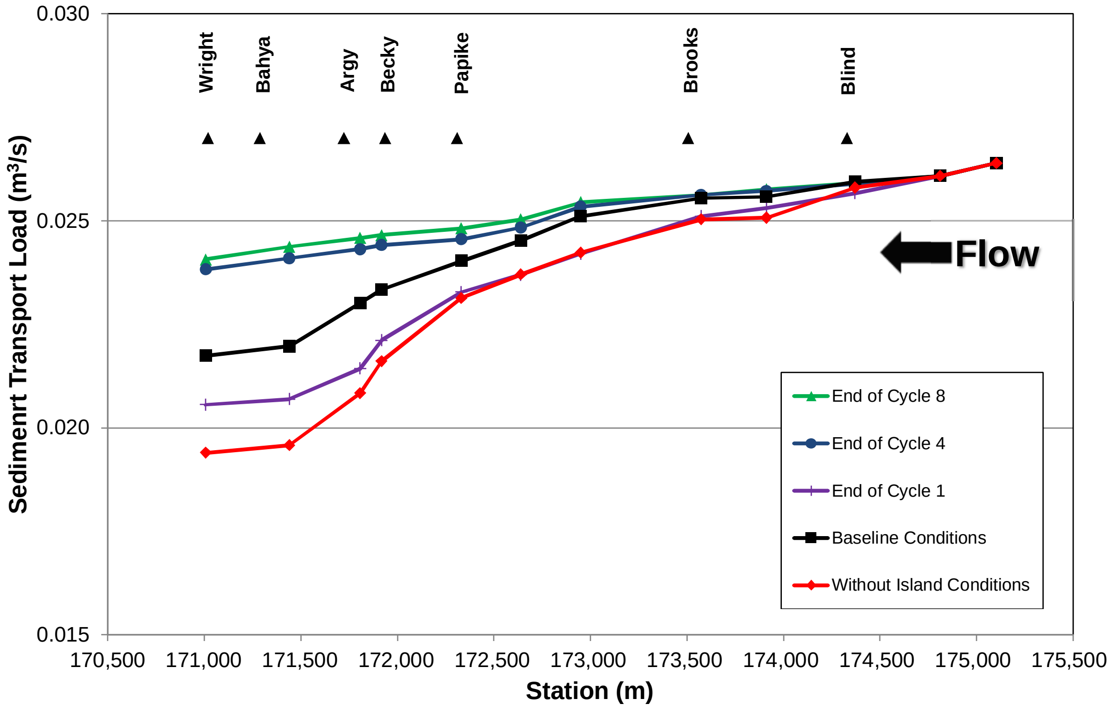

Figure 6.35 Variation in sediment transport along the Walters Ferry reach at the 2-year peak flow.

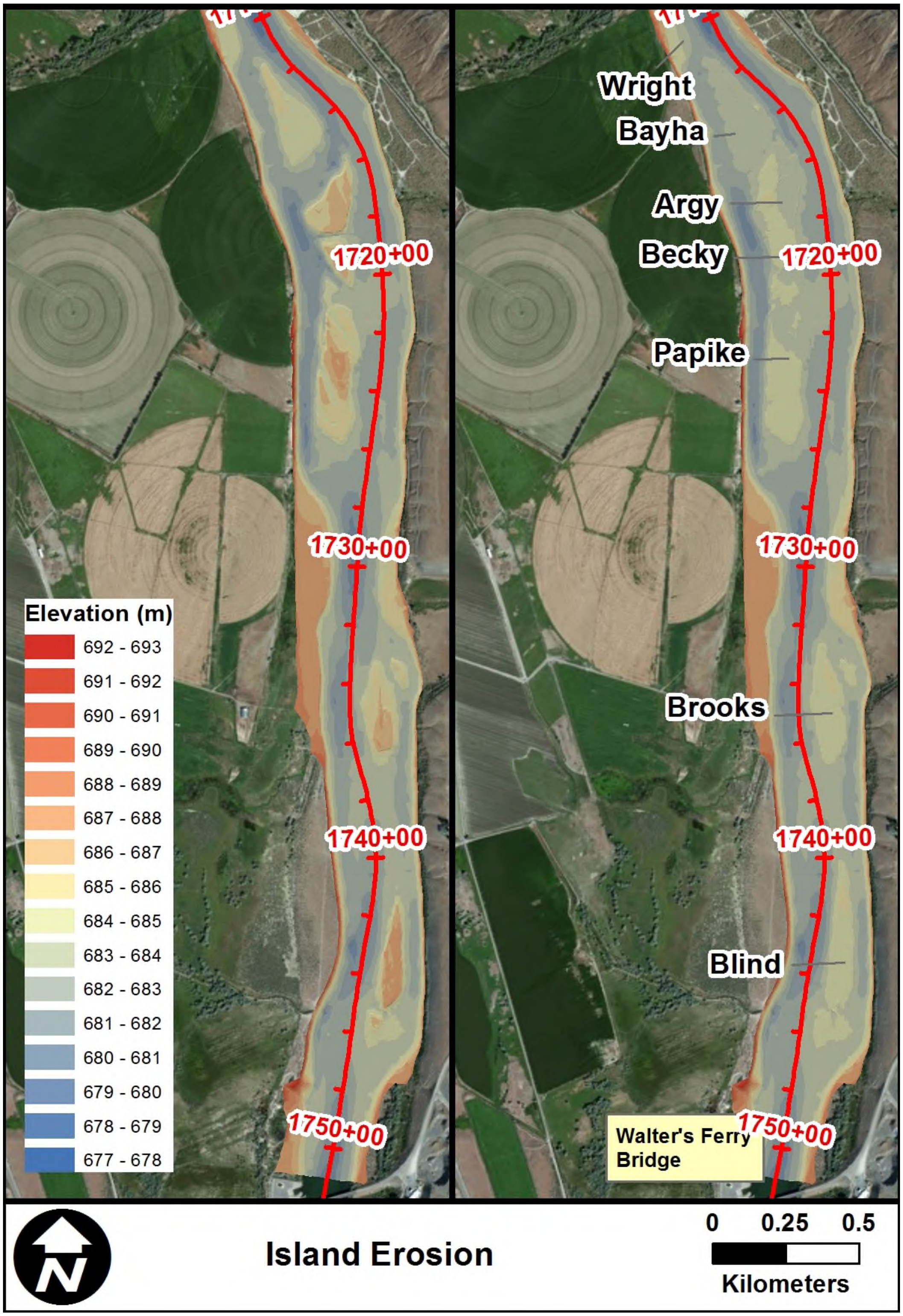

Figure 6.36. Comparison of the channel geometry between baseline conditions and following erosion of the islands in the Walters Ferry reach.

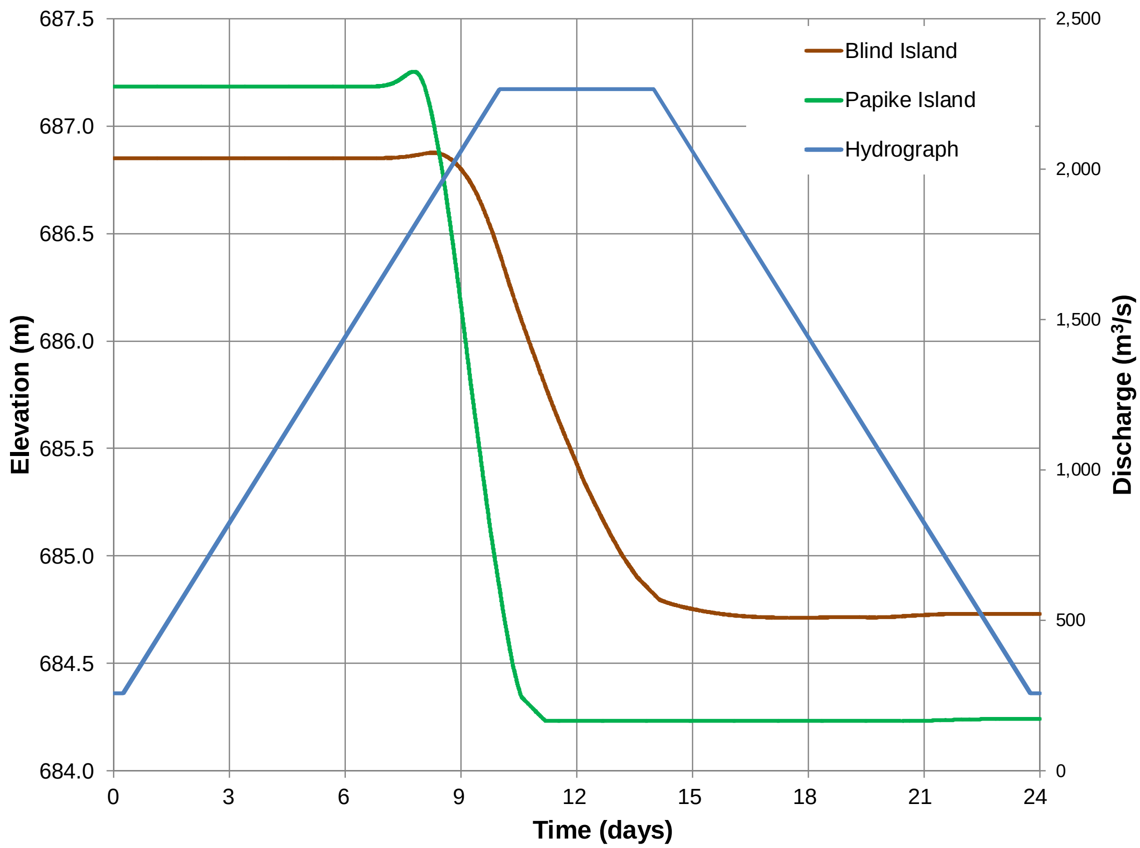

Figure 6.37 Rate of erosion at Papike Island and Blind Island over the duration of the 2,250 m^3/s hydrograph. The Walters Ferry model was with islands comprised of cohesionless sand-sized material.

7. Conclusions and Recommendations

7.1. Conclusions

This study was conducted to evaluate the island dynamics and their role in regulating sediment flux along the Middle Snake River (MSR), Idaho. The following conclusions were drawn from the study:

1. The MSR was selected for the study and contains approximately 300 islands along the 200-km reach. The three geomorphic subreaches of the MSR are primarily distinguished by the degree and character of anasotmosing. The up- and downstream subreaches are entrenched and contain a mostly single-thread channel with multiple flow paths around the islands, which occur as single islands, island groups, and island chains. The middle subreach has an anastomosing planform with occasional multiple channels. Dams on the Snake River upstream of the study reach and on tributaries within the study have altered the hydrology and sediment supply to the MSR compared to pre-dam conditions.
2. Review of the available literature indicates that most studies regarding river islands are concerned with the anastomosing channels that experience relatively frequent overbank flooding such as those located in Australia and Canada. No studies were found regarding river islands in entrenched conditions similar to the up- and downstream geomorphic reaches of the MSR. The majority of the reviewed studies emphasized the important role of vegetation for the development and maintenance of islands and/or anastomosing channels.
3. Historical analysis of aerial photography from 1938/1939 to present and topographic mapping from the 1890s show clear evidence of activity along the entire study reach including: erosion of older islands, formation of new islands, reworking of island chains to form new configurations, and shifting and reworking of the MSR channel itself. The

persistent pattern of change along the entire study reach strongly suggests an active channel with forming and reforming islands.

4. A recent sequence of aerial photography showed that new island surfaces can be stabilized in a few years supported by vegetation colonization in combination with a period of relatively low flows.

5. Analysis of the lateral constrictions and island patterns around the various controls (Mussetter and Harvey, 2001b) showed that almost all larger islands and island groups are located either upstream and/or downstream of lateral constrictions along the main channel.

6. Morphostratigraphic mapping, soil profile data, pollen analysis, and ^{14}C dating showed the dynamics of the islands and provide an estimate of the age of the islands. The soil profile data showed a large variation in age between the young soils (on the order of 100 of years) and the older gravel cores (on the order of 1,000's of year) in many islands. The soil profiles also showed evidence of truncated soil profiles.

7. The results from a 1-D hydraulic model analysis (Mussetter and Harvey, 2001b) indicates the up- and downstream reaches of the MSR have a pool/island morphology that is analogous to the pool riffle morphology found on smaller rivers. At frequent, low discharges, typical of those overtopping the low (and typically younger) elevation islands, shear stresses are relatively high in the wide and shallow island reaches compared to the pool reaches. At higher discharges, typical of those overtopping the higher (and typically older) surfaces, the islands areas are depositional zones.

8. The model output from a 2-dimensional hydraulic models of the baseline (1997/1999 geometry) conditions were used to perform and incipient motion analysis that indicated the bed material is not mobilized, thus indicating that the bed is armored. The channel bed armored during a previous hydrologic flow regime (including pre-dam) such as following the Bonneville flood and the gravel cores are relic bar features. The islands

along the MSR formed in response to more recent flood hydrology and to the silt-sand sized sediment supply, not the gravel- to cobble-sized material comprising island core; this explains why there are relatively young soils overlying older gravel cores.

9. The shear stress patterns at the bankfull discharge indicated that the shear stresses are typically highest at the heads of the islands and over the surface of the islands. During large floods, the shear stresses may have been sufficiently high to erode the surface of the islands. Subsequent deposition on the islands would appear as a truncated soil, as observed in the soil profiles.

10. Two-dimensional sediment-transport modeling was performed to simulate the dynamics and processes of island development. Without-island models were developed by modifying the Ketchup and Walters Ferry baseline models to represent the geometry of the reach without the islands and by incorporating the required sediment-transport parameters, which include the sediment-transport equation, representative bed-material sediment gradations and input discharge versus sediment transport rating curve. The sediment rating curve was developed to represent the input of the sand-sized material that comprises the islands. The models were run over a repeating series of representative flood hydrographs. The predicted island geometry at the end of the simulations approximated the baseline conditions reasonably well, both validating the modeling procedures and the applicability of applying 2-D models to simulate island development. The models predicted island formation in the low shear stress areas located up- and downstream of the channel constrictions, which supports the 1-D model results and the study hypotheses that where the hydraulic controls are fixed, islands form, erode and reform in the same general locations following a disturbance or a change in sediment supply.

11. The 2-D modeling predicted rapid initial aggradation of the islands, followed by a decrease in aggradation over time due to less frequent overtopping. This pattern is

consistent with the rate law (Wu et al. 2012) and studies by Wolman and Leopold (1967). The rate of island formation was shown to be on the order of decades.

12. Results from the 2-D model were used to evaluate the variation in bed-material transport along the reach. Under the without-islands (initial) conditions, the sediment-transport load is significantly higher at the upstream end of the reach compared to the downstream end, indicating the reach is significantly depositional. Over the duration of the simulations, the variation in sediment transport decreased due to the formation of the islands, which reduce the channel width, confine the flow path, and increase the sediment-transport capacity in the vicinity of the islands, resulting in more uniform sediment transport through the reach. This result shows that the islands regulate sediment flux through the reach.

13. Together, with the result that the islands locations are controlled by the lateral constrictions, these results support the study hypotheses that river islands form part of a temporal-spatial continuum of bedforms.

14. The results of the 2-D modeling showed the important interaction between fluvial process and vegetation in stabilizing the islands.

15. During low-sediment supply conditions, the channel will adjust from dynamic to a regime type channel, and the islands will remain stable. During large floods, the river may erode the margins and/or the surfaces of the islands, thereby partially restoring the sediment deficit. During subsequent higher sediment-load periods, the islands will reform in locations fixed by hydraulic controls and re-establish sediment flux through the reach.

7.2. Recommendations

The results of this study provide an improved understanding of the dynamics of river islands and the role of islands in regulating sediment flux along the MSR. An analysis was conducted that showed the dynamic nature of the islands within the MSR over the last approximately 100 years. This analysis showed that the larger islands and island groups are located either up- and/or downstream of lateral constrictions along the main channel. The geomorphic analysis also showed the response of the river to the post-dam hydrology, which includes the stabilization of the islands, due to vegetation and altered hydrology and the formation of berms around the islands.

One- and 2-D hydraulic models were used in the study and the results were integrated with the results from the geomorphic analyses and field data to develop a conceptual model of island dynamics. The results from the 2-D modeling showed how islands adjust their geometry in response to changes in sediment supply or a disturbance, and thereby form part of a temporal-spatial continuum of bedforms by adjusting their geometry to regulate sediment flux. The 2-D model also showed the importance of vegetation in stabilizing the islands.

Specific areas for future studies may include:

1. River islands have been reported in many environments, including the anastomosing rivers in Australia and Canada. Future studies could focus on the role of islands in other environments such as those observed in glacial-fed rivers in Alaska.
2. The 2-D sediment-transport modeling was conducted using a model considered state of the art at the time. Numerical modeling is developing rapidly and the models are becoming faster and more sophisticated at modeling complex processes, including sediment transport and the effects of vegetation. Future studies could include 3-D sediment-transport modeling of the development of islands and account for the effects of vegetation, sediment cohesion and change in roughness over time.

8. References

Abbado, D., Slingerland, R.L., and Smith, N.D., 2005. The origin of anastomosis in the upper Columbia River, British Columbia, Canada. In Fluvial Sedimentology VII, Blum, M.D., Marriott, S., and Leclair. S. (eds), Internat. Assoc. Sedim. Special Publ. 35.

Abbe, T.B. and Montogomery, D.R., 1996. Large woody debris jams, channel hydraulics and habitat formation in large rivers. Regulated Rivers: Research and Management, 12, pp. 201-221.

Andrews, E.D., 1984. Bed material entrainment and hydraulic geometry of gravel-bed rivers in Colorado. Geological Society of America Bulletin 95, March, pp. 371-378
.

Aquaveo, 2010. SMS Surface-water Modeling System, Version 10.1, User's Manual.

Ayres and Associates, 1997. Snake River Survey. Prepared for Mussetter Engineering, Inc., Fort Collins, CO.

Ayres and Associates, 1999. Snake River Survey. Prepared for Mussetter Engineering, Inc., Fort Collins, CO.

Bagnold, R.A. 1977. Bed load Transport by natural Rivers. Water Resources Research, 13, 2, pp. 303-312.

Baker, V.R., 1979. Erosional processes in channelized water flows on Mars. Journal of Geophysical Research. 84, pp. 7961-7983.

Barnes, H.H., 1967. Roughness characteristics of natural channels. U.S. Geological Survey Water-Supply Paper 1849.

Bates, R.L. and Jackson, J.A. (eds), 1997. *Glossary of Geology*, 4th ed. American Geological Institute, Alexandria, VA.

Bridge, J.S., 2003. Rivers and floodplains: forms, processes, and sedimentary record. Blackwell Science Ltd, Oxford, UK

Brice, J.C. and Blodgett, J.C., 1978. Countermeasures for hydraulic problems at bridges, Vol. 1, Analysis and Assessment. Federal Highway Administration FHWA/RD-78-162, Washington, DC, 184 p.

Buffington, J.M. and Montgomery, D.R., 2013. Geomorphic classification of rivers. In Shroder, J. and Wohl, E. (eds), Treatise on Geomorphology. Academic Press, San Diego, CA, vol. 9, Fluvial Geomorphology, pp. 730–767.

Chow, V.T. 1959. *Open Channel Hydraulics*. McGraw-Hill, Inc.

Cummings, L. and Moutoux, T.E., 2001. Pollen and phytolith analysis of sediment from islands in the Snake River, Idaho. Prepared for Mussetter Engineering. Inc., Fort Collins, Colorado.

Davis, W.M., 1899. The geographical cycle. Geographical Journal 14, pp. 481–504.

Davis, O.K., 1987. Spores of the Dung Fungus Sporomiella: Increased abundance in historic sediments and before Pleistocene Megafaunal Extinction. Quaternary Research 28, pp. 290-294.

Engelund, F. and Hansen, E., 1972. A Monograph for sediment transport and alluvial streams. Teknisk Forlag, Copenhagen.

Federal Geodetic Control Subcommittee, 1988. First order control specifications, v. 5.0.
Fetherston, K.L., Naiman, R.J., and Bilby, R.E., 1995. Large wood debris, physical processes, and riparian forest development in montane river networks of the Pacific Northwest. Geomorphology, 13, pp.133-144

Frye, J.C. and Willman, H.B., 1962. Morphostratigraphic units in pleistocene stratigraphy. American Association of Petroleum Geologists Bulletin, v. 46, pp. 112-113.

Garbrecht, J., Kuhnle, R.A., and Alonso, C.V., 1995. A sediment-transport formulation for large channel networks. J. Soil and Water Conservation. 50(5), pp. 527-529.

Gautier, E. and Grivel, S., 2006. Multi-scale analysis of island formation and development in the Middle Loire River, France. In Rowan, R., Duck, W., and Werrity, A. (eds), Sediment dynamics and the hydromorphology of fluvial systems, IAHS Pub, vol. 306, pp. 179-187.

Gile, L. H., Hawley, J. W., & Grossman, R. B. (1981). Soils and geomorphology in the Basin and Range area of Southern New Mexico: Guidebook to the Desert Project [Memoir 39]. Socorro, NM: New Mexico Bureau of Mines and Mineral Resources.

Gregory, K.J. and Walling, D.E., 1973. Drainage basin form and process. London: Arnold.
Greimann, B., Yong Lai, Y., and Huang, J., 2008. Two-dimensional total sediment load model equations. J. Hyd. Eng. 134:8

Tockner., K., 2001. Riparian vegetation and Island formation along the gravel-bed Fiume Tagliamento, Italy. Earth Surf. Process. Landforms 26, 31–62 (2001)

Hicks, D.M. and Mason, P.D., 1991. Roughness characteristics of New Zealand rivers. Water Resources Survey, DSIR Marine and Freshwater, Wellington, New Zealand.

Horton, R.E., 1945. Erosional development of streams and their drainage basin; hydrophysical approach to quantitative morphology. Bull. Geol. Soc. America, 56, pp. 275-370.

Huang, H. Q., and Nanson, G. C., 2007. Why some alluvial rivers develop an anabranching pattern. Water Resour. Res., 43, W07441.

Idaho Water Resource Board, 1993. Comprehensive state water plan: Snake River, Milner Dam to King Hill. The Board.

Jansen, J.D. and Nanson, G.C., 2010. Functional relationships between vegetation, channel morphology, and flow efficiency in an alluvial (anabranching) river. J. Geophys. Res., 115.
Jansen, J. D., and Nanson, G. C., 2004. Anabranching and maximum flow efficiency in Magela Creek, northern Australia, Water Resour. Res., 40,

Johnson, W.C., Dixon, M., Larson, G., and Simons, R.K., 1992. Final Report: Riparian vegetation along the Snake River, Idaho, below Swan Falls Dam: past, present and future. Prepared for the U.S. Fish and Wildlife Service, January.

Julien P.Y., 1995. Erosion and sedimentation. Cambridge University Press, 280 p.
Keller, E.A., 1971. Areal sorting of bed-load material: The hypothesis of velocity reversal. Geological Society of America Bulletin, v. 82, pp. 753-756.

Keller, E.A. and Melhorn, W.N., 1978. Rhythmic spacing and origin of pools and riffles. Geol. Soc. of America Bulletin, v. 89, pp. 723-730.

Kellerhals, R., Church, M., and Bray, D.I., 1976. Classification and analysis of river processes. Am. Soc. Civil. En. J. Hydraulics Div , 102, pp. 813-829.

Kjelstrom, L.C., 1992. Simulation of water-surface elevations for the Snake River in the Deer Flat National Wildlife Refuge. U.S. Geological Survey Water-Resources Investigations Report No. 91-4198, 105 p.

Knighton, A.D. and Nanson, G.C., 1993. Anastomosis and the contiuum of channel pattern. Earth Surface process and landforms (18), pp. 613-625.

Nanson, G. C., and Knighton, A. D., 1996. Anabranching rivers; their cause, character and classification. Earth Surface Processes and Landforms, 21, 217-239.

Knopf, F.L. and Olson, T.E., 1984. Naturalization of Russian-olive implications to Rocky Mountain wildlife. Wildlife Soc. Bull. 12, pp. 289-298

Komar, P.D., 1983. Shapes of streamlined islands on Earth and Mars: experiments and analyses of the minimum-drag form. Geology , 11, pp. 651-654.

Komar, P.D., 1984. The leminscape loop: Comaprisons with the shapes of streamlined landforms. The Journal of Geology , 92 (2), pp. 133-145.

Lane, E.W., 1955. The importance of fluvial geomorphology in hydraulic engineering. Proceedings of the American Society of Civil Engineers, 81, pp. 745-761.

Lane, E.W., 1957. A study of the shape of channels formed by natural streams flowing in erodible material. U.S. Army Engineer Division, Missouri River, Corps of Engineers, MRD Sediment Series no. 9, Omaha, Nebraska, 106 p.

Leopold, L.B. and Maddock, T., 1953. The hydraulic geometry of stream channels and some physiographic implications. Geological Survey Professional Paper 252.

Leopold, L.B. and Wolman, M.G., 1957. River channel patterns: braided, meandering, and straight. U.S. Geological Survey Professional Paper 282-B, Washington, DC, pp. 39–84

Leopold, L.B., Wolman, M.G., and Miller, J.P., 1964. Fluvial processes in geomorphology. San Francisco: Freeman.

Mack, R.N., 1986. Alian plant invasion into the Intermountain West: A case history. In Mooney, H.A. and Drake J.A. (eds.), Ecology of Biological Invasions of North America and Hawaii, Springer Verlag.

Maidment, D.R., 1992. Handbook of hydrology. McGraw-Hill, Inc., New York, NY, pp 17-48.
Makaske, B., 2001. Anastomosing rivers: a review of their classification, origin and sedimentary products. Earth-Science Reviews. 53, pp. 149–196.

Malde, H.E., 1968. The catastrophic late Pleistocene Bonneville Flood in the Snake River Plain, Idaho. U.S. Geological Survey Professional Paper 596
.
Maser, C. and Sedell, J.R., 1994. *From the forest to the sea. Delray Beach, Florida*. St. Lucie Press.

McDonald, R.R., Nelson, J.M., and Bennett, J.P., 2006, Multi-dimensional surface-water modeling system user's guide. U.S. Geological Survey Techniques and Methods, 6-B2, 136 p.

McKenney, R., Jacobson, R.B., and Werteimer, R.C., 1995. Woody vegetation and channel morphogenesis on low-gradient, gravel-bed streams in the Ozark Plateaus, Missouri and Arkansas. Geomorphology , 13, pp. 175-198.

Müller, N. 1995. River dynamics and floodplain vegetation and their alteration due to human impact. Archiv für Hydrobiologie Suppl. 101, pp. 477–512.

Meyer-Peter, E. and Müller, R., 1948. Formulas for bed-load transport. Proceedings, third meeting of International Association for Hydraulic Research, Stockholm, pp39-64.

Mussetter, R.A. and Harvey, M.D., 2001a. Expert report of Dr. Robert A. Mussetter and Dr. Michael D. Harvey regarding identification of the ordinary high-water marks along the Snake River from the upper end of Brownlee Reservoir to Sign Island. Prepared for the State of Idaho v. United States of America Case No. CIV97-0426-S-BLW in the United Stated District Court for the District of Idaho, February.

Mussetter, R.A. and Harvey, M.D., 2001b. Expert report of Dr. Robert A. Mussetter and Dr. Michael D. Harvey regarding the Age of Islands in the Snake River Sector of the Deerflat National Wildlife Refuge. Prepared for the State of Idaho v. United States of America Case No. CIV97-0426-S-BLW in the United Stated District Court for the District of Idaho, May.

Nadler, C.T. and Schumm, S.A, 1981. Metamorphosis of South Platte and Arkansas Rivers, eastern Colorado. Phys. Geog. 2, pp. 95-115.
Nanson, G.C., 1981. New evidence of scroll-bar formation on the Beatton River. Sedimentology 28, pp. 889-891.

Nanson, G.C. and Knighton, A.D., 1996. Anabranching rivers; their cause, character and classification. Earth Surface Processes and Landforms, 21, pp. 217-239.
Nanson, G.C. and Huang, H.Q., 1999. Anabranching rivers: divided efficiency leading to fluvial diversity. In Miller, A.J. and Gupta, A. (eds), Varieties of Fluvial Form, New York: Wiley, pp. 477-494.
National Center for Computation Hydroscience and Engineering (NCCHE), 2006. CCHE2D User's Manual. University of Mississippi, School of Engineering, 158 p.

North American Commission on Stratigraphic Nomenclature, 1983. North American stratigraphic code. American Association of Petroleum Geologists Bulletin, v. 67, no. 5, pp. 841-875.

O'Connor, J.E., 1993. Hydrology, hydraulics, and geomorphology of the Bonneville Flood. Boulder: Geological Society of America Special Paper 274.

Olsen, N.R.N, 2009. A three-dimensional numerical model for the simulation of sediment movements in water intakes with multiblock option. Department of Hydraulic and Environmental Engineering, The Norweigian University of Science and Technology.

Osterkamp, W.R., 1998. Processes of fluvial-island formation, with examples from Plum Creek, Colorado, and Snake River, Idaho. Wetlands v.18, no.4, pp. 530-545.

Osterkamp, W.R., Johnson, W.C., and Dixon, M.D., 2001. Biophysical Gradients Related to Channel Islands, Middle Snake River, Idaho. Geomorphic Processes and Riverine Habitat Water Science and Application v. 4, American Geophysical Union, pp. 73-83.

Osterkamp, W.R., Green, T.J., Reid, K.C., and Cherkinsky, A., 2011. Adjustment and interpretation of ^{14}C dates of bivalve shells from archaeological sites, Snake River Basin: unpublished report, contact authors.

Othberg, K.L. and Fosberg, M.A., 2001. Expert Report on the Geomorphology, Soils, and Age of Snake River Islands from the Upper End of Brownlee Reservoir to Sign Island, Prepared for the State of Idaho v. United States of America, Case No. CIV97-0426-S-BLW, in the U.S. District Court for the District of Idaho, May.

Othberg, K.L. and Stanford, L.R., 1992. Geologic map of the Boise Valley and adjoining area, Ada and Canyon Counties, Idaho. Idaho Geological Survey, Geologic Map Service, scale 1:100,000.
Othberg, K.L., 1994. Geology and Geomorphology of the Boise Valley and adjoining areas, Western Snake River Plain, Idaho. Idaho Geological Survey Bulletin 29, January, 54 p.

Othberg, K.L., McDaniel, P.A., and Fosberg, M.A., 1997. Soil development on a Pleistocene terrace sequence, Boise Valley, Idaho. Northwest Science, v. 71, no. 4, pp. 318-329.

Parker, G., 1990. Surface-based bed-load transport relation for gravel rivers. J. Hydraul. Res., 28(4), pp. 417-436.

Parker, G., Klingeman, P.C., and McLean, D.G., 1982. Bed load and size distribution in paved gravel-bed streams. Journal of the Hydraulics Divisions, American Society of Civil Engineers, 108(HY4), Proc. Paper 17009, pp. 544-571.

Pickup, G.,1976. Adjustment of stream-channel shape to hydrologic regime. J. Hydrol., 30, pp. 365-373.
Pizzuto, J.E., 1987. Sediment diffusion during overbank flows. Sedimentology 34, pp. 301-317.

Proffitt, G.T., and Sutherland, A.J., 1983. Transport of non-uniform sediments. Journal of Hydraulic Research, vol 21, No. 1, pp. 33-43.
Richards, K.S., 1976. Channel width and the riffle-pool sequence. Geological Society of America Bulletin, v. 87, June, pp. 883-890.

Robinson, T.W., 1969. Introduction, spread, and areal extent of saltcedar (Tamarix) in the western states. USDI Geological Survey Prof. Paper 491-A, 12 p.
Rouse, H., 1937. Modern Conceptions of mechanics of fluid turbulence. Transactions, ASCE, 102, pp. 436-505.

Rust, B.R., 1981. Sedimentation in an arid-zone anastomosing fluvial systemL Cooper creek, central Australia. Journal of Sedimentary Petrology, 51, 745-755.
Shields, A., 1936. Application of similarity principles and turbulence research to bed-load movement. California Institute of Technology, Pasadena; Translation from German Original; Report 167.

Schumm, S.A., 1985. Patterns of Alluvial Rivers. Ann. Rev. Earth Planet. Sci. 13 : 5-27.

Schumm, S.A., 1973. Geomorphic thresholds and complex response of drainage systems.

Schumm, S.A., 1977. *The Fluvial System*. New York: Wiley.

Schumm, S.A., Erskine, W.D., and Tilleard, J.W., 1996. Morphology, hydrology, and evolution of the anastomosing Ovens and King Rivers, Victoria, Australia. Geological Society of America Bulletin 108, pp. 1212–1224.

Simons, D.B., 1957. Theory and design of stable channels in alluvial material. Ph.D. Dissertation, Department of Civil Engineering, Colorado State University, Fort Collins, Colorado.

Sipos, G. and Kiss, T., 2004. Island development and morphological stability on the lowland reach of the River Maros, Hungary. Geomorphologia Slovaca, 1, pp. 52-61.

Smith, D.G. 1976. Effect of vegetation lateral migration of anastomosed channels of a glacial meltwater river. Geological Society of America Bulletin. Vol. 87, p 857-860.

Smith, D.G., 1983. Anastomosed fluvial deposits: modern examples from Western Canada. In Collinson, J. and Lewin, J. (eds), Modern and Ancient Fluvial Systems. Special Publication of the International Association of Sedimentologists 6, Blackwell, Oxford, pp. 155–168.

Smith, D.G., 1986. Anastomosing river deposits, sedimentation rates and basin subsidence, Magdalena River, northwestern Colombia, South America. Sedimentary Geology 46, pp. 177–196.

Smith, D.G. and Smith, N.D., 1980. Sedimentation in anastomosing river systems: examples from alluvial valleys near Banff, Alberta. Journal of Sedimentary Petrology, 50, pp. 157-164.

Smith, N.D., Cross, T.A., Dufficy, J.P., and Clough, S.R., 1989. Anatomy of an avulsion. Sedimentology 36, pp. 1–23.
Tabata, K.K. and Hikin, E.J., 2003. Interchannel hydraulic geometry and hydraulic efficiency of the anastomosing Columbia River, Southeastern British Columbia, Canada. Earth Surf. Process. Landforms 28, pp. 837–852.

Thompson, D.M., Wohl, E.E., and Jarrett, R.D., 1999. Velocity reversals and sediment sorting in pools and riffles controlled by channel constrictions. Geomorphology 27, pp. 239-241.

Tooth, S. and Nanson, G.C, 1999. Anabranching rivers on the Northern Plains of arid central Austrailia. Geomorphology 29, p 211-233.

Tooth, S. and Nanson, G.C., 2000. The role of vegetation in the formation of anabranching channels in an ephemeral river, Northern Plains, arid central Australia. Hydrol. Processes, 14, pp. 3099–3117.

U.S. Army Corps of Engineers, 1990. HEC-2, flood hydrograph package, Version 4.0, Hydrologic Engineering Center, Davis, California.

U.S. Bureau of Reclamation, 2006. Erosion and sedimentation manual. Technical Service Center, Denver Colorado.

Vanoni, V.A., 1977. Sedimentation Engineering, ASCE Manuals and Reports on Engineering Practice - No. 54. Prepared by the ASCE Task Committee for the Preparation of the Manual on Sedimentation of the Sedimentation Committee of the Hydraulics Division.

Van Rijn, L.C., 1984a. Sediment transport, part I. Bed load transport. Journal of Hydraulic Engineering 110, pp. 1431-1456.

Van Rijn, L.C., 1984b. Sediment transport, part II. Suspended load transport. Journal of Hydraulic Engineering 110, pp. 1613-1641.

Ward, J.V., Tockner. K., Edwards, P.J., Kollmann, J., Bretschko,G., Gurnell A.M., Petts, G.E., and Rossaro, B., 1999. A reference system for the Alps: the ‘Fiume Tagliamento’. Regulated Rivers 15: pp. 63–75.

Weiming Wu, Dalmo A. Vieira, and Sam S.Y. Wang (2000). New capabilities of the CCHE1D channel network model. Proc., ASCE’s 2000 Joint Conference on Water Resources Engineering and Water Resources Planning and Management, Minneapolis, USA, July 30-August 3. (on CD-ROM).

Wende, R. and Nanson, G.C., 1998. Anabranching rivers: Ridge-forming alluvial channels in tropical northern Australia. Geomorphology, 22, pp. 205–224.

Wilcock, P.R. and Kenworthy, S.T., 2002. A two-fraction model for the transport of sand/gravel mixtures. Water Resour. Res., 38(10).

Wilcock, P.R., and Crowe, J.C., 2003. Surface-based transport model for mixed-size sediment. Journal of Hydraulic Engineering 129, pp. 120-128.

Wolman, M.G., 1954. A method for sampling coarse river bed material, Transactions of American Geophysical Union, v.35 (6), pp. 951-956.

Wolman, M.G. and Brush, L.M., 1961. Factors controlling the size and shape of stream channels in coarse uncohesive sands. U.S. Geol. Surv.Prof. Paper 282-G.

Wolman, M.G. and Leopold, L.B., 1957. River floodplains: some observations and their formation. U.S. Geological Survey Professional Paper 282-C, pp. 87-107.

Wu, W., Wang, S.S.Y, and Jia, Y., 2000. Nonuniform sediment transport in alluvial rivers. J. Hydr. Res., IAHR, 38(6), pp. 427-434.

Wu B., Zheng, S., and Thorne, C.R., 2012. A general framework for using the rate law to simulate morphological response to disturbance in the fluvial system. Progress in Physical Geography. 36(5), pp. 575-597.

Yalin, M.S., 1963. An expression for bed-load transportation. Proc. ASCE, 89, pp. 221-250.

Yang, C.T., 1971. On river meanders. Journal of Hydrology 13: pp. 231–253.

APPENDIX A1 – List of Identified Islands

Appendix A1. List of identified islands located within the study reach.

Island Number	Island Name	AKA	Easting (m)	Northing (m)	Station (m)	Geomorphic Subreach	Hydraulic Subreach	Hydrologic Subreach
1	Whitehill		683855.71	291569.19	2604	IIIB	DS	H5
	Huffman		685480.48	289636.87	5215	IIIB	DS	H5
1a	Unamed at RM335.5		683951.23	291458.33	2725	IIIB	DS	H5
2	Fenzl		686916.14	289035.79	6808	IIIB	DS	H5
	Rapids #2		688219.25	288678.08	8151	IIIB	DS	H5
	Rapids #1		688488.46	288402.25	8408	IIIB	DS	H5
3	Waunch's		689775.67	289568.40	10054	IIIB	DS	H5
4	Rock		689862.31	290034.08	10626	IIIB	DS	H5
	Porters		691671.74	290946.57	13078	IIIB	DS	H5
	Westlake		694072.84	287370.71	17562	IIIB	DS	H5
4a	Unamed at RM342.3		692250.07	291018.08	13500	IIIB	DS	H5
5	Jackass	W-11	692532.59	290740.01	13869	IIIB	DS	H5
5a	Unamed at RM342.7		692763.87	290209.68	14436	IIIB	DS	H5
5b	Unamed at RM345.2		694631.66	287390.16	18006	IIIA	DS	H5
	Aulbach #1		696826.16	286856.30	22274	IIIA	DS	H5
6	Aulbach #2		696622.25	286752.18	22122	IIIA	DS	H5
7	Aulbach #3		696688.91	286913.65	22281	IIIA	DS	H5
7a	Unamed at RM349		698332.59	287763.89	24032	IIIA	DS	H5
8.1	McRea Group	W-8, Mason	698747.29	287451.09	24650	IIIA	DS	H5
8.2	McRea Group #2	W-10	698413.33	287690.68	24126	IIIA	DS	H5
8.3	McRea Group #3		698610.67	287744.95	24248	IIIA	DS	H5
8.4	Schledewitz	W-7	700441.34	287340.70	26383	IIIA	DS	H5
8.5	Unamed at RM 351.9	W-6	702551.93	286105.45	28991	IIIA	DS	H5
8a	Unamed at RM352.6		702336.62	285016.19	30161	IIB	DS	H4
8b	Unamed at RM352.9		702441.63	284656.15	30564	IIB	DS	H4
8c	Unamed atRM 353.1	W-5	702625.48	284325.38	30909	IIB	DS	H4
10	Goat		702356.22	284001.26	31280	IIB	DS	H4
	Patch		701932.88	284100.47	31346	IIB	DS	H4
	Long		702634.05	283776.35	31388	IIB	DS	H4
11.1	Smith Group #4		702470.83	282047.92	33257	IIB	DS	H4
11.2	Smith Group #3	W-3	702606.58	281802.18	33730	IIB	DS	H4
11.3	Smith Group #2		702918.93	281776.80	34171	IIB	DS	H4
11	Smith Group#1		702895.41	281283.90	34215	IIB	DS	H4
11a	Unamed at RM356.6		705338.27	281422.68	36684	IIB	DS	H4
11b	Unamed at RM357		706231.30	281081.76	37524	IIB	DS	H4
	Nadeau		705211.93	281194.90	36583	IIB	DS	H4
14	Larsen		705557.69	281074.96	36976	IIB	DS	H4
	Buttermilk		705905.93	281080.51	37333	IIB	DS	H4
15	Sundstrom	W-1	706293.51	280772.17	37909	IIB	DS	H4
	Grafton		706172.87	280511.20	38032	IIB	DS	H4
	Pruit		707656.73	279760.94	39670	IIB	DS	H4
	Resch		707929.68	279438.27	40168	IIB	DS	H4
	Oglesbee		708285.75	277040.28	42780	IIB	DS	H4
15a.1	Unamed at RM357.3		706515.16	280738.16	38130	IIB	DS	H4
15a.2	Unamed at RM357.4		706535.62	280614.38	38234	IIB	DS	H4
15a.3	Unamed at RM357.4		706534.73	280552.65	38272	IIB	DS	H4
15b	Unamed at RM359.8		708553.31	277488.77	42266	IIB	DS	H4
15c	Annear	P-20	708307.54	276749.63	42999	IIB	DS	H4
16	Ketchup	P-19	708097.87	276474.15	43358	IIB	DS	H4
17	Horse		706836.52	275110.87	45258	IIB	DS	H4
17a.1	Unamed at RM362.9		706232.71	273181.60	47339	IIB	DS	H4
17a.2	Unamed at RM362.9		706195.79	273152.95	47386	IIB	DS	H4
17a.3	Unamed at RM362.9		706207.25	273145.57	47382	IIB	DS	H4
18	Scarecrow		706003.53	272733.82	48018	IIB	DS	H4
18a	Sylvia		705680.71	272407.86	48378	IIB	DS	H4
	Duncan		705221.01	271660.40	49314	IIB	DS	H4
Pool	Pool		706077.59	271991.14	48739	IIB	DS	H4
18a.1	Unamed (side channel)		706421.29	272558.98		IIB	DS	H4
18b	Unamed at RM363.6		705794.25	272259.21	48528	IIB	DS	H4
18c	Unamed at RM364.1		705870.45	271362.92	49297	IIB	DS	H4

Island Number	Island Name	AKA	Easting (m)	Northing (m)	Station (m)	Geomorphic Subreach	Hydraulic Subreach	Hydrologic Subreach
18d	Unamed at RM364.3		705600.91	271181.56	49559	IIB	DS	H4
18d.1	Unamed at RM365.5		703855.99	270123.04	51546	IIB	DS	H4
18e	Unamed at RM365.7		703475.78	270080.56	51927	IIB	DS	H4
18e.1	Unamed at RM365.8		703324.92	269956.64	52095	IIB	DS	H3
18f	Unamed at RM366.6		702219.18	269656.46	53348	IIB	DS	H3
	Banks		702148.53	269074.11	54304	IIB	DS	H3
18f.1	Little Banks	P-14	701972.17	269505.77	53670	IIB	DS	H3
18f.2	Unamed at RM366.7		701907.28	269630.22	53627	IIB	DS	H3
18f.3	Unamed at RM366.7		701817.82	269600.68	53717	IIB	DS	H3
18f.4	Unamed at RM366.8		701793.31	269445.30	53884	IIB	DS	H3
18g	Unamed at RM366.9		701993.79	269256.64	54203	IIB	DS	H3
18h	Unamed at RM367.8		701856.59	267717.01	55650	IIB	DS	H3
	Ontario		702671.08	264930.04	58791	IIB	DS	H3
	Johnson		702644.62	264579.49	58894	IIB	DS	H3
	Welch		703173.79	264235.52	59814	IIB	Mid	H2B
18h.1	Unamed at RM 370.1	P-10	703502.79	264605.79	59729	IIB	Mid	H2B
	Ramey		704754.67	260442.03	64350	IIA	Mid	H2A
	Morton		703925.21	258841.31	68101	IIA	Mid	H2A
	McPhersons		702718.69	257179.72	70036	IIA	Mid	H2A
18i	Unamed at RM373.7		704537.16	260670.36	64394	IIA	Mid	H2A
18j	Unamed at RM374.3		704325.96	259932.53	65361	IIA	Mid	H2A
18k	Unamed at RM374.7		704631.22	259465.09	65915	IIA	Mid	H2A
18l	Unamed at RM375.7		704321.06	258049.59	67688	IIA	Mid	H2A
18m	Unamed at RM375.8		704121.38	258114.21	67882	IIA	Mid	H2A
18m.1	Unamed at RM377.2		702828.05	256558.72	70105	IIA	Mid	H2A
18m.2	Unamed at RM378.9		702250.30	255178.10	73204	IIA	Mid	H2A
18n	Unamed at RM380.1		702554.71	253626.08	75195	IIA	Mid	H2A
18n.1	Crow	P-6	702458.79	252674.59	76555	IIA	Mid	H2A
18o	Unamed at RM380.8		702593.08	252703.48	76690	IIA	Mid	H2A
18o.1	Unamed at RM380.8		702614.94	252672.30	76725	IIA	Mid	H2A
18p	Unamed at RM382.1		702576.21	250592.15	78766	IIA	Mid	H2A
	Perrin		702524.96	252135.48	77090	IIA	Mid	H2A
	Gamble		701865.68	249808.42	80121	IIA	Mid	H2A
19	Beaver		702659.95	250449.45	78957	IIA	Mid	H2A
19a	Unamed at RM382.3		702598.18	250321.86	79152	IIA	Mid	H2A
19a.1	Unamed at RM383		701222.27	250532.02	80094	IIA	Mid	H2A
19b	Unamed at RM383		701958.25	249404.31	80338	IIA	Mid	H2A
19b.1	Unamed at RM 383.1	P-2	701827.82	249226.53	80567	IIA	Mid	H2A
19c	Unamed at RM383.2		701738.42	249108.82	80760	IIA	Mid	H2A
	Unamed at RM384.1	P-1	701421.43	247648.00	82328	IIA	Mid	H2A
20	Quail #2	C-16, U	700591.81	244955.76	85342	IIA	Mid	H2A
21	Quail #1		700632.19	244840.26	85367	IIA	Mid	H2A
22	Cliff		699693.99	244882.34	86263	IIA	Mid	H2A
	Prati		699332.02	245024.73	86616	IIA	Mid	H2A
	Bridge		698845.19	244077.53	87403	IIA	Mid	H2A
23.1	Cable Group		700134.93	244332.27	85819	IIA	Mid	H2A
23.2	Cable Group		700181.20	244269.01	85794	IIA	Mid	H2A
23.3	Cable Group		700063.24	244182.32	85849	IIA	Mid	H2A
23.4	Cable Group		700305.50	244117.41	85741	IIA	Mid	H2A
23a.1	Cable Group		700097.68	244004.56	85833	IIA	Mid	H2A
23a.2	Cable Group		700133.01	244004.23	85817	IIA	Mid	H2A
23a.3	Cable Group		700178.58	243942.89	85803	IIA	Mid	H2A
23a.4	Cable Group		700255.46	243924.38	85773	IIA	Mid	H2A
23a.5	Cable Group		700302.38	243889.51	85753	IIA	Mid	H2A
23b	No RM (side channel)		699909.74	243389.99		IIA	Mid	H2A
24	Hoffman	M	699589.24	243686.78	89714	IIA	Mid	H2A
24a.1	Hoffman Group		699688.70	243547.67	89788	IIA	Mid	H2A
24a.2	Hoffman Group		699598.90	243518.16	89790	IIA	Mid	H2A
24a.3	Hoffman Group		699446.72	243543.91	89753	IIA	Mid	H2A
24a.4	Hoffman Group		699462.53	243528.51	89763	IIA	Mid	H2A

Island Number	Island Name	AKA	Easting (m)	Northing (m)	Station (m)	Geomorphic Subreach	Hydraulic Subreach	Hydrologic Subreach
24a.5	Hoffman Group		699444.50	243478.55	89784	IIA	Mid	H2A
24b	Unamed at RM392.6		698737.51	242697.73	90304	IIA	Mid	H2A
25	Ross	K	698692.18	242369.64	90632	IIA	Mid	H2A
25a	Unamed at RM392.7		698697.52	242265.61	90711	IIA	Mid	H2A
25b	Unamed at RM393.2		697851.73	242315.11	91441	IIA	Mid	H2A
25c	Unamed at RM393.3		697710.85	242379.67	91604	IIA	Mid	H2A
25d.1	Unamed at RM393.9		696979.42	241706.03	92722	IIA	Mid	H2A
25d	Unamed at RM394.1		696944.35	241390.14	93080	IIA	Mid	H2A
	Gold		697668.72	241691.74	92353	IIA	Mid	H2A
27a	Unamed at RM394.2		697145.47	241301.06	93128	IIA	Mid	H2A
27	Little Cottonwood		697061.62	241251.45	93164	IIA	Mid	H2A
26	Squatter's		697013.89	241076.10	93563	IIA	Mid	H2A
28	Big Cottonwood	C-7, F	697230.27	240864.87	93871	IIA	Mid	H2A
28a	Unamed at RM394.5		697302.17	240898.43	93904	IIA	Mid	H2A
28b	Unamed at RM394.5		697189.48	240838.42	93854	IIA	Mid	H2A
28c	Unamed at RM394.5		697188.05	240745.85	93906	IIA	Mid	H2A
29b	No RM (side channel)		698426.40	241344.23		IIA	Mid	H2A
29a.1	Heron Group		697572.65	241048.61	94024	IIA	Mid	H2A
29a.2	Heron Group		697597.86	241233.44	93929	IIA	Mid	H2A
29a.3	Heron Group		697844.56	241291.38	94295	IIA	Mid	H2A
29a.4	Heron Group		697910.19	241197.78	94338	IIA	Mid	H2A
29a.5	Heron Group		698087.03	241071.59	94430	IIA	Mid	H2A
29a.6	Heron Group		698109.37	241071.25	94423	IIA	Mid	H2A
29a.7	Heron Group		698108.89	241040.38	94442	IIA	Mid	H2A
29	Heron		697837.58	240964.57	94365	IIA	Mid	H2A
30	Rick	C-11, D	697903.54	240765.69	94445	IIA	Mid	H2A
30a	Unamed (side channel)		697971.05	240795.53		IIA	Mid	H2A
31.1	Boise Group		697532.23	240522.17	94318	IIA	Mid	H2A
31.2	Boise Group		697645.53	240347.35	94563	IIA	Mid	H2A
31.3	Boise Group		697799.42	240085.80	94863	IIA	Mid	H2A
9.1	Barney Group		697846.09	239933.10	94991	IIA	Mid	H2A
9.2	Barney Group		697774.79	239656.37	95289	IIA	Mid	H2A
9.2a	Barney Group		697810.01	239691.84	95246	IIA	Mid	H2A
9.2b	Barney Group		697832.38	239696.13	95236	IIA	Mid	H2A
9.2c	Barney Group		697797.14	239656.03	95284	IIA	Mid	H2A
9.3	Barney Group		697750.07	239502.41	95446	IIA	Mid	H2A
9.3a	Barney Group		697726.76	239441.03	95505	IIA	Mid	H2A
9.3b	Barney Group		697883.29	239381.52	95538	I	US	H1
32	Kline		696956.86	235019.77	100312	I	US	H1
33	Goose Egg		697248.71	234009.27	101347	I	US	H1
12	Big Willow		697273.91	233428.77	101919	I	US	H1
12a	Unamed at RM399.1		697307.27	233381.33	101962	I	US	H1
12b	Unamed at RM399.1		697251.21	233332.90	102013	I	US	H1
34.1	Billy Goat Group		697323.04	233294.55	102040	I	US	H1
34.2	Billy Goat Group		697252.33	233255.59	102085	I	US	H1
34.3	Billy Goat Group	P-5	697283.15	233245.28	102088	I	US	H1
34.4	Billy Goat Group		697229.53	233223.51	102116	I	US	H1
35	Main & East Shack		695794.05	231779.27	104078	I	US	H1
36	Rhubarb		694749.52	231251.06	105215	I	US	H1
37	Adrian		694013.89	230880.70	106055	I	US	H1
38	Suzy		693024.35	229367.28	107904	I	US	H1
39	Airport		692373.48	228134.33	109316	I	US	H1
	Peachtree		691948.15	226158.53	111322	I	US	H1
	Grassland		694449.14	224584.92	115853	I	US	H1
	Border		696385.88	224976.50	117937	I	US	H1
39a.1	Tule Group		698848.95	223697.95	120730	I	US	H1
39a.2	Tule Group		698946.50	223706.14	120823	I	US	H1
39a	TULE		699031.33	223683.88	120922	I	US	H1
39b.1	Unamed at RM411		700592.31	223414.29	122511	I	US	H1
39b	Unamed at RM411.9		701684.75	222805.01	123924	I	US	H1

Island Number	Island Name	AKA	Easting (m)	Northing (m)	Station (m)	Geomorphic Subreach	Hydraulic Subreach	Hydrologic Subreach
39c	Channel Island #3	C-4	701773.02	222711.10	124062	I	US	H1
39d	Channel Island #2	C-3	701854.76	222407.86	124387	I	US	H1
40	Silo		702181.81	221014.21	125891	I	US	H1
40a.1	Avocet	C-1	702471.96	220025.90	126939	I	US	H1
	Helton's	O-1	704326.77	218217.64	129606	I	US	H1
40a	Unamed at RM414.8		703778.05	218754.51	128862	I	US	H1
41	Homedale		705970.91	216665.50	131886	I	US	H1
42	Wegman		705964.22	216389.41	132169	I	US	H1
43.2	Rabbit Group		706139.53	216091.16	132520	I	US	H1
43.3	Rabbit Group		706208.27	215968.36	132663	I	US	H1
43.1	Rabbit		706334.84	215984.58	132723	I	US	H1
43.4	Rabbit Group		706447.80	215991.51	132787	I	US	H1
43.5	Rabbit Group		706543.01	215925.28	132911	I	US	H1
43.5a	Rabbit Group		706473.35	215883.84	132898	I	US	H1
43.6	Rabbit Group		706425.03	215637.56	133072	I	US	H1
43.6a	Rabbit Group		706491.91	215605.77	133154	I	US	H1
43.6b	Rabbit Group		706454.65	215575.10	133135	I	US	H1
44	Black Crowned		708442.54	214827.55	135253	I	US	H1
	Clark's		709281.11	214890.50	136089	I	US	H1
45.1	Olive Group		709416.65	214577.92	136232	I	US	H1
45.2	Olive Group		709663.39	214574.60	136470	I	US	H1
45a	Unamed at RM420		711012.92	214834.35	137832	I	US	H1
46	Feral		711570.04	214549.21	138448	I	US	H1
47	Pheasant #2		711861.03	214330.61	138867	I	US	H1
47a	Unamed at RM420.6		711729.24	214334.97	138746	I	US	H1
48	Pheasant #1		712113.77	214260.44	139120	I	US	H1
48a	Unamed at RM420.8		712014.83	214275.26	139032	I	US	H1
48b	Unamed at RM420.8		712023.64	214216.73	139081	I	US	H1
49	Pheasant #3		712209.17	214134.74	139288	I	US	H1
49a	Unamed at RM421.4		712967.73	213406.21	140330	I	US	H1
49b	Unamed at RM421.4		712978.19	213403.43	140340	I	US	H1
49c	Unamed at RM421.4		712986.33	213400.02	140349	I	US	H1
50	Tiny		713098.43	213302.00	140497	I	US	H1
50a	Unamed at RM421.5		713150.22	213245.00	140572	I	US	H1
51a	Unamed at RM421.7		713222.42	213022.53	140761	I	US	H1
51	Gosling		713453.80	212963.52	140984	I	US	H1
51b	Unamed at RM421.9		713657.50	212930.90	141171	I	US	H1
52	Jensen		713945.29	212573.77	141652	I	US	H1
52a	Unamed at RM422.5		714528.96	212042.12	142412	I	US	H1
53	Cigar		714504.75	211602.38	142791	I	US	H1
53a	Unamed at RM423.1		714712.59	211144.16	143319	I	US	H1
54	Marsing		715082.77	209426.18	145065	I	US	H1
55	Poison Ivy		715487.73	208797.14	145801	I	US	H1
56	Feedlot		716101.33	207845.81	146924	I	US	H1
57	Gem		716640.85	206407.42	148575	I	US	H1
58	Center		716345.41	204580.10	150497	I	US	H1
	Fruit		716793.56	201555.35	153629	I	US	H1
58a	Unamed at RM429.4		716571.05	201706.99	153396	I	US	H1
58b	Unamed at RM429.4		716571.05	201706.99	153396	I	US	H1
58c	Unamed at RM429.4		716638.11	201675.29	153446	I	US	H1
58d	Unamed at RM429.4		716682.67	201643.86	153494	I	US	H1
58e	Unamed at RM429.4		716705.14	201643.59	153503	I	US	H1
60	Dilley #2		717227.50	201338.95	154165	I	US	H1
59	Dilley #1		717268.96	201101.04	154336	I	US	H1
60a	Unamed at RM430.7		718770.74	199581.37	156457	I	US	H1
61a	Unamed at RM430.7		718838.56	199611.42	156503	I	US	H1
61	Cottontail		718961.73	199510.74	156665	I	US	H1
62	Foglers		719848.97	198769.53	157842	I	US	H1
63	Blackburn		720482.96	197893.93	158934	I	US	H1
63a	Unamed at RM432.1		720413.83	197838.79	158937	I	US	H1

Island Number	Island Name	AKA	Easting (m)	Northing (m)	Station (m)	Geomorphic Subreach	Hydraulic Subreach	Hydrologic Subreach
64	Dredge		720821.14	197289.53	159604	I	US	H1
64a	Stanley		721477.86	196493.83	160706	I	US	H1
65	Goldeneye		721956.88	196175.13	161252	I	US	H1
65a	Williams		722119.13	195901.72	161594	I	US	H1
66	Raccoon		723601.49	194218.61	163851	I	US	H1
66a	Unamed at RM434.7		723520.29	194427.60	163644	I	US	H1
66b	Unamed at RM434.9		723743.42	194185.07	163985	I	US	H1
66c	Unamed at RM435		723805.74	194056.06	164151	I	US	H1
66d	Unamed at RM435.3		724045.71	193748.28	164515	I	US	H1
66e	Unamed at RM435.6		724555.52	193439.76	165122	I	US	H1
67	Hermit		724771.27	193124.10	165486	I	US	H1
68.1	Rippee Group		724565.82	193093.56	165338	I	US	H1
68.1a	Rippee Group		724593.59	193022.52	165419	I	US	H1
68.2	Rippee Group		724696.73	192924.25	165616	I	US	H1
68.3	Rippee Group		724894.58	192803.15	165864	I	US	H1
68.4	Rippee		725048.05	192385.12	166329	I	US	H1
68.5	Rippee Group		725296.33	192335.43	166445	I	US	H1
69	Current		726396.82	191183.26	168182	I	US	H1
70	Fisher		726935.89	190995.62	168686	I	US	H1
71	Ware		727196.13	190759.80	169085	I	US	H1
72	Richards		727462.37	190445.94	169544	I	US	H1
72a	Unamed at RM439.1		728359.92	190028.82	170576	I	US	H1
73	Wright		728667.28	189705.55	171019	I	US	H1
74	Bayha		728989.10	189544.93	171332	I	US	H1
75	Argy		729248.75	189401.51	171722	I	US	H1
76	Becky		729353.17	189227.56	171936	I	US	H1
76a	Unamed at RM439.9		729320.53	189308.89	171848	I	US	H1
77a	Unamed at RM440		729386.12	189123.05	172046	I	US	H1
77b	Unamed at RM440		729385.48	189061.33	172106	I	US	H1
77c	Unamed at RM440		729521.54	189152.49	172096	I	US	H1
77d	Unamed at RM440		729565.92	189090.31	172174	I	US	H1
77e	Unamed at RM440.1		729429.56	188968.27	172220	I	US	H1
77	Papike		729511.00	188920.17	172308	I	US	H1
78.1	Brooks Group		730227.14	188110.67	173351	I	US	H1
78.2	Brooks Group		730251.73	188020.43	173447	I	US	H1
78.3	Brooks		730254.53	187961.45	173506	I	US	H1
79.1	Blind		730713.16	187261.75	174329	I	US	H1
79.2	Blind Group		730760.96	187041.08	174556	I	US	H1
80	Walters		730866.81	186027.86	175555	I	US	H1
81	Jim's		731221.08	185771.06	175850	I	US	H1
82	Kim's		731197.92	185709.56	175909	I	US	H1
83	Big Rocky		731272.04	185381.73	176295	I	US	H1
84	Little Rocky		731302.25	185074.75	176681	I	US	H1
84a	Unamed at RM442.7		731281.61	185165.11	176595	I	US	H1
84b	Unamed at RM442.7		731339.85	185123.46	176678	I	US	H1
84c	Unamed at RM442.7		731372.20	185121.41	176713	I	US	H1
85	Menning		732281.88	183515.24	178552	I	US	H1
	Noble		732826.80	182701.36	179555	I	US	H1
85a	Unamed at RM444.1		732310.50	183249.33	178827	I	US	H1
85a.1	Unamed at RM445.3		733735.84	182032.26	180796	I	US	H1
85b	Unamed at RM445.7		734285.76	181959.56	181355	I	US	H1
85c	Unamed at RM446.1		734920.48	181568.26	182072	I	US	H1
86a	Unamed at RM446.7		735887.12	181869.04	182974	I	US	H1
86	Guffy		736099.57	181734.93	183235	I	US	H1
87a	Unamed at RM447.9		737645.73	181496.85	184752	I	US	H1
87b	Unamed at RM447.9		737708.61	181458.08	184825	I	US	H1
87	Rail		737632.72	181361.61	184843	I	US	H1
88a	Unamed at RM447.9		737759.39	181418.24	184912	I	US	H1
88b	Unamed at RM		737780.94	181391.57	184951	I	US	H1
88	Sign		737974.45	181081.84	185267	I	US	H1

APPENDIX A2 – Mapping of Identified Islands

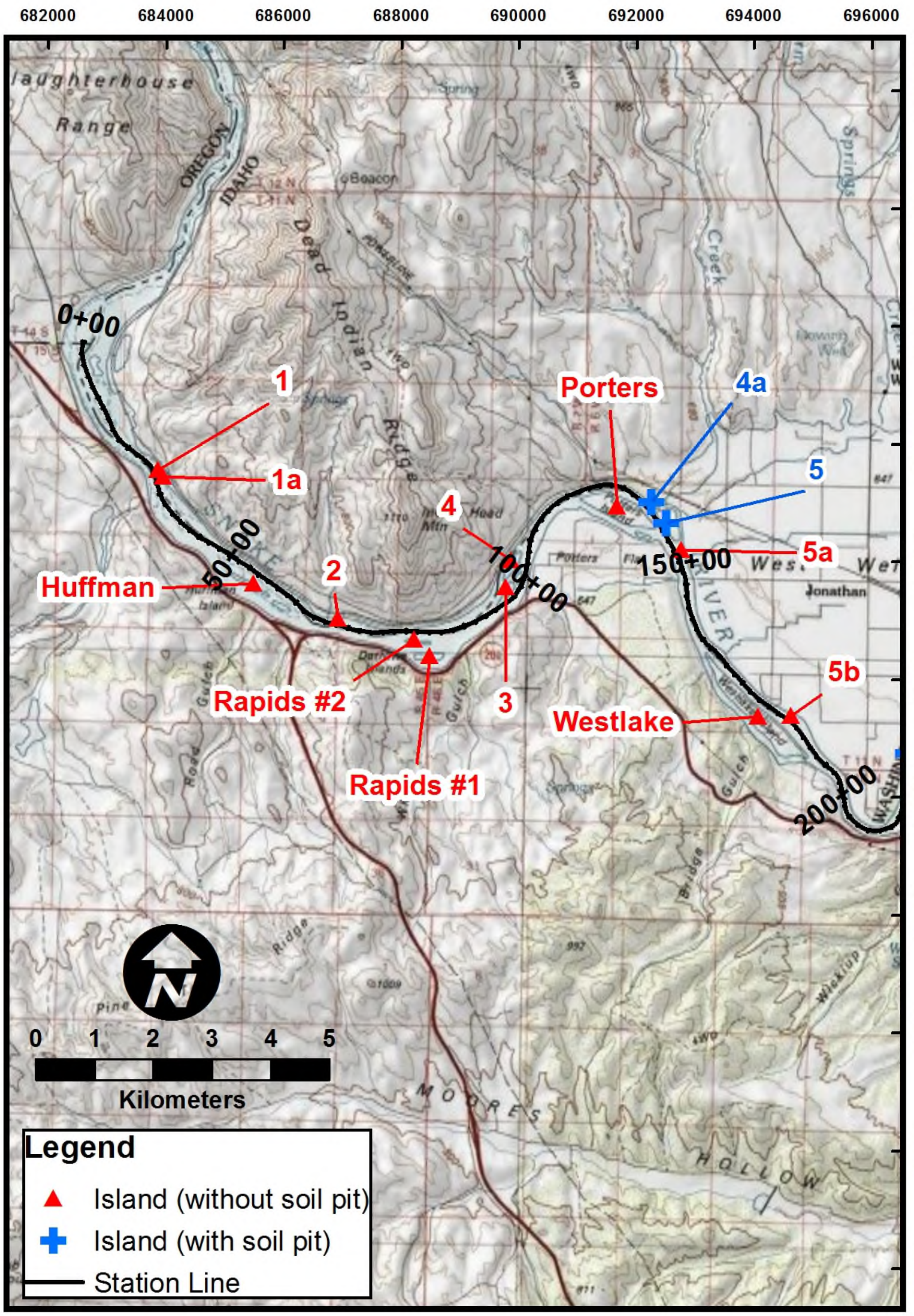

Figure A2.1 Location of named islands along the Middle Snake River.

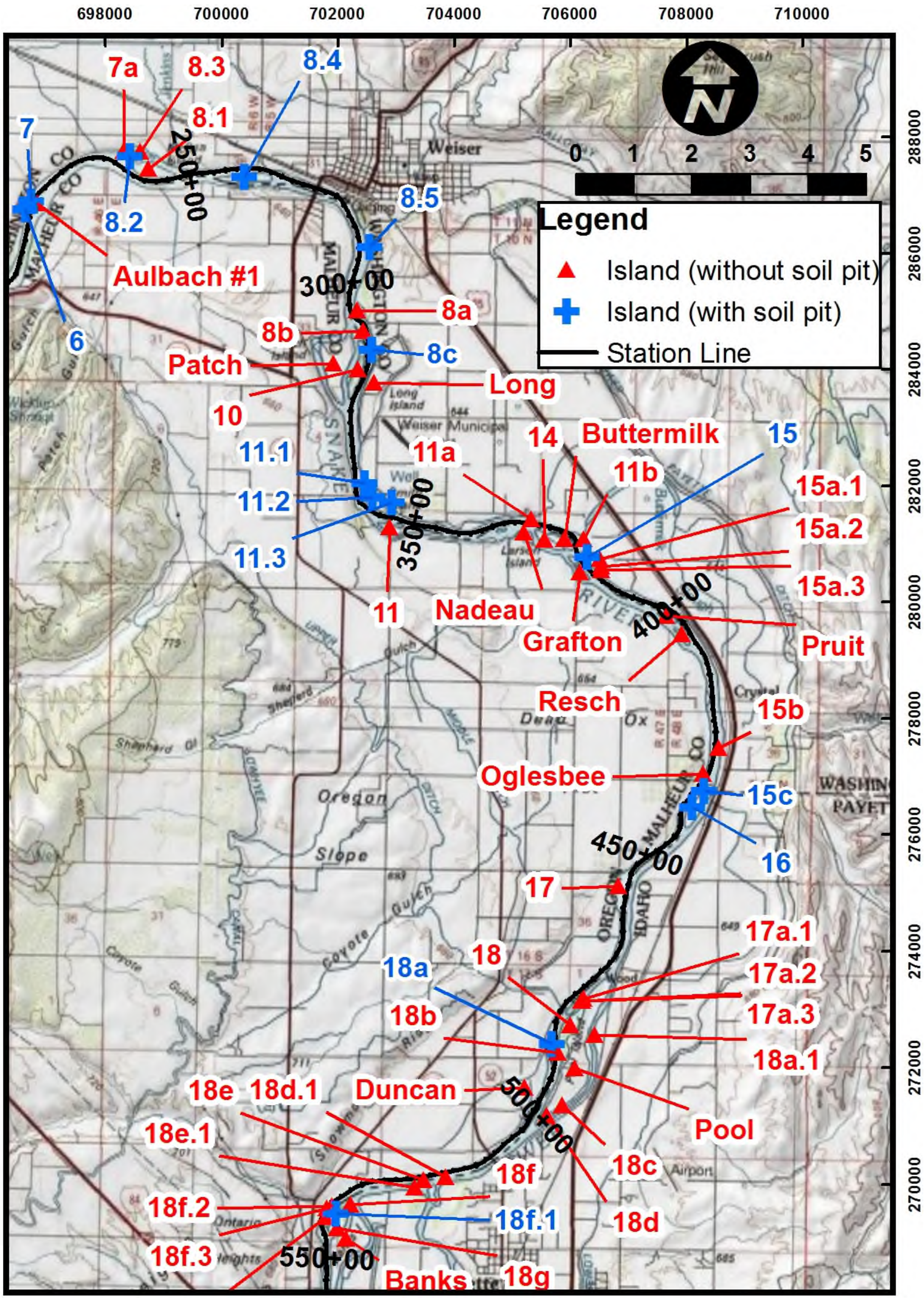

Figure A2.2 Location of named islands within the Middle Snake River.

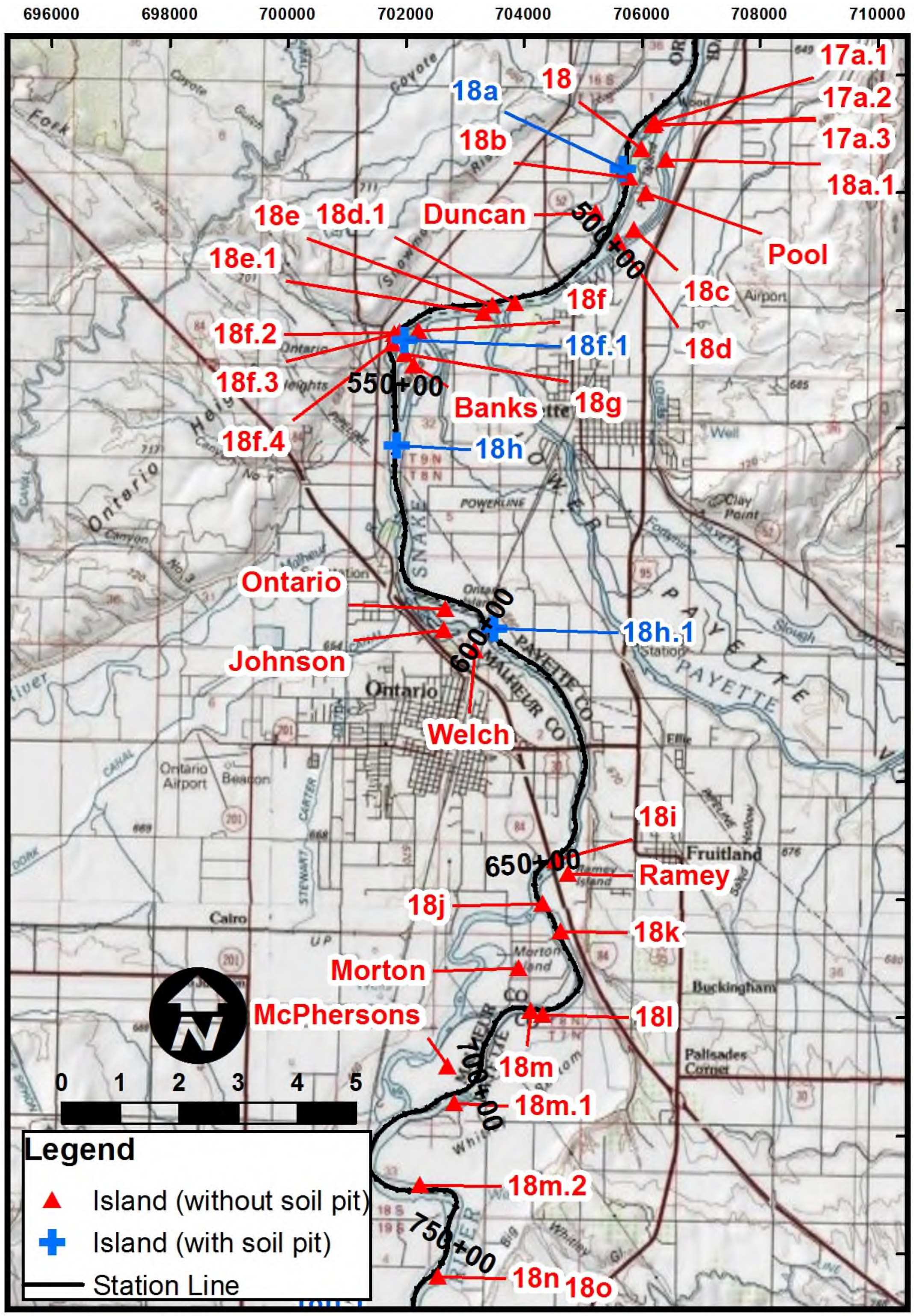

Figure A2.3 Location of named islands within the Middle Snake River.

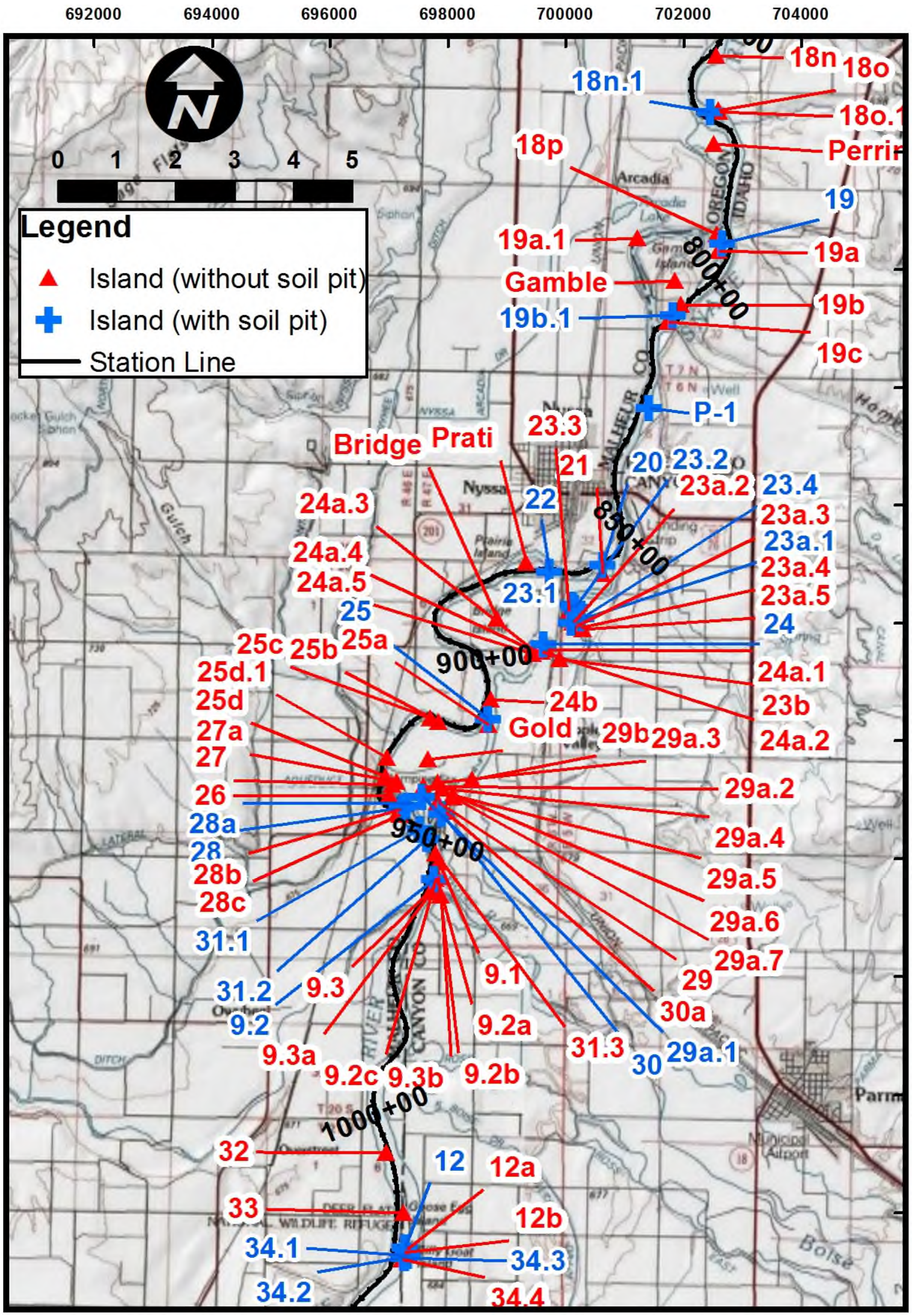

Figure A2.4 Location of named islands within the Middle Snake River.

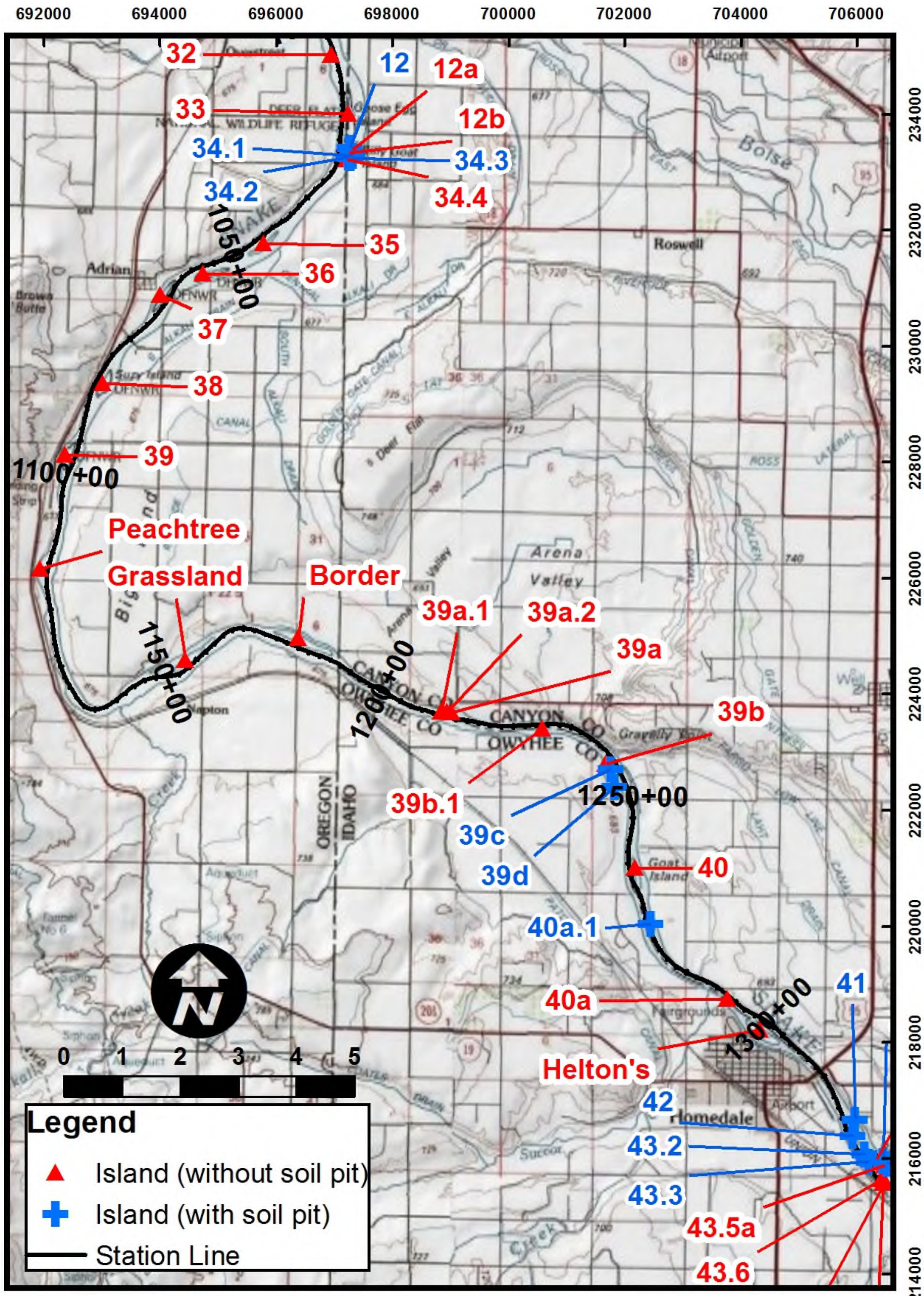

Figure A2.5 Location of named islands within the Middle Snake River.

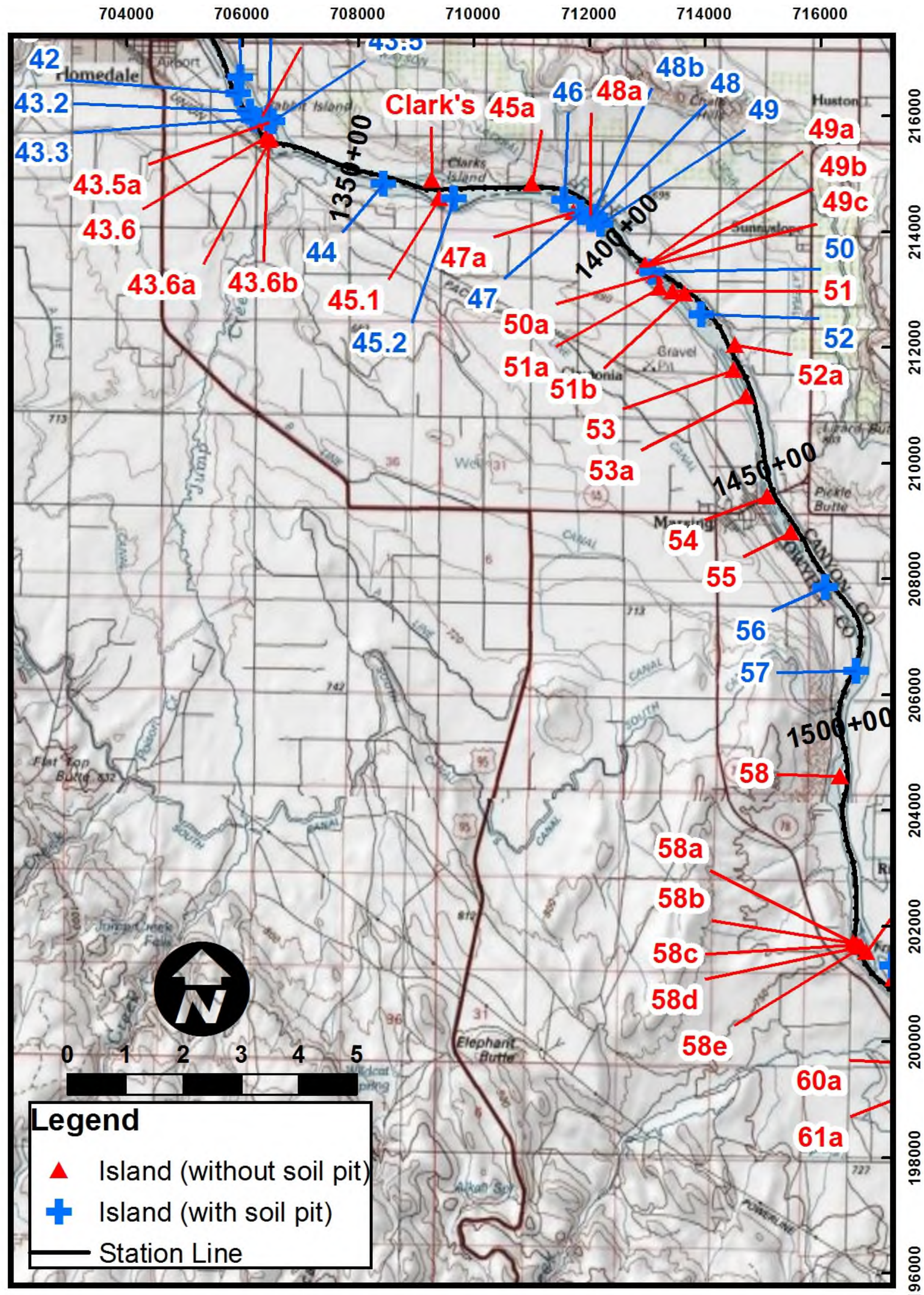

Figure A2.6 Location of named islands within the Middle Snake River.

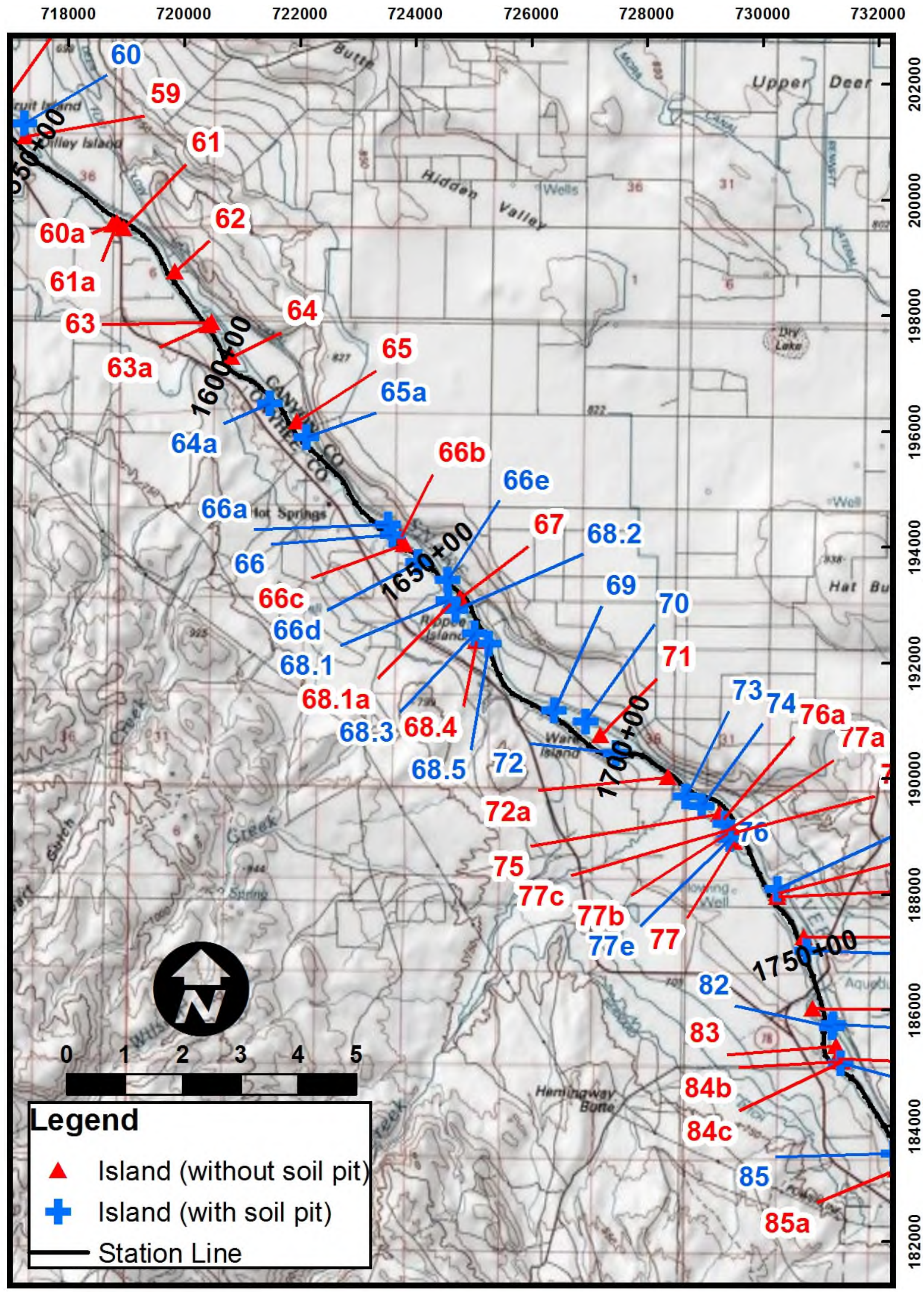

Figure A2.7 Location of named islands within the Middle Snake River.

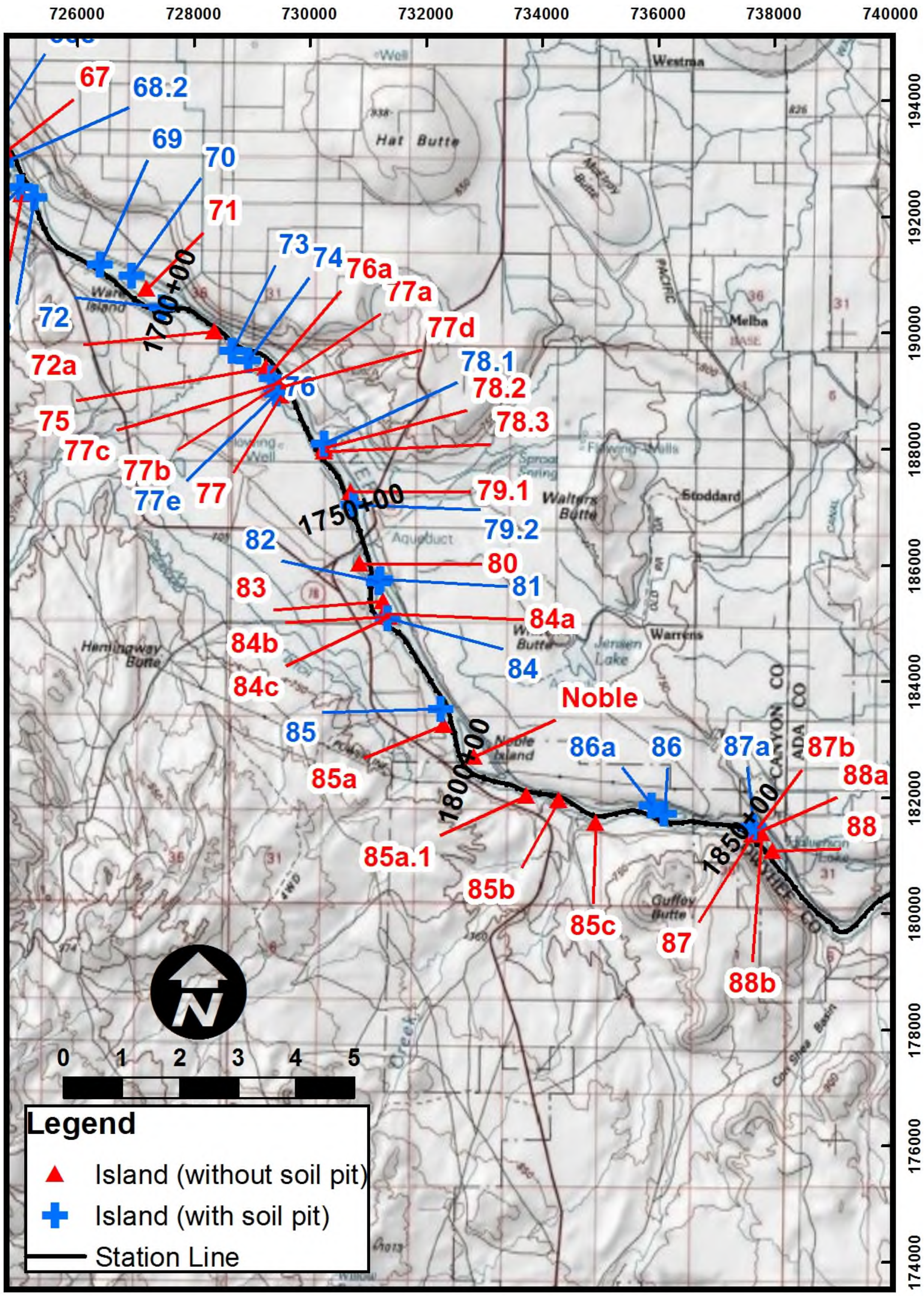

Figure A2.8 Location of named islands within the Middle Snake River.

APPENDIX B – Historic Topographic Mapping

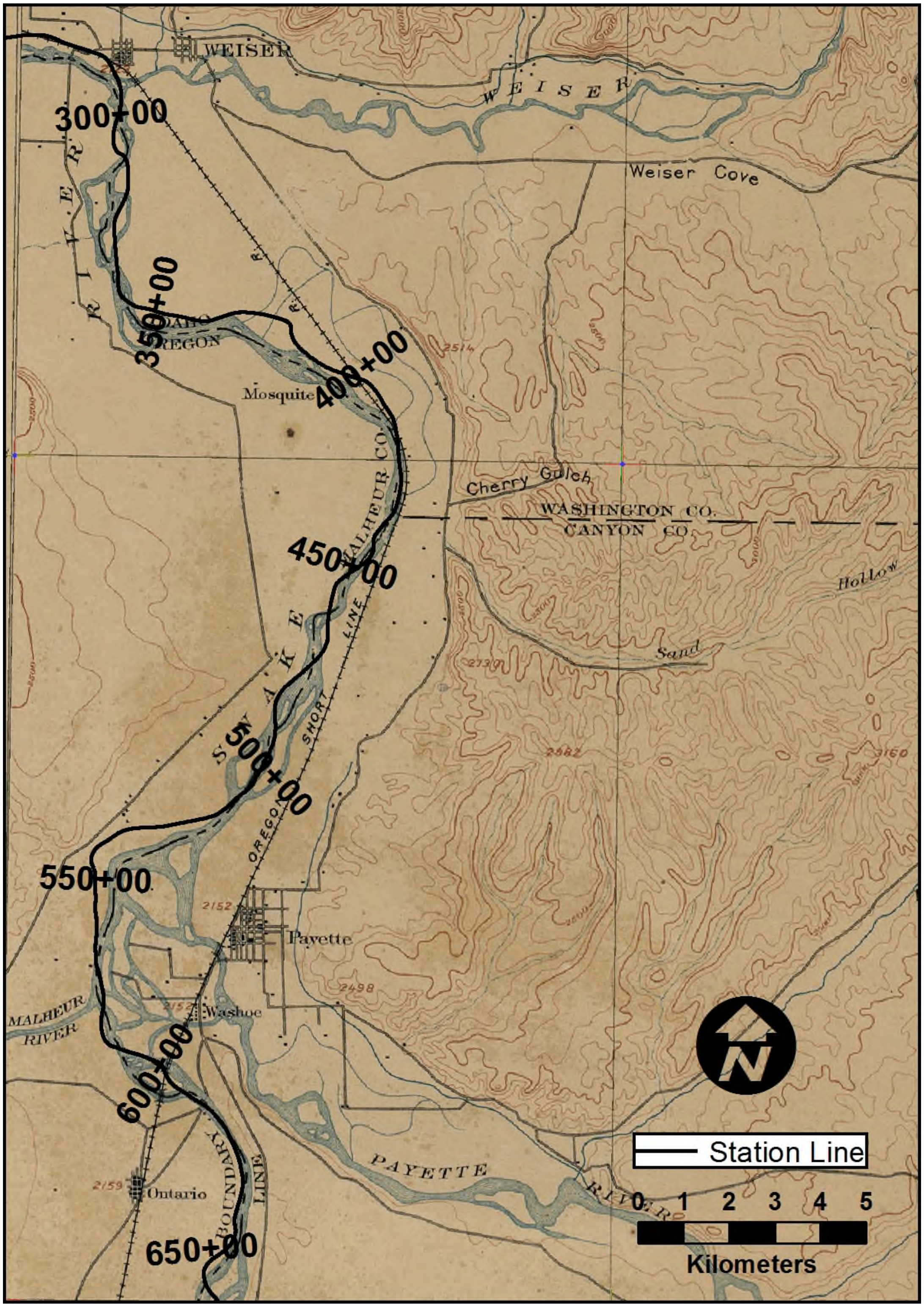

Figure B.1. A portion of the Weiser, Idaho-Oregon 30-minute topographic map, printed in 1897, reprinted in 1948. The study station line is overlain to show the current alignment and accuracy of the geo-referenced quad map.

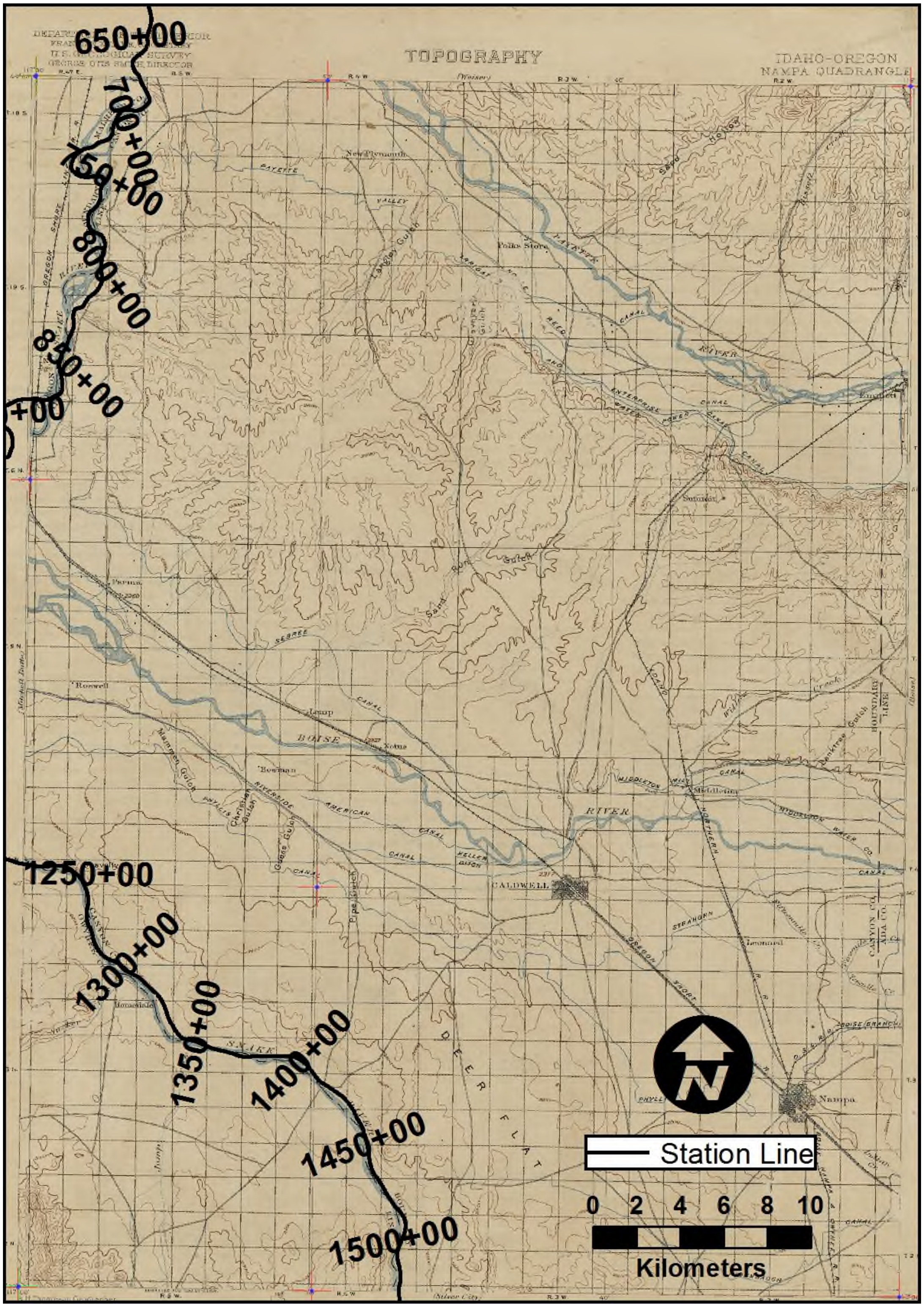

Figure B.2. A portion of the Nampa, Idaho-Oregon 30-minute topographic map, printed in 1898, reprinted in 1948.

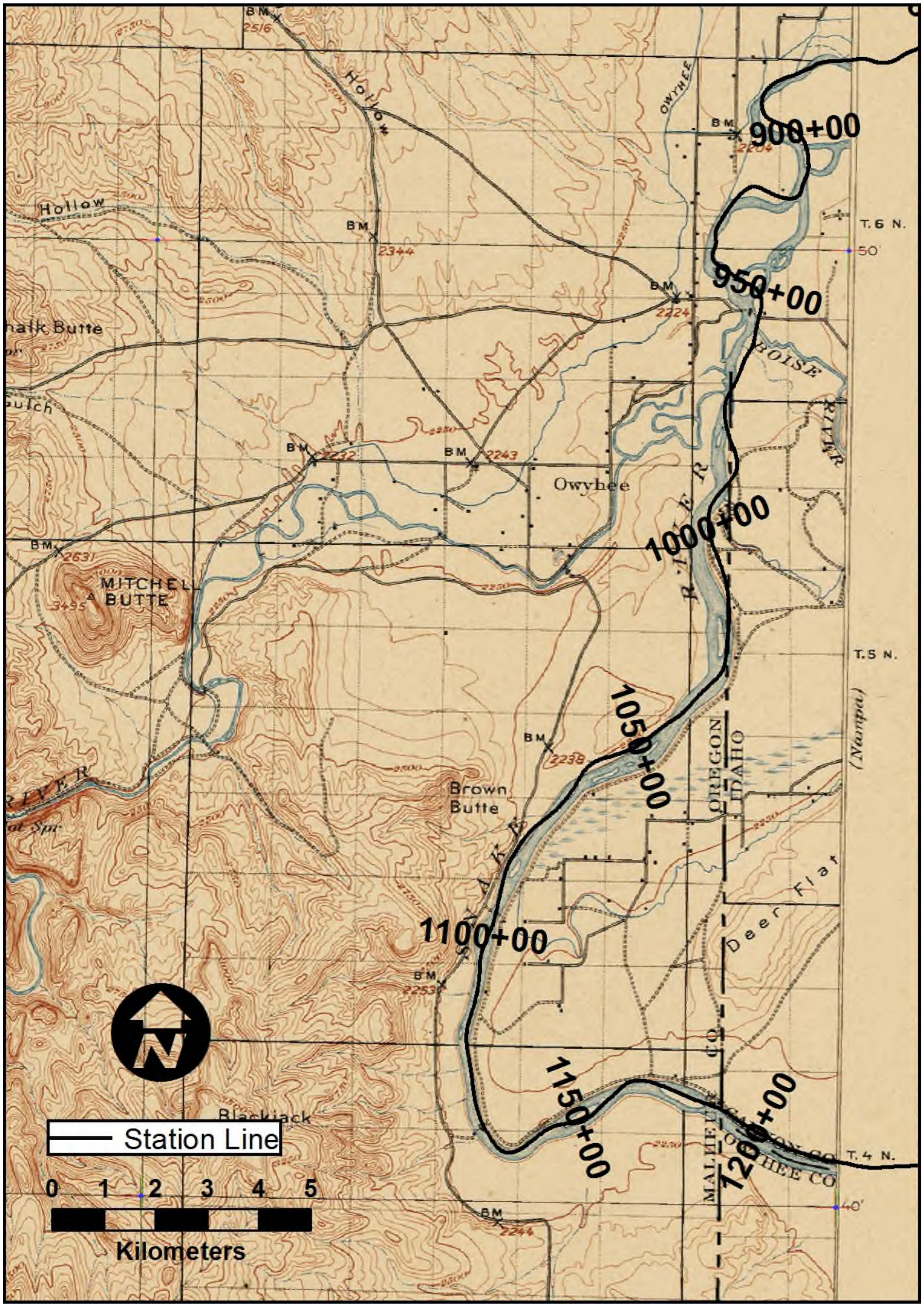

Figure B.3. A portion of the Mitchell Butte, Idaho-Oregon 30-minute topographic map, printed in 1906, reprinted in 1948.

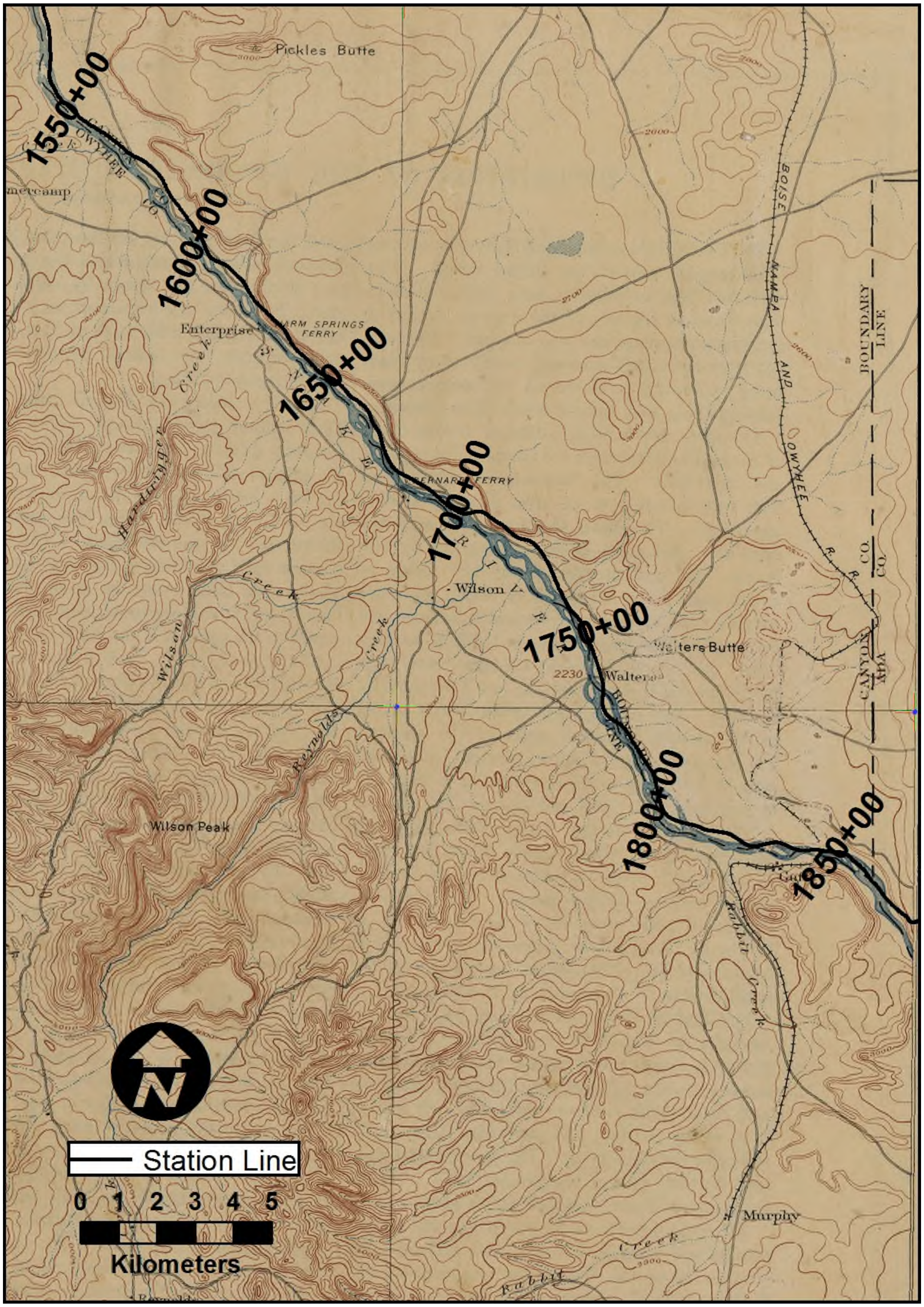

Figure B.4. A portion of the Silver City, Idaho 30-minute topographic map, printed in 1898, reprinted in 1943.

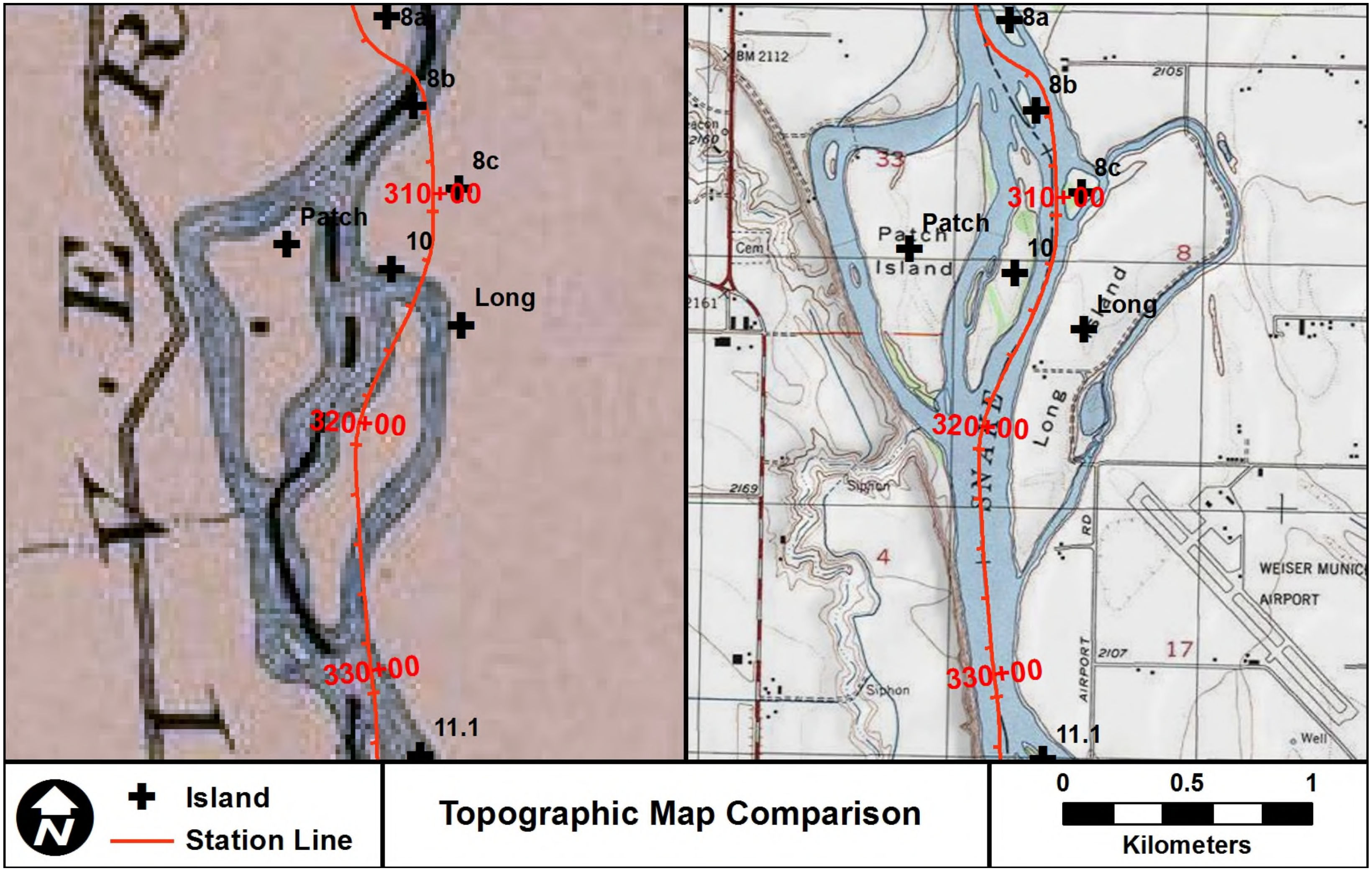

Figure B.5. Comparison of the between the 1894 (left figure) and the 2010 topographic map (right figure) of Patch, Goat (10) and Long Islands.

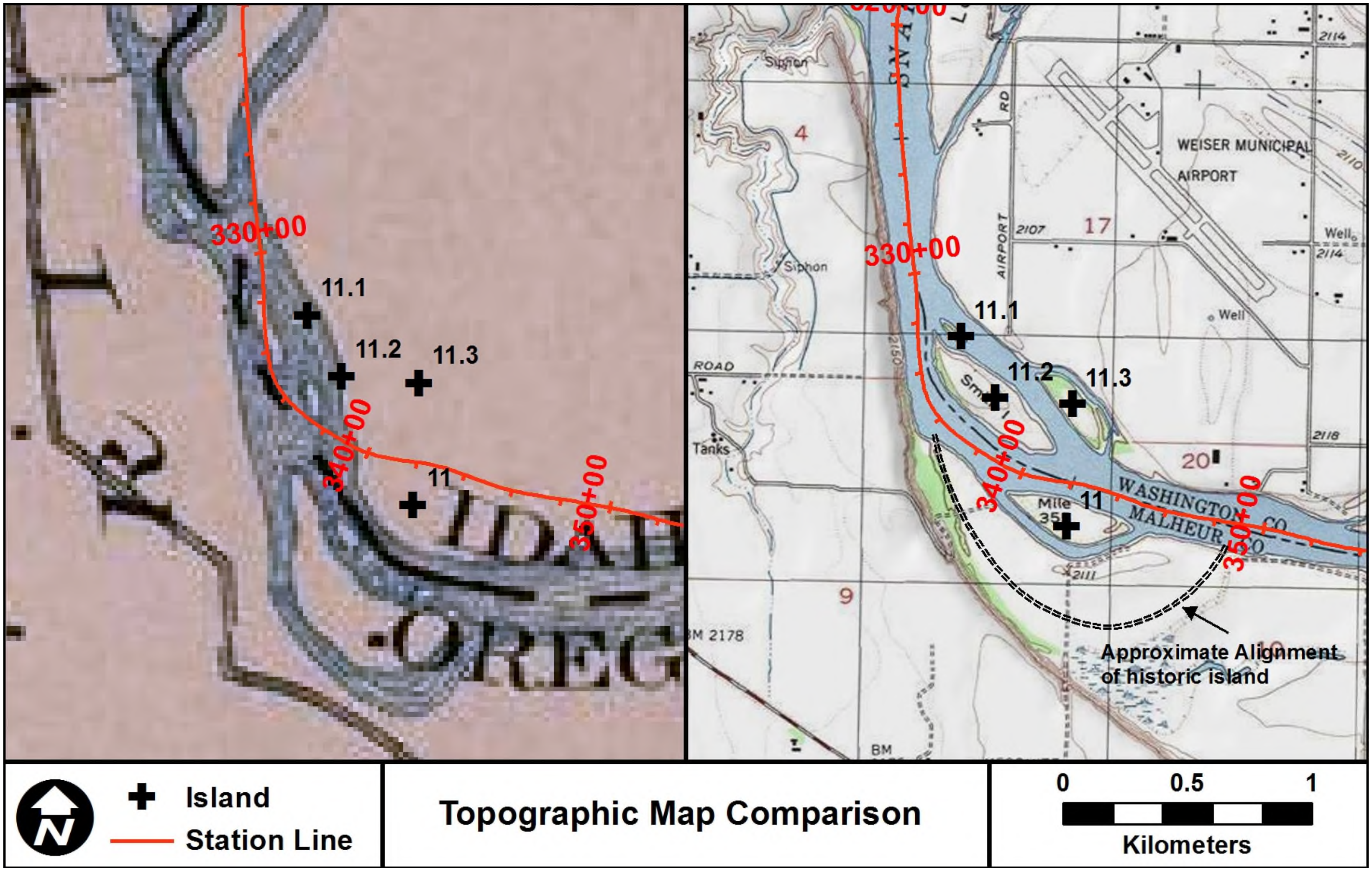

Figure B.6. Comparison of the between the 1894 (left figure) and the 2010 topographic map (right figure) of the Smith Group (11 to 11.3).

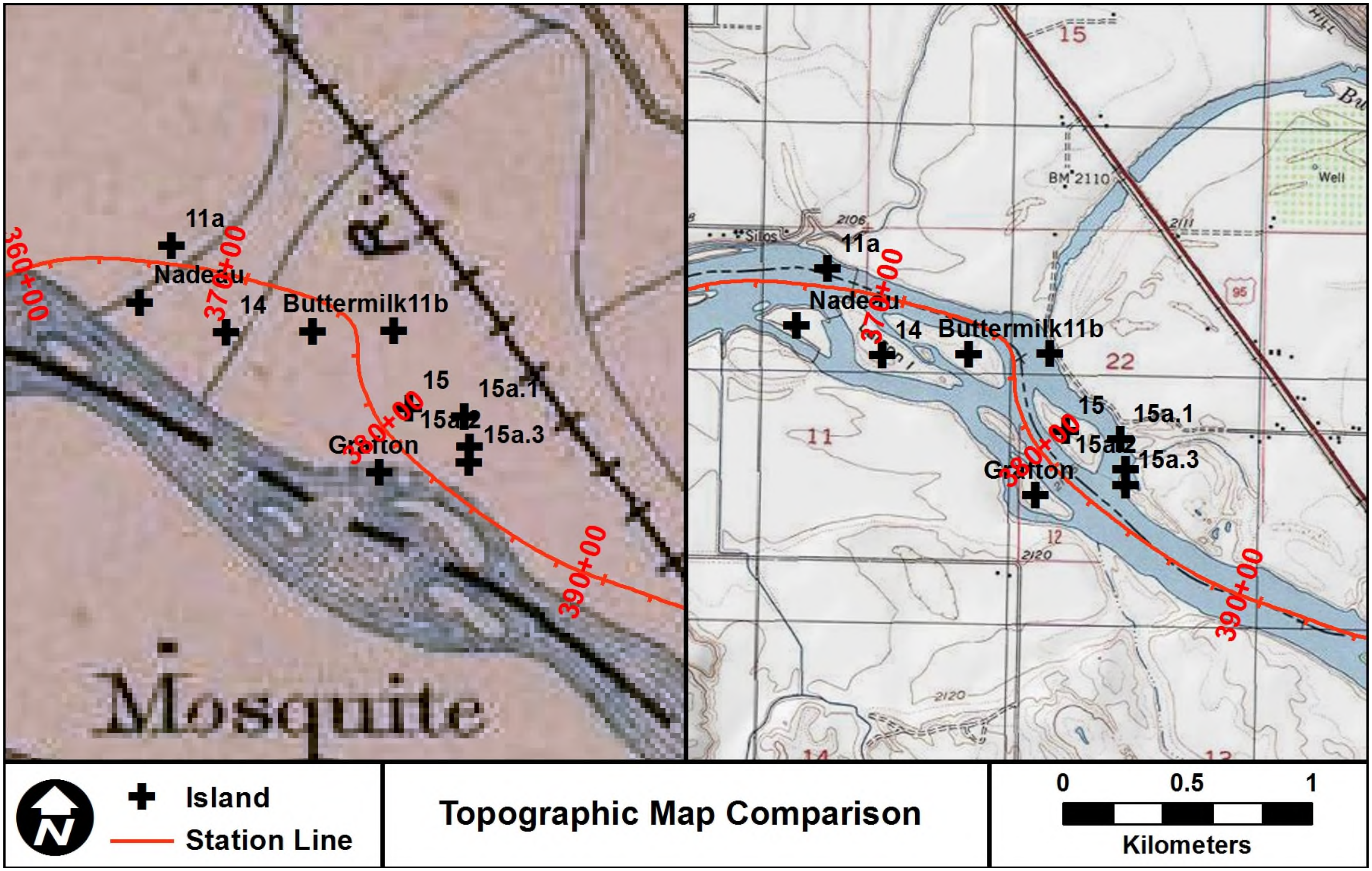

Figure B.7. Comparison of the between the 1894 (left figure) and the 2010 topographic map (right figure) showing Larson (14), Grafton and Sunstrom (15) Islands.

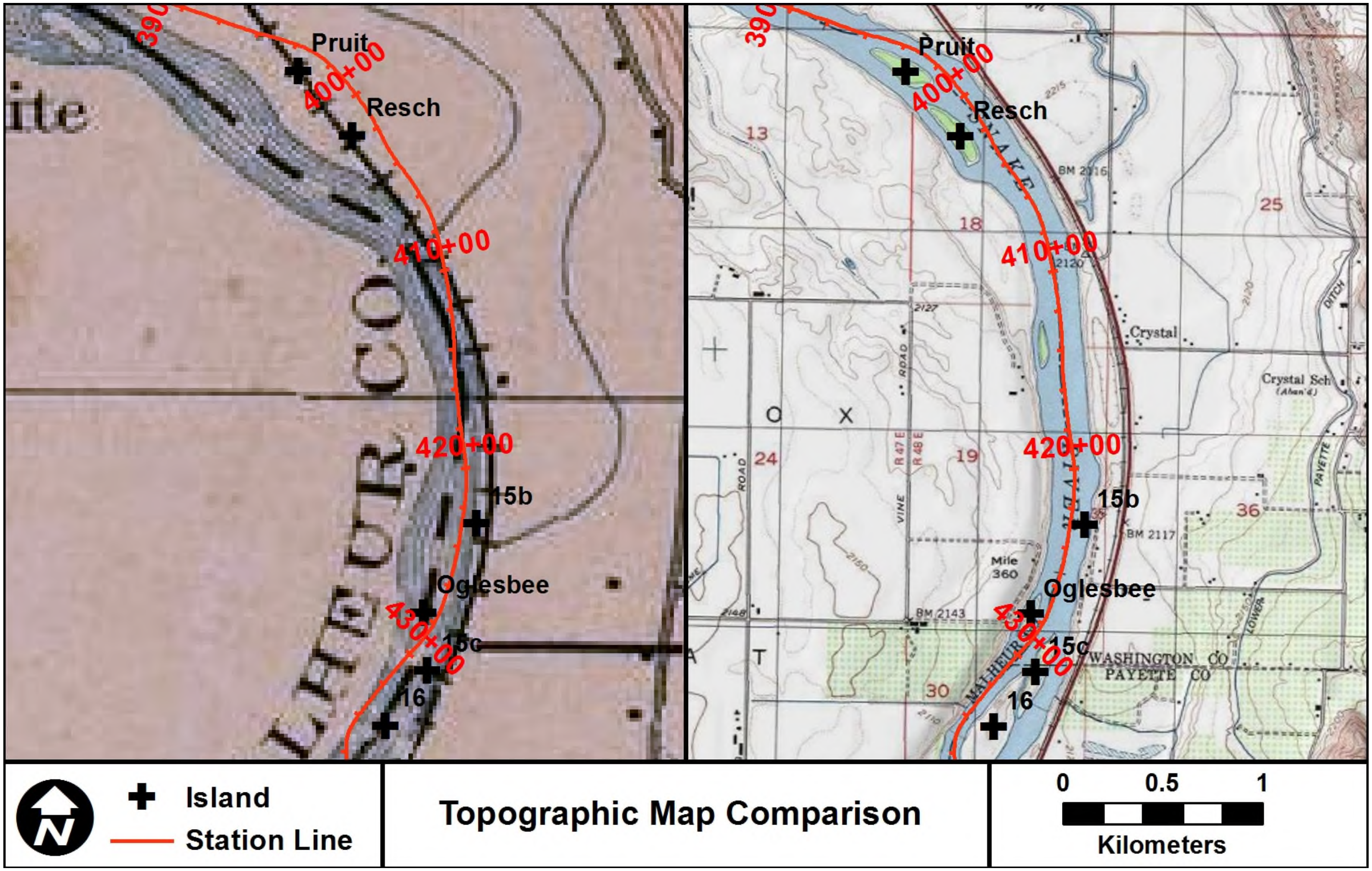

Figure B.8. Comparison of the between the 1894 (left figure) and the 2010 topographic map (right figure) showing Pruit, Resch, Oglesbee, Ketchup (16) and Annear (15c) Islands.

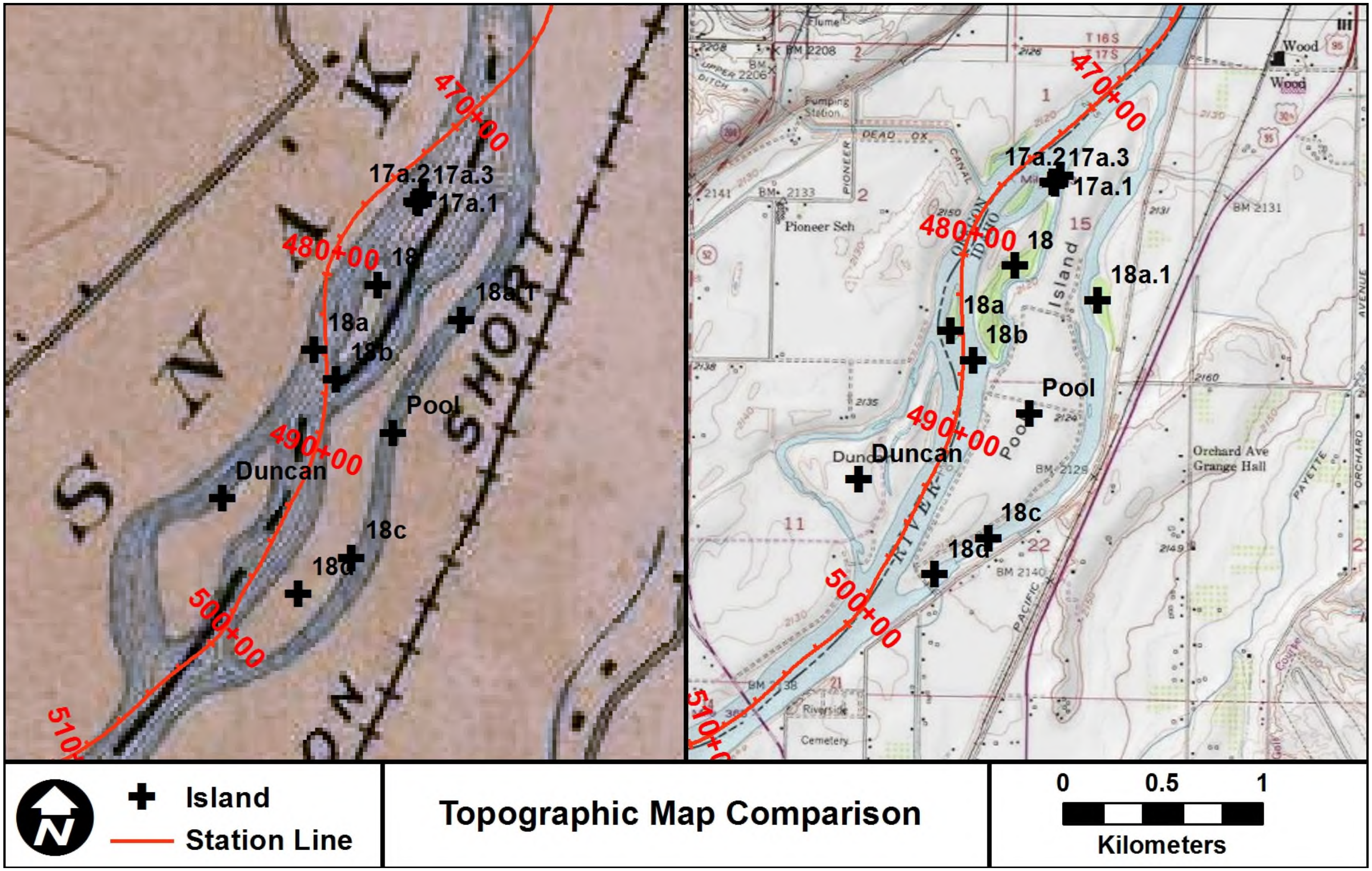

Figure B.9. Comparison of the between the 1894 (left figure) and the 2010 topographic map (right figure) showing Pool, Duncan and Scarecrow (18) Islands.

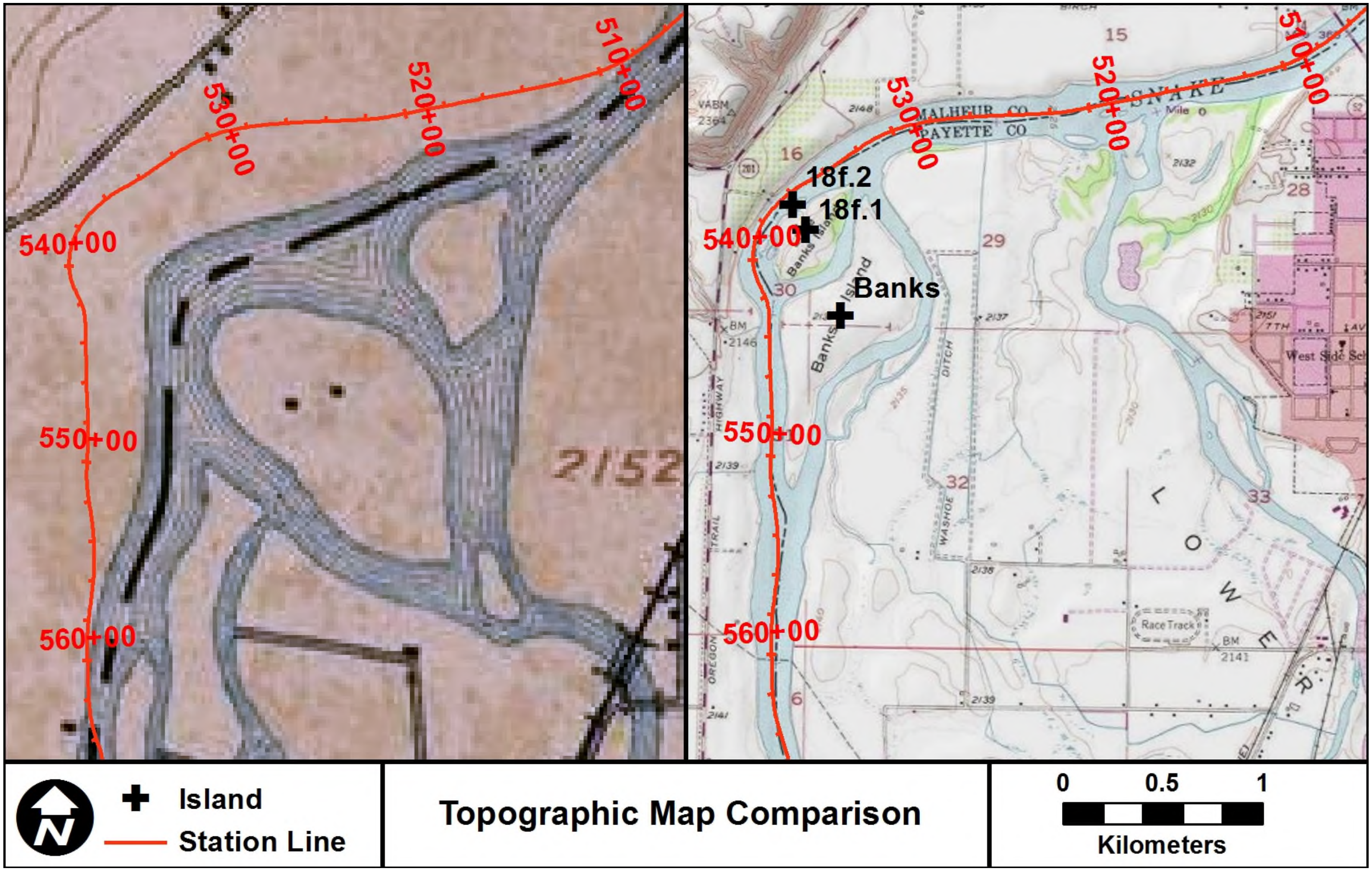

Figure B.10. Comparison of the between the 1894 (left figure) and the 2010 topographic map (right figure) in the vicinity of Banks and Little Banks (18f.1) islands. Note: there have been significant changes in the channel alignment in the vicinity of the Payette River confluence.

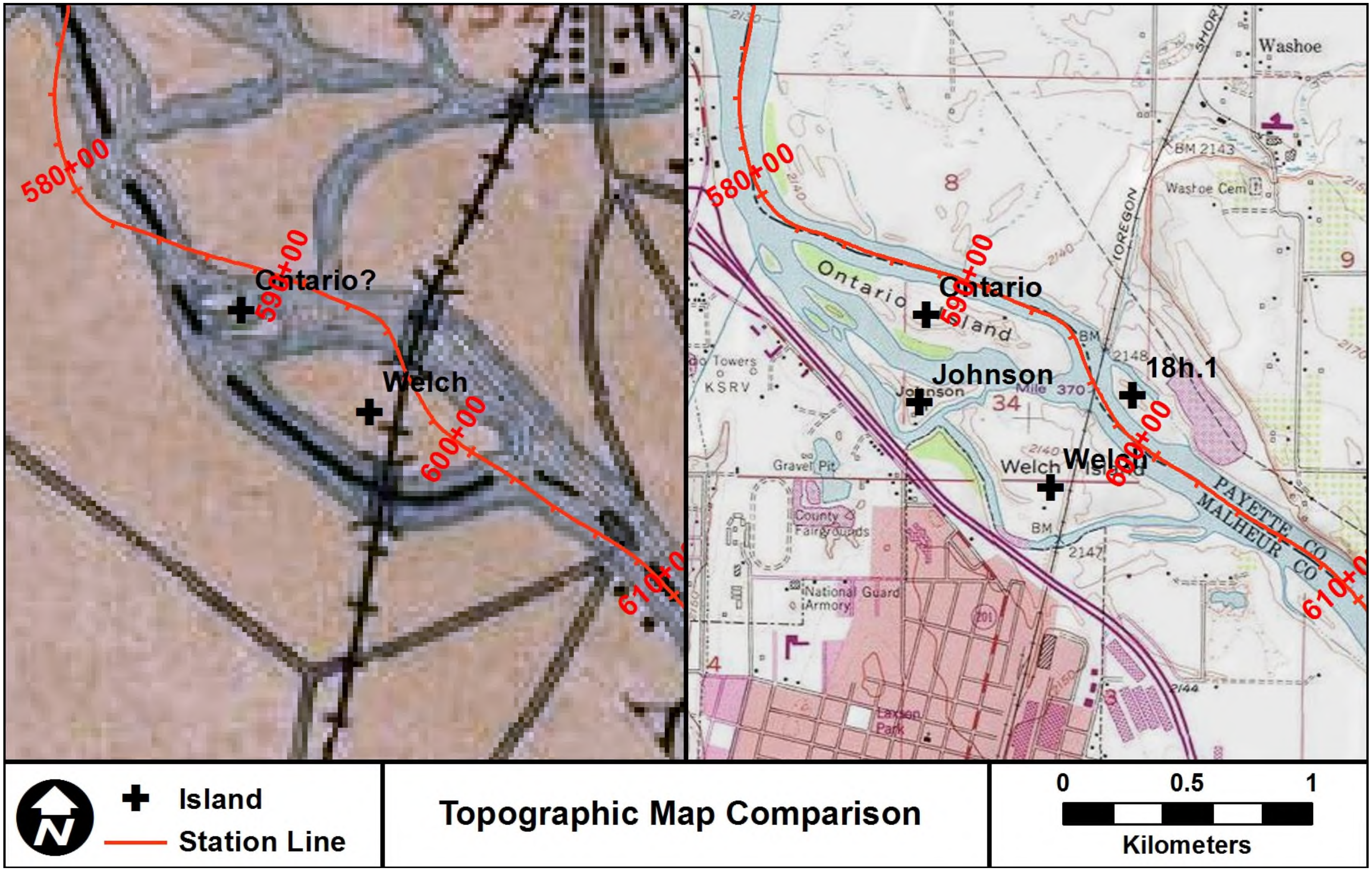

Figure B.11. Comparison of the between the 1894 (left figure) and the 2010 topographic map (right figure) in the Welch Island.

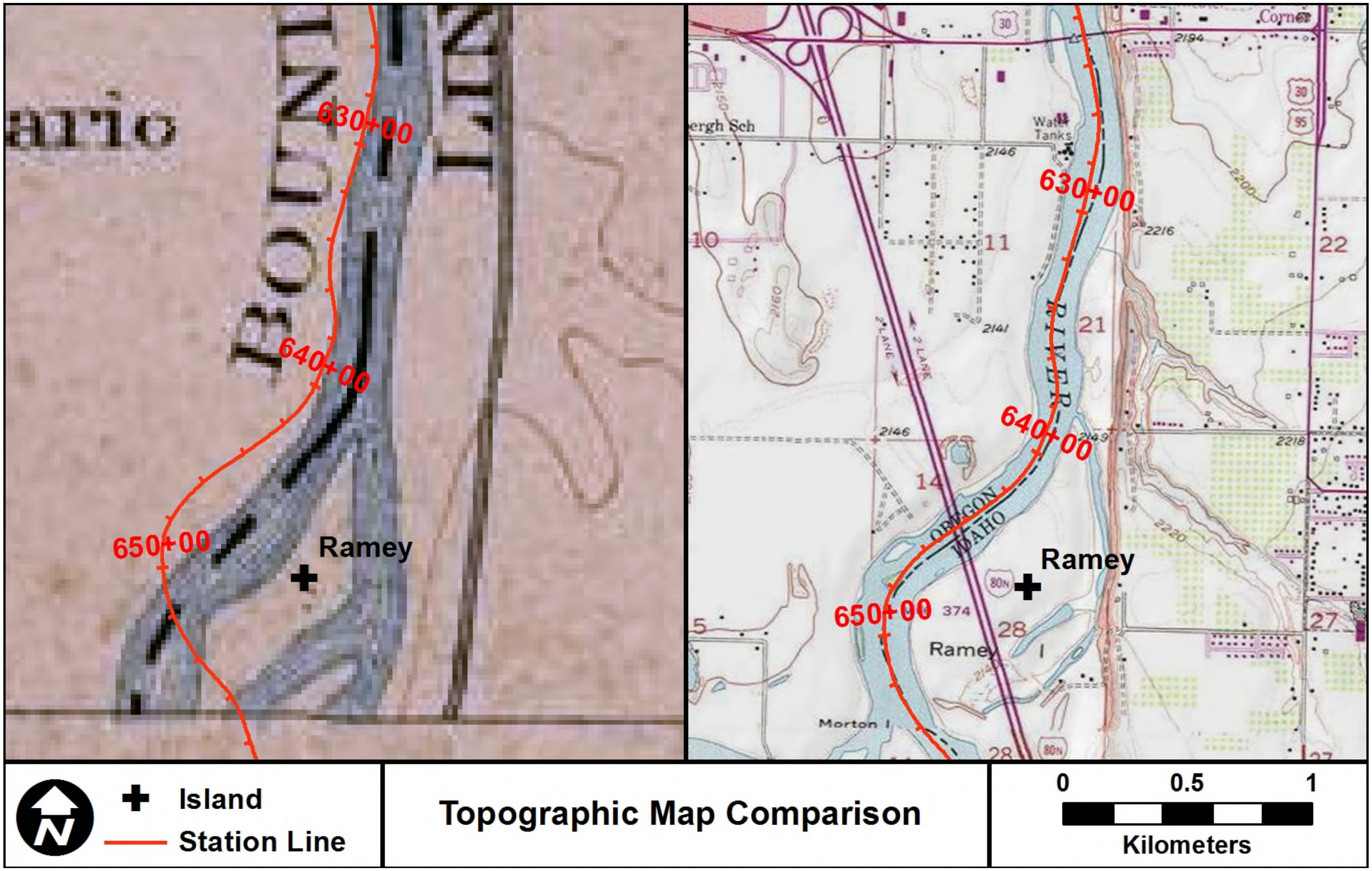

Figure B.12. Comparison of the between the 1894 (left figure) and the 2010 topographic map (right figure) in the Ramey Island.

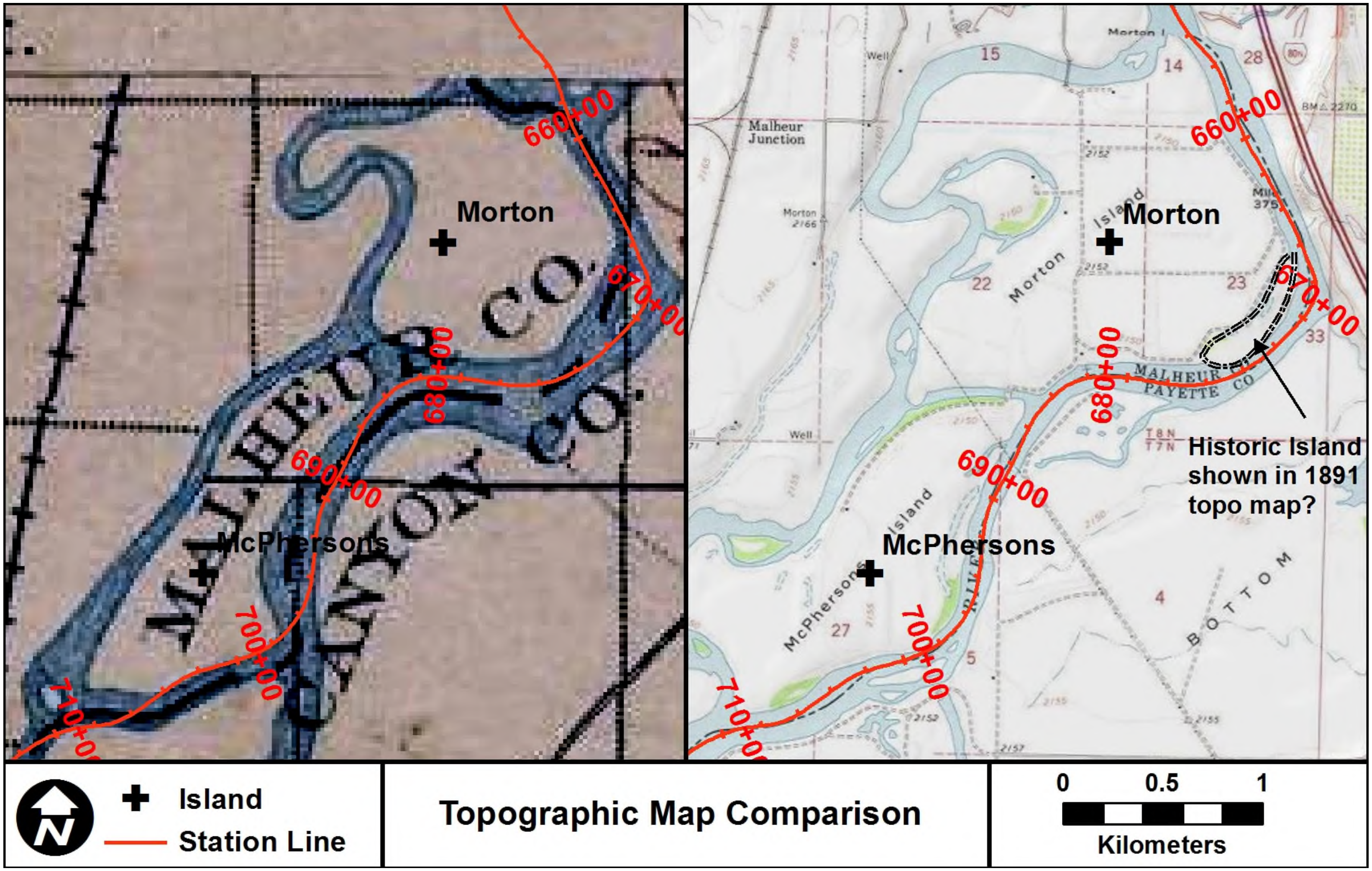

Figure B.13. Comparison of the between the 1891 (left figure) and the 2010 topographic map (right figure) showing Morton and McPhersons Island.

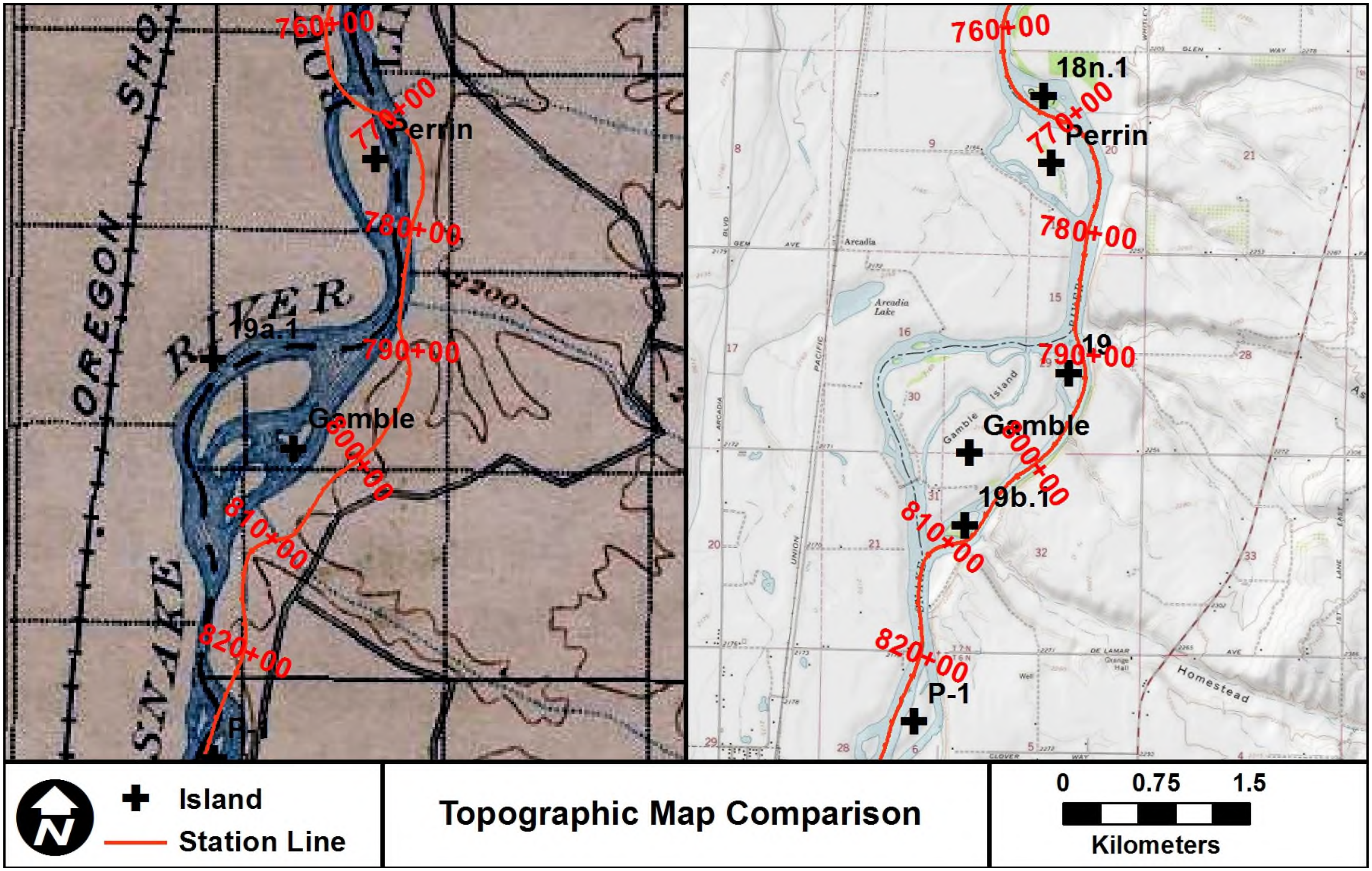

Figure B.14. Comparison of the between the 1891 (left figure) and the 2010 topographic map (right figure) showing Perrin, Gamble and P-1.

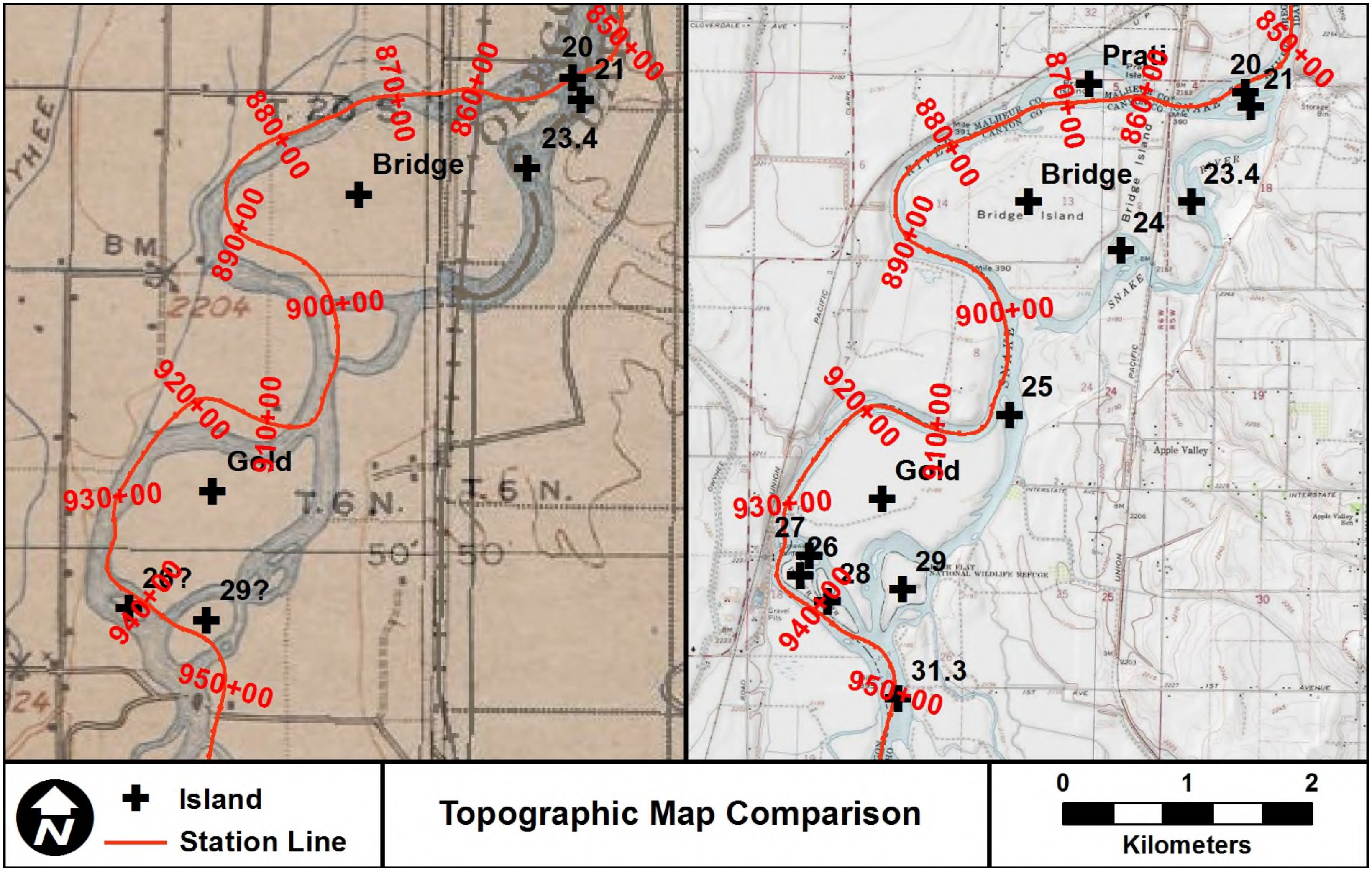

Figure B.15. Comparison of the between the 1905 (left figure) and the 2010 topographic map (right figure) showing the Quail Islands (20,21), Cable (23.4), Bridge, Gold and possibly Squatters (26) and Heron Island (29).

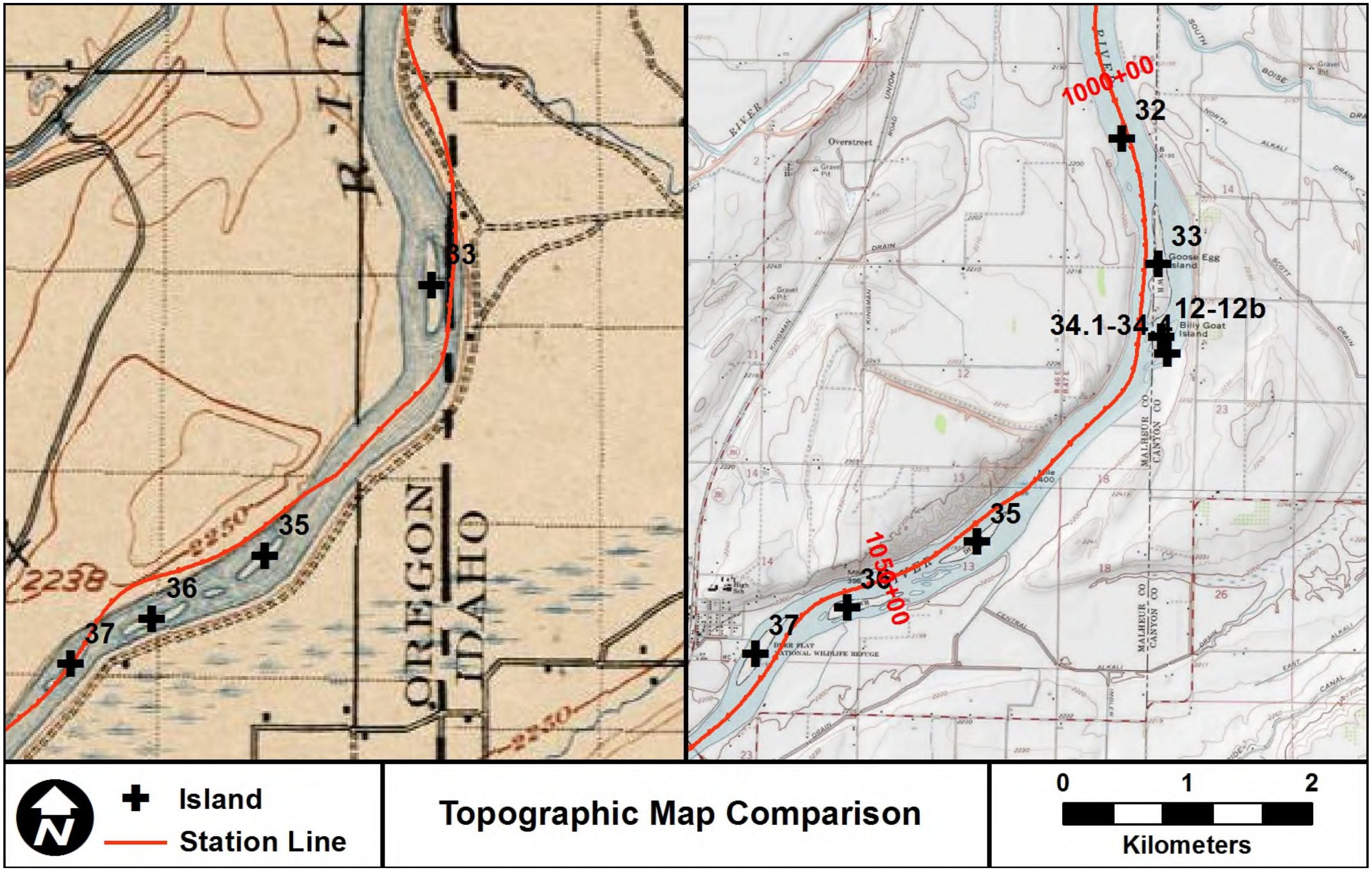

Figure B.16. Comparison of the between the 1905 (left figure) and the 2010 topographic map (right figure) showing the Goose Egg Island (33). Note: Kline Island (32), the Bill Goat Group (31.1-34.4) and the Islands 12 and 12b are not shown on the historic maps.

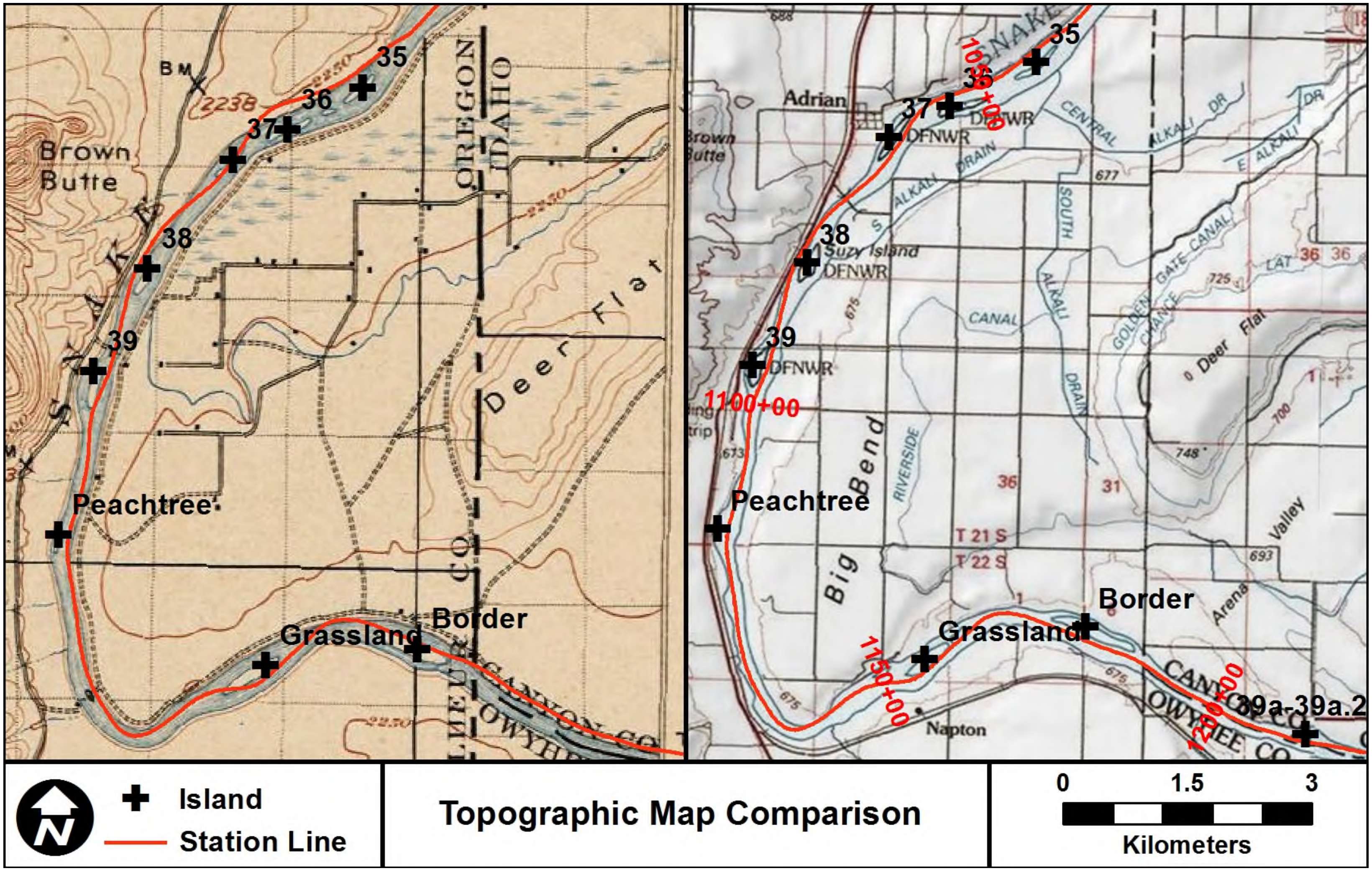

Figure B.17. Comparison of the between the 1905 (left figure) and the 2010 topographic map (right figure) showing Main & East Shack (35), Rhubarb (36, Adrian (37), Suzy (38), Airport (39), Peachtree, Grassland and Border Islands. The Tule Group (39a-39a.2) is not present.

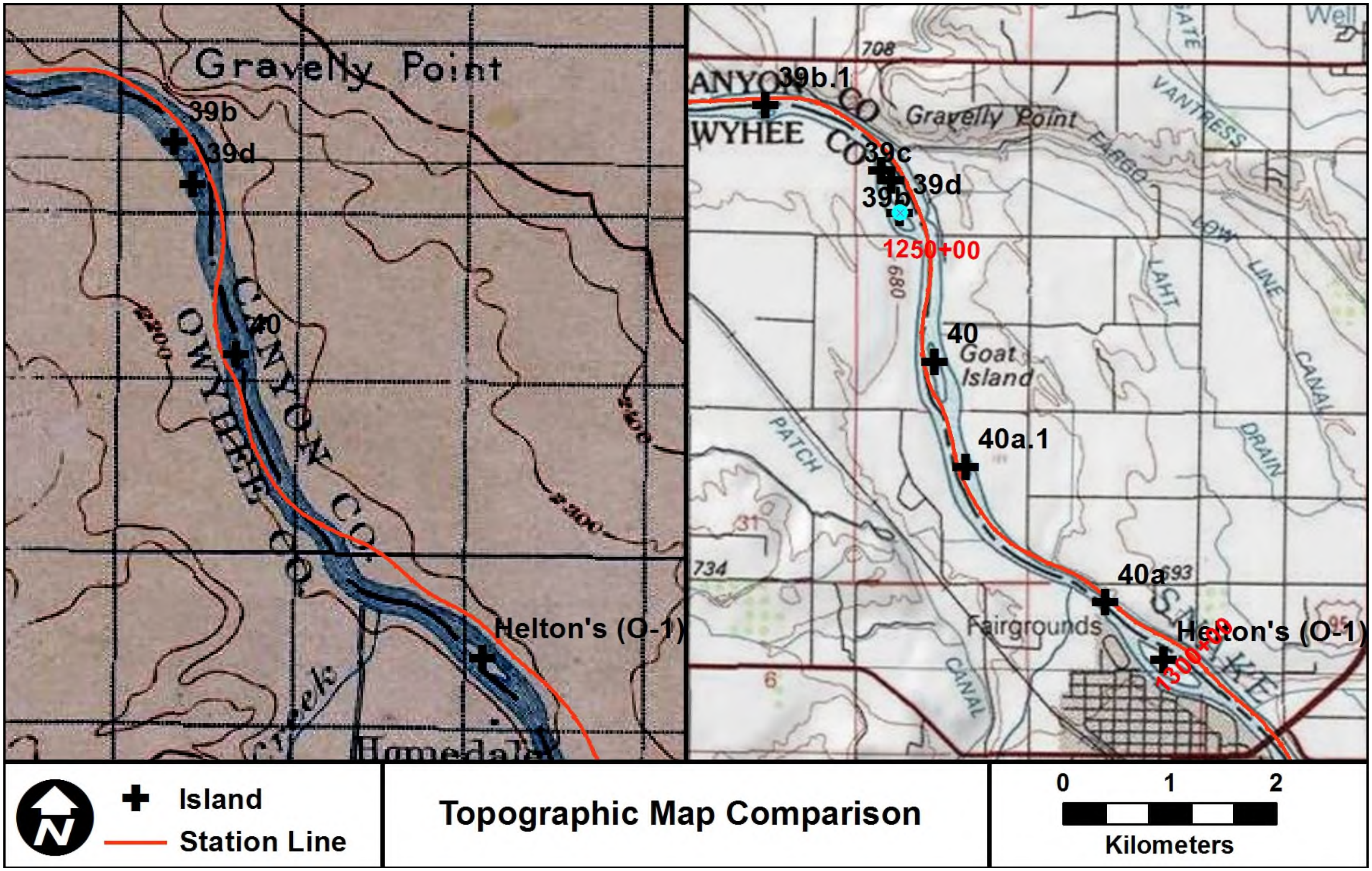

Figure B.18. Comparison of the between the 1891 (left figure) and the 2010 topographic map (right figure) showing the Channel island Group (39b, 39d, Silo 40) and Helton's Island.

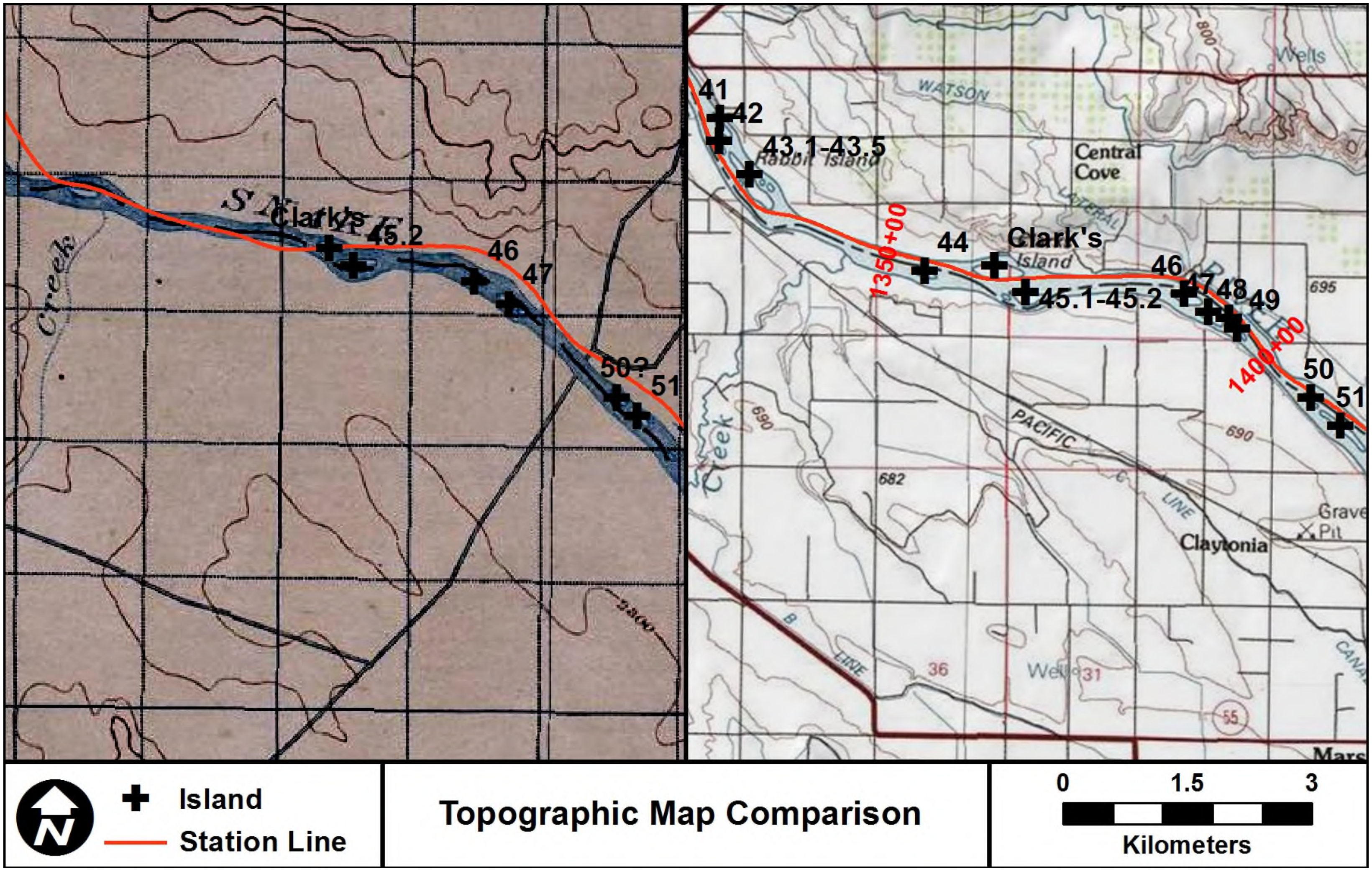

Figure B.19. Comparison of the between the 1891 (left figure) and the 2010 topographic map (right figure) showing Clarks's Olive (45), Feral (46), Phesant#2 (47) and Gosling Island (51). The location of Tiny (50) is uncertain. Homedale (40), Wegman (41), Black Crowned (44), Pheasant #1 (47), Pheasant #3 (49) are not shown on the older maps.

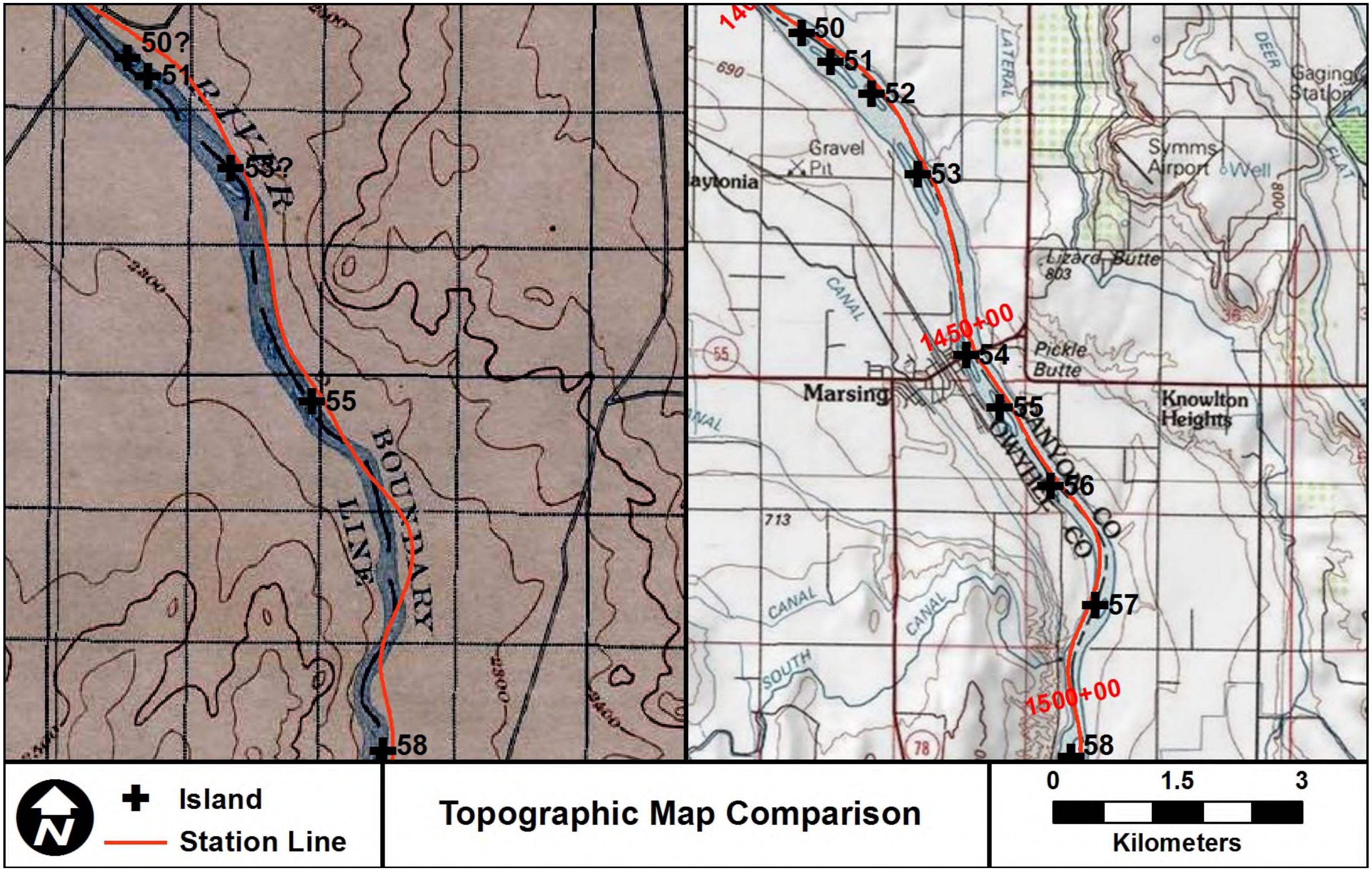

Figure B.20. Comparison of the between the 1891 (left figure) and the 2010 topographic map (right figure) showing Gosling (51), Cigar (53), Poison Ivy (55) and Center (58). Marshing (54), Feedlot (56) and Gem (57) are not shown on the older map.

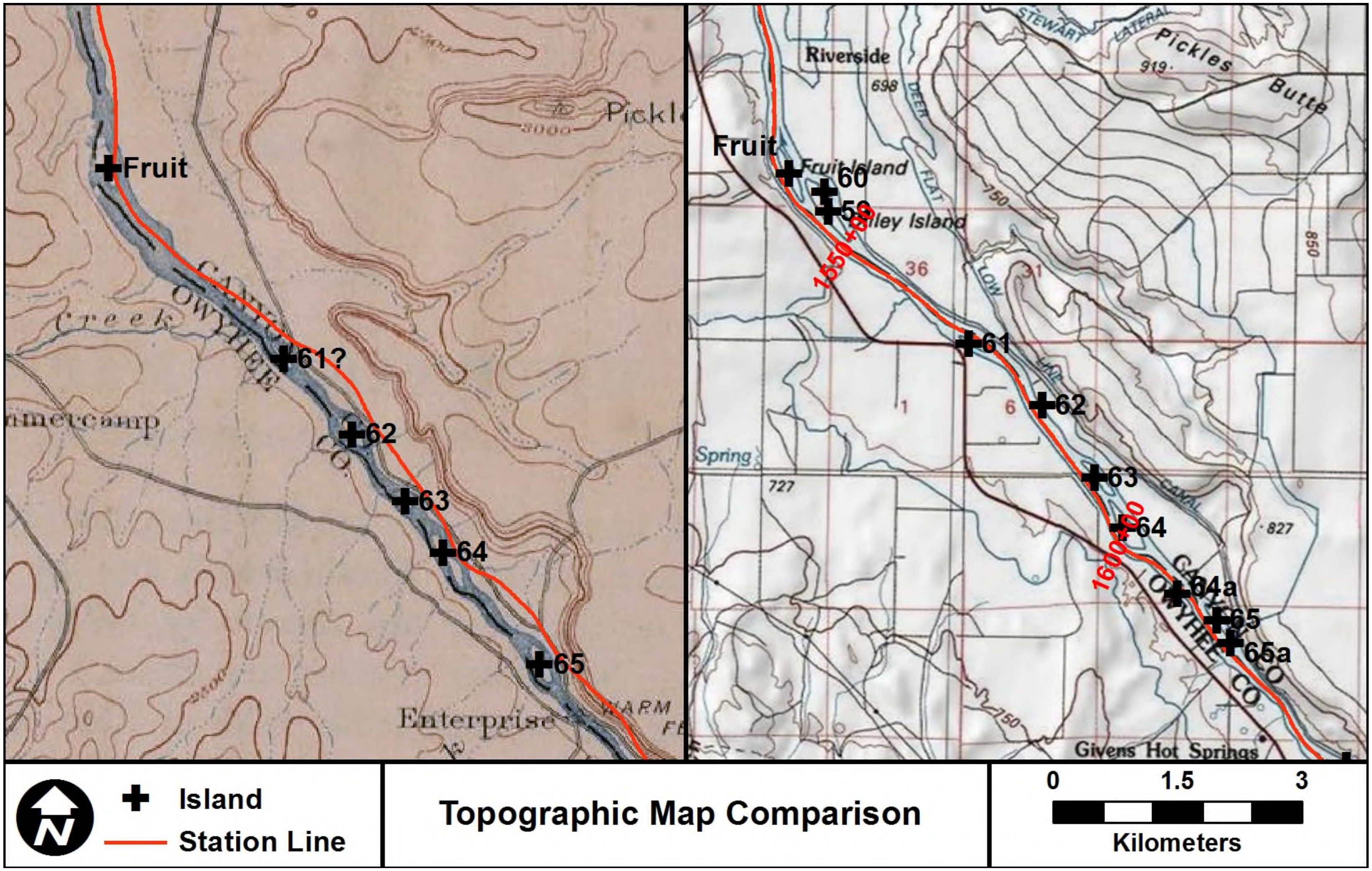

Figure B.21. Comparison of the between the 1892 (left figure) and the 2010 topographic map (right figure) showing Fruit, possibly Cottontail (61), Folgers (62), Blackburn (63), Dredge (64) and Goldeneye (65).

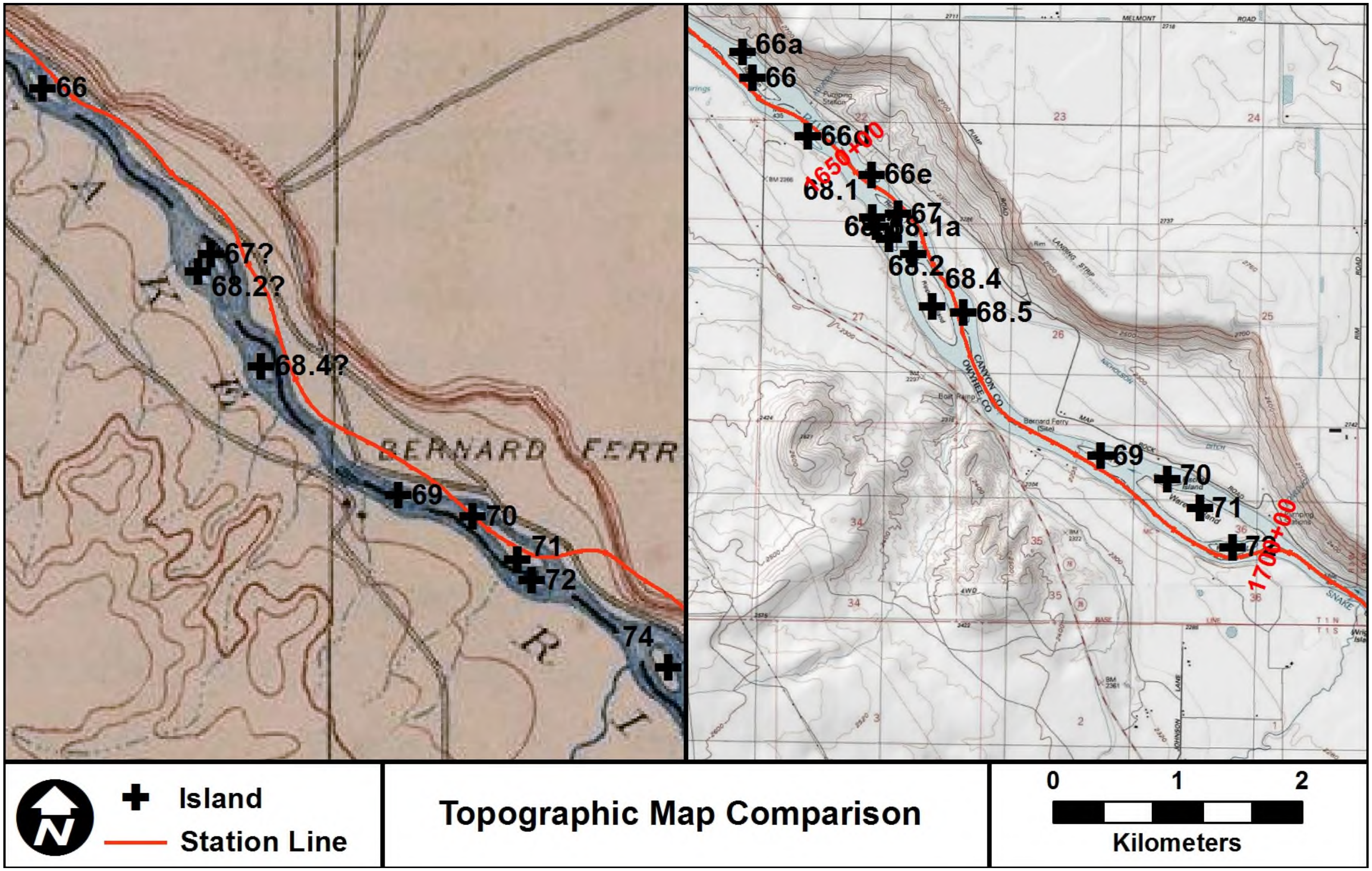

Figure B.22. Comparison of the between the 1892 (left figure) and the 2010 topographic map (right figure) showing Raccoon (66), probably Hermit (67) and Rippee Group (66.2, 66.4), Current (69), Fisher (70, Ware (71), Richards (72) and Bayha (74). Many of the smaller islands are not shown on the older map.

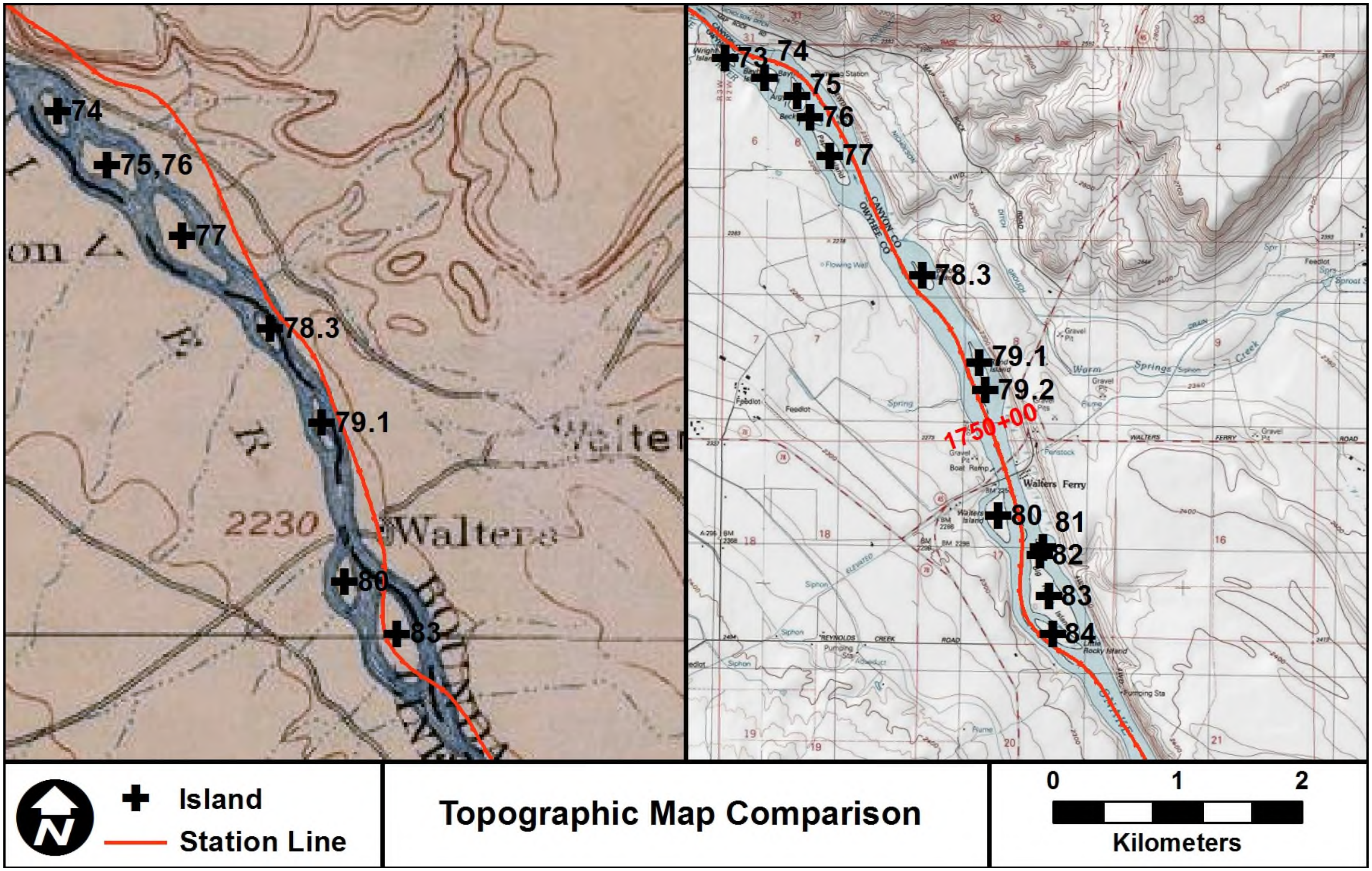

Figure B.23. Comparison of the between the 1892 (left figure) and the 2010 topographic map (right figure) showing Bayha (74), Argy (75), Becky (76), Brooks (78.3), Blind (79.1), Walters (80) and Big Rocky (83).

APPENDIX C – 1914 Water Supply Mapping

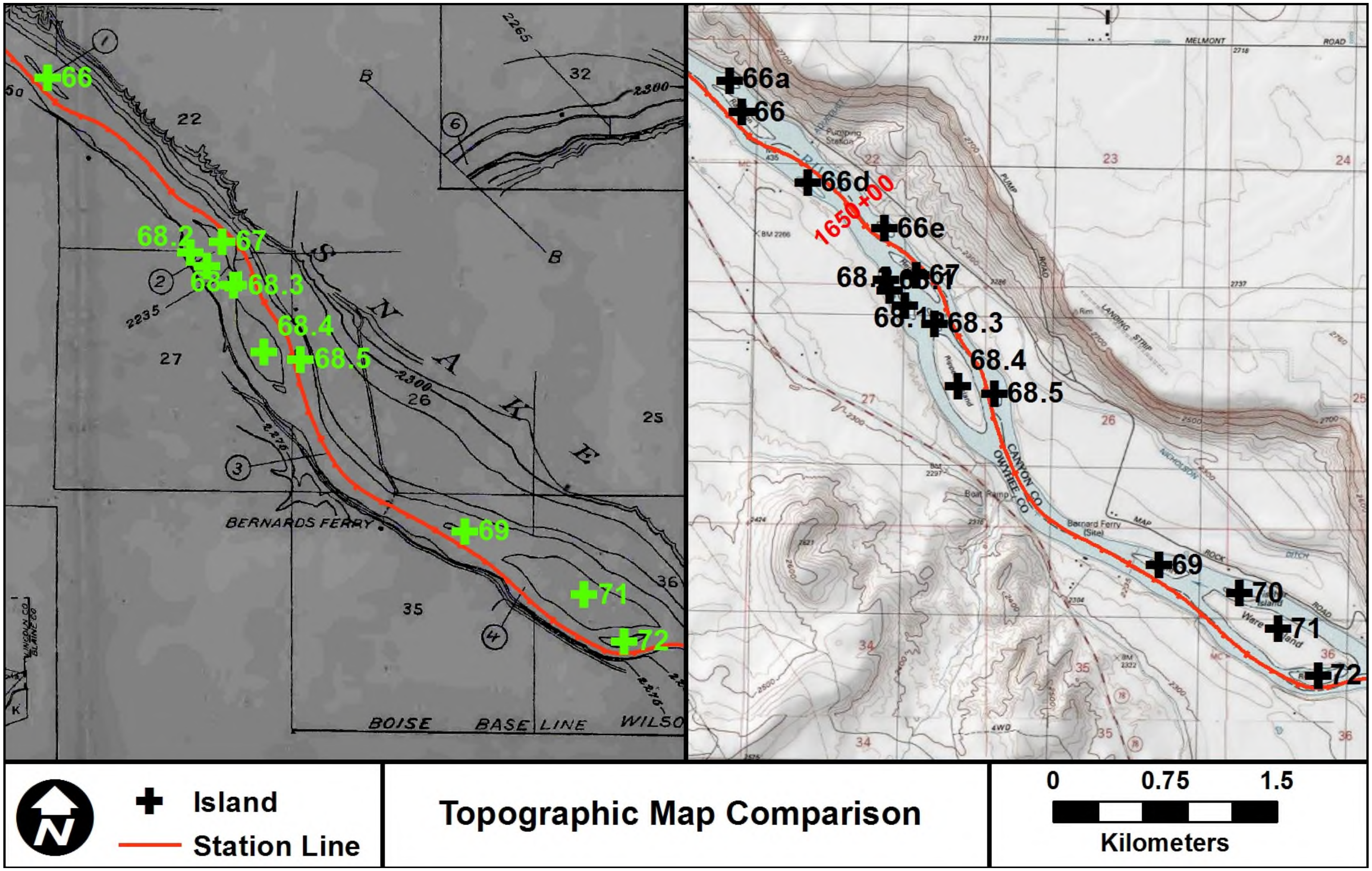

Figure C.1. Comparison of the between the Water Supply Paper (1914) (left figure) and the 2010 topographic map (right figure) showing Raccoon (66), Hermit (67), Rippee Group (68), Current (69), Ware (71) and Richards (72). Fischer (70) is not shown, but may have been mapped as part of Ware.

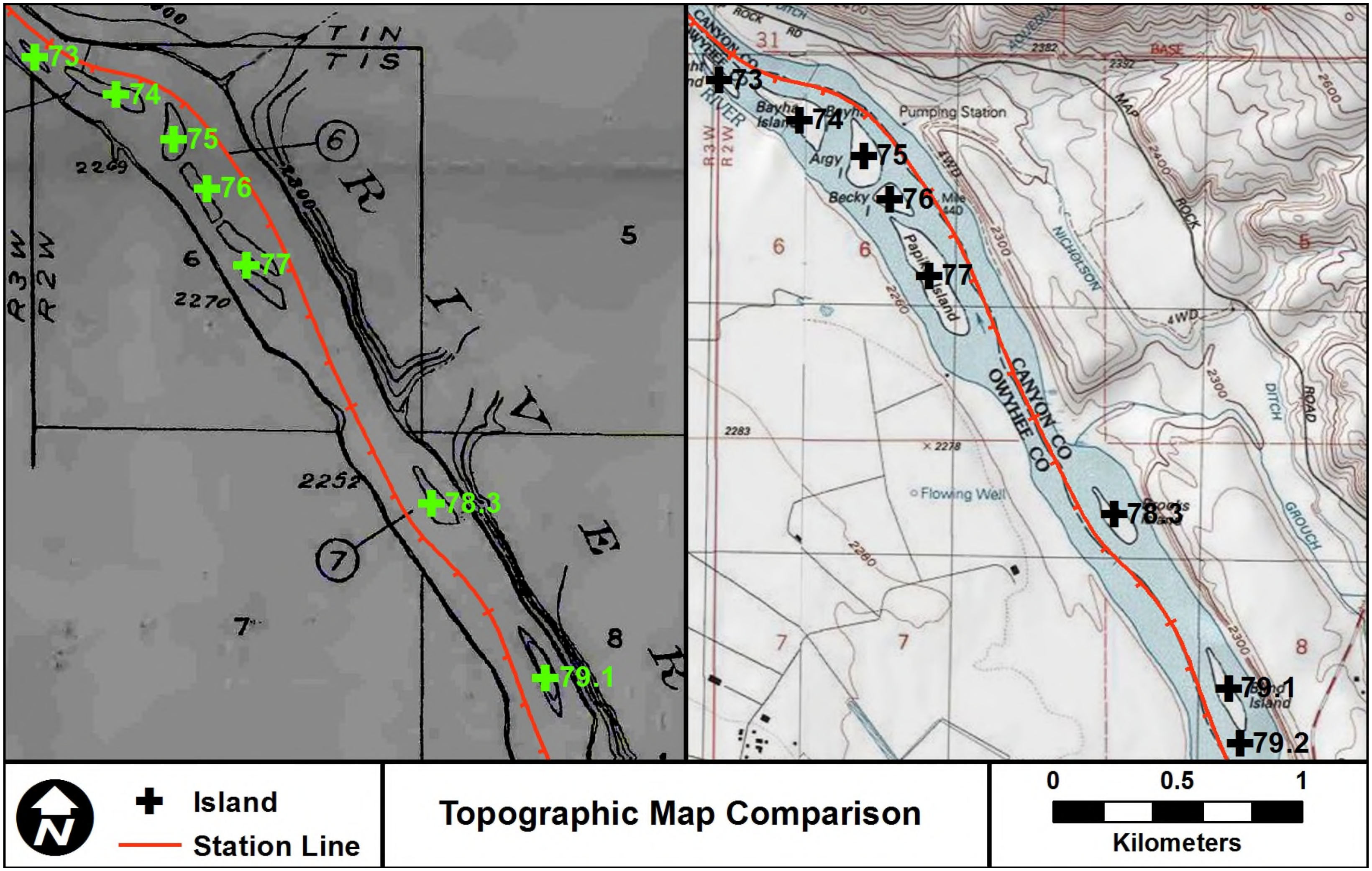

Figure C.2. Comparison of the between the Water Supply Paper (1914) (left figure) and the 2010 topographic map (right figure) showing the islands between Wright (73) and Blind (79.1). On the older maps, the islands around Becky (76) and Papike (77) have a different shape compared to the recent mapping.

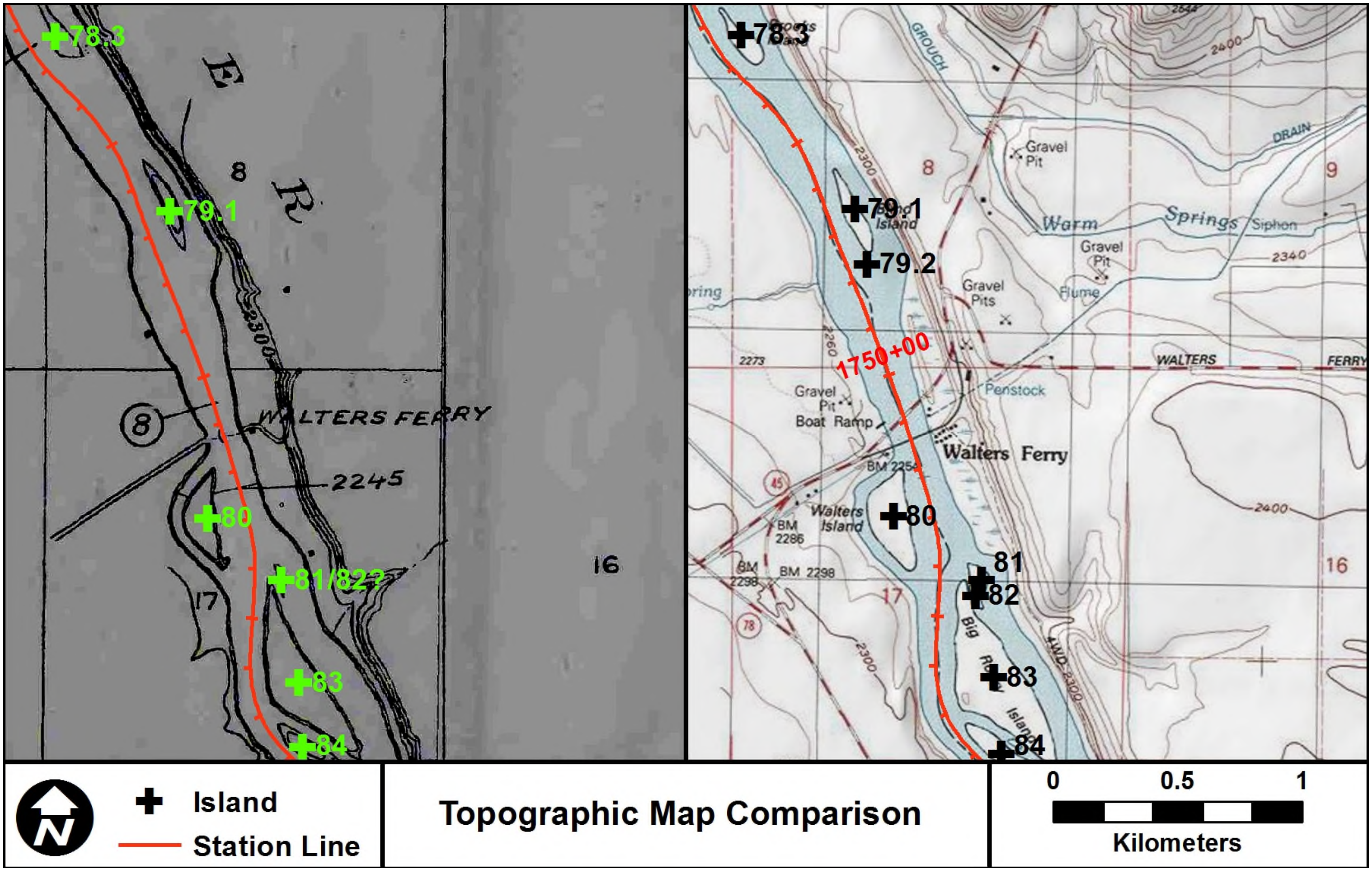

Figure C.3. Comparison of the between the Water Supply Paper (1914) (left figure) and the 2010 topographic map (right figure) showing the islands between Brooks (78.3) and Little Rocky (78.4).

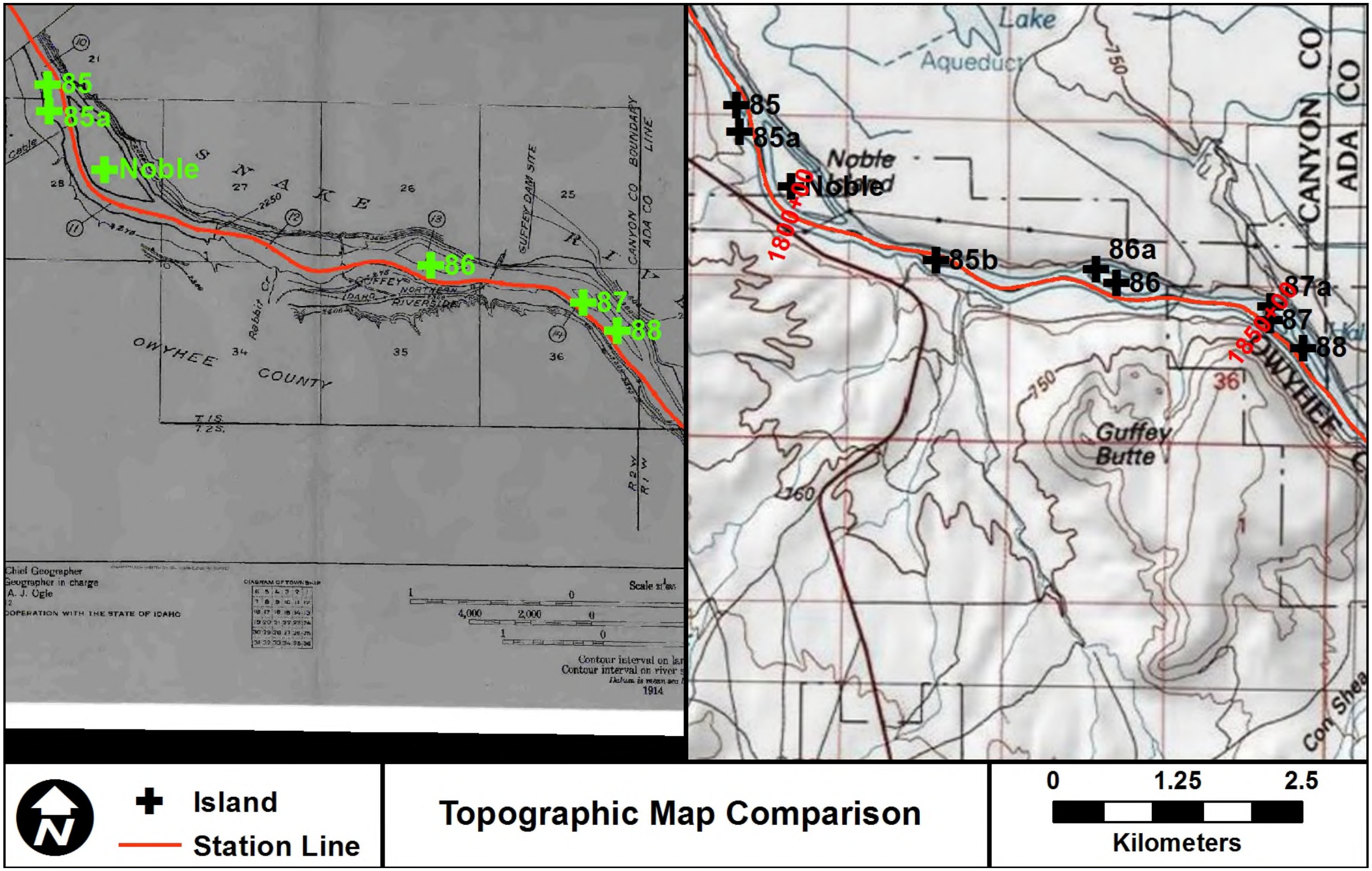

Figure C.4. Comparison of the between the Water Supply Paper (1914) (left figure) and the 2010 topographic map (right figure) showing the islands between Menning (85) and Sign Island (88).

APPENDIX D – 1938/1939 Aerial Photography Comparisons

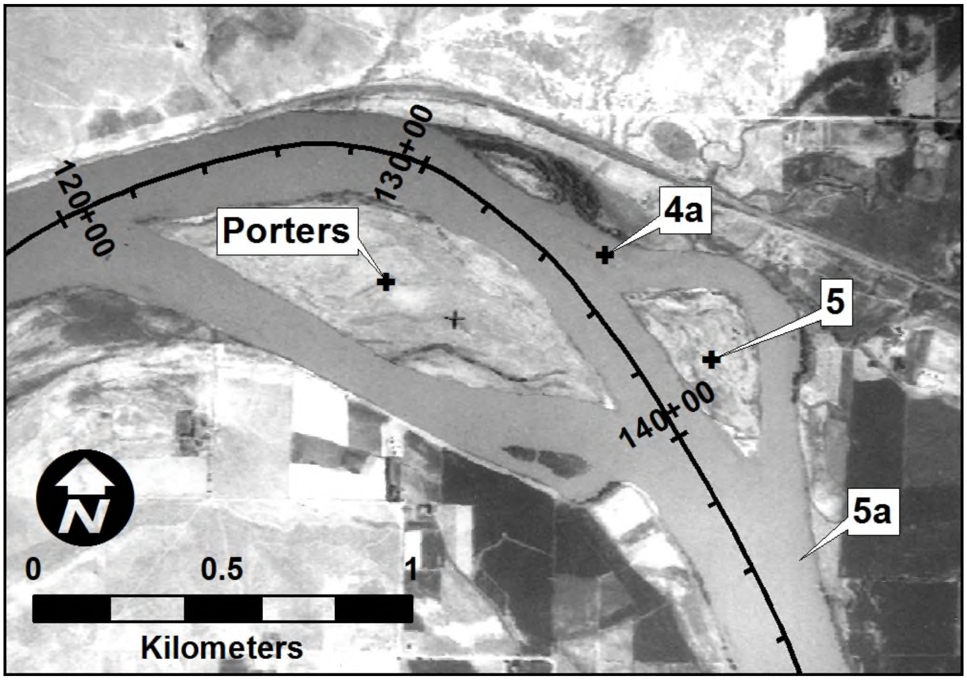

Figure D.1a. An early aerial photograph (taken on 7-7-38) showing Jackass Island (5) and Porter's Island. The upstream berm on Jackass Island (5) is small, and Island 4a is forming.

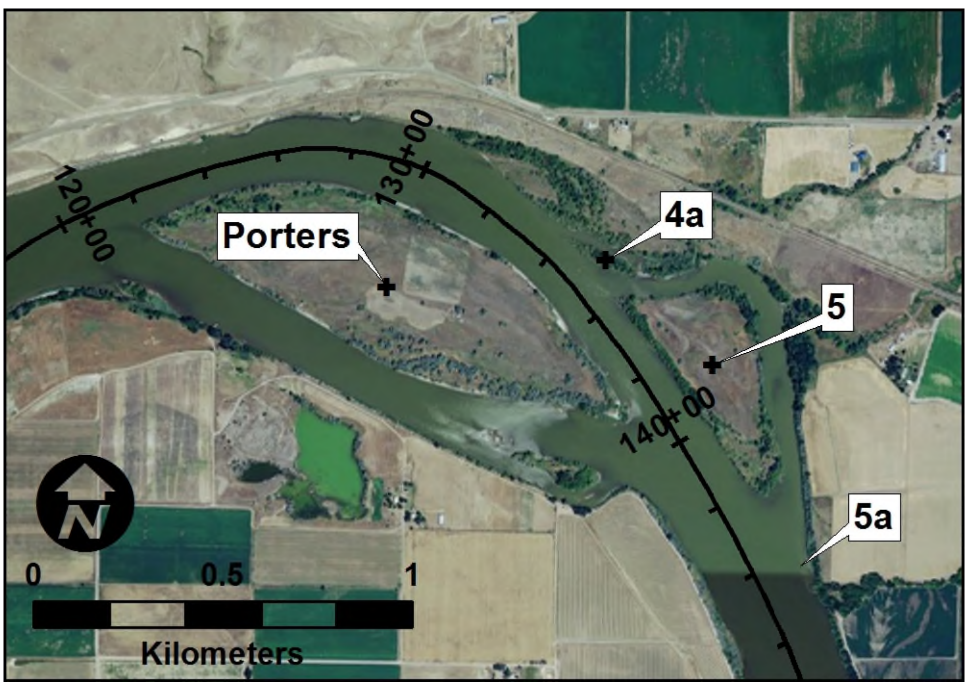

Figure D.1b. Aerial photograph taken in 2012 showing Jackass Island (5), 4a, and Porter's Island. The upstream berm on Jackass Island has grown considerably since 1938, and 4a is completely formed. Note also lateral berm growth on Jackass Island and riparian vegetation growth on berms and low islands.

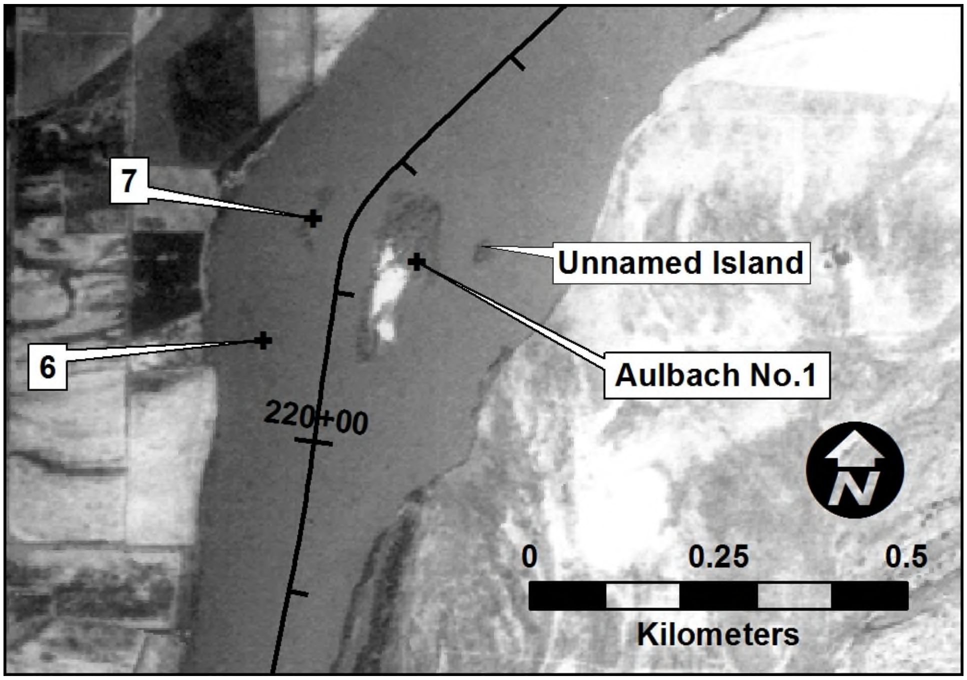

Figure D.2a. An early aerial photograph (taken on 7-7-38) showing the Aulbach Group (6, 7, Aulbach No.1, and an unnamed island). Note that some riparian vegetation growth has occurred on these islands

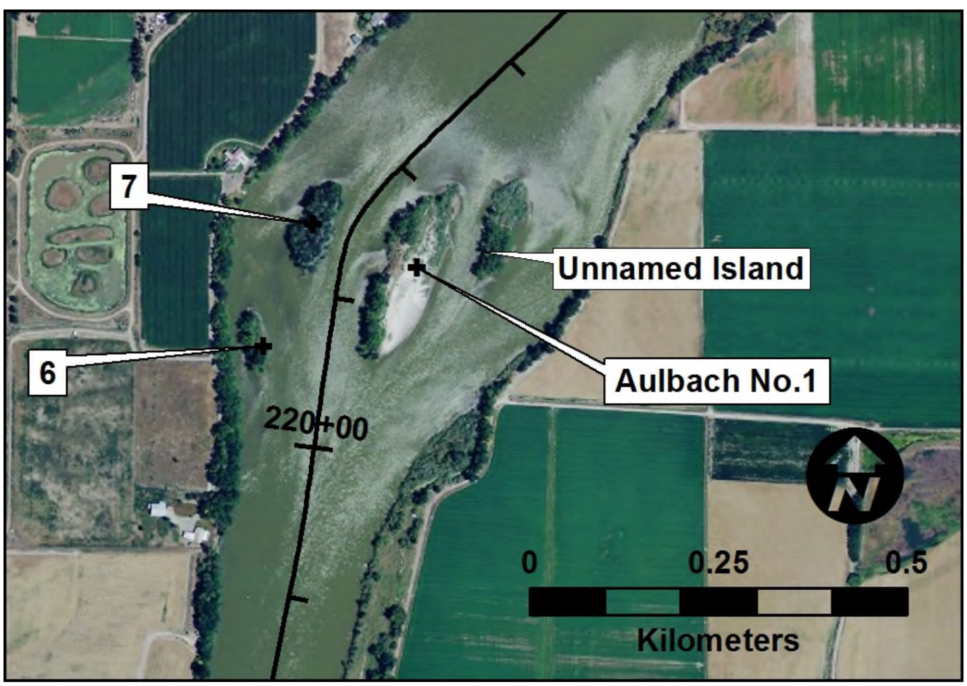

Figure D.2b. Aerial photograph taken in 2012 showing the Aulbach Group (6, 7, Aulbach No.1, and an unnamed island). Note that 6, 7, and the unnamed island have grown and Aulbach #1 has recently experienced dramatic erosion.

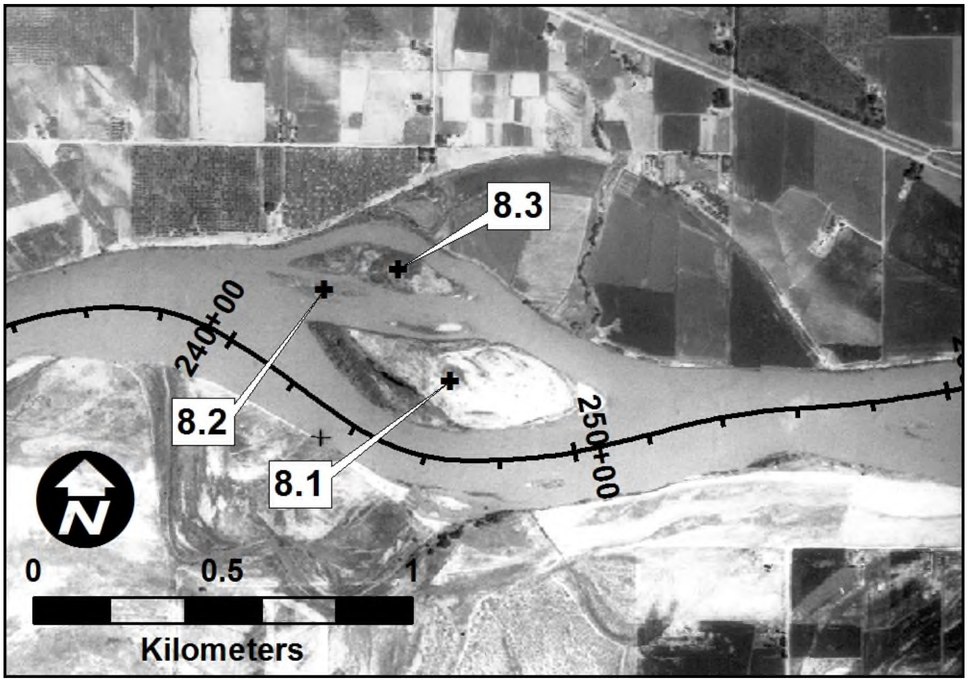

Figure D.3a. An early aerial photograph (taken on 7-6-38) of the McRea Group (8.1 through 8.3) shows Island 8.2 as low elevation gravel bars.

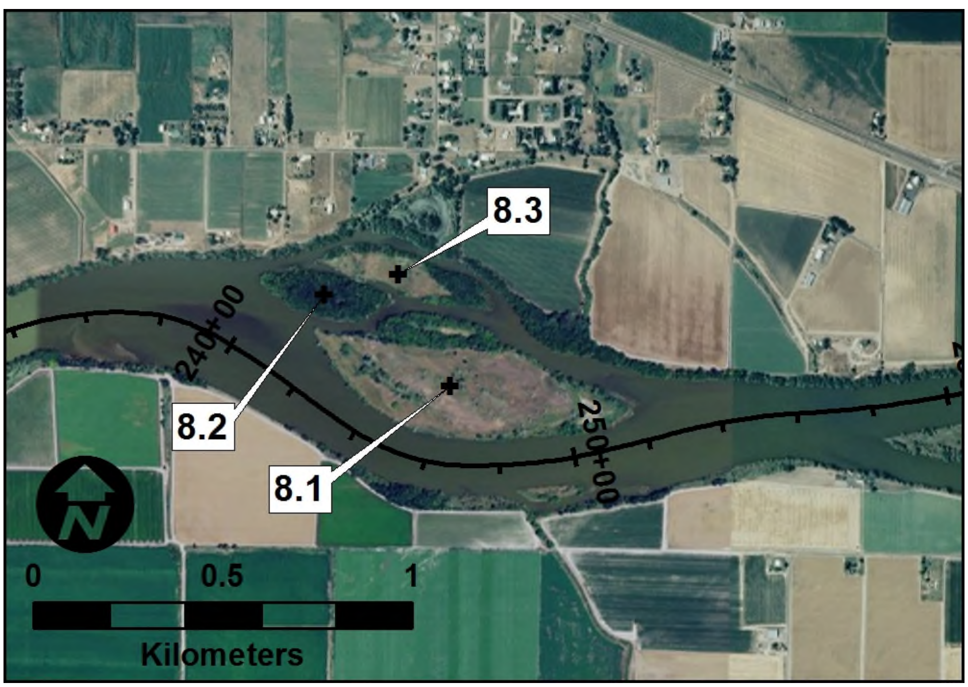

Figure D.3b. Aerial photograph taken in 2012 showing the McRea Group (8.1 through 8.3) fully formed. Note also riparian vegetation growth on low elevation islands and berms, and the growth of the upstream berm on Island 8.3.

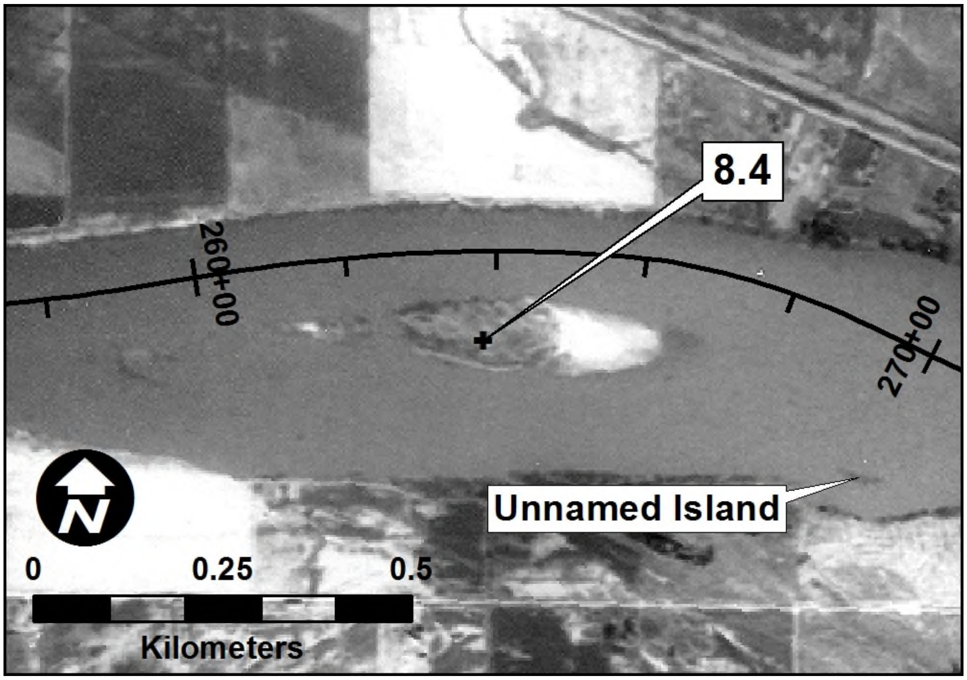

Figure D.4a. An early aerial photograph (BBC-6-32, taken on 7-6-38) showing the Snake River downstream of the Weiser River. This photograph shows half of the current island known as Schledewitz Island (8.4). Note moderate riparian vegetation growth on the left side of the island (downstream half) and a small island forming upstream.

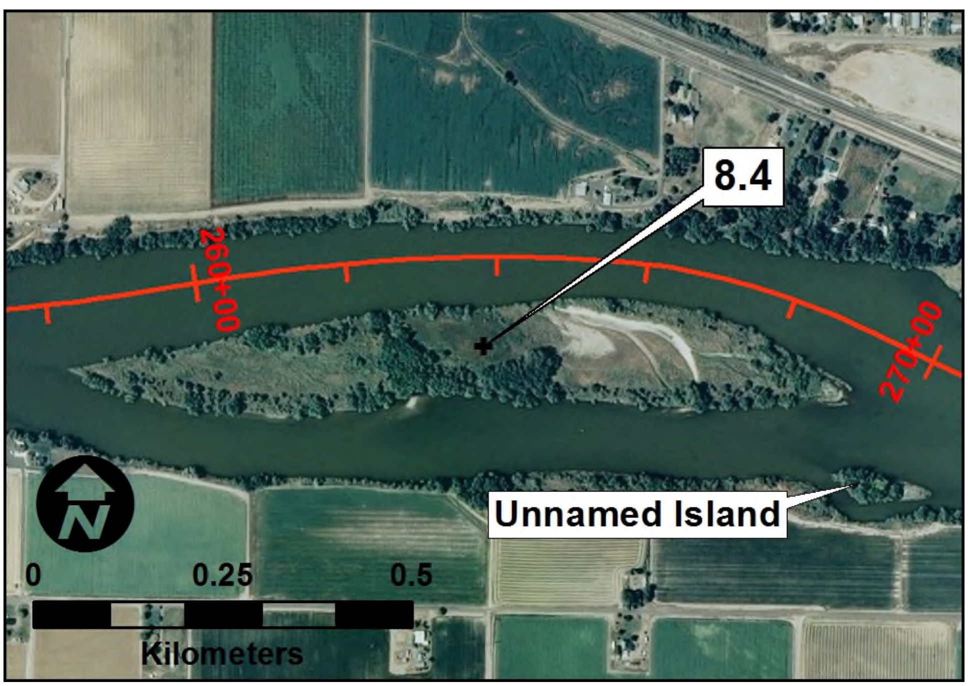

Figure D.4b. Aerial photograph taken in 2012 showing Schledewitz Island (8.4). Note the dramatic growth of this island and growth of riparian vegetation.

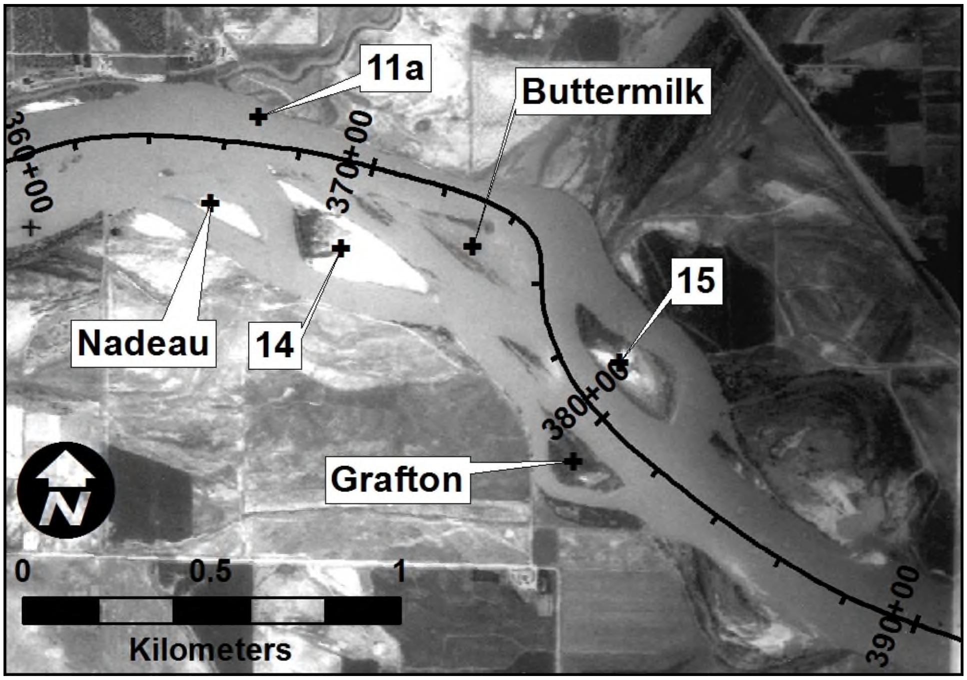

Figure D.5a. An early aerial photograph (BBC-6-53, taken on 7-10-38) showing Nadeau, Larson (14), Buttermilk, Sundstrom (15), and Grafton Islands. Note that the future Buttermilk Island is just shallow shoals, and that some riparian vegetation growth on 14, 15, and Grafton. (REMOVE 11B)

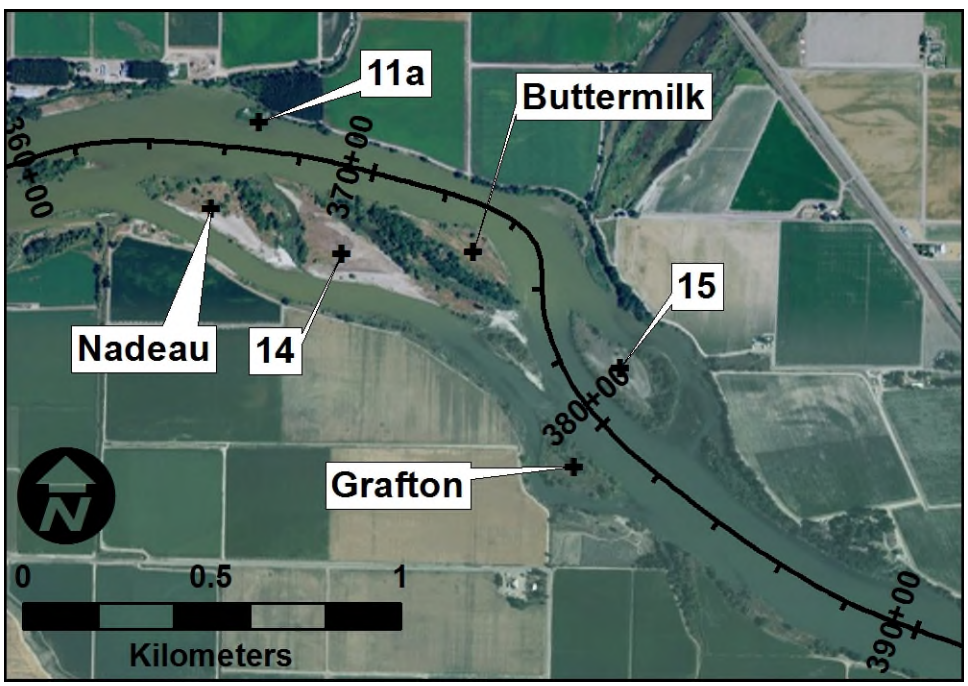

Figure D.5b. Aerial photograph taken in 2012 showing the Nadeau-Grafton Island chain. Note the growth of all islands since 1938, and the increase in riparian vegetation.

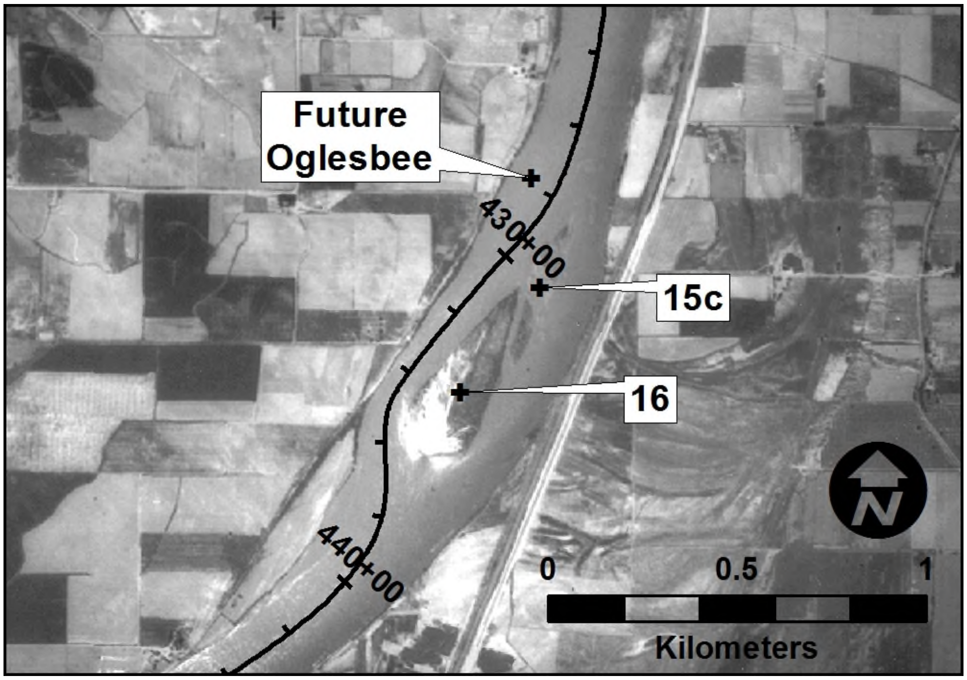

Figure D.6a. An early aerial photograph (taken on 6-10-38) showing Ketchup Island (16) and Annear Island (15c). Oglesbee Island has not yet formed.

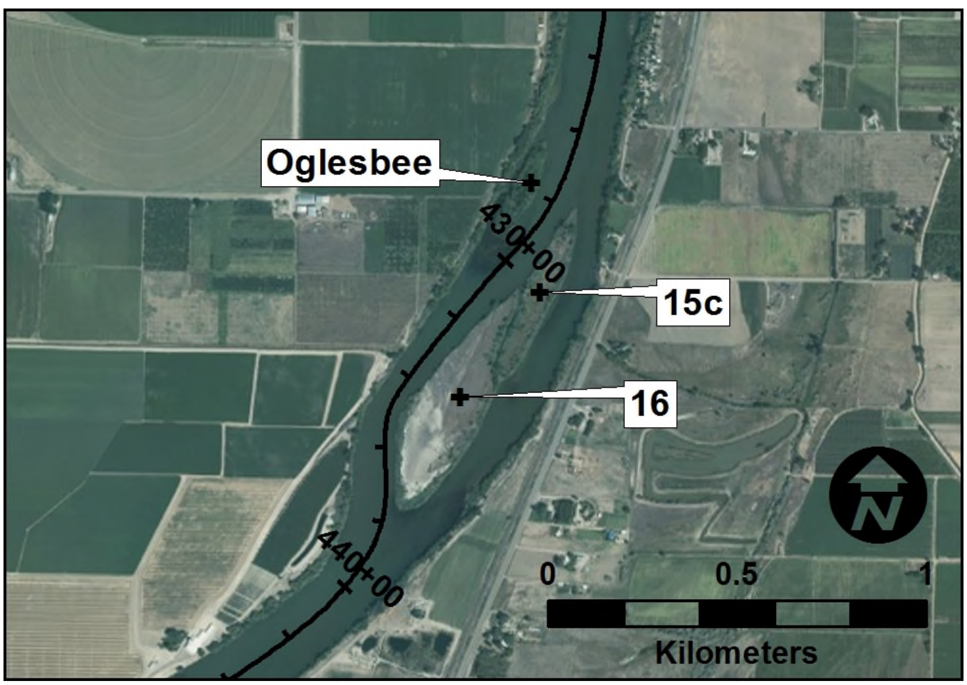

Figure D.6b. Aerial photograph taken in 2012 showing Ketchup (16), Annear (15c), and Ogelsbee Islands. Note that the upstream berm on Ketchup Island has grown, Annear Island is fully formed, and Oglesbee Island is now present.

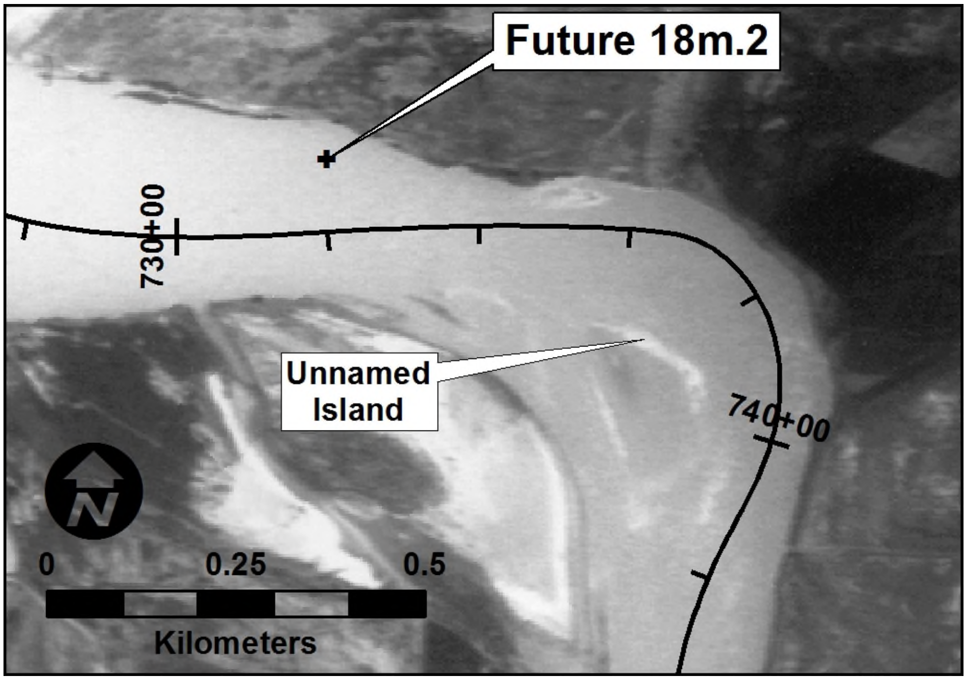

Figure D.7a. An early aerial photograph (taken on 7-6-1938) shows no island where 18m.2 currently exists, and an island forming at the apex of the upstream bend.

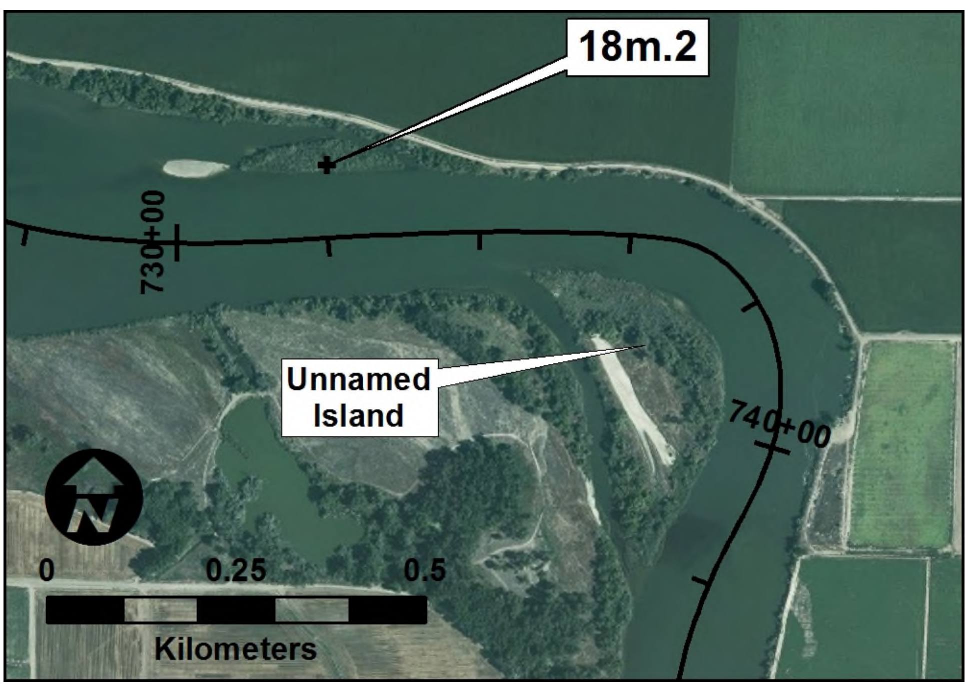

Figure D.7b. Aerial photograph taken in 2012 showing Unnamed Island (18m.2) and the island in the upstream bend fully formed.

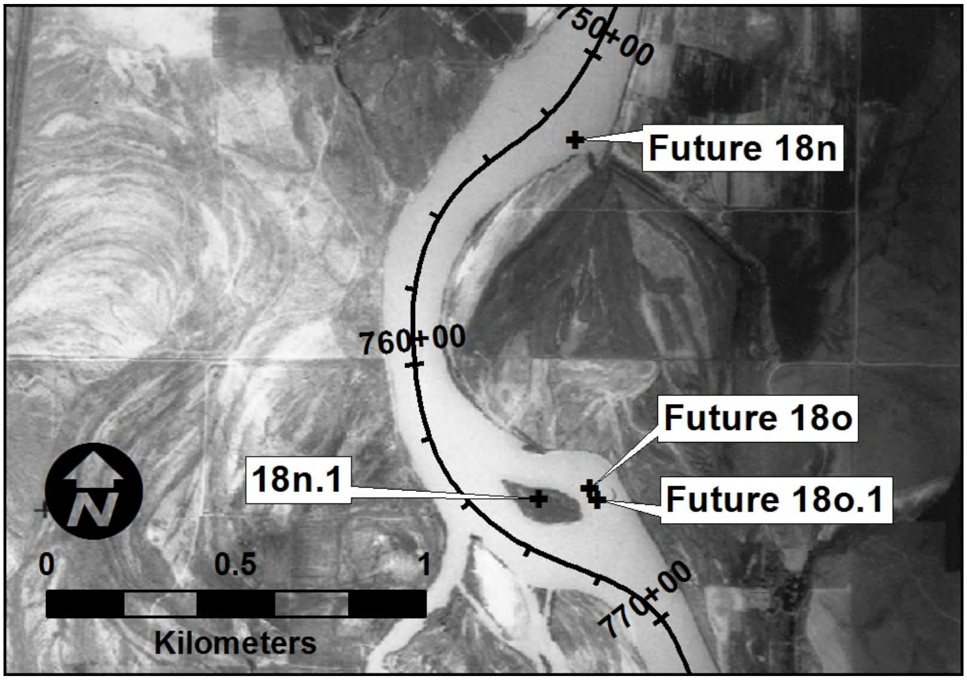

Figure D.8a. An early aerial photograph (taken 7-6-38) showing Crow Island (18n.1) and no islands at the present locations of 18n, 18o, and 18o.1.

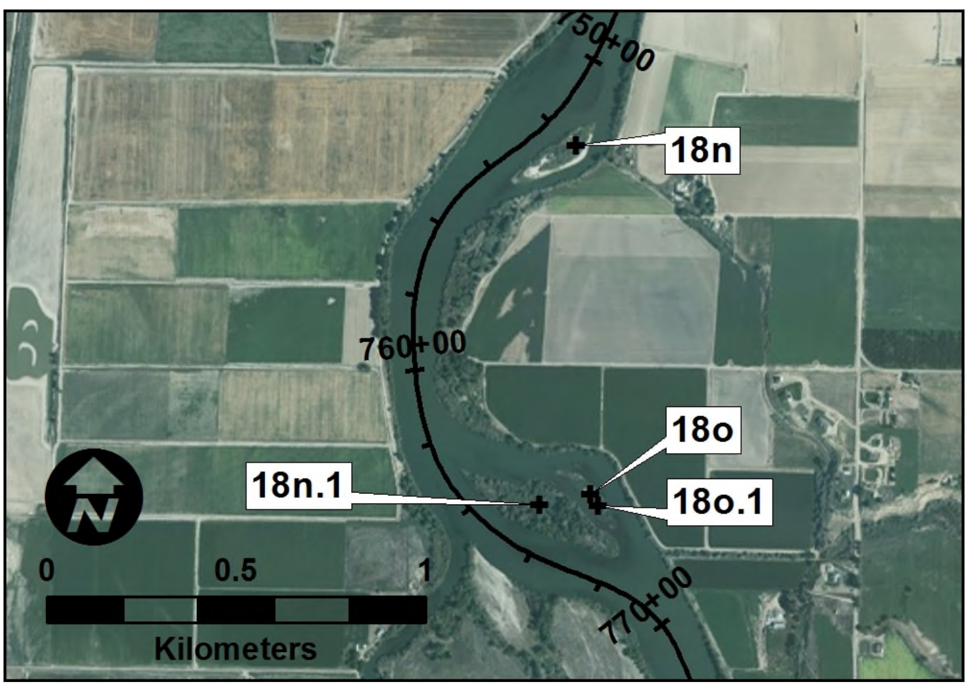

Figure D.8b. Aerial photograph taken in 2012 showing Crow Island (18n.1) and Unnamed Islands 18n, 18o, and 18o.1, now present. Note the upstream growth of Crow Island (18n.1).

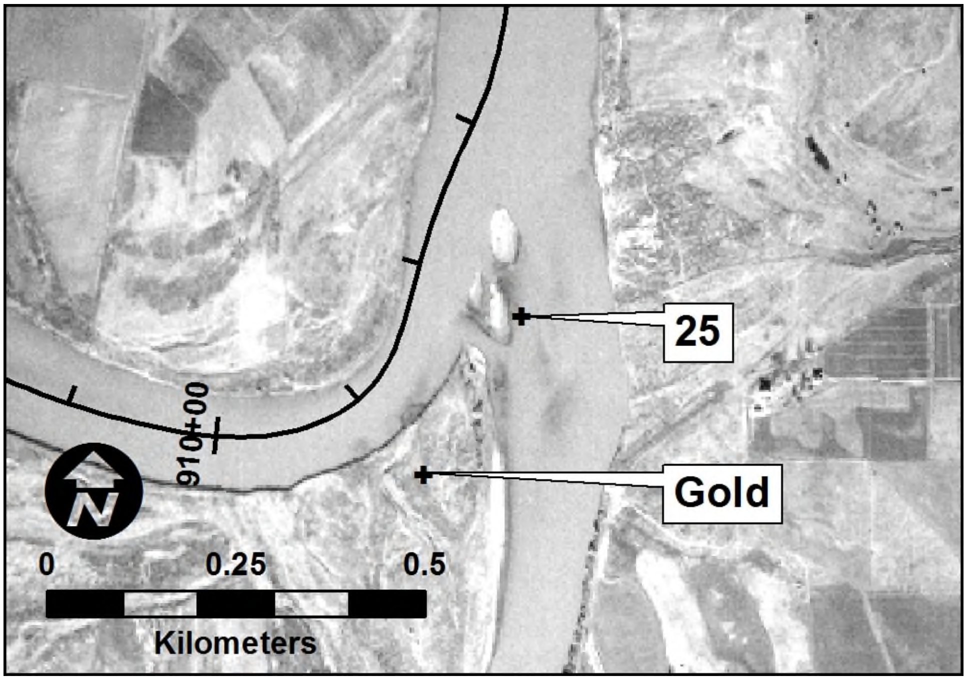

Figure D.9a. An early aerial photograph (taken on 7-6-38) showing the downstream end of Gold Island and the Ross Island (25) as shoals.

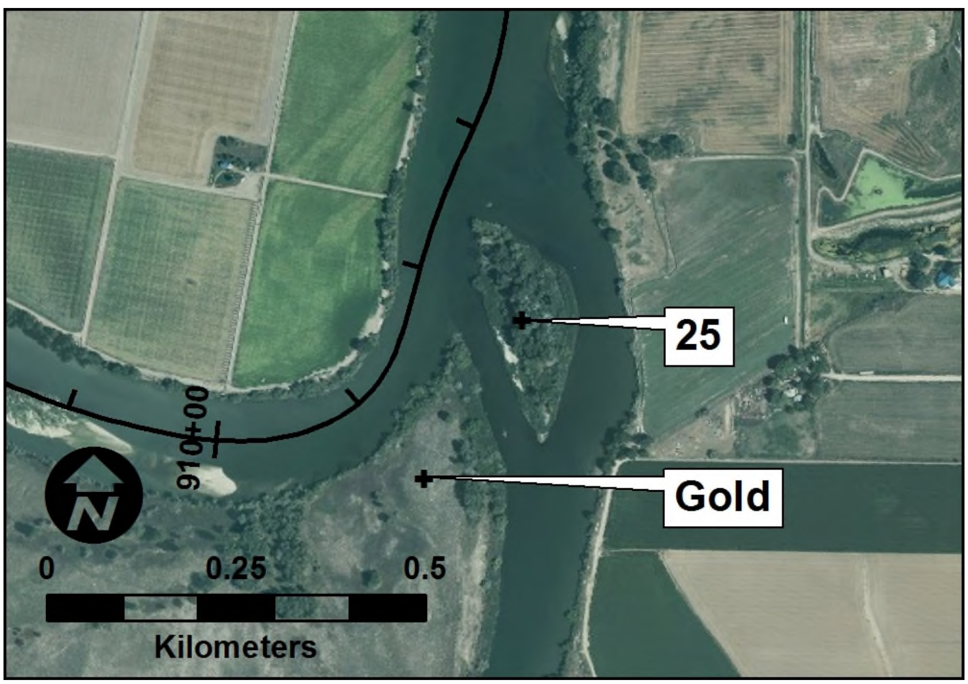

Figure D.9b. Aerial photograph taken in 2012 showing the downstream end of Gold Island and the fully-formed Ross Island (25).

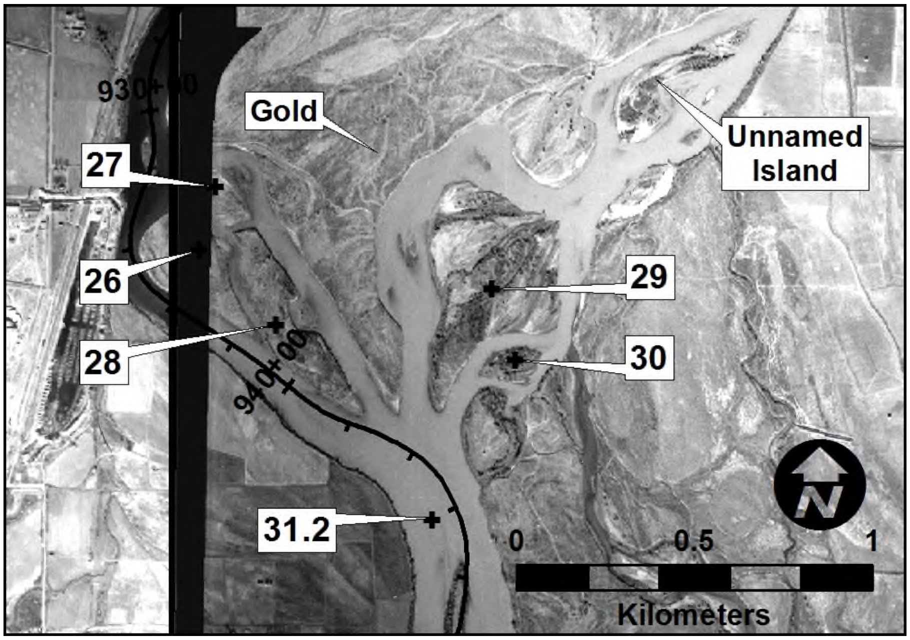

Figure D.10a. An early aerial photograph (taken on 11-6-38) showing the confluence of the Boise River, Big Cottonwood (28), Heron (29). Note the riparian vegetation on Heron (29), Ross (30), and the Unnamed Island, and the ridges of sediment on Ross showing sequential accretion. No island is shown at the location of the largest island in the current Boise Group (31.2).

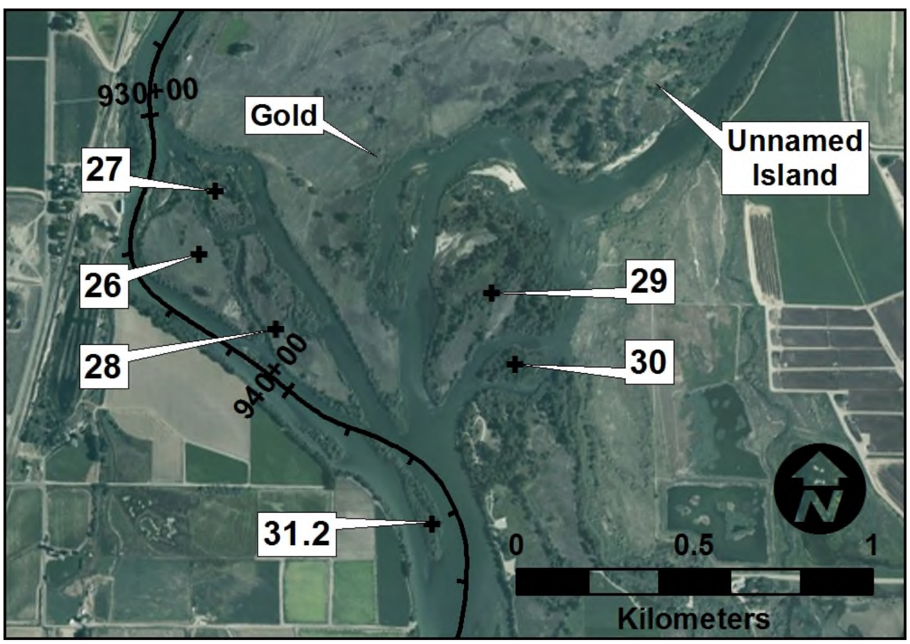

Figure D.10b. Aerial photograph taken in 2012 showing the channel downstream of the confluence with the Boise River, and the upstream end of Big Cottonwood (28), Gold, and Heron (29) Islands. The Boise Group (31.2) in its present location is also shown. Note the change in channel geometry downstream of Heron Island (29) and the increase in riparian vegetation.

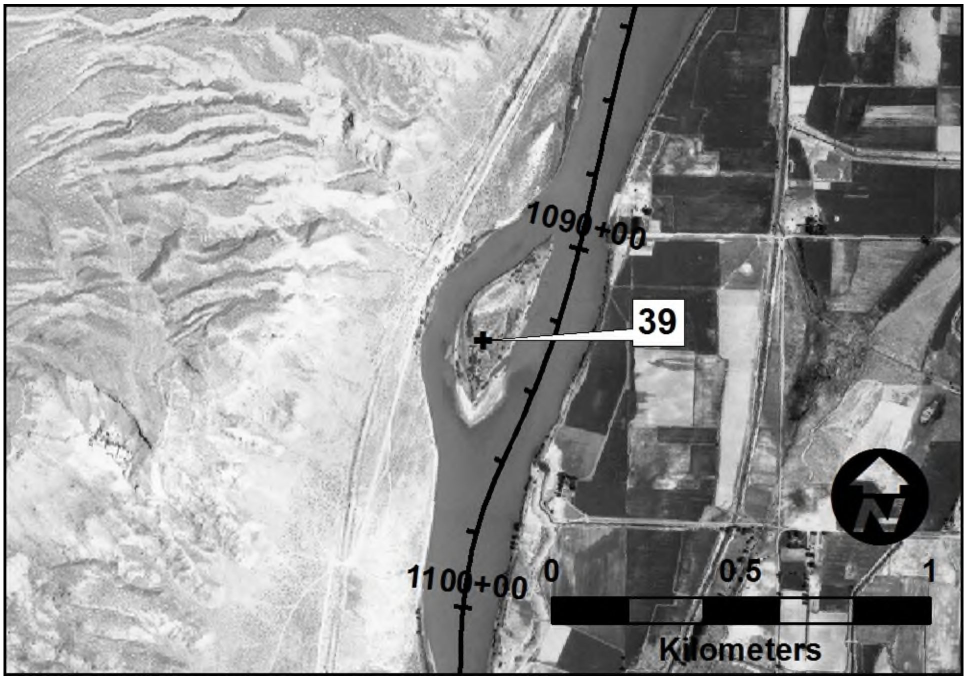

Figure D.11a. An early aerial photograph (taken on 5-27-39) of Suzy Island (39). Note exposed sediment on the upstream berm and erosional edges along the downstream end of the island

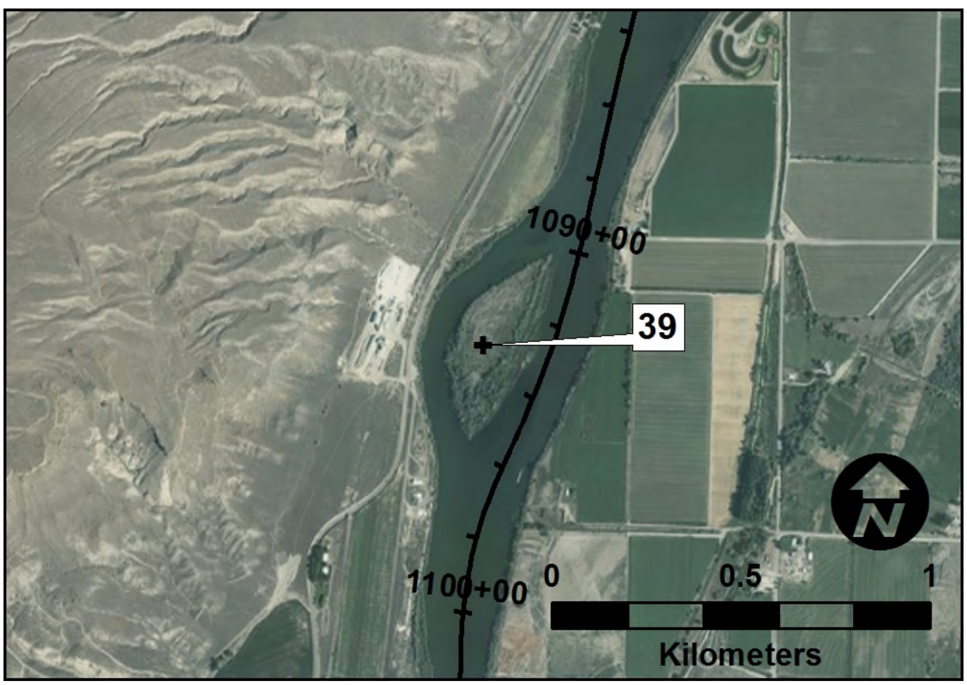

Figure D.11b. Aerial photograph taken in 2012 showing Suzy Island (39). Note upstream berm growth, minor lateral berm growth, and riparian vegetation increase.

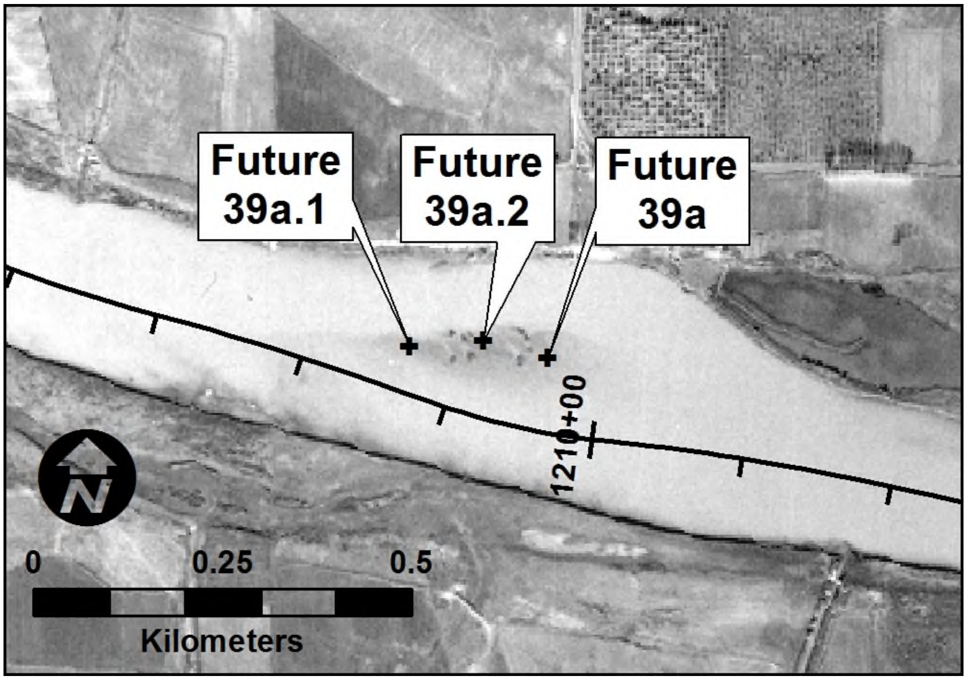

Figure D.12a. An early aerial photograph (taken on 11-6-38). Shoals and gravel bars are present at the current location of the Tule Island Group (39a, 39a.1, and 39a.2).

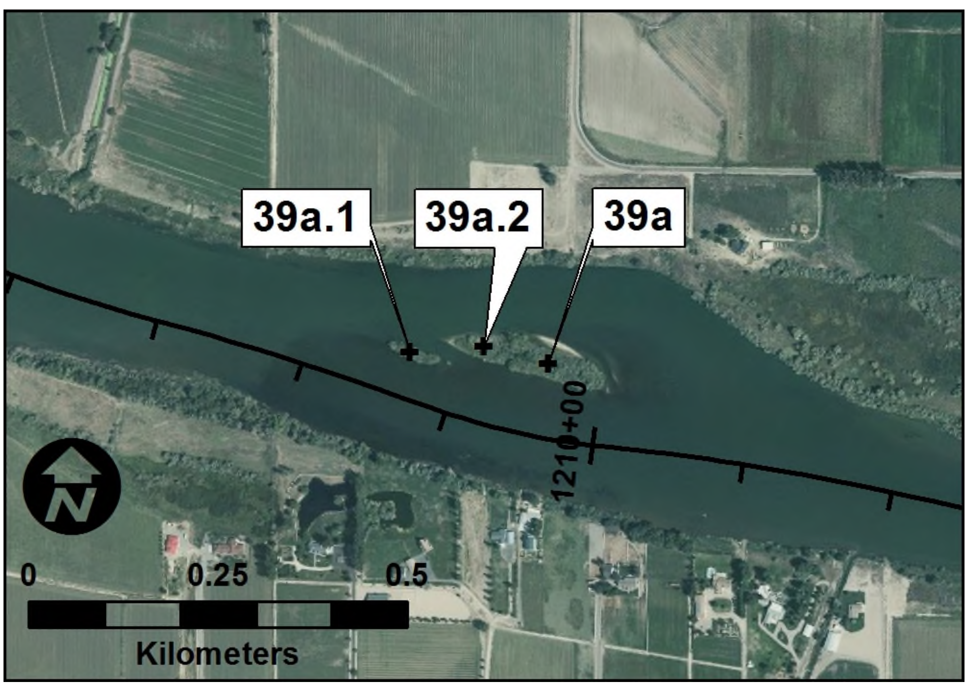

Figure D.12b. Aerial photograph taken in 2012 showing the current Tule Group (39a, 39a.1, and 39a.2).

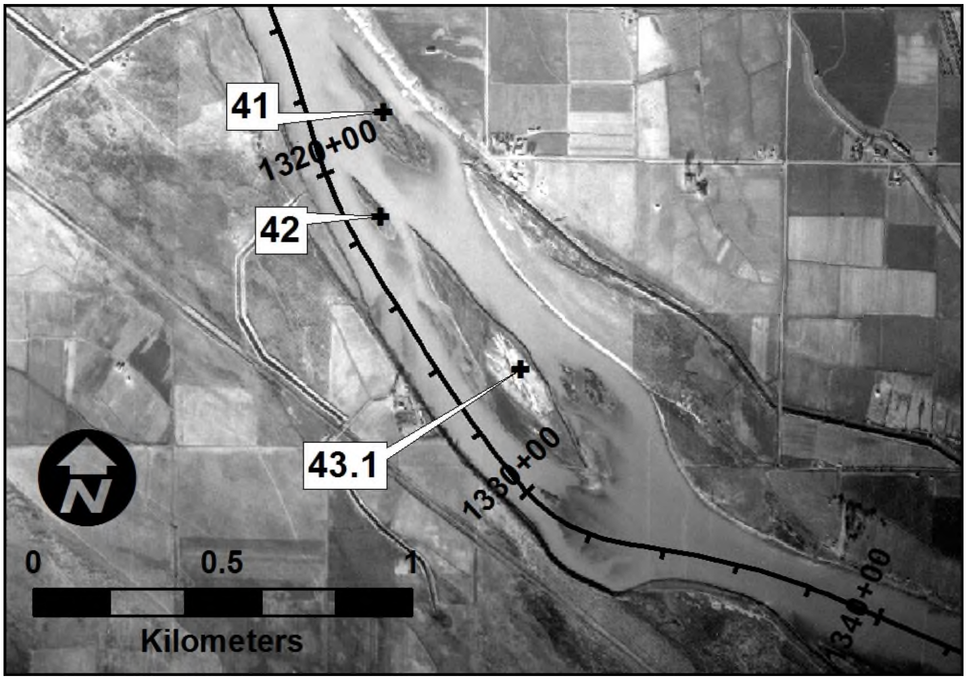

Figure D.13a. An early aerial photograph (taken on 11-6-38) of the Rabbit Island chain [Homedale (41), Wegman (42), Rabbit (43.1), and smaller islands and shoals]. Note the erosional edge around the high core of Rabbit Island

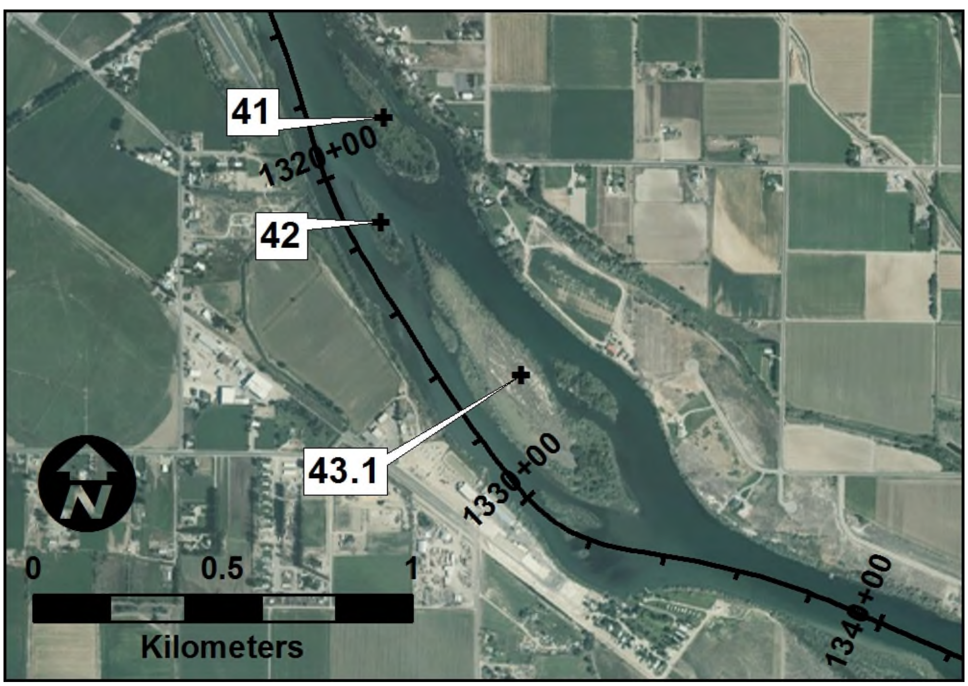

Figure D.13b. Aerial photograph taken in 2012 showing the Rabbit Island chain. Note the increase in the number of smaller islands and in the lateral berm around Rabbit Island (43.1). Also note the increase in riparian vegetation.

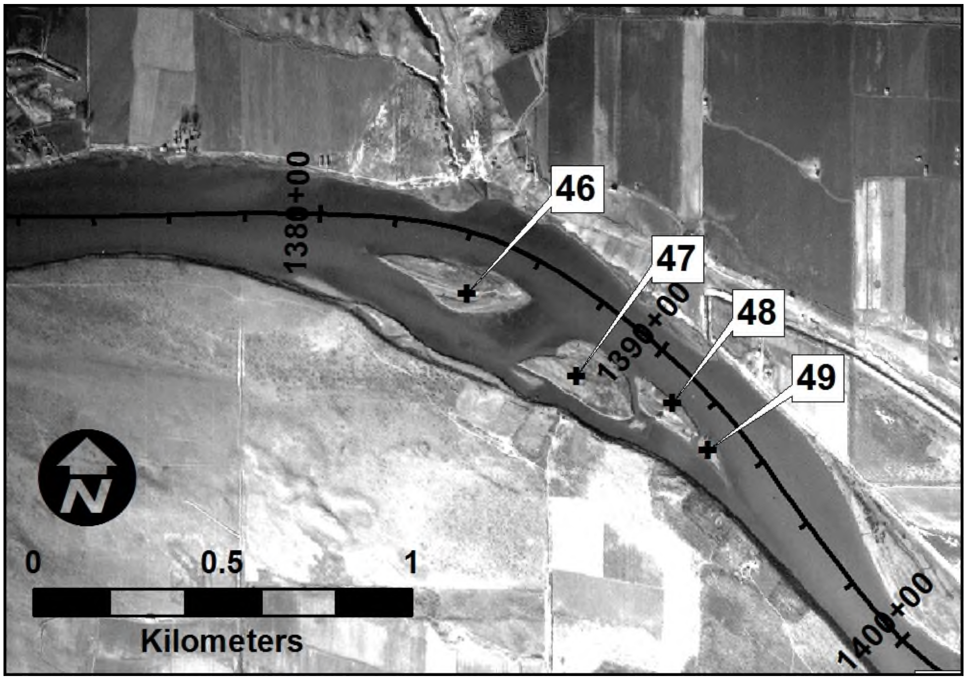

Figure D.14a. An early aerial photograph (taken on 11-18-38) of the Feral/Pheasant Island chain (46-49). Note the erosional edge on Pheasant Island #2 (47), and the lack of vegetated berms on all islands.

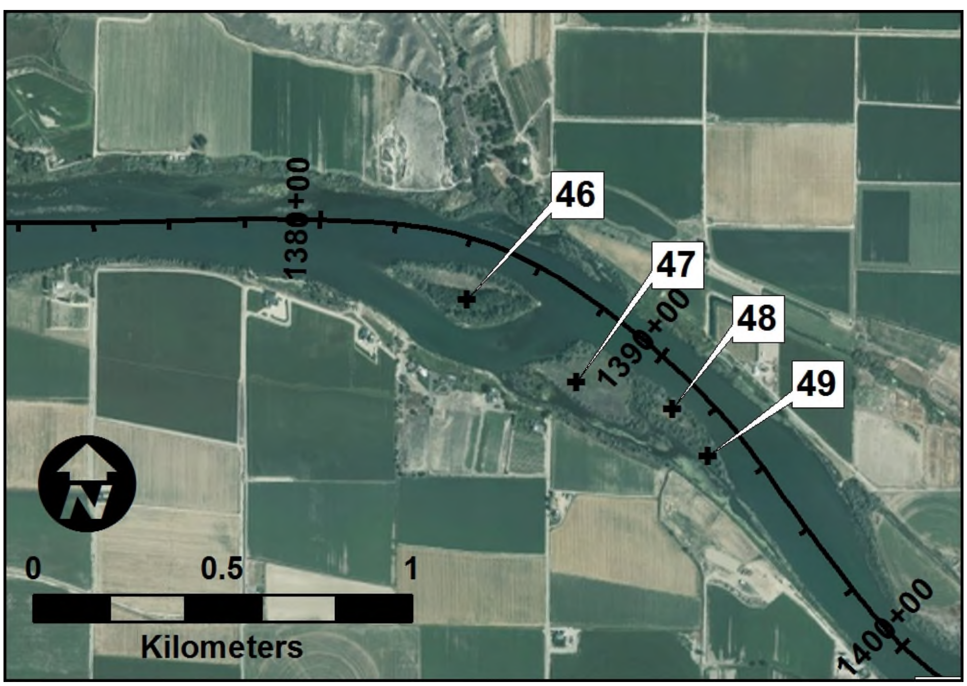

Figure D.14b. Aerial photograph taken in 2012 showing the Feral/Pheasant Island chain (46-49). Note the growth of berms around each island and the increase in riparian vegetation on the berms.

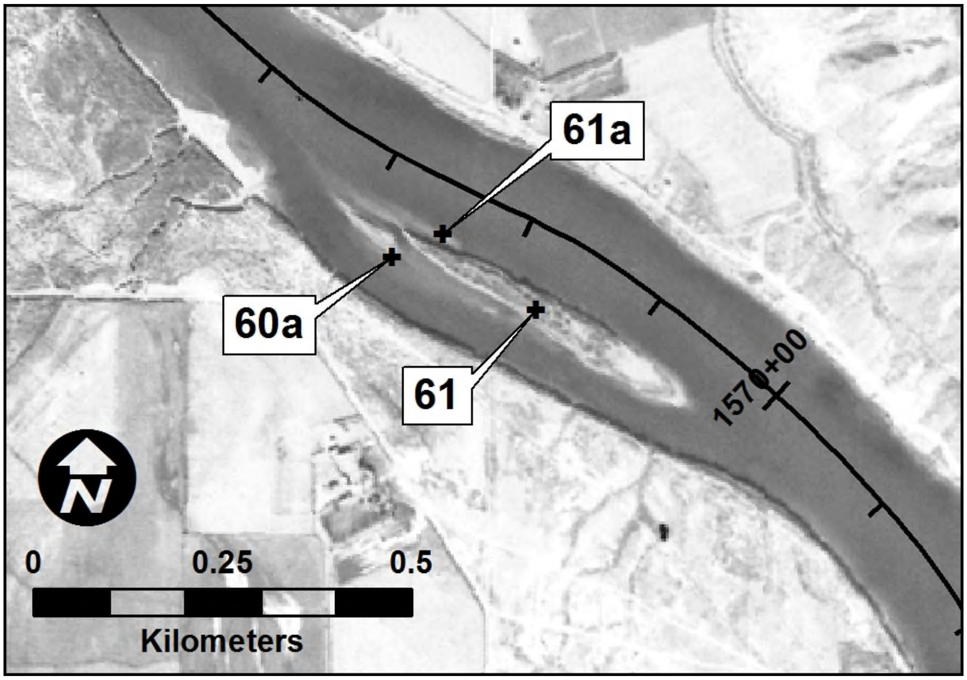

Figure D.15a. An early aerial photograph (taken on 11-27-38) of Cottontail Island (61) and smaller surrounding islands (60a and 61a).

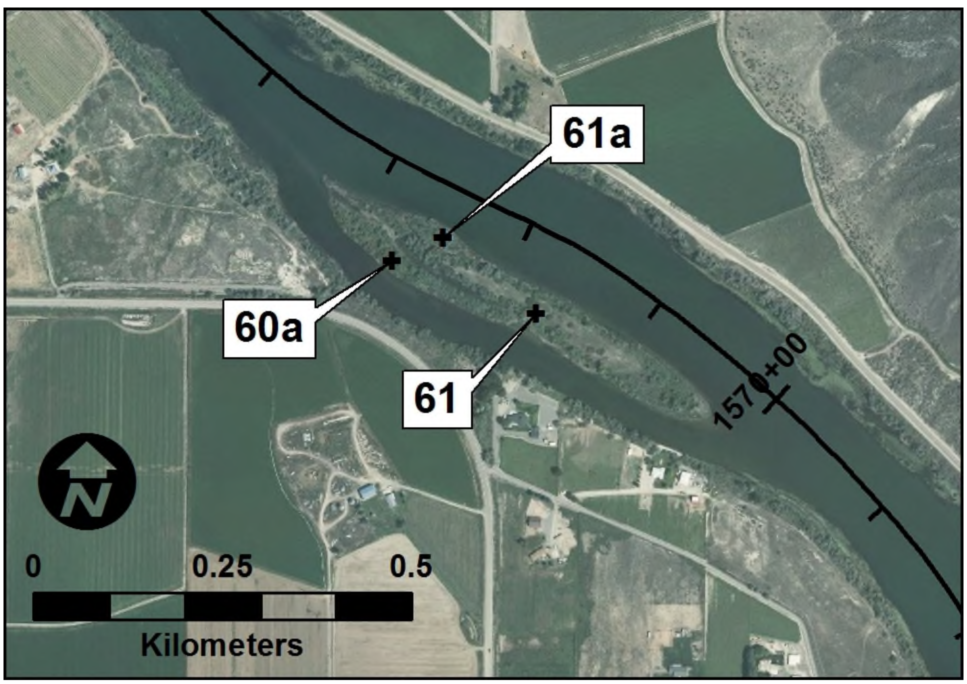

Figure D.15b. Aerial photograph taken in 2012 showing Cottontail Island (61). Note that island 61a has formed and 60a is much larger. Cottontail Island has experienced berm growth, and some erosion of the higher core, especially at the upstream end.

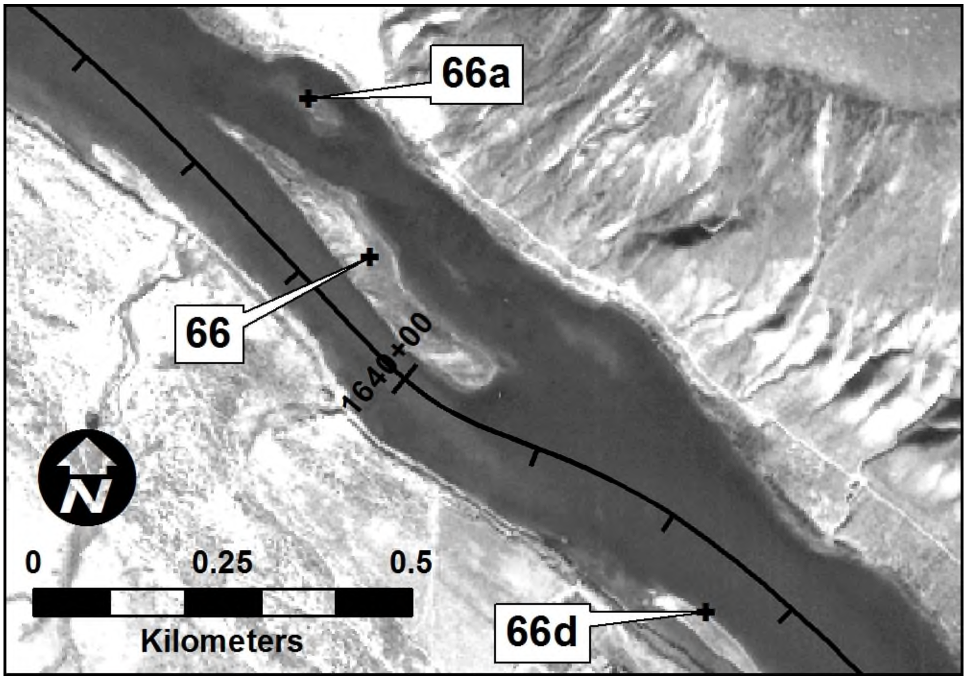

Figure D.16a. An early aerial photograph (taken on 7-31-39) showing Raccoon Island (66) and shoals at the present location of Island 66a.

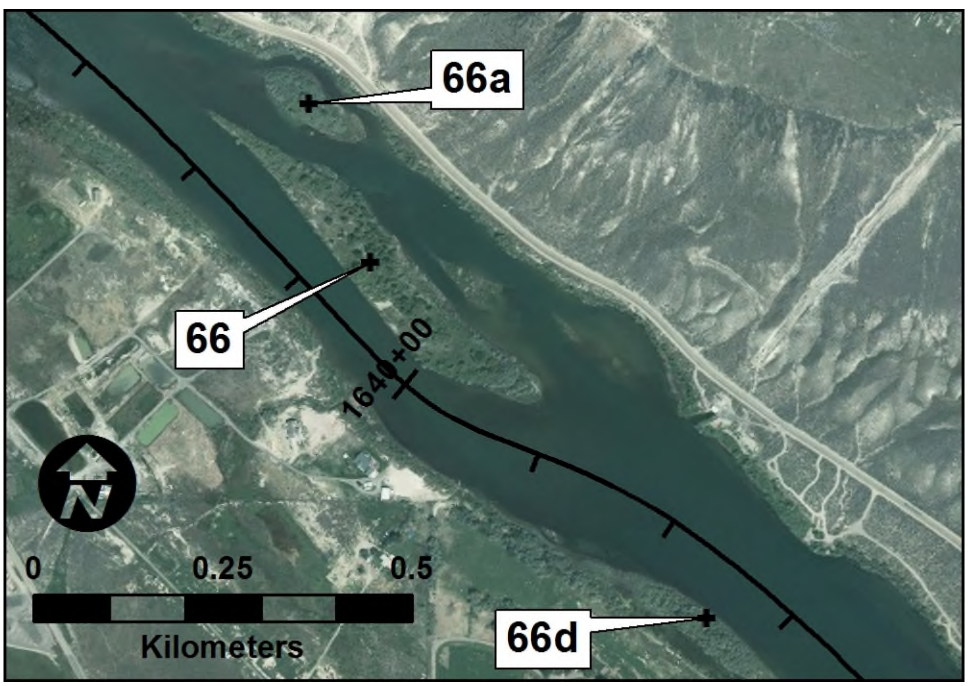

Figure D.16b. Aerial photograph taken in 2012 showing Raccoon Island (66) and Unnamed Island (66a). Note the merger of the two islands now making up Raccoon Island and the growth of the upstream berm.

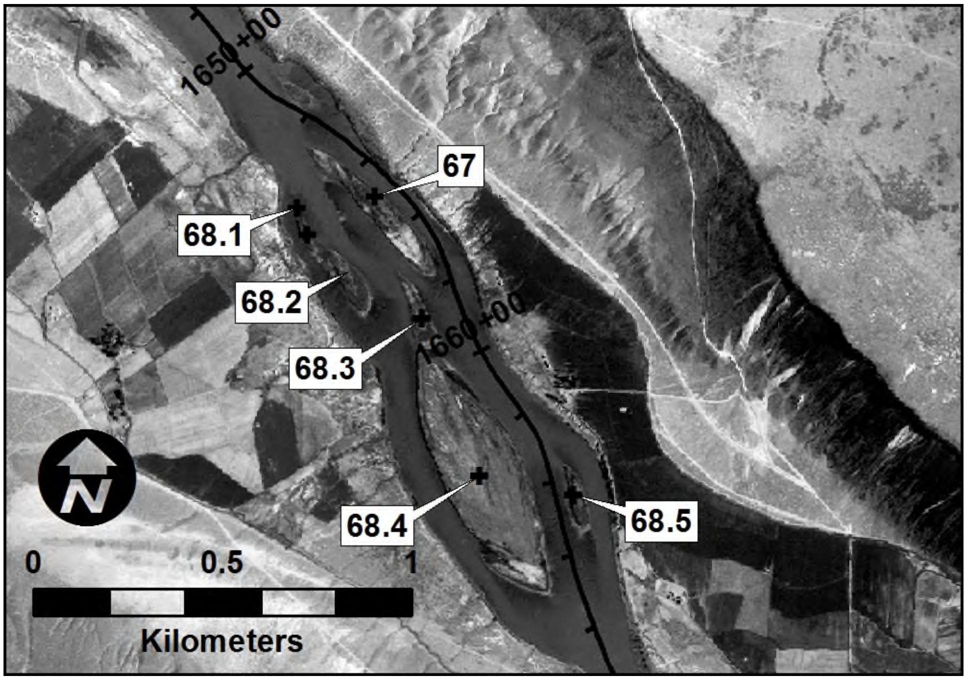

Figure D.17a. An early aerial photograph (taken on 7-23-39) of the Rippee/Hermit Island Group (67 through 68.5).

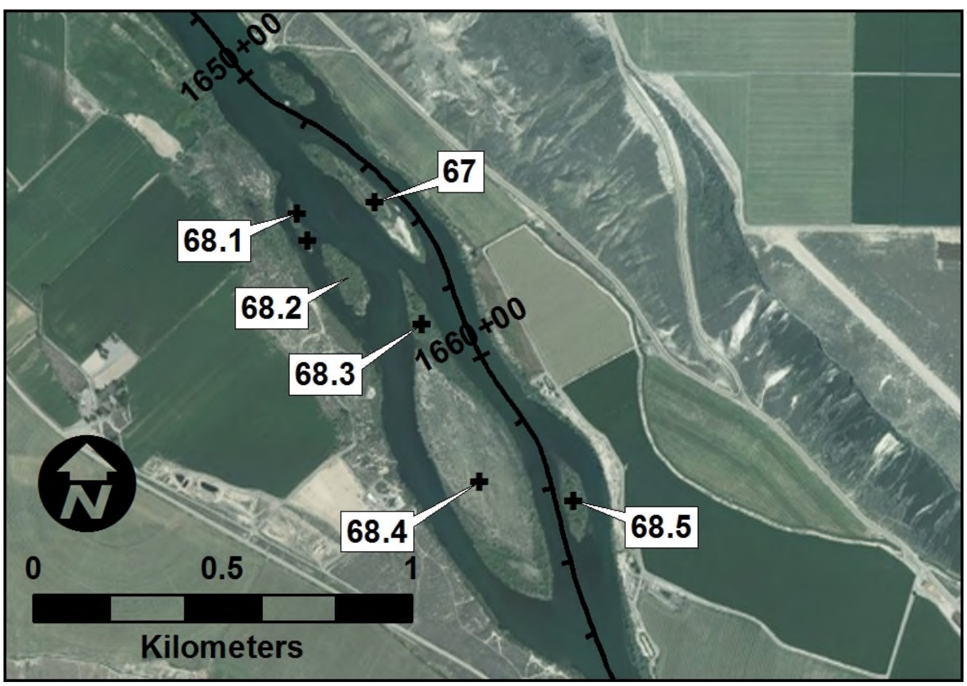

Figure D.17b. Aerial photograph taken in 2012 showing the Rippee/Hermit Group (67 through 68.5). Note the moderate increase in riparian vegetation, and the erosion of the core of Hermit Island (67).

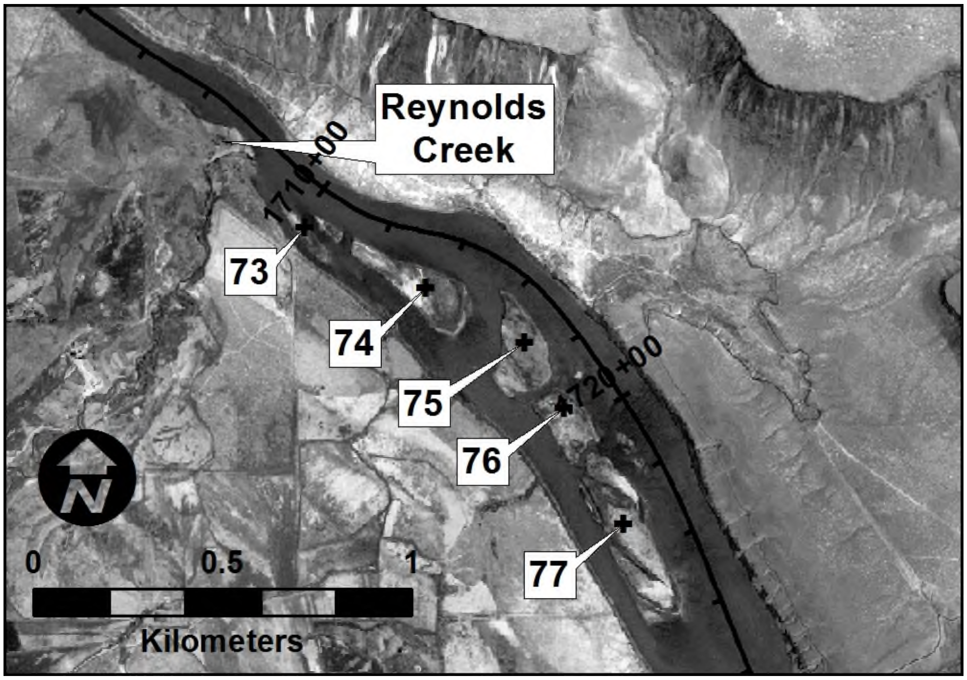

Figure D.18a. An early aerial photograph (taken on 7-23-39) of the Papike Chain: Papike (77), Becky (76), Argy (75), Bayha (74), and Wright (73) Islands.

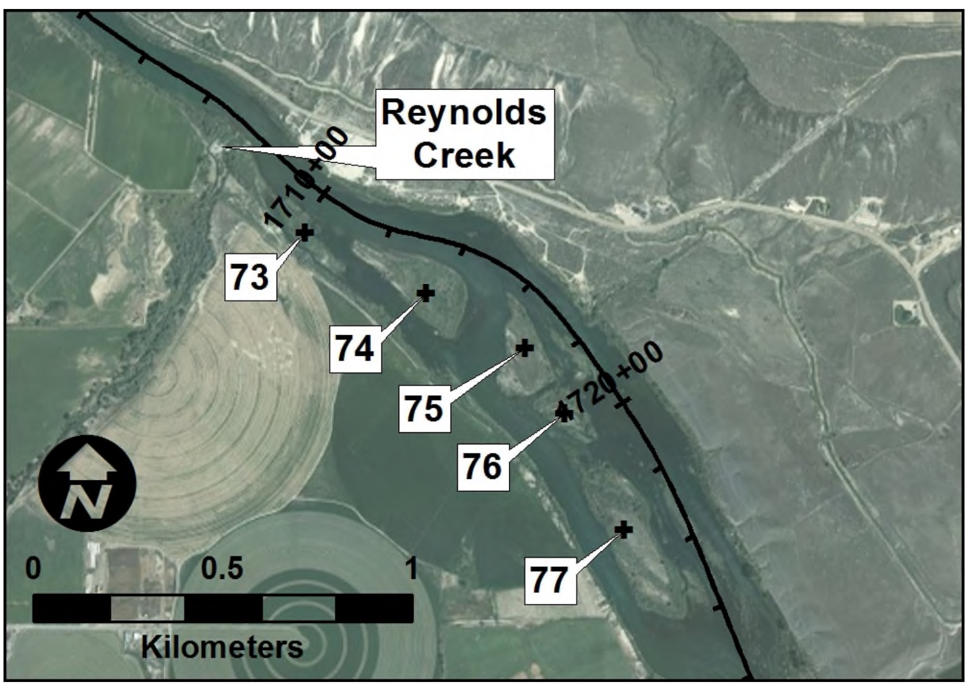

Figure D.18b. Aerial photograph taken in 2012 showing the Papike Chain (73 through 77). Note the addition to Papike (77), the erosion of Becky (76), the erosion of the downstream end of Bayha (74), and the removal of the island downstream of Bayha (74).

APPENDIX E – Soil Profiles

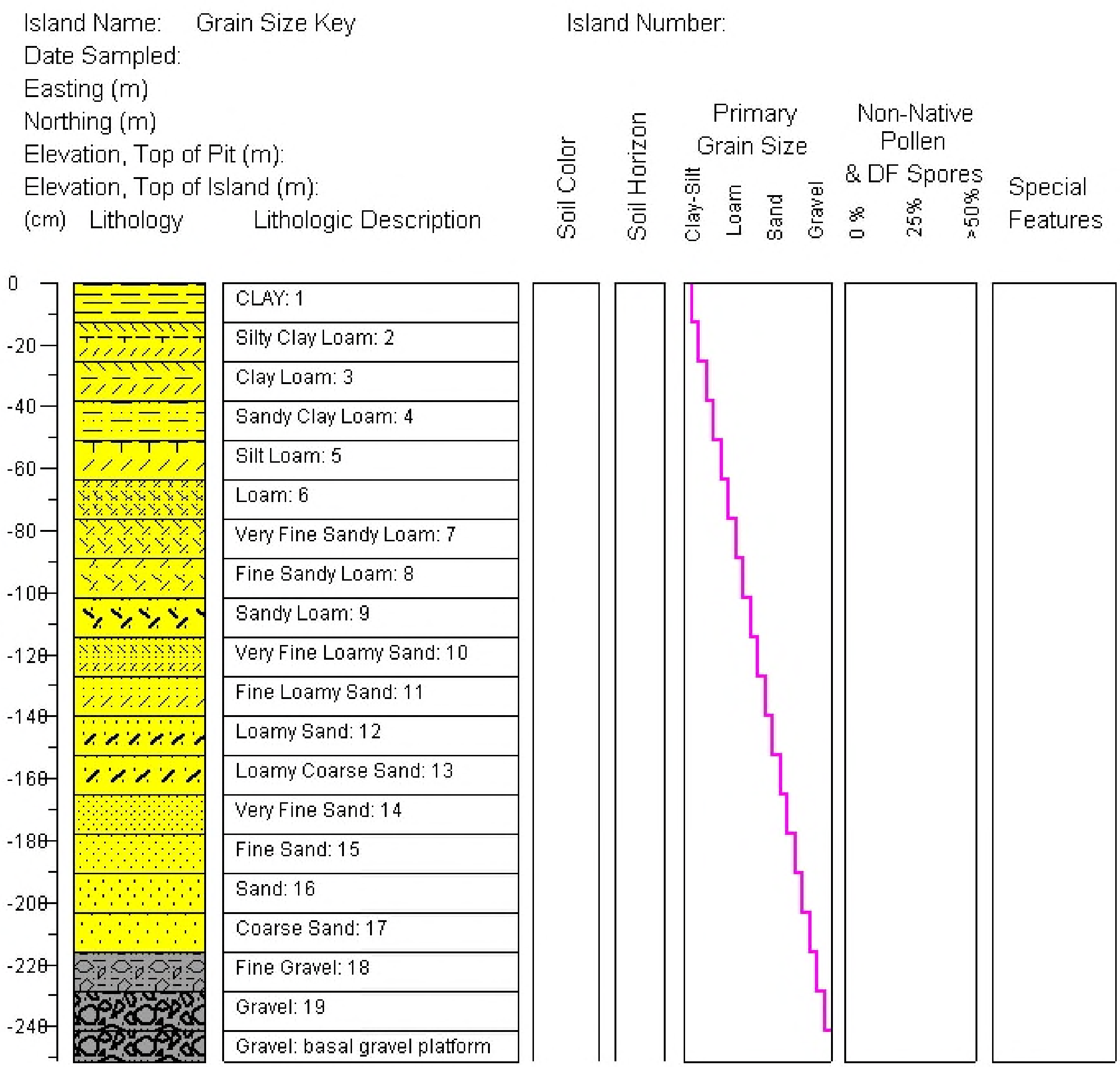

Figure E1. Grain-size Key.

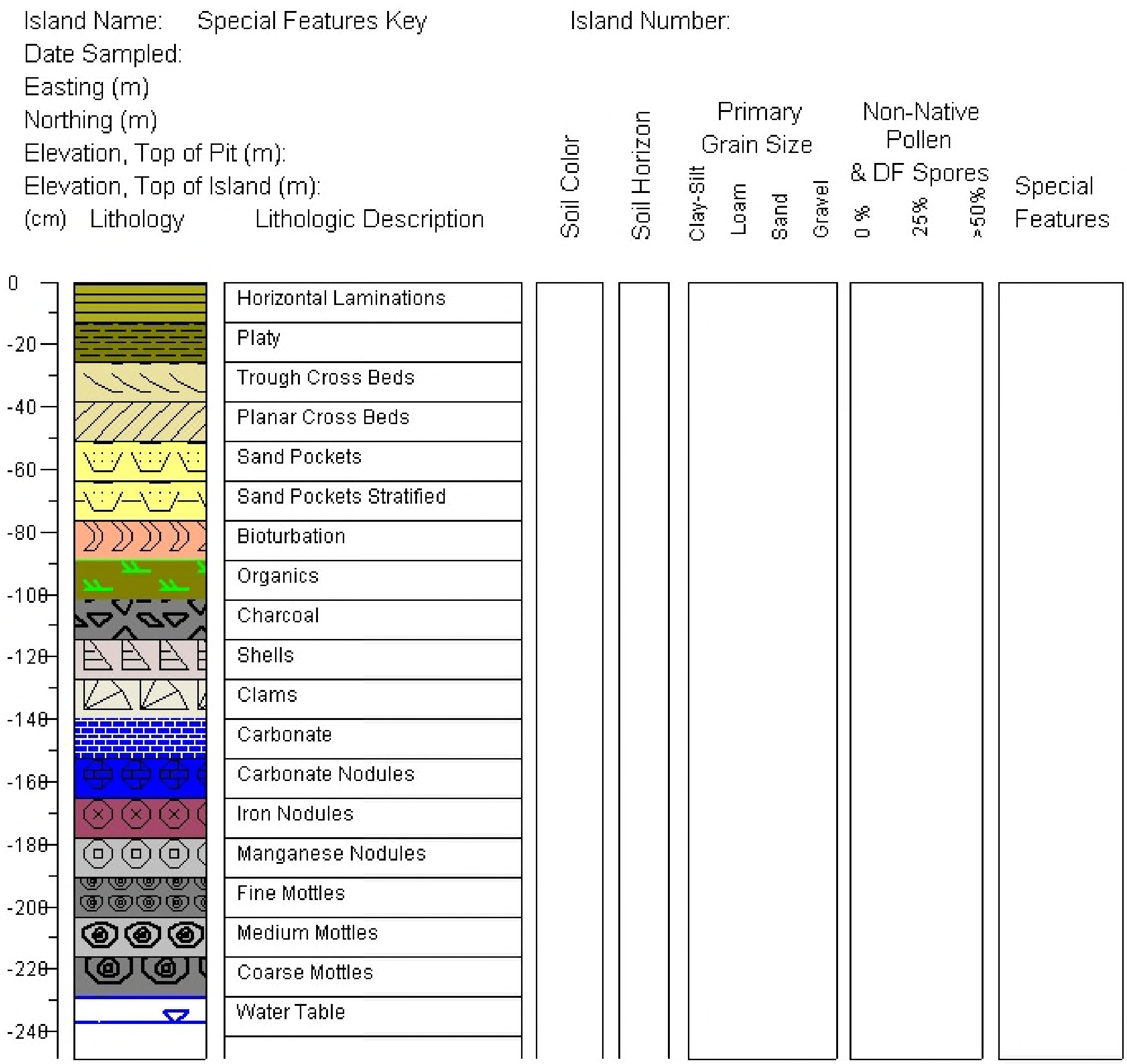

Figure E2. Special Features Key.

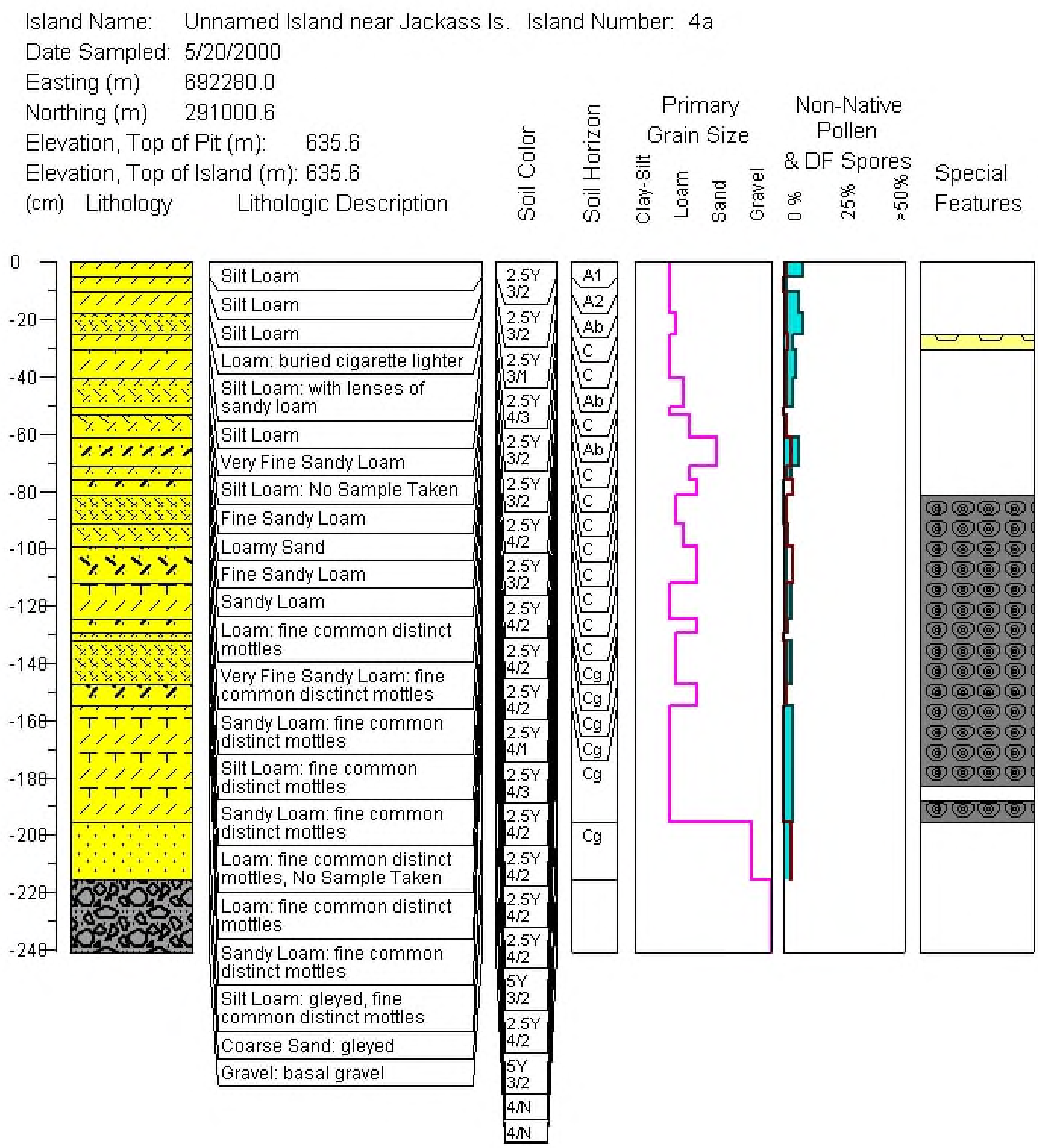

Figure E3. Unnamed Island near Jackass Island (4a) soil profile.

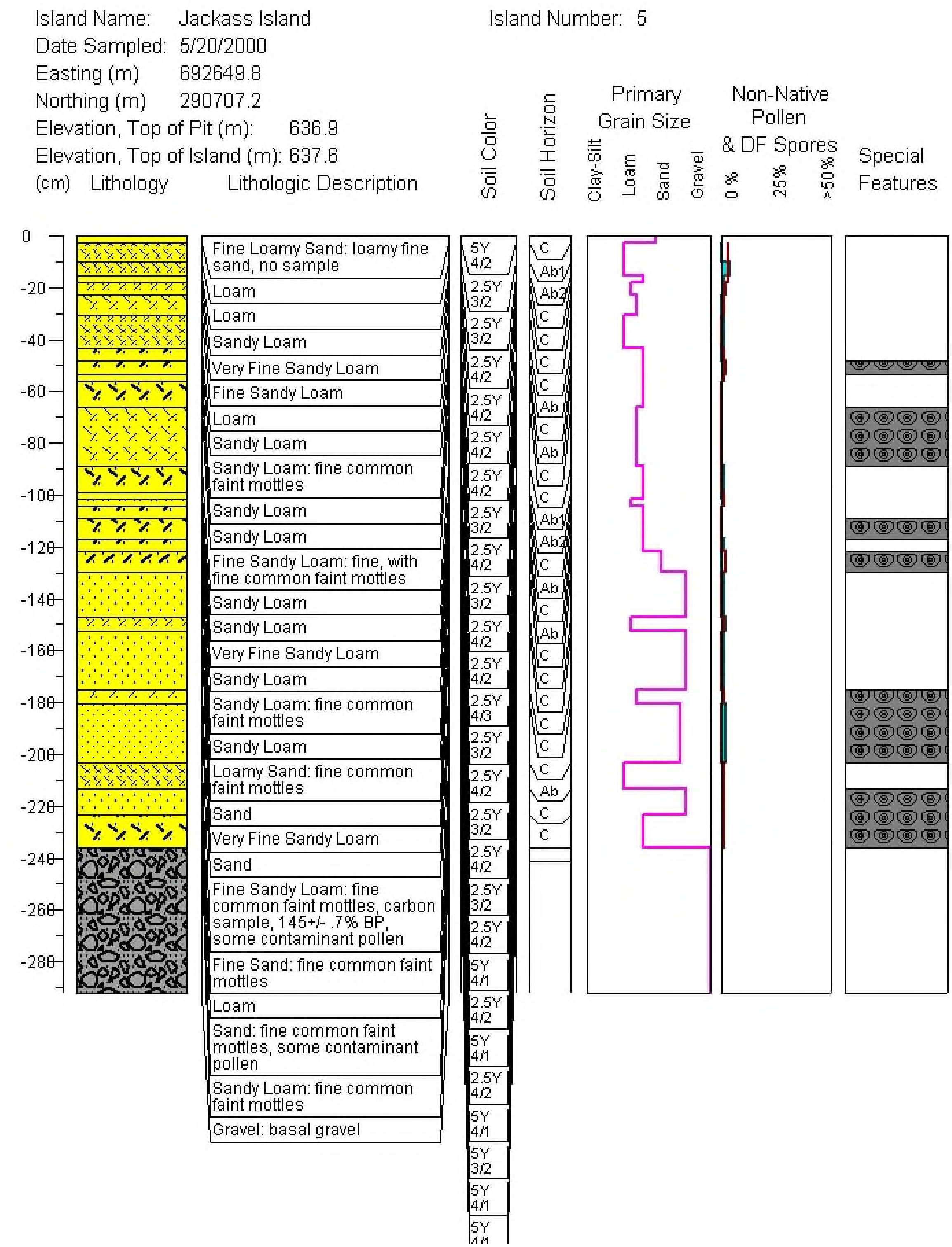

Figure E4. Jackass Island (5) soil profile.

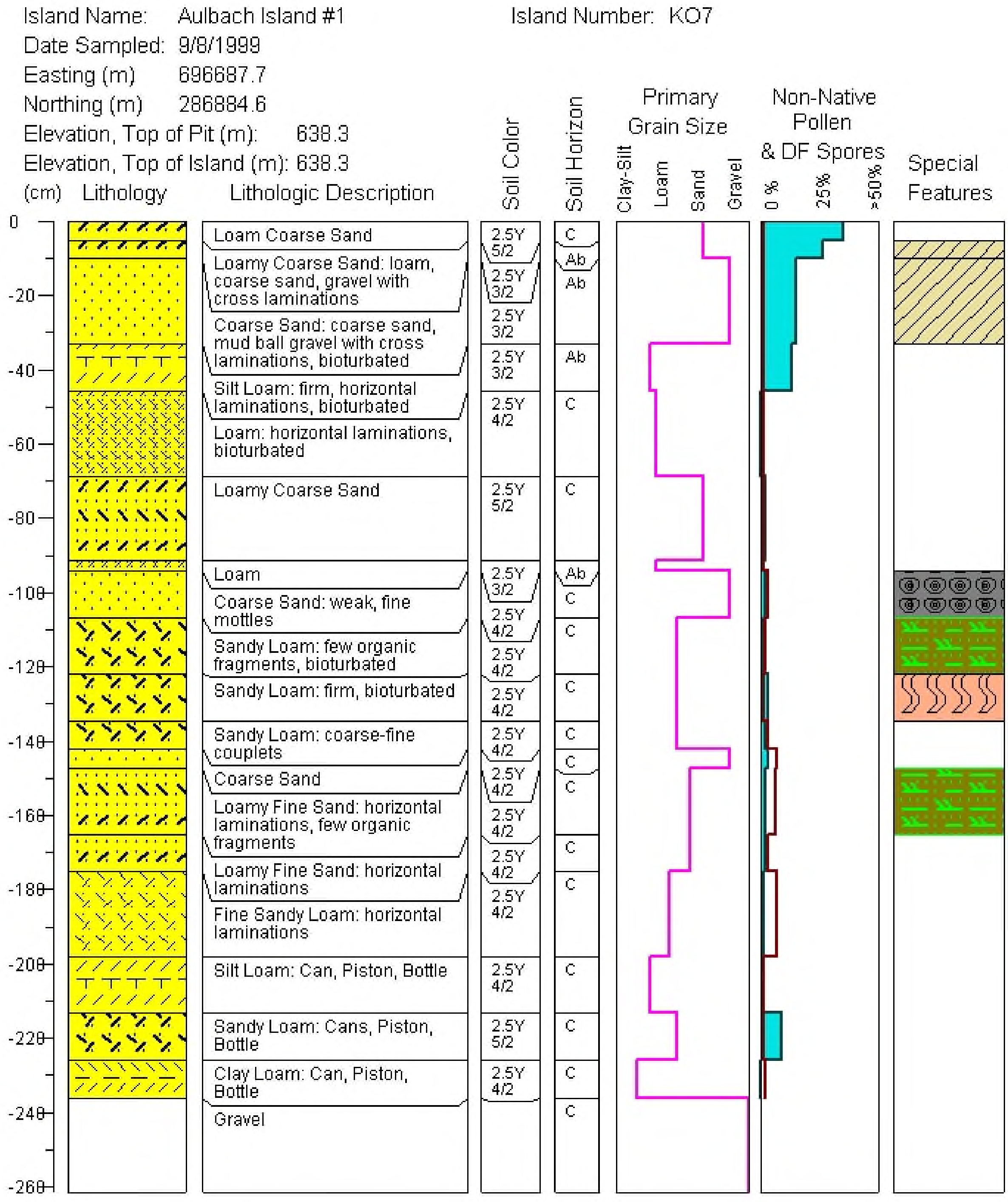

Figure E5. Aulbach Island #1 (KO7) soil profile.

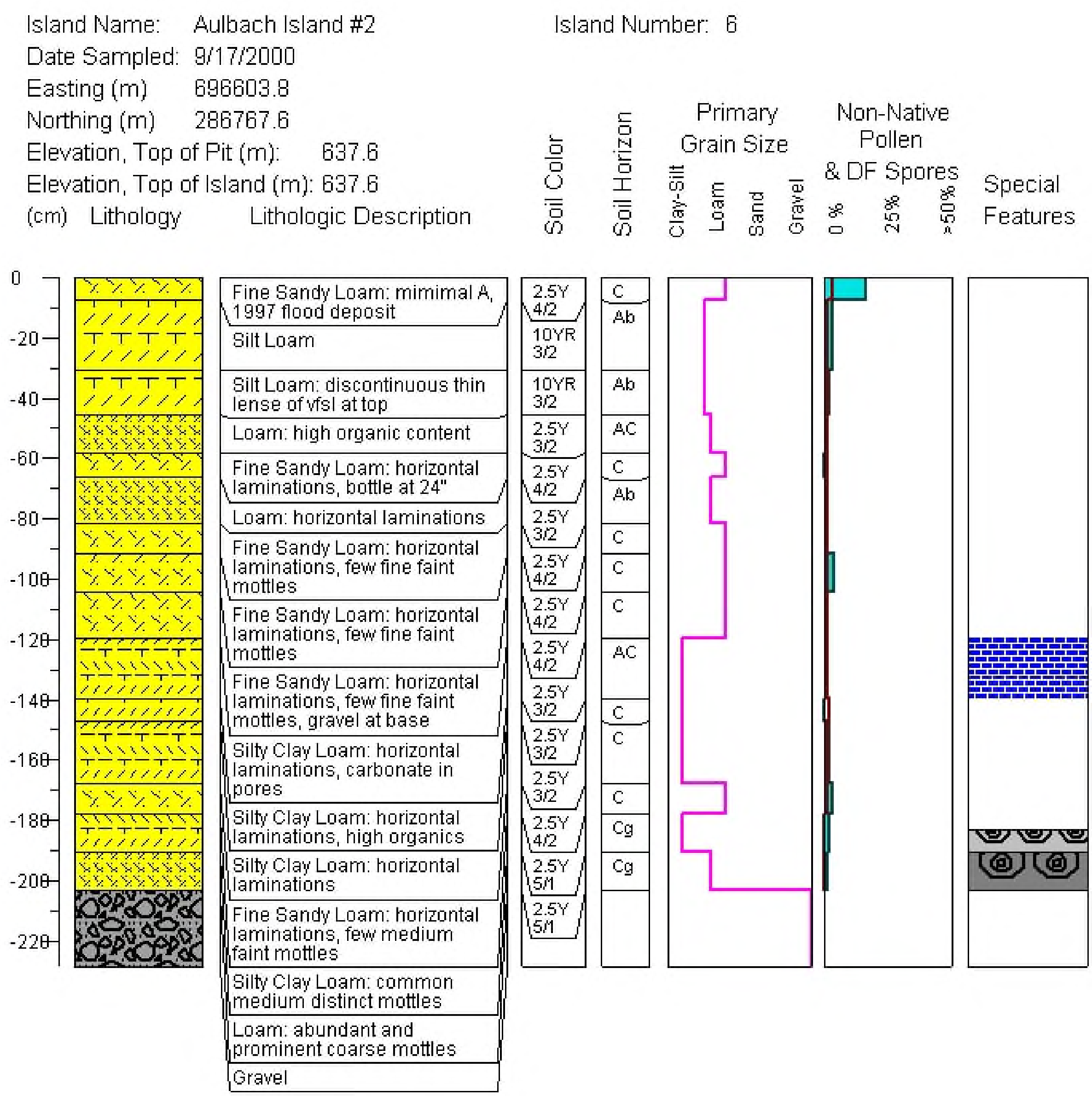

Figure E6. Aulbach Island #2 (6) soil profile.

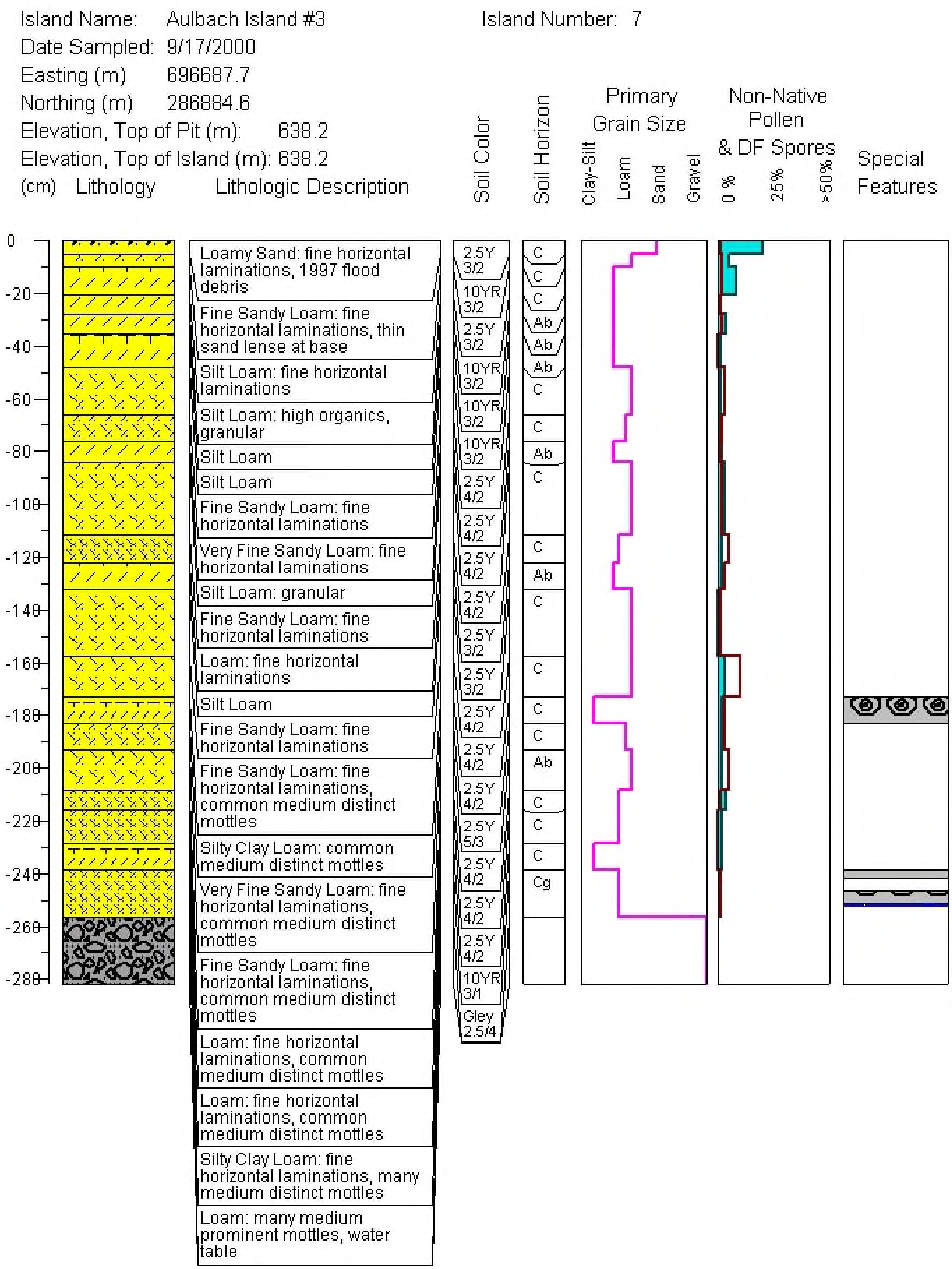

Figure E7. Aulbach Island #3 (7) soil profile.

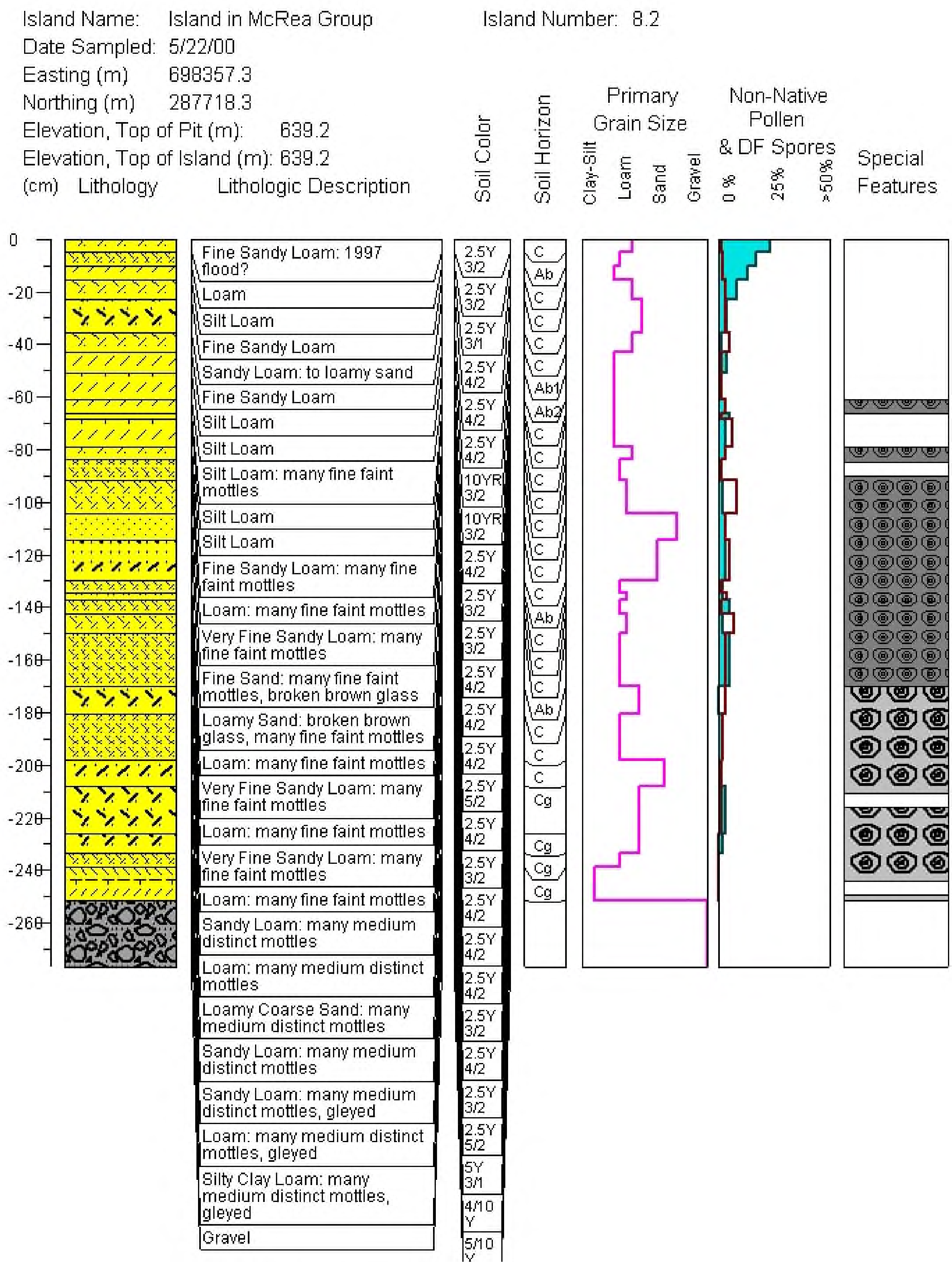

Figure E8. Island in McRea Group (8.2) soil profile.

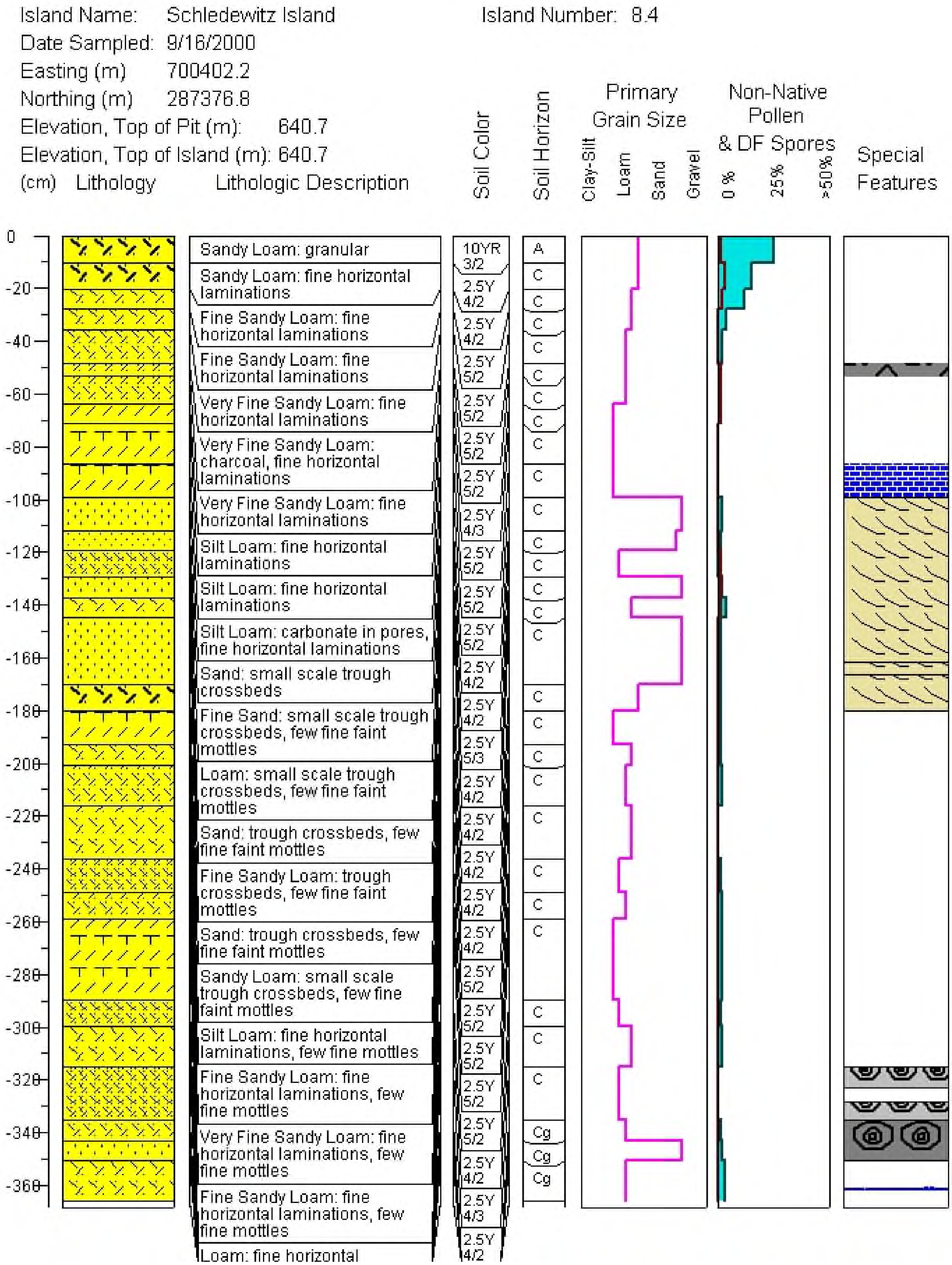

Figure E9. Schledewitz Island (8.4) soil profile.

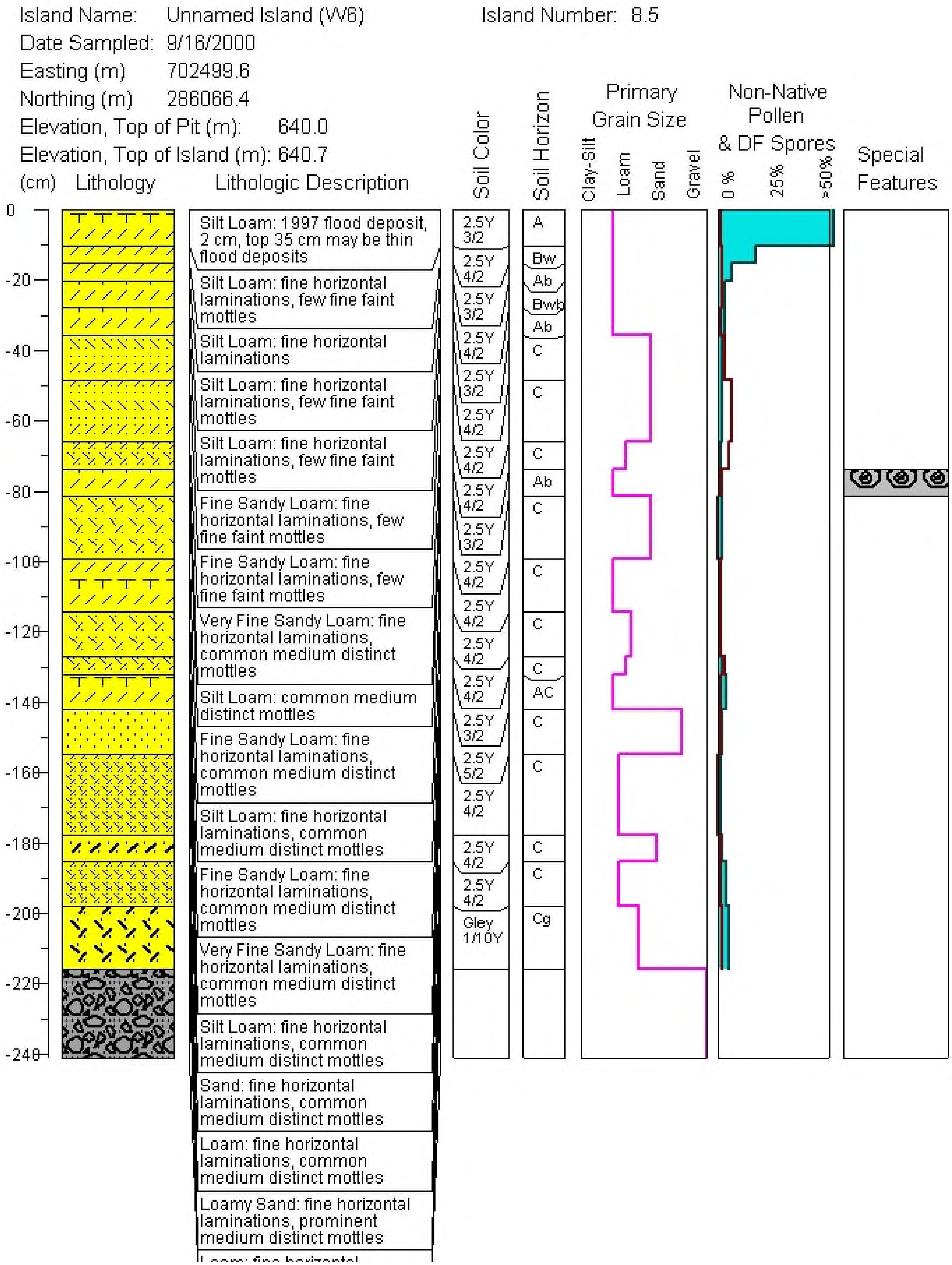

Figure E10. Unnamed Island, W6 (8.5) soil profile.

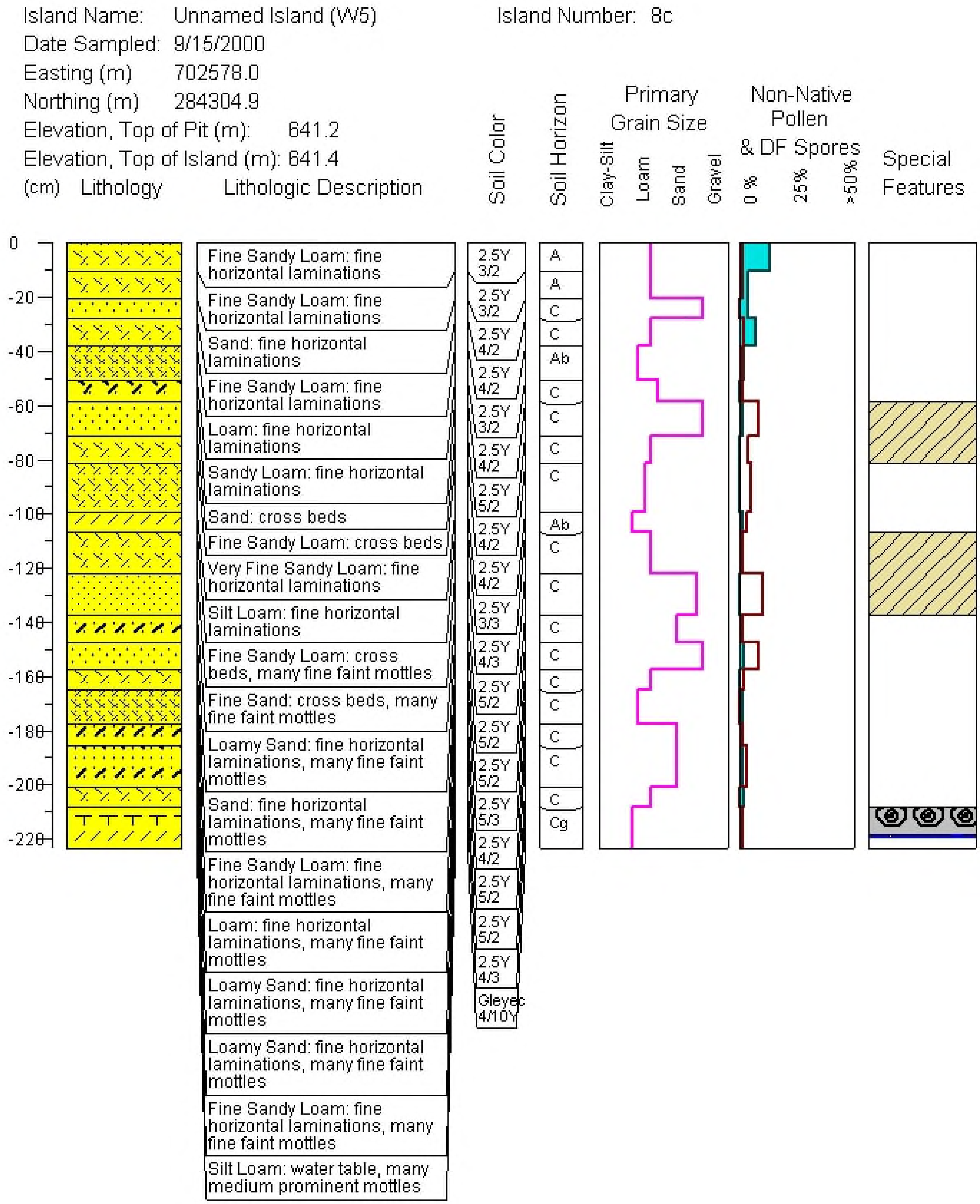

Figure E11. Unnamed Island, W5 (8C) soil profile.

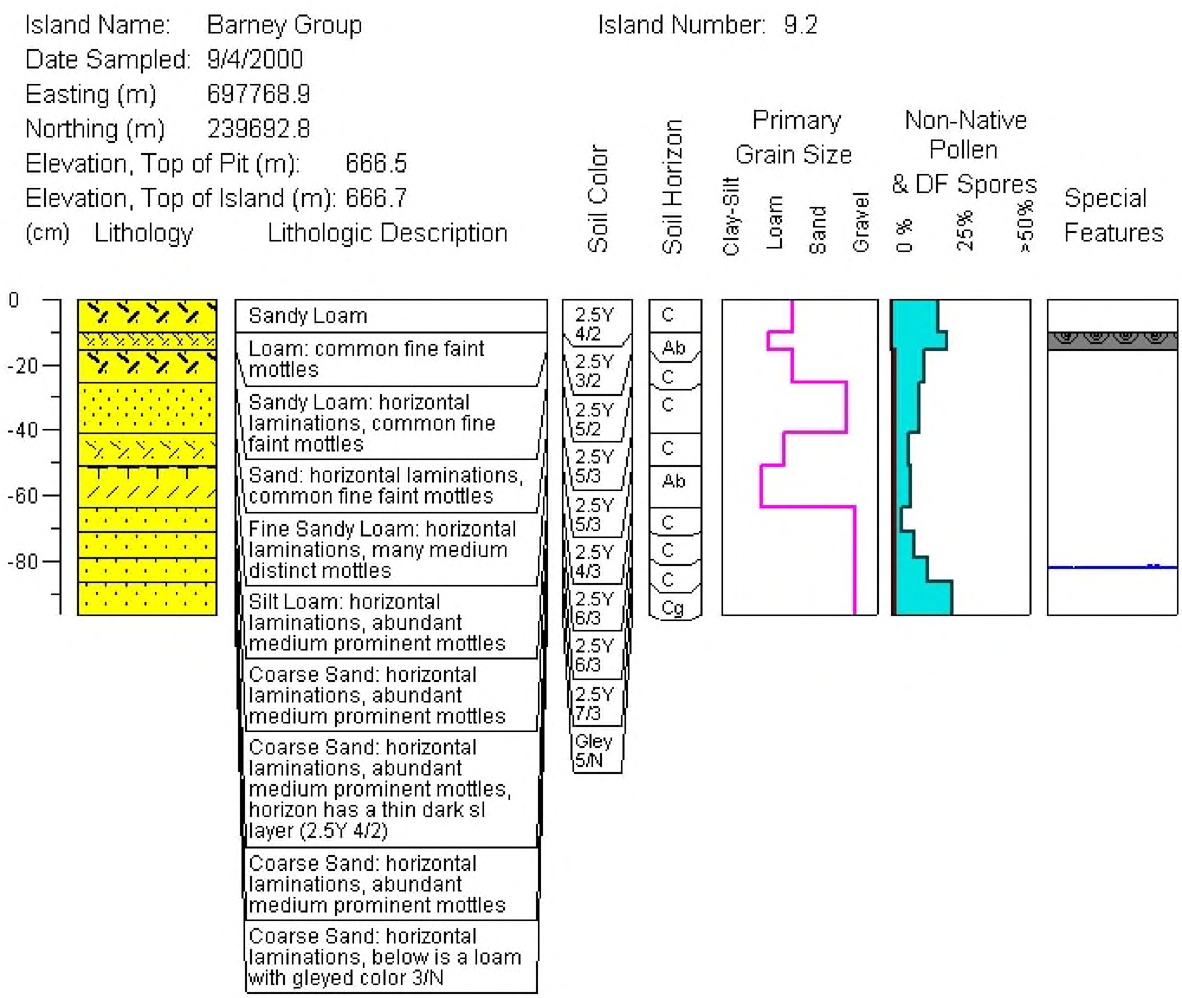

Figure E12. Barney Group (9.2) soil profile.

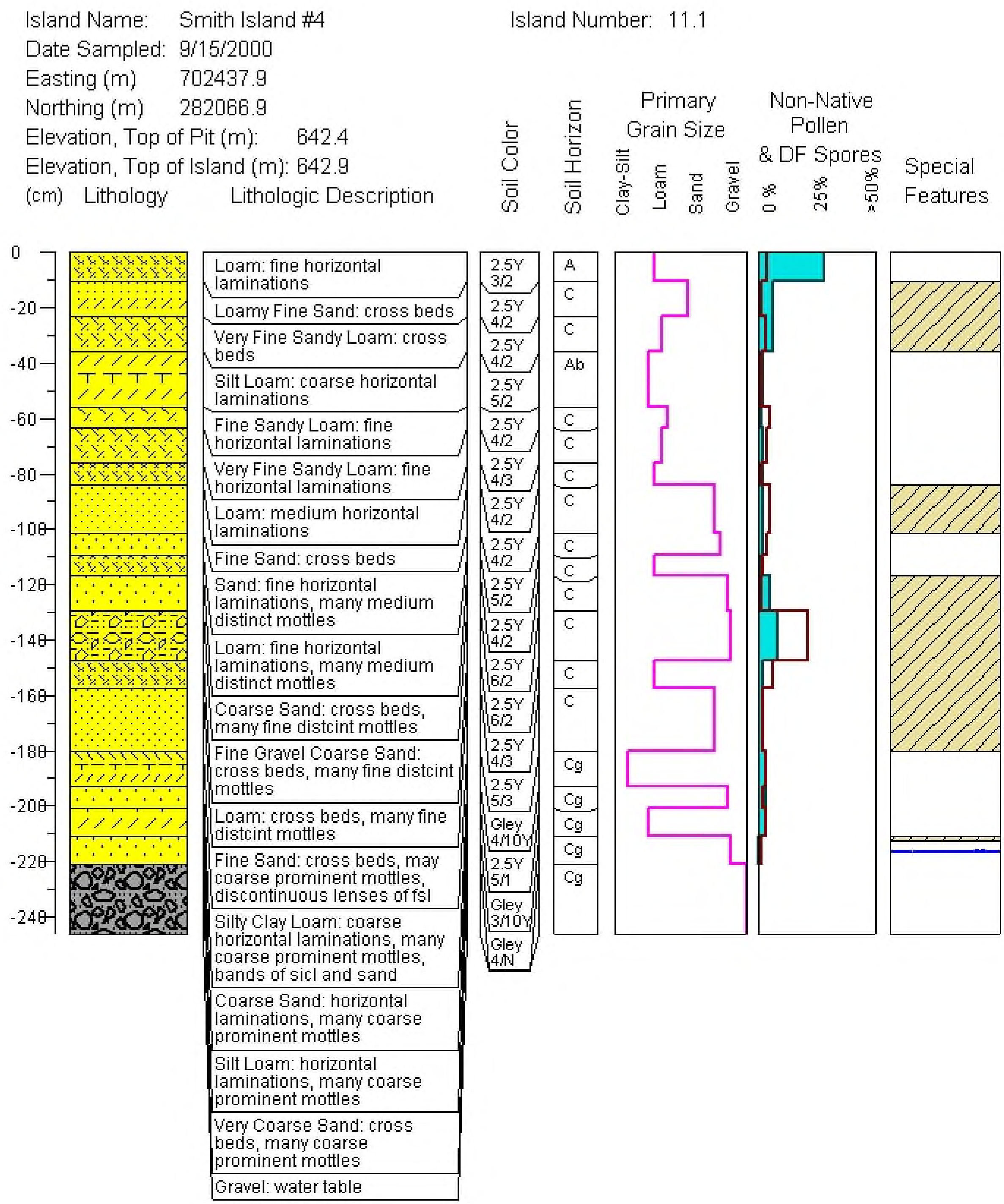

Figure E13. Smith Island #4 (11.1) soil profile.

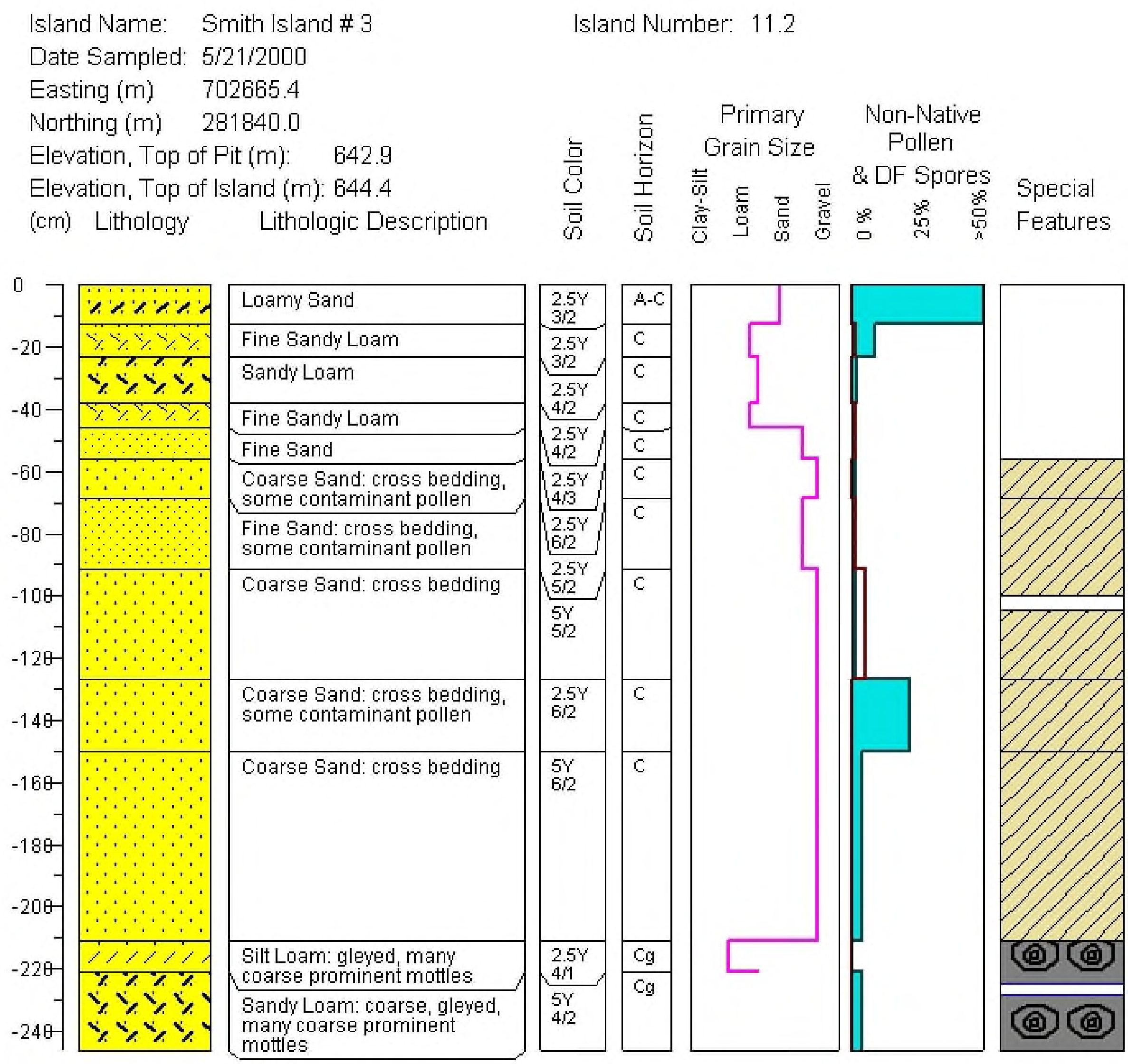

Figure E14. Smith Island #3 (11.2) soil profile.

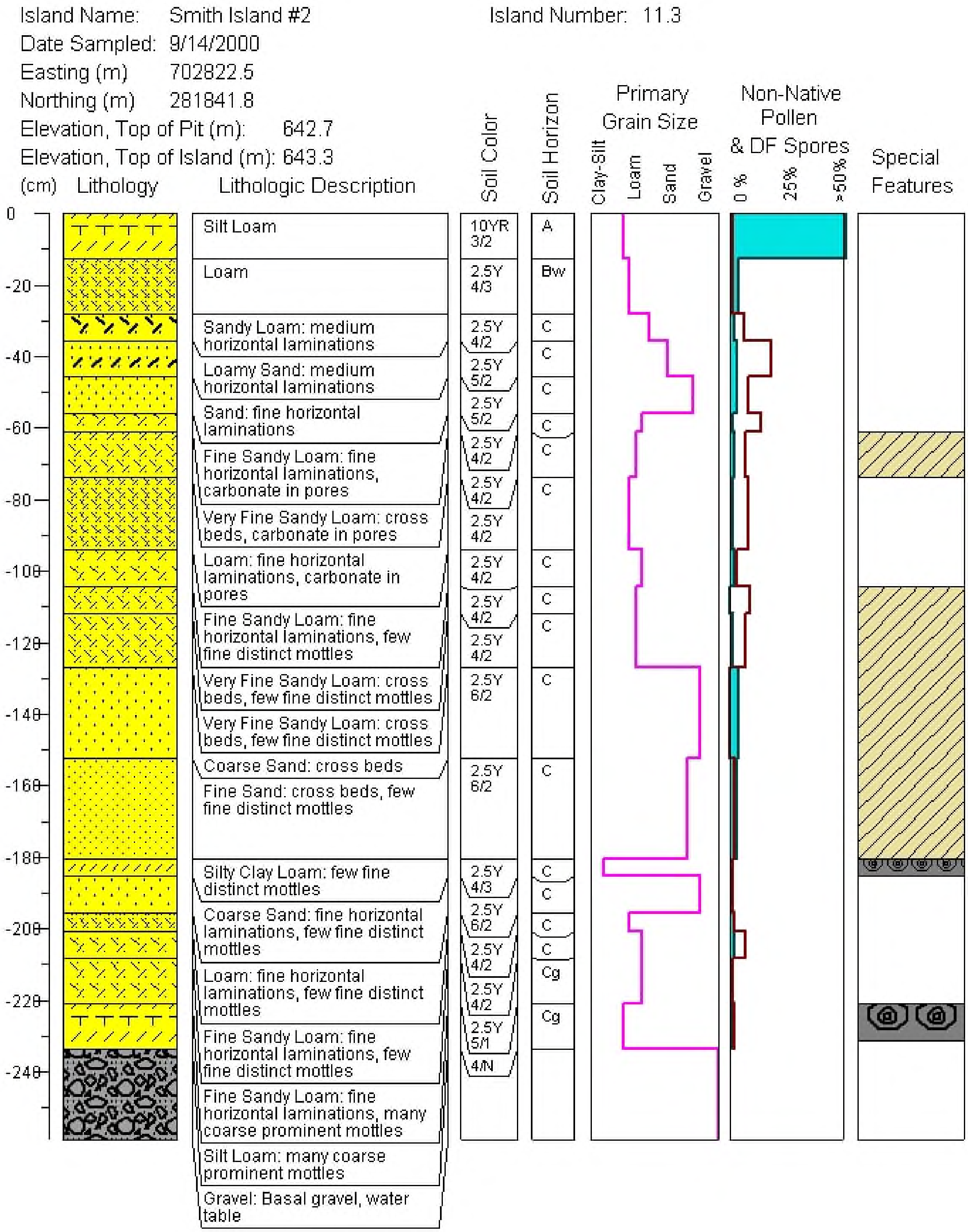

Figure E15. Smith Island #2 (11.3) soil profile.

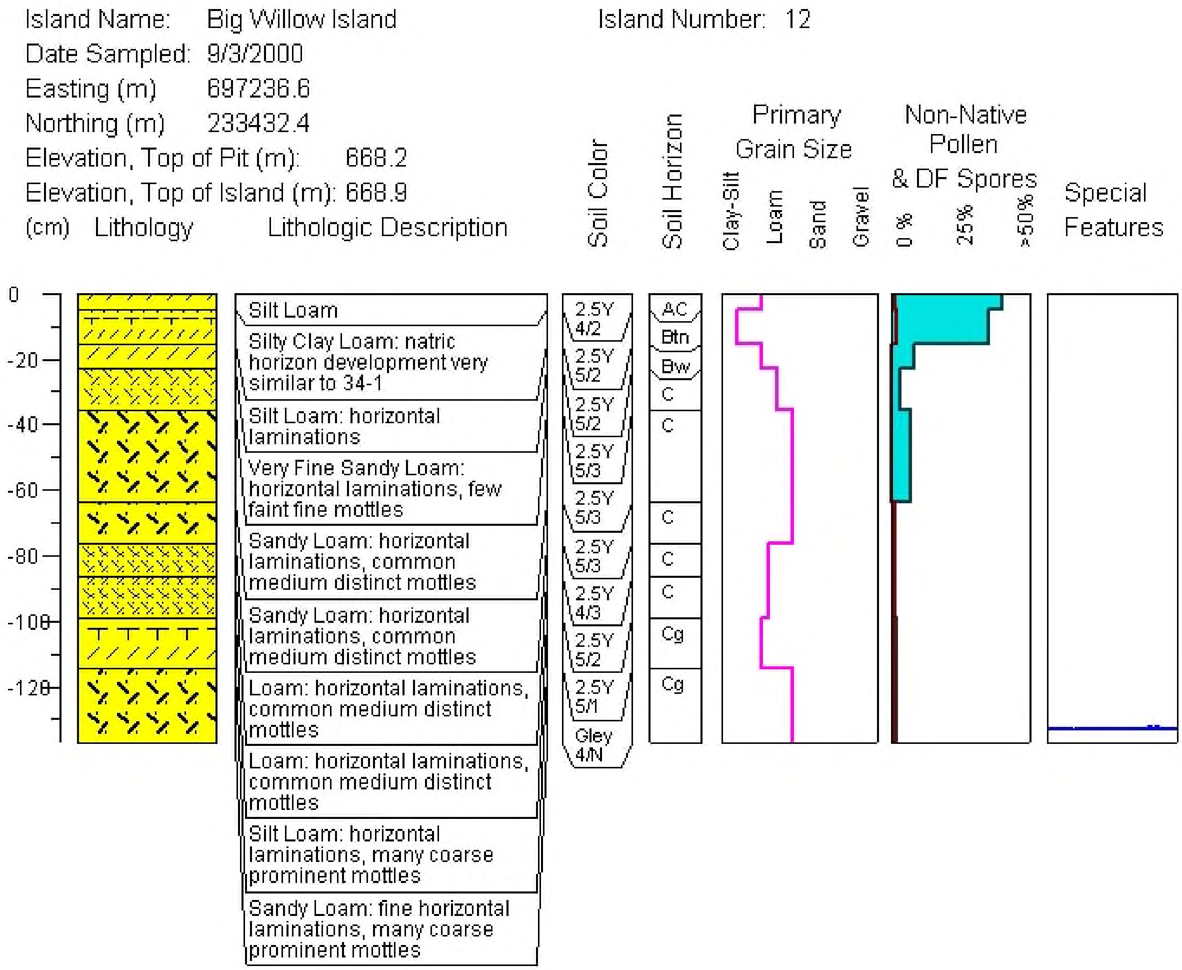

Figure E16. Big Willow Island (12) soil profile.

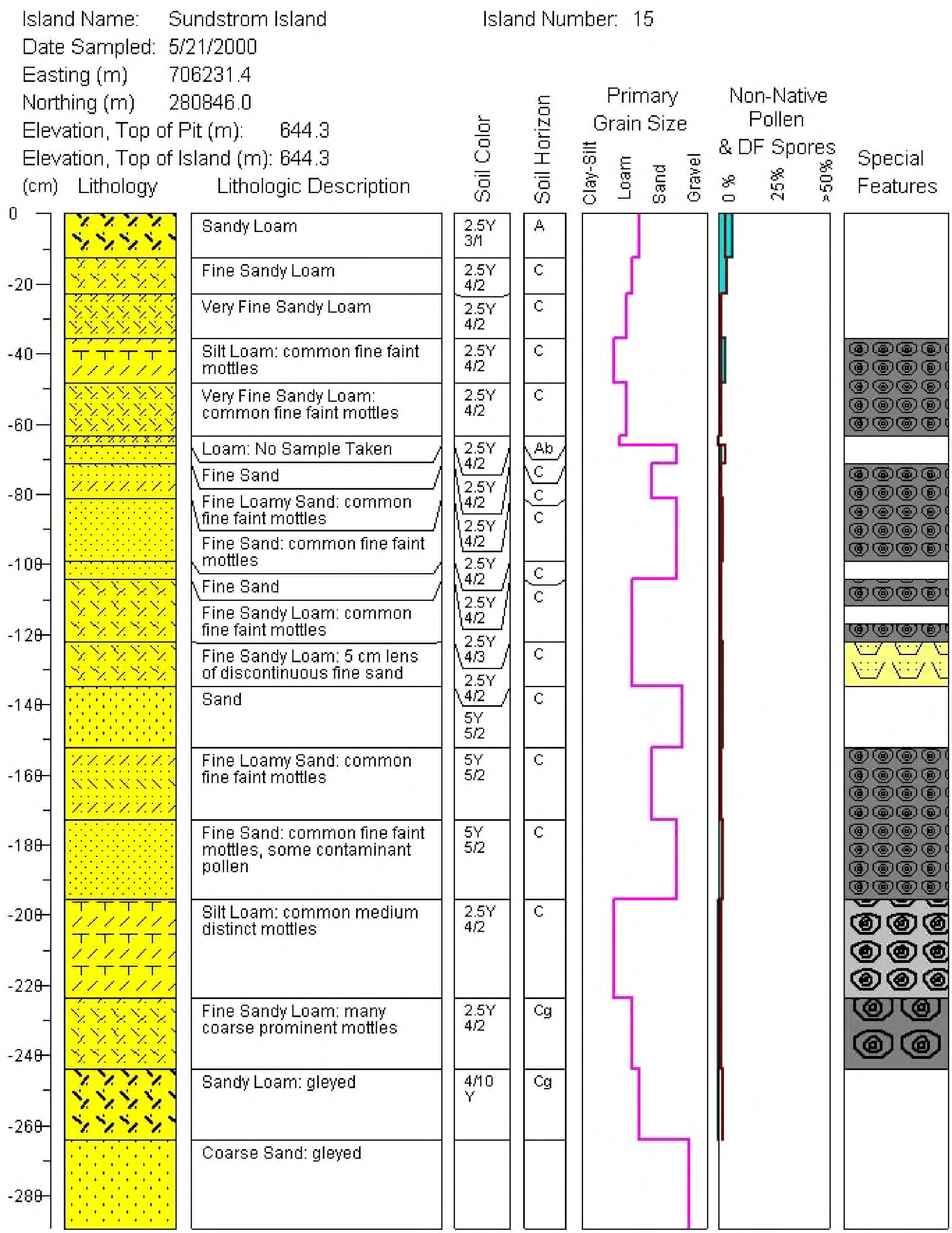

Figure E17. Sundstrom Island (15) soil profile.

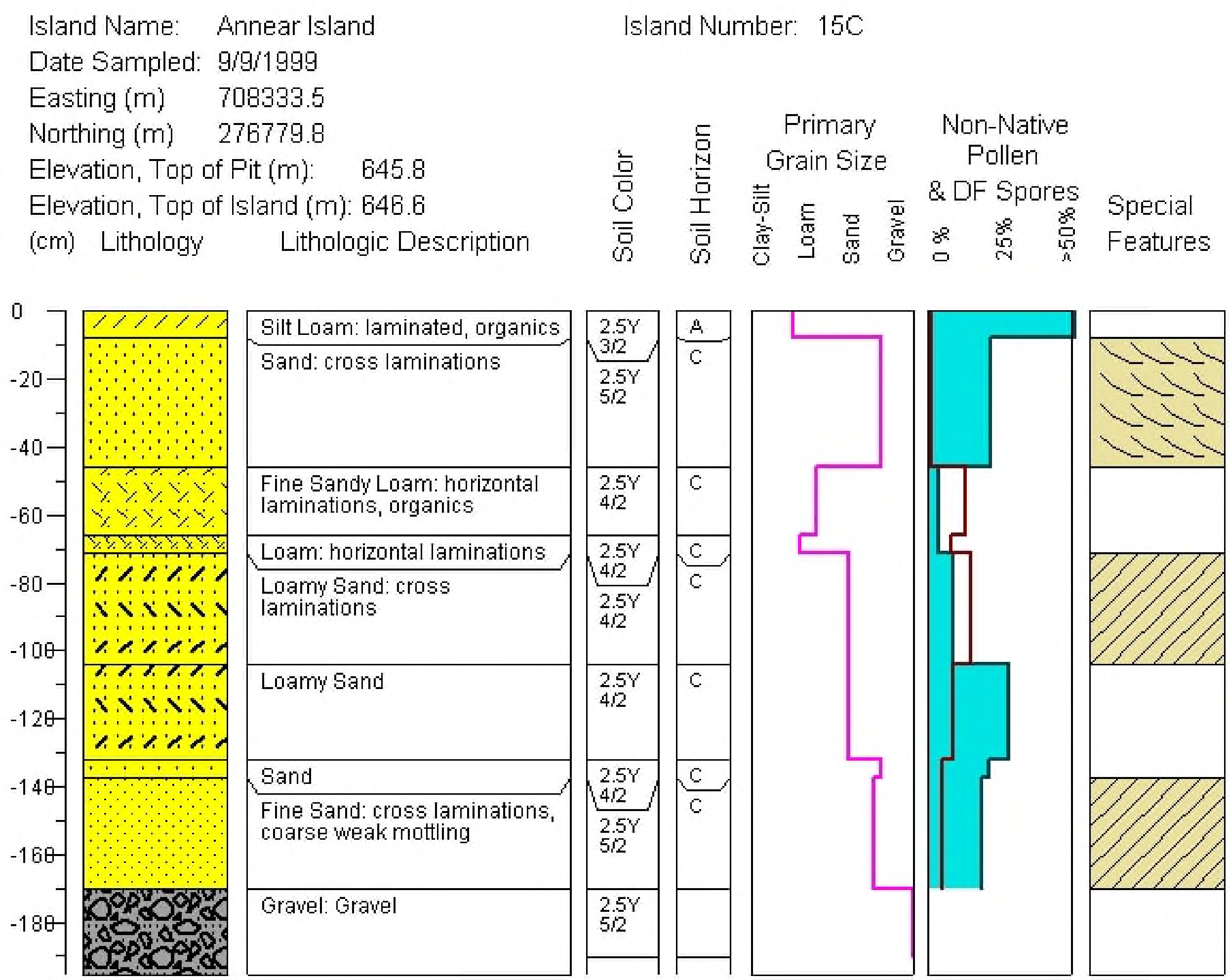

Figure E18. Annear Island (15C) soil profile.

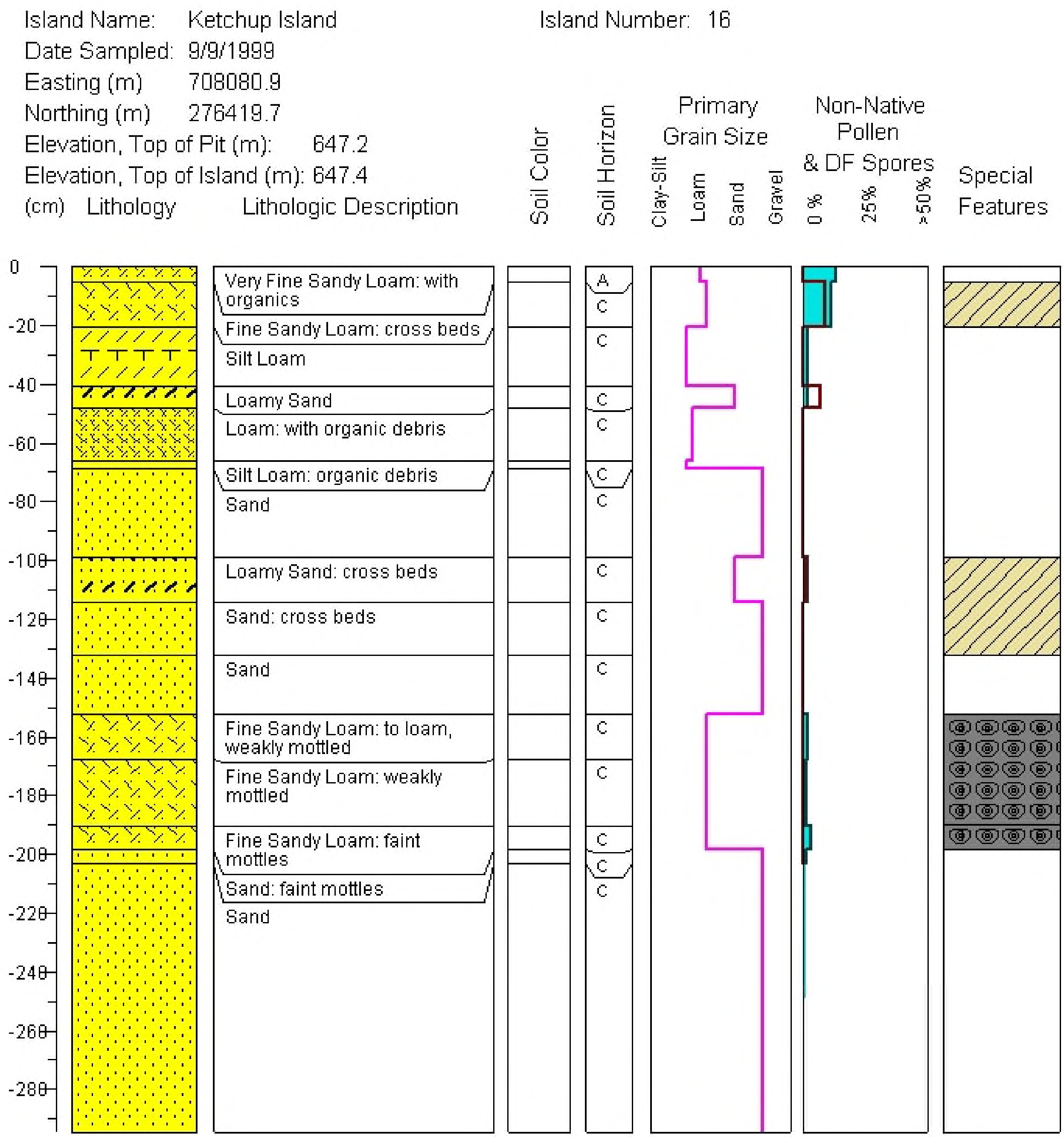

Figure E19. Ketchup Island (16) soil profile.

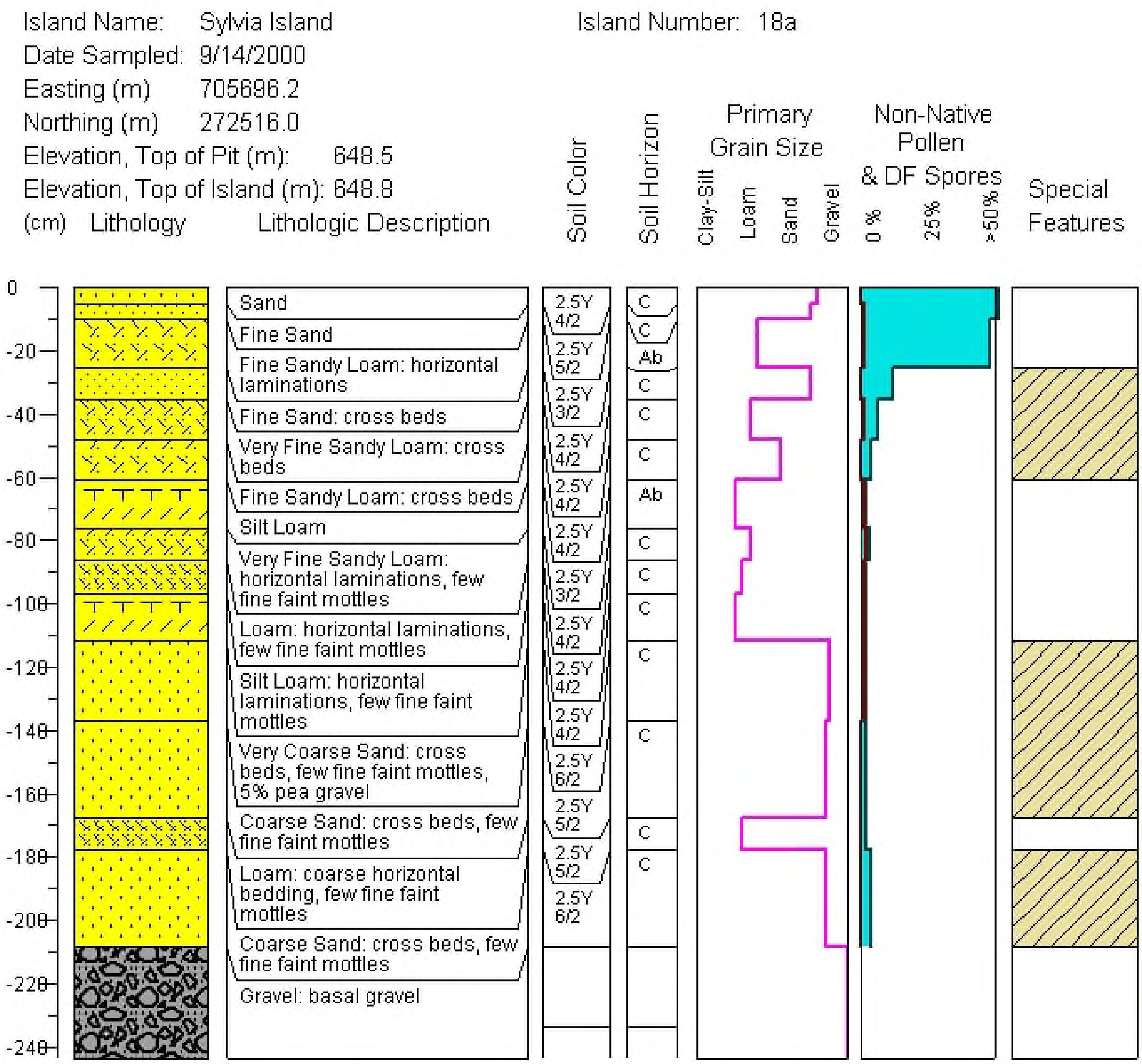

Figure E20. Sylvia Island (18a) soil profile.

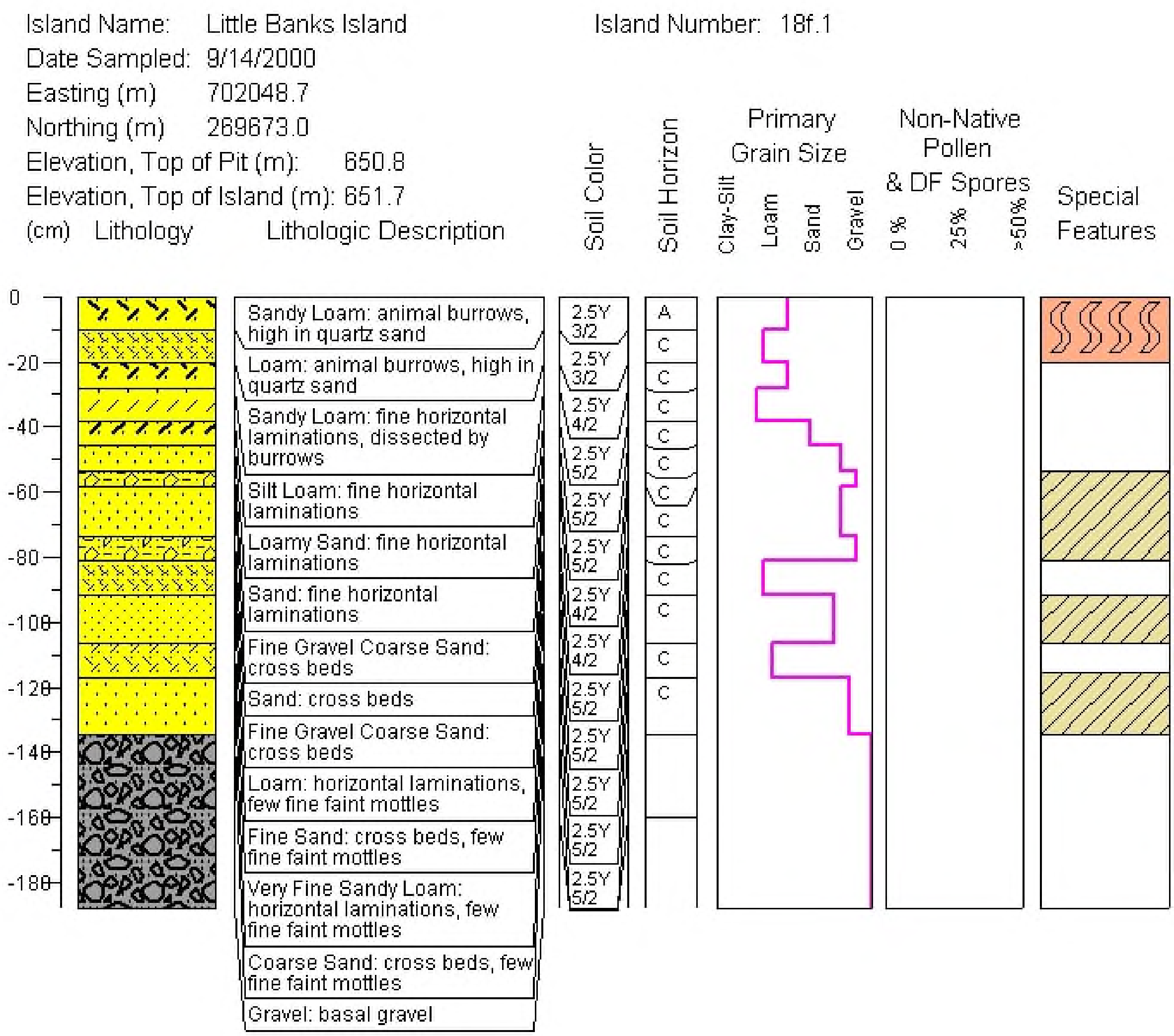

Figure E21. Little Banks Island (18f.1) soil profile.

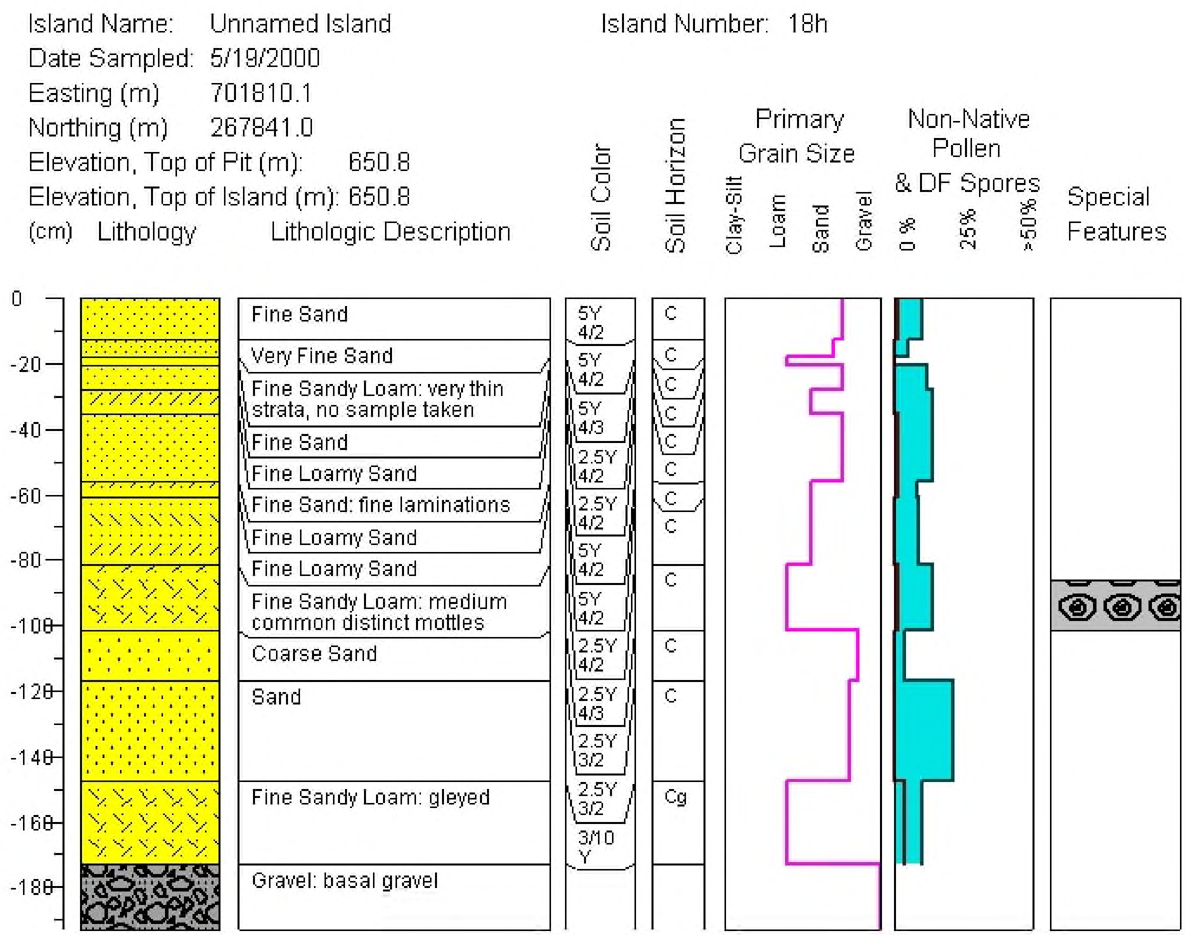

Figure E22. Unnamed Island (18h) soil profile.

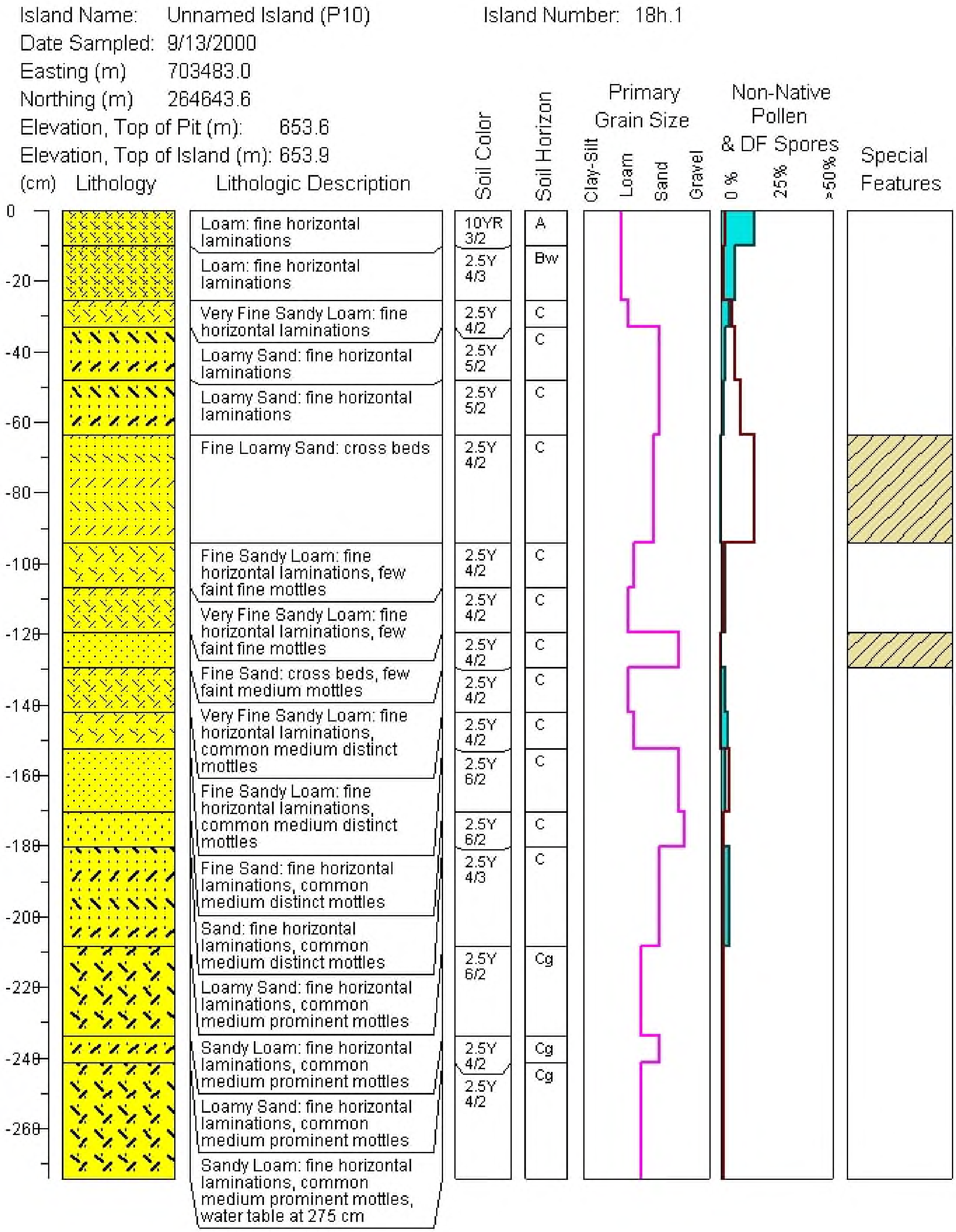

Figure E23. Unnamed Island, P10 (18h.1) soil profile.

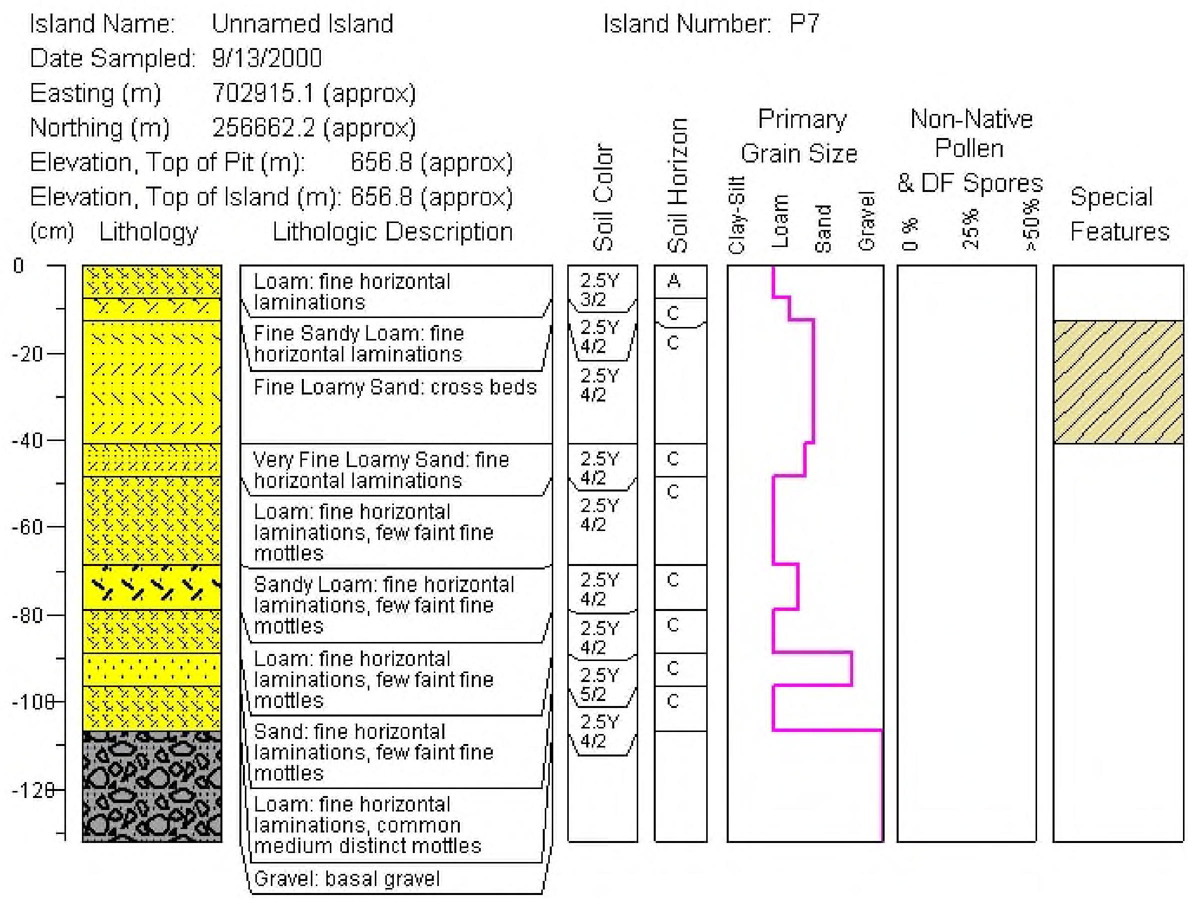

Figure E24. Unnamed Island (P7).

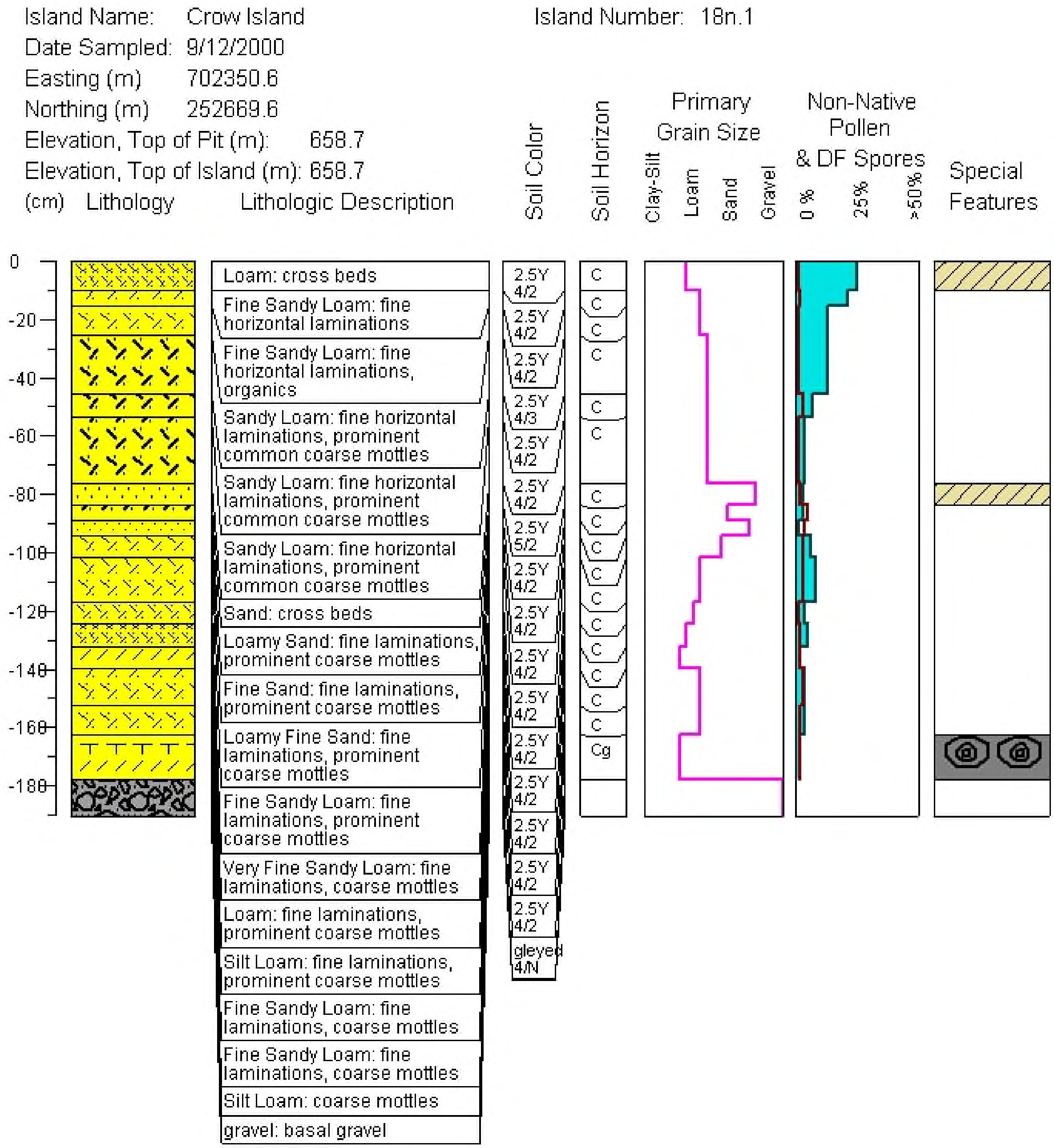

Figure E25. Crow Island (18n.1) soil profile.

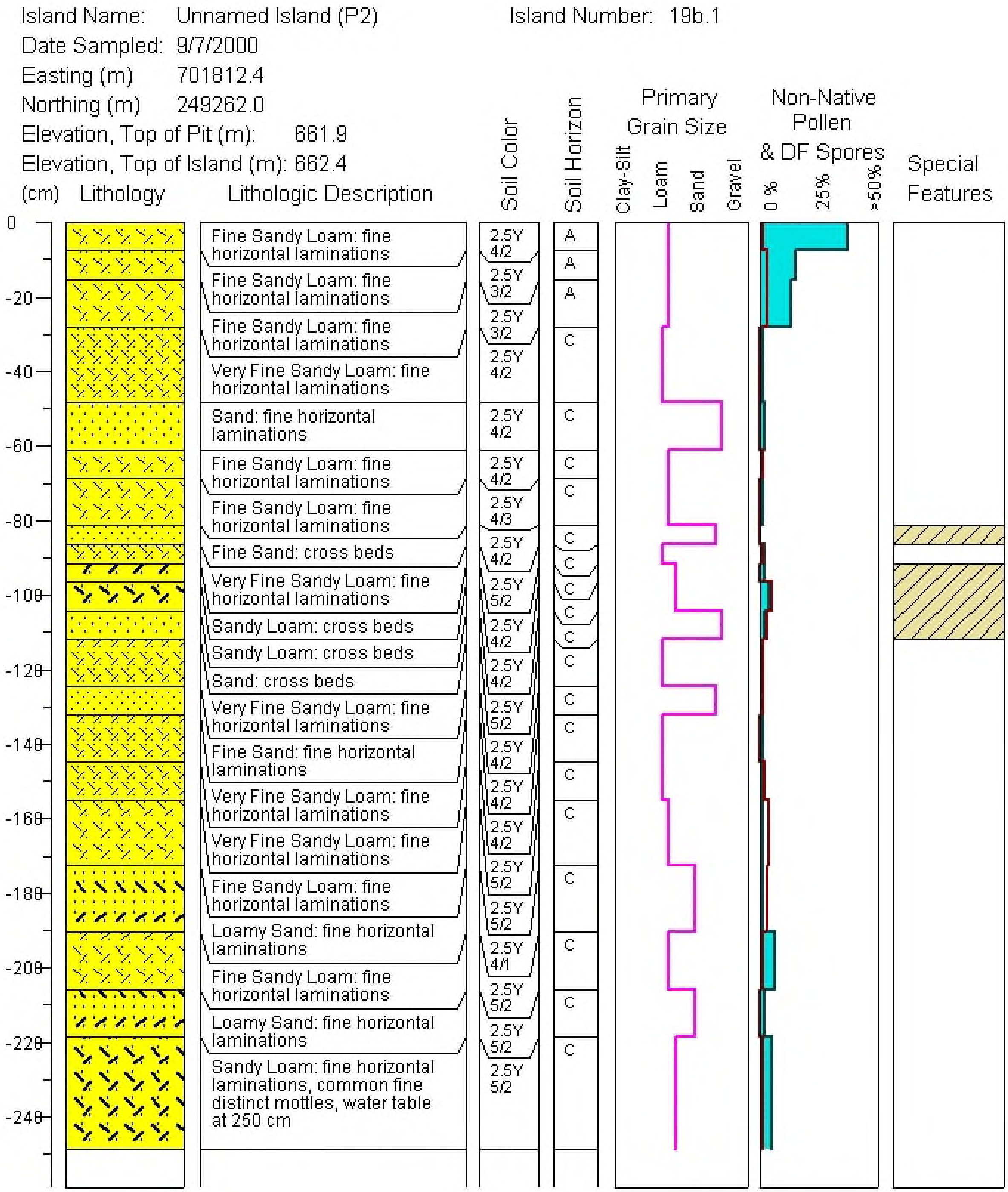

Figure E26. Unnamed Island, P2 (19b.1) soil profile.

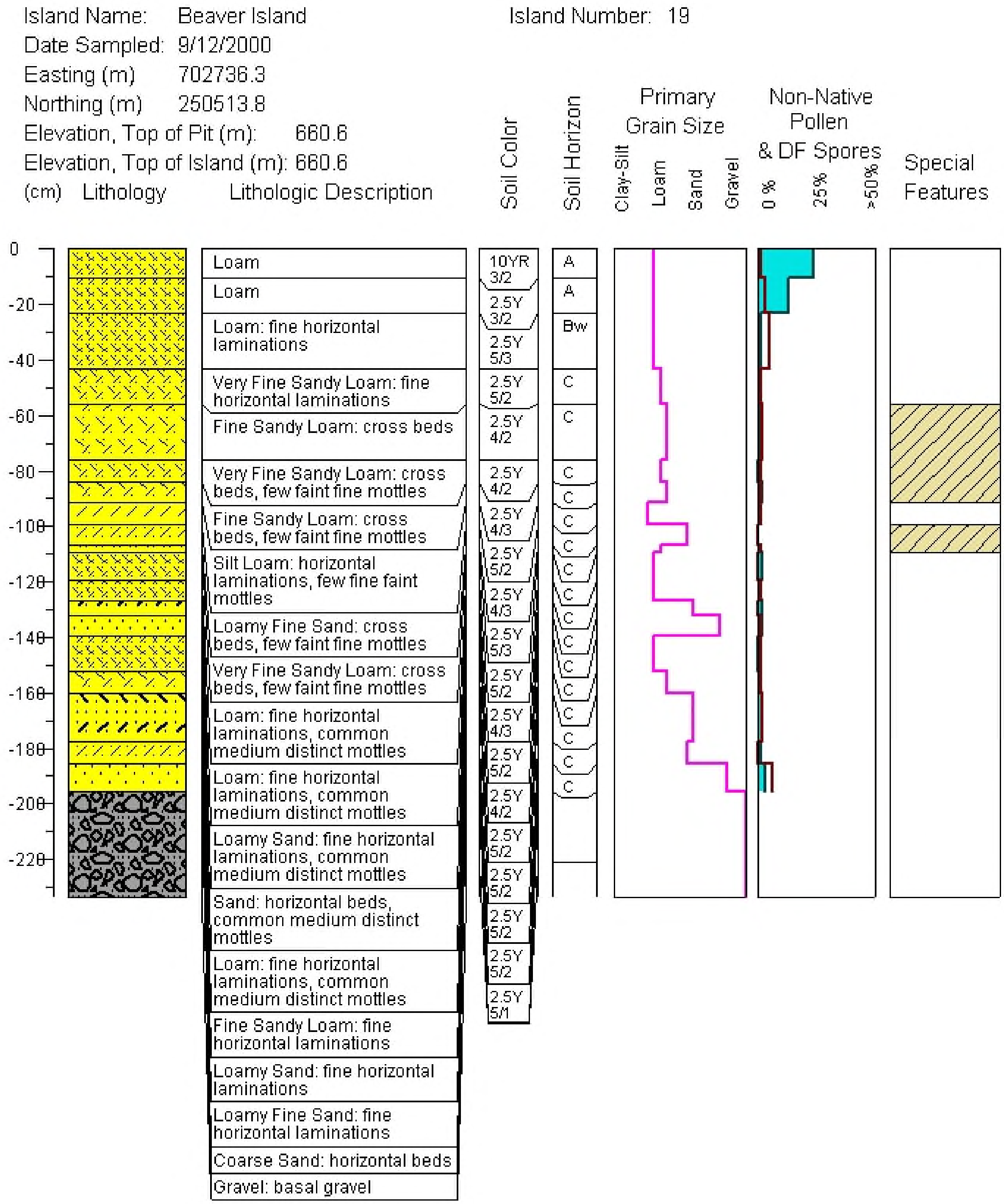

Figure E27. Beaver Island (19) soil profile.

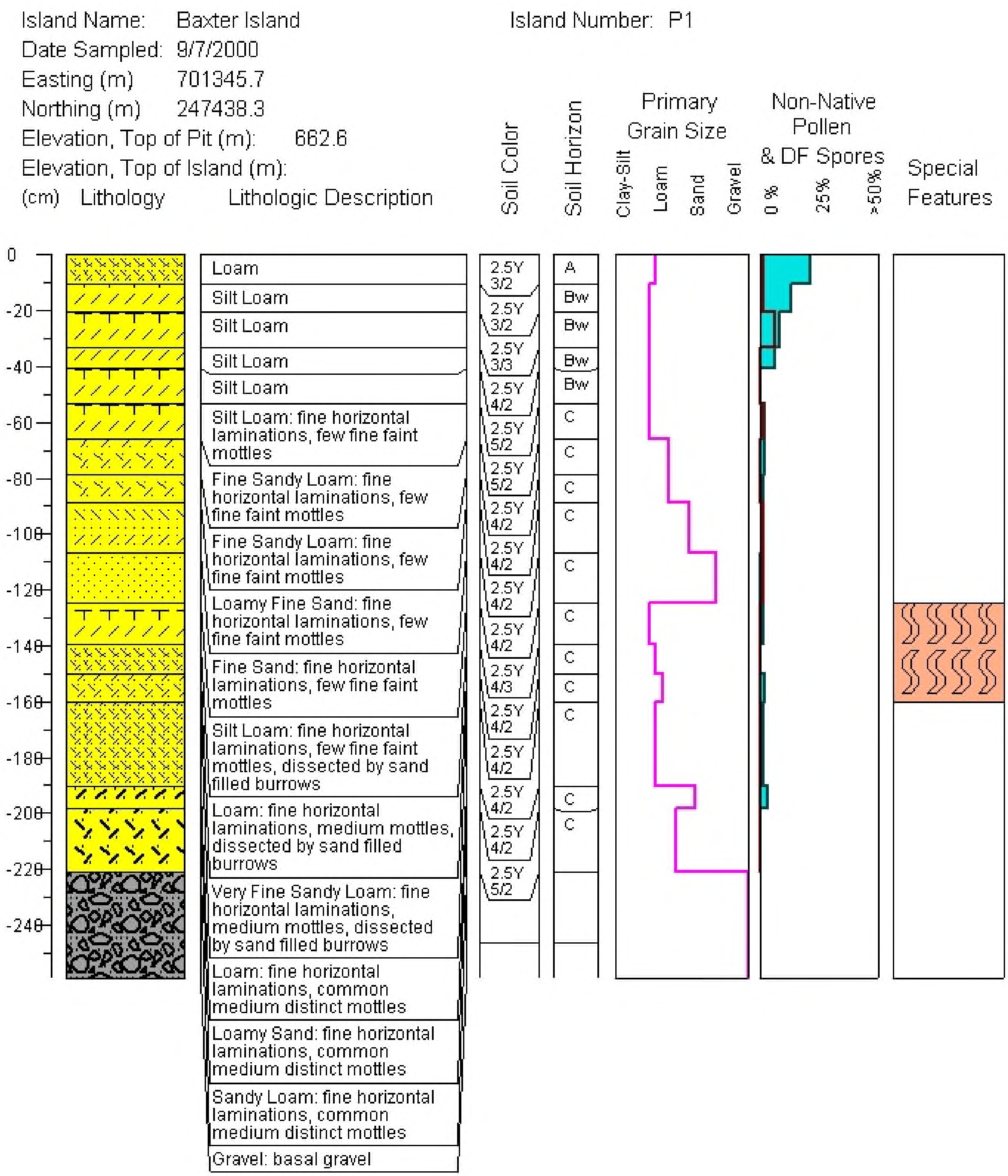

Figure E28. Baxter Island (P1) soil profile.

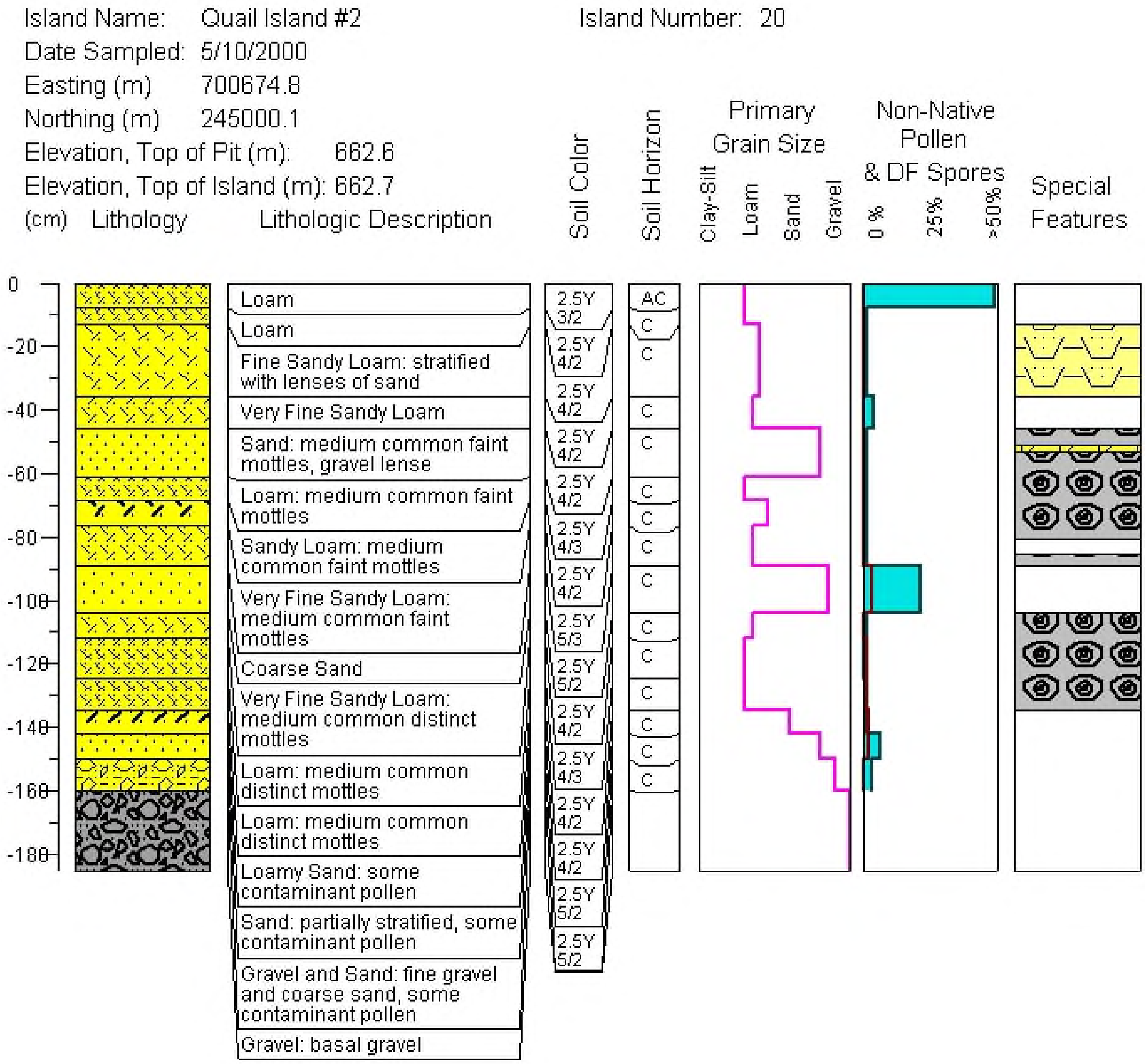

Figure E29. Quail Island #2 (20) soil profile.

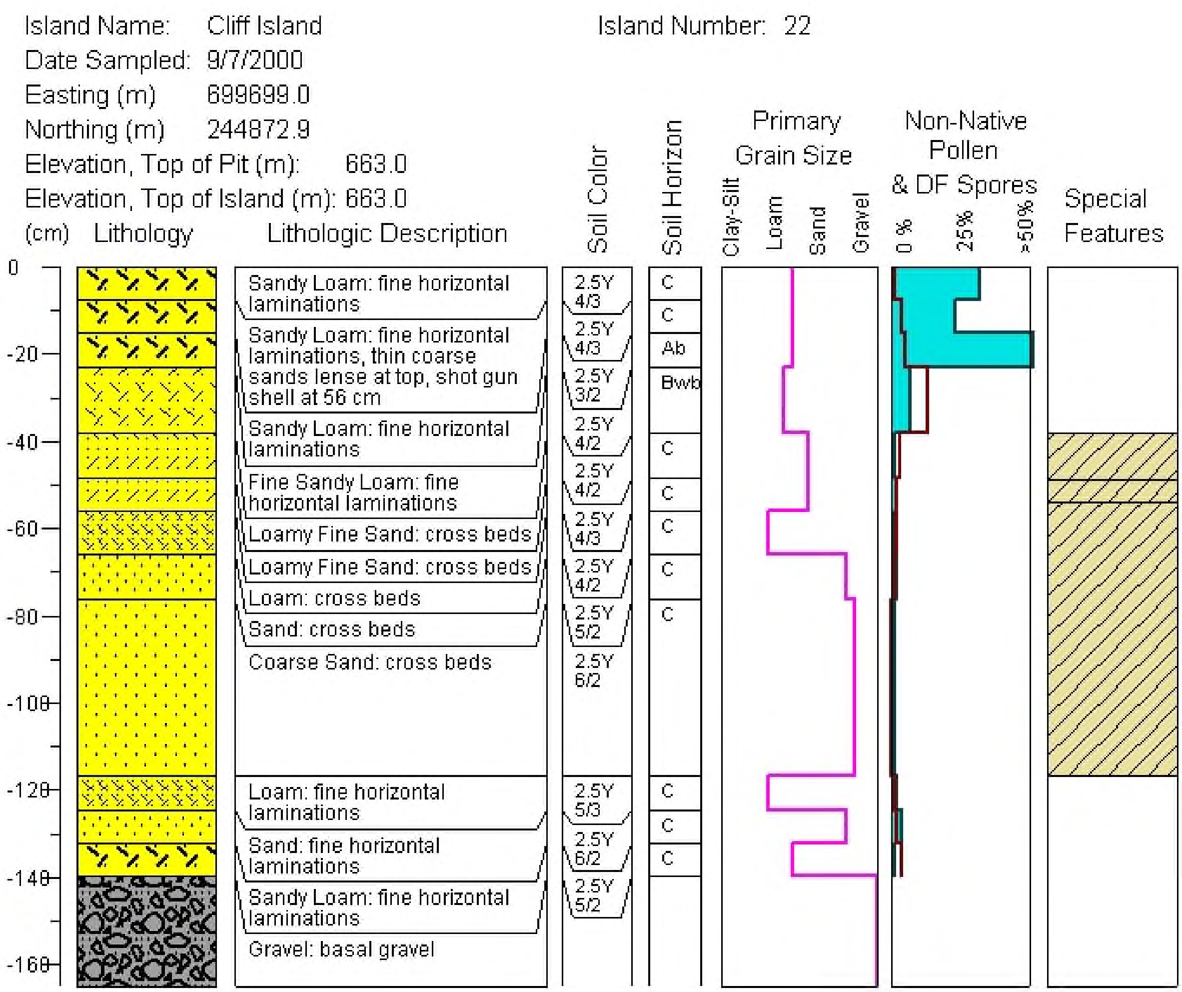

Figure E30. Cliff Island (22) soil profile.

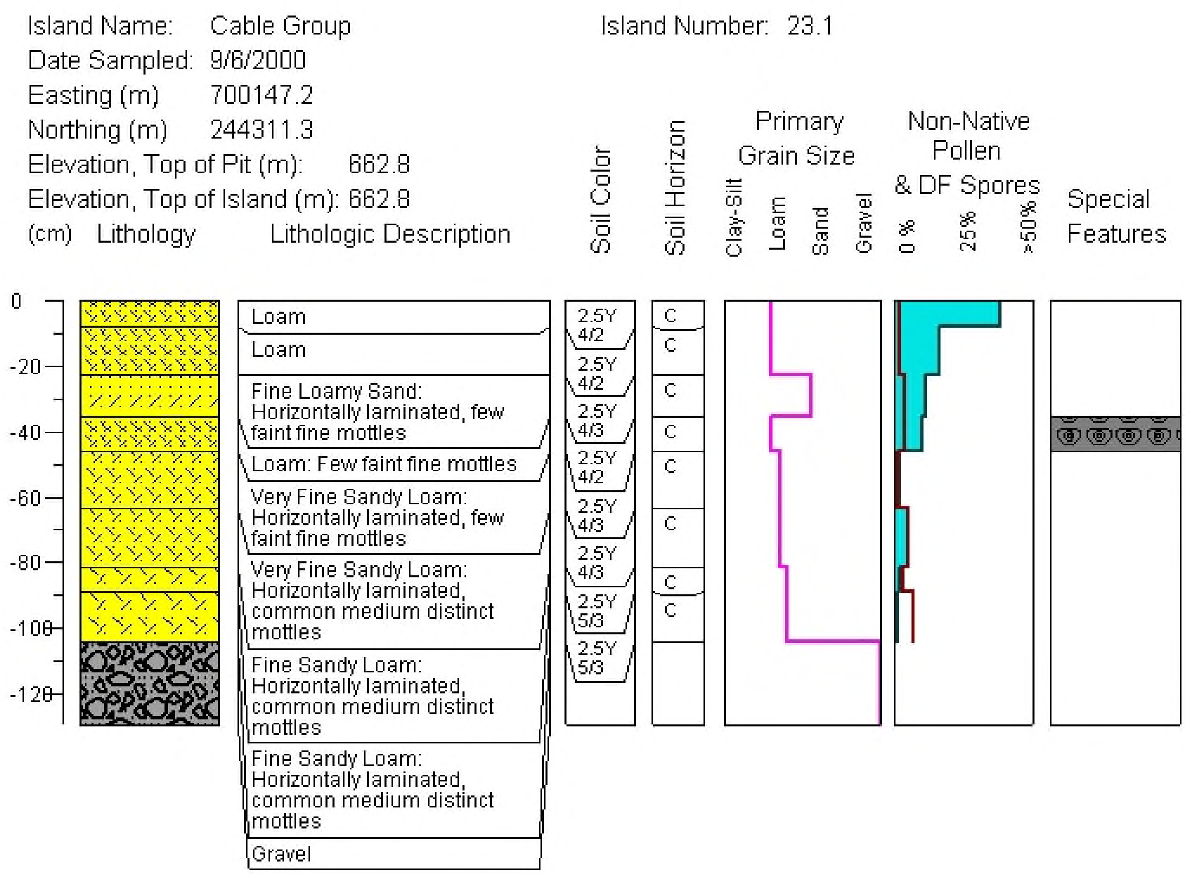

Figure E31. Cable Group (23.1) soil profile.

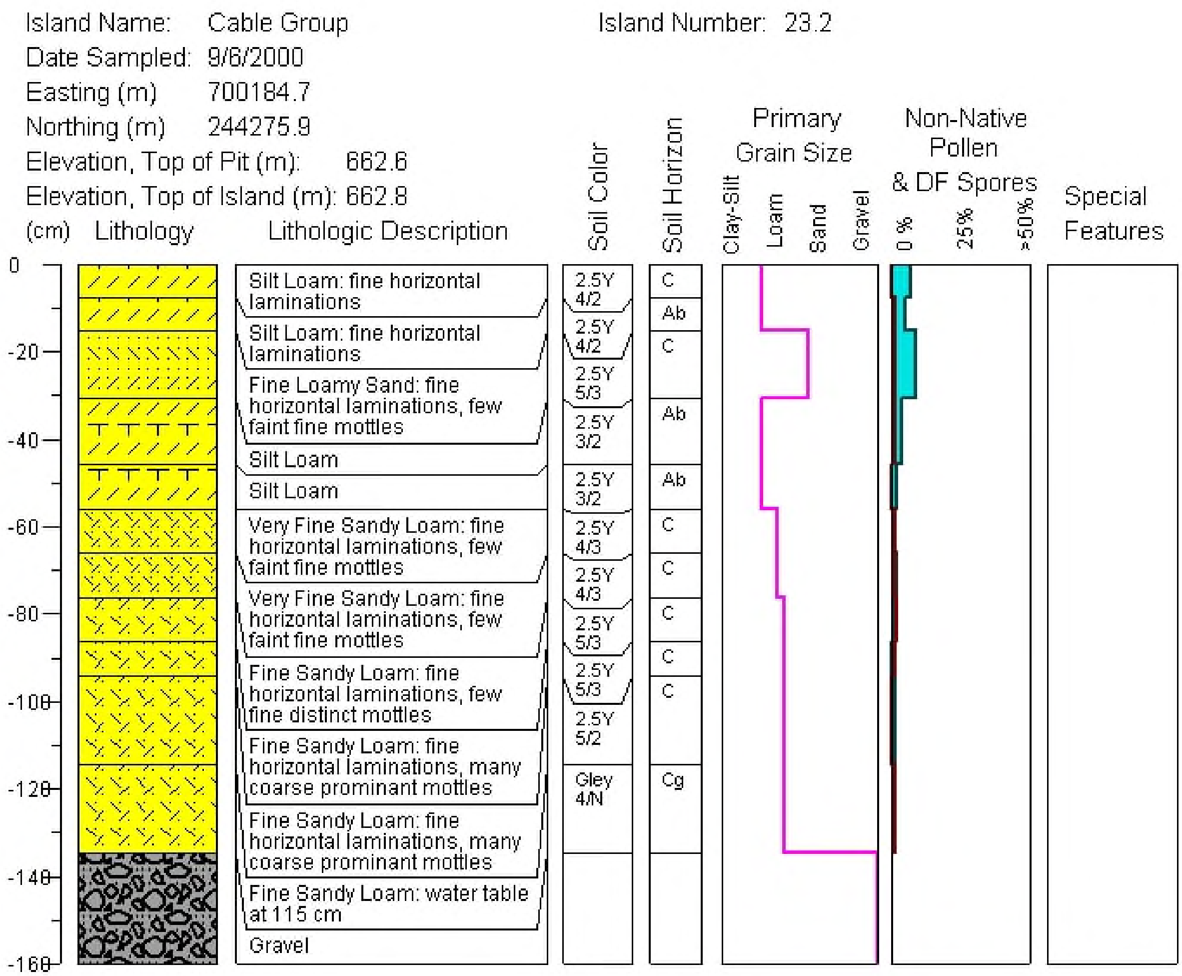

Figure E32. Cable Group (23.2) soil profile.

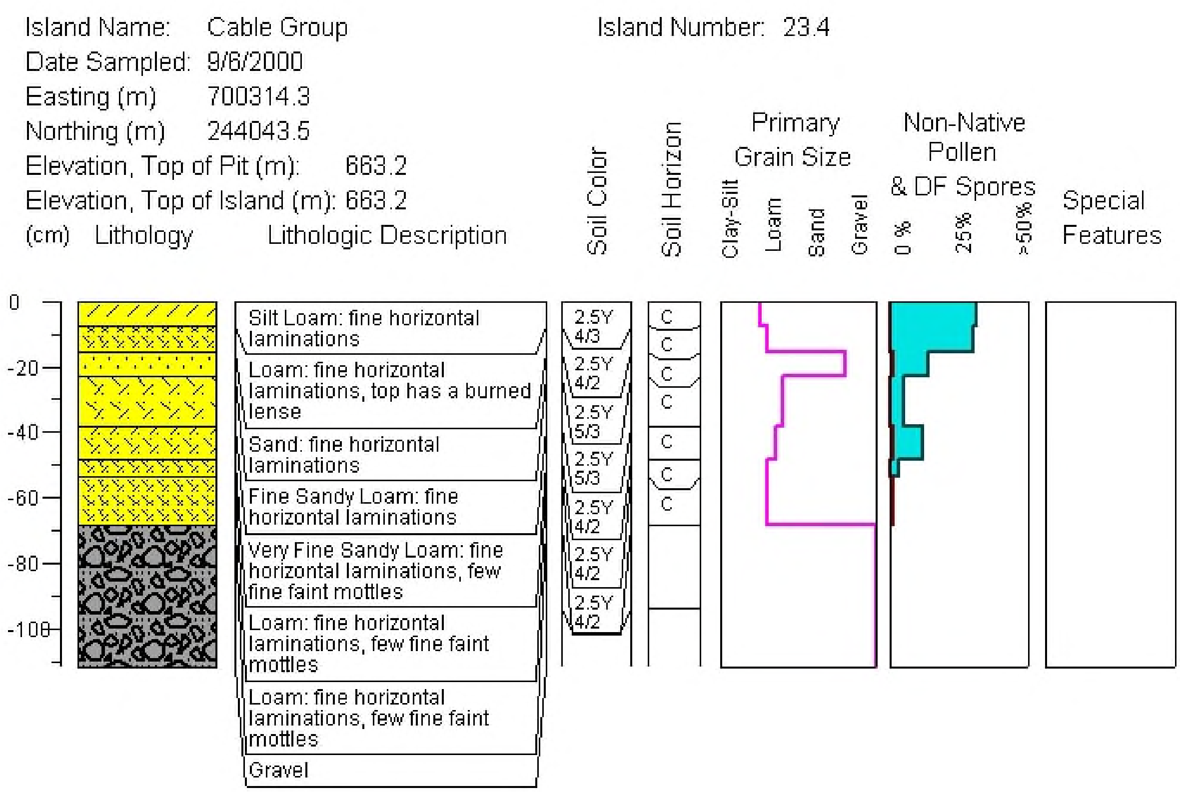

Figure E33. Cable Group (23.4) soil profile.

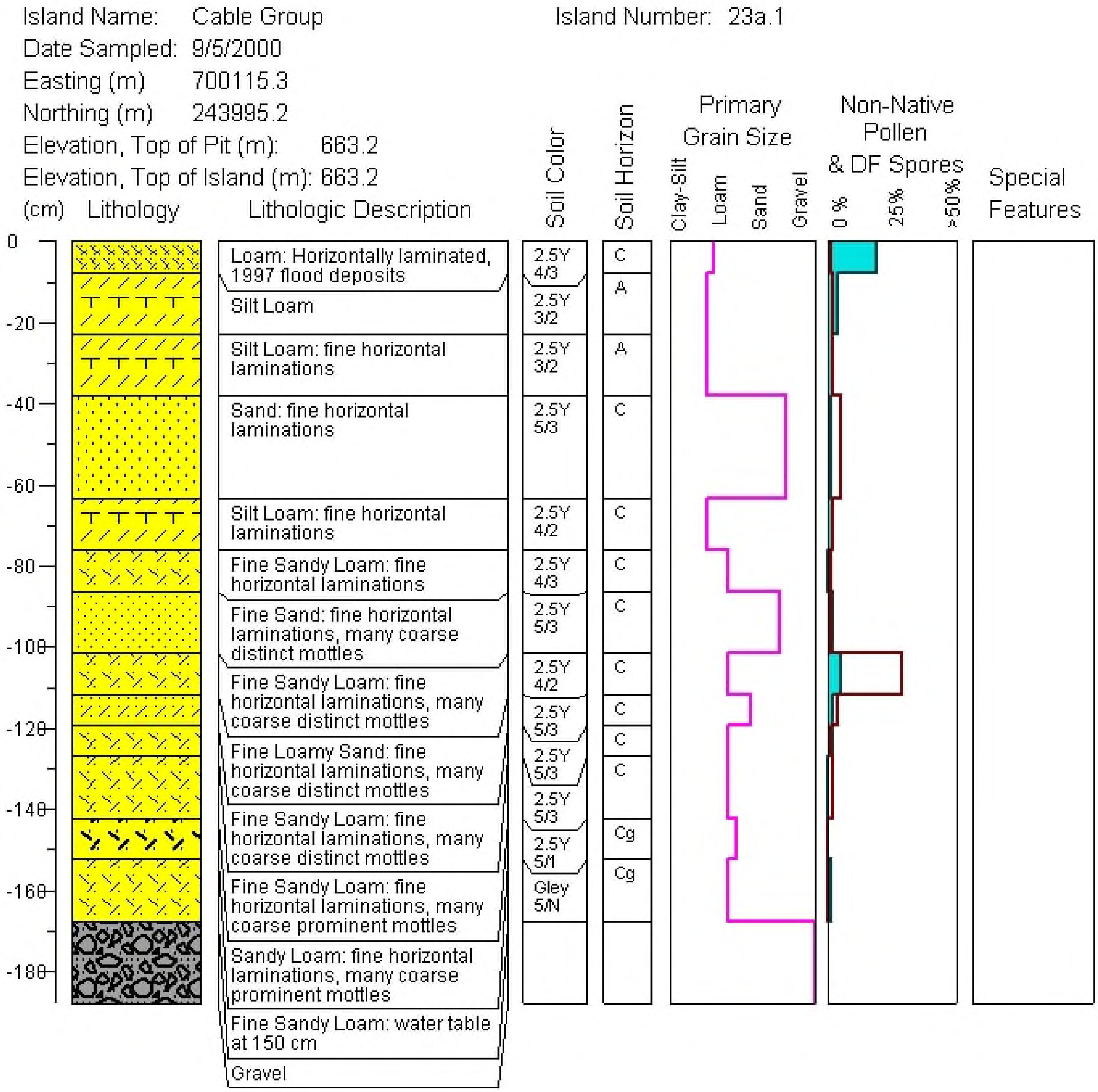

Figure E34. Cable Group (23a.1) soil profile.

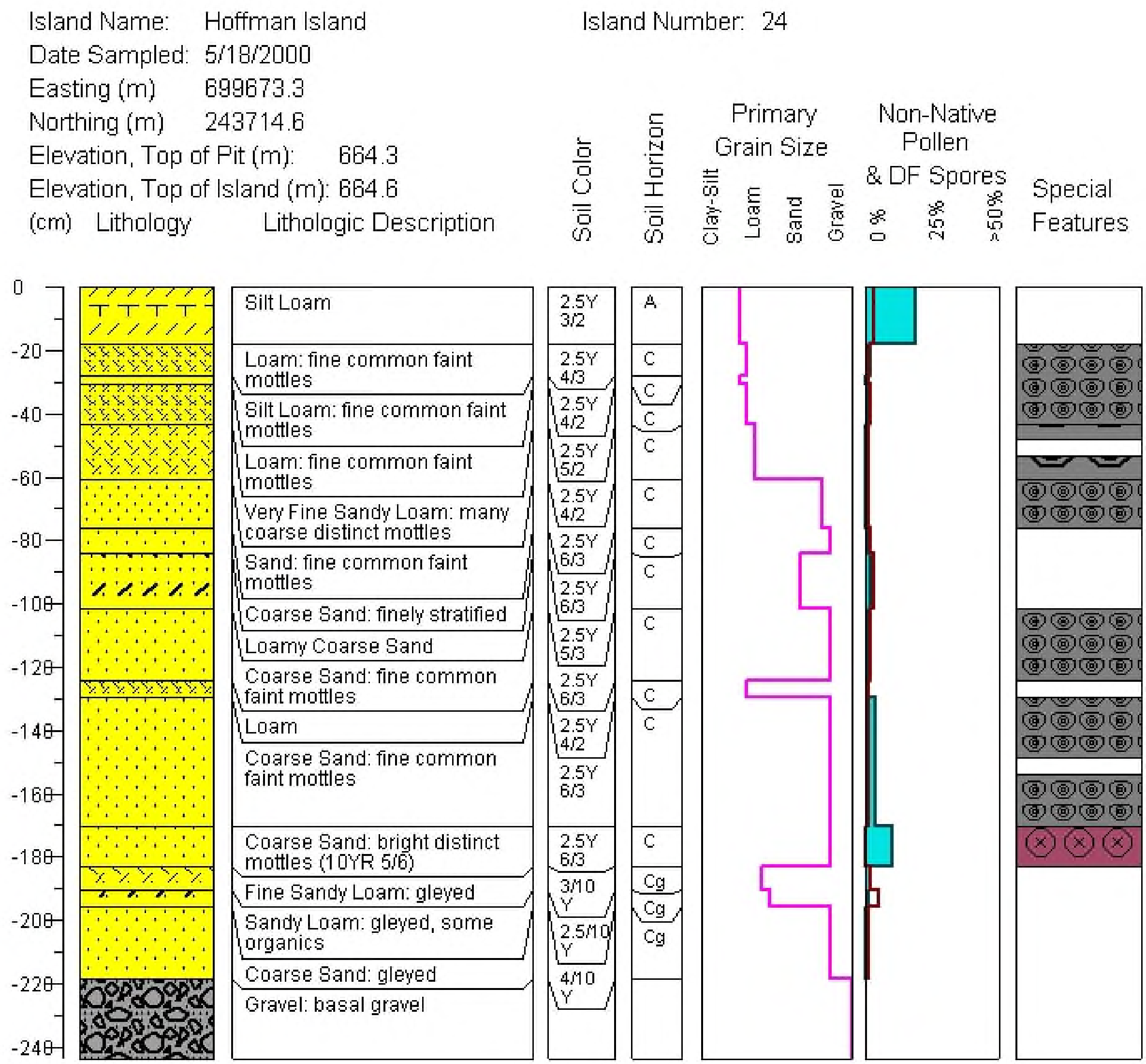

Figure E35. Hoffman Island (24) soil profile.

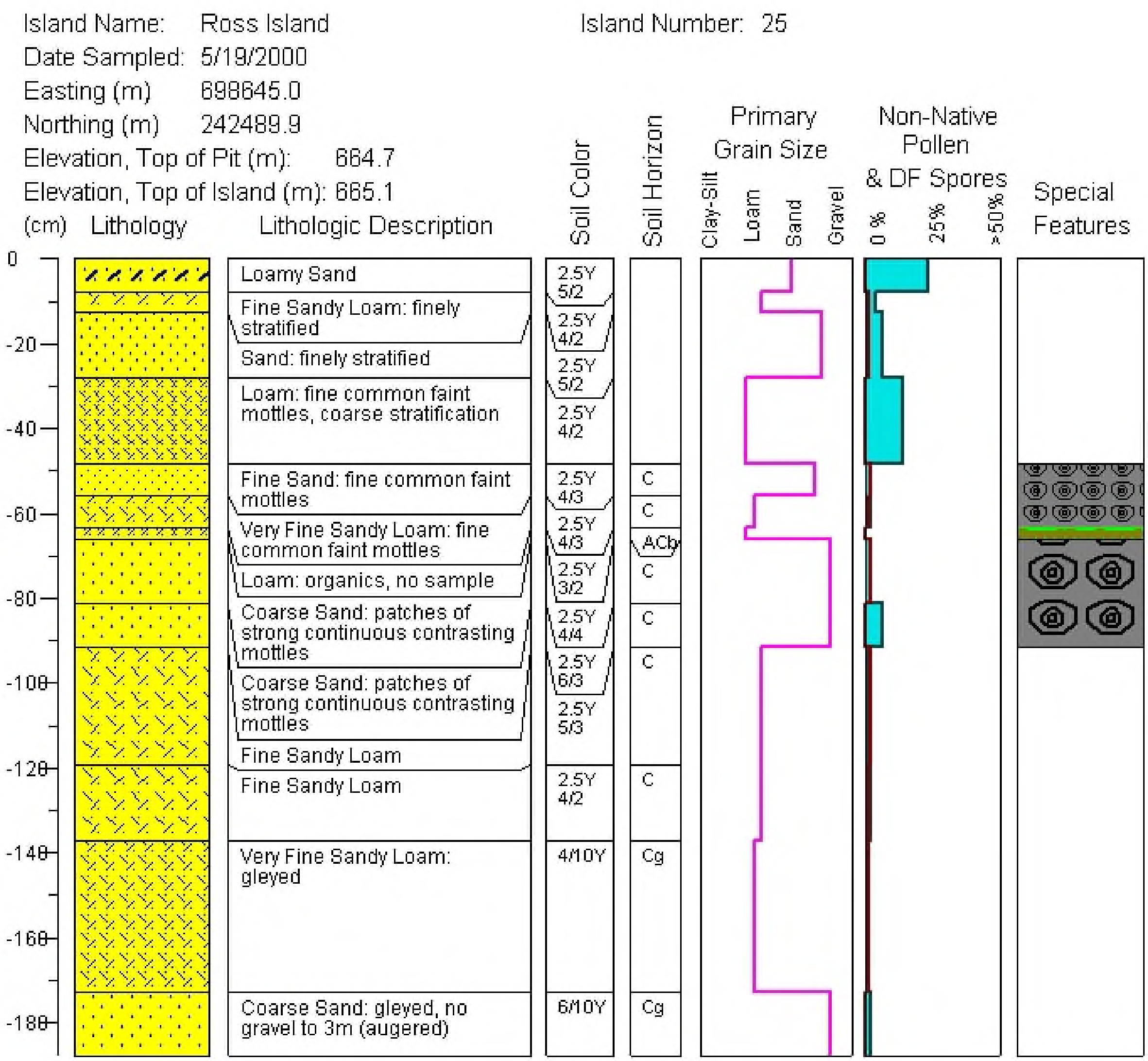

Figure E36. Ross Island (25) soil profile.

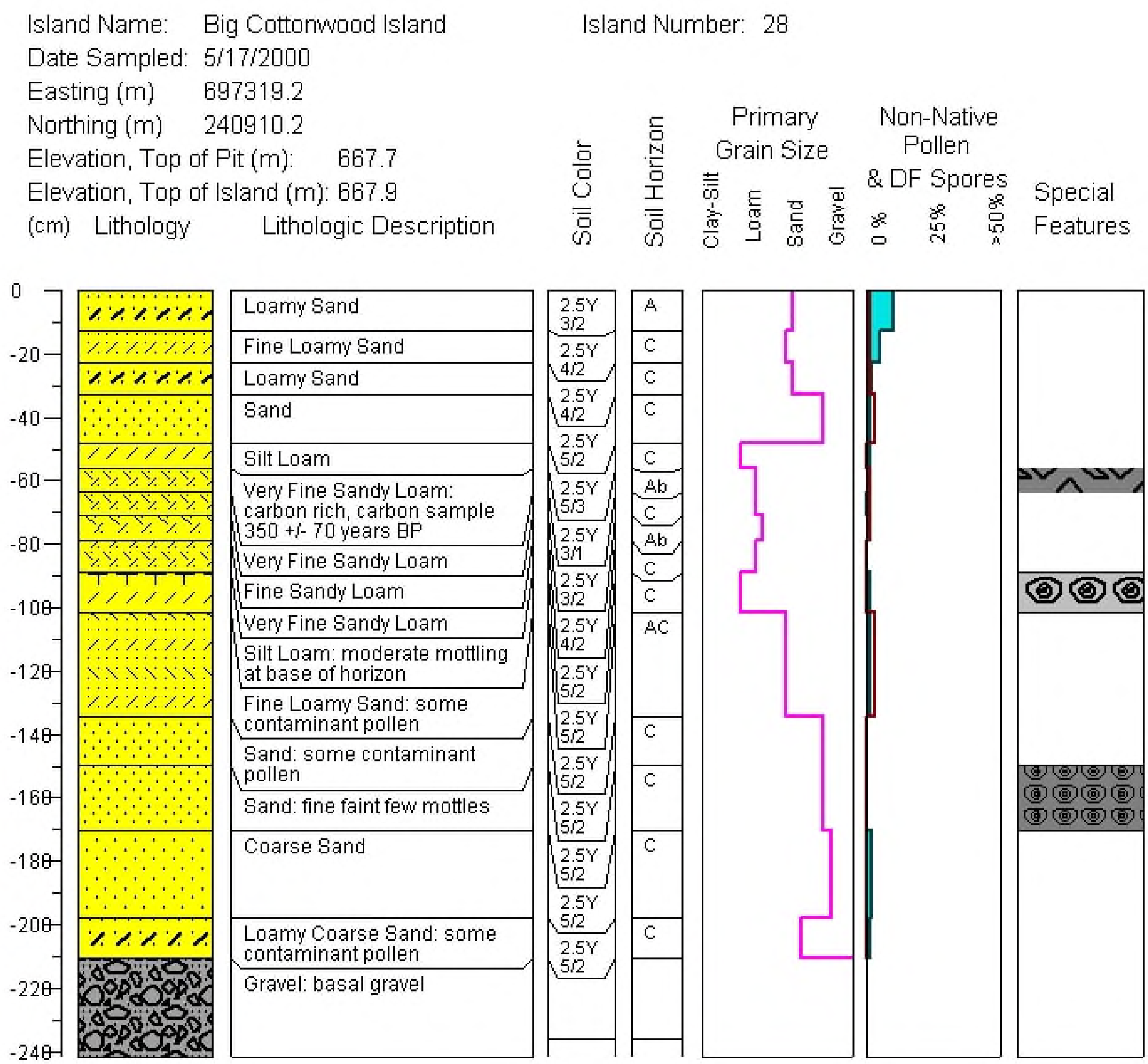

Figure E37. Big Cottonwood Island (28) soil profile.

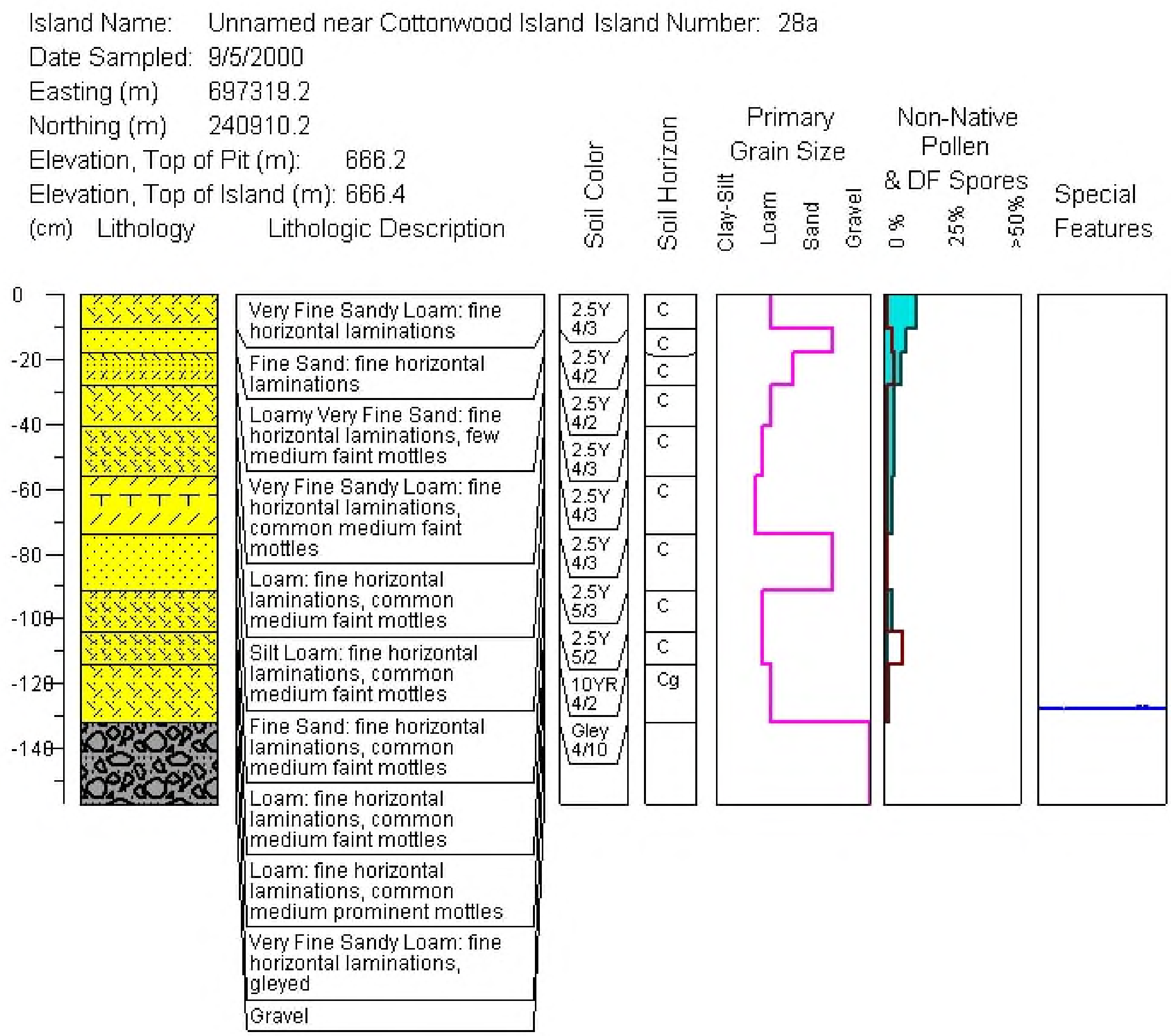

Figure E38. Unnamed Island near Cottonwood Island (28a) soil profile.

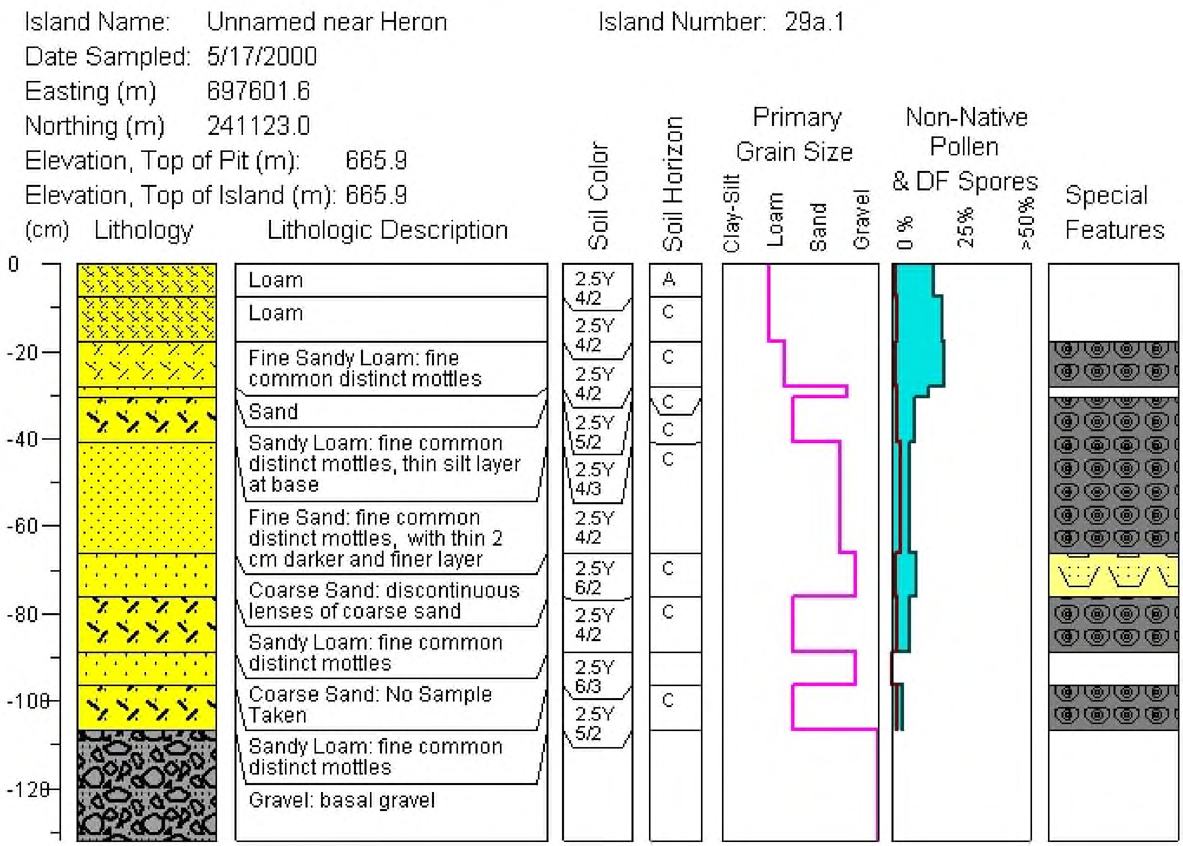

Figure E39. Unnamed Island near Heron Island (29a.1) soil profile.

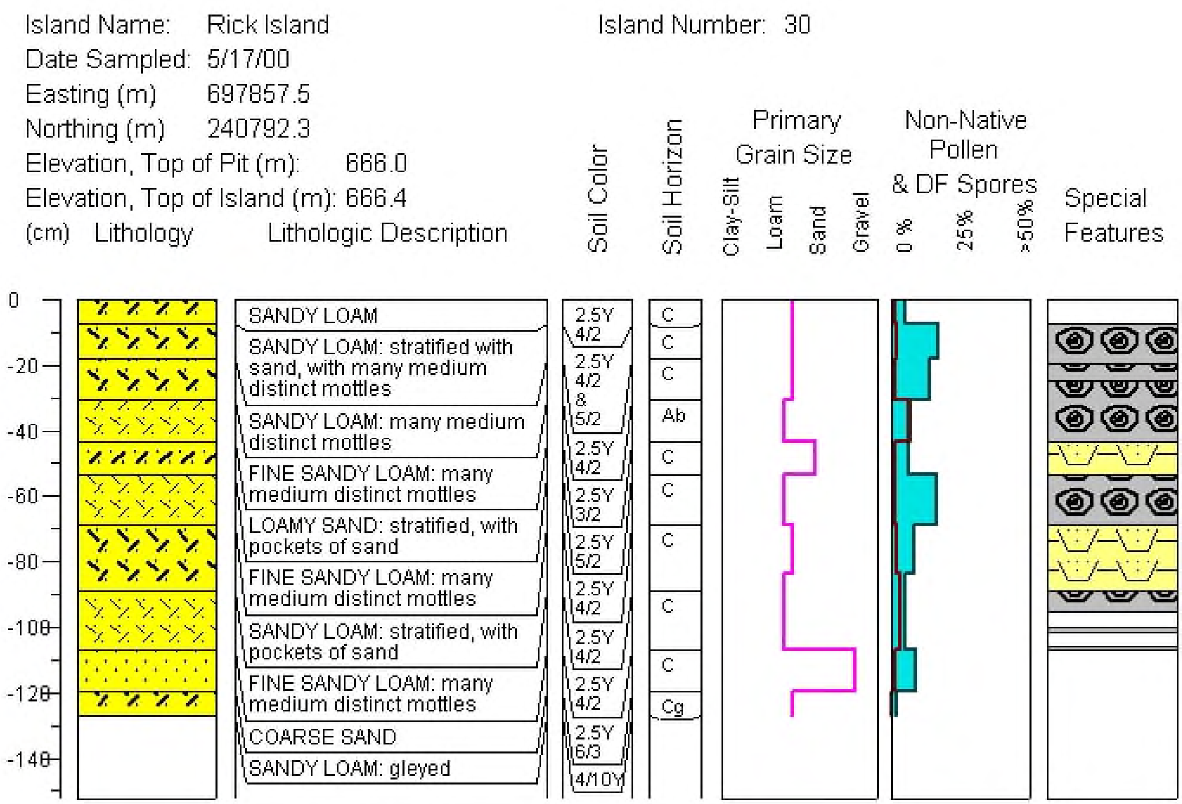

Figure E40. Rick Island (30) soil profile.

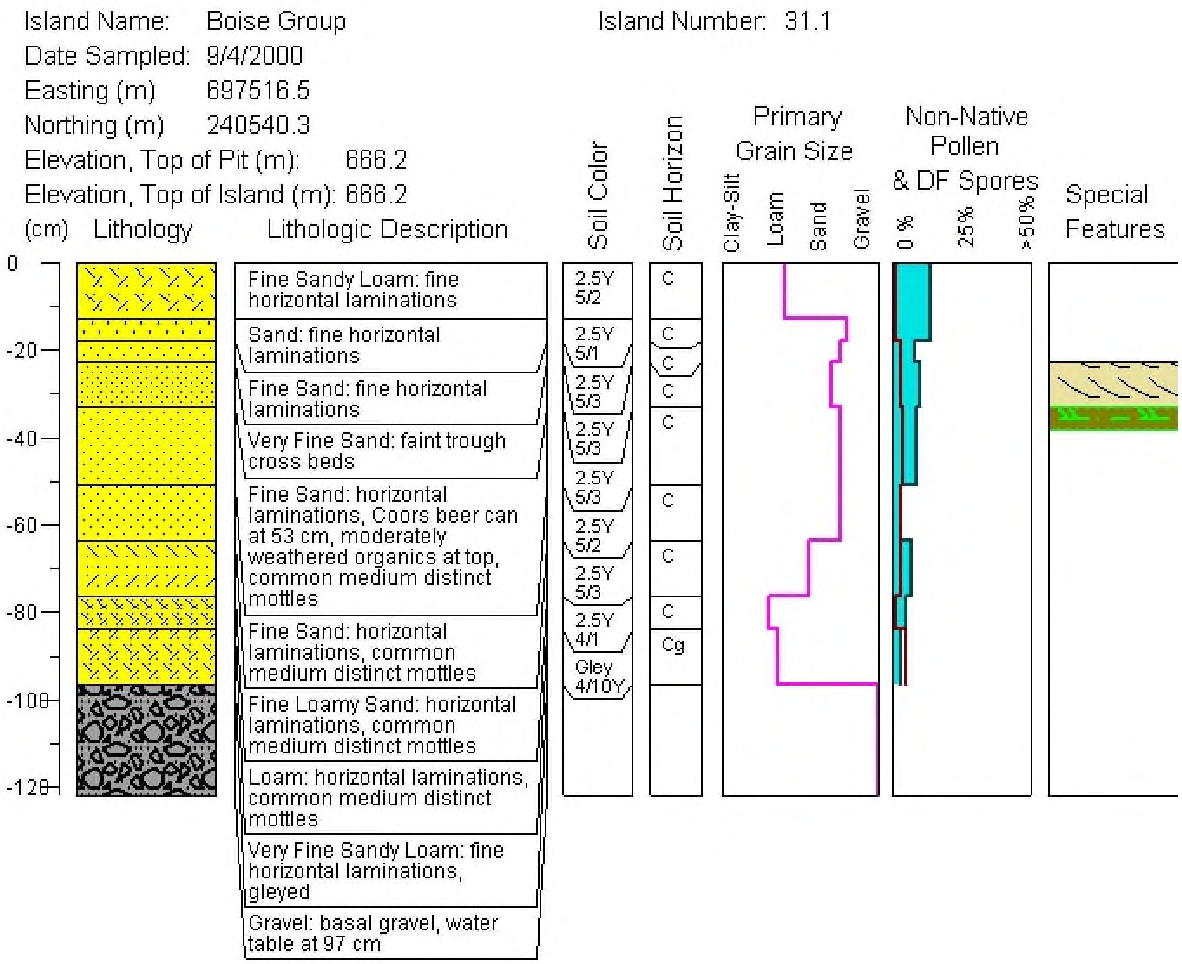

Figure E41. Boise Group (31.1) soil profile.

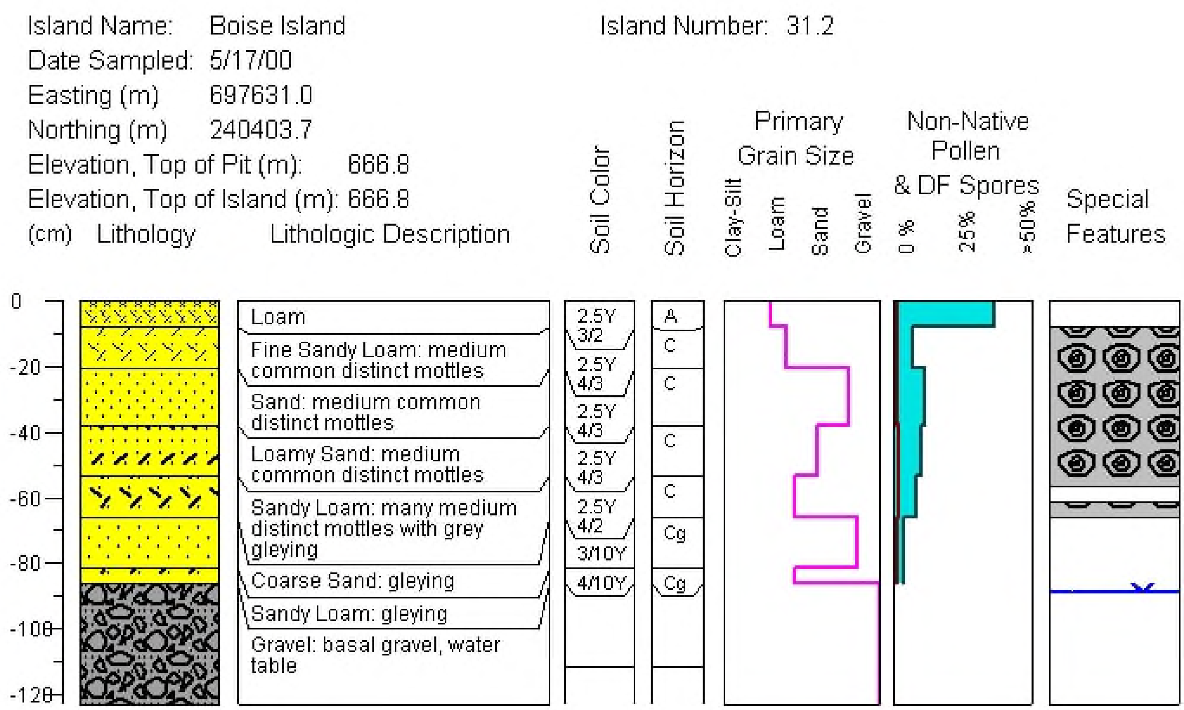

Figure E42. Boise Group (31.2) soil profile.

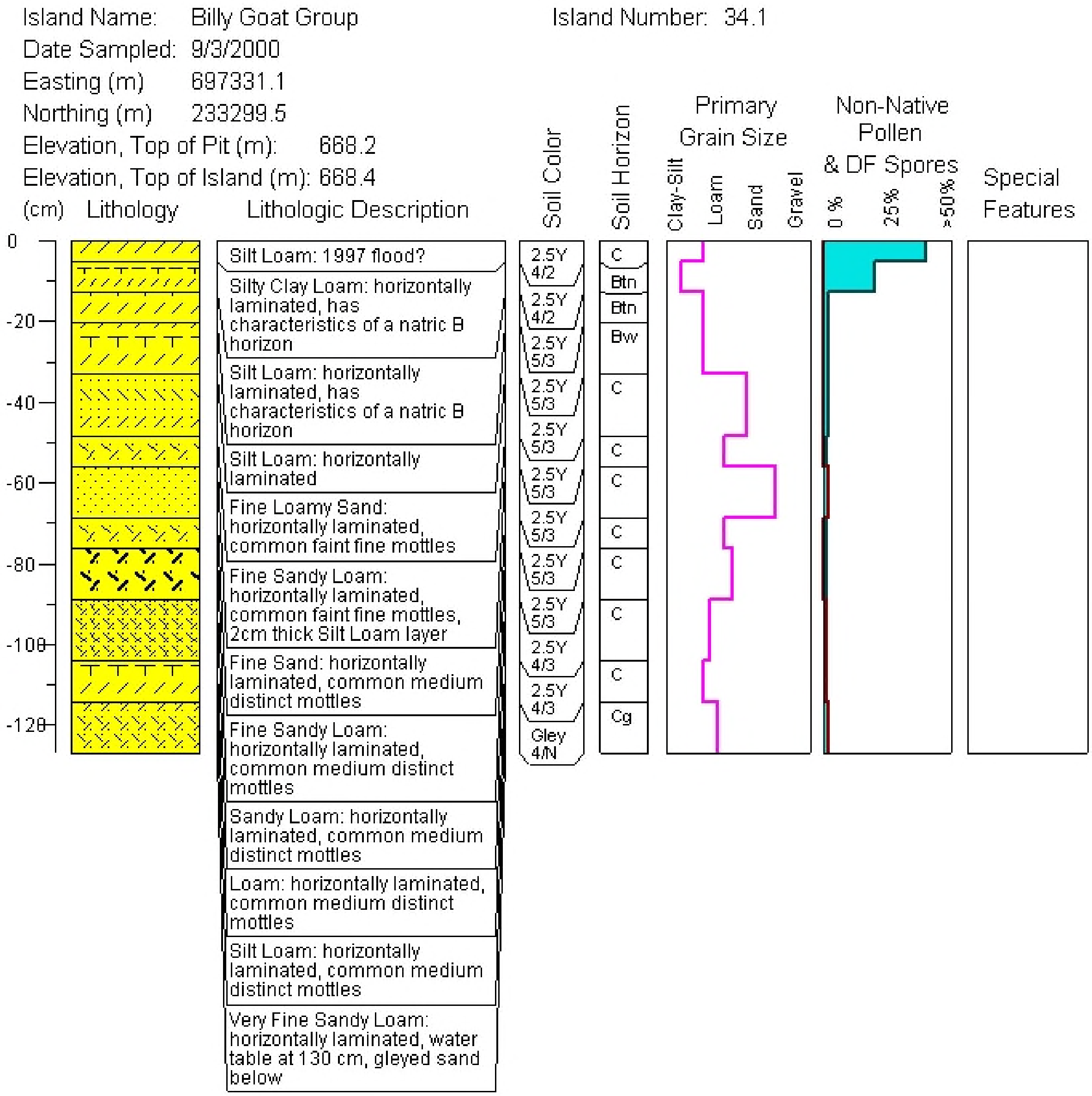

Figure E43. Billy Goat Group (34.1) soil profile.

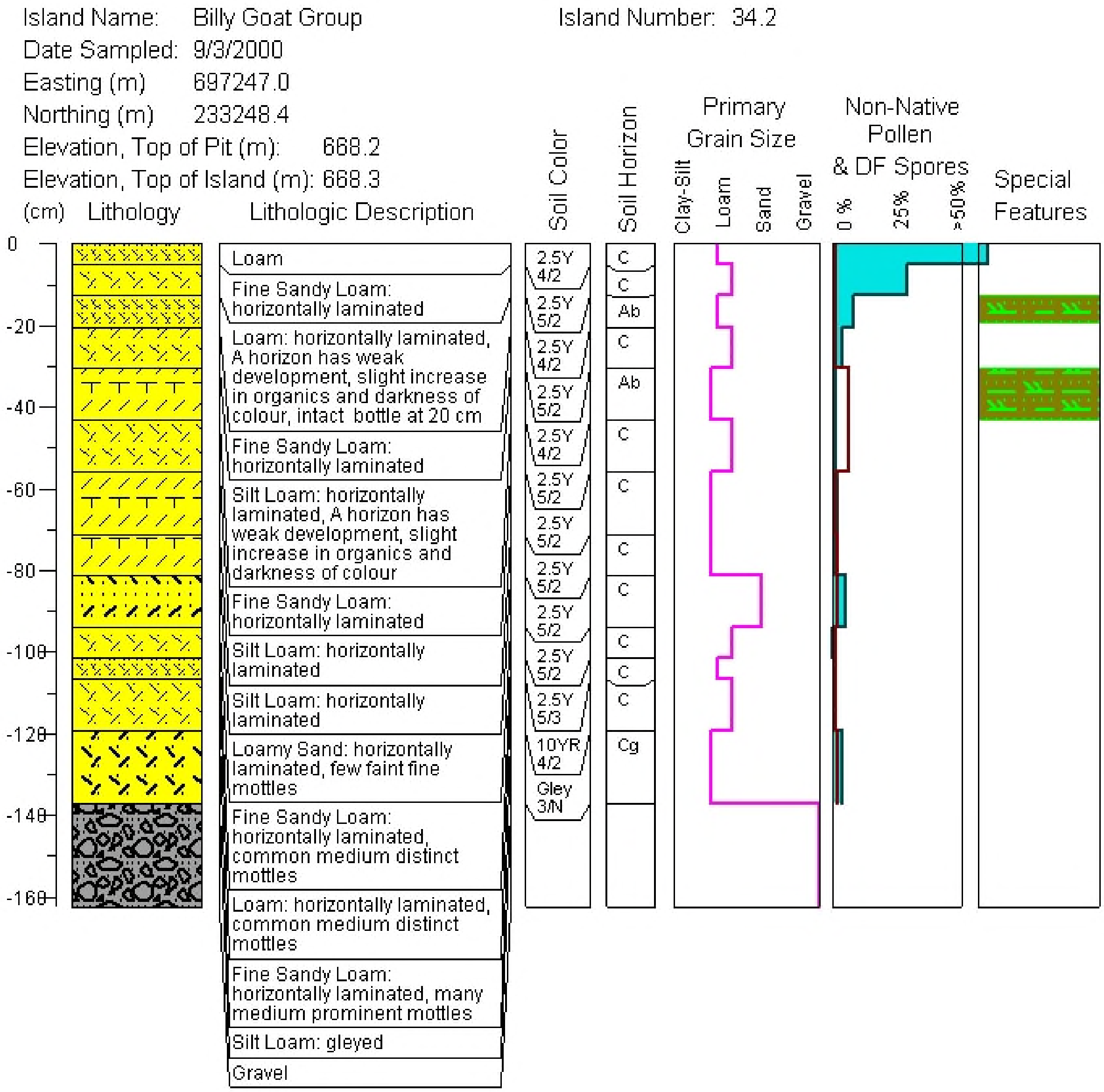

Figure E44. Billy Goat Group (34.2) soil profile.

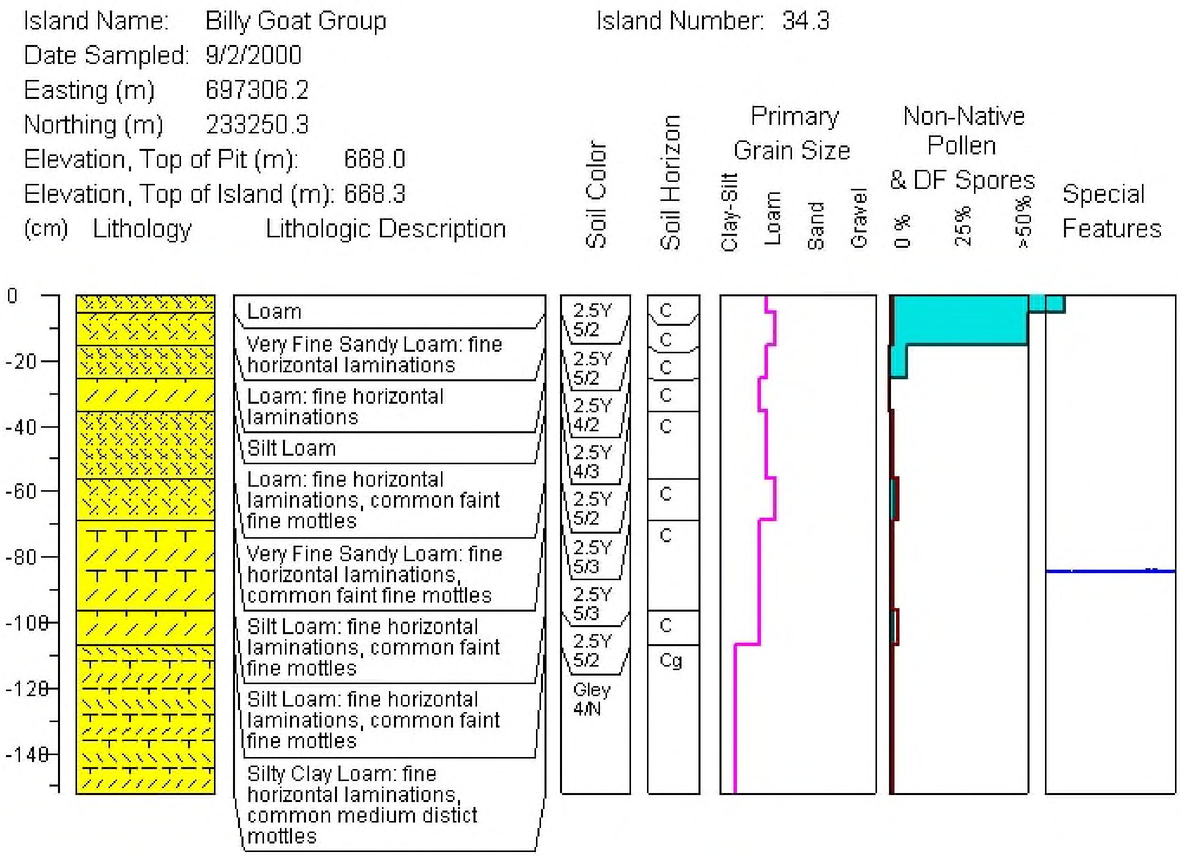

Figure E45. Billy Goat Group (34.3) soil profile.

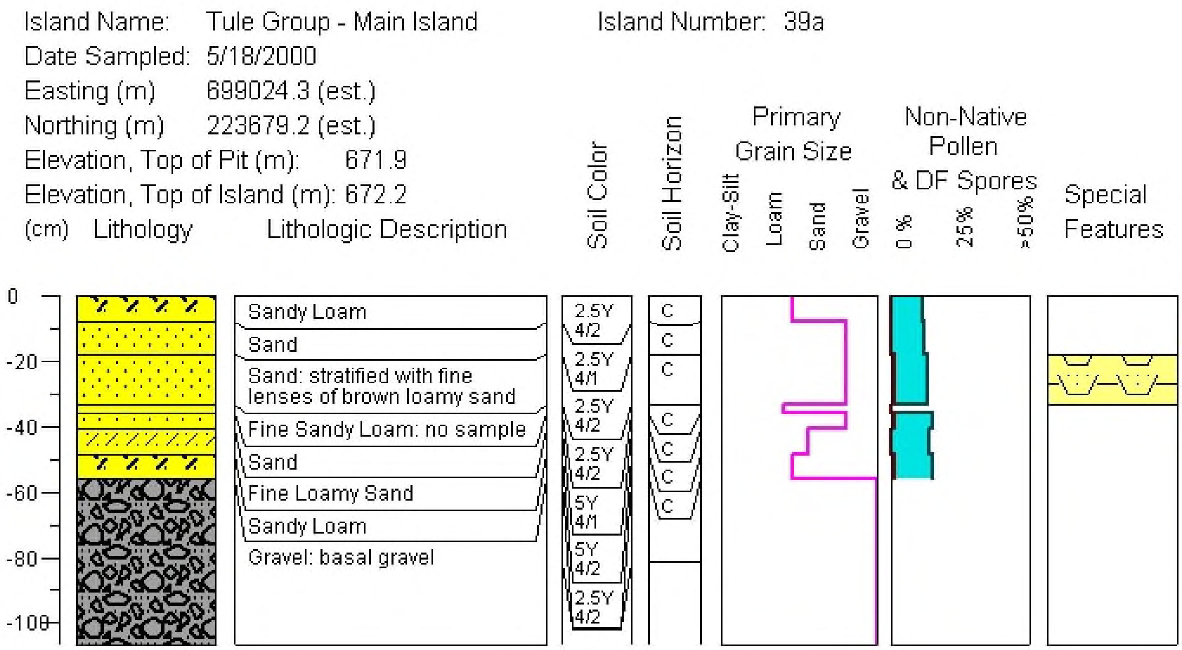

Figure E46. Tule Group, Main Island (39a) soil profile.

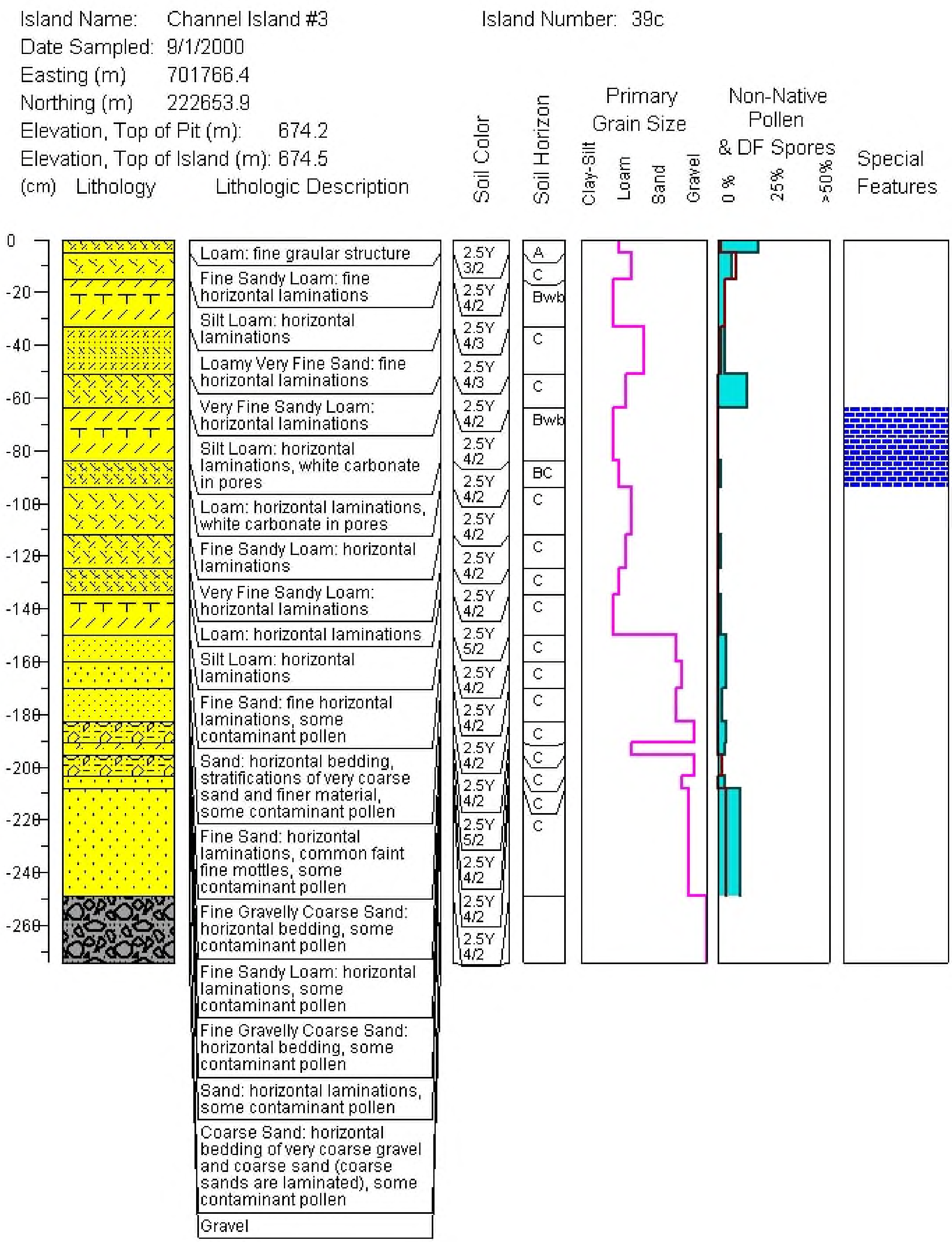

Figure E47. Channel Island #3 (39c) soil profile.

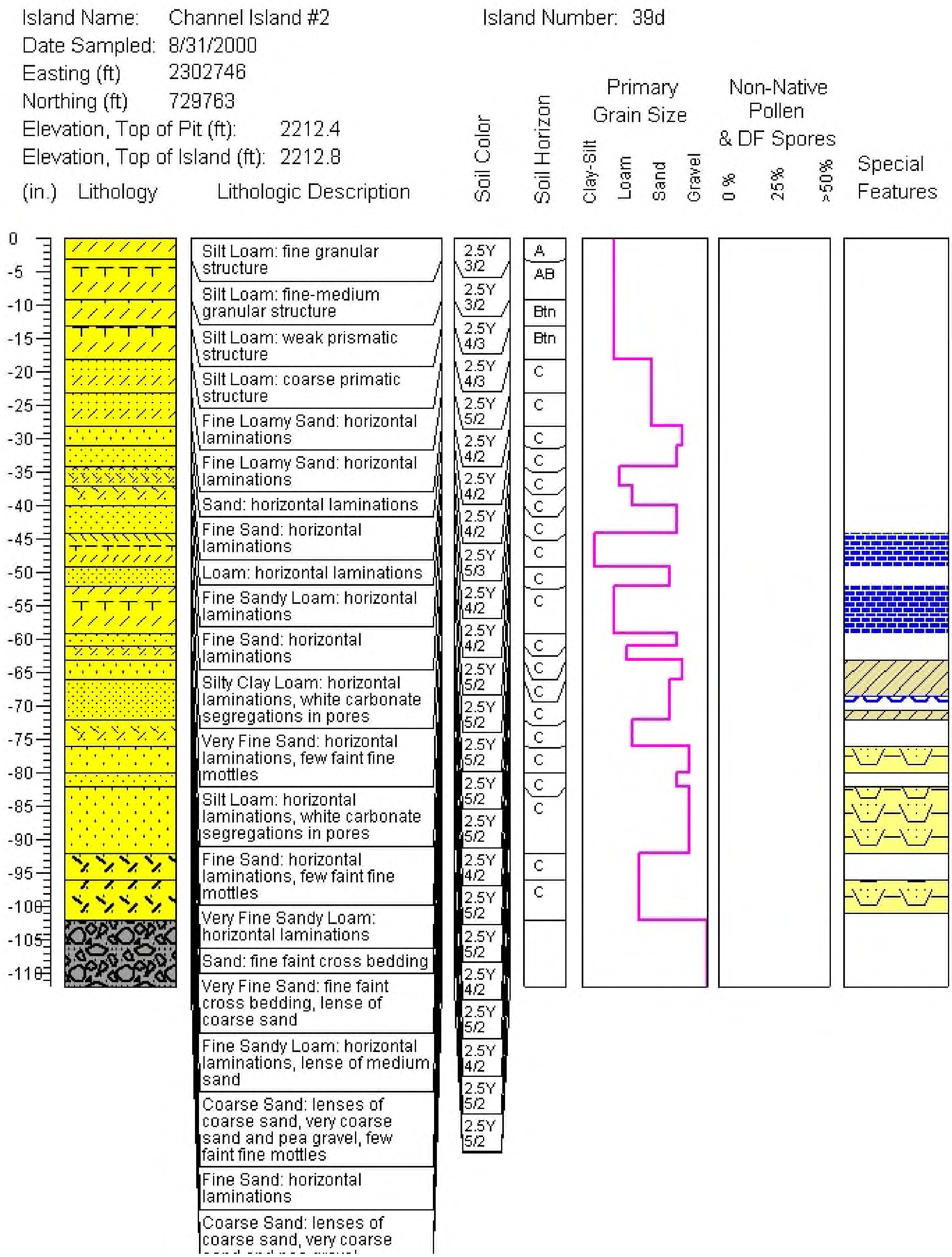

Figure E48. Channel Island #2 (39d) soil profile.

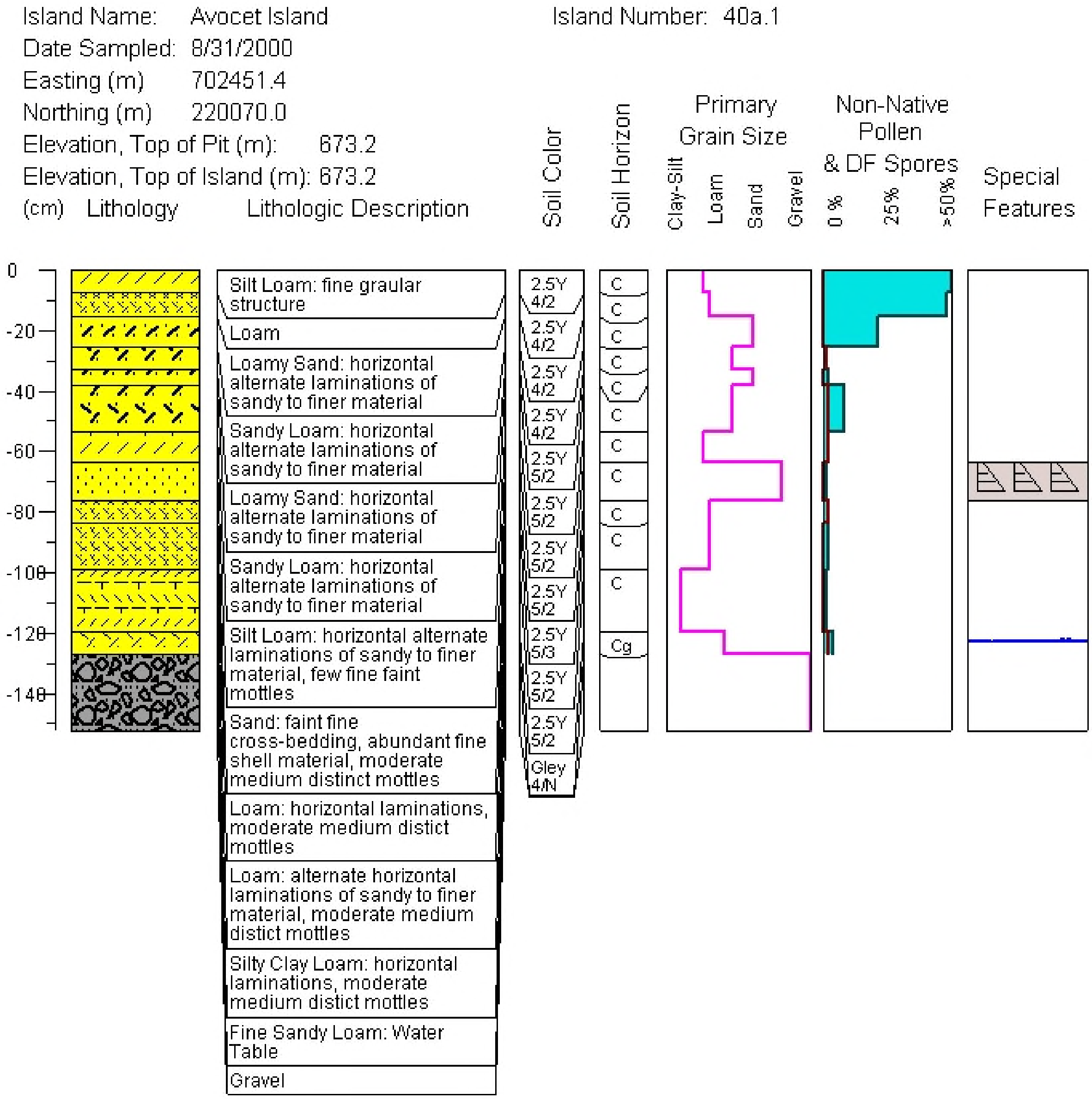

Figure E49. Avocet Island (40a.1) soil profile.

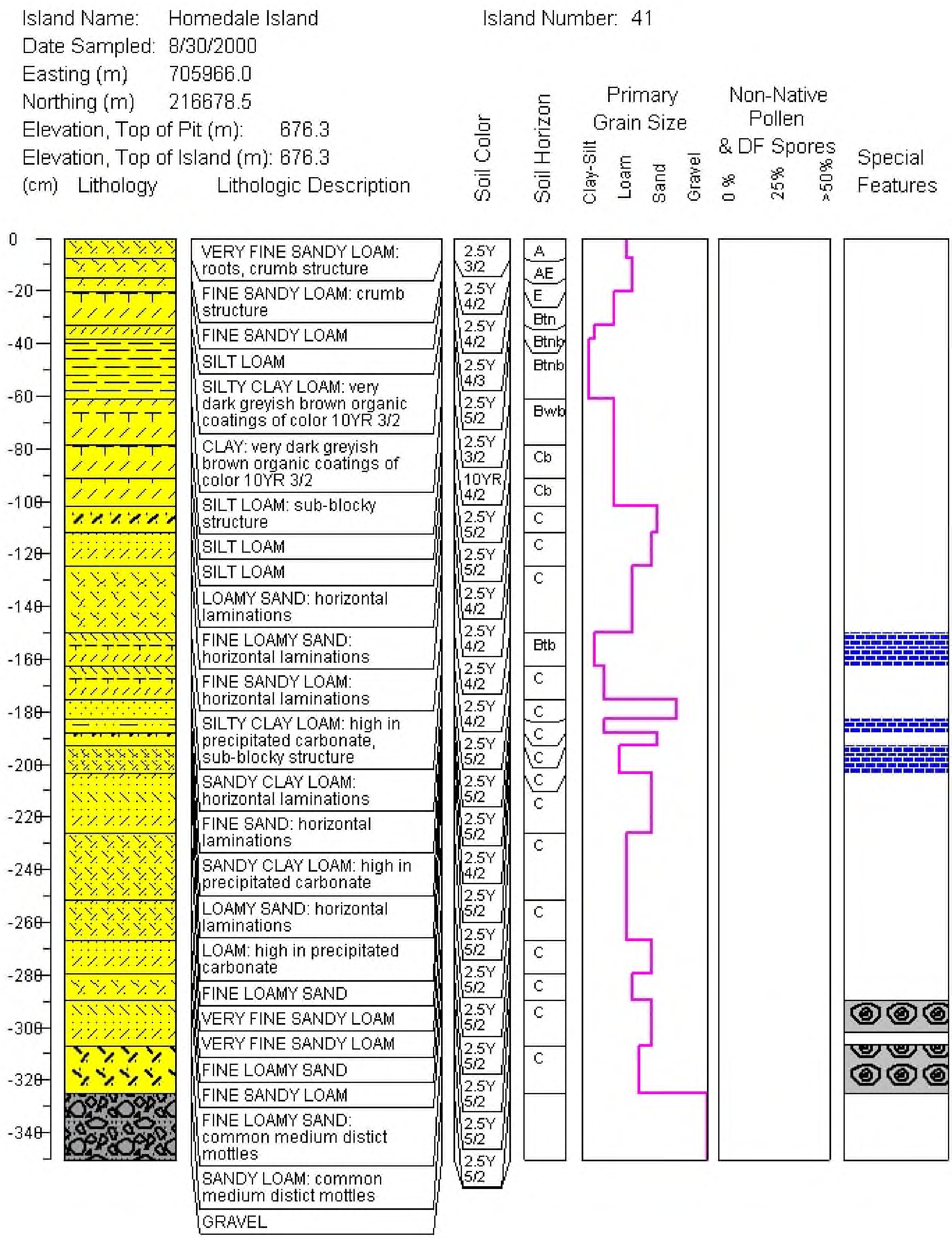

Figure E50. Homedale Island (41) soil profile.

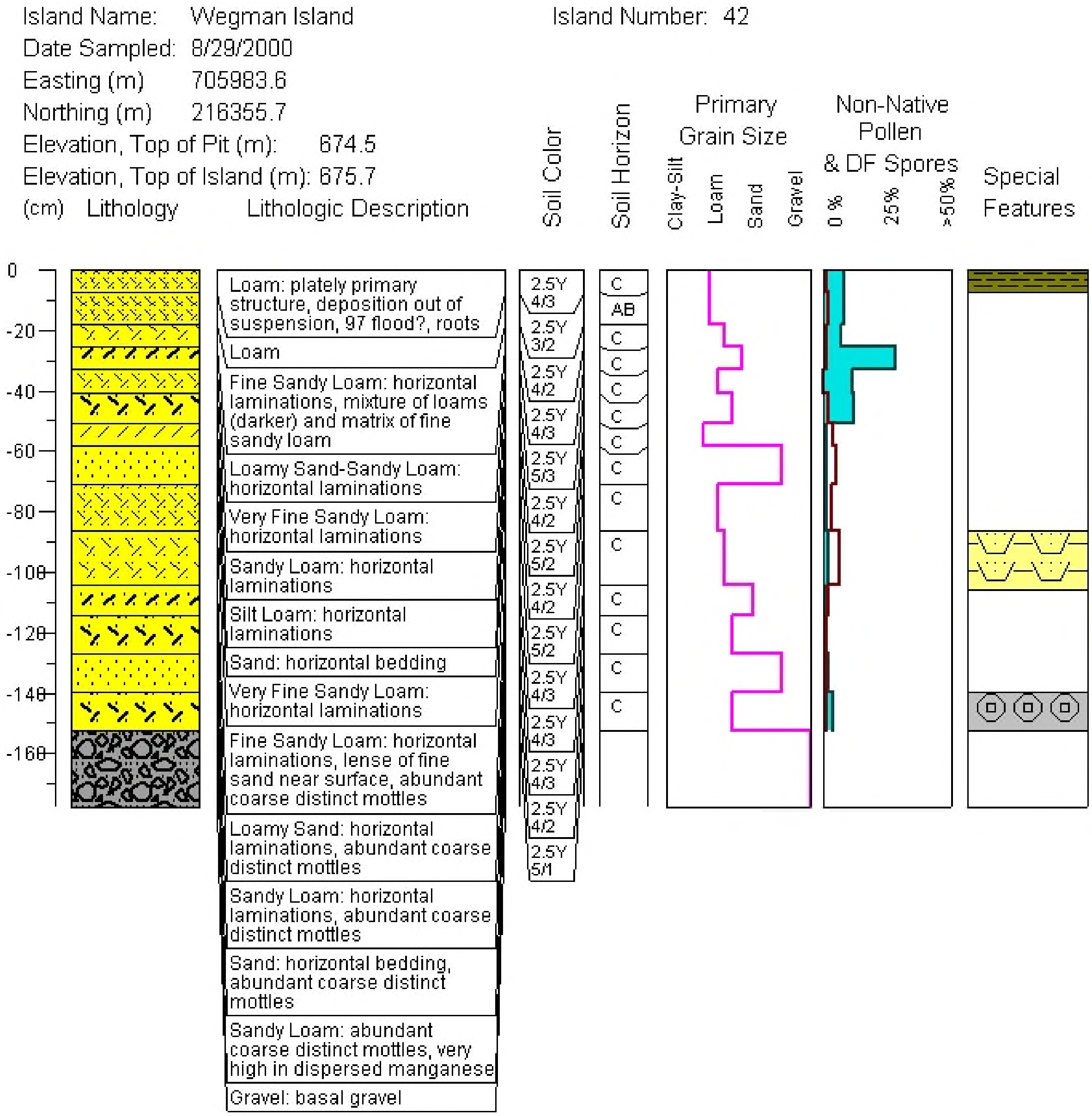

Figure E51. Wegman Island (42) soil profile.

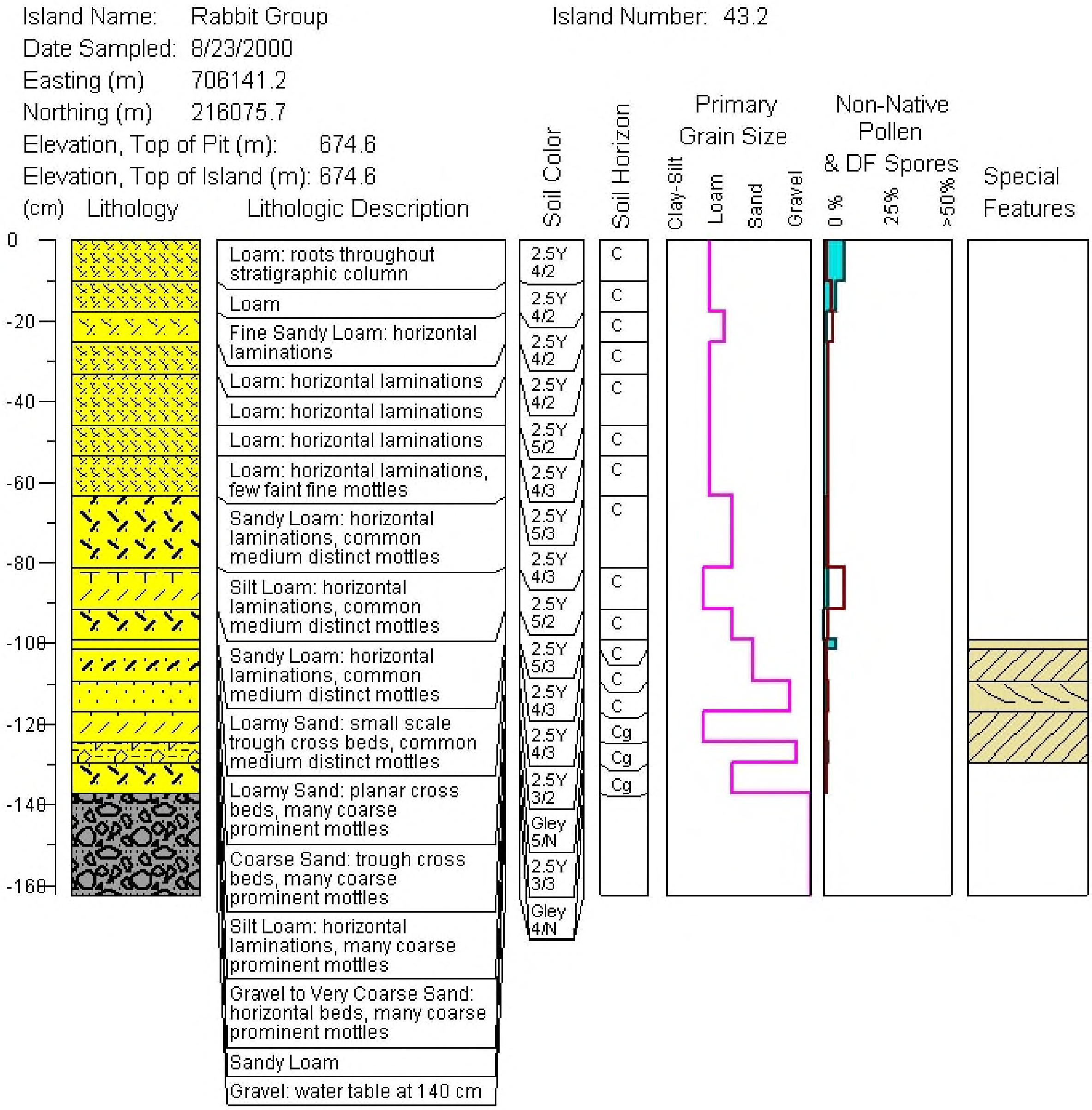

Figure E52. Rabbit Group (43.2) soil profile.

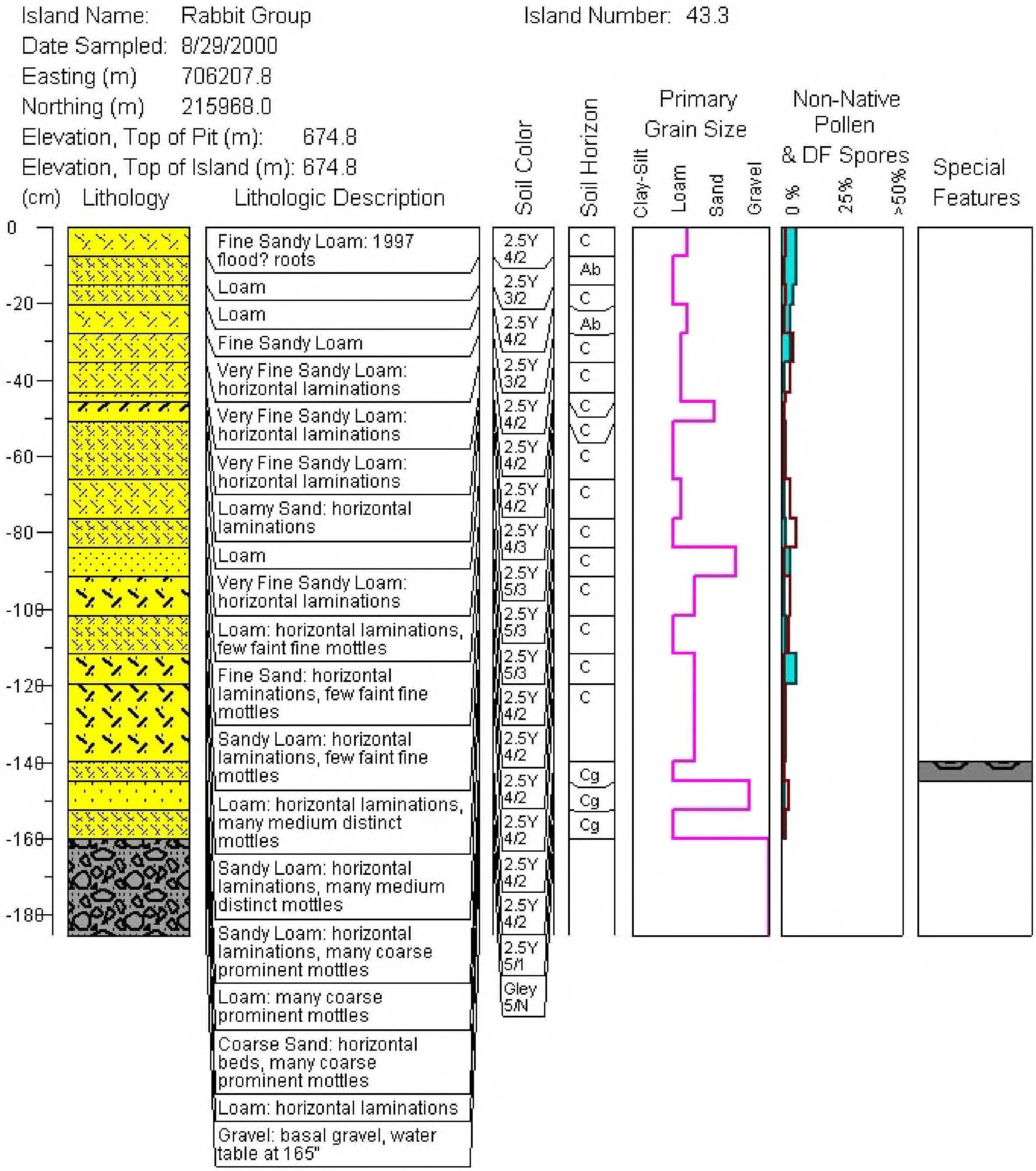

Figure E53. Rabbit Group (43.3) soil profile.

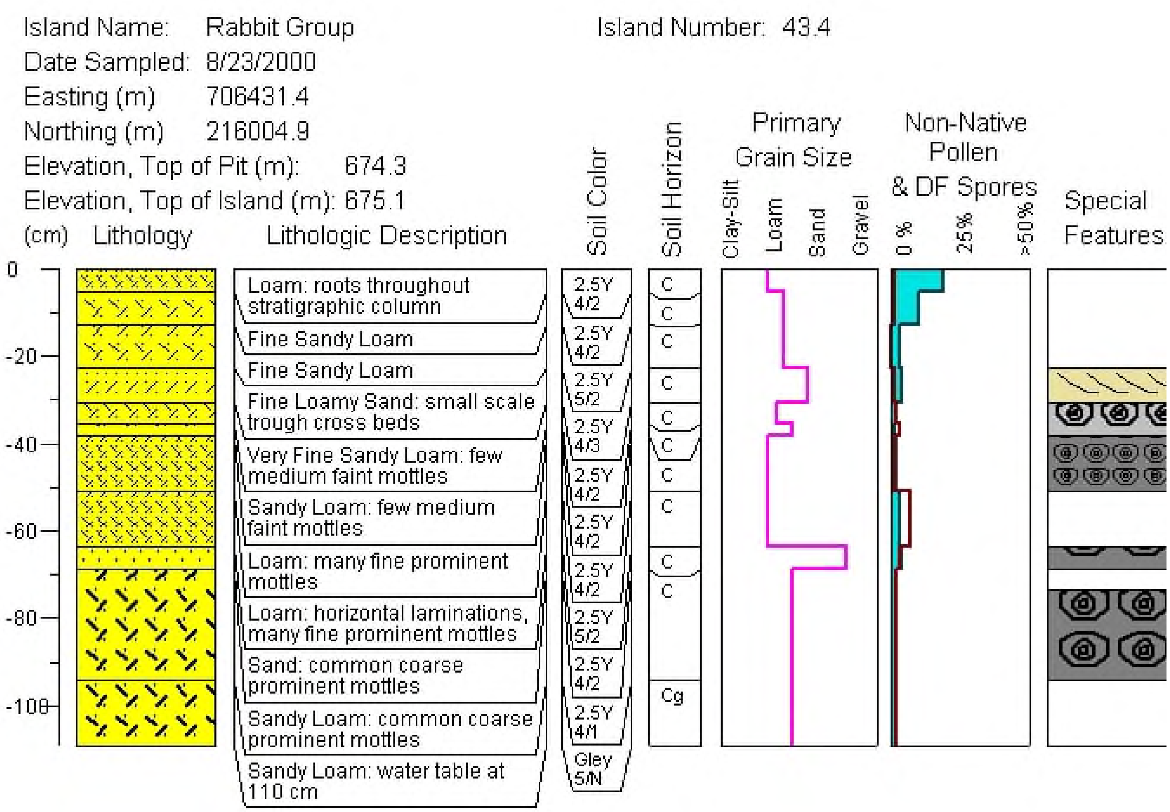

Figure E54. Rabbit Group (43.4) soil profile.

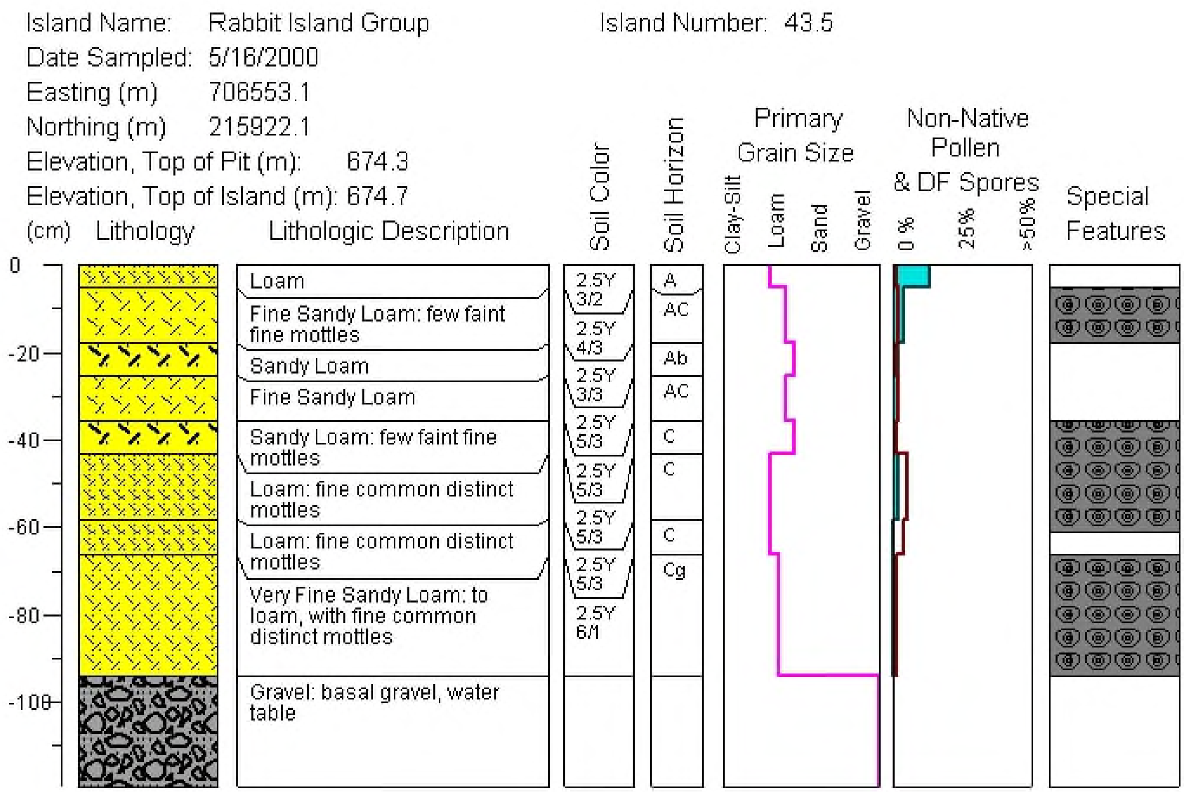

Figure E55. Rabbit Group (43.5) soil profile.

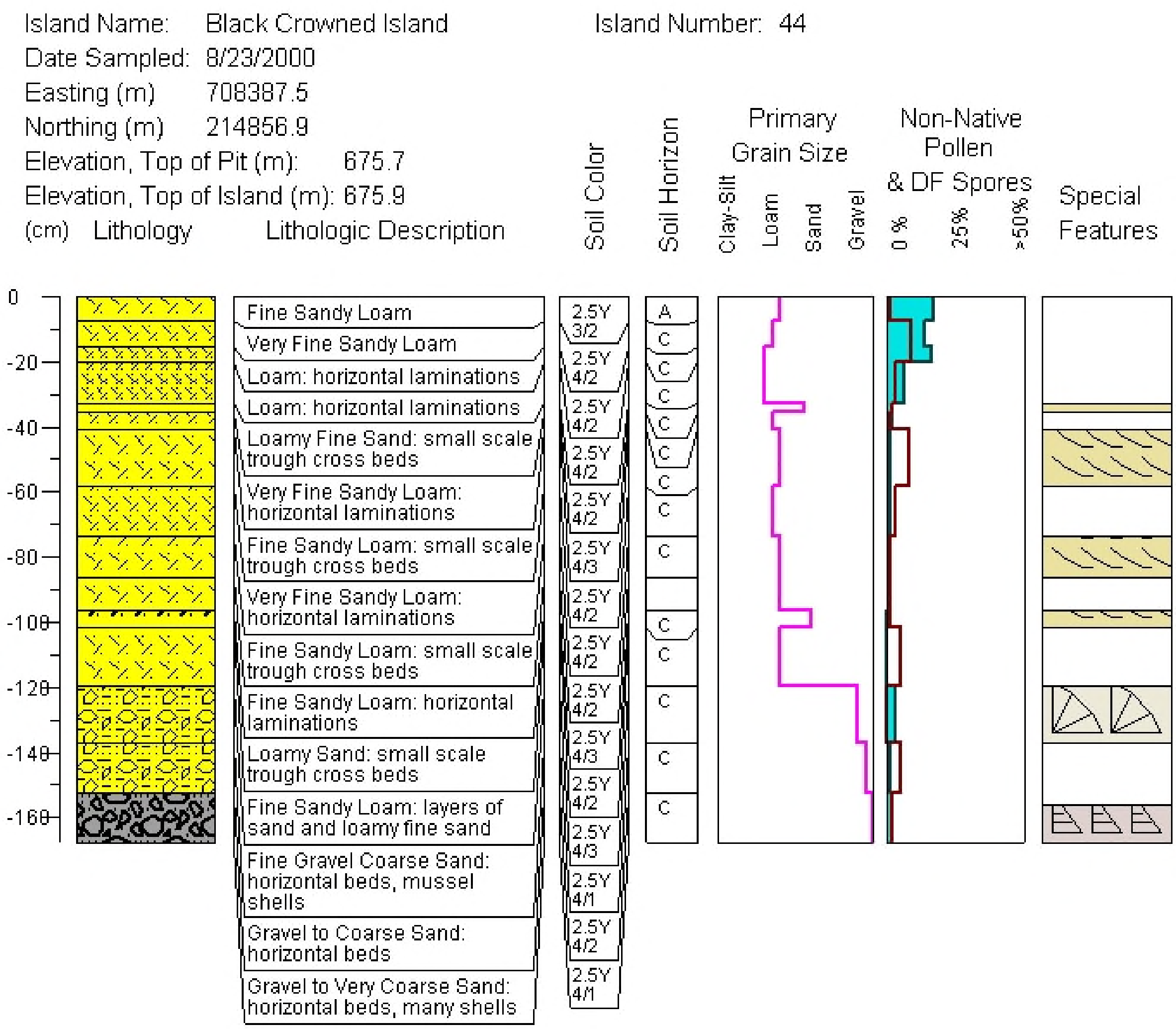

Figure E56. Black Crowned Island (44) soil profile.

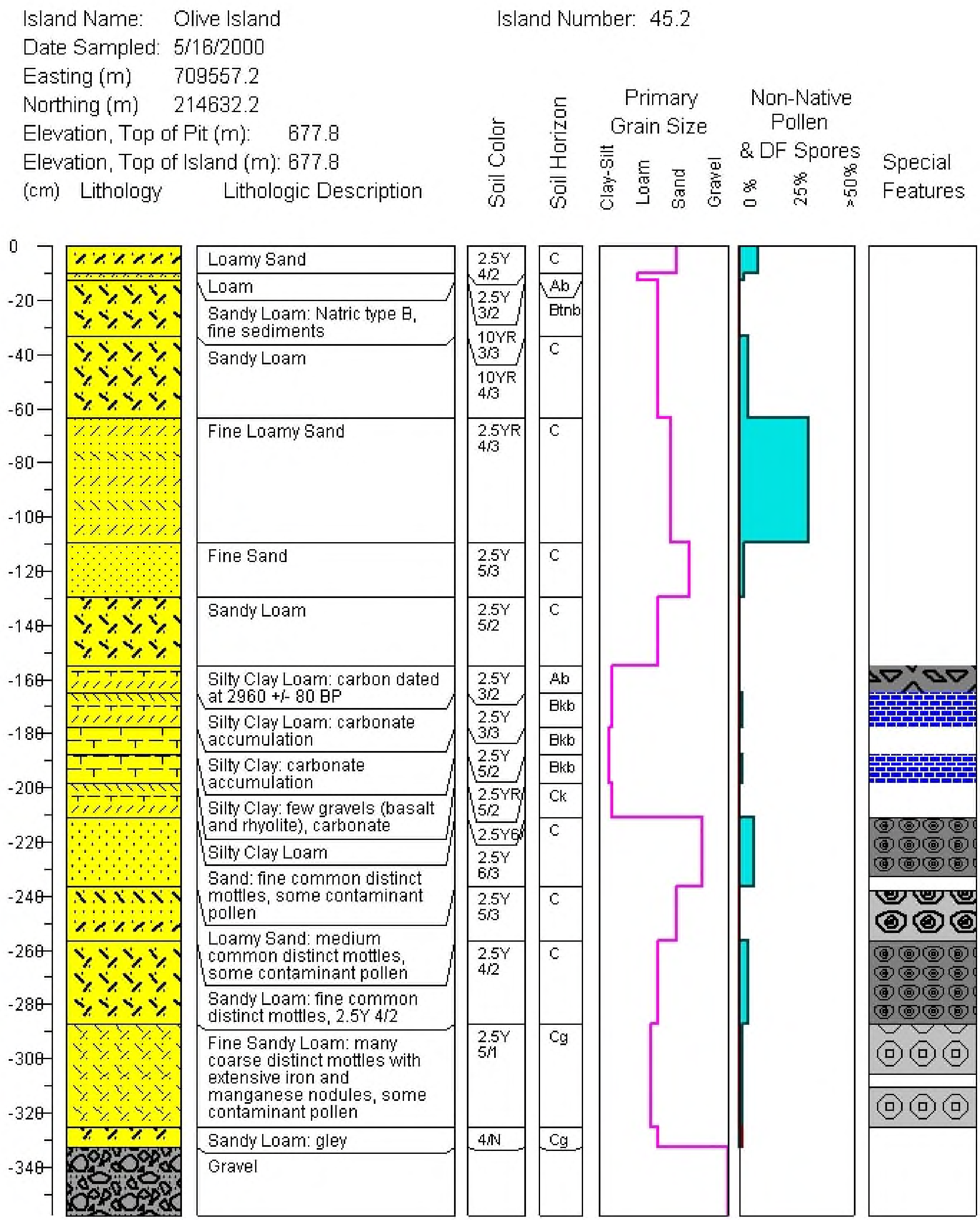

Figure E57. Olive Island (45.2) soil profile.

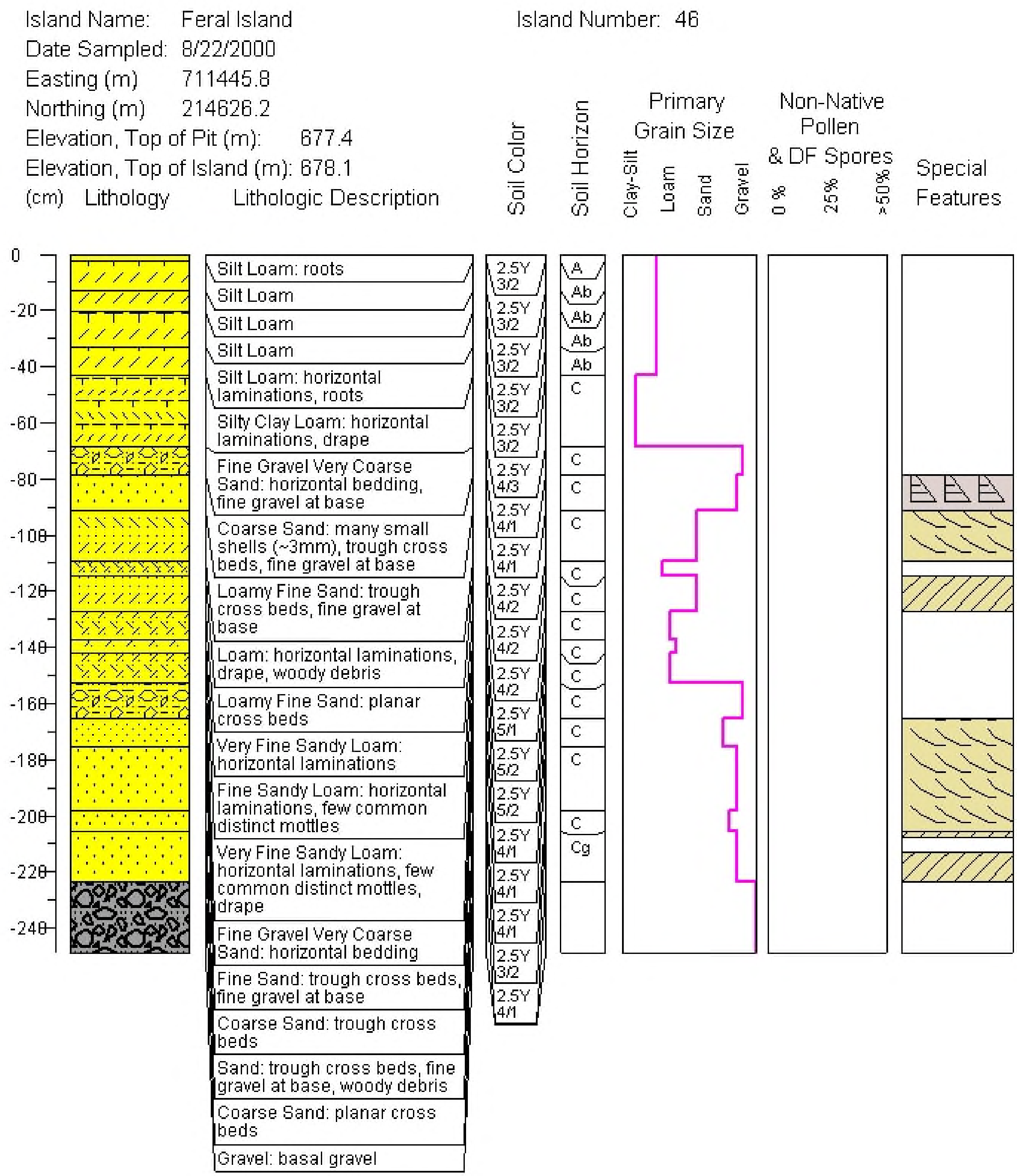

Figure E58. Feral Island (46) soil profile.

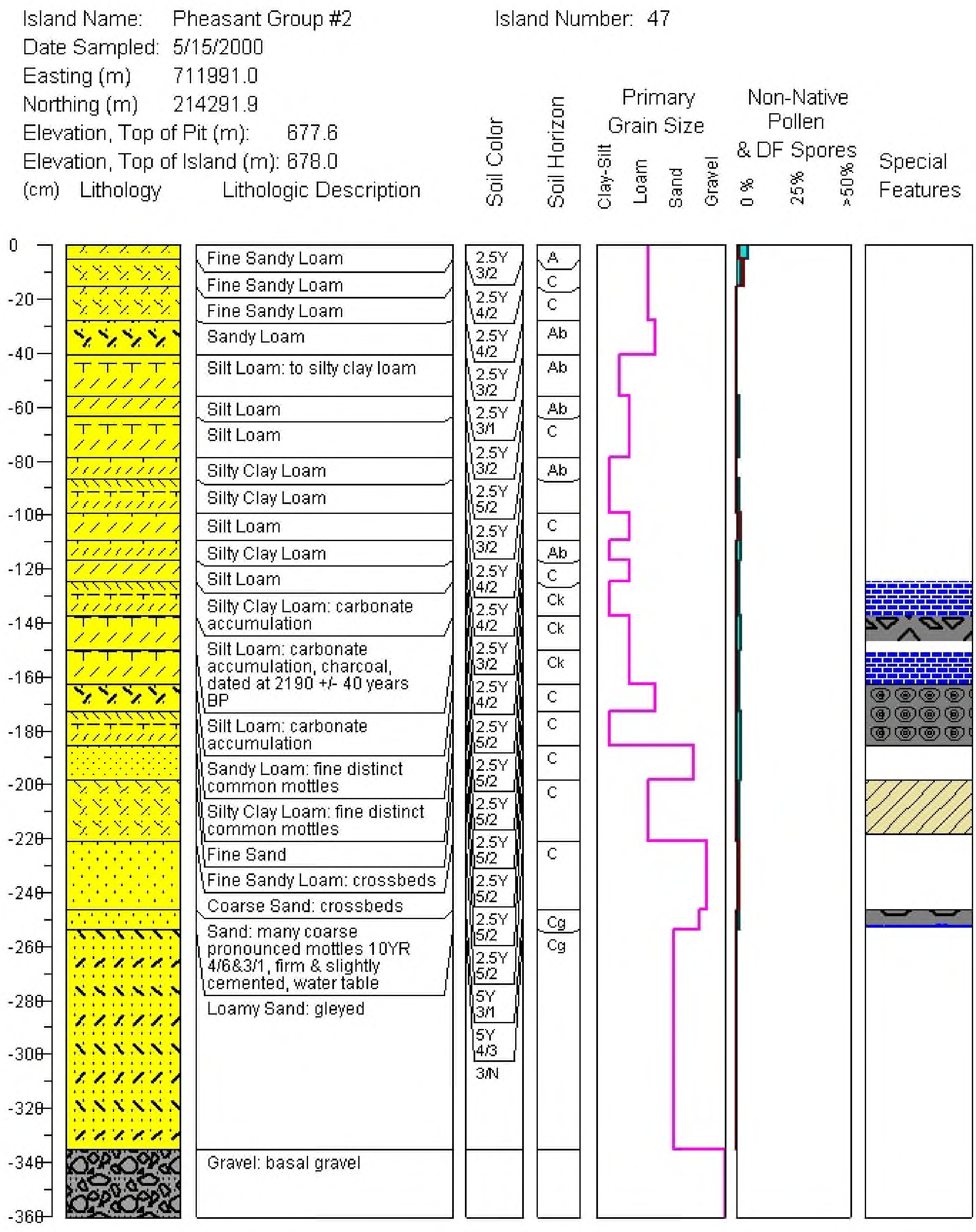

Figure E59. Pheasant Group #2 (47) soil profile.

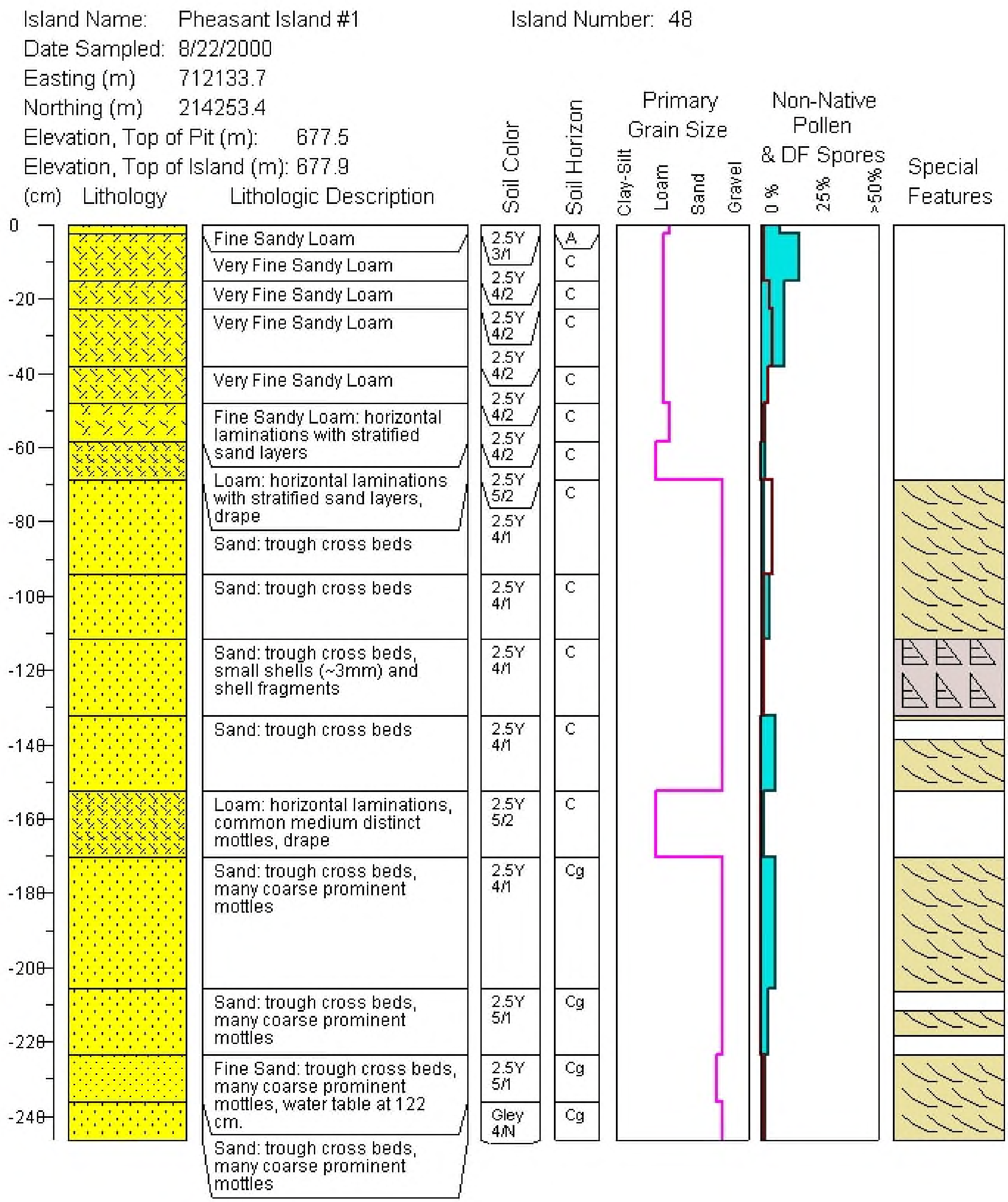

Figure E60. Pheasant Island #1 (48) soil profile.

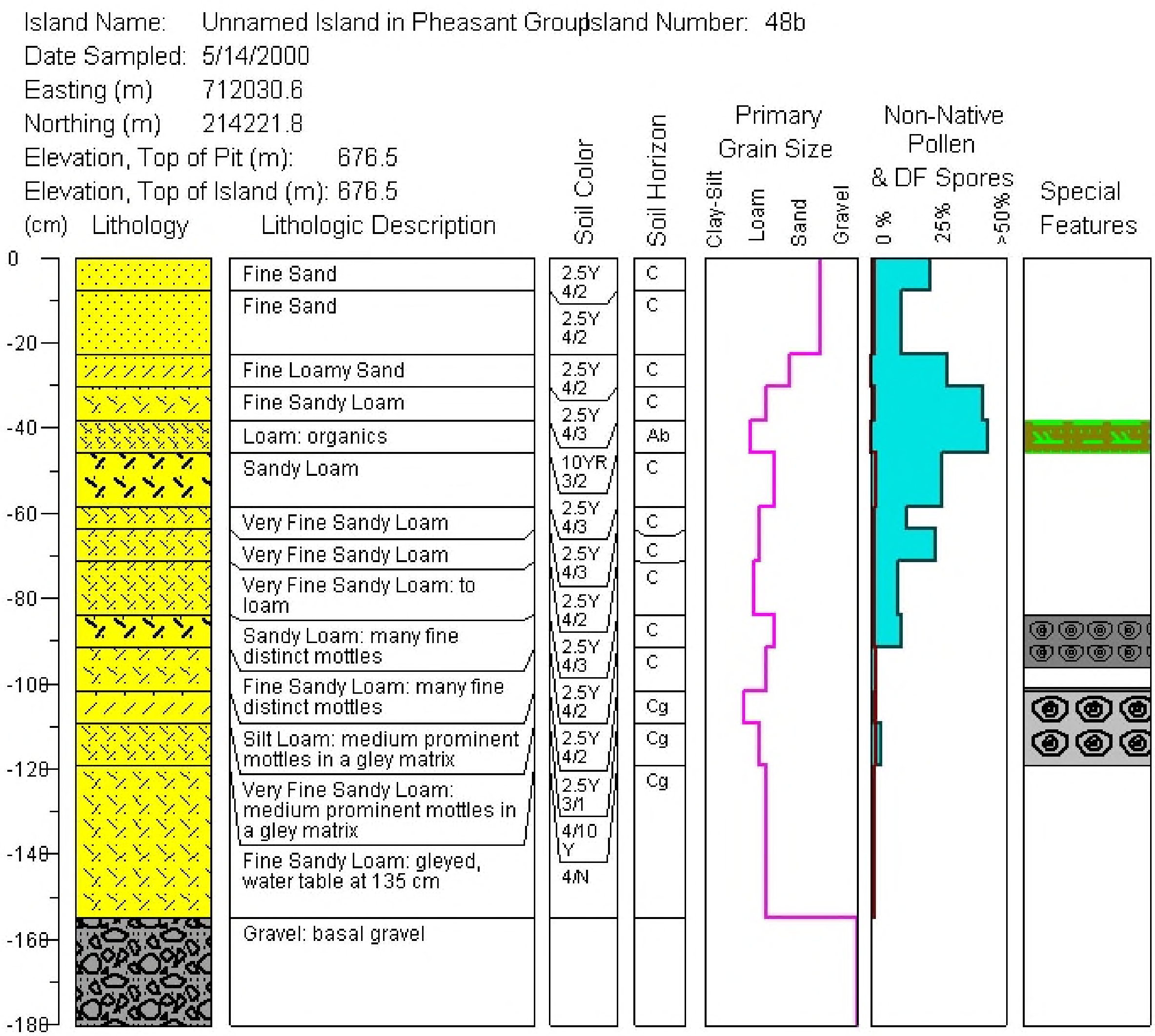

Figure E61. Unnamed Island in Pheasant Group (48bb) soil profile.

Island Name: Pheasant Island #3
Date Sampled: 5/15/2000
Easting (m) 712222.2
Northing (m) 214140.7
Elevation, Top of Pit (m): 676.4
Elevation, Top of Island (m): 676.4

Island Number: 49

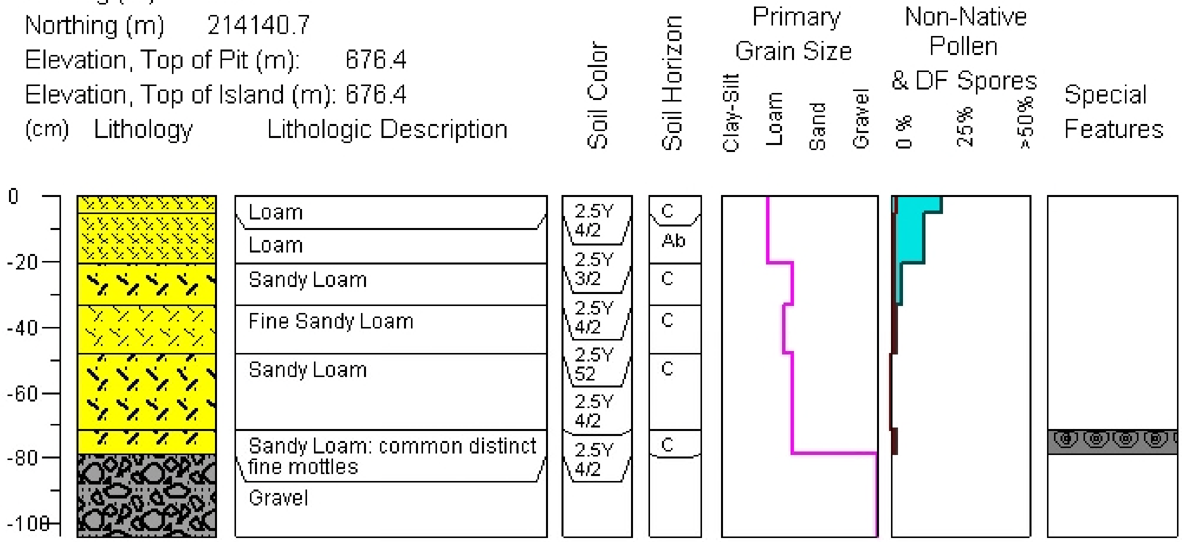

Figure E62. Pheasant Island #3 (49) soil profile.

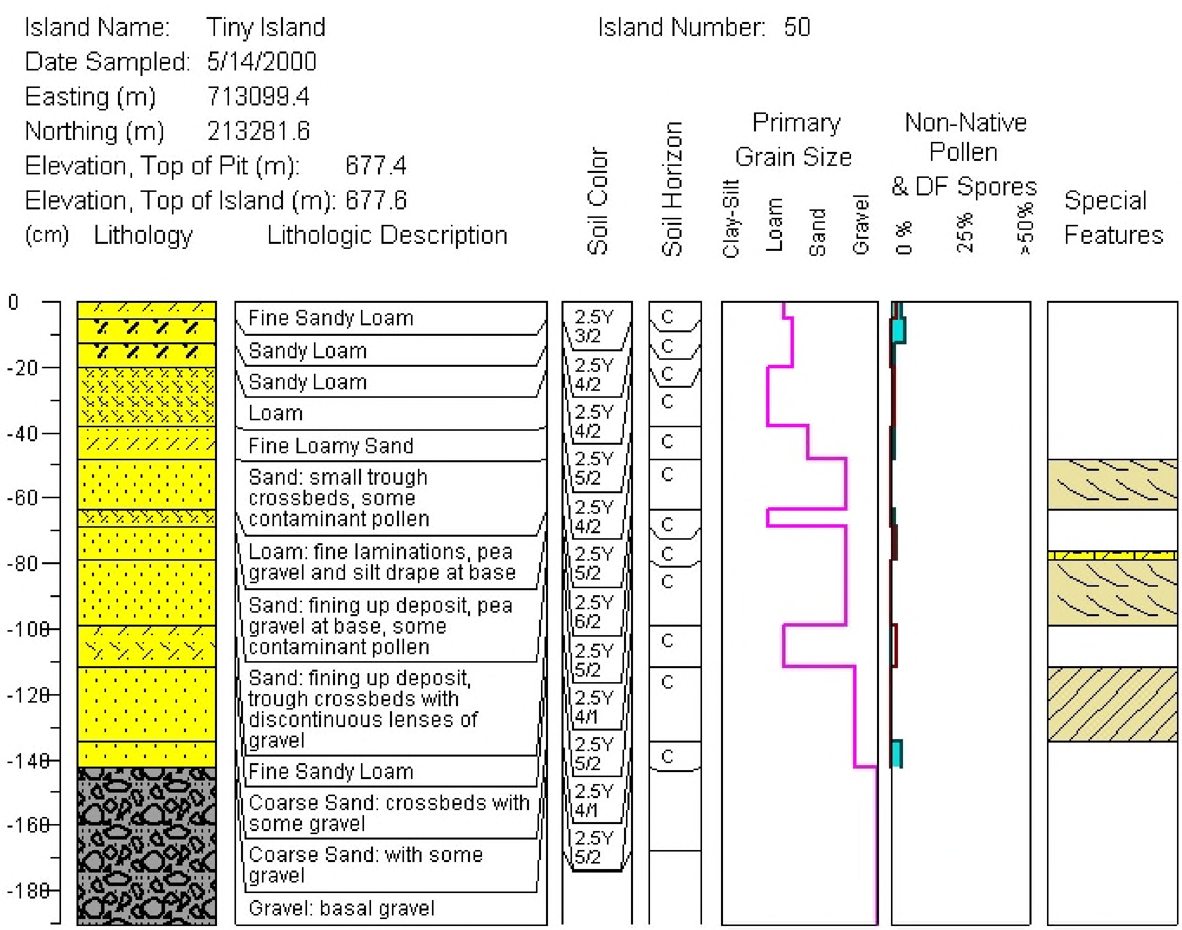

Figure E63. Tiny Island (50) soil profile.

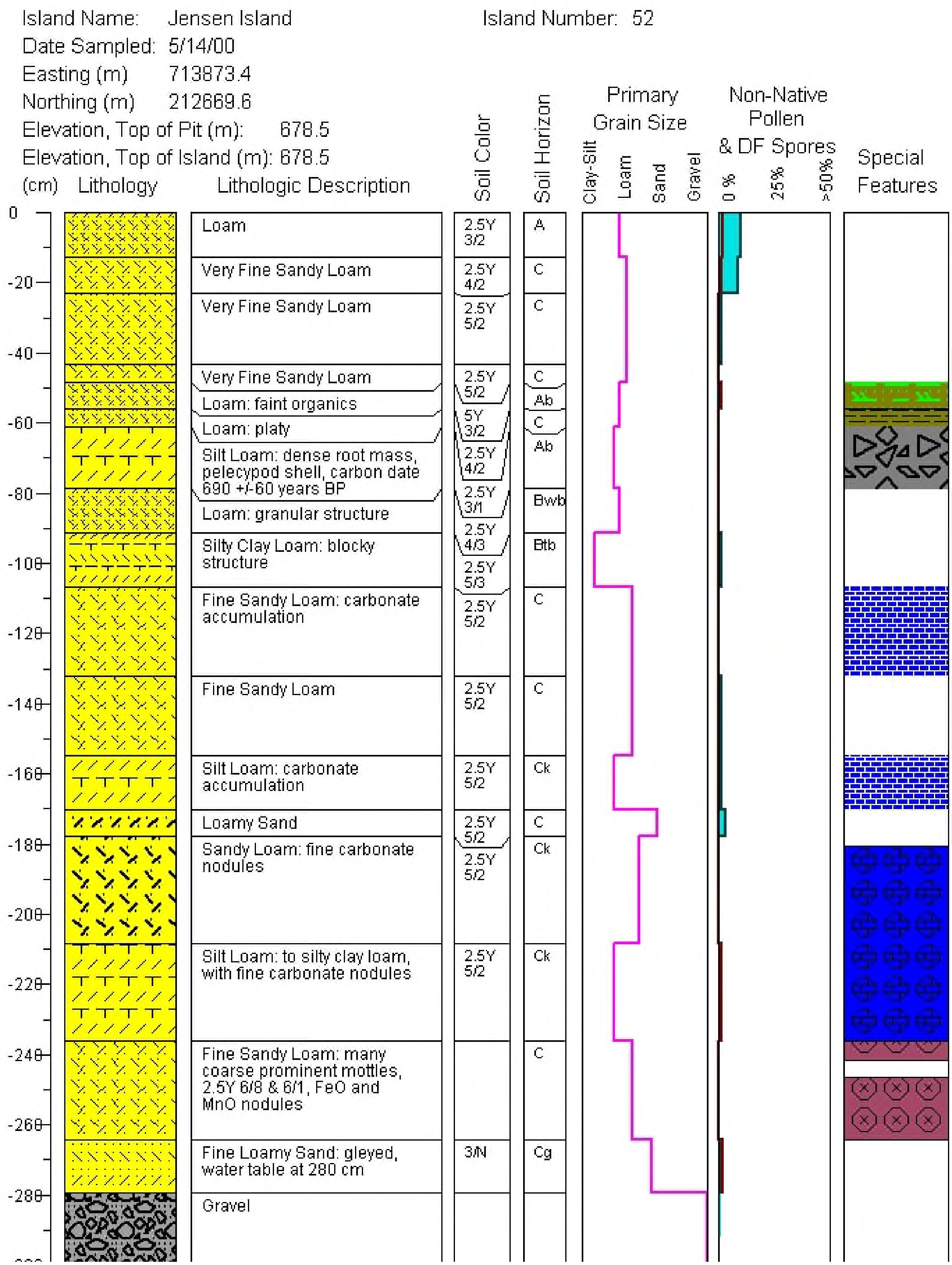

Figure E64. Jensen Island (52) soil profile.

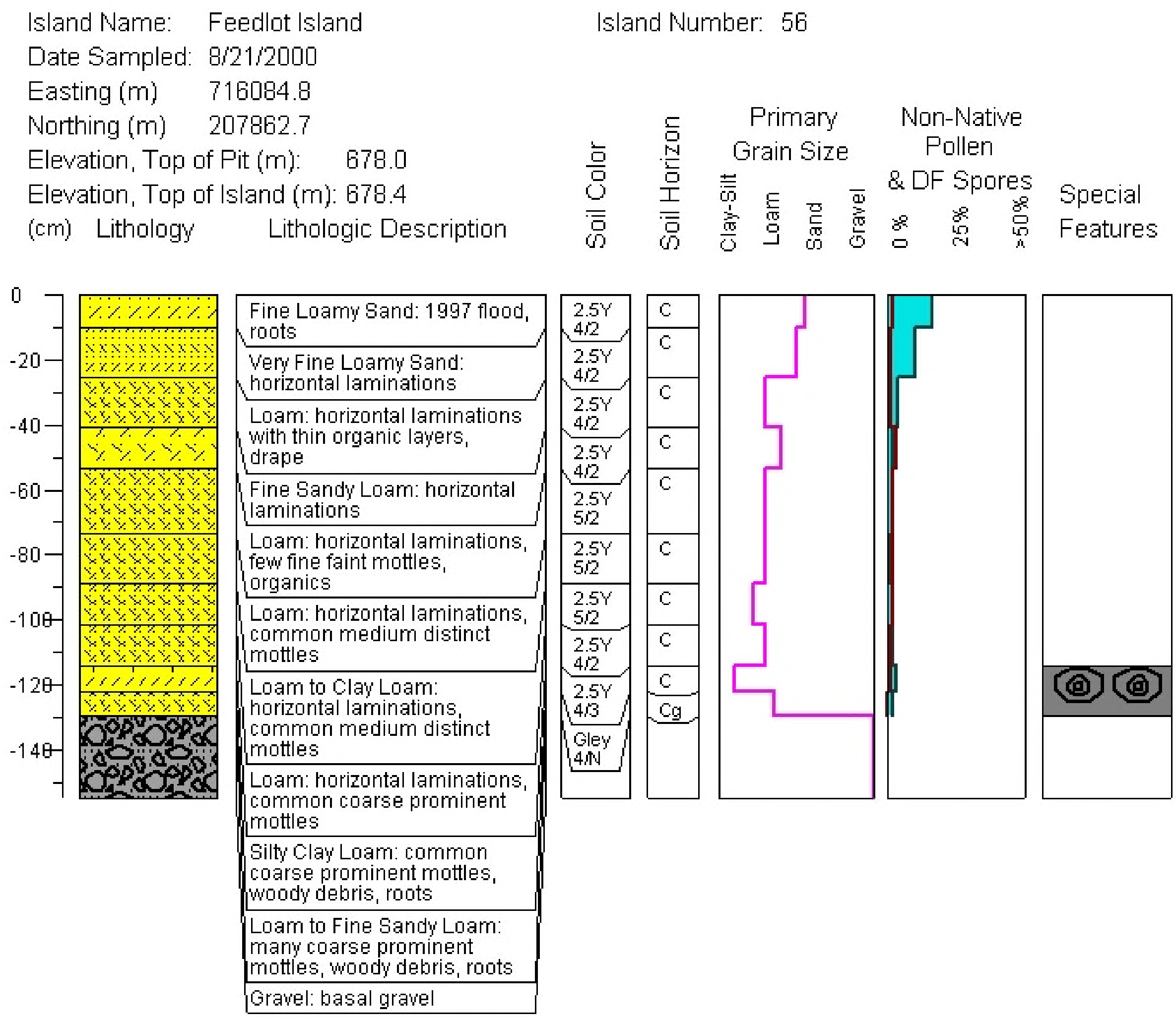

Figure E65. Feedlot Island (56) soil profile.

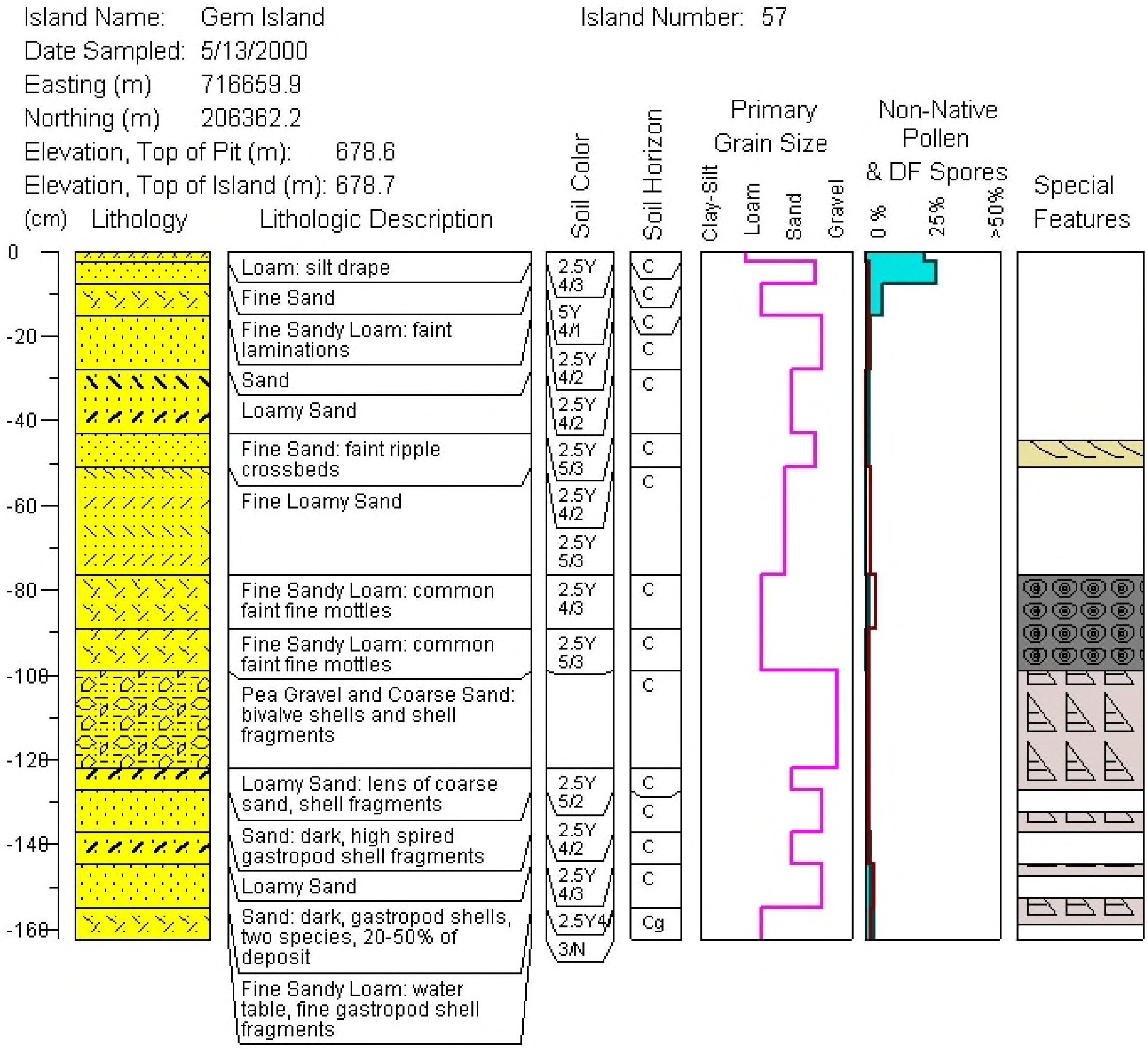

Figure E66. Gem Island (57) soil profile.

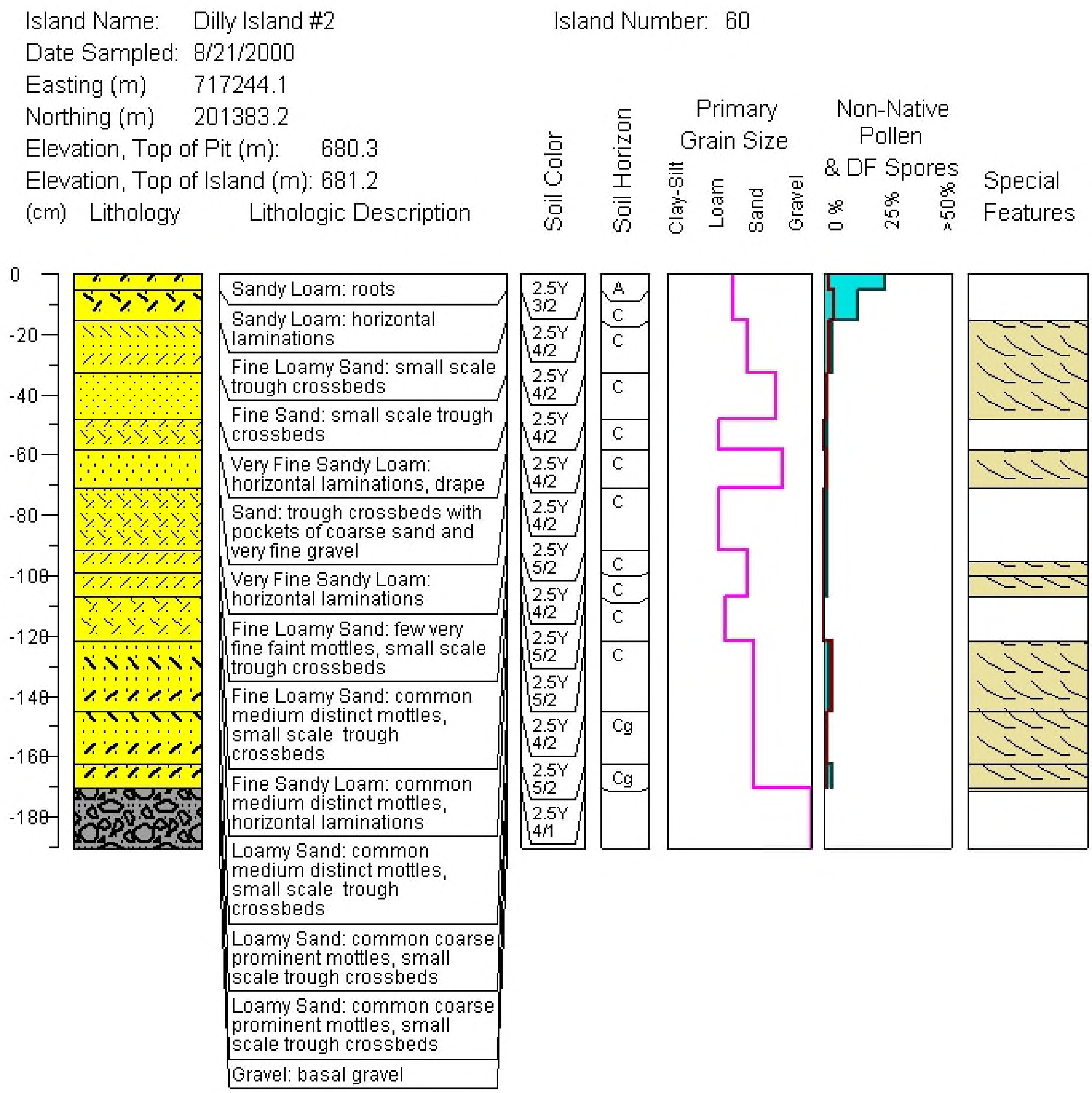

Figure E67. Dilly Island #2 (60) soil profile.

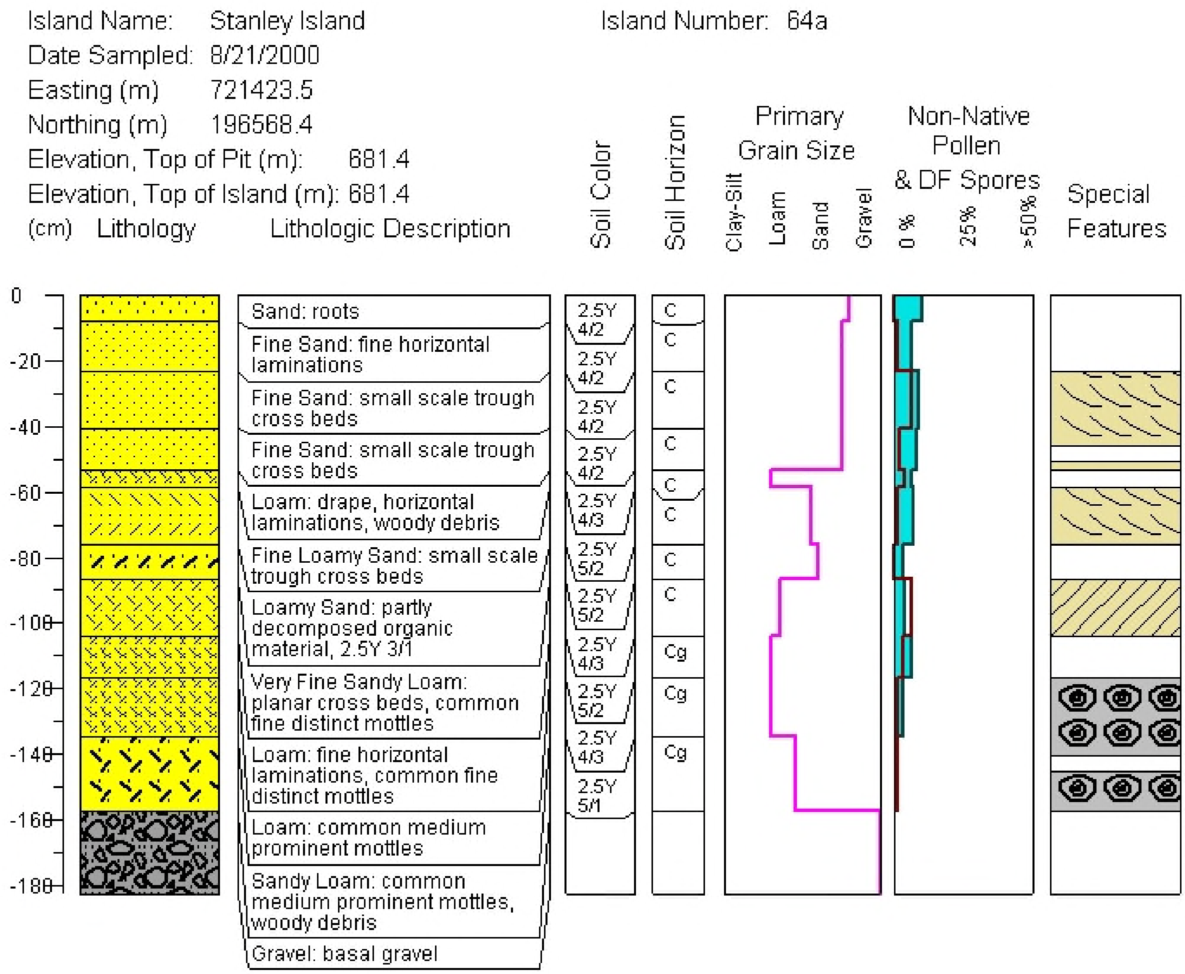

Figure E68. Stanley Island (64a) soil profile.

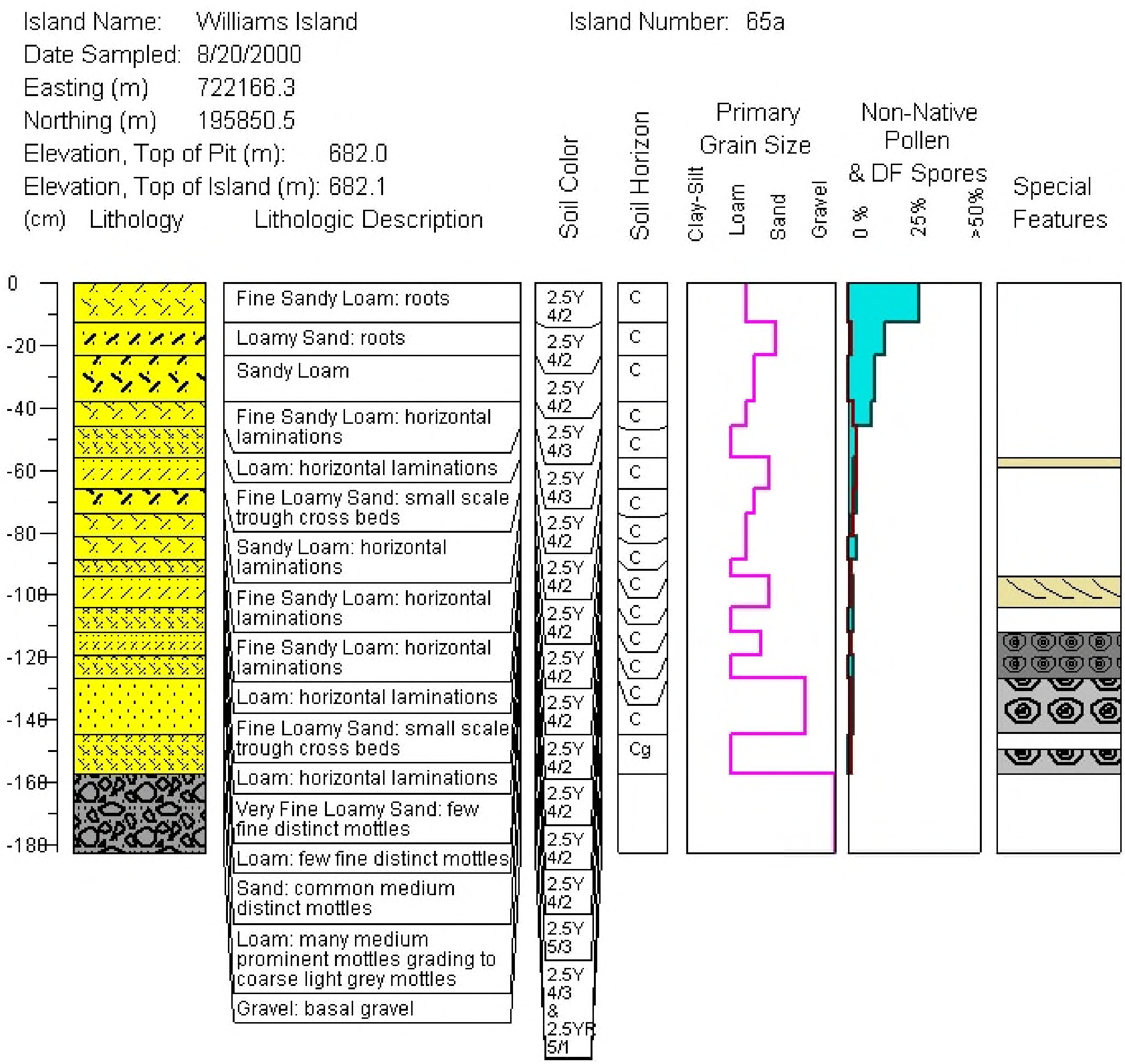

Figure E69. Williams Island (65a) soil profile.

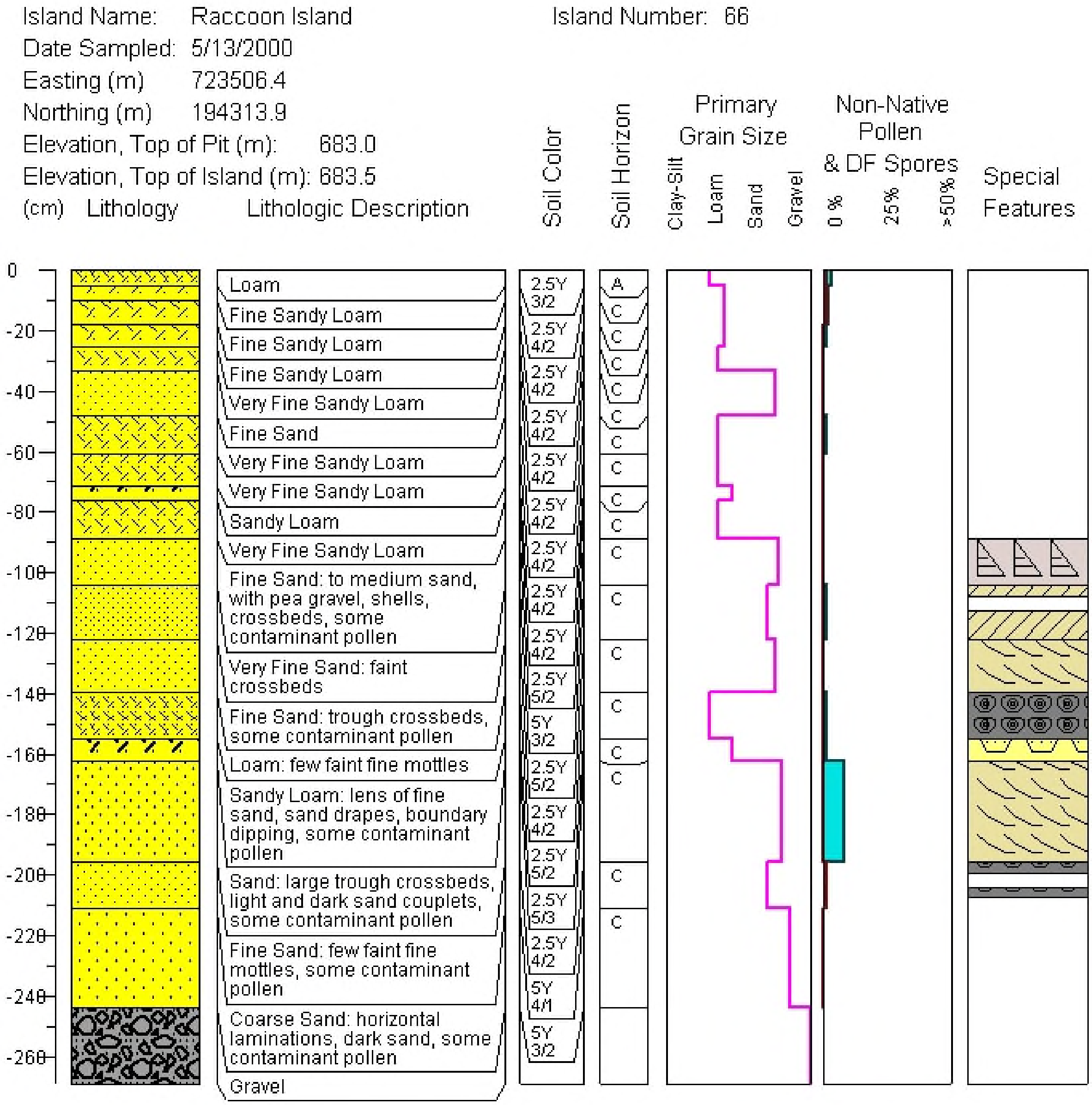

Figure E70. Raccoon Island (66) soil profile.

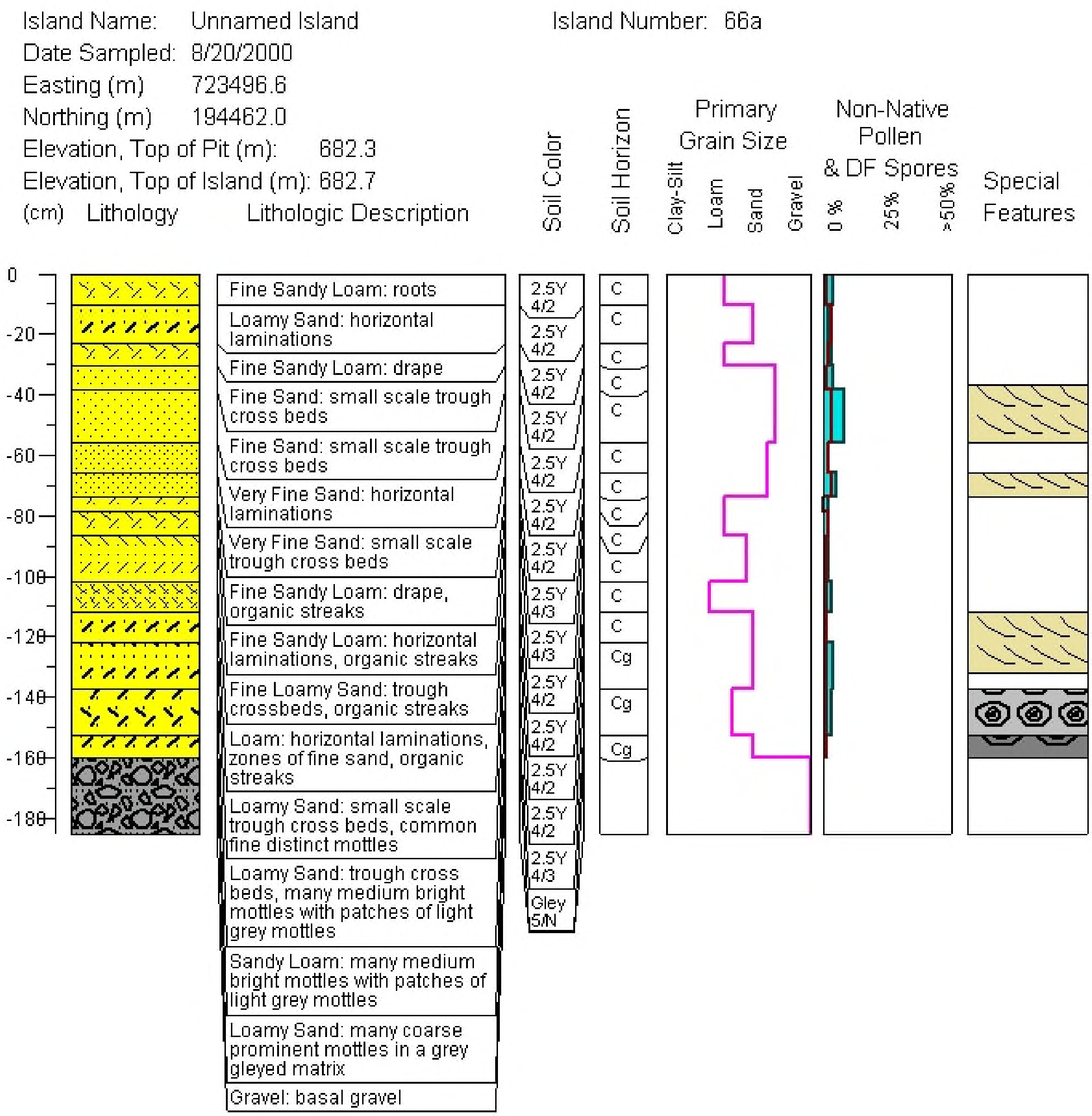

Figure E71. Unnamed Island (66a) soil profile.

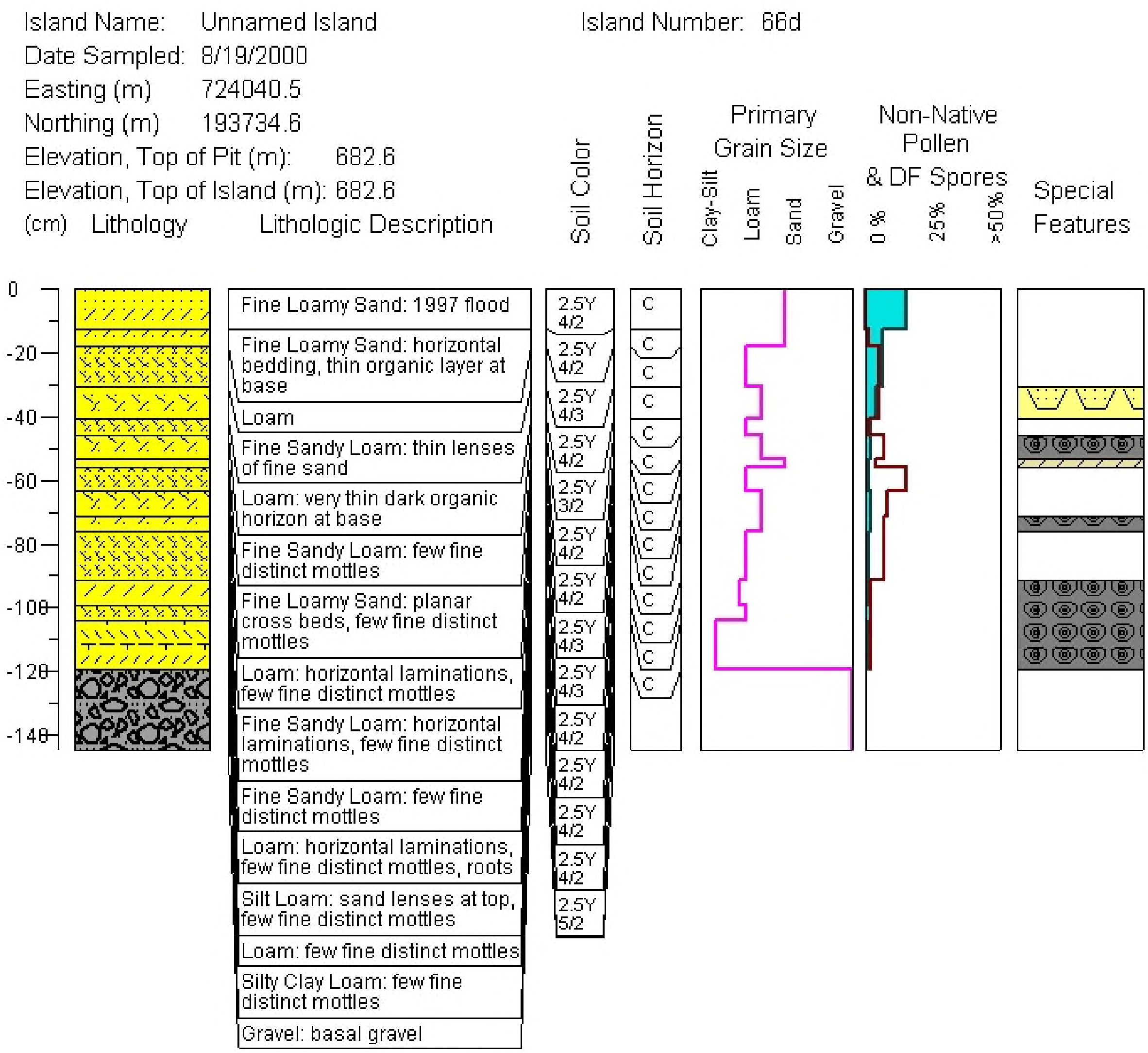

Figure E72. Unnamed Island (66d) soil profile.

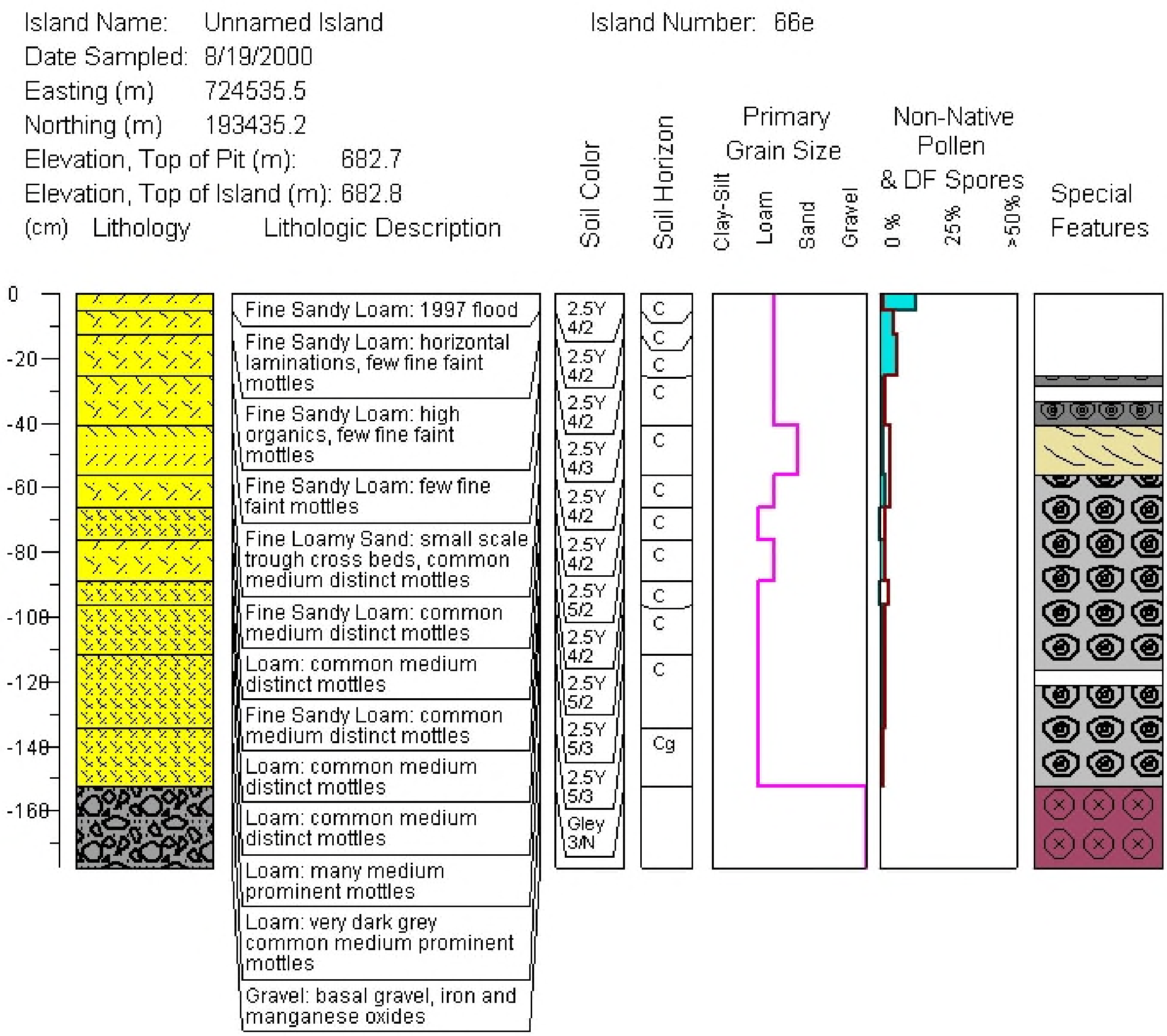

Figure E73. Unnamed Island (66e) soil profile.

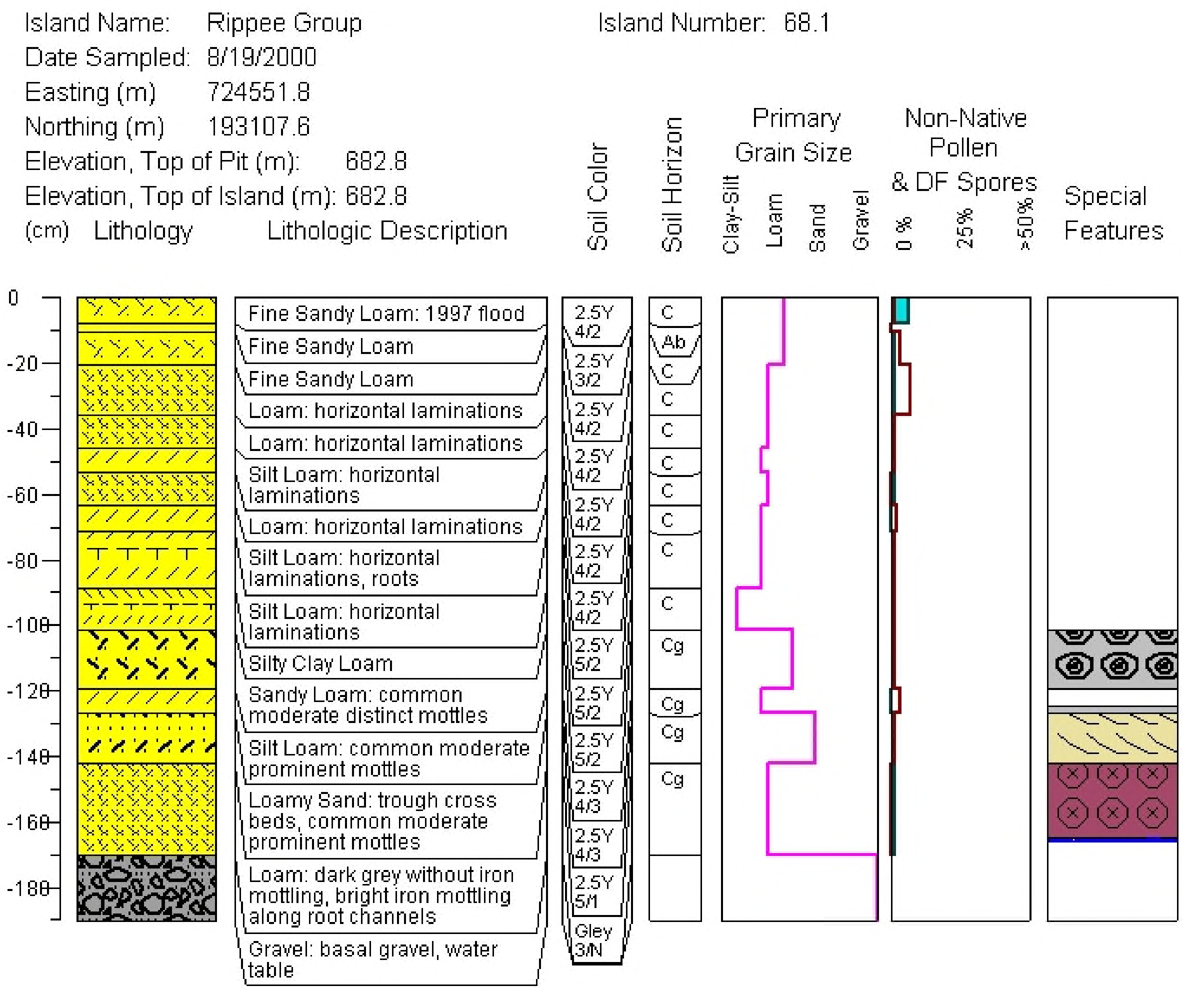

Figure E74. Rippee Group (68.1) soil profile.

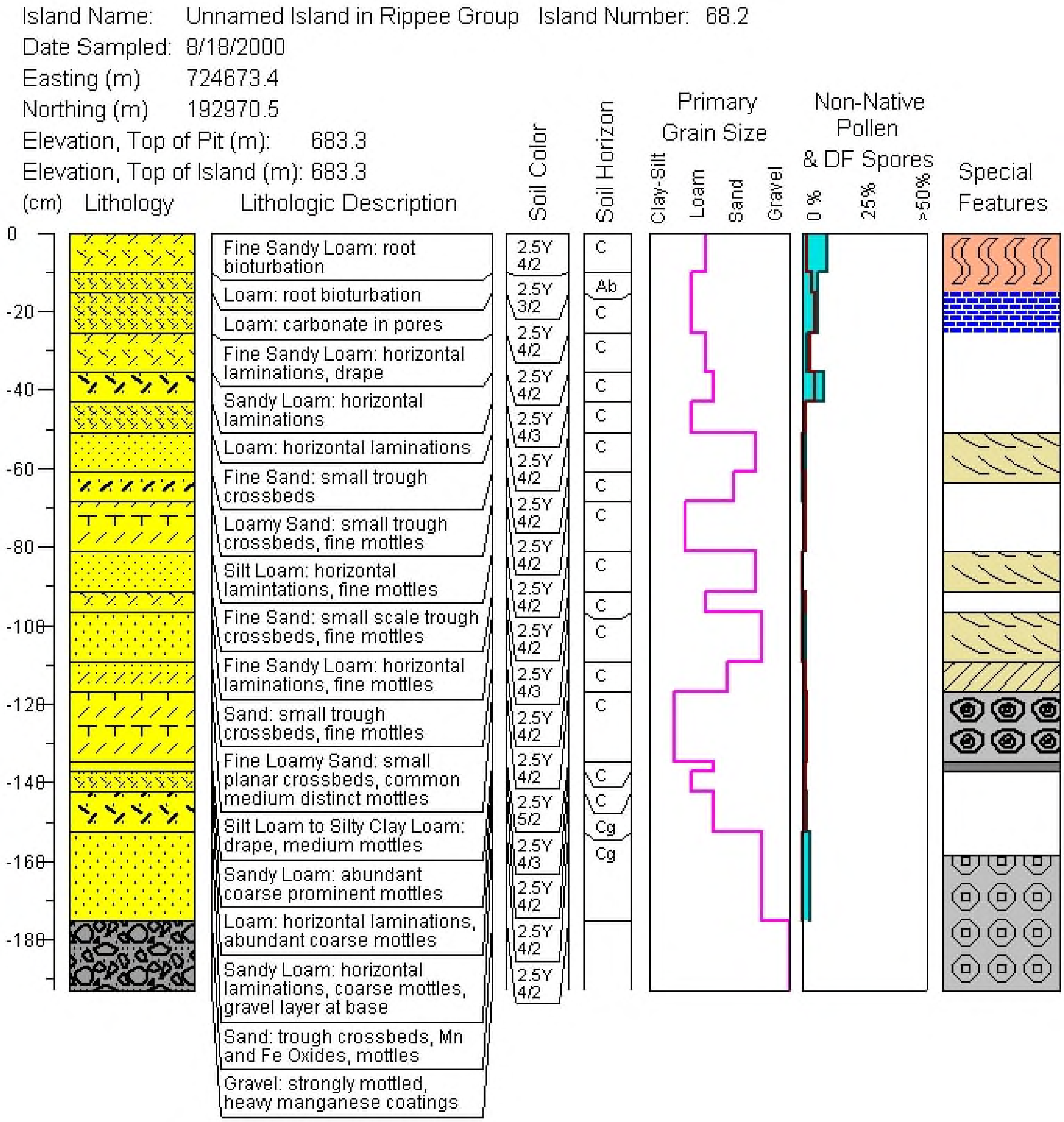

Figure E75. Unnamed Island in Rippee Group (68.2) soil profile.

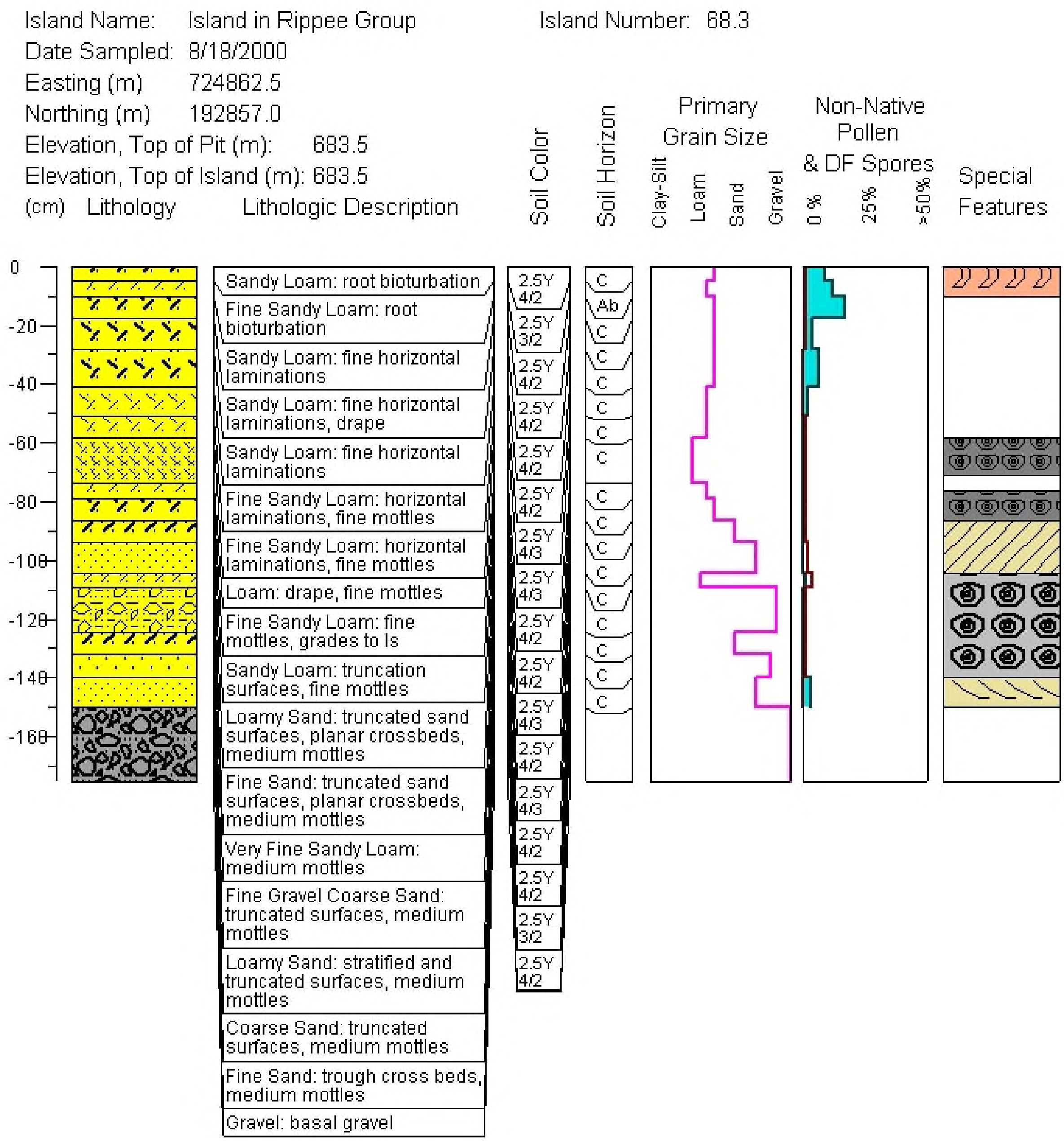

Figure E76. Unnamed Island in Rippee Group (68.3) soil profile.

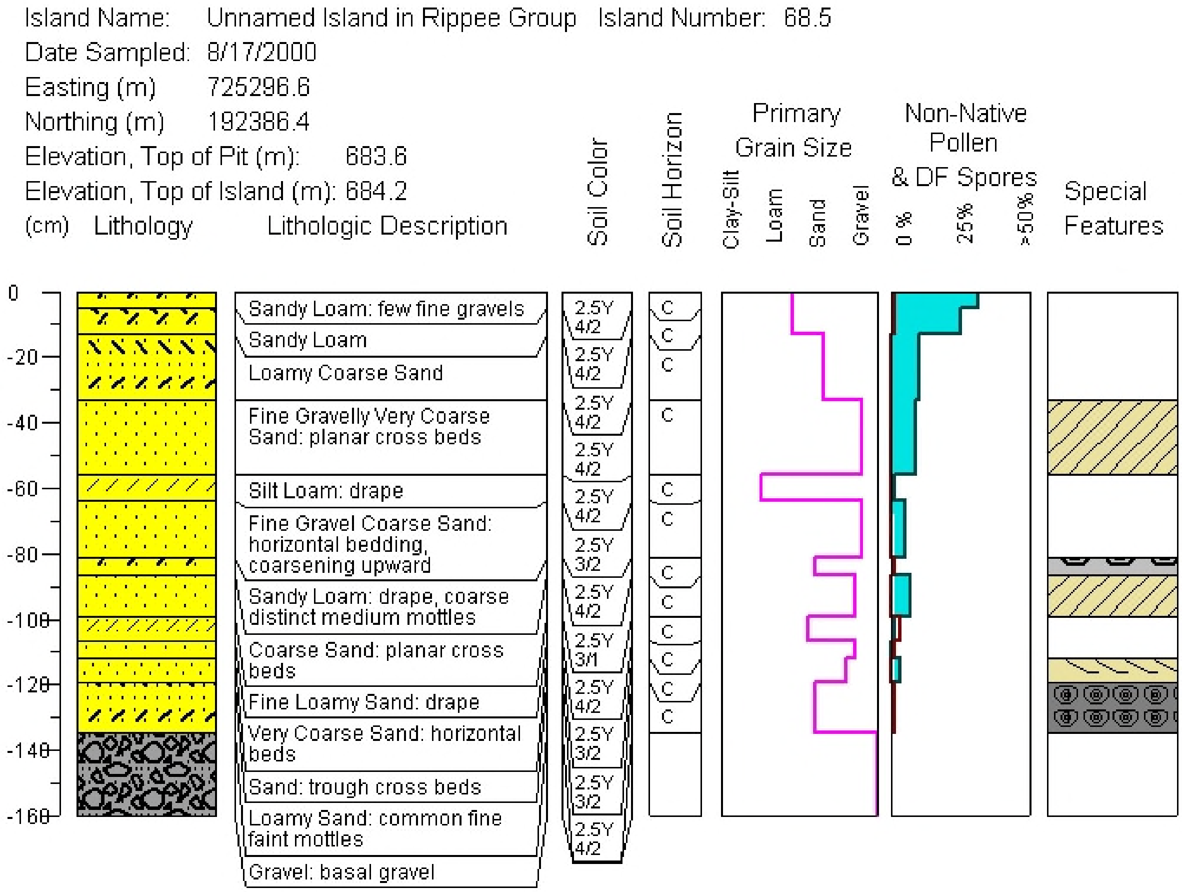

Figure E77. Unnamed Island in Rippee Group (68.5) soil profile.

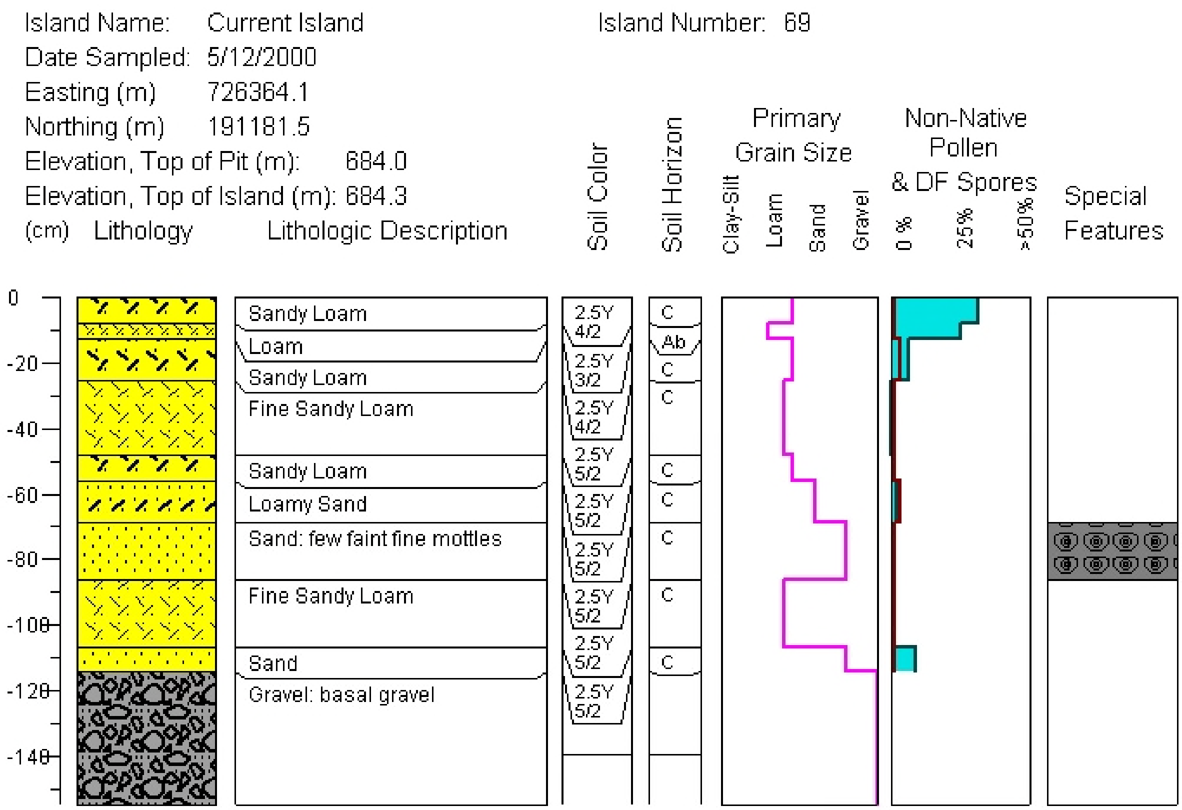

Figure E78. Current Island (69) soil profile.

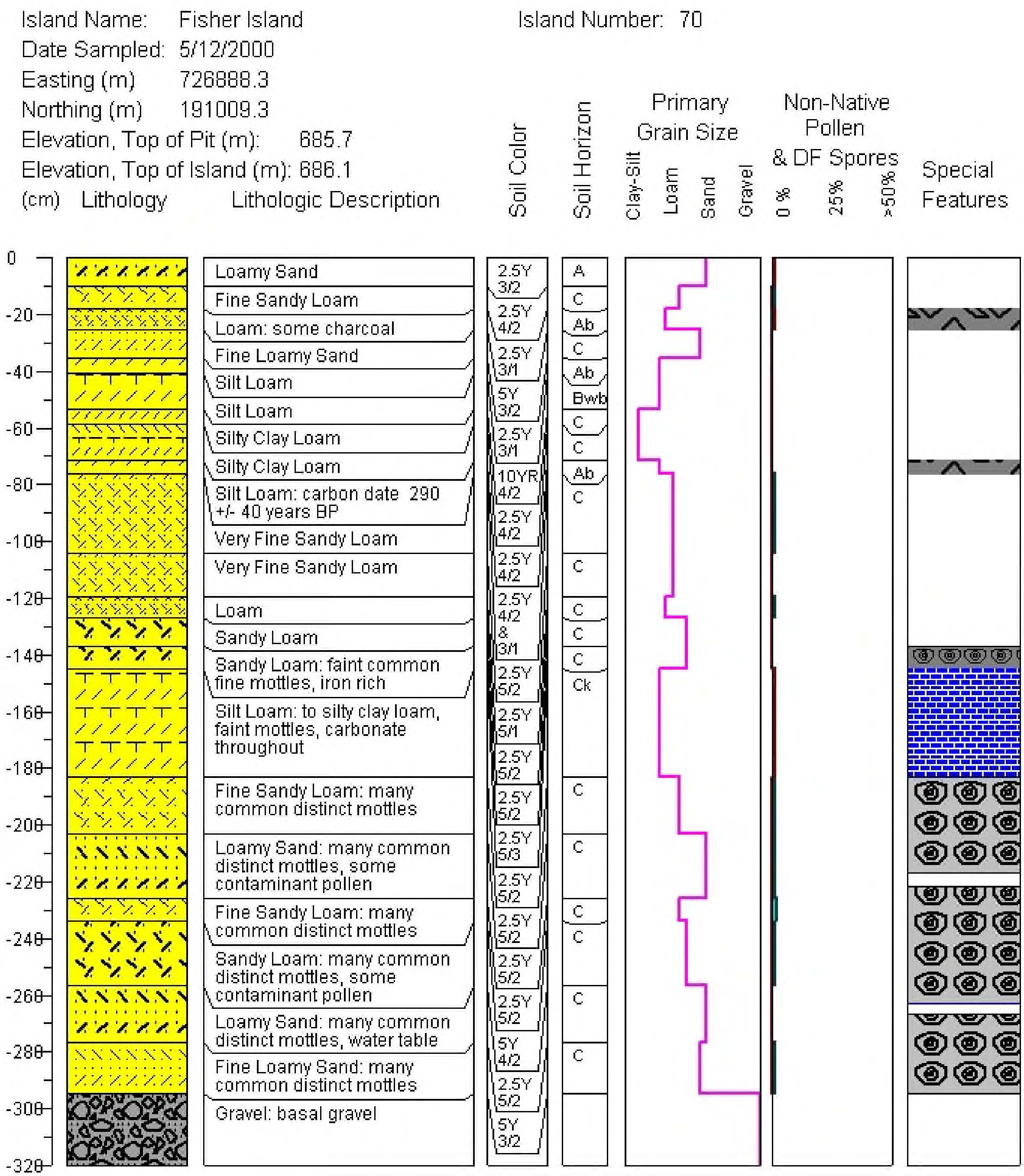

Figure E79. Fisher Island (70) soil profile.

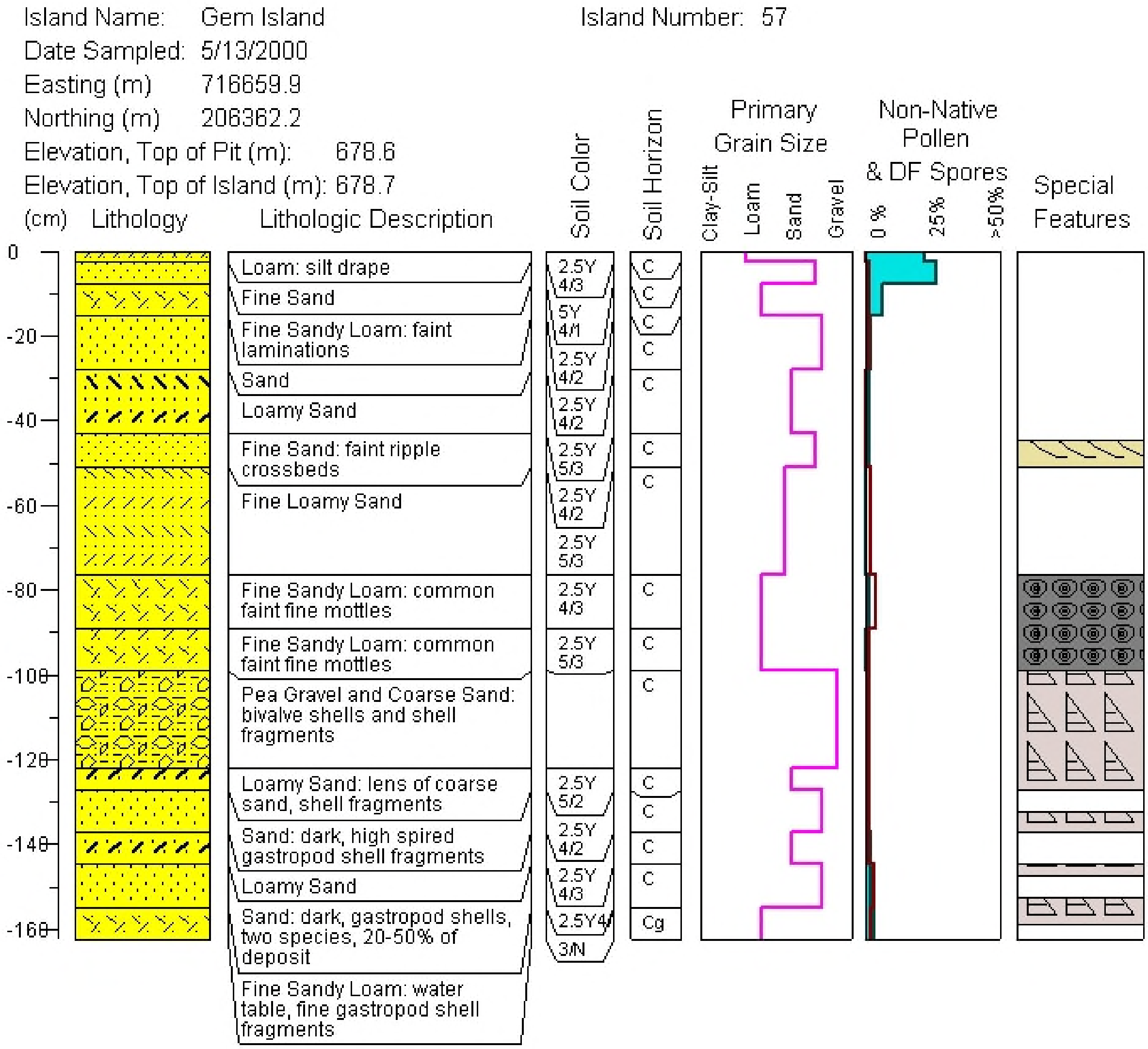

Figure E80. Richards Island (72) soil profile.

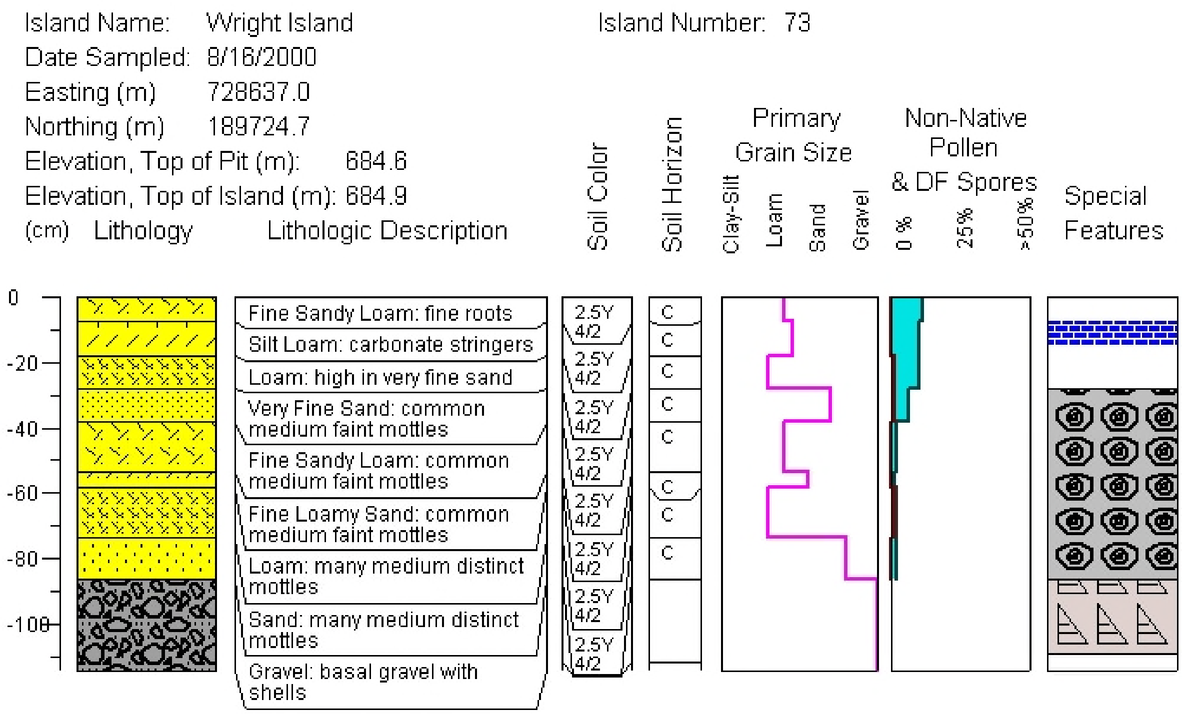

Figure E81. Wright Island (73) soil profile.

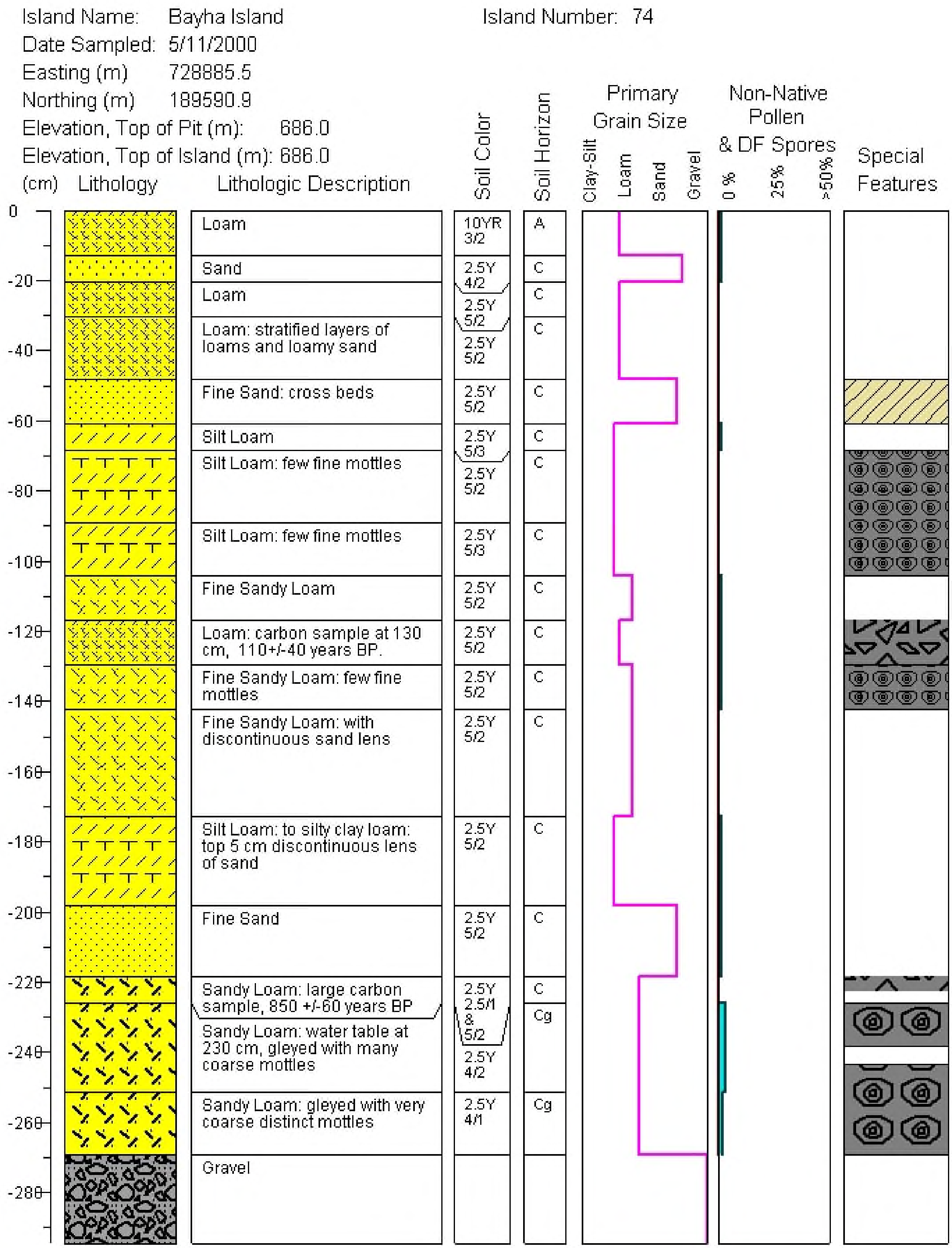

Figure E82. Bayha Island (74) soil profile.

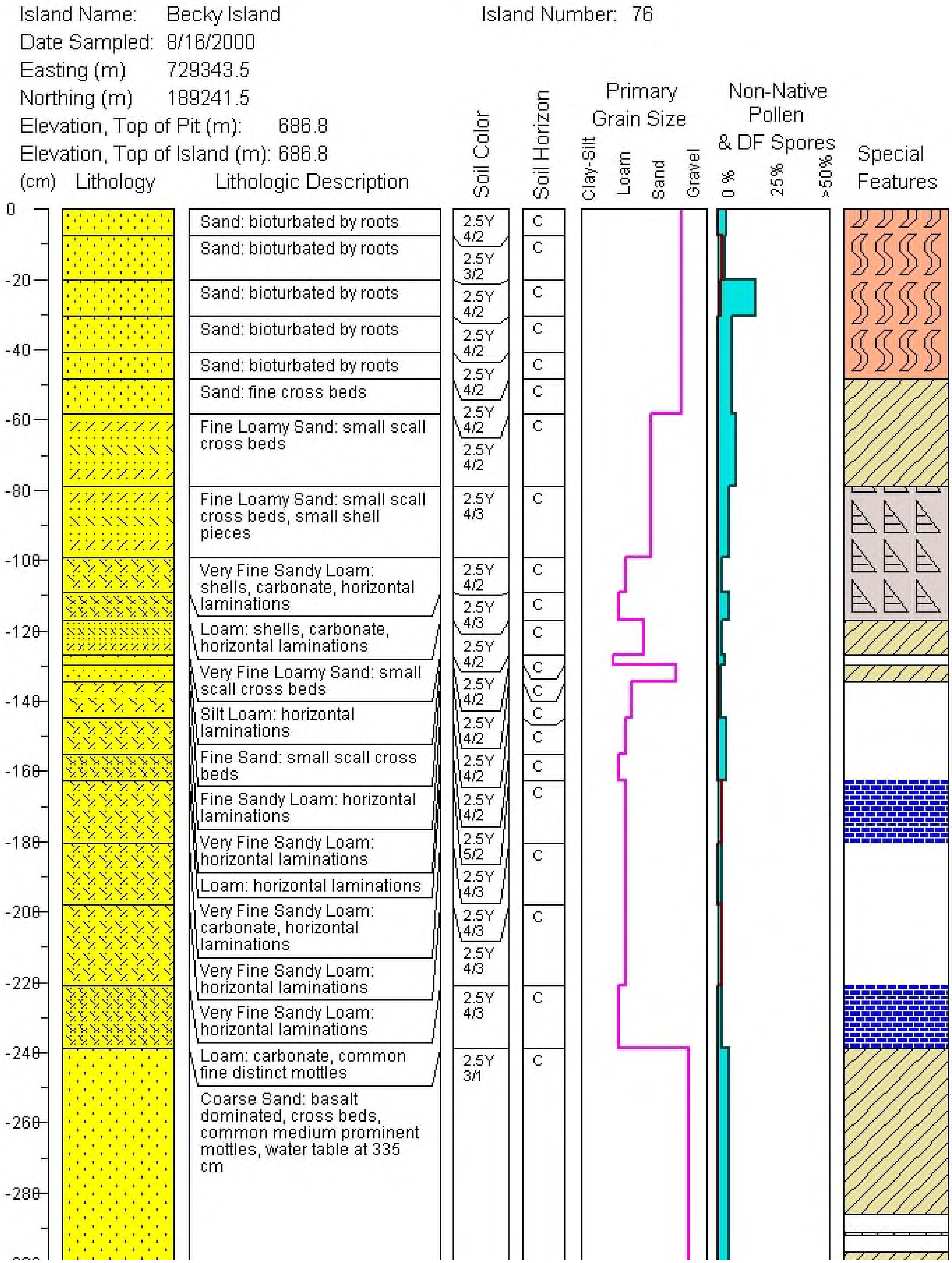

Figure E83. Becky Island (76) soil profile.

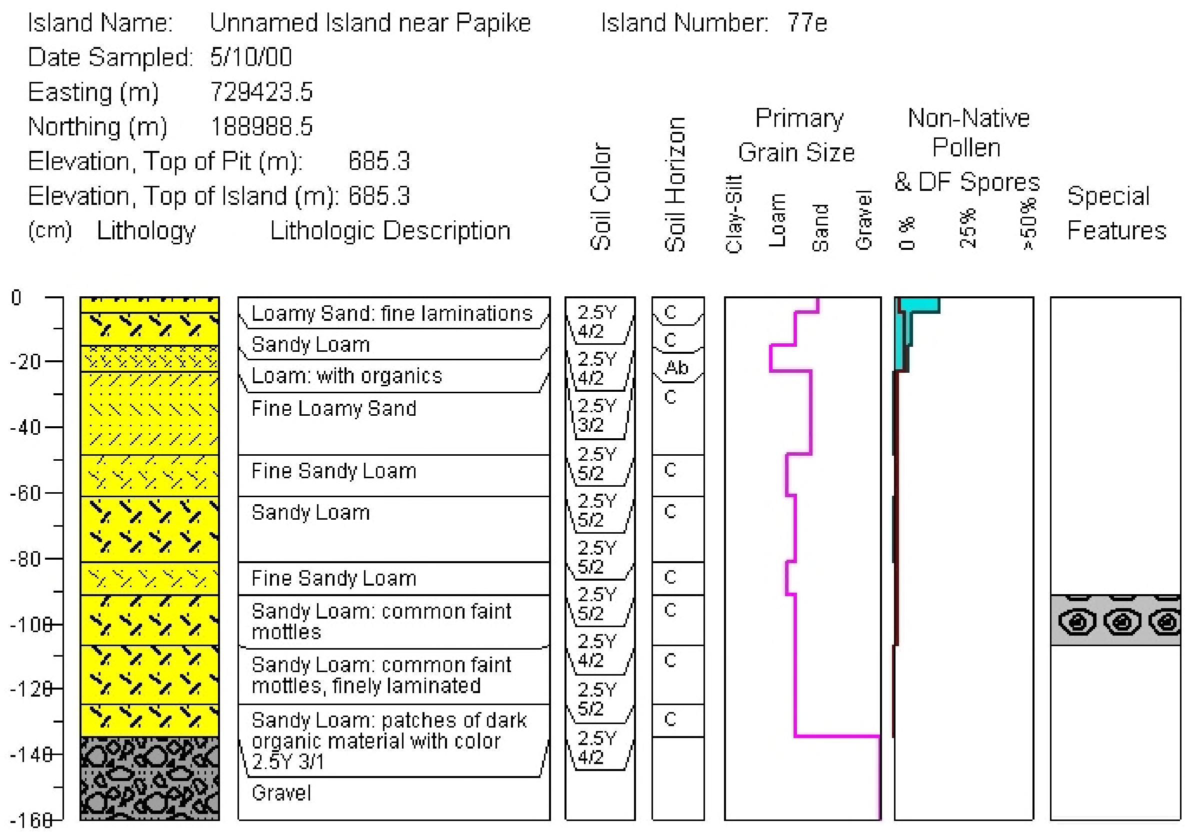

Figure E84. Unnamed Island near Papike Island (77e) soil profile.

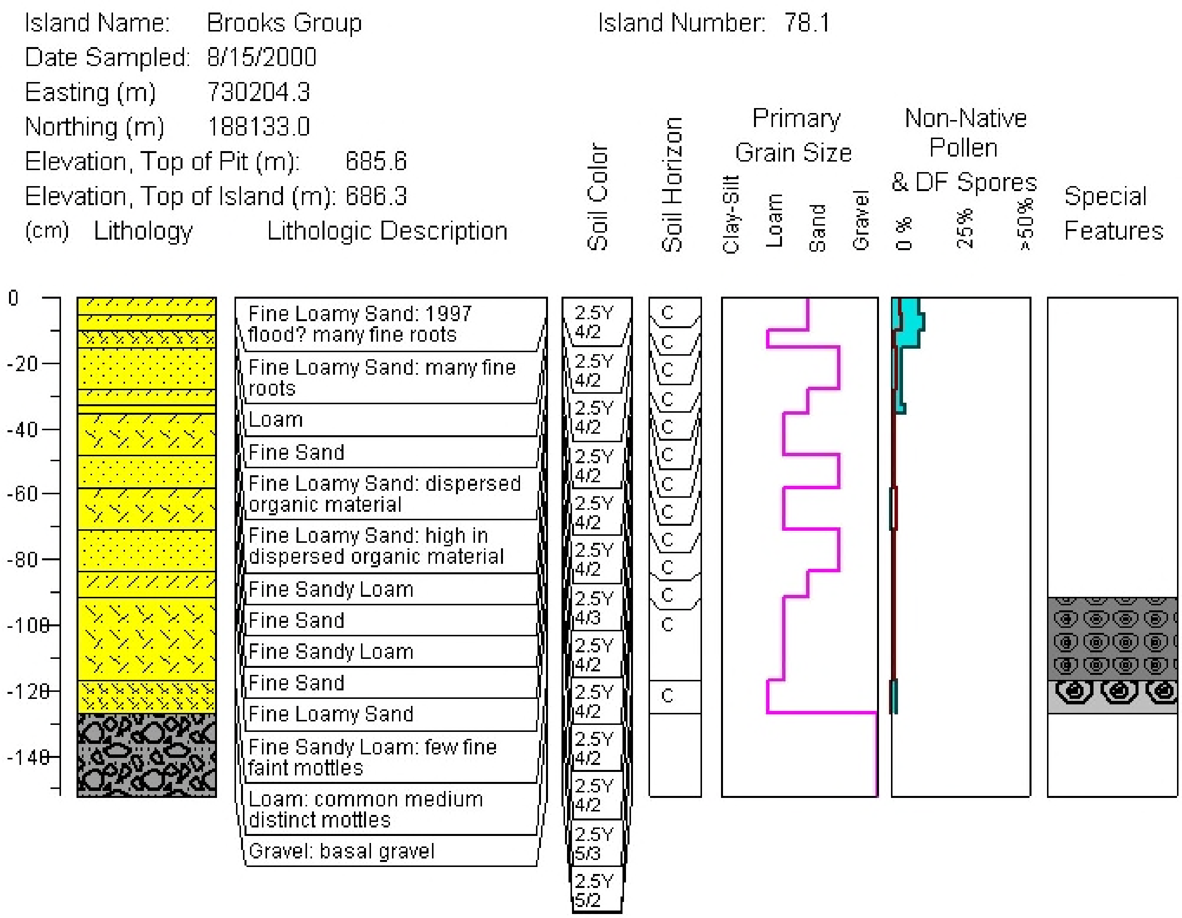

Figure E85. Brooks Group (78.1) soil profile.

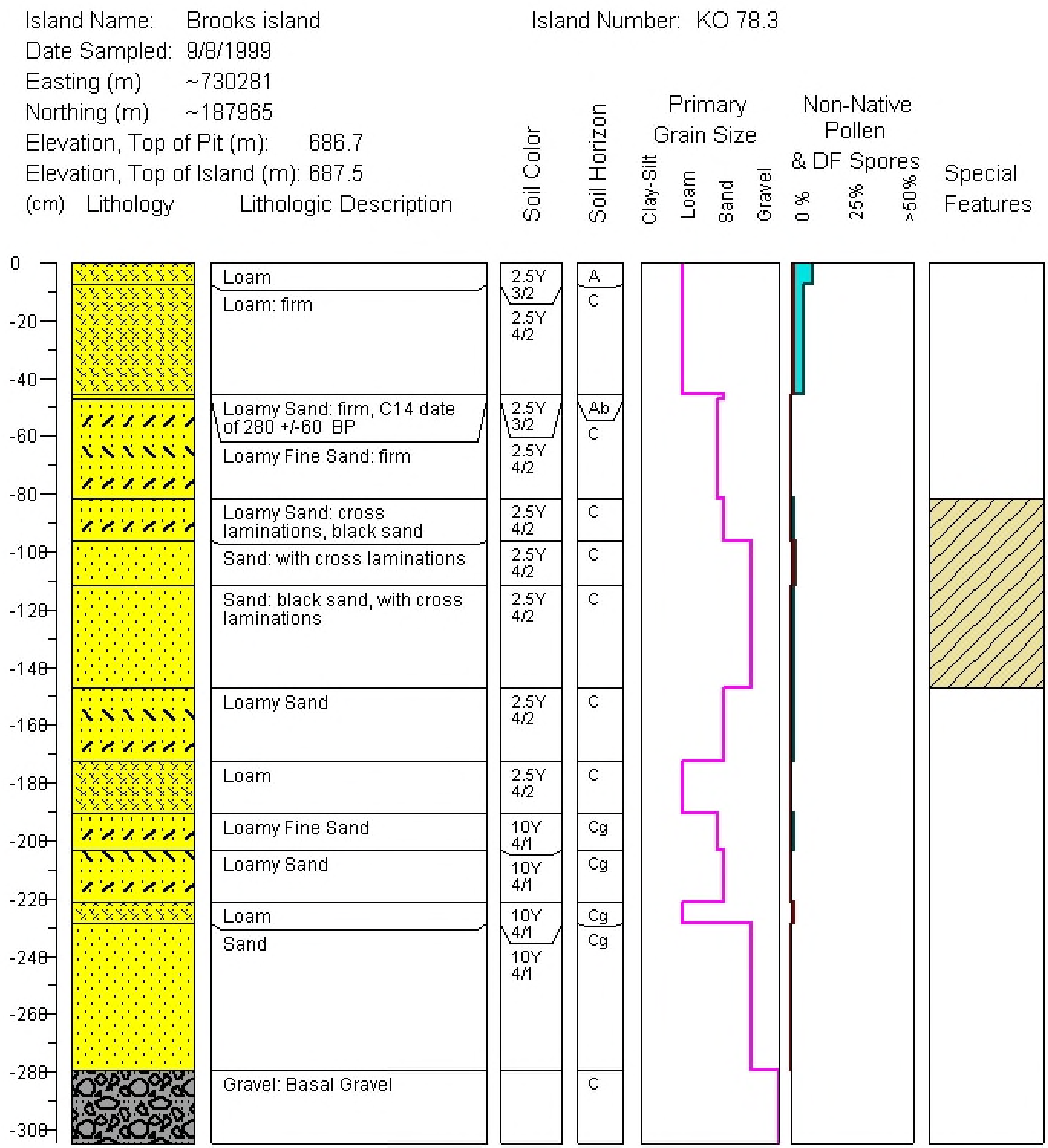

Figure E86. Brooks Island (78.3) soil profile.

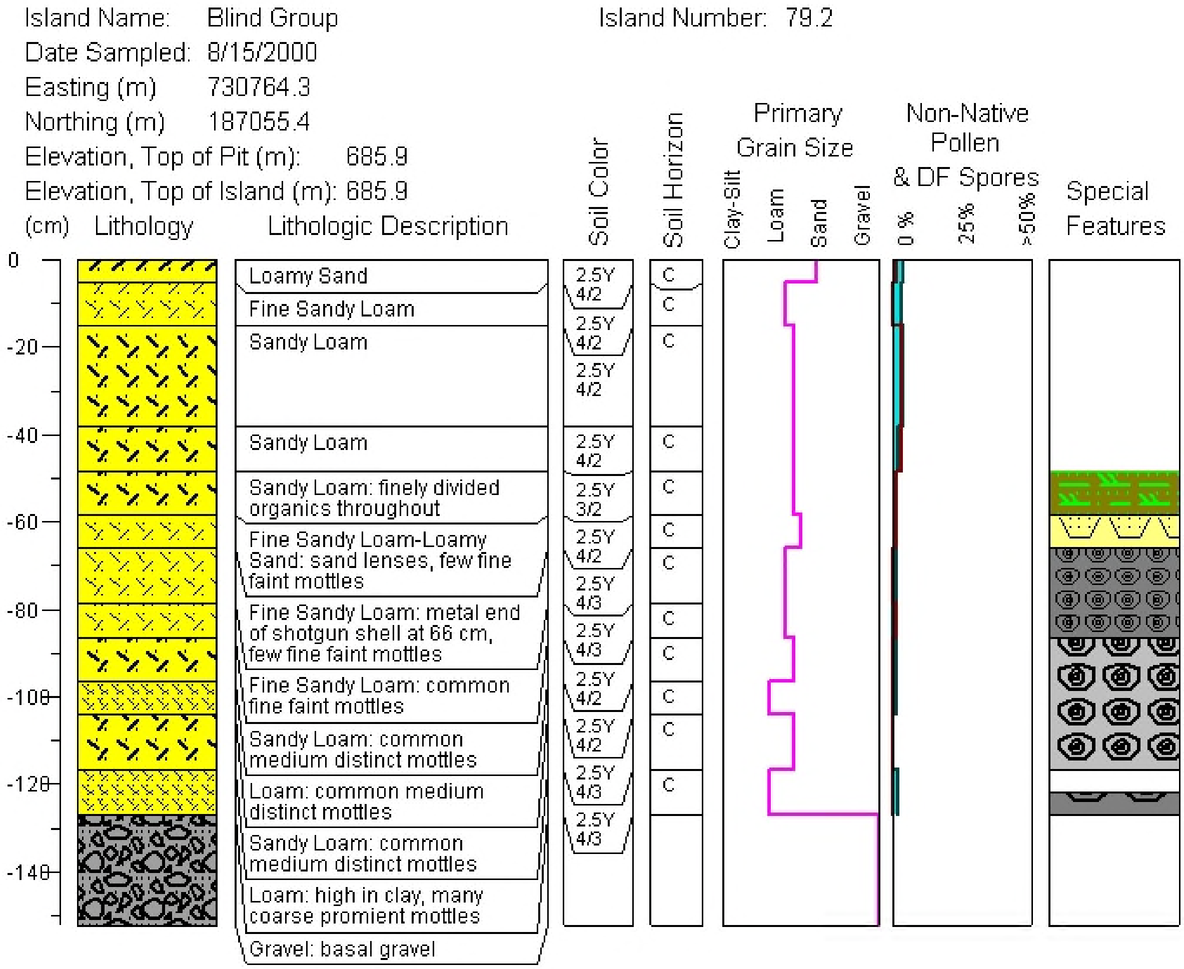

Figure E87. Blind Group (79.2) soil profile.

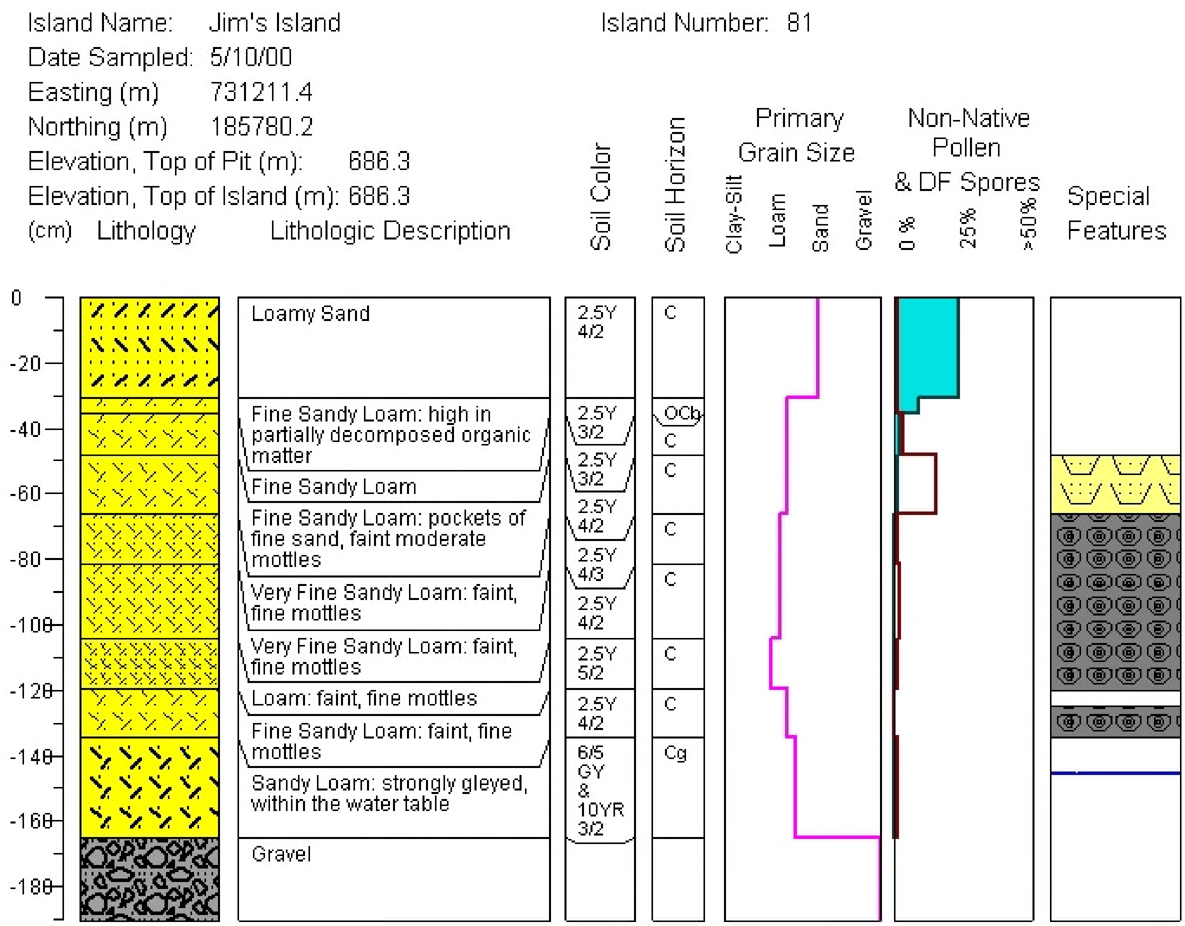

Figure E88. Jim’s Island (81) soil profile.

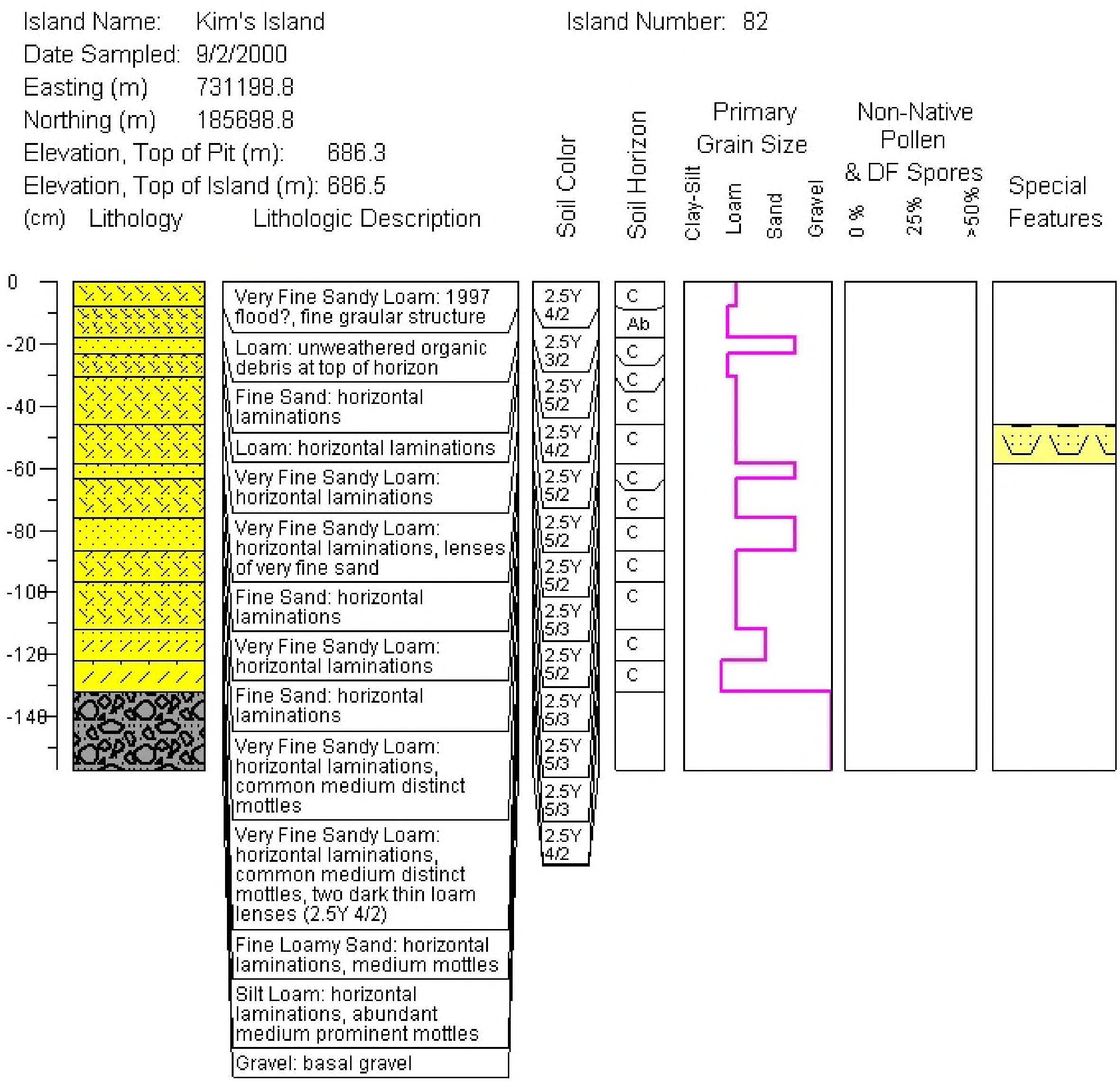

Figure E89. Kim’s Island (82) soil profile.

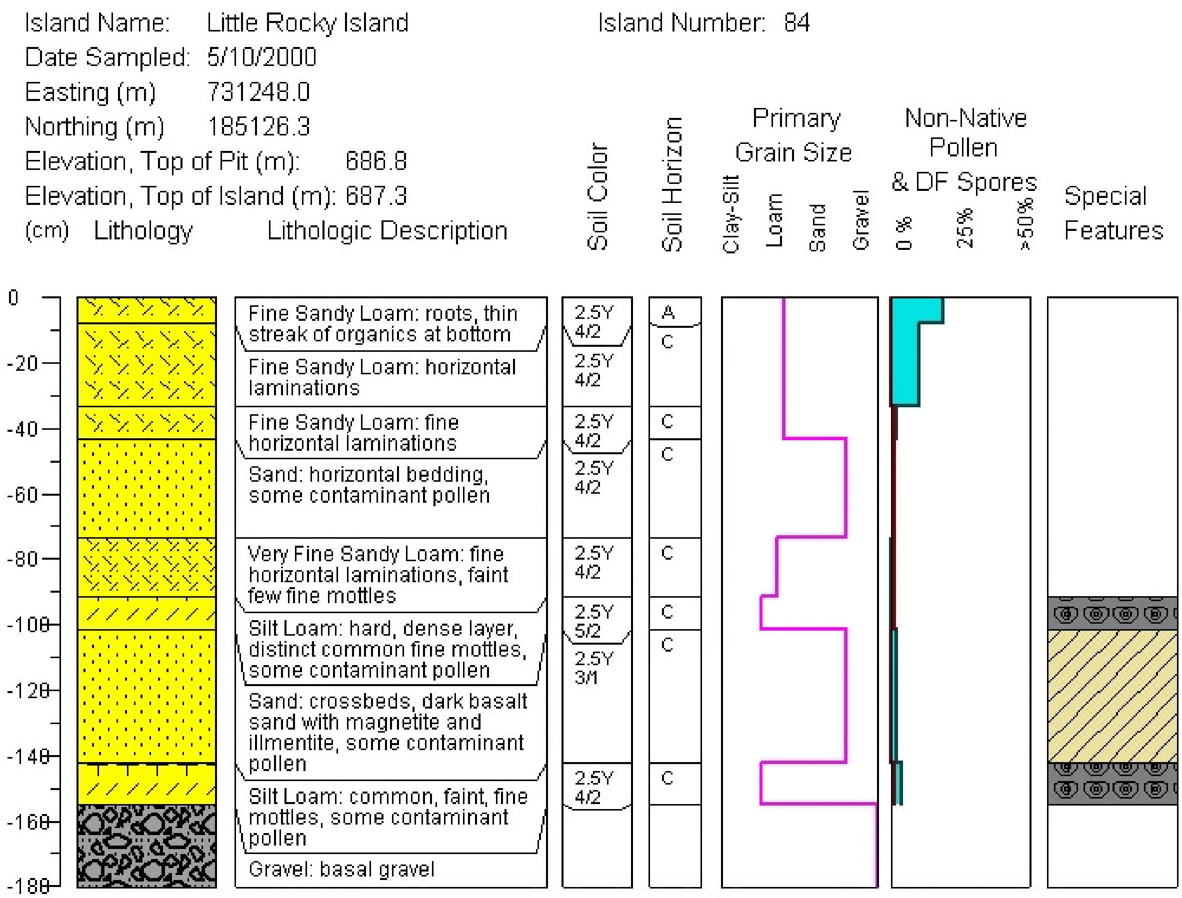

Figure E90. Little Rocky Island (84) soil profile.

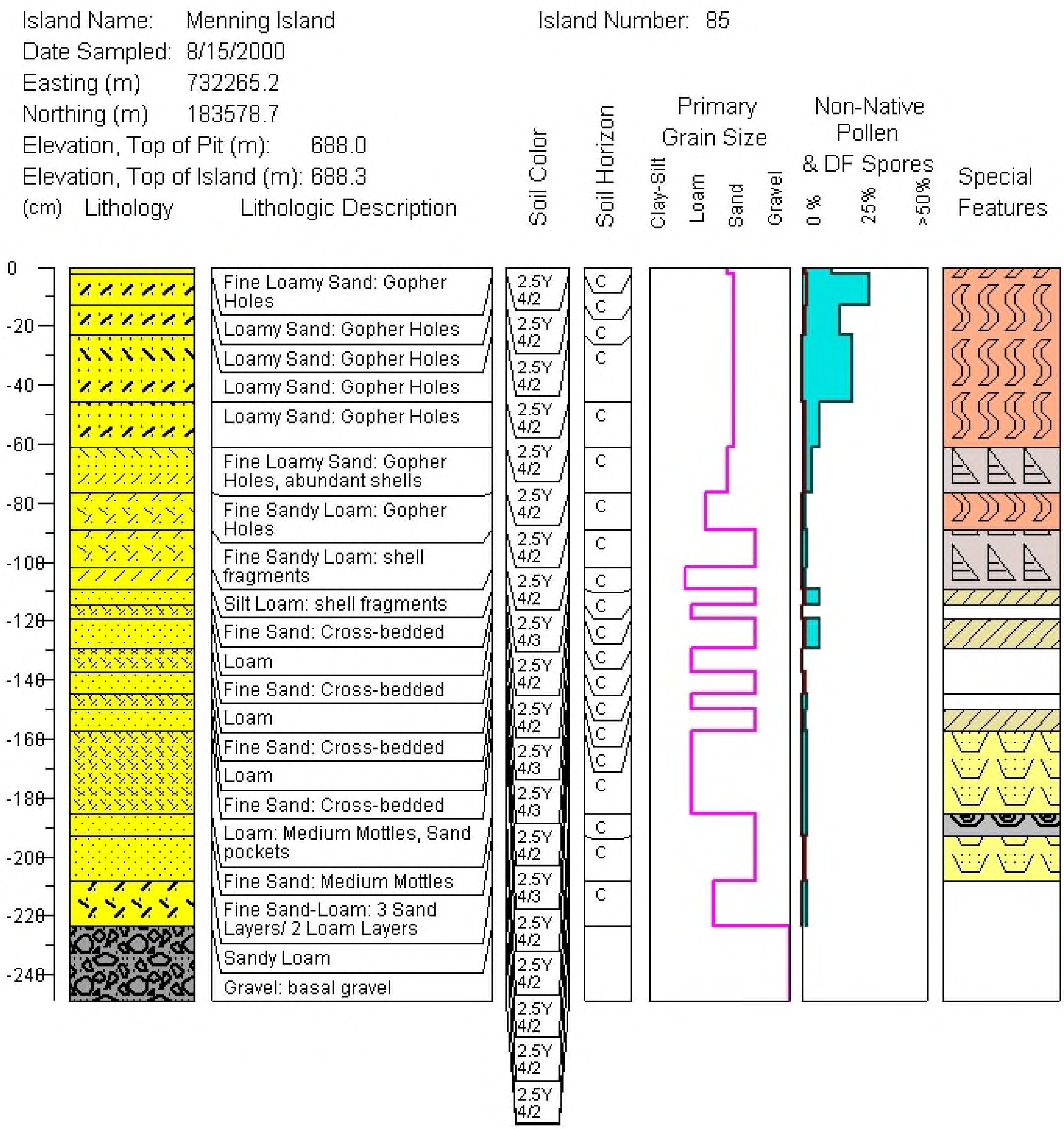

Figure E91. Menning Island (85) soil profile.

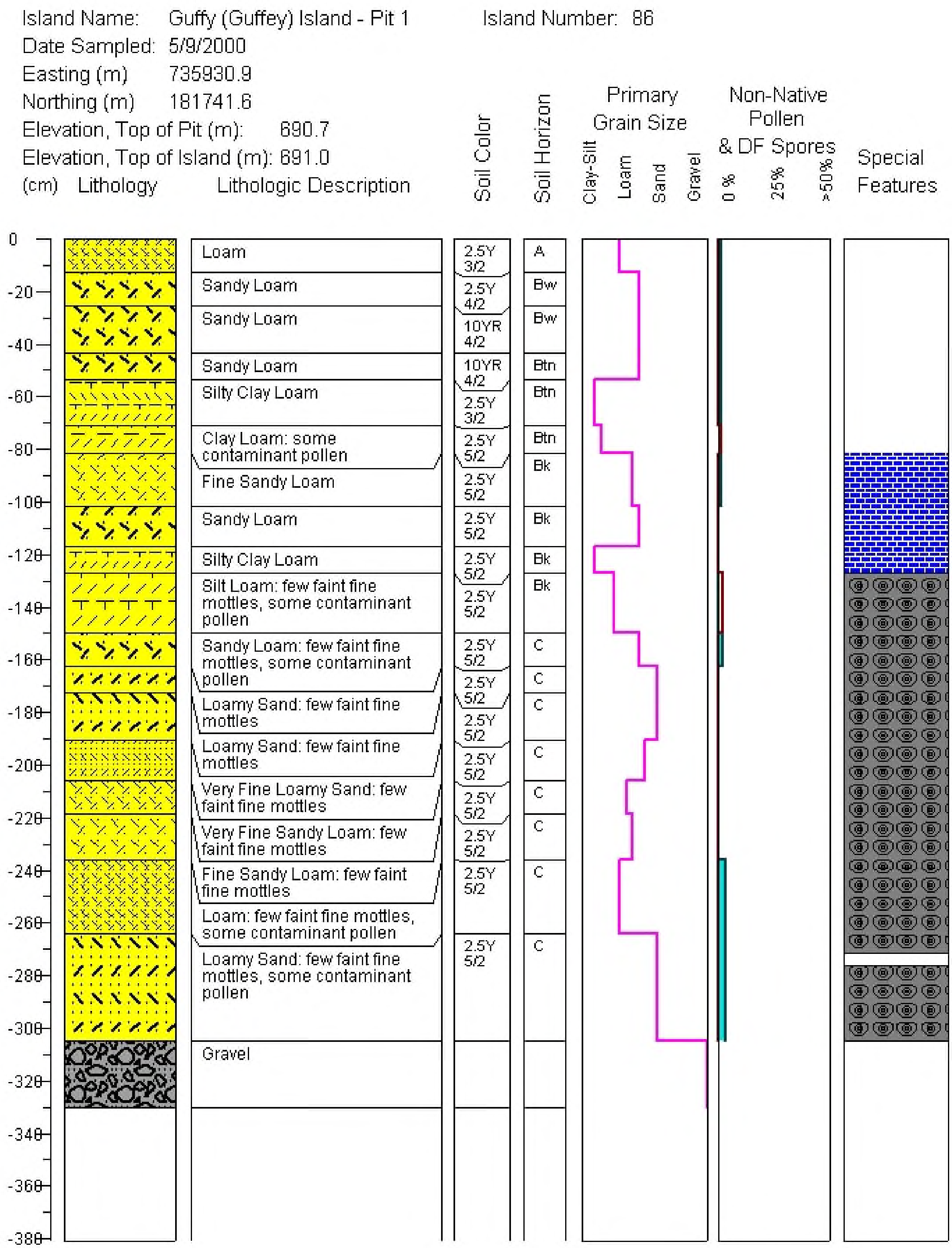

Figure E92. Guffey Island – Pit 1, (86) soil profile.

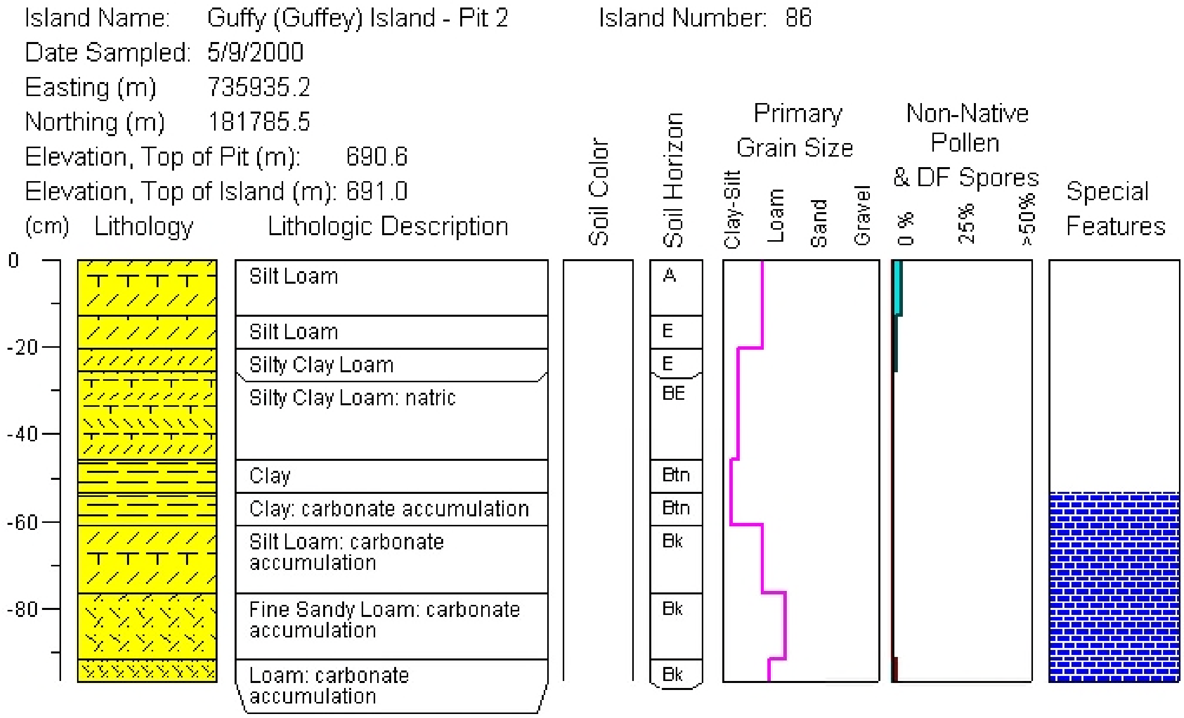

Figure E93. Guffey Island – Pit 2, (86) soil profile.

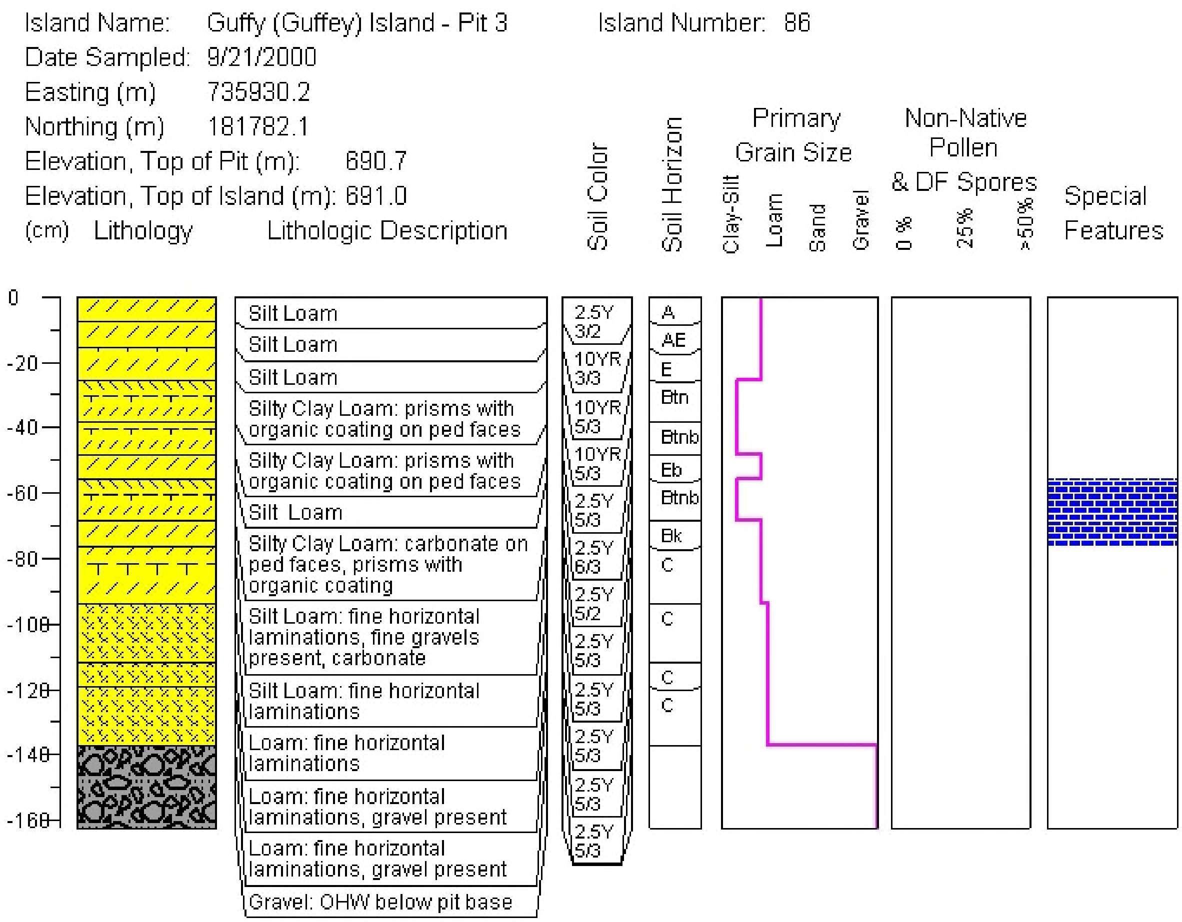

Figure E94. Guffey Island – Pit 3, (86) soil profile.

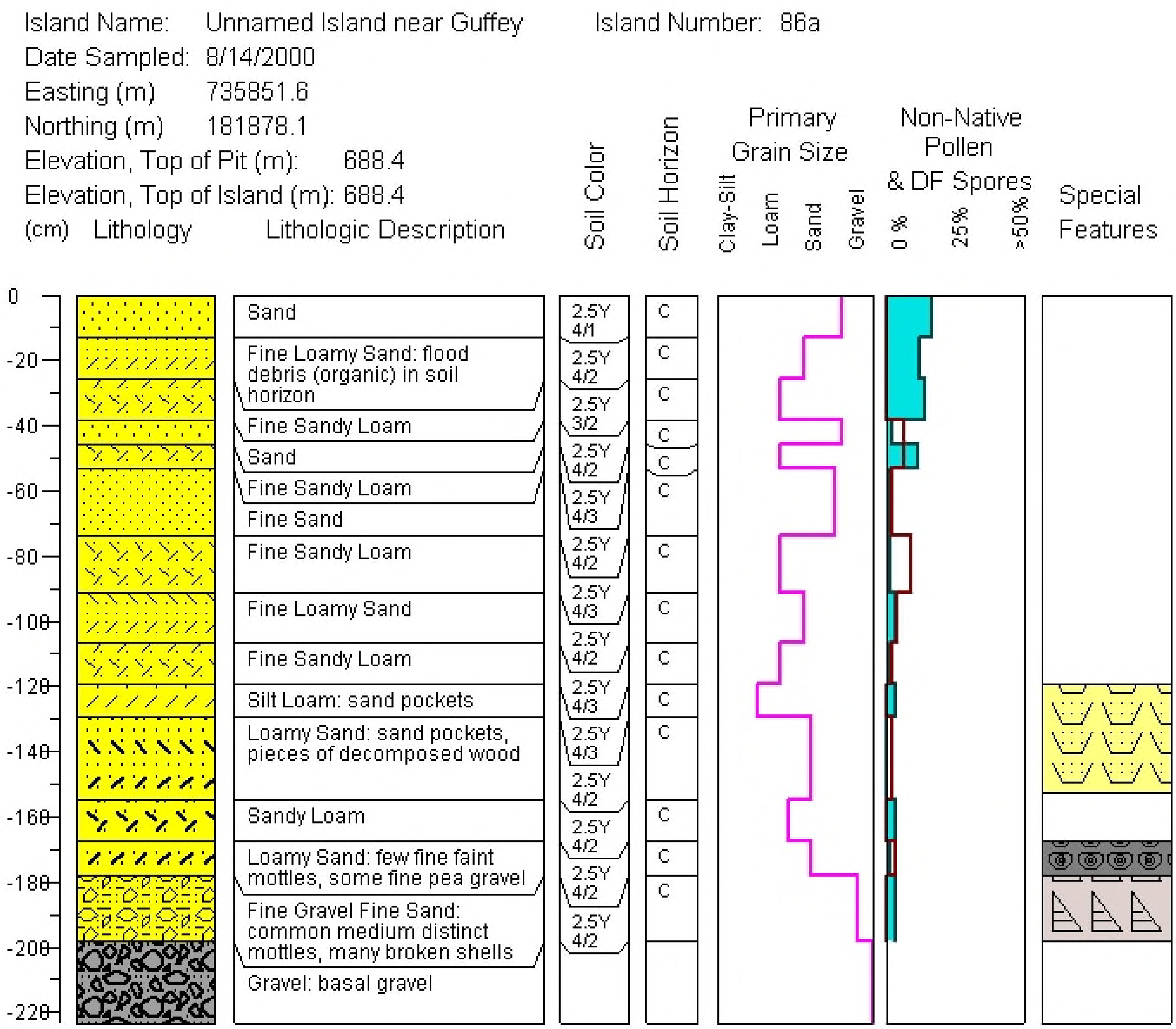

Figure E95. Unnamed Island near Guffey Island (86a) soil profile.

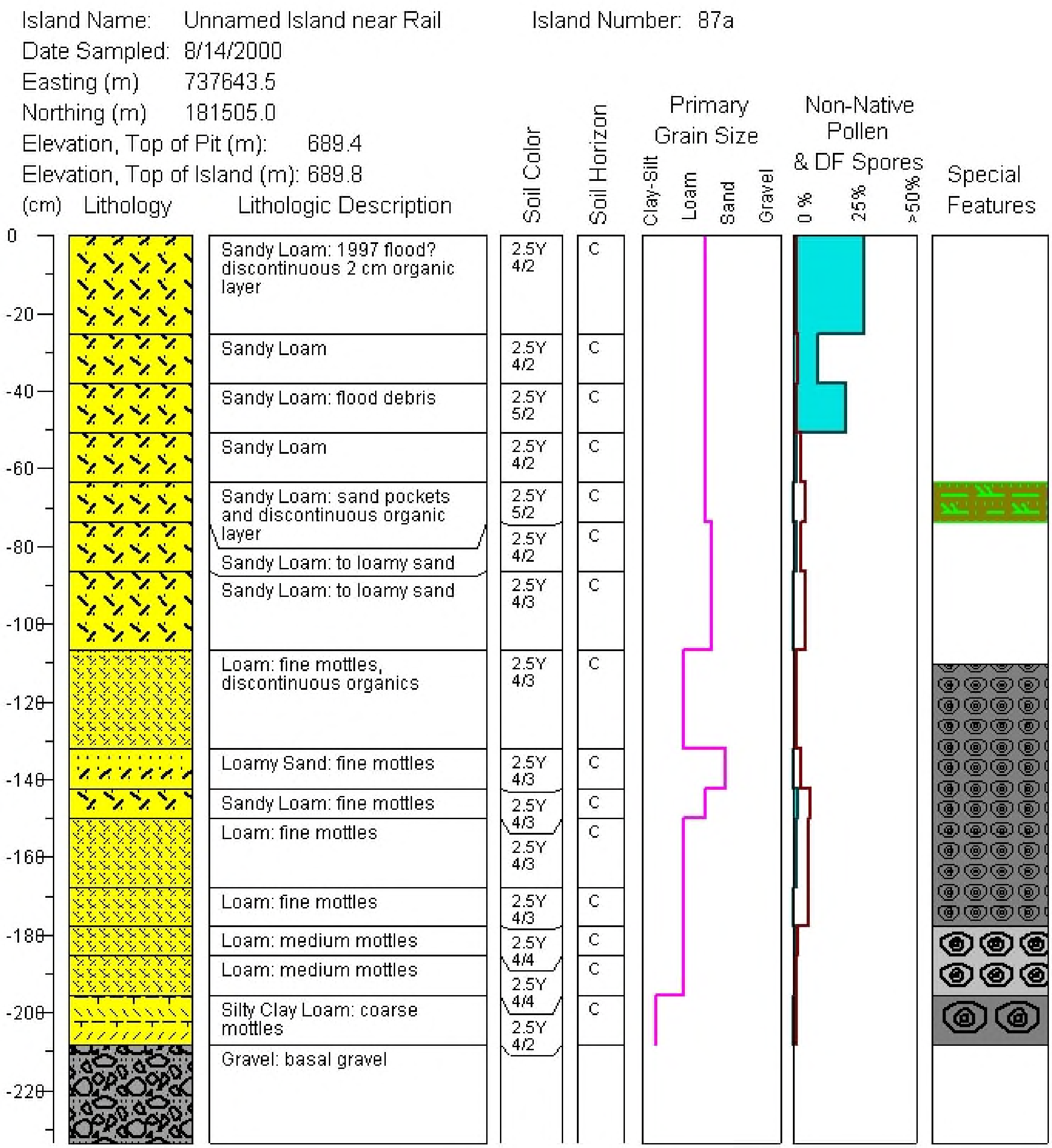

Figure E96. Unnamed Island near Rail (87a) soil profile.

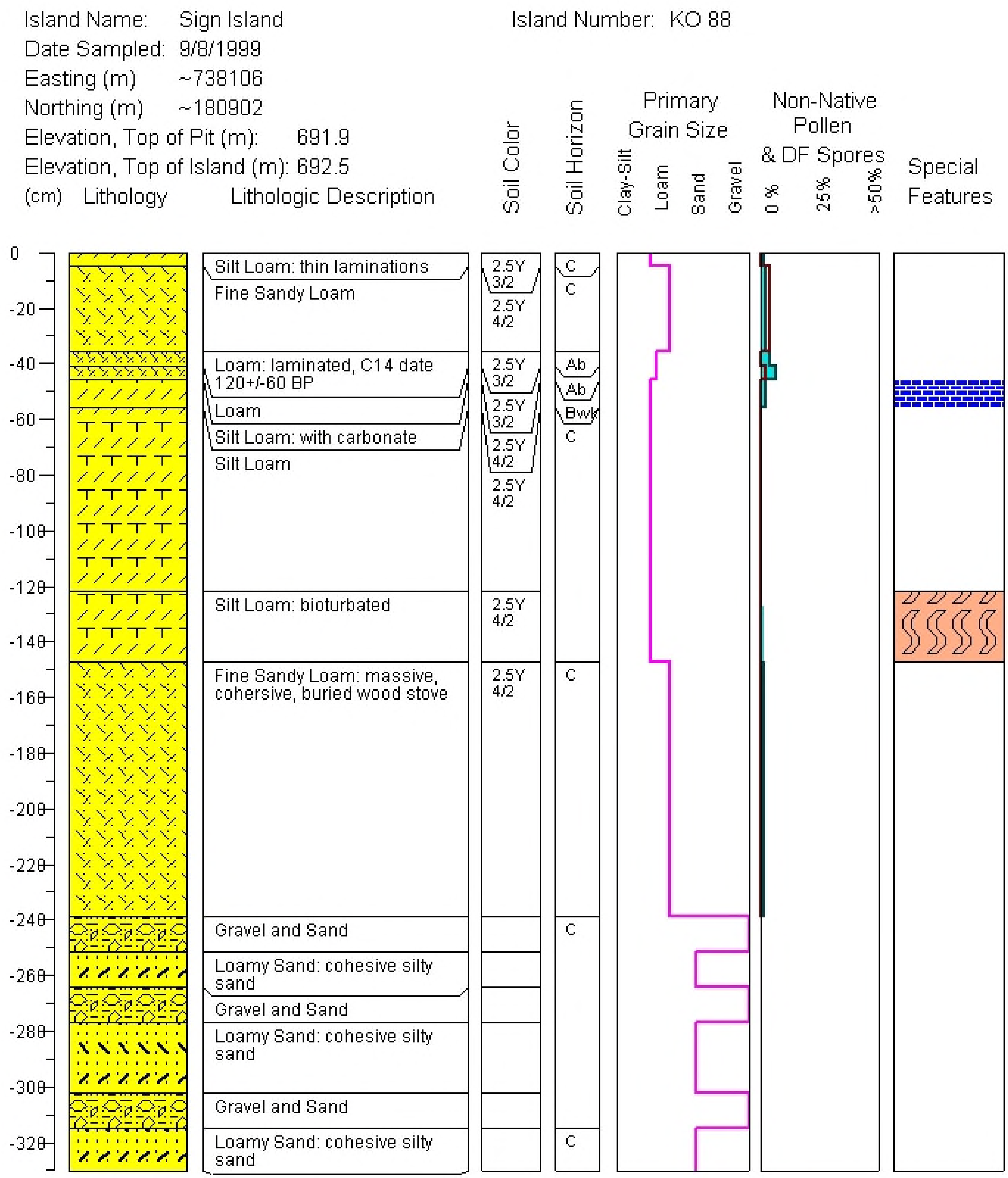

Figure E97. Sign Island (KO 88).

APPENDIX F1 – Tables

Table F.1 Summary of the islands observed in the review of early maps and aerial photography.

Island Number	Island Name (AKA)	1894-1906 USGS Maps*	1914 USGS Water Supply Paper 347*	1938 and 1939 Aerial Photos*
1	Whitehill	No Map	No Map	No Photo
	Huffman	No Map	No Map	No Photo
1a	Unnamed at RM335.5	No Map	No Map	No Photo
2	Fenzl	No Map	No Map	F
	Rapids #2	No Map	No Map	P
	Rapids #1	No Map	No Map	P
3	Waunch's	No Map	No Map	F
4	Rock	No Map	No Map	P
	Porters	No Map	No Map	P
	Westlake	No Map	No Map	P
4a	Unnamed at RM342.3	No Map	No Map	F
5	Jackass (W-11)	No Map	No Map	P
5a	Unnamed at RM342.7	No Map	No Map	NP
5b	Unnamed at RM345.2	No Map	No Map	NP
	Aulbach #1	No Map	No Map	F
6	Aulbach #2	No Map	No Map	NP
7	Aulbach #3	No Map	No Map	F
7a	Unnamed at RM349	No Map	No Map	NP
8.1	Mason	No Map	No Map	P
8.2	McRea Group #2	No Map	No Map	F
8.3	McRea Group #3	No Map	No Map	P
8.4	Schledewitz	?	No Map	1/2 F
8.5	Unnamed at RM 351.9	NP	No Map	F
8a	Unnamed at RM352.6	NP	No Map	NP
8b	Unnamed at RM352.9	NP	No Map	NP
8c	Unnamed at RM 353.1	NP	No Map	F
10	Goat	?	No Map	P
	Patch	P	No Map	P
	Long	P	No Map	P
11.1	Smith Group #4	NP	No Map	F
11.2	Smith Group #3	?	No Map	P
11.3	Smith Group #2	?	No Map	P
11	Smith Group#1	P	No Map	P
11a	Unnamed at RM356.6	NP	No Map	NP
11b	Unnamed at RM357	NP	No Map	NP
	Nadeau	F	No Map	F
14	Larsen	?	No Map	F
	Buttermilk	?	No Map	P
15	Sundstrom	P	No Map	P
	Grafton	?	No Map	P
	Pruit	NP	No Map	F
	Resch	NP	No Map	NP

Island Number	Island Name (AKA)	1894-1906 USGS Maps*	1914 USGS Water Supply Paper 347*	1938 and 1939 Aerial Photos*
	Oglesbee	NP	No Map	NP
15a.1	Unnamed at RM357.3	NP	No Map	NP
15a.2	Unnamed at RM357.4	NP	No Map	NP
15a.3	Unnamed at RM357.4	NP	No Map	NP
15b	Unnamed at RM359.8	NP	No Map	NP
15c	Annear	NP	No Map	F
16	Ketchup	NP	No Map	P
17	Horse	NP	No Map	P
17a.1	Unnamed at RM362.9	NP	No Map	NP
17a.2	Unnamed at RM362.9	NP	No Map	NP
17a.3	Unnamed at RM362.9	NP	No Map	NP
18	Scarecrow	P	No Map	P
18a	Sylvia	NP	No Map	P
	Duncan	P	No Map	P
Pool	Pool	P	No Map	P
18a.1	Unnamed (side channel)	NP	No Map	F
18b	Unnamed at RM363.6	NP	No Map	NP
18c	Unnamed at RM364.1	NP	No Map	NP
18d	Unnamed at RM364.3	NP	No Map	NP
18d.1	Unnamed at RM365.5	NP	No Map	NP
18e	Unnamed at RM365.7	NP	No Map	NP
18e.1	Unnamed at RM365.8	NP	No Map	F
18f	Unnamed at RM366.6	NP	No Map	NP
	Banks	P	No Map	P
18f.1	Little Banks	?	No Map	P
18f.2	Unnamed at RM366.7	NP	No Map	NP
18f.3	Unnamed at RM366.7	NP	No Map	NP
18f.4	Unnamed at RM366.8	NP	No Map	NP
18g	Unnamed at RM366.9	NP	No Map	NP
18h	Unnamed at RM367.8	NP	No Map	NP
	Ontario	?	No Map	P
	Johnson	?	No Map	P
	Welch	P	No Map	P
18h.1	Unnamed at RM 370.1	NP	No Map	P
	Ramey	P	No Map	P
	Morton	P	No Map	P
	McPhersons	P	No Map	P
18i	Unnamed at RM373.7	NP	No Map	NP
18j	Unnamed at RM374.3	NP	No Map	NP
18k	Unnamed at RM374.7	NP	No Map	NP
18l	Unnamed at RM375.7	NP	No Map	NP
18m	Unnamed at RM375.8	NP	No Map	NP

Island Number	Island Name (AKA)	1894-1906 USGS Maps*	1914 USGS Water Supply Paper 347*	1938 and 1939 Aerial Photos*
18m.1	Unnamed at RM377.2	NP	No Map	F
18m.2	Unnamed at RM378.9	NP	No Map	NP
18n	Unnamed at RM380.1	NP	No Map	NP
18n.1	Crow	NP	No Map	P
18o	Unnamed at RM380.8	NP	No Map	NP
18o.1	Unnamed at RM380.8	NP	No Map	NP
18p	Unnamed at RM382.1	NP	No Map	NP
	Perrin	P	No Map	P
	Gamble	P	No Map	P
19	Beaver	NP	No Map	F
19a	Unnamed at RM382.3	NP	No Map	NP
19a.1	Unnamed at RM383	NP	No Map	NP
19b	Unnamed at RM383	NP	No Map	F
19b.1	Unnamed at RM 383.1	NP	No Map	P
19c	Unnamed at RM383.2	NP	No Map	NP
	Unnamed at RM384.1	P	No Map	P
20	Quail #2	?	No Map	P
21	Quail #1	NP	No Map	P
22	Cliff	NP	No Map	F
	Prati	NP	No Map	P
	Bridge	P	No Map	P
23.1	Cable Group	NP	No Map	F
23.2	Cable Group	NP	No Map	F
23.3	Cable Group	NP	No Map	P
23.4	Cable Group	P?	No Map	P
23a.1	Cable Group	NP	No Map	F?
23a.2	Cable Group	NP	No Map	NP
23a.3	Cable Group	NP	No Map	NP
23a.4	Cable Group	NP	No Map	NP
23a.5	Cable Group	NP	No Map	NP
23b	No RM (side channel)	NP	No Map	F
24	Hoffman	NP?	No Map	P
24a.1	Hoffman Group	NP	No Map	NP
24a.2	Hoffman Group	NP	No Map	NP
24a.3	Hoffman Group	NP	No Map	NP
24a.4	Hoffman Group	NP	No Map	NP
24a.5	Hoffman Group	NP	No Map	NP
24b	Unnamed at RM392.6	NP	No Map	NP
25	Ross	NP	No Map	F
25a	Unnamed at RM392.7	NP	No Map	NP
25b	Unnamed at RM393.2	NP	No Map	NP
25c	Unnamed at RM393.3	NP	No Map	NP
25d.1	Unnamed at RM393.9	NP	No Map	NP

Island Number	Island Name (AKA)	1894-1906 USGS Maps*	1914 USGS Water Supply Paper 347*	1938 and 1939 Aerial Photos*
25d	Unnamed at RM394.1	NP	No Map	NP
	Gold	P	No Map	P
27a	Unnamed at RM394.2	NP	No Map	NP
27	Little Cottonwood	?	No Map	F
26	Squatter's	?	No Map	P
28	Big Cottonwood	?	No Map	P
28a	Unnamed at RM394.5	?	No Map	F
28b	Unnamed at RM394.5	NP	No Map	NP
28c	Unnamed at RM394.5	NP	No Map	NP
29b	No RM (side channel)	NP	No Map	F
29a.1	Heron Group	NP	No Map	NP
29a.2	Heron Group	NP	No Map	NP
29a.3	Heron Group	NP	No Map	NP
29a.4	Heron Group	NP	No Map	NP
29a.5	Heron Group	NP	No Map	NP
29a.6	Heron Group	NP	No Map	NP
29a.7	Heron Group	NP	No Map	NP
29	Heron	P	No Map	P
30	Rick	?	No Map	P
30a	Unnamed (side channel)	NP	No Map	NP
31.1	Boise Group	NP	No Map	NP
31.2	Boise Group	NP	No Map	NP
31.3	Boise Group	NP	No Map	NP
9.1	Barney Group	NP?	No Map	NP
9.2	Barney Group	NP?	No Map	NP
9.2a	Barney Group	NP?	No Map	NP
9.2b	Barney Group	NP?	No Map	NP
9.2c	Barney Group	NP?	No Map	NP
9.3	Barney Group	NP?	No Map	NP
9.3a	Barney Group	NP?	No Map	NP
9.3b	Barney Group	NP?	No Map	P
32	Kline	NP	No Map	F
33	Goose Egg	P	No Map	P
12	Big Willow	NP	No Map	P
12a	Unnamed at RM399.1	NP	No Map	F?
12b	Unnamed at RM399.1	NP	No Map	F
34.1	Billy Goat Group	NP	No Map	P
34.2	Billy Goat Group	NP	No Map	P
34.3	Billy Goat Group	NP	No Map	F
34.4	Billy Goat Group	NP	No Map	F
35	Main & East Shack	P	No Map	P
36	Rhubarb	P	No Map	P
37	Adrian	P	No Map	P

Island Number	Island Name (AKA)	1894-1906 USGS Maps*	1914 USGS Water Supply Paper 347*	1938 and 1939 Aerial Photos*
38	Suzy	P	No Map	P
39	Airport	P	No Map	P
	Peachtree	P	No Map	P
	Grassland	P	No Map	P
	Border	P	No Map	P
39a.1	Tule Group	NP	No Map	F
39a.2	Tule Group	NP	No Map	F
39a	TULE	NP	No Map	F
39b.1	Unnamed at RM411	NP	No Map	F
39b	Unnamed at RM411.9	NP	No Map	NP
39c	Channel Island #3	F?	No Map	P
39d	Channel Island #2	F?	No Map	P
40	Silo	P	No Map	P
40a.1	Avocet	NP	No Map	F
	Helton's	P	No Map	P
40a	Unnamed at RM414.8	NP	No Map	F
41	Homedale	NP	No Map	P
42	Wegman	NP	No Map	P
43.2	Rabbit Group	NP	No Map	F
43.3	Rabbit Group	NP	No Map	F
43.1	Rabbit	NP	No Map	P
43.4	Rabbit Group	NP	No Map	F
43.5	Rabbit Group	NP	No Map	P
43.5a	Rabbit Group	NP	No Map	F?
43.6	Rabbit Group	NP	No Map	F
43.6a	Rabbit Group	NP	No Map	NP
43.6b	Rabbit Group	NP	No Map	NP
44	Black Crowned	NP	No Map	P
	Clark's	P	No Map	P
45.1	Olive Group	NP	No Map	P
45.2	Olive Group	P	No Map	P
45a	Unnamed at RM420	NP	No Map	NP
46	Feral	P	No Map	P
47	Pheasant #2	P	No Map	P
47a	Unnamed at RM420.6	NP	No Map	F
48	Pheasant #1	?	No Map	P
48a	Unnamed at RM420.8	NP	No Map	NP
48b	Unnamed at RM420.8	NP	No Map	F
49	Pheasant #3	NP	No Map	P
49a	Unnamed at RM421.4	NP	No Map	NP
49b	Unnamed at RM421.4	NP	No Map	NP
49c	Unnamed at RM421.4	NP	No Map	NP
50	Tiny	NP?	No Map	P

Island Number	Island Name (AKA)	1894-1906 USGS Maps*	1914 USGS Water Supply Paper 347*	1938 and 1939 Aerial Photos*
50a	Unnamed at RM421.5	NP	No Map	NP
51a	Unnamed at RM421.7	NP	No Map	F
51	Gosling	?	No Map	P
51b	Unnamed at RM421.9	NP	No Map	NP
52	Jensen	NP	No Map	P
52a	Unnamed at RM422.5	NP	No Map	NP
53	Cigar	?	No Map	P
53a	Unnamed at RM423.1	NP	No Map	NP
54	Marsing	NP	No Map	P
55	Poison Ivy	P	No Map	P
56	Feedlot	NP	No Map	P
57	Gem	NP	No Map	P
58	Center	NP	No Map	P
	Fruit	P	No Map	P
58a	Unnamed at RM429.4	NP	No Map	NP
58b	Unnamed at RM429.4	NP	No Map	NP
58c	Unnamed at RM429.4	NP	No Map	F
58d	Unnamed at RM429.4	NP	No Map	NP
58e	Unnamed at RM429.4	NP	No Map	NP
60	Dilley #2	NP?	No Map	P
59	Dilley #1	NP	No Map	P
60a	Unnamed at RM430.7	NP	No Map	F
61a	Unnamed at RM430.7	NP	No Map	F
61	Cottontail	P	No Map	P
62	Foglers	P	No Map	P
63	Blackburn	P?	No Map	F?
63a	Unnamed at RM432.1	NP	No Map	F
64	Dredge	P	No Map	P
64a	Stanley	NP	No Map	NP
65	Goldeneye	P	No Map	P
65a	Unnamed at RM433.5 (Williams)	NP	No Map	P
66	Raccoon	P?	F?	P
66a	Unnamed at RM434.7	NP	NP	F
66b	Unnamed at RM434.9	NP	NP	F
66c	Unnamed at RM435	NP	NP	NP
66d	Unnamed at RM435.3	NP	NP	F
66e	Unnamed at RM435.6	NP	NP	F
67	Hermit	P	P	P
68.1	Rippee Group	NP	P	P
68.1a	Rippee Group	NP	NP	F
68.2	Rippee Group	P	F?	P
68.3	Rippee Group	NP	P	P

Island Number	Island Name (AKA)	1894-1906 USGS Maps*	1914 USGS Water Supply Paper 347*	1938 and 1939 Aerial Photos*
68.4	Rippee	P	P	P
68.5	Rippee Group	NP	F?	P
69	Current	P?	P?	P
70	Fisher	P	?	P
71	Ware	P	P	P
72	Richards	P	P	P
72a	Unnamed at RM439.1	NP	NP	NP
73	Wright	NP	P	P
74	Bayha	P?	P	P
75	Argy	P	P	P
76	Becky	?	P	P
76a	Unnamed at RM439.9	NP	NP	NP
77a	Unnamed at RM440	NP	NP	NP
77b	Unnamed at RM440	NP	NP	NP
77c	Unnamed at RM440	NP	NP	F
77d	Unnamed at RM440	NP	NP	F
77e	Unnamed at RM440.1	?	NP	P
77	Papike	P?	P	P
78.1	Brooks Group	NP	NP	F
78.2	Brooks Group	NP	NP	F?
78.3	Brooks	P?	P	P
79.1	Blind	P	P	P
79.2	Blind Group	NP	NP	F
80	Walters	P	P	P
81	Jim's	NP	?	F
82	Kim's	NP	?	F
83	Big Rocky	P	P	P
84	Little Rocky	?	P	P
84a	Unnamed at RM442.7	NP	NP	NP
84b	Unnamed at RM442.7	NP	NP	NP
84c	Unnamed at RM442.7	NP	NP	F
85	Menning	?	P	P
	Noble	P	P	P
85a	Unnamed at RM444.1	?	NP	F
85a.1	Unnamed at RM445.3	NP	NP	NP
85b	Unnamed at RM445.7	NP	NP	NP
85c	Unnamed at RM446.1	NP	NP	NP
86a	Unnamed at RM446.7	NP	NP	F
86	Guffy	P	P	P
87a	Unnamed at RM447.9	?	NP	P
87b	Unnamed at RM447.9	NP	NP	NP
87	Rail	P	P	P
88a	Unnamed at RM447.9	NP	NP	NP

Island Number	Island Name (AKA)	1894-1906 USGS Maps*	1914 USGS Water Supply Paper 347*	1938 and 1939 Aerial Photos*
88b	Unnamed at RM	NP	NP	NP
88	Sign	P	P	P
P-Present	NP-Not Present	F-Forming	?=Designation Uncertain	

Table F.2 Geomorphic Characteristics of the Middle Snake River Valley in the study reach. Modified from Mussetter and Harvey (2001b).

Island Number	Island Name	AKA	Valley Form (1)	Channel Form (2)	Tributary Locations (3)	Upstream Constriction (4)	Downstream Constriction (4)	Larger Constriction (4)	Floodplain constriction (4)	Fan Construction (4)
1	Whitehill	W-13	En ff	S	Mu Md	A	G	ds		B
	Huffman		En ff	S	Mu Sd	A	G	us	ds	us
2	Fenzl	W-12	En ff	S	Su Md	G	A	ds		B
	Rapids #2		En ff	S	Mu Md	A	A	ds	us	B
	Rapids #1		En ff	S	Mu Md	A	A	ds	us	B
3	Waunch's		En ff	S	Su Md	G	A	us	B	
4	Rock		En ff	S	Su Md	G	A	us	B	
	Porter's		En nf	S	Su Sd	A	G	us	B	
5	Jackass	W-11	En nf	S	Su Sd	A	G	us	B	
	Westlake		nf wf	S		A	A	us	B	
	Aulbach #1		nf hwf	S	Sd	G	A	ds	B	
6	Aulbach #2		nf hwf	S	Sd	G	A	ds	B	
7	Aulbach #3		nf hwf	S	Sd	G	A	ds	B	
8.1	McRea Group	W-8, Mason	nf hwf	S	Lu	G	G	ds	B	
8.2	"	W-10	nf hwf	S	Lu	G	G	ds	B	
8.3	"	W-9	nf hwf	S	Lu	G	G	ds	B	
8.4	Schledewitz	W-7	nf hwf	S	Lu	G	G	eq	B	
10	Goat		wf	A	Su Ld	A	A	ds	B	
11.2	Smith #3	W-3	nf hwf	S	Sd	A	A	ds	B	
11.3	Smith #2	W-2	nf hwf	S	Sd	A	A	ds	B	
	Smith #1		nf hwf	S	Sd	A	A	ds	B	
	Nadeau		nf hwf	S	Su	A	A	ds	B	
14	Larsen		nf hwf	S	Su	A	A	ds	B	
	Buttermilk		nf hwf	S	Su	A	A	ds	B	
15	Sundstrom	W-1	nf hwf	S	Su	A	A	ds	B	
	Grafton		nf hwf	S	Su	A	A	ds	B	
	Pruit		nf hwf	S		A	G	eq	B	
	Resch		nf hwf	S		A	G	eq	B	
	Oglesbee		nf hwf	S		A	G	us	B	
15c	Annear	P-20	nf hwf	S		A	G	us	B	
16	Ketchup	P-19	nf hwf	S		A	G	us	B	
17	Horse		nf hwf	SA	Su	G	G	eq	B	
	Pool		nf hwf	A	Lu	G	G	eq	B	
18	Scarecrow	P-17, P-18	nf hwf	A	Lu	G	G	eq	B	
18a	Sylvia	P-16	nf hwf	A	Lu	G	G	eq	B	
	Duncan		nf hwf	A	Lu	G	G	eq	B	
18n.1	Crow	P-6	wf	sA	Su	A	A	ds	B	
19	Beaver	P-5	wf	sA	Su Sd	A	G	ds	B	
20	Quail No. 2	C-16, U	wf	A	Md	A	G	eq	B	
21	Quail No. 1	C-15, T	wf	A	Md	A	G	eq	B	
22	Cliff	V	wf	A		A	A		B	
23.1	Cable Group	C-14?, R	wf	A	Su Sd	A	A		B	
23.2	"	Q	wf	A	Su Sd	A	A		B	

Island Number	Island Name	AKA	Valley Form (1)	Channel Form (2)	Tributary Locations (3)	Upstream Constriction (4)	Downstream Constriction (4)	Larger Constriction (4)	Floodplain constriction (4)	Fan Construction (4)
23.3	"	C-14, O	wf	A	Su Sd	A	A		B	
23.4	"	C-14, P	wf	A	Su Sd	A	A		B	
24	Hoffman	M	wf	A	Sd	G	A	us	B	
25	Ross	K	wf	A						
26	Squatter's	C-8, G	wf (nf)	A	Lu Md	G	A	ds	ds	
27	Little Cottonwood	C-9, H	wf (nf)	A	Lu Md	G	A	ds	ds	
28	Big Cottonwood	C-7, F	wf (nf)	A	Lu Md	G	A	ds	ds	
29	Heron	C-10, E	wf (nf)	A	Lu	A	A	ds	B	
30	Rick	C-11, D	wf (nf)	A	Lu	A	A	us	B	
31.1	Boise Group		wf (nf)	A	Lu Ld					
31.2	"		wf (nf)	A	Lu Ld					
31.3	"	C-6, B	wf (nf)	A	Lu Ld					
9.1	Barney Group		wf (nf)	A	Lu Ld					
9.2	"	A?	wf (nf)	A	Lu Ld					
9.2a	"		wf (nf)	A	Lu Ld					
9.2b	"		wf (nf)	A	Lu Ld					
9.2c	"		wf (nf)	A	Lu Ld					
9.3	"	A?	wf (nf)	A	Lu Ld					
9.3a	"		wf (nf)	A	Lu Ld					
9.3b	"	in Boise R?	wf (nf)	A	Lu Ld					
	Kline		wf (htf)	S	Ld	G	G	us	us	
33	Goose Egg	C-5	wf (htf)	S	Ld	G	G	us	us	
12	Big Willow		wf (htf)	S	Ld	G	G	us	us	
34.1	Billy Goat Group		wf (htf)	S	Ld	G	G	us	us	
34.2	"		wf (htf)	S	Ld	G	G	us	us	
34.3	"		wf (htf)	S	Ld	G	G	us	us	
34.4	"		wf (htf)	S	Ld	G	G	us	us	
35	Main & East Shack		En ff (hsct & hwt)	S		G	G	us	B	
36	Rhubarb		En ff (hsct & hwt)	S		G	G	us	B	
37	Adrian		En ff (hsct & hwt)	S		G	G	us	B	
38	Suzy		En ff (hsct)	S	Mu Md	G	A	us	B	B
39	Airport		En ff (hsct)	S	Su Md	A	A	us eq	B	B
	Peachtree		En ff (hsct)	S	Mu Sd	A	A	us	ds	B
	Grassland		En ff (hsct)	S	Md	G	G	ds		
	Border		En ff (hsct)	S		A	A	us	B	
39a.1	Tule Group		En ff (hsct)	S		A	G	us	us	
39a.2	Tule Group		En ff (hsct)	S		A	G	us	us	
39a	Tule		En ff (hsct)	S		A	G	us	us	
39c	Channel #3	C-4	En ff (hsct)	S		A	A	eq	B	
39d	Channel #2	C-3	En ff (hsct)	S		A	A	eq	B	
40	Silo	Goat C-2	En ff (hsct)	S	Mu	A	G	ds	B	
40a.1	Avocet	C-1	En ff (hsct)	S	Mu	G	G	ds	ds	us
	Helton's	O-1	En ff (hsct)	S	Md	A	A	ds	us	ds

Island Number	Island Name	AKA	Valley Form (1)	Channel Form (2)	Tributary Locations (3)	Upstream Constriction (4)	Downstream Constriction (4)	Larger Constriction (4)	Floodplain constriction (4)	Fan Construction (4)
41	Homedale		En ff (hsct)	S	Mu	A	G	us	B	us
42	Wegman		En ff (hsct)	S	Mu	A	G	us	B	us
43.1	Rabbit Group	Rabbit	En ff (hsct)	S	Mu	A	G	us	B	us
43.2	"		En ff (hsct)	S	Mu	A	G	us	B	us
43.3	"		En ff (hsct)	S	Mu	A	G	us	B	us
43.4	"		En ff (hsct)	S	Mu	A	G	us	B	us
43.5	"		En ff (hsct)	S	Mu	A	G	us	B	us
43.5a	"		En ff (hsct)	S	Mu	A	G	us	B	us
43.6	"		En ff (hsct)	S	Mu	A	G	us	B	us
43.6a	"		En ff (hsct)	S	Mu	A	G	us	B	us
43.6b	"		En ff (hsct)	S	Mu	A	G	us	B	us
44	Black Crowned		En ff (hsct)	S	Md	G	G	ds		
	Clark's		En ff (hsct)	S	Mb	A	A	us	B	
45.2	Olive	Smith's	En ff (hsct)	S	Mb	A	A	us	B	
46	Feral		En ff (hnt)	S		A	G	us	us	
47	Pheasant No. 2		En ff (hnt)	S	Md	A	G	us	us	
48	Pheasant No. 1		En ff (hnt)	S	Md	A	G	us	us	
49	Pheasant No. 3		En ff (hnt)	S	Md	A	G	us	us	
50	Tiny		En (hsct)	S	Su	G	A	ds	ds	us
51	Gosling		En (hsct)	S	Su	G	A	ds	ds	us
52	Jensen		En (hsct)	S	Su	G	A	ds	ds	us
53	Cigar		En (hsct)	S	Su, Sd	G		us		B
54	Marsing		En ff (hsct)	S	Sd	A	G	us eq	us	ds
55	Poison Ivy		En ff (hsct)	S		A	G	us eq	us	
56	Feedlot		En ff (hsct)	S		G	G	eq	us	
57	Gem		En ff (hsct)	S	Su	G	G	eq	B	us
58	Center		En ff (hsct)	S	Mu Sd	A	A	us	us	B
	Fruit		En ff	S	Mu Md	G	G	us	ds	us
59	Dilly #1		En ff	S	Mu Md	G	G	us	ds	us
60	Dilly #2		En ff	S	Mu Md	G	G	us	ds	us
61	Cottontail		En ff	S	Md	G	G	ds	us	ds
62	Foglers		En	S	Su					
63	Blackburn		En ff	S	Sd	A	A	ds	B	ds
64	Dredge		En ff	S	Sd	A	A	ds	B	ds
65	Goldeneye		En ff	S	Mu	G	G-A	us	ds	us
65a	Williams	13	En ff	S	Mu	G	G-A	us	ds	us
66	Raccoon		En ff	S	Md	G	G	ds	us	ds
67	Hermit		En	S	Mu	A	G	us	B	us
68.1	Rippee Group		En	S	Mu	A	G	us	B	us
68.1a	"		En	S	Mu	A	G	us	B	us
68.2	"		En	S	Mu	A	G	us	B	us
68.3	"		En	S	Mu	A	G	us	B	us
68.4	"	Rippee	En	S	Mu	A	G	us	B	us

Island Number	Island Name	AKA	Valley Form (1)	Channel Form (2)	Tributary Locations (3)	Upstream Constriction (4)	Downstream Constriction (4)	Larger Constriction (4)	Floodplain constriction (4)	Fan Construction (4)
68.5	"		En	S	Mu	A	G	us	B	us
69	Current		En ff	S	Lu Md	A	G	us	ds	us
70	Fisher		En ff	S	Lu Md	A	G	us	ds	us
71	Ware		En ff	S	Lu Md	A	G	us	ds	us
72	Richards		En ff	S	Lu Md	A	G	us	ds	us
73	Wright		En ff	S	Lu Ld	A	A	ds	B	B
74	Bayha		En ff	S	Lu Ld	A	A	ds	B	B
75	Argy		En ff	S	Lu Ld	A	A	ds	B	B
76	Becky		En ff	S	Lu Ld	A	A	ds	B	B
77	Papike		En ff	S	Lu Ld	A	A	ds	B	B
78.3	Brooks	Brooks	En ff	S	Ld	G	A	ds	B	ds
79.1	Blind	Blind	En ff	S	Su	G	G	us	us	
80	Walters		En ff	S		A	A	us	ds	
81	Jim's		En ff	S		A	A	us	ds	
82	Kim's		En ff	S		A	A	us	ds	
83	Big Rocky		En ff	S	Su	A	A	us	ds	us
84	Little Rocky		En ff	S	Mu	A	A	us		us
85	Menning		En ff	S	Mu	G	G	us	ds	us
	Noble		En ff	S	Mu Md	A	A	us	ds	us
86	Guffy		En	S	Su Md	A	A	us	ds	us
87	Rail		En	S	Mu Sd	A	A	us		B
88	Sign		En	S	Mu Sd	A	A	us		B

1 Valley Form:	En - entrenched
	ff - floodplain fragments
	nf - narrow floodplain
	wf - wide floodplain
	htf - high terrace fragments
	hsct - high, semi-continuous terrace
	hwt - high wide terrace
2 Channel Form:	S - single channel with islands
	A - Anastamosing
3 - Tributarys:	S, M, L - small, medium, large
	u - upstream
	d - downstream
4 - Constrictions:	A - abrupt
	G - gradual
	us - upstream
	ds- downstream
	B- both

Table F.3 Geomorphic characteristics of the Islands in the Middle Snake River study reach (Mussetter and Harvey, 2001b).

Island Number	Island Name	AKA	Island Form *	Core Form *	Upstream Berm Form *	Lateral Berm Form *	Downstream Berm Form *	Core Change or Whole Island if No Core**	Ustream Bern Change**	Lateral Berm Change**	Downstream Berm Change**	Chute Change**
1	Whitehill	W-13	A(43)									
	Huffman		Ir	Ir	A							
2	Fenzl	W-12	S									
	Rapids #2		Ir	Ir		Ir		V	V	V		f
	Rapids #1		A	A	A	N Ir		e	gV	gV		
3	Waunch's		Ir (A)	A Ir	A	W N Ir			GV	gV		
4	Rock		A Ir	A	A				g			
	Porter's		A	A	A Ir	N	A(87)		g		GV	
5	Jackass	W-11	A	A	A	W N			GV	GV		f
	Westlake		Ir	Ir	A	N			gv	gv		
	Aulbach #1		Ir (A)	A Ir	S	W N		E				f
6	Aulbach #2		Ir					Gv				
7	Aulbach #3		Ir					Gv				
8.1	McRea Group	W-8, Mason	A	A	S	W N			gv	GV		f
8.2	McRea Group	W-10	A(87)					GV				
8.3	McRea Group	W-9	Ir	Ir	A	N			GV			f
8.4	Schledewitz	W-7	Ir	A(38) Ir(97)	A Ir		A	GV			GV	f
10	Goat		Ir	Ir	Ir	Ir	A		V	g	g	f
11.2	Smith #3	W-3	A	Ir	A	all	D		g	g	G	
11.3	Smith #2	W-2	A	Ir	A	N W	A					f
	Smith #1		A	A Ir	A	N R			V	V		f
	Nadeau		Ir					GV				f
14	Larsen		Ir	Ir	Ir (97)		A (97)		GV			f
	Buttermilk		Ir					GV				f
15	Sundstrom	W-1	A	Ir	S A	W R				g		

Island Number	Island Name	AKA	Island Form *	Core Form *	Upstream Berm Form *	Lateral Berm Form *	Downstream Berm Form *	Core Change or Whole Island if No Core**	Ustream Bern Change**	Lateral Berm Change**	Downstream Berm Change**	Chute Change**
	Grafton		A	Ir	A	W R						
	Pruit		SA					GV				
	Resch		A Ir					GV				
	Ogelsbee		S(87) A(97)					GV				
15c	Annear	P-20	A Ir (87)	Ir ?	Ir (A)				eGV			f
16	Ketchup	P-19	S(38) A(97)	Ir	A	W Ir	Annear		Gv	e		f
17	Horse		Ir	A	Ir(97)	W Ir		e	gV	GV		f
	Pool		Ir	Ir	A	N(97)	S D			gV		f
18	Scarecrow	P-17, P-18	Ir	Ir	Ir	W Ir	A D		gV	gV	GV	f
18a	Sylvia	P-16	S(38) A(97)					GV				f
	Duncan		Ir									
18n.1	Crow	P-6	A					G				
19	Beaver	P-5	A(38) Ir(97)	Ir	Ir	W Ir		e	egV	GV	GV	
20	Quail No. 2	C-16, U	Ir	A(38) Ir(97)	S A	Ir	A	e	eV	V		
21	Quail No. 1	C-15, T	Ir	A Ir	A	Ir N	A	e	eV	gV	V	
22	Cliff	V	S(38) A(97)					gV				
23.1	Cable Group	C-14?, R	Ir					V				
23.2	Cable Group	Q	Ir					V				
23.3	Cable Group	C-14, O	Ir	Ir	A Ir	N	A	E	V	V	V	f
23.4	Cable Group	C-14, P	Ir					V				
24	Hoffman	M	Ir	?	A	W N		e	V	gV		f
25	Ross	K	A Ir					GV				f
26	Squatter's	C-8, G	Ir	Ir	S	W N Ir	A D	e	V	gV		f
27	Little Cottonwood	C-9, H	A Ir	A	A	W N Ir	A D	e	V	eV	GV	
28	Big Cottonwood	C-7, F	Ir	Ir	S	N(97)			gV			

Island Number	Island Name	AKA	Island Form *	Core Form *	Upstream Berm Form *	Lateral Berm Form *	Downstream Berm Form *	Core Change or Whole Island if No Core**	Ustream Bern Change**	Lateral Berm Change**	Downstream Berm Change**	Chute Change**
29	Heron	C-10, E	Ir	Ir	A Ir	W N Ir		e	gV	GV		f
30	Rick	C-11, D	S					E	GV			f
31.1	Boise Group		A(97)					GV				
31.2	Boise Group		A(97)					GV				
31.3	Boise Group	C-6, B	Ir(97)					EV				
9.1	Barney Group		Ir(97)					GV				
9.2	Barney Group	A?	Ir(97)					GV				
9.2a	Barney Group		Ir(97)					GV				
9.2b	Barney Group		Ir(97)					GV				
9.2c	Barney Group		Ir(97)					GV				
9.3	Barney Group	A?	Ir(97)					GV				
9.3a	Barney Group		Ir(97)					GV				
9.3b	Barney Group	in Boise R?	Ir(97)									
	Kline		S					GV				
33	Goose Egg	C-5	A Ir	A	Ir	N		e	V			f
12	Big Willow		A (Ir)	?				e?	gV	gV		
34.1	Billy Goat Group		A Ir						gV			f
34.2	Billy Goat Group		A Ir									
34.3	Billy Goat Group		A Ir									
34.4	Billy Goat Group		A Ir									
35	Main & East Shack		A Ir	A	Ir	W N Ir		e	eV	V		
36	Rhubarb		A Ir	S	A Ir	N		e	GV	GV		f
37	Adrian		S	S	S	N R			V	gV		
38	Suzy		A	A	A	N-Ir(97)		e?	gV	gV		f
39	Airport		A	A	A	N(97)		E	gV	gV		f

Island Number	Island Name	AKA	Island Form *	Core Form *	Upstream Berm Form *	Lateral Berm Form *	Downstream Berm Form *	Core Change or Whole Island if No Core**	Ustream Bern Change**	Lateral Berm Change**	Downstream Berm Change**	Chute Change**
	Peachtree		A	A	SA	N(97)		E	gV	gV		f
	Grass		A Ir	A	I	N(87)	A D	e	GV			
	Border		A Ir	A Ir	A	N(97)		e	gV	gV		A
39a.1	Tule Group		Ir(97)					GV				
39a.2	Tule Group		Ir(97)					GV				
39a	Tule		A-Ir(97)					GV				
39c	Channel #3	C-4	A Ir	Ir	A	N Ir	A			gV	V	
39d	Channel #2	C-3	A Ir	Ir	Ir	N Ir	A(97)	e?	GV			f
40	Silo	Goat C-2	A Ir	A	A	N Ir	A		V	V	GV	
40a.1	Avocet	C-1	S					gV				
	Helton's	O-1	A	Ir	A	N R			gV	gV		
41	Homedale		A Ir	Ir	A	N(97)		e	GV			f
42	Wegman		S					gV				
43.1	Rabbit Group	Rabbit	A Ir	A	A	N(97)		E	GV	gV		
43.2	Rabbit Group		A Ir					GV				
43.3	Rabbit Group		A Ir					GV				
43.4	Rabbit Group		A Ir					GV				
43.5	Rabbit Group		A Ir					GV				
43.5a	Rabbit Group		A Ir (97)					GV				
43.6	Rabbit Group		A Ir					GV				
43.6a	Rabbit Group		A Ir (97)					GV				
43.6b	Rabbit Group		A Ir (97)					GV				
44	Black Crowned		A(38) Ir(97)					GV				
	Clark's		A	A	S	N Ir		e		V		
45.2	Olive	Smith's	A	A	A	N(97)		e	V	gV		

Island Number	Island Name	AKA	Island Form *	Core Form *	Upstream Berm Form *	Lateral Berm Form *	Downstream Berm Form *	Core Change or Whole Island if No Core**	Ustream Bern Change**	Lateral Berm Change**	Downstream Berm Change**	Chute Change**
46	Feral		A	S	A	N Ir		e	V	V		
47	Pheasant No. 2		Ir	A-Ir		N Ir		e		V		
48	Pheasant No. 1		Ir	Ir		N W Ir	S	e		gV	gV	f
49	Pheasant No. 3		A(38) Ir(97)					gV				f
50	Tiny		A	A	Ir	Ir N (97)	A (97)	e	g	V		f
51	Gosling		Ir	Ir	A	W N Ir		e?	gV	gV		f
52	Jensen		Ir	A	A	W Ir(97)		E	g	g		
53	Cigar		Ir	Ir		N(97)			V	V		
54	Marsing		Ir					g				f
55	Poison Ivy		A	S	A			V	GV			
56	Feedlot		S					g				
57	Gem		S A					G				
58	Center		A	A	A	all (97)	A D (97)	e	GV	GV	GV	
	Fruit		Ir	Ir	A	N-W R	A D	V	gV	GV	GV	f
59	Dilly #1		Ir	Ir	A	all		V	GV	GV		
60	Dilly #2		A	Ir	A			E	gV			f
61	Cottontail		A(38) Ir(97)	Ir	S	N Ir	A D	E	gV	gV	GV	
62	Foglers		Ir A	A Ir		N R		e		V		f
63	Blackburn		A Ir	A Ir		N Ir	S		GV	gV	gV	f
64	Dredge		A	A	S	N Ir	A		gV	gV	V	f
65	Goldeneye		A	A (38) Ir (97)	A	N Ir	A	e?	V	gV	gV	f
65a	Williams	13	A					V				
66	Raccoon		A(39) Ir(97)									f
67	Hermit		A(39) Ir(97)	A(39) Ir(97)	S(39) A(97)	N	A	E			GV	
68.1	Rippee Group		A(39) Ir(97)					gV				

Island Number	Island Name	AKA	Island Form *	Core Form *	Upstream Berm Form *	Lateral Berm Form *	Downstream Berm Form *	Core Change or Whole Island if No Core**	Ustream Bern Change**	Lateral Berm Change**	Downstream Berm Change**	Chute Change**
68.1a	Rippee Group		A(39) Ir(97)					gV				
68.2	Rippee Group		A(39) Ir(97)					gV				
68.3	Rippee Group		A(39) Ir(97)					gV				
68.4	Rippee-Main	Rippee	S	S	A	N(97)	A	e?			gV	f
68.5	Rippee Group		A					gV				
69	Current		S A	S(39) Ir(97)	A	N R	S	E?				
70	Fisher		S A	S	S	N			g			
71	Ware		A Ir	Ir	S	N(97)	A		v	gv	Gv	f
72	Richards		A Ir	A Ir	S	N R	A (97)		v	Gv	Gv	f
73	Wright		A									
74	Bayha		Ir	Ir	A	N R (97)			gv			
75	Argy		Ir	Ir			A(97)	v				
76	Becky		Ir	Ir		N R (97)	A(97)	E		Gv	Gv	
77	Papike		Ir	Ir	S	N Ir (97)	A		v	Gv	gv	
78.3	Brooks	Brooks	Ir	Ir		N Ir	A	e?		V		
79.1	Blind	Blind	A	A	Ir	N Ir (97)			G	Gv		
80	Walters		A	A	A	N R			v			
81	Jim's		A					G				
82	Kim's		A					g				
83	Big Rocky		A	A Ir	Ir	N R	A D		g	gv		
84	Little Rocky		A	A	Ir	W R	AD		g	Gv		
85	Menning		Ir	Ir	S	W R	A		Gv	gv	gv	
	Noble		A	A	A	N R		e	g	gv		
86	Guffy		A	A	A	N R	AD		g		G	
87	Rail		A	A		N Ir						
88	Sign		Ir	Ir	A	N R			g	g		

* Island Form

A - assymetric, streamlined
S - symmetric, streamlined
R - regular
Ir - irregular
N - narrow
W - wide
D - detached

**Island Change

V= Vegetation increase
e= Limited erosion
E= Prominent erosion
f= Filling
g= Limited growth
G= Prominent growth

Numbers in parentheses refer to date of aerial photogra

Table F.4 Overtopping Discharge with Return Intervals and Exceedence Percent for Selected Islands in the MSR. (Modified from Mussetter and Harvey (2001b).

Island Number	Island Elevation (m)*	Overtopping Discharge (m^3/s)	Exceedence Percent	Return Interval (years)	MSU Soil Number
1	629.23	357	57.82	<1	3
1a	630.02	392	47.83	<1	3
2	631.76	406	44.76	<1	3
3	635.81	2,866	0.00	>55	
4	637.64	>3,681	0.00	>55	
4a	635.57	1,561	1.32	3.8	2-
5	637.64	>3,681	0.00	>55	2+
USB5	635.81	1,601	1.09	3.9	2-
5a	632.61	<141.6	99.88	<1	4
5b	636.24	1,179	5.50	2.0	4
6	637.58	1,347	3.12	2.5	3
7	638.19	1,666	0.71	4.4	2-
7a	638.01	1,133	6.24	2.0	3
8.1	640.69	3,079	0.00	>55	2+
USB8.1	638.86	1,477	1.87	3.2	2-
8.2	639.20	1,922	0.13	8.3	2-
8.3	640.69	3,024	0.00	>55	2+
USB8.3	637.95	938	10.16	1.5	2-
8.4	640.72	2,586	0.00	>55	2-
8.5	640.69	1,513	1.61	3.4	2-
8a	640.90	1,365	1.97	3.2	3
8b	640.93	1,266	3.06	3.0	
8c	641.39	1,336	2.25	3.2	2-
10	642.52	2,027	0.00	40.8	
11.1	642.88	1,906	0.02	25.5	2-
11.2	644.41	3,060	0.00	>55	2-
USB11.2	643.13	1,933	0.02	29.9	3
11.3	643.31	2,024	0.00	40.4	2-
Nad	643.13	1,305	2.58	3.1	3
11a	642.06	679	15.72	1.4	
14	643.74	1,676	0.25	6.3	
But	643.74	1,542	0.69	4.1	
11b	642.46	710	14.45	1.4	4
15	644.26	1,853	0.06	16.2	2-
15a.1	642.21	472	30.50	1.1	4
15a.2	641.15	<140.1	99.86	<1	4
15a.3	642.95	823	10.90	1.6	4
15b	642.91	199	98.29	<1	3
Ogl	646.18	1,817	0.08	13.7	
15c	646.57	2,013	0.00	39.0	2-

Island Number	Island Elevation (m)*	Overtopping Discharge (m^3/s)	Exceedence Percent	Return Interval (years)	MSU Soil Number
16	647.40	2,716	0.00	>55	2+
USB16	645.87	1,415	1.58	3.4	2-
17	648.00	2,550	0.00	>55	
17a.1	645.35	281	82.38	<1	4
17a.3	645.41	290	78.93	<1	4
17a.2	645.54	335	59.62	<1	4
18a.1	648.95	2,219	0.00	>55	2-
18	649.83	2,944	0.00	>55	2+
18a	648.77	1,867	0.05	17.2	2-
18b	645.66	<140.1	99.86	<1	4
18c	648.71	1,416	1.57	3.4	3
18d	649.13	1,485	1.03	4.0	5
18d.1	649.77	1,591	0.48	4.3	
18e	649.22	897	9.20	1.8	3
18e.1	649.83	1,227	0.92	3.7	
18f	648.80	495	19.89	1.4	3
18f.2	650.41	1,256	0.73	3.9	
18f.1	651.72	2,297	0.00	>55	2-
18f.3	650.44	1,250	0.77	3.9	
18f.4	650.72	1,315	0.44	4.8	
18g	649.89	808	6.61	2.0	3
18h	650.81	934	4.40	2.4	3
18h.1	653.92	2,001	0.00	>55	2-
18i	653.25	675	9.33	1.8	3
18j	651.57	<141.6	99.75	<1	3
18k	651.85	<141.6	99.75	<1	3
18l	655.59	1,252	0.59	3.9	3
18m	656.17	1,596	0.00	29.5	3
18m.1	655.96	806	5.99	2.0	
18m.2	656.84	858	5.03	2.1	
18n	658.28	1,228	0.70	4.8	3
18n.1	658.68	1,194	0.89	4.4	3
18o	658.64	1,115	1.53	3.2	3
18o.1	658.70	1,136	1.34	3.3	3
18p	657.73	284	54.11	1.0	5
19	660.56	1,819	0.00	>55	2-
19a	658.03	281	55.16	1.0	4
19a.1	660.14	1,247	0.61	5.0	
19b	660.49	1,209	0.80	4.6	3
19b.1	662.39	2,531	0.00	>55	2-

Island Number	Island Elevation (m)*	Overtopping Discharge (m^3/s)	Exceedence Percent	Return Interval (years)	MSU Soil Number
19c	659.13	315	43.43	1.1	3
20	662.70	1,522	0.00	34.2	2-
21	664.28	2,489	0.00	>55	2+
22	663.00	1,343	0.26	6.4	2-
23.1	662.82	1,073	2.01	3.1	3
23.2	662.82	1,032	2.62	3.0	3
23.3	664.56	2,315	0.00	>55	2+
23.4	663.18	1,231	0.68	4.8	3
23a.1	663.21	1,252	0.59	5.0	3
23a.2	661.78	360	33.01	1.2	4
23a.3	661.87	391	28.21	1.2	5
23a.4	662.06	492	18.56	1.4	5
23a.5	662.51	756	7.11	2.0	4
23b	663.85	1,173	1.03	3.5	
24	664.62	1,509	0.00	32.3	2-
24a.1	664.04	1,161	1.12	3.4	3
24a.2	664.28	1,279	0.48	5.6	3
24a.3	663.58	848	5.20	2.3	4
24a.4	663.28	693	8.78	1.9	4
24a.5	662.94	516	16.89	1.5	4
24b	663.03	348	35.33	1.1	3
25	665.13	1,467	0.00	25.3	3
25a	663.70	421	24.43	1.2	4
25b	663.49	395	27.66	1.2	4
25c	665.29	1,373	0.19	7.0	3
25d.1	665.29	1,042	2.45	3.1	
25d	664.16	386	28.82	1.2	3
26	667.21	2,327	0.00	>55	2+
27	666.57	1,718	0.00	>55	2+
27a	664.77	650	10.18	1.8	3
28	667.91	>2,690.1	0.00	>55	2+
USB28	665.99	989	3.11	3.0	3
28a	666.38	1,517	0.00	33.4	3
28b	664.95	403	26.63	1.2	5
28c	665.23	599	12.39	1.7	3
29	667.36	2,309	0.00	>55	2+
29a.1	665.90	1,086	1.85	3.1	3
29a.2	666.17	1,343	0.26	6.4	3
29a.3	666.05	1,310	0.37	6.0	4
29a.4	664.46	398	27.19	1.2	5

Island Number	Island Elevation (m)*	Overtopping Discharge (m^3/s)	Exceedence Percent	Return Interval (years)	MSU Soil Number
29a.5	664.10	218	86.46	<1	4
29a.6	664.86	605	12.10	1.7	5
29a.7	664.56	394	27.82	1.2	5
29b	665.35	1,179	0.99	3.5	
30	666.41	1,495	0.00	30.5	3
30a	665.01	574	13.62	1.7	4
31.1	666.23	1,110	1.58	3.2	3
31.2	666.78	1,531	0.00	35.4	3
31.3	666.38	1,009	2.87	3.0	5
9.1	666.63	1,166	1.08	3.4	4
9.2a	666.41	996	3.01	3.0	4
9.2	666.66	748	7.31	2.0	3
9.2b	666.48	679	9.20	1.8	4
9.2c	666.48	675	9.33	1.8	4
9.3	666.84	794	6.24	2.0	4
9.3a	666.45	631	10.95	1.8	4
9.3b	666.93	816	5.79	2.1	3
32	667.85	681	3.50	2.2	
33	670.10	1,954	0.00	>55	1
USB33	668.12	716	2.63	2.3	2-
12	668.88	1,070	0.00	26.1	1
12a	668.18	726	2.43	2.4	3
12b	667.33	374	21.68	1.2	4
34.1	668.40	819	0.83	3.5	1
34.2	668.30	771	1.59	2.7	3
34.3	668.30	774	1.54	2.7	3
34.4	668.12	688	3.31	2.2	3
35	670.10	1,642	0.00	>55	
36	670.19	1,592	0.00	>55	
USB36	668.12	485	12.14	1.5	
37	670.07	1,411	0.00	>55	
USB37	668.12	428	17.02	1.3	
38	670.90	1,738	0.00	>55	2+
USB38	668.73	563	7.46	1.6	3
39	671.32	1,806	0.00	>55	
USB39	669.04	569	7.22	1.7	
39a.2	671.32	448	15.14	1.4	
39a.1	671.84	652	4.26	2.0	
39a	672.24	815	0.88	3.4	3
39b.1	672.42	771	1.60	2.7	

Island Number	Island Elevation (m)*	Overtopping Discharge (m^3/s)	Exceedence Percent	Return Interval (years)	MSU Soil Number
39b	671.93	448	15.16	1.4	3
39c	674.49	1,594	0.00	>55	2+
USB39c	672.69	686	3.36	2.2	
39d	674.46	1,546	0.00	>55	2+
USB39d	672.69	658	4.10	2.0	
40	674.49	1,353	0.00	>55	2+
USB40	672.69	498	11.22	1.5	2-
40a.1	673.24	628	5.06	1.9	3
40a	672.94	385	20.61	1.2	4
41	676.29	1,577	0.00	>55	1
USB41	674.22	604	5.84	1.8	3
42	675.65	1,213	0.00	>55	3
43.1	677.02	1,844	0.00	>55	1
USB43.1	674.74	655	4.17	2.0	3
43.2	674.61	676	3.62	2.1	3
43.3	674.80	729	2.37	2.4	3
43.4	675.13	887	0.36	5.9	3
43.5	674.74	693	3.20	2.2	3
43.5a	674.03	418	17.92	1.3	5
43.6	674.61	607	5.74	1.8	3
43.6a	674.13	406	18.80	1.3	5
43.6b	674.16	419	17.86	1.3	4
44	675.86	972	0.13	10.5	2-
Clarks	679.55	>1,982.2	0.00	>55	
USBClarks	675.44	628	5.05	1.9	
45.1	675.65	739	2.16	2.5	3
45.2	677.75	1,875	0.00	>55	1
45a	675.22	327	27.59	1.1	4
46	678.12	1,836	0.00	>55	2+
USB46	675.74	466	13.59	1.4	3
47	678.00	1,697	0.00	>55	2+
47a	676.32	687	3.35	2.2	3
48	677.88	1,603	0.00	>55	2-
48a	675.62	373	21.77	1.2	3
48b	676.47	735	2.24	2.5	3
49	676.41	711	2.76	2.3	3
49a	676.11	499	11.17	1.5	4
49b	676.11	498	11.20	1.5	4
49c	676.11	498	11.22	1.5	4
50	677.60	1,230	0.00	>55	3

Island Number	Island Elevation (m)*	Overtopping Discharge (m^3/s)	Exceedence Percent	Return Interval (years)	MSU Soil Number
50a	676.41	608	5.69	1.8	4
51	678.48	1,671	0.00	>55	2+
USB51	676.96	730	2.34	2.4	2-
51a	676.11	447	15.27	1.4	4
51b	676.17	394	19.81	1.2	5
52	678.55	1,631	0.00	>55	2+
USB52	676.66	480	12.47	1.5	3
52a	676.23	211	70.20	<1	
53	679.22	1,980	0.00	>55	1
USB53	677.57	827	0.74	3.7	3
53a	676.53	280	36.92	1.1	5
55	679.89	1,949	0.00	>55	1
USB55	678.24	872	0.43	5.0	3
56	678.42	877	0.41	5.4	3
57	678.73	879	0.39	5.6	3
58	681.62	>1,982.2	0.00	>55	1
USB58	679.03	830	0.71	3.8	2-
58a	678.45	406	18.84	1.3	4
58b	678.94	577	6.85	1.7	4
58c	677.94	228	59.08	1.0	3
58d	678.06	250	47.84	1.0	3
58e	678.12	260	43.14	1.1	4
Fruit	681.69	1,949	0.00	>55	
USBFruit	679.70	806	0.99	3.2	
59	681.90	1,947	0.00	>55	1
USB59	679.98	805	1.00	3.2	2-
60	681.20	1,561	0.00	>55	2-
60a	680.44	860	0.49	4.8	3
61	682.33	1,903	0.00	>55	2+
USB61	680.77	997	0.09	17.3	2-
61a	679.52	471	13.20	1.4	3
63	683.51	>1,982.2	0.00	>55	1
USB63	681.14	929	0.23	8.4	3
63a	680.50	674	3.65	2.1	5
64	683.61	>1,982.2	0.00	>55	1
USB64	681.01	769	1.65	2.7	2-
64a	681.38	806	0.99	3.2	3
65	683.67	1,893	0.00	>55	1
65a	682.11	977	0.12	10.8	3
66	683.54	1,293	0.00	>55	2-

Island Number	Island Elevation (m)*	Overtopping Discharge (m^3/s)	Exceedence Percent	Return Interval (years)	MSU Soil Number
66a	682.66	895	0.33	6.1	3
66b	681.87	549	8.15	1.6	5
66c	681.26	339	25.80	1.2	4
66d	682.63	789	1.24	2.8	3
66e	682.75	762	1.79	2.7	5
67	684.58	1,591	0.00	>55	2+
USB67	682.81	680	3.51	2.2	2-
68.1	682.84	752	1.95	2.7	3
68.1a	683.03	811	0.92	3.3	3
68.2	683.27	868	0.45	5.0	2-
68.3	683.45	922	0.25	8.2	2-
68.4	685.71	>1,982.2	0.00	>55	1
USB68.4	683.24	669	3.80	2.0	2-
68.5	684.18	1,173	0.00	>55	2-
69	684.28	984	0.11	11.8	2-
70	686.14	1,887	0.00	>55	2+
USB70	683.97	718	2.60	2.4	3
71	687.48	>1,982.2	0.00	>55	1
USB71	684.89	1,049	0.00	23.7	2-
72	686.04	1,727	0.00	>55	2-
USB72	684.28	736	2.24	2.5	3
72a	683.97	522	9.65	1.5	
73	684.86	789	1.25	2.8	3
74	685.98	1,272	0.00	>55	2-
75	686.71	1,617	0.00	>55	2+
76	686.84	1,621	0.00	>55	2-
76a	684.25	419	17.84	1.3	4
77	687.11	1,733	0.00	>55	2+
USB77	685.37	772	1.57	2.7	2-
77a	684.76	612	5.57	1.9	4
77b	684.86	647	4.42	2.0	5
77c	684.18	363	22.86	1.2	4
77d	684.25	375	21.55	1.2	4
77e	685.31	840	0.62	4.0	3
78.1	686.29	1,077	0.00	27.0	3
78.2	685.43	671	3.75	2.0	3
78.3	687.54	1,807	0.00	>55	2+
79.1	688.15	>1,982.2	0.00	>55	2+
79.2	685.89	764	1.77	2.7	3
80	687.78	1,617	0.00	>55	1

Island Number	Island Elevation (m)	Overtopping Discharge (m^3/s)*	Exceedence Percent	Return Interval (years)	MSU Soil Number
USB80	686.10	731	2.32	2.4	3
81	686.32	777	1.47	2.8	3
82	686.47	829	0.72	3.8	3
83	693.60	>1,982.2	0.00	>55	1+
84	687.29	1,181	0.00	>55	2-
USB84	685.95	535	8.89	1.5	3
84a	685.92	547	8.25	1.6	4
84b	685.92	539	8.69	1.5	4
84c	686.17	636	4.80	2.0	3
85	688.27	1,455	0.00	>55	2-
USB85	687.11	837	0.64	3.9	3
85a	686.23	459	14.18	1.4	4
Noble	689.09	1,878	0.00	>55	
USBNoble	687.29	681	3.50	2.2	
85a.1	687.05	529	9.23	1.5	4
85b	688.15	873	0.42	5.0	2-
85c	687.69	587	6.45	1.8	
86	690.98	>1,982.2	0.00	>55	1
USB86	688.54	790	1.23	2.8	2-
86a	688.42	800	1.07	3.0	3
87	693.82	>1,982.2	0.00	>55	1+
87a	689.76	1,156	0.00	>55	2-
87b	688.51	655	4.18	2.0	4
88	692.51	>1,982.2	0.00	>55	2+
USB88	689.91	1,010	0.08	19.6	2-
88a	688.54	653	4.26	2.0	4
88b	688.73	713	2.71	2.3	4

* if discharge values are preceded by a >, the island top was higher than the highest discharge profile created by the HEC-2 model, and the discharge listed is that highest discharge. If the discharge is preceded by a <, the overtopping discharge was below the lowest discharge profile.

Table F.5 Soil and Pollen Information. (Modified from Mussetter and Harvey (2001b).

Island No.	Island Name	Review of Aerial Photos 1938 & 1939	Core Soil MSU No.	Soil Horizons	Pollen Distribution*	Dung Fungal Spore Distribution*	Low Charcoal Abundance Depth (cm)	Comments
4a		F	2-	2A, 3Ab	A-M to base	M-L to base	to base	Cigarette Lighter at 25cm
5	Jackass (W-11)		2+	9Ab	L-S to base	M-L to 56cm, SB	48	C14 date, 146 BP at 1.8m
	Aulbach No. 1		2-	4Ab	A-L to base	M-L to base	to base	Cans, Bottle, Piston at 2-2.3m
6	Aulbach No. 2		3	A, 3Ab, 2AC	A-L to base	M-L to 1.8m	147	Intact Bottle at 61cm
7	Aulbach No. 3		2-	6Ab	A-L to base	A-L to 2.2m	173	
8.2	McRea Group (W-10)	F	2-	5Ab	A-M to base	A-M to base	150	Broken Brown Glass at 1.1m
8.4	Schledewitz (W-7)	1/2 F	2-	A/C	A-S to base	L-S to 1.5m	53,119	
8.5	W-6	F	2-	2A/Bw, 2Ab	A-L to base	M-L to base	48, 114	
8c	W-5	F	2-	2A, 2Ab	A-L to 51cm, SB	A-S to base	147	
11.1	Smith No. 4	F	2-	A, Ab	A-L to 2.1m	A-L to base	102	
11.2	Smith No.3 (W-3)		2-	A/C	A-L to base	S to base	221	
11.3	Smith No.2 (W-2)		2-	A/Bw	A-L to base	A-L to base	180	
15	Sundstrom (W-1)		2-	A, Ab	M-L to 2m	M-L to base	few	
15c	Annear (P-20)	F	2-	A/C	A-M to base	L-S to base	104	
16	Ketchup (P-19)		2+	A/C	A-L to 48cm, SB	L-S to base	99	
18a	Sylvia (P-16)		2-	2Ab	A-M to base	L to base	76	
18f.1	Little Banks (P-14)		2-	A/C	A-L to base	M-L to base	91	
18h		NP	3	all C's	A-M to base	S to base	to base	
18h.1	P-10		2-	A/Bw	A-L to base	A-S to base	94	
	P-7		2-	A/C	A-L to 1m	A-L to base	to base	
18n.1	Crow (P-6)		3	all C's	A-L to base	M-L to base	to base	
19	Beaver (P-5)		2-	A,A/Bw	A-S to base	M-S to base	56	
19b.1	P-2		2-	3A	A-L to base	M-S to base	86	
	Baxter (P-1)		2+	> Bw	A-S to base	A-S to 1.2m	20	

Island No.	Island Name	Review of Aerial Photos 1938 & 1939	Core Soil MSU No.	Soil Horizons	Pollen Distribution*	Dung Fungal Spore Distribution*	Low Charcoal Abundance Depth (cm)	Comments
20	Quail No. 2 (C-16)		2-	A/C	A-L to base	S below 89cm	124	
22	Cliff (V)		2-	Ab/Bwb	A-L to base	A-L to base	to base	Shotgun Shell at 15cm
23.1	Cable Group (C-14?, R)		3	all C's	A-L to base	M-L to base	64	
23a.1	Cable Group		3	2Ab	A-L to 1.3m	A-L to 1.4m	64	
23.2	Cable Group (Q)		3	3Ab	M-L to base	L-S to base	30	
23.4	Cable Group		3	all C's	A-L to base	Few	no info	
24	Hoffman (M)		2-	A/C	A-S to 2m	M-L to base	few	
25	Ross (K)	F	3	Ab	A-M to base	S to base	to base	
28	Big Cottonwood (F)		2+	A, 2Ab, AC	M-L to 64cm, SB	S to 1.4m	64	C14 date, 350 BP at 64cm
28a	Unnamed		3	all C's	A-L to base	A-L to base	to base	
29a.1	Heron Group		3	all C's	A-M to base	L to base	to base	
30	Rick (C-11, D)		3	Ab	A-M to base	M-L to base	to base	
31.1	Boise Group	NP	3	all C's	A-M to base	M-L to base	to base	Coors Beer Can at 53cm
31.2	Boise Group	NP	3	A/C	A-M to base	L to base	to base	
9.2	Barney Group (A?)		3	2Ab	A-M to base	L-S to base	to base	
12	Big Willow		1	> Bw	A-L to base	L-S to base	15	
34.1	Billy Goat Group		1	> Bw	A-L to base	Few	20	
34.2	Billy Goat Group		3	2Ab	A-L to base	M-L to base	to base	Intact Bottle at 20cm
34.3	Billy Goat Group		3	all C's	A-L to base	M-S to base	36	
39a	Tule	F	3	all C's	A-M to base	S to base	to base	
39c	Channel No. 3 (C-4)		2+	>Bw	A-S to 1.4m	M-L to 51cm	64	
39d	Channel No. 2 (C-3)		2+	>Bw	no info	no info	no info	
40a.1	Avocet (C-1)		3	all C's	no info	no info	no info	
41	Homedale		1	>Bw	no info	no info	no info	

Island No.	Island Name	Review of Aerial Photos 1938 & 1939	Core Soil MSU No.	Soil Horizons	Pollen Distribution*	Dung Fungal Spore Distribution*	Low Charcoal Abundance Depth (cm)	Comments
42	Wegman		3	Ab	A-L to base	M-L to base	to base	
43.2	Rabbit Group		3	all C's	M-L to base	A-L to base	to base	
43.3	Rabbit Group		3	2Ab	no info	no info	no info	
43.4	Rabbit Group		3	all C's	no info	no info	no info	
43.5	Rabbit Group		3	A, Ab	M-L to 58cm	L to base	to base	
44	Black Crowned		2-	A/C	M-L to 1m, SB	M-L to base	to base	
45.2	Olive Group		1	> Bw	M-L to 1.3m, SB	one	10	C14 date, 2960 BP at 1.6m
46	Feral		2+	A, 3Ab	no info	no info	no info	
47	Pheasant No. 2		2+	> Bw	S to base	few	28	C14 date, 2190 BP at 1.5m
48	Pheasant No. 1		2-	A/C	A-L to base	M-L to 1.3m, SB	to base	
48b	Pheasant Group	F	3	Ab	A-L to base	L-S to base	to base	
49	Pheasant No. 3		3	Ab	A-L to 48cm, SB	S to base	to base	
50	Tiny		3	all C's	L-S to base	S to base	to base	
52	Jensen		2+	> Bw	M-L to 43cm, SB	very S to base	48	C14 date, 690 BP at 71cm
56	Gem		3	all C's	A-L to base	M-L to 1.2m	to base	
57	Gem		3	all C's	A-L to base	S-51cm, L to base	to base	
60	Dilley No. 2		2-	A/C	A-L to base	S to base	99	
64a	Stanley	NP	3	all C's	no info	no info	no info	
65a	Williams		3	all C's	A-L to 1.5m	L-S to base	to base	
66	Raccoon		2-	A/C	L-S to base	only above 18cm	122	
66a	Unnamed		3	all C's	M-L to base	M-L to base	to base	
66d			3	all C's	A-L to base	A-L to base	71	
66e	Hermit No. 2		3	all C's	A-S to base	M-L to base	to base	
68.1	Rippee Group		3	Ab	M-S to base	M-S to base	to base	

Island No.	Island Name	Review of Aerial Photos 1938 & 1939	Core Soil MSU No.	Soil Horizons	Pollen Distribution*	Dung Fungal Spore Distribution*	Low Charcoal Abundance Depth (inches)	Comments
68.2	Rippee Group		2-	Ab	A-L to 61cm, SB	M-S to base	69	
68.3	Rippee Group		2-	Ab	A-L to 51cm, SB	L-S to base	to base	
68.5	Rippee Group		2-	all C's	A-L to base	S to base	to base	
69	Current		2-	Ab	A-L to base	L to base	to base	
70	Fisher		2+	> Bw	S to base	few	18	C14 date, 290 BP at 76cm
72	Richards		2-	all C's	A-L to base	A-L to base	89	
73	Wright		3	all C's	A-L to base	few	to base	
74	Bayha		2-	A/C	L-S to base	none	30	Two C14 dates: 110 BP at 1.3m, and 850 BP at 2.2m
76	Becky		2-	all C's	A-L to base	few	58	
77e	Papikee Group		3	Ab	A-M to 23cm, SB	L to 1.1m	to base	
78.1	Brooks Group		3	all C's	A-L to base	M-L to 1.2m	to base	
78.3	Brooks Group		2+	A, Ab	M-L to 46cm, SB	Few	47	C14 date, 280 BP at 46cm
79.2	Blind Group		3	all C's	M-S to base	L-S to 86cm	to base	end of shotgun shell at 66cm
81	Jim's		3	all C's	A-L to 66cm	L-S to base	to base	
82	Kim's		3	Ab	no info	no info	no info	
84	Little Rocky		2-	A/C	A-L to base	S to base	to base	
85	Menning		2-	all C's	A-L to base	S to base	145	
86	Guffey		1	> Bw	L to 102cm	Few	150	
86a	Guffey Group	F	3	all C's	A-L to base	A-S to base	to base	
87a	Rail Group		2-	all C's	A-M to 64cm SB	M-L to base	to base	
88	Sign		2+	> Bw	M-L to 51cm	to 46cm	not listed	Wood Stove, Bottle, Battery, 1.5-2.3m C14 date, 120 BP at 41cm

* For Pollen and Spore Information:

A - Abundant
M - Moderate
L - Low
S – Sporatic
SB - Sporatic Below